Anti-coronavirus potential of halophytes and invasive plants from Northern France : discovery of active terpenoids from Hippophae rhamnoides and Senecio inaequidens

Malak Al Ibrahim

THÈSE DE DOCTORAT DE L'UNIVERSITÉ DE LILLE

Ecole Doctorale Biologie–Santé

Pour l'obtention du grade de :
Docteur de L'UNIVERSITÉ DE LILLE

Anti-coronavirus potential of halophytes and invasive plants from Northern France: discovery of active terpenoids from *Hippophae rhamnoides* and *Senecio inaequidens*

Halophytes et plantes invasives du Nord de la France avec un potentiel anti-coronavirus : découverte de terpénoïdes actifs isolés *d'Hippophae rhamnoides* et de *Senecio inaequidens*

Directrices de Thèse : **Dr. Karin Séron & Pr. Céline Rivière**

Présentée et soutenue publiquement par

Malak Al Ibrahim

le 25 Janvier 2024

Membres du Jury :

Pr. Angèle Lengo Mambu, Université de Limoges	Rapportrice
Pr. Chaker El Kalamouni, Université de La Réunion	Rapporteur
Pr. François Helle, Université de Picardie Jules-Verne	Examinateur
Pr. Nicolas Blanchemain, Université de Lille	Président
Dr. Karin Séron, Centre d'Infection et d'Immunité de Lille	Directrice de thèse
Pr. Céline Rivière, Université de Lille	Co- directrice de thèse

"There must be no barriers to freedom of inquiry. There is no place for dogma in science. The scientist is free, and must be free to ask any question, to doubt any assertion, to seek for any evidence, to correct any errors. Our political life is also predicated on openness. We know that the only way to avoid error is to detect it and that the only way to detect it is to be free to inquire. And we know that as long as men are free to ask what they must, free to say what they think, free to think what they will, freedom can never be lost, and science can never regress." ***J. ROBERT OPPENHEIMER, 1945***

Acknowledgments

I would like to express my sincere gratitude to all those who have contributed to and supported me throughout the completion of PhD thesis.

Thank you Jean for welcoming me into the MCV lab. I truly appreciate the opportunity to be a part of your team. Your ideas and advice have allowed me to improve my thesis project.

Thank you Jean-Louis Hilbert for welcoming me into the UMRT BioEcoAgro.

Thanks to the members of the PhD jury for accepting the invitation to be part of my committee and dedicating their time to review and assess my thesis. Your willingness to contribute your expertise and insight to evaluate my work is greatly valued.

To my supervisor Karin, thank you for your confidence and trust and for guiding and training me over these three years, thank you for your great patience, your help, and your advice. Your belief in my abilities and the opportunity provided have been pivotal in shaping my academic pursuits and professional growth. I am immensely grateful for your support, guidance, and the invaluable learning experience gained under your mentorship.

To my co-supervisor Céline, I want to express my deepest gratitude to your unwavering patience, exceptional guidance, and tireless support throughout my doctoral journey. Thank you for extraordinary commitment, going above and beyond by conducting structural characterization NMR during your personal time and days off. I am sincerely honored and privileged to have been mentored by someone as dedicated and knowledgeable as you.

Big thank you to Jennifer who's been a total legend, helping me out with HPLC and CPC. Your patience and gentle guidance, even when things went overtime, made a world of difference. Seriously, couldn't have managed without your expertise and cool-headed support. Thanks a ton for always having my back!

A huge shout out to Evariste for being an absolute rock star in assisting with experiments and analyses. Your hard work and expertise has been a game-changer, seriously lightening my load and making a huge difference in this project. I couldn't have done it

without their expertise and dedication, and I'm incredibly grateful for everything you've done to make this research journey smoother.

Thanks for Loweise and Imelda for running the experiments in the BSL 3 for me. Your help was a total lifesaver and I really appreciate you tackling that for me. Couldn't have done it without you!

I also want to thank Gabriel for his diligent effort in collecting and identifying the plant specimens and for his assistance in pulverizing and preparing the crude extracts at the beginning of the PhD.

Massive thanks to Mariam, Asma, Abda, Orfeas, Esther, Djamila, and Augustin for all the laughs and creating such an awesome environment. Those crazy moments and talks we've shared together have been a blast, and I'm grateful for the fun times and fantastic memories we've made. Cheers to our great memories!

A big thank you goes out to all the members of the MCV lab and the pharmacognosy lab. I am sincerely thankful for your active engagement and support throughout my research journey. Your attentive presence during my presentations, insightful questions, and willingness to offer assistance or guidance whenever needed have been invaluable to me. This expression of thanks extends to both former PhD students and other members who were part of the lab during my doctoral studies.

I also want to thank the members of my CSI jury, Madame Sevser, Sandrine, Chaker, and Catherine, for their constructive feedback, and valuable suggestions provided, which have undoubtedly enriched the quality and depth of my research.

I would also like to extend my gratitude to Professor Johan Neyts for graciously welcoming me into his lab at the Rega Institute and including me in their meetings. I am sincerely grateful for the invaluable experience and unwavering support I received during my time there. Additionally, I am thankful for the hospitality shown by providing us with complimentary food during the lab meetings.

I want to express my heartfelt appreciation to Dirk Jochmans for dedicating his time generously, engaging in insightful discussions, and consistently following up during my secondement at the Rega Institute.

I am deeply grateful to the European Union's Horizon 2020 Research and Innovation program and I-Site ULNE under the Marie Sklodowska-Curie grant agreement (PEARL program No. 847568) for funding my PhD. Additionally, I extend my gratitude to the Centre National de la Recherche Scientifique (CNRS: COVID and ViroCrib programs), FEDER-FSE Hauts-de-France region (AP09 REACT-EU 22003058), and CPER BiHauts Eco de France, funded by both the French State and the Hauts-de-France region, for their support of this work.

I would like to extend my deepest appreciation to my parents, Hussein and Fatima, whose unwavering love and encouragement have been the cornerstone of my academic pursuit. Your belief in me during moments of self-doubt and the strength you provided during challenging times have been invaluable. Dad, affectionately calling me 'Queen' with every step I take in life, your belief in me and encouragement have been a crown I wear proudly. Mom, your endless love, encouragement, and support have shaped my character and propelled me through the challenges of academic life. You both sacrificed so much to provide me with the best education possible. This achievement stands as a testament to your dedication, sacrifices, and unwavering belief in my dreams. I hope I have made you proud by the end of this journey.

I extend my heartfelt gratitude to my sisters, Sokaina and Farah, and my brothers, Ali and Ahmad. This PhD journey has been a rollercoaster ride filled with highs and lows, and I wouldn't have made it this far without your unwavering support and encouragement. Your consistent belief in my abilities, words of encouragement during challenging times, and endless patience have been an immense source of strength and motivation for me.

MALAK AL IBRAHIM

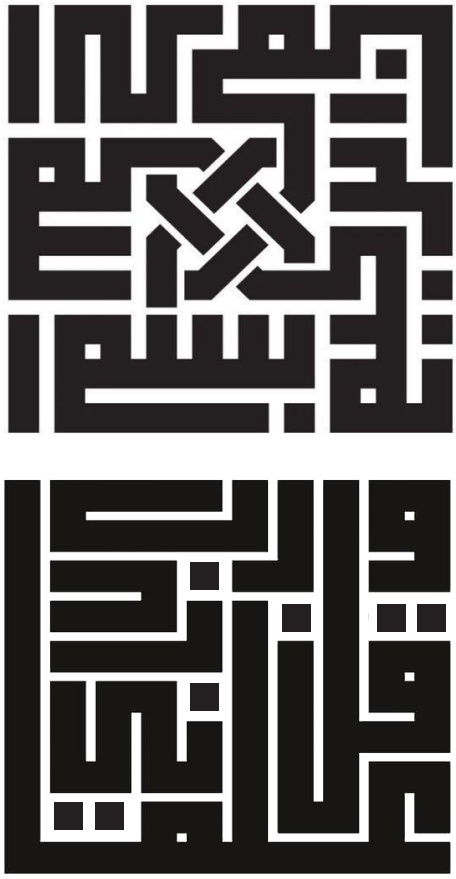

“I dedicate this work to my beloved family whose unconditional love, encouragement, and support have been the cornerstone of my journey, inspiring me to achieve this milestone. I also dedicate this work to the land of resilience and resistance, to my beloved Lebanon . May its enduring spirit forever shine as a beacon of hope and perseverance.”

Table of Contents

List of Figures

List of Tables

List of Abbreviations

Abbreviation	Definition
3CLpro or Mpro	Chymotrypsin-Like Protease
6-HB	6-Helix Bundle
ABTS	2,2′-Azino-Bis(3-Ethylbenzthiazoline-6-Sulfonic Acid
ACE2	Angiotensin-Converting Enzyme 2
ADRS	Acute Respiratory Distress Syndrome
APN	Aminopeptidase N
Aq	Aqueous
BCoV	Bovine Coronavirus
BoCoV	Bovine Coronaviruses
CC50	50% Cytotoxic Concentration
CCL2	Chemokine Ligands 2
CCL4	Chemokine Ligands 4
CCoV	Canine Coronavirus
CD	Connector Domain
CFR	Case-Fatality Rate
CH	Central Helix
CM	Convoluted Membranes
COVID-19	Coronavirus Disease 2019
CPC	Centrifugal Partition Chromatography
CQ	Chloroquine
CRCoV	Canine Respiratory Coronavirus
CSG	Coronavirus Study Group
CT	Cytoplasmic Tail
CTD	C- Terminal Domain
CTLs	Cytotoxic T Lymphocytes
DCM	Dichloromethane
DHP	Dehydropyrrolizidine
DMAPP	Dimethylallyl-Pyrophosphate
DMSO	Dimethyl Sulfoxide
DMV	Double-Membrane Vesicles
DPP4	Dipeptidyl Peptidase-4
DPPH	Diphenyl-1-Picrylhydrazyl
dsRNA	Double-Stranded
E	Envelope Protein
ECoV	Equine Coronavirus
EMA	European Medicines Agency
ER	Endoplasmic Reticulum

ERGIC	Endoplasmic Reticulum-Golgi Intermediate Compartment
EtOAc	Ethyl Actete
EUA	Emergency Use Authorization
FCoV	Feline Coronavirus
FECV	Feline Enteric Coronavirus
FIP	Feline Infectious Peritonitis
FP	Fusion Peptide
GGPP	Geranylgeranyl-Pyrophosphate
GPP	Geranyl-Pyrophosphate
gRNA	Gemonic Rna
HAEC	Human Airway Epithelial Cells
HCQ	Hydroxychloroquine
HE	Hemagglutinin-Esterase
HEV	Hemagglutinating Encephalomyelitis Virus
HR1	Heptad Repeat 1
HR2	Heptad Repeat 2
HSV-1	Herpes Simplex Type 1
HSV-2	Herpes Simplex Type 2
HR DCM SE	DCM sub-extract of *Hippophae rhamnoides*
HT	Hydroxytyrosol
IAS	Invasive Alien Species
IBV	Infectious Bronchitis Virus
IC50	The 50% Inhibitory Concentration
ICTV	International Committee On Taxonomy Of Viruses
IDR	Inherently Disordered Region
IFN-I	Type I Interferon
IFN-γ	Interferon Gamma
IL-15	Interleukin 15
IL-17	Interleukin 17
IL-6	Interleukin 6
IPP	Isopentenyl-Pyrophosphate
L	Leaves
LKR	Central Linking Region
LPV/r	Lopinavir And Ritonavir
M	Membrane Protein
MA	Maslinic Acid
MD	Molecular Docking
MERS-CoV	Middle East Respiratory Syndrome Coronavirus
MHV	Murine Hepatitis Virus
MIC	Minimal Inhibitory Concentration
MIS	Multisystem Inflammatory Syndrome
MS	Spectrometry

MTS	3-(4,5-Dimethylthiazol-2-Yl)-5-(3-Carboxymethoxyphenyl)-2-(4-Sulfophenyl)-2H-Tetrazolium
N	Nucleocapsid Protein
NCoV	Novel Coronavirus
NHC	Beta-D-N4-Hydroxycytidine
NIH	National Institute Of Health
NMR	Nuclear Magnetic Resonance
NP	Natural Products
Nsps	Nonstructural Proteins
NTD	N-Terminal Domain
OA	Oleanolic Acid
O-ac Sia	O-Acetylated Sialic Acid
ORF	Open Reading Frames
PDCoV	Porcine Deltacoronavirus
PEDV	Porcine Epidemic Diarrhea Virus
PhCoV	Pheasant Coronavirus
PHEIC	Public Health Emergency Of International Concern
PHEV	Porcine Hemagglutinating Encephalomyelitis Virus
Plpro	Papain-Like Proteases
PPE	Personal Protective Equipment
PRCV	Porcine Respiratory Coronavirus
PS	Packaging Signal
PSM	Plant Specialized Metabolites
PV	Poliovirus Type 2
R	Roots
RBD	Receptor-Binding Domains
RdRp	Rna-Dependent Rna Polymerase
RNP	Ribonucleoprotein Complex
ROS	Reactive Oxygen Species
RTC	Randomized Controlled Trial
RtCoV	Rat Coronavirus
RVNA	Rabies Virus Neutralizing Antibodies
S	Spike Protein
S	Stesms
S1/S2	S1/S2 Protease Cleavage Site
SADSCoV	Swine Acute Diarrhea Syndrome Coronavirus
SARS-CoV	Severe Acute Respiratory Syndrome Coronavirus
SARS-CoV-2	Severe Acute Respiratory Syndrome Coronavirus-2
SCSP	Cucumber Sulfated Polysaccharide
SD1	Subdomain 1
SD2	Subdomain 2

SI	Selectivity Index
SI DCM SE	DCM sub-extract of *Senecio inaequidens*
SL-CoVs	Sars-Like CoVs
SS	Single Sequence
SSE	Super-Spreading Events
TCM	Traditional Chinese Medicine
TCoV	Turkey Coronavirus
TGEV	Transmissible Gastroenteritis Virus
TMD	Transmembrane Domain
TMPRSS2	Transmembrane Protease, Serine 2
TNF	Tumor Necrosis Factor
TRS	Transcriptional Regulatory Sequence
UA	Ursolic Acid
UHPLC	Ultra-High Performance Liquid Chromatography
VLP	Virus-Like Particles
VOC	Variant Of Concern
VOI	Variant Of Interest
VUM	Variant Under Monitoring
WHO	World Health Organization

Scientific Contribution

Publications

1. **Malak Al Ibrahim**, Zachee Louis Evariste Akissi [†], Lowiese Desmarets[†], Gabriel Lefèvre, Jennifer Samaillie, Imelda Raczkiewicz, Sevser Sahpaz, Jean Dubuisson, Sandrine Belouzard, Céline Rivière[‡], and Karin Séron[‡].
   Discovery of Anti-Coronavirus Cinnamoyl Triterpenoids Isolated from *Hippophae rhamnoides* during a Screening of Halophytes from the North Sea and Channel Coasts in Northern France.

   International Journal of Molecular Sciences, 24(23), Article 23. https://www.mdpi.com/1422-0067/24/23/16617

2. Abda Ba, Vincent Roumy, **Malak Al Ibrahim**, Imelda Raczkiewicz, Jennifer Samaillie, Asma Hakem, Sevser Sahpaz, Sandrine Belouzard, William Diatta, Mamadou Sidybé, Christel Neut, Karin Séron, Matar Seck, Céline Rivière.

   Antibacterial and anti-coronavirus investigation of selected Senegalese plant species according to an ethnobotanical survey (*Journal of Ethnopharmacology*, submitted,)

Communications

1. **Malak Al Ibrahim**, Lowiese Desmarets, Gabriel Lefèvre, Jennifer Samaillie, Nathan François, Sevser Sahpaz, Jean Dubuisson, Sandrine Belouzard, Céline Rivière[‡], Karin Séron[‡].
   Exploration of the antiviral activity of halophytes and salt tolerant plant species in the North of France against human coronaviruses, One Health International Day (OHID), June 2002, Lille, France- **Oral**

2. **Malak Al Ibrahim**, Lowiese Desmarets, Gabriel Lefèvre, Jennifer Samaillie, Nathan François, Sevser Sahpaz, Jean Dubuisson, Sandrine Belouzard, Céline Rivière[‡], Karin Séron[‡].
   In vitro antiviral potential of an Asteraceae plant species collected in northern France against coronavirus, 24th Annual Conference of the European Society for Clinical Virology, September 2022, Manchester, United Kingdom- **Poster**

3. **Malak Al Ibrahim**, Lowiese Desmarets, Gabriel Lefèvre, Jennifer Samaillie, Nathan François, Sevser Sahpaz, Jean Dubuisson, Sandrine Belouzard, Céline Rivière[‡], Karin Séron[‡].
   1st Joint Meeting on Natural Products Pharmacology SIF-SIPHAR-IMGNPP, Italian Society of Pharmacology and Pharmacognosy, February 2022, Naples, Italy- **Poster**

This page is intentionally left blank.

Abstract

Coronaviruses are responsible for mild to severe respiratory tract illnesses in humans. Despite significant advancements in understanding coronavirus pathology and clinical management, these viral diseases remain a public health concern due to recurrent outbreaks driven by the emergence of variants, unequal access to COVID-19 treatments, inadequate vaccination rates and untreated high-risk populations. Thus, it is imperative to proactively develop specific and affordable antiviral solutions to control and prevent future pandemics. Plants exposed to abiotic stress factors and new environments represent a vast source of bioactive compounds. In this project, we investigated the antiviral potential *in vitro* of different halophytes, less salt-tolerant plants and invasive plants collected in the North of France against different coronaviruses.

In the first part of the project, a variety of strictly halophytes and relatively salt-tolerant plants growing on the coastline in northern France were screened for their *in vitro* antiviral activity against different coronaviruses. The most active plant species, *Hippophae rhamnoides* L. (Eleagnaceae), underwent bioguided fractionation to identify active natural products. Six compounds were isolated from the three most active fractions using preparative HPLC and were identified as cinnamoyl triterpenoids through HRMS and mono- and bi-dimensional NMR. Infection tests demonstrated a dose-dependent inhibition of these triterpenes against HCoV-229E and SARS-CoV-2, notably highlighting their activity against both viruses.

In the second part of the project, the antiviral potential against coronaviruses of *Senecio inaequidens* (Asteraceae), an invasive plant species, was explored. Six compounds purified by CPC and preparative HPLC were identified as sesquiterpenoid derivatives. They displayed a dose-dependent inhibitory effect on HCoV-229E and four of them also exhibited inhibition against SARS-CoV-2.

Our findings suggest that *Hippophae rhamnoides* and *Senecio inaequidens* could represent potential sources of antiviral agents against human coronaviruses.

Keywords: coronaviruses; bioguided fractionation; SARS-CoV-2; natural products; terpenoids; screening

Résumé

Les coronavirus sont responsables de maladies des voies respiratoires bénignes à graves chez l'Homme. Malgré des progrès significatifs dans la compréhension de la pathologie et de la gestion clinique des coronavirus, ces maladies virales restent un problème de santé publique en raison d'épidémies récurrentes provoquées par l'émergence de variants, d'un accès inégal aux traitements contre la COVID-19, de taux de vaccination inadéquats et de populations à haut risque non vaccinées. Il est donc impératif de développer des solutions antivirales spécifiques et abordables pour contrôler et prévenir de futures pandémies. Les plantes exposées à des facteurs de stress abiotiques et à de nouveaux environnements représentent une vaste source de composés bioactifs. Dans ce projet, nous avons étudié le potentiel antiviral *in vitro* contre différents coronavirus de plantes halophytes et invasives récoltées dans le nord de la France.

Dans la première partie du projet, des halophytes strictes et d'autres relativement tolérantes au sel poussant sur le littoral du nord de la France ont été sélectionnées et testées pour leur activité antivirale *in vitro* contre différents coronavirus. L'espèce végétale la plus active, *Hippophae rhamnoides* L. (Eléagnacées), a subi un fractionnement bioguidé pour identifier les composés actifs. Six composés ont été isolés des trois fractions les plus actives par HPLC préparative et ont été identifiés par HRMS et RMN mono- et bidimensionnelle comme étant des triterpènes substitués par des dérivés d'acide cinnamique. Les tests d'infection ont démontré une inhibition dose-dépendante de ces triterpènes contre le HCoV-229E et le SARS-CoV-2, mettant notamment en évidence leur activité contre les deux virus.

Dans la deuxième partie du projet, le potentiel antiviral contre les coronavirus de *Senecio inaequidens* (Asteraceae), une espèce végétale envahissante, a été exploré. Six composés purifiés par CPC et CLHP préparative ont été identifiés comme étant des dérivés de sesquiterpènes. Ils ont présenté un effet inhibiteur dose-dépendant sur le HCoV-229E, et quatre d'entre eux se sont montrés également actifs contre le SARS-CoV-2.

Nos résultats suggèrent que *Hippophae rhamnoides* et *Senecio inaequidens* pourraient représenter des sources potentielles d'agents antiviraux contre les coronavirus humains

Mots clés : coronavirus, fractionnement bioguidé, SARS-CoV-2, produits naturels, terpénoïdes, criblages

I. Aims of the PhD project

Previous collaborative studies on extremophile plants, conducted by my two supervisors, have enabled the discovery of natural compounds possessing antiviral properties. Notably, dehydrojuncusol, isolated from the halophyte *Juncus maritimus*, has demonstrated its ability to inhibit the replication of the hepatitis C virus (Sahuc et al., 2019). In this context, we further investigated the antiviral capacities of halophytes and invasive plant species. This research project aims to explore the potential of natural compounds from plant species collected in Northern France for their antiviral effects against human coronaviruses such as HCoV-229E and SARS-CoV-2. The project is divided into two main parts:

1. **Study of the anti-coronavirus potential of halophytes and less salt tolerant plant species, with focus on *Hippophae rhamnoides*:** The initial phase involves the investigation of various plant species, particularly emphasizing halophytes and less salt-tolerant species. Special attention is given to the antiviral activity of cinnamoyl triterpenoids isolated from *Hippophae rhamnoides*.
2. **Investigation of the anti-coronavirus potential of *Senecio inaequidens*:** The second part focuses on exploring the antiviral properties of the invasive plant species *Senecio inaequidens*.

To identify potential bioactive compounds with antiviral effects against coronaviruses, plant samples were collected from different regions along the northern French coast. Crude methanolic extracts were prepared using solid-liquid extraction methods. The extracts cytotoxicity was assessed via the MTS assay, while antiviral activity was evaluated using assays such as luciferase assays and western blot analysis on the crude extracts derived from all collected plants. Further steps involved liquid-liquid partitioning of the most active extracts to isolate and identify the active components against human coronaviruses. The active partition was then subjected to purification processes, including bio-guided assay fractionation and purification by means of preparative chromatography (CPC and preparative HPLC). The purified bioactive compounds responsible for the observed antiviral effects were identified by HR-MS and NMR spectroscopy. This comprehensive methodology integrated various extraction, testing, and purification techniques to isolate and characterize potential antiviral compounds from the collected plants. The aim was to identify novel natural compounds that could serve as potential antiviral agents against coronaviruses, thereby contributing to the development of new therapeutic strategies.

II. Introduction

Part 1

1. Coronavirus: History, classification, epidemiology, pathogenesis, transmission, viral cycle

1.1. History of coronaviruses

Coronaviruses are enveloped viruses with a linear, non-segmented, positive sense, single-stranded RNA genome. They are large RNA viruses, with genome size ranging from 25 to 32 kb, and virion size between 120 nm to 140 nm in size. Coronavirus virions are pleomorphic although often spherical, composed of an outer lipid layer covered with a crown of club-shaped spikes. The name "coronavirus" is derived from the Latin word corona, meaning "crown". *Corona* is derived from the Ancient Greek κορώνη *(korōnè),* meaning “garland” or “wreath,” coming from a proto-Indo-European root, *sker- or ker-*, meaning “to turn" or “to bend” (Cavanagh, 2005). CoVs belong to the subfamily *Orthocoronavirinae* of the *Coronaviridae* family in the *Cornidovirineae* suborder of the *Nidovirales* order (Payne, 2017). The *Coronaviridae* subfamily comprises four genera, *Alphacoronavirus, Betacoronavirus, Gammacoronavirus* and *Deltacoronavirus*. *Alpha-* and *Betacoronaviruses* are known to infect mammals, whereas *Gamma-* and *Deltacoronaviruses* circulate primarily in birds with the exception of porcine deltacoronavirus (PDCoV) of pigs and a gammacoronavirus of beluga whales **(Figure 1)**. Coronaviruses were initially grouped on serological cross-reactivity which has subsequently been refined by gene sequencing.

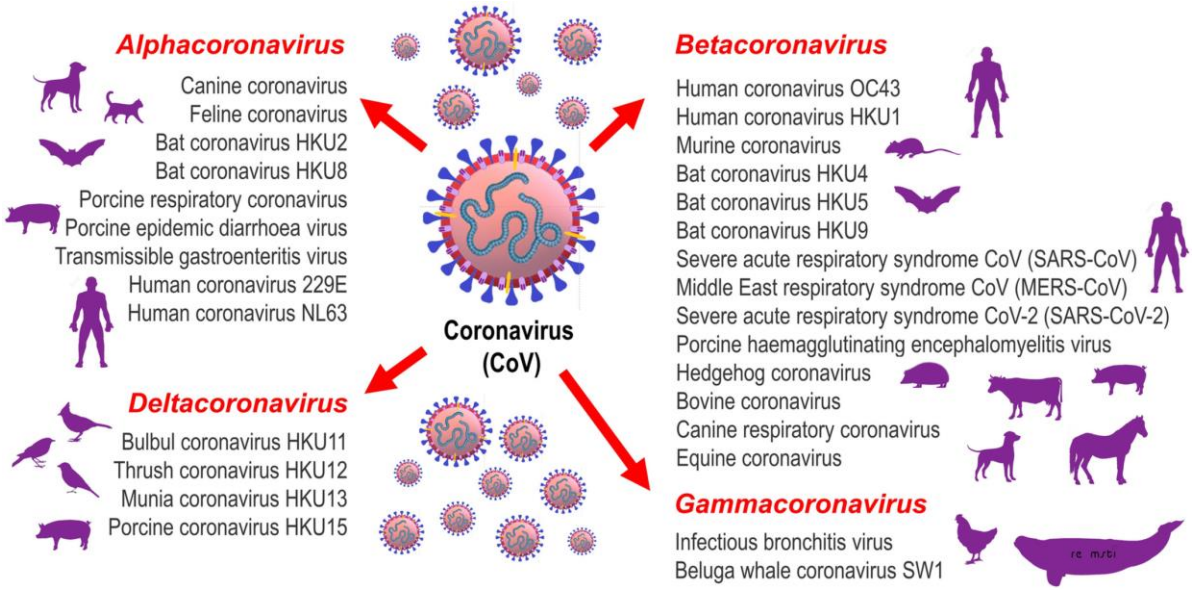

Figure 1. Classification of CoV genera – *Alphacoronavirus*, *Betacoronavirus*, *Gammacoronavirus*, and *Deltacoronavirus* (Sharun et al., 2020).

1.2. Animal coronaviruses

Coronaviruses are globally spread pathogens that infect a wide range of mammals, including humans, and various species of birds. They have been isolated from bovine, dromedary camel, porcine, feline, canine, and avian species. The major group of CoVs comprises porcine transmissible gastroenteritis virus (TGEV), feline coronavirus (FCoV), canine coronavirus (CCoV), HCoV-229E, and porcine epidemic diarrhea virus (PEDV). The second group consists of murine hepatitis virus (MHV), bovine coronavirus (BCoV), HCoV-OC43, porcine hemagglutinating encephalomyelitis virus (HEV), rat coronavirus (RtCoV), and equine coronavirus (ECoV). The third group comprises infectious bronchitis virus (IBV), turkey coronavirus (TCoV), and pheasant coronavirus.

1.2.1. Bovine coronaviruses

Bovine coronaviruses (BoCoVs) are known as the ancestor of many other coronaviruses that affect other species including humans (HCoV-OC43), swine (Porcine Hemagglutinating Encephalomyelitis virus—PHEV), equids (ECoV), and dogs (CRCoV). BoCoVs are known to infect mice and several domestic and wild ruminants. BoCoV has tropism for the intestinal tract causing neonatal calf diarrhea and winter dysentery in adult cattle (Decaro et al., 2008). Besides, BoCoVs can cause respiratory disease complex calf pneumonia and contribute to shipping fever (Storz et al., 2000).

1.2.2. Feline coronaviruses

Two major biotypes of feline coronaviruses with different pathogenicity exist: feline enteric coronavirus (FECV) (ubiquitous enteric biotype), and feline infectious peritonitis (FIP) viruses (virulent biotype) (Pedersen, 2009). Both FECV and FIPV are divided into two types I and II, based on Ab neutralization of spike (S) protein and the genetic divergence in the S gene. FCoV type I poorly propagates in cells, whereas type II can grow well in many different cell lines, thus it is mostly used as a model in cell (Pedersen et al., 1984). FECVs are highly contagious and are transmitted horizontally via the fecal–oral route. Most infections with FECV infections are benign, undetected, or cause mild diarrhea. However, FECVs can occasionally induce severe enteritis. Approximately 20–60% of domestic cats are seropositive. In contrast, FIPV are known to be fatal causing FIP which a lethal disease characterized by fibrinous and granulomatous serositis, vasculitis, protein-rich serous effusion in body cavities, and fibrinous and granulomatous inflammatory lesions (pyogranulomas) (Hayashi et al., 1977).

1.2.3. Canine coronaviruses

Canine coronavirus disease, known as CCoV are known to infect dogs and were first identified in 1971. Three different canine coronaviruses have been identified. CCoV type I and type II are included in group 1 coronaviruses. Genetic analysis of several CCoVs type I revealed genetic similarity to FCoV type I than to CCoV type II (Pratelli et al., 2003). Sequence analysis of the genome of FCoVs revealed that type II originated by a template switch between CCoV type II and FCoV type I.

1.2.4. Porcine coronaviruses

Porcine coronaviruses are known to infect piglets of all ages. So far, six CoVs infect pigs, including four that belong to the genera alphacoronaviruses: transmissible gastroenteritis virus (TGEV), porcine respiratory coronavirus (PRCV), the porcine epidemic diarrhea virus (PEDV), and the swine acute diarrhea syndrome coronavirus (SADSCoV), one belongs to the genus *Betacoronavirus*, porcine hemagglutinating encephalomyelitis virus (PHEV), and one to the *Deltacoronavirus*, the porcine deltacoronavirus (PDCoV) (Q. Wang et al., 2019). TGEV, PRCV, and PHEV have been circulating in swine for decades, whereas PEDV, PDCoV and SADS-CoV are considered newly emerging coronaviruses.

Transmissible gastroenteritis virus (TGEV)

Transmissible gastroenteritis virus (TGEV) was first reported in the US in 1946 after an epidemic of transmissible gastroenteritis (Doyle & Hutchings, 1946). Subsequently, outbreaks of TGEV have been reported in many countries with large swine industries as Canada, China, Australia Japan, China, Belgium, and Africa (Kemeny & Woods, 1977; Pritchard, 1987; Wood et al., 1981).

Porcine respiratory coronavirus (PRCV)

PRCV is common in the swine population and is not associated with significant problems. Unlike TGEV, PRCV is an airborne virus that infects the respiratory tract of pigs. PRCV has been observed in many European countries including the Netherlands, Denmark, Great Britain, Spain, Belgium and France as well as the United States (Enjuanes & van der Zeijst, 1995). Interestingly, cross protection exists between PRCV and TGEV, thereby, the antibodies formed as a result of infection with PRCV protect pigs against TGEV infection. This explains how TGEV became less present and is no longer a significant problem for pig farmers in Europe.

Porcine epidemic diarrhea virus (PEDV)

PEDV was identified in 1974 after sporadic outbreak Porcine epidemic diarrhea (PED) in Europe, since 1971, leading to substantial economic losses on breeding farms due to the high mortality among piglets (Song & Park, 2012). In Asia, PEDV was first reported in Asia in the 1980s and is still a concerning virus and a major pig pathogen, causing more severe outbreak than those occurring in Europe (H. Fan et al., 2012; Luo et al., 2012). Since its appearance in the US in April 2003, it has rapidly spread across the country, causing high death cases in swine farms (Stevenson et al., 2013). PEDV is mainly transmitted through direct contact through the fecal–oral route or indirect contact, particularly in farms with low biosecurity measures (Jung & Saif, 2015). Airborne PDEV transmission through the fecal–nasal route is another route for the virus to spread, particularly among neonatal piglets (Niederwerder et al., 2016). PED is a disease characterized by acute diarrhea, dehydration, and/or vomiting in newborn pigs.

Currently, no vaccine is available to prevent PEDV circulation in pigs, therefore, future PED outbreaks are still predictable to occur in pigs.

It is worth noting that a chimeric swine enteric coronavirus (SeCoV), reported in Germany and Italy, Slovakia, and Spain, is a novel recombinant between TGEV and PEDV, with most of the genome originating from TGEV, and the S and 3A genes being derived from PEDV (Akimkin et al., 2016; Boniotti et al., 2016; de Nova et al., 2020; Mandelik et al., 2018).

Porcine hemagglutinating encephalomyelitis virus (PHEV)

PHEV, a member of the genus *Betacoronavirus*, is known as an etiological agent of vomiting and wasting disease in pigs. The first clinical outbreak of PHEV was reported in Ontario Canada (Roe & Alexander, 1958), but it was not until 1962 that PHEV was isolated and identified (Greig et al., 1962). PHEV replicates in the nasal mucosa and tonsils, causing nonspecific respiratory symptoms as cough and sneezing at the beginning of infection. Replication in the primary sites of replication allows it to spread through the peripheral nervous system to the central nervous system (CNS) causing encephalomyelitis in piglets. There is no vaccine available against PHEV, however, dithiothreitol and ether are considered effective in PHEV disinfection (Mora-Díaz et al., 2021).

Swine acute diarrhea syndrome coronavirus (SADS-CoV)

SADS-CoV, emerged first in China, Guangdong province, in 2016 with high mortality among baby pigs (Gong et al., 2017). The SADS-CoV genome isolated from severe outbreaks in piglets has been closely related to bat CoV HKU2 identified in 2007 (95 % nucleotide identity), suggesting that it originates from bats (P. Zhou et al., 2018). Like other enteric swine coronaviruses, infection with SADS-CoV is associated with acute diarrhea and vomiting leading to weight loss, dehydration, and with 90% mortality rates in piglets under five days of age (L. Zhou et al., 2019).

Porcine deltacoronavirus (PDCoV)

PDCoV belongs to the genus *Deltacoronavirus*, was first identified and reported in Hong Kong and China in 2012 (Woo et al., 2012) and was first introduced in the US in

2014 spreading throughout the country (Marthaler et al., 2014). Infection with PDCoV, like TGEV, displays a similar pattern by propagating in intestinal epithelia causing enterocyte loss, villus atrophy, which is manifested by acute, watery diarrhea and vomiting, leading to dehydration and body weight loss with increased mortality in young piglets.

1.2.5. Avian coronavirus

Infectious bronchitis virus (IBV)

Avian CoVs belong to the genus *Gammacoronavirus* that includes three major species: IBV, which was the first coronavirus isolated from an outbreak in chicken flocks in 1937. The virus can infect wild birds and domestic fowl (*Gallus gallus*), both gallinaceous and non-gallinaceous species. Chickens (*Gallus gallus*) and pheasants are the only natural hosts for IBV. On the other hand, IBV has been detected in other bird species as turkeys, quails and penguins, pigeons, geese (Circella et al., 2007; Dea & Tijssen, 1989; Karesh et al., 1999).

IBV or IBV-like *Gammacoronaviruses* are a major cause of severe economic loss in the poultry industry by causing bronchitis, urinary tract infection, and reproductive problems in chickens. The clinical signs and severity of infection depend on the age group, immunity and virus virulence. Young chicks develop the most severe respiratory forms of the infection, whereas IBV causes older birds most reproductive lesions and drops in egg production in adult birds. Given the highly infectious nature of the virus, continual emergence of antigenic variants, and its omnipresence in wild and domestic bird species, controlling its spread in the poultry industry globally, even with the strictest preventative measures applied, is very challenging. Despite the vaccination programs and procedures to eradicate the virus, no countries with intensive poultry industry are free from IBV. Outbreaks of IBV continue to occur due to the continual emergence of antigenic variants that evade the immune response, as well as increased virus virulence. Therefore, multiple vaccines are required to control the spread of IBV and provide cross protection. Two types of vaccine, live and inactivated vaccines, are used. Live vaccines cause a reduction in virus virulence; however, the risk of high attenuations might make the vaccine highly virulent. On the other hand, inactivated vaccines production is more expensive, less protective thus requires continuous dosing and application to achieve long term protection (Cavanagh, 2007).

Pheasant coronavirus (PhCoV)

PhCoV had a great similarity to IBV on the morphological and genetic level; however, they differ in terms of antigenicity, replication, and viral pathogenicity by causing respiratory and kidney disease.

Turkey coronavirus (TCoV)

TCoV causes enteric disease in turkeys (Day et al., 2014). Outbreak of TCoV infection has been occurring sporadically worldwide, with the main method of protection relying on conventional biosecurity measures and depopulation upon the disease outbreak (Jindal et al., 2014).

1.3. Human coronaviruses

The era of human coronaviruses began in the mid-1960s by Tyrrell and Bynoe (Tyrrell & Bynoe, 1966) who successfully isolated a virus from the nasal washings of a male child, naming it as B814. Within the same period, Hamre and Procknow characterized other etiological agent of respiratory tract infections, 229E, in medical graduates with symptoms of common cold (Hamre & Procknow, 1966). Subsequently, McIntosh et al. were able to isolate two viruses, OC38 and 43, using an organ culture method similar to the technique adapted by Tyrrell and Bynoe (McIntosh et al., 1967). HCoV-229E and HCoV-OC43 were classified as *Alphacoronavirus* and *Betacoronavirus*, respectively. They were recognized as mild respiratory tract pathogens, causing flu-like infection, thus they were not further explored or investigated in the research field. It was until 2002–2003, a highly pathogenic *Betacoronavirus* named severe acute respiratory syndrome coronavirus (SARS-CoV) emerged in Guangdong province in South China causing severe acute respiratory infection with high morbidity and mortality rates that were not reported with the previously discovered coronaviruses (Zhong et al., 2003). Even though the outbreak has ended a year after its appearance, two new CoVs have been discovered, the *Alphacoronavirus* HCoV-NL63 and the *Betacoronavirus* HCoV-HKU1. HCoV-NL63 was isolated in 2004 from a child suffering from bronchiolitis and conjunctivitis in the Netherlands, however, HCoV-HKU1 was discovered in 2005 from a 71-year-old man with pneumonia in Hong-Kong (van der Hoek et al., 2005; Woo et al., 2005). A decade after the discovery of SARS-CoV, another highly pathogenic human *Betacoronavirus* that causes severe respiratory syndrome has emerged in the Middle East

thus named Middle East respiratory syndrome coronavirus (MERS-CoV). The virus was isolated in Saudi Arabia from an old man who developed pneumonia and renal failure (Zaki et al., 2012). In late December 2019 a novel human CoV, SARS-CoV-2, similar to SARS-CoV, was discovered in Wuhan, China, when some patients were diagnosed with pneumonia. Since then, the virus has rapidly widespread across all countries worldwide becoming the major pandemic since the 21st century **(Figure 2)**.

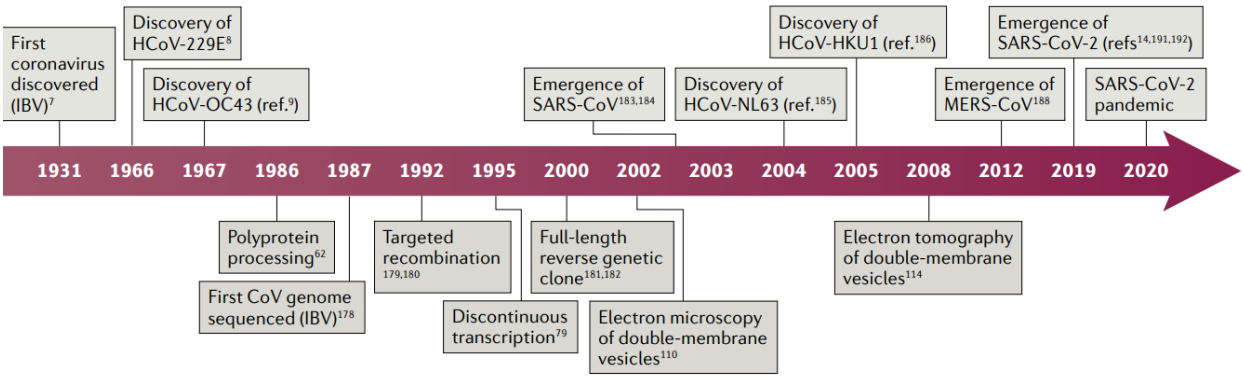

Figure 2. Timeline of CoV discovery (V'kovski et al., 2021).

1.3.1. Mild human coronaviruses

HCoV-229E

HCoV-229E (named after a student specimen coded 229E) was first isolated in 1965 from the nasal discharge of a medical student. The discovery of the isolate B814 led to the discovery of HCoV-229E. It is one of the four mild human coronaviruses that circulate worldwide and was the first HCoV to be fully sequenced (Thiel et al., 2001).

HCoV-229E has been previously associated with various human diseases, leading to various clinical syndromes, ranging from self-resolving common cold in adults to pneumonia in children and the elderly. HCoV-229E infection has generally been associated with mild upper respiratory tract infections such as common colds in immunocompetent individuals, and severe and life-threatening lower respiratory tract infections in immunocompromised individuals (Walsh et al., 2013; Pene et al., 2003). Additionally, serological tests have suggested the involvement of HCoV-229E in the development of Kawasaki disease (Shirato et al., 2014).

The incidence of HCoV-229E is usually lower than that of other types of circulating coronaviruses. A synopsis of the seasonality of HCoVs between 2014 and 2021 in the

United States showed that HCoV-229E accounted for 12.2% of HCoV positive cases, were HCoV-229E being the lowest in percentage among children <5 years of age (M. M. Shah et al., 2022). Similarly, in the United Kingdom, HCoV-229E represented 12.4% of all HCoV positive cases (Gaunt et al., 2010). This observation was also reported in Hong Kong in 2006, with HCoV-229E representing 4.5% of all HCoV-229E positive specimens (Lau et al., 2006).

HCoV-229E tends to be epidemic, predominantly circulating during the winter season in temperate climate countries. In the USA, infections with HCoV-229E occurred in winter and spring (Hendley et al., 1972). Similarly, in Belgium, an HCoV-229E case was detected during winter and early spring (Moës et al., 2005). A previously published report indicated that an HCoV-229E laboratory strain remained viable on various surfaces for 7 days, suggesting its relative stability in the environment (Bonny et al., 2018).

Symptoms of HCoV-229E infection in adults are mostly common cold-like and include general malaise, headache, nasal discharge, sneezing, a sore throat and sometimes cough and fever. Typically, symptoms peak on day 3 or 4 of illness and are self-limited (Poutanen, 2018). While the HCoV-229E was detected in stool specimens, this does not necessarily imply its involvement in acute gastroenteritis (Risku et al., 2010). Sequence analysis of HCoV-229E isolates circulating in Victoria, Australia, between 1979 and 2004 did not reveal distinct subtypes of HCoV-229E suggesting minimal genetic divergence (Chibo & Birch, 2006).

HCoV-OC43

First isolated in 1967, HCoV-OC43 is more prevalent than other HCoVs and is generally associated with mild upper respiratory tract infections in pediatrics and adults, although it has adopted neuro-invasive properties such as fatal encephalitis (Dijkman et al., 2012; Morfopoulou et al., 2016). Even though HCoV-OC43 has no serological cross-reactivity with HCoV-229E, the two viruses could not be distinguished based solely on clinical symptoms. Similar to HCoV-229E, HCoV-OC43 is also primarily transmitted during the winter and spring seasons in temperate climates.

However, in contrast to HCoV-229E, phylogenetic and evolutionary analyses of spike protein of HCoV-OC43 isolates in Belgium and China have showed the presence of genetically divergent strains (Vijgen, Keyaerts, Lemey, et al., 2005; Y. Zhang et al., 2015).

Since its emergence, seven genotypes (A–G) have been identified by phylogenetic analysis, which might explain the ability of HCoV-OC43 to infect mice as well as other ruminant species. The genetic sequence of HCoV-OC43 shows a high similarity of 96% to the bovine coronavirus.

Molecular clock analysis of HCoV-OC43 suggested it has a zoonotic origin and was transmitted from bovine to humans in the 1890s (Vijgen, Keyaerts, Moës, et al., 2005).

HCoV-NL63

HCoV-NL63 was identified in 2004. The majority of HCoV-NL63 infections are mild, although it has been associated with pneumonia or neurological diseases, particularly in children, the elderly, and immunocompromised individuals. NL63 is the most frequently identified respiratory virus for croup in children (van der Hoek et al., 2005). Along with HCoV-OC43, it is responsible for most hospitalizations among all mild HCoVs. Coinfection with NL-63 and other respiratory viruses is very frequent; however, mixed viral infection is not necessarily associated with increased disease severity.

Phylogenetically, HCoV-NL63 and HCoV-229E are more closely related to each other than to any other human coronavirus, sharing 65% sequence homology. HCoV-NL63 circulates and peaks in winter and spring in temperate regions, which contrasts with the summer-to-autumn seasonality reported in tropical and subtropical regions (Lau et al., 2006; Moës et al., 2005).

HCoV-HKU1

HCoV-HKU1 was first discovered shortly after HCoV-NL63, and has roughly the same clinical presentation. The virus usually causes upper respiratory infections, but pneumonia or acute bronchiolitis were also observed (Lau et al., 2006). Considering the symptoms they cause, these human coronaviruses are clinically indistinguishable from rhinoviruses or influenza viruses.

1.3.2. Highly pathogenic human coronaviruses

Severe acute respiratory syndrome coronavirus (SARS-CoV)

The severe acute respiratory syndrome (SARS) caused by the SARS-CoV was first detected in Guangdong, China, in 2002 (Peiris et al., 2003). SARS began to spread globally after a patient traveled from mainland China to Hong Kong. Since then, it has spread rapidly to 29 other countries causing more than 8000 cases with a 10% mortality rate between November 2002 and July 2003 (World Health Organization, 2015). Generally, the number of death cases was much higher in elderly people than in pediatrics and adults (Donnelly et al., 2003; So et al., 2004). The high mortality rate within this age group was linked to a history of chronic diseases such as heart and respiratory illnesses. SARS was mainly characterized by flu-like signs and symptoms including fever, chills, muscle aches, headache, and occasionally diarrhea. The incubation period of SARS was usually 2-7 days but could be as long as 10 days. Patients were most contagious during the second week of illness (Center for Disease Control and Prevention, 2005). SARS-CoV was transmitted via close personal contact through respiratory droplets and perhaps by airborne transmission. Previous reports detected the presence of SARS-CoV in respiratory secretions and stool and urine specimens of infected individuals (Chan et al., 2004). Even though this rate does not reflect evidence of multiple infections over a short time span, super-spreading events (SSE) have been reported for SARS-CoV.

Nosocomial transmission was the primary accelerator of SARS infections. A highly effective episode of viral transmission occurred in Hong Kong when one patient was responsible for transmitting the virus to 138 persons (mostly healthcare workers) who had been in contact with him (R. S. M. Wong & Hui, 2004). Superspreading events have also been reported in Singapore (CDC, 2003) and Toronto (Poutanen et al., 2003). Before public measures were introduced, the R_0 for the SARS outbreak was estimated to be 2-3. This rate was decreased to 1 after implementing unprecedented global public health efforts aided by the rise in summer temperatures, thus halting the spread of the virus (Petersen et al., 2020).

Phylogenetic studies suggested that SARS-CoV was closely related to a virus isolated from palm civets, harboring a nucleic acid identity higher than 99.6% suggesting animal-to-human transmission.

Middle East respiratory syndrome coronavirus (MERS-CoV)

The second coronavirus epidemic began in 2012 in the Middle East, specifically in Jeddah, Saudi Arabia. The virus was isolated from a 60-years-old man with acute pneumonia and renal failure (Zaki et al., 2012). Since its discovery, the virus has been described under several names, with 'novel coronavirus' (NCoV) being the most commonly used. Later, the virus was named 'Middle East respiratory syndrome coronavirus' (MERS-CoV) by the Coronavirus Study Group (CSG).

A series of clinical illnesses is associated with MERS-CoV, ranging from mild upper respiratory symptoms such as cough and fever to severe lower respiratory tract infections such as pneumonia and multi-organ failure. As of May 2023, a total of 2604 cases of Middle East respiratory syndrome (MERS) were reported globally by health authorities, with 936 associated deaths, resulting in a case-fatality rate (CFR) of 36%, compared to 10% for SARS-CoV (World Health Organization, 2023b). From April 2012 till October 2023, a total of 2608 cases of MERS-CoV have been reported, including 945 deaths (European Centre for Disease Prevention and Control, 2023). The majority of death cases were reported within the elderly group, immunocompromised patients, and patients with comorbidities as renal failure, diabetes, hypertension, cardiovascular disease, etc. (Alotaibi & Bahammam, 2021).

MERS-CoV cases have been detected in over 27 countries, with the majority of reported cases mainly detected in countries in or near the Arabian Peninsula, where the risk of infection remains ongoing. Recently, sporadic cases were also reported in America, Europe, North Africa, and Asia (Aly et al., 2017). Even though the virus was detected in several countries, the majority of cases were reported in Saudi Arabia accounting for 84.3 % of all cases (World Health Organization, 2023b).

The transmission route of MERS-CoV includes human-to-human transmission transmitted through respiratory droplets or through direct contact with a surface contaminated with infected respiratory droplets, making it is as the main mode of virus transmission. However, host-to-host as well as host-to-human could possibly occur. In South Korea, MERS-CoV outbreaks occurred due to super-spreader index case-patients who visited healthcare facilities, thus spreading the virus to healthcare workers and other patients (Hui, 2016). The healthcare environment and families are recorded as the major source of the virus outbreak. Therefore, preventing transmission could be achieved by

implementing control strategies and measures to halt the spread of the virus. This could be achieved by isolating and quarantining of infected cases and setting up administrative controls, safer work practices, and personal protective equipment (PPE), particularly in hospitals.

Severe acute respiratory syndrome coronavirus-2 (SARS-CoV-2)

In late December 2019, a novel coronavirus outbreak happened in Wuhan, China, and swiftly spread across different countries, aggressively infecting people worldwide. The primary cluster of patients showed pneumonia-like symptoms and were found to be epidemiologically linked a seafood market where wildlife animals (bats, pangolin, and rabbits) are traded (Zhu et al., 2020). This market is considered one of the largest seafood wholesale markets in central China and visited by 10,000 people on a daily basis. To determine the etiological agent and better understand the origin of the disease, a surveillance system was launched, and samples from the lower respiratory tract of infected patients were characterized and examined (D. Wang et al., 2020).

Retrospective contact tracing and deep sequencing analysis ruled out several causative agents of respiratory disease, as SARS, MERS, influenza, etc., and indicated the presence of a novel coronavirus. The novel virus given the name of 2019-nCoV by the Chinese authorities on the 7th of January. Later, the International Committee on Taxonomy of Viruses (ICTV) announced the virus name SARS-CoV-2 because the virus is genetically related to the coronavirus responsible for the SARS outbreak of 2003, and the World Health Organization (WHO) named the disease “COronaVIrus Disease 2019” (COVID-19).

By January 30 2020, 7834 confirmed has been reported, with 98 cases detected in 18 different countries outside China, 8 of which are due to human-to-human transmission. Thus WHO declared this rapid spread as a public health emergency of international concern (PHEIC) (World Health Organization, 2020b). The continues assessment of the outbreak revealed alarming levels of virus spread and severity; within two weeks, the WHO noticed a 13-fold increase in the number of cases outside in China and a 3-fold increase in the number of countries with cases. Therefore, on March 11 2020, the WHO decided to officially characterize COVID-19 as a “very-high risk” global

pandemic (World Health Organization, 2020c) and confinement is imposed in many countries such as France from March 17 2020.

As of today, the overall number of global Covid-19 cases has surpassed 772 million cases, while the death toll is estimated to exceeded 6.9 million (World Health Organization, 2023c). However, this number was underestimated by at least 35% (Kung et al., 2021). It is now accounted as the worse-hit and most dreaded pandemic since the Spanish flu in 1920. Although SARS-CoV-2 appears to be less lethal than SARS-CoV or MERS-CoV, it has much higher transmissibility potential. The R0 of COVID-19 was initially estimated by the WHO between 1.4 and 2.4; however, other reports estimated R0 as high as 5.7 (Sanche et al., 2020). Even though all these estimations are based on intrinsic factor as virus infectivity and transmissibility potential, the wide ranges reported are affected by other extrinsic factors such as the incidence of the virus, testing strategies implemented, estimation model used, population density, etc. The incubation period for COVID-19 is, on average 5-6 days, and it may take up to 14 days. However, with the emergence of new variants that are more contagious, this period was shortened (Galmiche et al., 2023). The quarantine and isolation duration of exposed or suspected cases was then set at 14 days thereby accommodating the incubation period of the virus.

Airborne transmission of SARS-CoV-2 via aerosols formation is suspected to be the main mode of transmission. Early in the pandemic, there was a debate on whether SARS-CoV-2 could transmit through air or not. The super-spreading events that happened in several countries, including China, United States, Germany and Italy, cannot occur with exposure to droplets or fomites and strongly support the dominance of aerosol transmission (Comber et al., 2021). Besides, the detection nosocomial infections, despite following protective measure and the use of personal protective equipment (PPE) designed against droplet transmission, can be adequately explained only by aerosols (Klompas et al., 2021). Transmission was also reported through other body fluids and secretions such as feces, urine, semen, and tears, as well as mother-to-child.

Infected individuals whether symptomatic or not, are considered highly contagious. Clinical manifestations of COVID-19 range from mild to severe illness, and patients can present as either symptomatic or asymptomatic. Like SARS-CoV and MERS-CoV, SARS-CoV-2 infect mainly the respiratory system. The majority of the population who contracted COVID-19 showed mild symptoms as fever, dry cough, fatigue, muscle

pain, diarrhea, and vomiting. However, in some cases, it may cause multisystem inflammatory syndrome (MIS) that include damage to the digestive system, urogenital system, central nervous system, circulatory system, cardiovascular system and results in elevated levels of inflammatory markers in children and adults (Chatzis et al., 2022; Morris et al., 2020; Zhang et al., 2020). Surprisingly, a significant proportion of mild and severe cases of infected people experienced post-acute sequelae of COVID-19, months after infection and even after recovery (da Costa e Silva et al., 2023; Munblit et al., 2021).

Coronavirus variants

Genetic sequencing of viral samples, epidemiological studies, and laboratory research allowed the detection SARS-CoV-2 variants of concern and interest with increased transmission capacities. Although the rate of evolution of coronavirus is much less than the rates of other RNA viruses, such as HIV-1 or influenza virus, however, the virus was estimated to have a high mutation rate and adjust to its host, leading in the generation of new variant strain (Markov et al., 2023). SARS-CoV-2 mutation rate is estimated to be approximatively 10^{-4} nucleotide mutations per site per year (González-Vázquez & Arenas, 2023). Even though, coronaviruses possess a 3′–5′ exonuclease proof reading activity; however, this does not exclude the possibility of deletions and mutations that might lead to virus diversity. For instance, the deletion that happened at position 69–70 within the spike gene results in an S-gene drop out; this deletion was pivotal in the identification of the SARS-CoV-2 Alpha variant (B.1.1.7), and has been associated with increased infectivity (Walker et al., 2021). SARS-CoV-2 variants were classified into variant of interest (VOI), variant of concern (VOC), and variant under monitoring (VUM) (CDC, 2020a).

The major viral mutants identified to date includes the Alpha (B.1.1.7), Beta (B.1.351), Gamma (P1), Delta (B.1.617.2), and Omicron (B.1.1.529) variants **(Table 1)** (European Centre for Disease Prevention and Control, 2021). Omicron has exhibited an unprecedented rate of spread since it first appeared in late 2021. At present, Omicron is the sole VOC in circulation. Within the omicron family, there exist several subvariants, including BA.1 (B.1.1.529.1), BA.2 (B.1.1.529.2), BA.3 (B.1.1.529.3), BA.4, BA.5, and related lineages. Notably, the BA.5 strain of omicron is the most highly transmissible and predominant subvariant on a global scale. Additionally, there are emerging subvariants

and lineages, such as BQ.1, BQ.1.1, BA.4.6, BF.7, BA.2.75.2, XBB.1, and BF.7, which have garnered international attention.

Table 1. Different variations and spike mutations, along with precise RBD mutations, and the countries where these variants were first identified (Scovino et al., 2022).

Variants	Deletions	Mutation S1+S2	RBD mutations	Earliest Documented in
Alpha (B.1.1.7)	ΔH69, ΔV70, ΔY144	N501Y, A570D, D614G, E484K, T716I, S982A, P681H, D1118H	E484K, S494P, N501Y	United Kingdon (10, 15)
Beta (B.1.351)	Δ241/4, Δ242, Δ243	N501Y, A701V, D614G, E84K, D215G, K417N, and D80A	K417N, E484K, N501Y	South Africa (10, 16)
Gamma (P1)		N501Y, L18F, D614G, E484K, T1027I, K417T, D138Y, R190S, H655Y, P26S, T20N	K417N, E484K, N501Y	Brazil (10, 17, 18)
Delta (B.1.617.2)	Δ156, Δ157	T478K, L452R, D614G, G142D, D950N, T19R, P681R, R158G, E484Q	L452R, E484Q	India (10, 19)
Omicron (B.1.1.529)	ΔH69-V70, Δ143-145, Δ211-212	A67V, T95I, G142D, G339D, S371L, S373P, S375F, K417N, N440K, G446S, S477N, T478K, E484A, Q493K, G496S, Q498R, N501Y, Y505H, T547K, D614G, H655Y, N679K, P681H, N764K, D796Y, N856K, Q954H, N969K, L981F	K417N, E484A, N501Y	South Africa (10, 20)

1.4. COVID-19 pathogenesis

The pathological characteristics of COVID-19 can vary in their distribution and severity. Most patients experience upper mild respiratory and lung symptoms including fever, cough, fatigue, muscle pain, headache, and disturbances in taste and smell, rather than severe pneumonia. However, those with severe cases can also develop widespread small and large vessel thrombosis (Baram et al., 2020), cardiac conduction abnormalities (Bhogadi et al., 2022), neurological issues (Ousseiran et al., 2023), diarrheal symptoms (Boniotti et al., 2016), and gastrointestinal bleeding (Cappell & Friedel, 2023), all of which can be life-threatening. In a study using hamsters, the virus temporarily damages cells in the olfactory epithelium, leading to a loss of taste and smell, which is commonly observed in COVID-19 (Reyna et al., 2022). The presence of angiotensin-converting enzyme 2 receptor (ACE2), an important receptor for virus-cell fusion, in various tissues can explain the locations of infection and patient symptoms. For instance, ACE2 receptors are found in organs like the intestine and the endothelial cells of the kidney and blood vessels, which may account for gastrointestinal symptoms and cardiovascular complications (Ni et al., 2020). Postmortem examinations have shown lymphocytic endotheliitis in the lungs, heart, kidneys, and liver, as well as liver cell necrosis and heart attacks in COVID-19 patients, indicating direct harm to multiple organs (Menter et al., 2020).

The initial immune response draws virus-specific T cells to the infection site, where they eliminate infected cells, leading to recovery in most individuals. It is clear that advanced age, male gender, specific racial groups, obesity, diabetes, cardiovascular diseases, chronic lung or kidney issues, and immunocompromised are associated with more severe disease, especially when multiple risk factors are present (Martono et al., 2023).

In individuals with severe disease, SARS-CoV-2 triggers an abnormal immune response. Histological examinations of lung tissues from died COVID-19 patients have confirmed the inflammatory nature of the injury, with features similar to acute respiratory distress syndrome (ARDS) (J. Zheng et al., 2022). COVID-19 can induce a cytokine storm in the lungs due to an overactive immune response, leading to excessive production of pro-inflammatory cytokines, which results in widespread inflammation, particularly in the lungs (Montazersaheb et al., 2022). Patients with severe COVID-19 often have elevated levels of certain pro-inflammatory cytokines such as interleukin 6 (IL-6), interferon gamma (IFN-γ), interleukin 15 (IL15), interleukin 17 (IL17), and chemokines such as chemokine ligands 2 (MCP1/CCL2), and chemokine ligands 4 (MIP1-beta/CCL4) (Gonçalves et al., 2022). This excessive inflammation reduces the effectiveness of cellular immunity, causing CD8+ T cells and natural killer cells to have difficulty to kill infected cells (Ghasemzadeh et al., 2022). This response prolongs the presence of infection markers and leads to abnormal increases in the quantity and duration of pro-inflammatory cytokine secretion by innate immune cells. These cytokines attract neutrophils and macrophages to the infection site, resulting in self-activation and a continuous high secretion of pro-inflammatory cytokines, making it challenging to restore homeostatic levels without anti-inflammatory treatment (Rabaan et al., 2021).

1.5. Inter-species transmission of coronaviruses

Virus spillover remains a major challenge to public health. Animal species play a significant role in the transmission cycle of CoVs by acting as hosts or reservoirs. They possess specific cell receptors essential for CoV replication and genome mutations. All seven HCoVs have their origins in animals, specifically bats, mice, or domestic animals. An animal is considered the evolutionary host of an HCoV when it houses a closely related ancestor with a high degree of genetic similarity at the nucleotide sequence level.

Similarly, a reservoir host continuously carries HCoVs, establishing a long term endemicity.

SARS-CoV-2

Regarding SARS-CoV-2, it exhibits a 96.2% nucleotide similarity with a bat CoV named CoV RaTG13, which was isolated from *Rhinolophus affinis* Horsfield (Rhinolophidae), and is considered one of the closest known relatives of SARS-CoV-2 (Cantoni et al., 2022). Recent studies based on metagenomic sequencing techniques have indicated that a group of endangered small mammals, known as pangolins (*Manis javanica* Desmarest, Manidae), might also harbor ancestral beta-CoVs related to SARS-CoV-2 (S. K. Gupta et al., 2022). These newly identified pangolin CoVs genomes share a nucleotide sequence homology ranging from 85% to 92% with SARS-CoV-2 (S. K. Gupta et al., 2022). However, they are equally closely related to CoV RaTG13, showing approximately 90% identity at the nucleotide sequence level. The highest sequence similarity is found in the receptor-binding domains (RBDs) between SARS-CoV-2 and SARS-CoV-2-related coronaviruses in pangolins and RaTG13, indicating the highest overall genome-wide sequence homology (S. Zhang et al., 2021). Presently, there is no conclusive evidence supporting a direct pangolin origin of SARS-CoV-2 due to the sequence differences between SARS-CoV-2 and pangolin SARS-CoV-2-related beta-CoVs **(Figure 3)**.

MERS-CoV

Phylogenetic analysis clusters MERS-CoV to the same group as bat CoV-HKU4 and bat CoV-HKU5. Both Bat CoV-HKU4 and MERS-CoV employ the same host receptor, dipeptidyl peptidase-4 (DPP4), for virus entry (Lau et al., 2013; van Boheemen et al., 2012). When examining the RdRp sequences of MERS-CoV, they are found to be more closely related, from a phylogenetic perspective, to those in bat beta-CoVs identified in Europe and Africa. Notably, MERS-CoV and its nearest relative, bat CoV-HKU25, share only 87% nucleotide sequence similarity (Xiong et al., 2022). Live MERS-CoV, indistinguishable from the virus found in humans, was obtained from nasal swabs of dromedary camels. However, the exact timeframe of the virus's introduction to dromedary camels remains uncertain. Yet, data from studies examining stored

dromedary camel sera and the geographical distribution of affected dromedary camel populations strongly suggest that the virus has been present in dromedary camels for several decades. While bats and alpacas are potential reservoirs for MERS-CoV, dromedary camels appear to be the sole animal host responsible for the transmission of the virus to humans, serving as the reservoir host for MERS-CoV **(Figure 3)** (Mohd et al., 2016).

SARS-CoV

Masked palm civets (*Paguma larvata* Smith, Viverridae) and raccoon dogs (*Nyctereutes procyonoides* Gray, Canidae) in live animal markets were initially found to harbor SARS-CoV-like viruses that closely resembled SARS-CoV. Subsequent investigations to identify the natural animal host of SARS-CoV led to the discovery of a closely related bat coronavirus known as SARS-related *Rhinolophus* bat CoV HKU3 (SARSr-Rh-BatCoV HKU3), which is prevalent in Chinese horseshoe bats (Li et al., 2005). The latter and other bat CoVs share a high nucleotide sequence homology of 88-92% with SARS-CoV. While several SARS-like CoVs (SL-CoVs) have been identified in bats, only one, named WIV1, has been successfully isolated as a live virus. WIV1, which was obtained from bat fecal samples, has been shown to use receptors for cell entry that are also used by bats, civets, and humans (Ge et al., 2013). Moreover, serum from individuals who had recovered from SARS is capable of neutralizing WIV1. To date, WIV1 is the closest known ancestor of SARS-CoV found in bats, sharing a 95% nucleotide sequence homology.

In addition to the highly pathogenic HCoVs, the origins of endemic HCoVs have also been investigated. Phylogenetic evidence suggests that both HCoV-NL63 and HCoV-229E may have emerged from bat CoVs **(Figure 3)** (Hu et al., 2015). In contrast, the paternal viruses for HCoV-OC43 and HCoV-HKU1 have been identified in rodents **(Figure 3)** (Corman et al., 2018). Notably, a bat CoVs referred to as Appalachian Ridge CoV (ARCoV.2,) found in North American tricolored bats, has shown a close genetic relationship with HCoV-NL63 (Huynh et al., 2012). On the other hand, HCoV-229E appears to have genetic ties to another bat CoVs known as Hipposideros/GhanaKwam/19/2008, initially detected in Ghana (Hu et al., 2015). There have also been suspicions that camelid could serve as an intermediate host for HCoV-229E **(Figure 3)**.

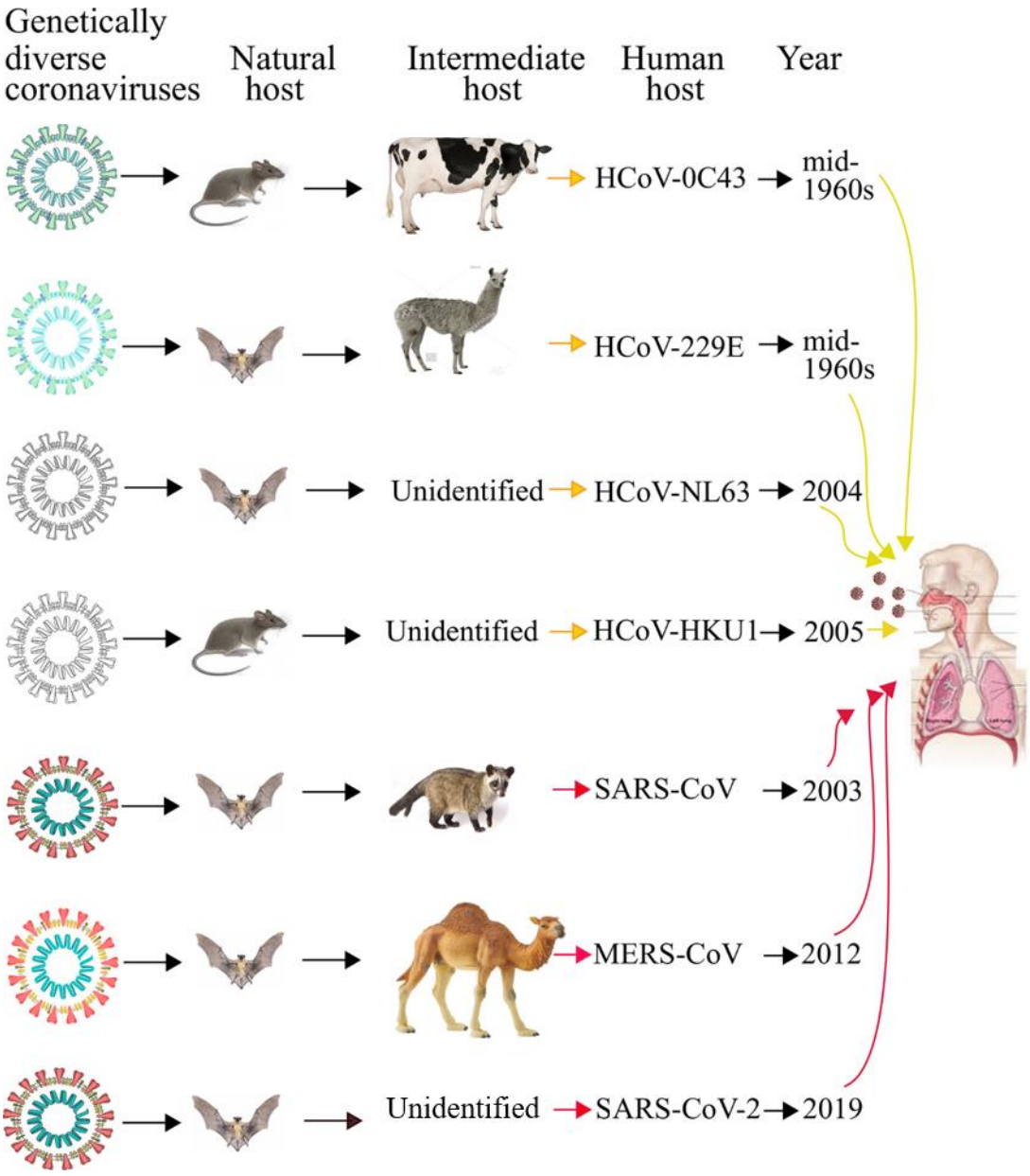

Figure 3. The transmission of HCoVs from their natural hosts (bats or rodents) to the intermediate hosts (camelids, civets, dromedary camels, pangolins or bovines), and eventually to the human population (Ye et al., 2020) (Edited).

1.6. Coronaviruses virion properties

Coronavirus particles are large, pleomorphic but roughly spherical, with a diameter ranging between 80–220 nm, having a buoyant density of approximately 1.18 g/ml in sucrose (MacLachlan & Dubovi, 2017). Coronaviruses have four common structural proteins: a large surface glycoprotein (S; 1150–1450 amino acids), a small envelope protein (E; 100 amino acids), integral membrane glycoprotein (M; 250 amino acids)

embedded in the envelope, and a phosphorylated nucleocapsid protein (N; 500 amino acids) associated with the genome **(Figure 4)**. Coronaviruses are distinguished by the club shaped bulbous projections of the homotrimic peplomer glycoprotein (20 nm deep) protruding from the viral membrane. In the case of embecoviruses like OC43 and BCoV, there is an additional feature — a second interspersed, homodimeric, shorter glycoprotein projections (5 nm deep) composed of the hemagglutinin-esterase (HE; 425 amino acids) protein (King & Brian, 1982). Inside the envelop, the N protein packages the viral genome into a ribonucleoprotein complex (RNP) known as the capsid. RNPs are helical and have been reported to have a diameter of 9–16 nm with 3–4 nm hollow interior **(Figure 4)** (Neuman et al., 2006).

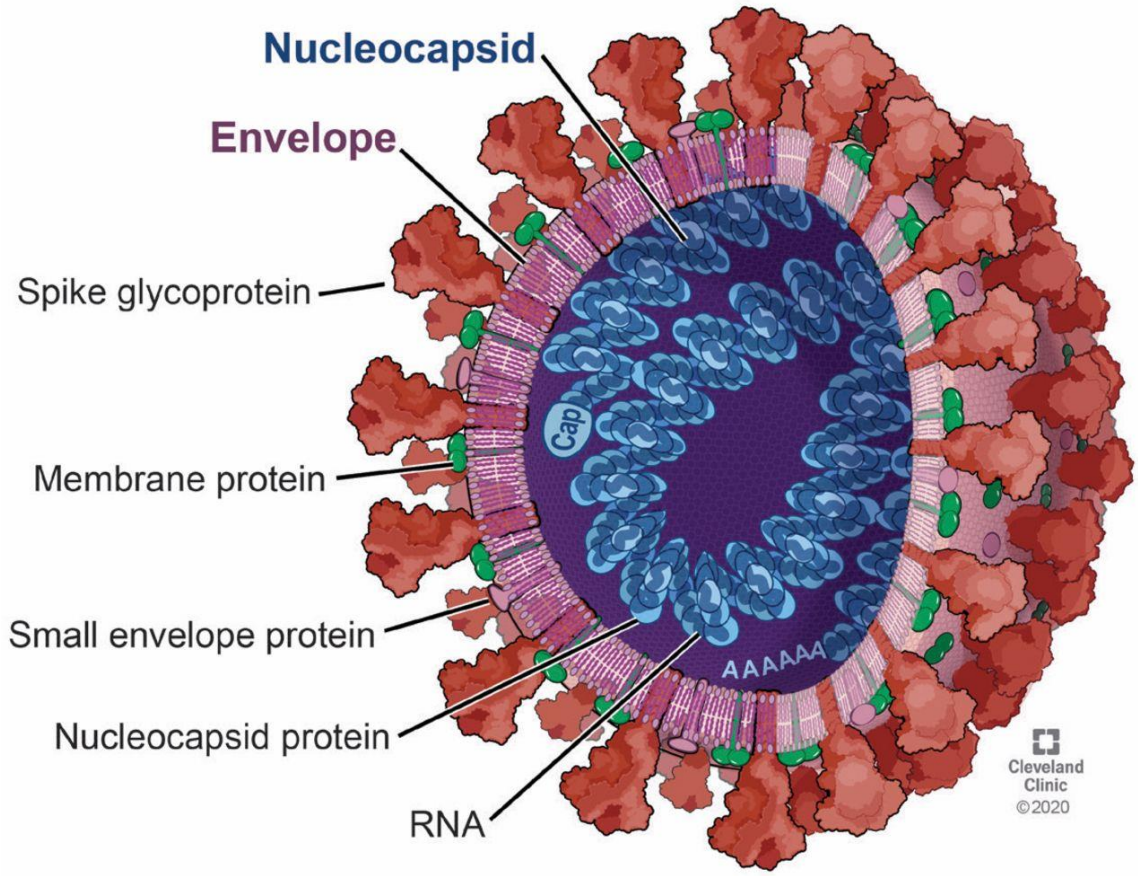

Figure 4. Structure of the SARS-CoV-2 viral particle and its genetic makeup. The virus comprises four key structural proteins: Spike protein (S), Membrane protein (M), Nucleocapsid protein (N), and Envelope protein (E) (Bergmann & Silverman, 2020).

1.6.1. Structural proteins

Genome

Coronavirus possess the largest known genome among RNA viruses, ranging from 27 to 31kb. The genome is non-segmented, positive-sense, single-stranded molecule. The polycistronic genome resemble the structure of most eukaryotic mRNAs structure by having a 5'-cap and 3'-poly(A) tail. However, unlike eukaryotic mRNAs, it contains multiple open reading frames (ORFs). The RNA is flanked by two untranslated regions that contain secondary RNA structures functionally important for RNA–RNA interactions and for the viral-cellular protein interaction during the replication, transcription, and transcription processes. The 5′UTR, ranges from 210 to 530 nucleotides contains the 5′ cap structure, followed by specific region of 70 nucleotides identified as the leader sequences, and cis-acting element, named transcriptional regulatory sequence (TRS), both of which are involved in subgenomic mRNA production (Mohammadi-Dehcheshmeh et al., 2021). Downstream the 5′ UTR, the genome features a replicase gene occupying two-thirds (20 kb), with two overlapping ORFs coding for two polyproteins named ORF1a and ORF1b. These latter are cleaved into 16 non-structural proteins (Nsps), and play a very crucial role in viral replication. The 3′ UTR ranges from 270 to 500 nucleotides and is preceded by a one-third (10 kb) region that encodes for structural and accessory proteins (V'kovski et al., 2021). The genome is organized in a highly conserved manner among coronaviruses in a 5'-leader-UTR-replicase-(HE)-S-E-M-N-3'-UTR-poly (A) tail gene arrangement, with interspersed ORFs that encode accessory proteins to form a nested subgenomic mRNAs. The SARS-CoV-2 genome share about 82% sequence identity with SARS-CoV and MERS-CoV and >90% sequence identity for essential enzymes and structural proteins **(Figure 5)**.

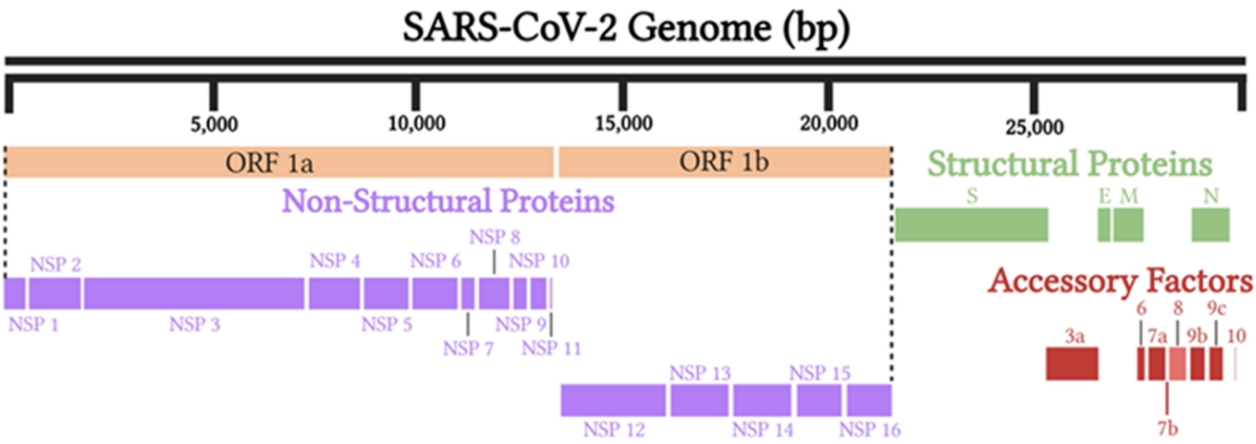

Figure 5. Schematic diagrams of the SARS-CoV-2 virus particle and genome. The genomic arrangement consists of ORF1a-ORF1b-S-ORF3-E-M-ORF6-ORF7 (with 7a and 7b)-ORF8-ORF9b-N in sequential order. ORF1a encodes eleven nonstructural proteins (nsp1–11), while ORF1b encodes five nonstructural proteins (nsp12–16). Additionally, there are eight accessory proteins identified (Jamison et al., 2022).

Spike protein (S)

The spike protein is the largest and the most prominent of the 4 major structural protein of coronavirus. It mediates the virus's attachment to the host cell receptor and the subsequent fusion of the virus envelop with the membrane of the host cell. The spike protein is heavily glycosylated with a size of 180–200 kDa and belongs to the type I membrane-protein family (Letko et al., 2020). It consists of an extracellular N terminus, a transmembrane domain, anchored in the viral membrane, and a short intracellular C-terminal tail **(Figure 6A)** (Bosch et al., 2003). S proteins are class I fusion glycoproteins synthesized as a single-chain precursors that assemble into trimers upon folding. The ectodomain is divided into two functionally distinct domains, S1 and S2. The surface exposed S1 subunit consists of a receptor-binding domain (RBD) that engages the host cell receptor **(Figure 6B)** (Costello et al., 2022). This domain is considered as the determinant of the host range, virus virulence, tropism, and pathogenicity. It also contains an amino-terminal (N-terminal) domain (NTD). The RBD is considered as a primary target for neutralizing antibodies (nAbs). SARS-CoV-2 and SARS-CoV RBD are considered ~73%–76% similar in sequence. The virus requires the proteolytic cleavage of the spike protein by host cell-derived proteases to permit fusion. Cleavage depends of the protein sequences of the S1/S2 junction and can occur through during trafficking in the producer cell by host furin-like enzymes or by the transmembrane protease, serine 2 (TMPRSS2) at the cell surface during attachment for priming and entry or by cathepsin

proteases in the late endosome/endolysosome, particularly in the S2 domain close to the S1/S2 site, termed the S2' site for membrane fusion (Peacock et al., 2021). The S2 fusion subunit is highly conserved, involved in fusion, and comprises four conserved structural regions: a fusion peptide, a transmembrane region (stem helix), and heptad repeats 1 and 2 (HR1-HR2) bundle, that is the hallmark of class I fusion proteins (S. Liu et al., 2004). The S protein is specific to each coronavirus and will therefore recognize cellular receptors that are also specific. The coronaviruses SARS-CoV and SARS-CoV-2 use the surface protein ACE2 (CD147) as a cellular receptor. HCoV-229E binds to aminopeptidase N (APN); *O*-acetylated sialic acid (O-ac Sia) for OC43 and HKU1; and DPP4 for MERS-CoV (Jackson et al., 2022).

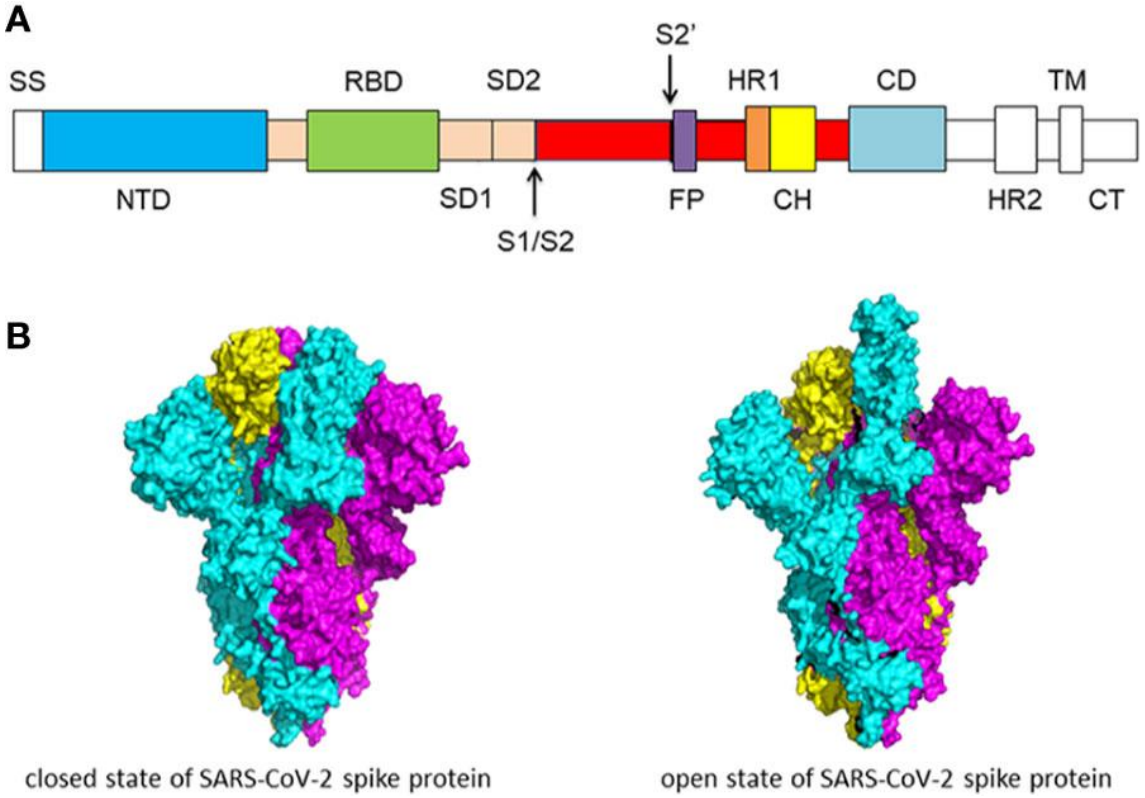

Figure 6. Schematic diagram illustrating the primary structure of the SARS-CoV-2 spike protein A. These sections include SS (single sequence), NTD (N-terminal domain), RBD (receptor-binding domain), SD1 (subdomain 1), SD2 (subdomain 2), S1/S2 (S1/S2 protease cleavage site), S2' (S2' protease cleavage site), FP (fusion peptide), HR1 (heptad repeat 1), CH (central helix), CD (connector domain), HR2 (heptad repeat 2), TM (transmembrane domain), and CT (cytoplasmic tail). The protease cleavage site is indicated by arrows B. Cryo-EM structure of the SARS-CoV-2 spike protein, with the left side representing the closed state and the right side representing the open state (M.-Y. Wang et al., 2020).

Hemagglutinin-esterase (HE)

The subgenus *Embecovirus* of the betacoronavirus family, including the human CoVs HKU1 and OC43, along with BCoV, express another viral surface protein identified as hemagglutinin-esterase HE. HEs are 40–50 kDa homodimeric class I membrane proteins, with a dual function encompassing of two functional domains: an *O*-ac Sia binding domain and a corresponding sialate *O*-acetylesterase domain (Hurdiss et al., 2020). HE protein binds to 9-*O*-acetylated sialic acids containing receptors and mediates a receptor-destroying enzyme activity through the sialate-9-*O*-acetylesterase domain, facilitating progeny release or escape from non-permissive host cells. It also plays a role during the very early stages of infection. Evolutionary studies revealed that CoV HE is closely related to influenza C and toroviruses HEs and is a result of relatively recent lateral gene transfer events (Zeng et al., 2008).

Envelop protein (E)

The envelop protein is a small, integral membrane polypeptide of 75–109 amino acids ranging from 8.4 to 12 kDa in size, making it a minor constituent of the viral envelop. Due to its small size and limited quantity, it was discovered and recognized as a virion component much later than the other structural proteins. The primary and secondary structure reveals that E has a short hydrophilic N terminal domain of 7- 12 amino acids, a transmembrane domain (TMD) of 25 amino acids, and a long hydrophobic C-terminal tail of 36-72 residues, comprising the majority of the protein (Masters, 2006). The envelop protein plays an essential role in different steps of the virus replication cycle including assembly, budding, envelope formation, and secretion. It is highly divergent across different coronaviruses. The SARS-CoV-2 E protein sequence is 95% and 36% identical to those of SARS-CoV and MERS-CoV E proteins, respectively.

Membrane protein (M)

M glycoprotein is considered the most abundant structural protein of the coronavirus virion, consisting of 217–230 amino acids ranging from 25 to 30 kDa in its preglycosylated form. The M protein plays a critical role in giving the virion its shape through interacting with other M, S, and N proteins. M is a multispanning membrane protein divided into 3 domains: a small N terminal domain located on the exterior of the virion or intracellularly in the ER lumen, a three transmembrane segments, and a large C-terminal domain that constitutes the majority of the protein molecule, located in the

interior of the virion or on the cytoplasmic side when inserted into the host cell membrane (Dolan et al., 2022). At the amino terminus, the tail has been shown to contain signals for localization of the M protein to the trans-Golgi network for MERS-CoV and the endoplasmic reticulum-Golgi intermediate compartment (ERGIC)/cis-Golgi for IBV (Perrier et al., 2019). The M protein has been also indicated for virus assembly (Desmarets et al., 2023). The C terminal tail contains a short hydrophilic region and an amphipathic domain closely associated with the membrane, while at the N terminus, it contains a highly conserved 12-amino-acid domain sequence just after the third TM domain (Arndt et al., 2010). This domain was identified to play a role in virion assembly. The M protein shows the same basic structure among different coronaviruses even though the amino acid protein sequence might differ.

Nucleocapsid protein (N)

The coronavirus N protein is a phosphorylated protein ranging from 43–46 kDa (419 amino acid), and is a component of the helical nucleocapsid. It is a highly conserved in structure and function and relatively consistent among different coronaviruses. The N protein possesses conserved distinctly folded domains connected by interspersed spacer region. The conserved domains are made up of N-terminal domain (NTD), responsible for RNA binding, and a C- terminal domain (CTD), responsible for dimerization and oligomerization. The NTD and the CTD are connected by an inherently disordered region (IDR) called the central linking region (LKR), responsible for regulating the RNA binding activity. Another two IDRs known as N-tail and C-tail are present on both sides of the NTD and the CTD (W. Wu et al., 2023). LKR regions have an arginine/serine-rich sites that undergo phosphorylation and are believed to play a role in binding to the membrane protein M and to the viral RNA with high affinity. The N protein bind to the viral RNA through its 140 amino acid RNA-binding domain in a bead-on-a-string manner. Due to the conserved regions, it is suggested that antibodies manufactured against the N protein of SARS-CoV could also recognize the N protein of SARS-CoV-2.

1.6.2. Non Structural proteins

As mentioned previously, the 5' end of the viral genome is occupied by two large open reading frames, ORF1a and ORF1b, which potentially encode for two polypeptides, pp1a and pp1ab. The final auto-proteolytic cleavage pp1a and pp1ab by chymotrypsin-like

protease (3CLpro or Mpro) and two papain-like proteases (PLpro) produce 16 nonstructural proteins (Nsps). The pp1a comprises Nsp1 to Nsp11, and pp1ab corresponds to Nsp12 to Nsp16. PLpro, a domain of Nsp3, cleaves the bond between Nsp1 and Nsp2, Nsp2 and Nsp3, Nsp3 and Nsp4, thus releasing Nsp1, Nsp2, and Nsp3. Mpro, corresponding to Nsp5, cleaves the 11 bonds between the remaining Nsps (Masters, 2006).

Nsp1

The Nsp1 proteins found in beta-CoVs consist of approximately 180 amino acids. They are distinguished by their flexible N- and C-terminal extensions and feature a distinctive hydrophobic β-barrel structure situated within the central part of the protein (Almeida et al., 2007). Nsp1 mediates RNA processing and replication. It has been shown to play a role in cell cycle arrest by interrupting the G-0 and G-1 phases of the cell cycle, its ability to inhibit translation, and promotes mRNA degradation (Finkel et al., 2021). Due to its role in inhibiting innate immunity, Nsp1 could serve as a target for pharmaceutical drugs and vaccines. SARS-CoV-2 Nsp1 shares ~91% similarity in protein sequence with SARS-CoV Nsp1.

Nsp2

The precise role of Nsp2 remains partially understood. Nsp2 is the most divergent Nsps among the coronavirus family, consisting of 638 amino acids (Woo et al., 2010). It plays a role in modulating the survival signaling pathway by interacting with host cell key proteins of autophagy and apoptosis regulators, and other kinases to achieve optimal virus replication (Bouhaddou et al., 2020). Besides, it promotes mitochondrial integrity, and reduces cellular stress to sustain the virus, contributing to the process of viral replication. Nsp2 deletion mutants showed delayed viral growth kinetics compared to wild type.

Nsp3

Nsp3 protein is largest multidomain non-structural protein encoded by the virus, with an average weight of 212 kDa (1945 amino acids) in SARS-CoV-2. Nsp3 is released by the cleavage of PLpro, which itself a domain of Nsp3 (Lei et al., 2018). Nsp3 plays a crucial role in the virus replication cycle by interacting with proteins involved in the

replication and transcription, assisting in the formation of a replicase-transcriptase complex crucial for the virus's replication cycle. Besides, it acts on post-translational modifications by counteracting the host's immune response, particularly the interferon system thereby blocking the innate immunity of the host and promotes cytokine expression. Due to its multifunctional implications, Nsp3 is considered the second most promising vaccine candidate besides S protein (Lundin et al., 2014).

Nsp4

Nsp4 is a membrane-spanning protein of molecular weight around 56 kDa (500 amino acid residues). It acts by anchoring the viral replication-transcription complex (RTC) to intracellular membranes, remodeling them to form double-membrane compartments used for viral RNA synthesis. Together with Nsp3 and Nsp6, this protein forms a complex to build fluid-filled bubbles within infected cells by inducing the formation double-membrane vesicles (DMVs) where components of newly formed viruses come together during virus replication (Sakai et al., 2017).

Nsp5

Nsp5 is also known as the main protease (Mpro) or 3CL protease. Mpro forms a dimeric structure, and each individual unit of this dimer exhibits a three-domain configuration. The active site is located within a gap between the first and second domains of each monomer. Nsp5 plays a central role in cleaving the viral polyproteins translated from the viral RNA, releasing various Nsps required for viral replication and transcription (Anderson-Daniels et al., 2022). Since Nsp5 is vital for viral replication and has a specific role in proteolytic processing, it has been targeted for drug development efforts.

Nsp6

Nsp6 is approximately 34 kDa membrane protein with six transmembrane helices, whose C-terminals are highly conserved. It is a common component in both alpha and beta coronaviruses and is typically located within the endoplasmic reticulum (ER) of the host cells. Nsp6 assists in the formation of double membranes together with Nsp3 and Nsp4.

Nsp7 and Np8

Nsp7 is an alpha helical protein of about 10 kDa, typically found in the cytoplasmic membrane. Nsp7 forms dimers and engages in interactions with other viral proteins, including Nsp5, Nsp8, Nsp9, and Nsp13. Nsp8 has a molecular weight approximately 22 kDa of 198 amino acids. Together, Nsp7-8 serve as a cofactor for SARS-CoV-2's RNA-dependent RNA polymerase (RdRp), which is also referred to as Nsp12. This interaction is a critical component of the machinery required for both viral replication and transcription.

Nsp9

Nsp9 is an ssRNA-binding protein Nsp9 that has different dimerization forms. This dimeric form increases its nucleic acid binding affinity and prevents RNA from degrading, ensuring that the replication process proceeds efficiently. Nsp9 amino acid sequence of SARS-CoV-2 is 97% similar to that of SARS-CoV.

Nsp10

Nsp10 is a small, single domain protein composed of approximately 148 amino acid residues. It plays an essential role in viral transcription by stimulating Nsp14 and Nsp16. Nsp10 acts as a cofactor for Nsp14; this partnership enhances the exoribonuclease activity of Nsp14. Nsp10 also interacts with Nsp16 which is involved in RNA cap methylation (Kakavandi et al., 2023).

Nsp11

Nsp11 is relatively small, consisting of 13 amino acids, and is a less characterized protein. Its precise function in the coronavirus life cycle is not well-defined.

Nsp12

Nsp12 is made up of 932 amino acids and is often referred to as the RNA-dependent RNA polymerase (RdRp). It has a minimal activity on its own and usually boosted with the presence of cofactors Nsp7 and Nsp8. Nsp12 is responsible for synthesizing RNA from an RNA template during the viral replication process. Due to its

essential role in viral replication, Nsp12 is a target for antiviral drug development such as remdesivir and molnupiravir.

Nsp13

Nsp13 is a helicase enzyme of 67 kDa, consisting of 596 amino acids. Nsp13 catalyzes the unwinding of double-stranded DNA or RNA intermediates in a 5′ to 3′ direction to produce single-stranded RNA templates for replication and transcription. Nsp13 interacts with several other non-structural proteins, such as Nsp7/Nsp8/Nsp12 (RdRp), which enhances the catalytic efficiency of Nsp13 by increasing the step size of nucleic acid unwinding (Newman et al., 2021). Due to its highly conserved sequence and crucial role in viral replication, Nsp13 is a potential target for antiviral drug development.

Nsp14

Nsp14 is a 60 kDa protein with key roles in viral RNA synthesis, proofreading, and immune evasion. The N-terminal region of Nsp14 contains an exonuclease domain, which is involved in proofreading and repairing the viral RNA genome during replication, whereas the C-terminal domain functions as a methyltransferase for mRNA capping. Exo domain activity contributes to enhancing the fidelity of viral RNA replication by removing misincorporated nucleotides from newly synthesized RNA strands, thus reducing the frequency of errors in the viral genome. The interaction of Nsp14 with Nsp10 (a cofactor of Nsp14) lead to its stabilization and enhancement of the enzymatic activity. Besides, Nsp14 interacts with Nsp16 which methylates the RNA cap structure contributing to immune escape (Zaffagni et al., 2022).

Nsp15

Nsp15 is an endoribonuclease, which means it has the ability to cleave the viral RNA at specific sites. It primarily targets double-stranded RNA (dsRNA) regions in the viral genome. It is hypothesized that this protein destroys the genome to help the virus evade host immune responses (Saramago et al., 2022). Nsp15 is relatively conserved among coronaviruses.

Nsp16

Nsp16 is an enzyme that acts as a methyltransferase. This protein forms a heterodimer with the Nsp10 cofactor, and this complex, Nsp10-Nsp16, forms the methyltransferase machinery responsible for modifying the viral RNA cap. Cap modification allows the virus to evade the host immunity (Gorkhali et al., 2021). In addition, it disguised the genetic material to make it look like human RNA, and thus, less likely to be recognized and targeted by the host's antiviral defenses.

1.6.3. Accessory proteins

Accessory genes are interspersed genes that fall between the set of canonical genes, replicase, S, E, M, N, that are considerably variable among different coronaviruses. These accessory gene range from one such as in HCoV-NL63 to 11 such as in SARS-CoV-2. ORFS are named after the name of their coding regions. Accessory proteins are generally small and dispensable for viral replication; their role is not fully elucidated, but seems to play a role in viral pathogenesis and regulating host defense.

ORF3a

ORF3a protein is encoded by the ORF3a gene located between the S and the E genes and is the largest among all accessory proteins with 275 amino acid residues. Structural analysis revealed that it is a viroporin, integral membrane protein involved in virus release, apoptosis and pathogenesis (Ren et al., 2020). ORF3a creates ion channels in the host cell membrane, altering the membrane permeability, homeostasis, and membrane remodeling, and facilitates virus escape (Kern et al., 2021). ORF3a induces pathogenesis by increasing the expression and secretion of fibrinogen thereby increasing cytokine production.

ORF3b

ORF3b protein is a relatively small protein, that accumulates in the nucleus and mitochondria of infected cells. This protein inhibits cell growth, and regulates the innate response by being a potent interferon antagonist (Konno et al., 2020).

ORF6

ORF6 is a 61amino-acid residues membrane associated protein, located in the Golgi and ER of infected cells. It is primarily involved in reducing the synthesis of primary IFN and blocking the transmission of signal to the immune system (Miorin et al., 2020).

ORF7a and ORF7b

ORF7a protein is a type-I transmembrane protein. ORF7a is a protein with the ability to antagonize the type I interferon (IFN-I) response. ORF7a helps viruses to escape outside the host cell by decrease the supply of tetherin which is a protein that prevents the diffusion of virus particles after budding from infected cells (Pekosz et al., 2006).
ORF7b protein is an integral membrane protein with 44 amino acids that is retained in the Golgi apparatus. Little is known about this protein but it is believed to play a role in inducing cellular apoptosis.

ORF8

This protein is 121-amino-acid long involved in ER-associated degradation and vesicle trafficking. The main role of ORF-8 remains unclear but it is shown to induce stress in the ER, supporting immune evasion.

ORF9b

It consists of 97 amino acid residues. It functions during virus assembly as a membrane-attachment point for other viral proteins. ORF9b interacts with the adaptor protein Tom70, a mitochondrial import, and thereby modulates the host immune response by compromising IFN-I synthesis (Jiang et al., 2020).

1.7. The SARS-CoV-2 infection cycle

Coronaviruses rely on various host factors to infect cells. Once inside the cell, they initiate a replication cycle in the cytoplasm, using numerous strategies to control viral gene expression at both the translational and transcriptional levels. The steps leading to the release of new viral particles are coordinated and heavily dependent on the host cell's infrastructure and metabolism.

Entry

Coronavirus infection starts with the binding of the virus particle to various host attachment and entry factors, which subsequently lead to viral entry and fusion with the host cell membrane **(Figure 9)**. Cell entry receptors differ between coronaviruses. FCoV, PEDV, HCoV-229E and other alpha coronaviruses employ APN as their receptor (Tresnan et al., 1996), SARS-CoV-2, SARS-CoV and HCoV-NL63 use ACE2 as their receptor (W. Li et al., 2003; K. Wu et al., 2009), MHV enters through CEACAM1 (R. K. Williams et al., 1991), and MERS-CoV binds to DPP4 (Raj et al., 2013). CoV-HKU1 (Huang et al., 2015) and human CoV-OC43 (Vlasak et al., 1988) use 9-O-ac-Sia as their receptor. The interaction between the S1 protein subunit through its RBD and ACE2 receptor is crucial step in this process, and also governs the tissue tropism and pathogenicity of the virus.

Following the receptor binding, fusion of the viral and cellular membrane is triggered either directly at the cell surface (early, non-endosomal pathway), through the acid-dependent proteolytic cleavage of the S protein by TMPRSS2, or in the endosomal compartment after endocytosis (late, endosomal pathway) via the endosomal cysteine proteases cathepsin B and cathepsin L. Proteolytic cleavage occurs at two sites within the S2 portion of the protein: at the interface between S1 and S2 domain (S1/S2 site), separating the RBD and fusion domains of the S protein, and another one within the S2 for exposing the fusion peptide **(Figure 7)** (Belouzard et al., 2009). The binding to the receptor and subsequent proteolytic cleavage will expose a hydrophobic fusion peptide will be inserted into the cell membrane, subsequently followed by the pairing of the two heptad repeats (HR1 and HR2) forming an antiparallel six-helix bundle **(Figure 7)**. This bundle formation facilitates the merging of viral lipid envelop and cellular membranes, leading to fusion and the eventual release of the viral nucleocapsid into the cytoplasm of the cell.

For, SARS-CoV-2, SARS-CoV, HCoV-229E and MERS-CoV, fusion of the viral and cellular membrane is triggered upon cleavage of the S protein by TMPRSS2 (Bertram et al., 2013; Glowacka et al., 2011; Shirato et al., 2013). While SARS-CoV-2 primarily relies on activation by TMPRSS2, if the target cells express insufficient TMPRSS2 or if a virus–ACE2 complex does not encounter TMPRSS2, the virus is internalized into the late endosome where cleavage at the S2′ site can also be occurs by cathepsins, particularly

cathepsin L (A. Bayati et al., 2021). Other proteases were shown to function in cleaving the spike protein such as furin, trypsin, and cathepsins B depending on the cell type.

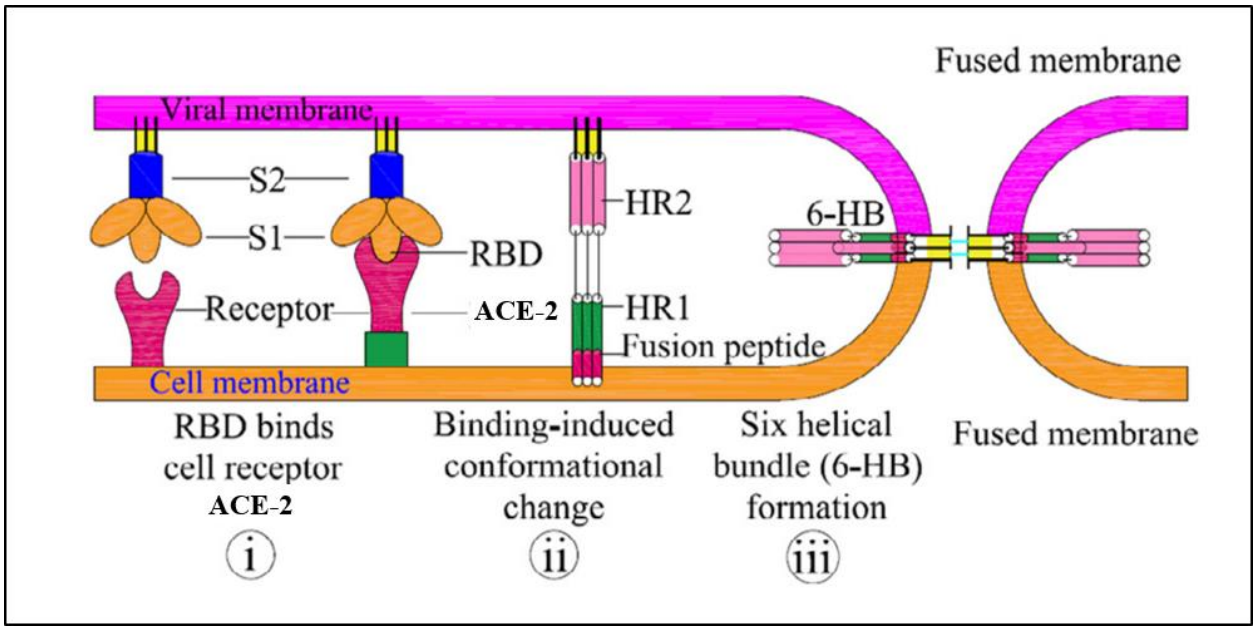

Figure 7. Visual representation of S-protein assisted membrane fusion mechanism of SARS-CoV2: RBD in the S1 subunit peptide interaction with the ACE-2 receptor results in. i) a pre-hairpin structure forms, exposing HR1 and inserting the fusion peptide into the host cell membrane. ii) Fusion intermediates are created as the fusion peptide becomes linked with the host cell membrane. iii) 6-HB (6-helix bundle) forms as HR2 refolds into stabilized trimer hairpins, bringing the virus and host cell closer together for fusion (Velusamy et al., 2021) (Edited).

Replication

Following the release of the viral genome in the cytoplasm, the viral gemonic RNA (gRNA) recruits host cell ribosomes and serves as an mRNA for the translation of the replicase gene, comprised of ORF1a and ORF1b for the synthesis of pp1a and pp1ab, two polyproteins. To translate both overlapping ORFs the virus employs a specific mechanism involving a "slippery sequence" (5'-UUUAAAC-3') and an RNA pseudoknot, consequently inducing a ribosomal frameshift, shifting the reading frame from ORF1a to ORF1b (Rehfeld et al., 2023). Pp1a and pp1ab are further cleaved by two cysteine proteases that are located within Nsp3 (papain-like protease; PLpro) and Nsp5 (chymotrypsin-like protease) to produce sixteen nonstructural proteins (Nsp1-11) from pp1a and (Nsp 1–16) from pp1ab (Yadav et al., 2021). The cleaved non-structural proteins will assemble to form the RTC and create a conducive environment for RNA synthesis, replication, and translation of sub-genomic RNAs **(Figure 9)**.

Following the translation and the assembly of the replication complex, viral RNA synthesis will begin by producing both gRNA and sgRNA. The full-length negative stranded form of gRNA produced from viral genome serves as a template for the production of the (+) gRNA that will packed later into newly formed virions **(Figure 8)** (Long, 2021).

In parallel, negative sgRNAs are also synthesized from the viral genome that serve as templates for production of high amounts of the positive-sense sgRNAs which in turn, acts as mRNA for the production of structural and accessory viral proteins. In the process of negative-strand RNA synthesis, the RTC halts transcription when it encounters transcription regulatory sequences (TRSs) found upstream of most ORFs in the 3' one-third of the viral genome (Malone et al., 2022). Transcription is then re-initiated at the TRS adjacent to a leader sequence (TRS-L) located at the 5′ end of the genome. The discontinuous step of negative strand RNA synthesis leads to the synthesis of a group of negative-strand sgRNAs, which are subsequently employed used as a template to generate a distinctive series of positive-sense sgRNAs **(Figure 8)** (Sola et al., 2015). These positive-sense sgRNAs are then translated into both structural and accessory proteins.

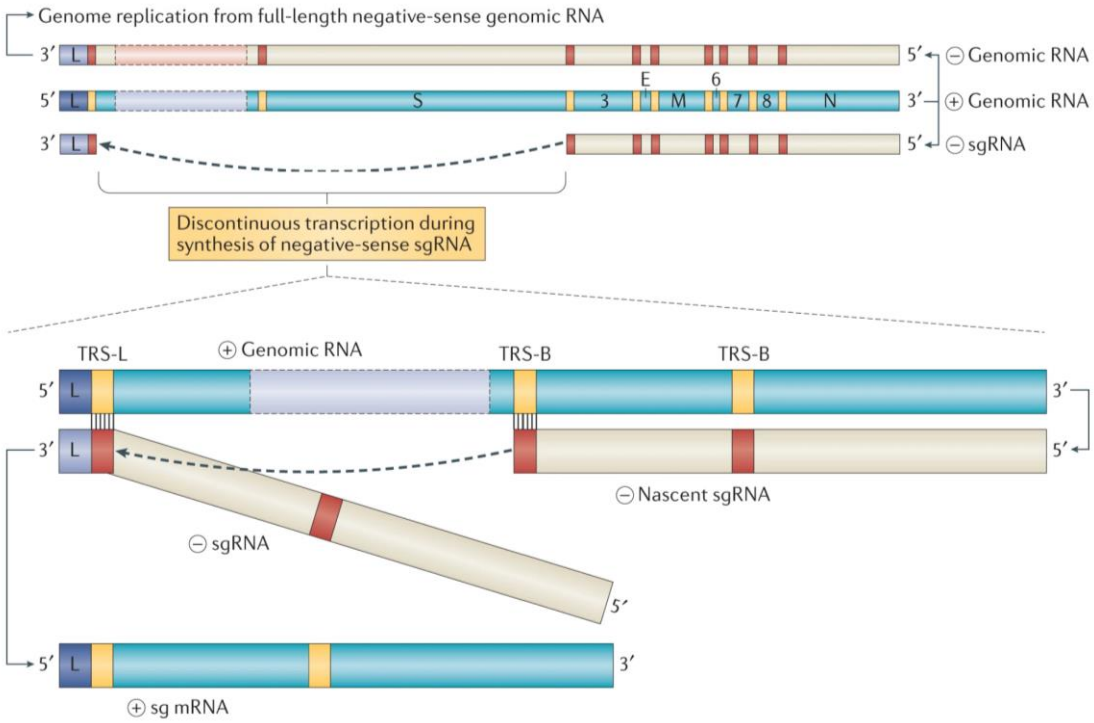

Figure 8. Schematic representation of coronavirus RNA synthesis. The full-length positive-sense genomic RNA serves as a template for creating both full-length negative-sense copies, used for genome replication, and subgenomic negative-sense RNAs (–sgRNA), which produce subgenomic mRNAs (sg mRNA). The synthesis of negative strand RNA, involving a template switch from body transcription regulatory sequences (TRS-B) to the leader TRS (TRS-L), leading to the production of one sg mRNA (V'kovski et al., 2021).

Assembly and release

Following replication and sgRNA synthesis, structural and accessory proteins are synthesized from their respective sgRNAs. Structural proteins, S, E, and M are translated, and through their intracellular trafficking signals, they are transported and inserted into the ER, whereas the N protein remains in the cytoplasm where it binds to the viral RNA. The S, E, and M proteins are transported through the secretory pathway and reach the ERGIC (Hardenbrook & Zhang, 2022). Within the ERGIC, viral genomes, encapsulated by the N protein, bud into membranes that also contain viral structural proteins. This process results in the formation of mature virions **(Figure 9)**.

Most of the protein-protein interactions required for coronavirus assembly are directed by the M proteins, however, the M protein alone is insufficient for virion formation. M protein interacts with E protein to form virus-like particles (VLPs) suggesting a conjugative role of the two protein to form the shape of the virus envelop (Z. Zhang et al.,

2022). The viral RNA encodes a packaging signal (PS) that facilitates the packaging of the viral genome into the ribonucleocapsid. The phosphorylation of the N protein is crucial for viral assembly and the organization the viral genome into a helical ribonucleocapsid via N-N interactions (Wu et al., 2023). The M protein interacts with the nucleocapsid, and this interaction contributes to the finalization of virion assembly. The particles are then transported to the cell membrane and released into the extracellular space through exocytosis or cell lysis.

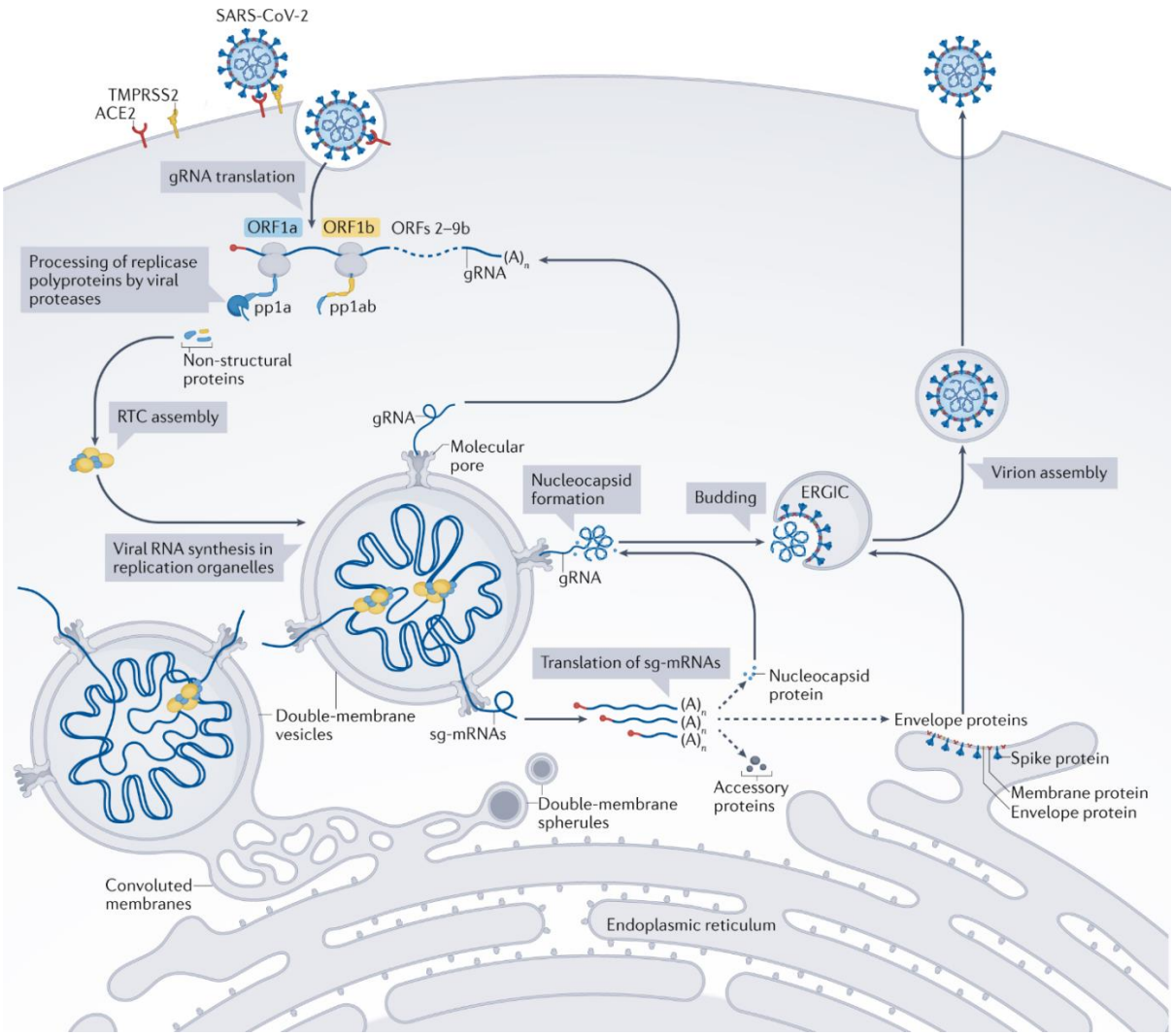

Figure 9. Coronavirus particles attach to cellular attachment factors, and their interactions with cellular receptors like ACE2 and host factors like the cell surface serine protease TMPRSS2 facilitate viral entry and fusion at the cell or endosomal membrane. Following entry, the viral genomic RNA is released and subjected to immediate translation of two large open reading frames, ORF1a and ORF1b. Polyproteins pp1a and pp1ab are processed into individual non-structural proteins (nsps) during both translation and post-translation processes in line with the production of non-structural proteins (nsps), the formation of specialized structures like double-membrane vesicles (DMVs), convoluted membranes (CMs), and small open double-membrane spherules (DMSs) occurs. The translated structural proteins move into the membranes of the endoplasmic reticulum (ER) and then pass through the ER-to-Golgi intermediate compartment (ERGIC). There, they interact with newly produced genomic RNA that is encapsulated by N proteins, leading to the formation of budding virions within secretory vesicular compartments. These virions are eventually released by exocytosis (Malone et al., 2022).

2. Treatment strategies for COVID-19

2.1. Vaccines (prophylactic treatment)

Despite all the preventive measures enacted to halt the spread of the virus, the pandemic has resulted in significant morbidity and mortality rates worldwide. Research into vaccines for SARS and MERS has provided valuable insights and a foundation for the development of COVID-19 vaccines. Several effective COVID-19 vaccines were tested in clinical trials of within a very short period. As of today, over 13.5 billion individuals across the globe have been administered at least one dose of a COVID-19 vaccine (WHO). Different types of vaccines exist: whole virus vaccine, viral vector vaccine, nucleic acid vaccine, recombinant subunit vaccine.

The AstraZeneca vaccine, also known as Vaxzevria or the Oxford-AstraZeneca vaccine contains the S protein gene in a chimpanzee adenovirus vector (ChAdOx1). This vaccine was administered in more countries than any other vaccine (Vanaparthy et al., 2021). Other viral vector vaccines against COVID-19 include Sputnik V, Sputnik Light produced in Russia. Besides, two highly effective mRNA vaccines were manufactured against COVID-19, Pfizer–BioNTech COVID-19 vaccine and Moderna COVID-19 vaccine. The vaccine is made up of a lipid nanoparticle encapsulating the mRNA of the S protein. The initial phase 3 clinical results for the Pfizer-BioNTech vaccine in December 2020 indicated a 95% efficacy in preventing symptomatic COVID-19 in adults after two doses (Polack et al., 2020), consequently, it was the first to receive FDA Emergency Use Authorization (EUA). Besides, it has shown between 90% and 100% effective against severe COVID-19 symptoms (Pfizer, BioNTech, 2021). However, with time, the vaccine efficacy decreases more rapidly, dropping to 75 percent after 90 days (Whitaker et al., 2022). Therefore, booster shots were recommended to help maintain strong and long-lasting protection against COVID-19. Similarly, the Moderna (mRNA-1273) vaccine was designed with the same goals and principles as that of Pfizer BioNTech. Moderna's Phase 3 clinical results in December 2020 was similar to Pfizer-BioNTech's, demonstrating approximately 94.1% efficacy in preventing COVID-19 at that stage (Baden et al., 2021). However, a comparative analysis of the two mRNA vaccines revealed that among older adults, mRNA-1273 was linked to a reduced likelihood of experiencing adverse events in contrast to BNT162b2 (Harris et al., 2023).

2.2. Strategies for discovery and development of new therapeutics for SARS-CoV-2 infection

Numerous antiviral medications are presently being investigated for their potential in combating SARS-CoV-2 infection. The repurposing of existing drugs like remdesivir and other neutralizing antibodies has proven effective in treating COVID-19 patients. Nonetheless, these drugs face challenges, including limited therapeutic effectiveness and noticeable side effects. Furthermore, it is assumed that the use of bi- or tri-therapy are necessary to avoid emergence of resistant viruses. To tackle the formidable task of rapidly developing new treatments for SARS-CoV-2, collaborative efforts among pharmaceutical companies, biotechnology firms, and research laboratories are crucial, with a careful focus on the target. A comprehensive understanding of the detailed SARS-CoV-2 life cycle is essential for identifying potential drug targets.

Small-molecule drug discovery involves various aspects and key strategies. Antiviral therapeutics can target either the host or the virus itself. Host-directed antivirals aim at human proteins essential in the viral life cycle, while viral proteins interfere with pathway components. Some approved drugs may inhibit SARS-CoV-2 endocytosis *in vitro*, including chlorpromazine (Vercauteren et al., 2010), fluvoxamine (Otomo et al., 2008), sertraline (Takahashi et al., 2010), promethazine (Sharma et al., 2019), nystatin (Vercauteren et al., 2010), amiloride, vinblastine, itraconazole, flubendazole, terfenadine, imipramine, and beta-methyl cyclodextrin (H. Lin et al., 2018; Tomkiewicz et al., 1993). TMPRSS2 mediates the cleavage of the viral spike protein, which constitutes a key mechanism in the activation of SARS-CoV-2 and facilitates host cell entry, thus making it a potential target for antiviral intervention. The clinical TMPRSS2 inhibitor, camostat mesylate, effectively inhibited SARS-CoV and MERS-CoV, as well as SARS-CoV-2 entry (Hoffmann et al., 2020). Several natural compounds, including baicalin, scutellarin, nicotianamine, and glycyrrhizin, also showed antiviral potential by blocking the attachment and entry of SARS-CoV-2 by binding to ACE2 *in vitro* (Chen & Du, 2020).

Virus-targeting drugs directly focus on viral components, thereby blocking replication. Conserved viral proteins are considered a target because they accumulate fewer mutation and are essential to the viral life cycle. Efforts to interfere with viral replication have centered on RdRp and the two viral proteases, PLpro and Mpro, using small-molecule inhibitors (Narayanan et al., 2022). While all viral enzymes involved in

coronavirus replication are potential candidates for therapeutic development, the role of Mpro in polyprotein processing is well-documented and assayable, making it a prime target for suppressing viral replication. The rapid availability of Mpro structures has facilitated structure-based drug design efforts. Covalent inhibition of SARS-CoV-2 Mpro cysteine 145 with selective antiviral drugs can stop the virus replication without affecting human catalytic pathways (La Monica et al., 2022). Furthermore, SARS-CoV and SARS-CoV-2 Mpro share 96% sequence similarity, allowing previously discovered SARS-CoV chemical probes targeting Mpro to be repurposed for SARS-CoV-2.

Similarly, RdRp has been validated as a target for several reasons: (i) its catalytic site sequence is broadly conserved across coronaviruses and SARS-CoV-2 variants, (ii) its structure and function are well-understood among RNA viruses, and (iii) there are precedent RdRp inhibitors for other RNA viruses, increasing confidence in its relevance as a target (Zhu et al., 2020). A variety of RdRp inhibitors with different mechanisms of action, such as remdesivir and molnupiravir, have been developed (Gordon et al., 2020; Hashemian et al., 2022).

Non-covalent inhibitors have been identified for SARS-CoV PLpro. Nsp3/PLpro cleaves ubiquitin and ISG15 modifications within host cells, compromising innate immune responses, making PLpro an excellent drug target for the next generation (Narayanan et al., 2022). The high sequence and structural similarity between SARS-CoV and SARS-CoV-2 PLpro suggests that already discovered SARS-CoV PLpro inhibitors can also effectively inhibit SARS-CoV-2 PLpro with almost identical activity profiles (Osipiuk et al., 2021).

2.3. Therapeutic treatment

With the emergence of coronaviruses outbreak, and since future epidemics and pandemics are predictable, it has become a necessity find effective antivirals to prevent future outbreaks that could jeopardize livestock and public health.

In the early phase of the SARS-CoV epidemic, efforts to design anti-SARS drugs were initiated, however soon after the virus was controlled and stopped spreading, research on antiviral development was not further continued. SARS-CoV patients were treated with several antiviral agents as corticosteroids, IFN-I, convalescent plasma or immunoglobulins, ribavirin, lopinavir and ritonavir (LPV/r).

2.3.1. Immunomodulatory Agents

Corticosteroids

Corticosteroids has been widely used to treat SARS-CoV due to its rationale contribution to suppress the "cytokine storm" by significantly reducing the production of early response cytokines such as IFN-γ, tumor necrosis factor (TNF), interleukin 1 (IL-1), and interleukin 6, thus preventing tissue damage. Other reports showed a rational use of corticosteroids to treat ARDS and septic shock (Keh et al., 2003; Meduri et al., 1998). On the other hand, a combination treatment of corticosteroids with interferon alpha I showed better oxygen saturation levels and resolved lung abnormalities compared to corticosteroids alone (Loutfy et al., 2003). However, based on the clinical evidence, the use of corticosteroids alone showed harmful effects outweighing the benefits. Necroscopic observations and autopsy of SARS patients had revealed fungal superinfection and aspergillosis upon treatment with high doses of corticosteroids or for prolonged periods. Besides, the potential of corticosteroids to suppress the innate immune system might delay the virus clearance, thus increasing the risk of virus-related complication. The use of corticosteroids in subjects with MERS delayed virus clearance but did not necessarily improve survival and reduce hospitalization duration. It is worth noting that most studied were performed in the urgency of the epidemics, and several limitations could be identified in the studies. Thus, corticosteroids were not recommended to be administrated alone and were usually prescribed empirically with ribavirin or interferon.

2.3.2. Virus targeting agents

Anti-SARS-CoV-2 Monoclonal Antibodies

Monoclonal antibodies have showed clinical benefits and have emerged as a treatment option for COVID-19. The FDA has granted authorization for bamlanivimab plus etesevimab, casirivimab plus imdevimab, sotrovimab, and bebtelovimab for the treatment of outpatients with mild to moderate COVID-19. Monoclonal Ab acts by neutralizing the virus by binding to the spike protein on its surface thus preventing it to enter the cell and cause infection (National Institutes of Health, 2023). Unfortunately, with the emergence of new variant strains, these monoclonal are unlikely to provide effectiveness.

Remdesivir

With the emergence of SARS-CoV-2 in late 2019 and the race to find an effective drug and vaccine to combat COVID-19, repurposing existing drugs was the fastest approach to mitigate the disease burden. Remdesivir, an anti-hepatitis C virus drug, has been studied in several clinical trials for the treatment of COVID-19 **(Figure 10)**. Remdesivir functions as a nucleoside analog that the RdRp incorporates into the emerging RNA product, enabling the addition of three additional nucleotides before RNA synthesis comes to a halt (Kokic et al., 2021). Remdesivir showed evidence of efficacy and safety, thus was granted approval by FDA for treating COVID-19. Treatment with remdesivir early during infection, showed a clinical benefit in rhesus macaques infected with SARS, suggesting that it could prevent progression of the disease to pneumonia in COVID-19 patients (Williamson et al., 2020). Meta-analysis comparing the efficacy of remdesivir vs placebo in RCTs showed a high probability of remdesivir reducing the mortality for non-ventilated patients with COVID-19 requiring supplemental oxygen therapy. By contrast, remdesivir causes harm to patients requiring ventilation (Lee et al., 2022). Interestingly, remdesivir combined with baricitinib was more effective than remdesivir alone in reducing the recovery time and improving the clinical status of patients with Covid-19 (Kalil et al., 2021). Another study highlighted the a 3-day course of remdesivir could significantly reduce the risk of hospitalization in non-hospitalized COVID-19 patients with mild to moderate symptoms who are at risk of progressing to severe disease (Gottlieb et al., 2022).

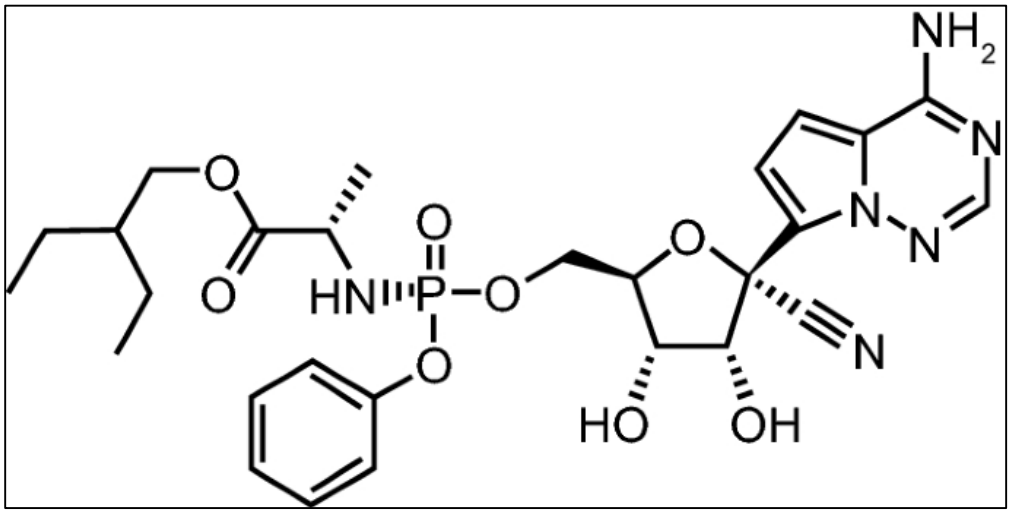

Figure 10. Remdesivir structure (Lamb, 2020).

Molnupiravir

In addition, Lagevrio, also known by its generic name molnupiravir, manufactured by Merck and Ridgeback Biotherapeutics, has been granted the FDA authorization to treat of mild-to-moderate coronavirus disease 2019 (COVID-19) in adults who are within 5 days of symptom onset and are at high risk of developing severe COVID-19. Molnupiravir is the oral prodrug of beta-D-N4-hydroxycytidine (NHC), a ribonucleoside that disrupt the replication of SARS-CoV-2 by introducing mutations into the viral genome, rendering the virus less infectious and less able to cause severe illness **(Figure 11)**. Molnupiravir has been tested *in vitro* and showed an EC_{50} ranging between 0.32 and 2.66 μM. This drug has shown activity against different SARS-CoV-2 variants of concern, including the highly transmissible Omicron B1.1.529 (Vangeel et al., 2022) and its sub-variants as the B.1.1.7 (alpha), B.1351 (beta), P.1 (gamma) and B.1.617.2 (delta) (Teli et al., 2023). Molnupiravir is a mutagenic agent and it has been reported that it could induce mutations in SARS-CoV-2 genome in patients that can be transmitted to other patients (Sanderson et al., 2023). There were debates and concerns regarding the long-term safety and efficacy of molnupiravir, as well as the potential for the emergence of resistant variants of the virus. the European Medicines Agency (EMA) considered that the benefit/risk balance of molnupiravir in the treatment of COVID-19 was not established and refused its marketing authorization (EMA, 2023). Continued close monitoring is required for a better assessment of the safety profile of molnupiravir.

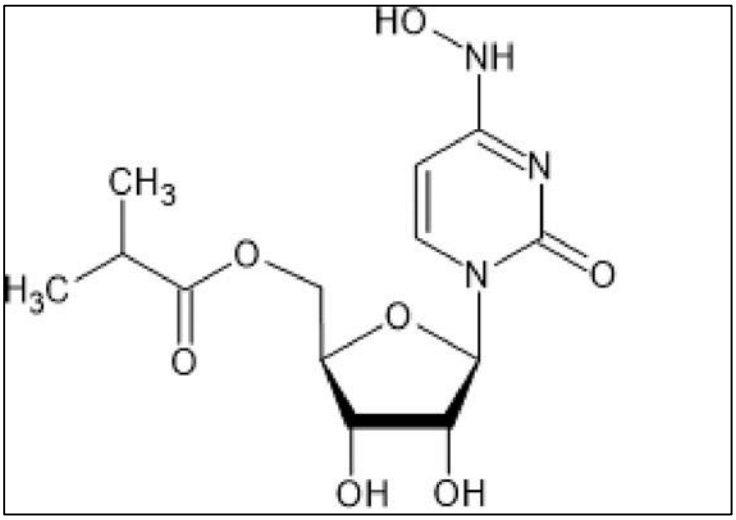

Figure 11. Molnupiravir structure (Oziminski & Bycul, 2023).

Nirmatrelvir/ritonavir (Paxlovid)

It was not until December 2021 that the FDA granted Emergency Use Authorization (EUA) for paxlovid for the treatment of mild-to-moderate COVID-19 in adults and pediatric patients (12 years of age and older weighing at least 40 kg). This medicine was also approved by the EMA and is used in the European Union (EMA, 2022). Paxlovid is comprised of nirmatrelvir, a SARS-CoV-2 main protease inhibitor (Mpro, also referred to as 3CLpro or Nsp5 protease), co packaged with ritonavir, an HIV-1 protease inhibitor and CYP3A inhibitor **(Figure 12)**. Ritonavir alone has no effect on SARS-CoV-2; however, it inhibits the CYP3A-mediated metabolism of nirmatrelvir, consequently maintaining high nirmatrelvir plasma concentrations. The drug was developed by Pfizer in collaboration with the pharmaceutical company, AstraZeneca, and has demonstrated an 89% decrease in the likelihood of hospitalization and mortality among individuals who were not vaccinated (Hammond et al., 2022).

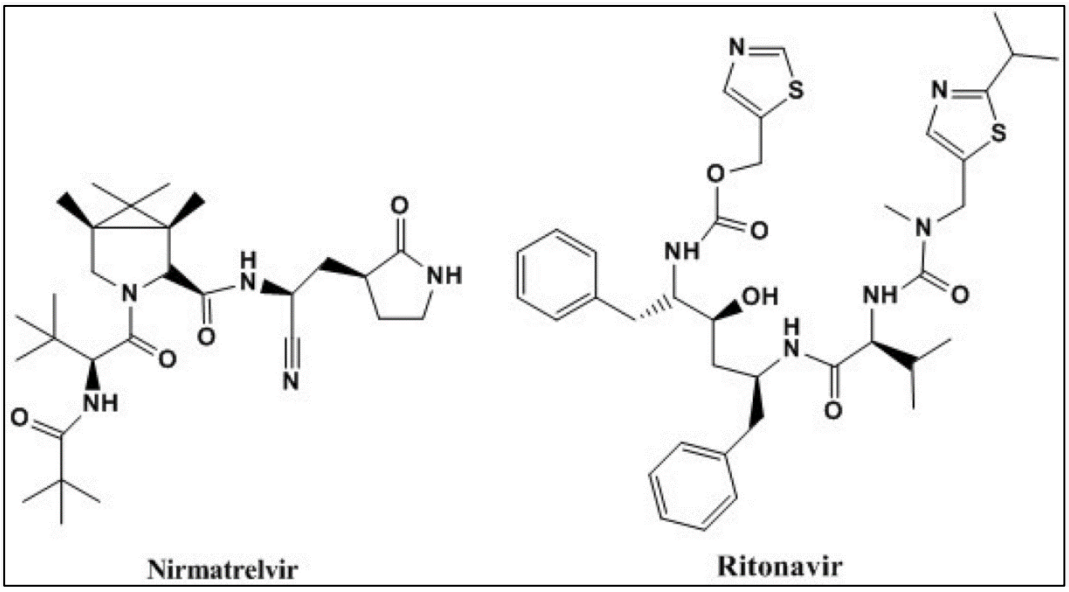

Figure 12. Structural formula of nirmatrelvir and ritonavir (Imam et al., 2023).

Ensitrelvir

Ensitrelvir fumaric acid (S-217622, referred to as ensitrelvir), a newly developed oral inhibitor of the SARS-CoV-2 3C-like protease **(Figure 13)**. Known as Xocova® in Japan, this compound was created in partnership between Shionogi and Hokkaido University and functions as an orally active 3C-like protease inhibitor (Shionogi & Co., 2023). The

findings of a randomized phase 2/3 study indicated that ensitrelvir administration led to a median time of approximately 1.5 days for fever resolution and around 6.5 days for the resolution of all COVID-19 symptoms (Shionogi Inc., 2023). Furthermore, administering ensitrelvir within the initial three days of experiencing COVID-19 symptoms may have contributed to preventing or improving issues related to taste and smell. Ensitrelvir is used in Japan with an emergency regulatory approval.

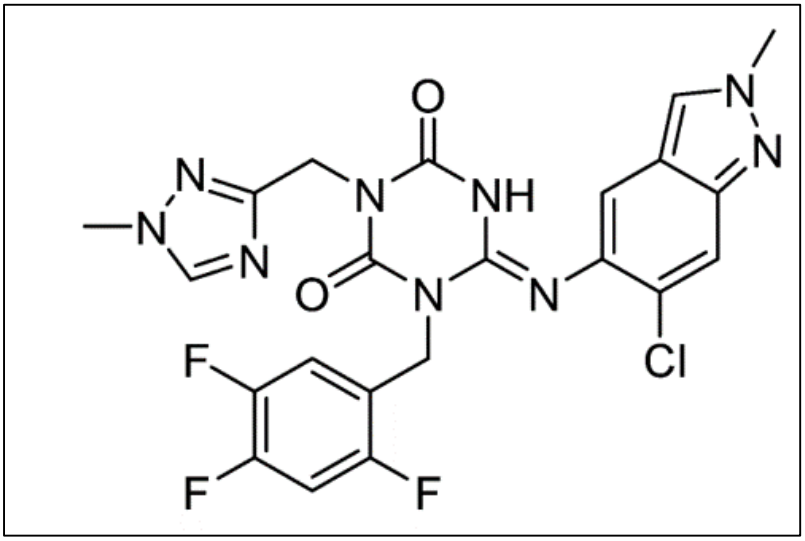

Figure 13. Ensitrelvir structure (Farkaš et al., 2023).

Ribavirin

Ribavirin, a nucleoside analogue, is well known for its wide spectrum of antiviral activity against DNA and RNA viruses and was widely prescribed as a treatment for SARS-CoV **(Figure 14)**. However, it failed as an effectiveness antiviral agent. Generally, ribavirin showed a lack for efficacy in clinical trials and was associated with adverse effects as anemia along with hypoxia, resulting in an increased risk of death in the treated SARS-CoV patients (Knowles et al., 2003). Although ribavirin has been given as part of treatment regimens for MERS patients, meta-analyses of case studied have found limited efficacy in treating patients with highly pathogenic coronavirus respiratory syndromes. A combination treatment of ribavirin with IFN-I might have efficacious effects with timely administration and monitoring of adverse effects (Al-Tawfiq et al., 2014). However, a combination treatment of interferons IFN-α2a or IFN-β1a and ribavirin did not consistently improve outcome of MERS disease, particularly in elderly individuals with comorbidities (Shalhoub et al., 2015). Even though ribavirin did not improve patients'

outcomes, it has shown an antiviral activity against SARS-CoV-2 *in vitro* (Unal et al., 2021).

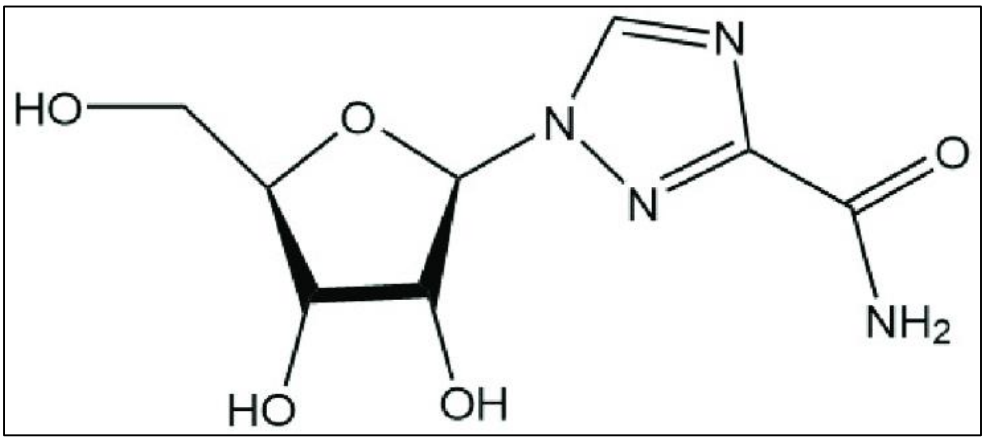

Figure 14. Chemical structure of ribavirin (Unal et al., 2021).

2.3.3. Host targeting agents

Chloroquine/ Hydroxychloroquine

The anti-malarial drugs chloroquine (CQ) and hydroxychloroquine (HCQ) have gained a wide spread attention and have been a topic of significant debate and research during the COVID-19 pandemic **(Figure 15)**. Due to their broad range of antiviral activity and inflammatory properties, they have consequently gained attention as a potent element in treating COVID-19 pneumonia patients. However, their non-effectiveness in treating COVID-19 is now clear. Chloroquine's mechanism of action against SARS-CoV-2 involves inhibition of the virus's endocytic fusion pathway rather than its membrane fusion pathway. The National Institute of Health (NIH) has halted trials on CQ, claiming that it is unlikely to be beneficial to hospitalized patients with COVID-19. The largest international RCT for COVID-19 treatments, "Solidarity Trial" reported little or no effect on overall mortality, initiation of ventilation, and duration of hospital stay in hospitalized patients (World Health Organization, 2020a). CQ/ HCQ are only effective in inhibiting SARS-CoV-2 infection *in vitro* (J. Liu et al., 2020).

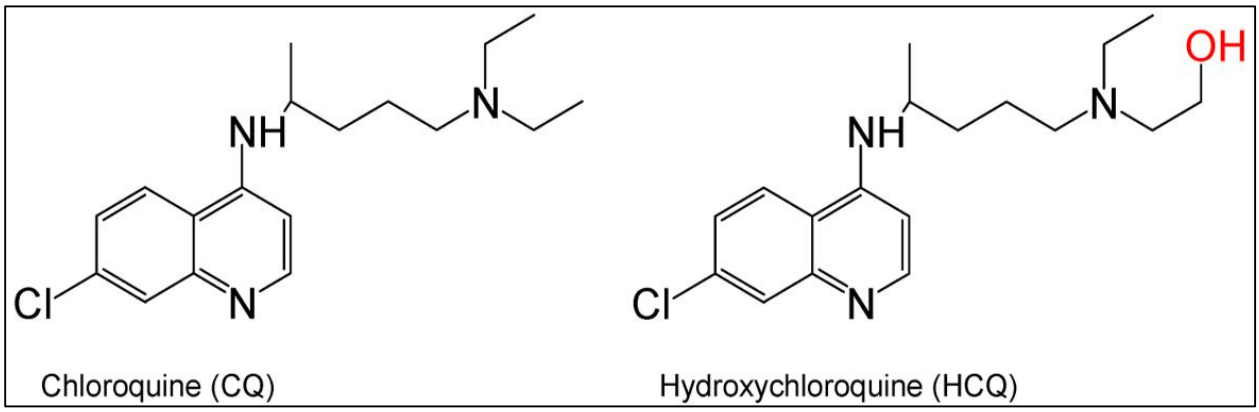

Figure 15. Chloroquine and Hydroxychloroquine structure (J. Liu et al., 2020).

2.4. *In vitro* models for studying HCoVs

The comprehension of coronavirus infection biology, growth kinetics and tropism, as well as the development of antivirals and vaccines, heavily relies on cell-based methods and animal models. Vero cells, derived from African green monkey kidney tissue, have gained prominence due to their susceptibility to a wide range of viruses, including SARS-CoV, MERS-CoV, and SARS-CoV-2, as they support viral replication to high titers (Hoffmann et al., 2022; Keyaerts et al., 2005). This high susceptibility is likely attributed to their elevated expression of the ACE2 receptor. Besides, Calu-3 cells, a human lung adenocarcinoma cell line, were initially considered highly permissive to SARS-CoV and SARS-CoV-2 (Baczenas et al., 2021). However, comparative studies revealed that SARS-CoV-2 production in Calu-3 was typically lower than that in Vero E6 cells (Chu et al., 2020). Additionally, Huh-7 cells, derived from human hepatoma, are frequently used for *in vitro* production of infectious HCV particles and anti-HCV drug assays. They are also permissive to various human coronaviruses, including HCoV-229E, HCoV-OC43, MERS-CoV, SARS-CoV, and SARS-CoV-2 (de Wilde et al., 2013; Freymuth et al., 2005). Despite their permissiveness to SARS-CoV-2, co-expression analyses of ACE2 and TMPRSS2 suggested that Huh-7 cells strongly expressed TMPRSS2 but lacked ACE2 expression, resulting in moderate viral replication (Nie et al., 2004). Other mammalian cell lines permissive to different human coronaviruses include Human embryonic kidney 293T cells (HEK 293T) and cancer coli 2 cells (Caco-2).

Human airway epithelial cells (HAEC) represent a primary target of coronaviruses, including SARS-CoV-2. HAEC exhibit the same structure and complexity as human lung

tissue, making them susceptible to various respiratory viral infections (Boda et al., 2018; Loo et al., 2020). With the inclusion of all pertinent cell types found in the lower respiratory tract—such as ciliated, goblet, and basal cells, including those expressing ACE2 and TMPRSS2—this system enables the detailed examination of interactions between hosts and pathogens at both molecular and cellular levels. Furthermore, it serves as a platform for evaluating the effectiveness of antiviral drugs.

Investigating viral envelope glycoproteins is crucial for understanding various aspects of a virus, including its lifecycle initiation, host and cellular tropism, interspecies transmission, viral pathogenesis, and host cell entry pathways. Pseudotyped particles, also known as pseudovirions, are valuable tools for studying viral fusion proteins. These pseudovirions consist of a surrogate viral core with a different viral envelope protein on their surface. Typically, pseudotyped particles are derived from model viruses, such as retroviruses (e.g., MLV and HIV) or rhabdoviruses (e.g., VSV), with essential genes removed to render them incapable of completing a full replication cycle (Fujioka et al., 2022; Millet & Whittaker, 2016; Xu et al., 2021). The S proteins of human coronaviruses are employed as examples of viral envelope proteins incorporated into MLV pseudotyped particles, resulting in HCoV S pseudovirions (HCoV-S) (Millet & Whittaker, 2016).

I*n vivo* models are indispensable for the study of coronaviruses, enabling researchers to explore virus behavior, transmission, and pathogenesis in living organisms. A variety of animal models have been employed to investigate coronaviruses, including SARS-CoV, MERS-CoV, and SARS-CoV-2. Common *in vivo* models include hACE2-transgenic mouse models, mouse-adapted SARS-CoV-2, hamsters, ferrets, and non-human primates (Rosa et al., 2021).

2.5. Bioactive natural products in COVID-19 therapy

Although vaccines and antiviral drugs have been developed, several significant challenges stand in the way of achieving herd immunity for COVID-19. These challenges encompass disparities in vaccine distribution, individuals who do not respond effectively to vaccines, the emergence of SARS-CoV-2 variants that can evade the immune response, and vaccine hesitancy among the global population (M. Bayati et al., 2022; Jing et al., 2023). Moreover, these interventions are primarily accessible to nations with the financial resources to secure early access. This limitation is largely attributed to patent

holders resisting the call for licensing agreements that would permit generic manufacturers to produce similar antivirals or vaccines (Kana et al., 2023). Consequently, low-income countries, which often have weaker healthcare systems, higher poverty rates, and limited access to critical resources like medical supplies and vaccines, have borne a disproportionate burden. Therefore, there is a critical need for effective, readily accessible, and cost-effective antiviral treatments targeting SARS-CoV-2, particularly in low-income countries.

Natural products (NPs) are a category of small-molecule drugs that can be either extracted as specialized metabolites from living organisms, including medicinal plants and microorganisms or artificially synthesized in a laboratory. Throughout history, NPs have played a pivotal role in the realm of drug discovery, particularly in the development of compounds with antimicrobial and antitumor properties. Their significance derives from the way they have been finely tuned structurally through evolution to fulfill specific biological roles, including defense mechanisms and interactions with other microorganisms. NPs offer a diverse array of chemical structures that set them apart from the more conventional approaches of combinatorial chemistry, thus providing opportunities to uncover entirely novel small-molecule lead compounds.

The WHO reports that nearly 80% of the global population relies on traditional medicines to treat various ailments (World Health Organization, 2023a). Previous experiences dealing with outbreaks like influenza (Eichberg et al., 2022), MERS-CoV (Xian et al., 2020), and HIV infections (Andersen et al., 2018) have emphasized the valuable role of NPs derived from medicinal plants and their derivatives in the development of new antiviral drugs. This value is attributed to their ready availability and the rich diversity of substances they offer, all of which possess therapeutic potential.

Numerous studies have been published, categorizing natural compounds as potential inhibitors of SARS-CoV-2. These inhibitors are categorized as either antiviral agents or Immunomodulatory therapies.

2.5.1. Antiviral agents

Antiviral agents primarily target different step of the viral infectious cycle such as the internalization phase of the virus, preventing the attachment and entry of the virus into host cells. They may also affect cellular endocytic mechanisms, modify environmental

conditions such as pH, or interact with cellular receptors and proteolytic enzymes to inhibit internalization and viral replication. Some natural compounds hold the potential to serve as antiviral agentsand may be used for prophylaxis against COVID-19. However, for most of these compounds, *in vivo* validation is needed.

Molecules in clinical trials

Researchers have reported that epigallocatechin gallate (EGCG) can simultaneously bind to the RBD of SARS-CoV-2 and compete with ACE2 binding, effectively blocking the recruitment of these viruses to the host cell surface (Henss et al., 2021). A Phase 2 randomized clinical trial (NCT04446065) is currently underway to assess the prophylactic effect of Previfenon, a drug containing EGCG, in high-risk healthcare workers.

Additionally, Echinaforce, an alcoholic extract derived from *Echinacea purpurea* (L.) Moench. (Asteraceae) known for its history in treating respiratory tract infections, exhibited virucidal activity against HCoV-229E, MERS-CoV, SARS-CoV, and SARS-CoV-2 (Signer et al., 2020). Due to its promising potential for prophylaxis, it is currently in a phase 4 clinical trial (NCT04999098) to assess its effectiveness in reducing viral shedding in COVID-19.

***In vitro* antiviral molecules and extracts**

RPI-27, a high-molecular-weight branched polysaccharide extracted from the seaweed *Saccharina japonica* (J.E. Areschoug) C.E. Lane, C. Mayes, Druehl & G.W. Saunders (Laminariaceae), exhibited potent antiviral activity against SARS-CoV-2 with an IC_{50} of 83 nM, surpassing the effectiveness of remdesivir (Kwon et al., 2020). Other sulfated polysaccharides like heparin, TriS-heparin, and non-anticoagulant low-molecular-weight heparin (NACH) also demonstrated promising antiviral activity against SARS-CoV-2 by binding to the S-protein RBD (Kwon et al., 2020). Similarly, marine sulfated polysaccharides such as cucumber sulfated polysaccharide (SCSP), extracted from *Stichopus japonicus* Selenka (=*Apostichopus japonicus* Selenka), brown and red algae belonging to Stichopodidae family, displayed dose-dependent antiviral activities against SARS-CoV-2.

Vitis vinifera L. (Vitaceae) leaf extract has been reported to possess a virucidal effect on SARS-CoV-2 by containing various bioactive flavonoids, primarily derivatives of quercetin, luteolin, kaempferol, apigenin, isorhamnetin, myricetin, chrysoeriol, biochanin, isookanin, and scutellarein. This extract significantly reduced the entry of SARS-CoV-2 into cells by preventing viral attachment (Zannella et al., 2021).
Additionally, a commercial product called HIDROX, which contains 40% hydroxytyrosol (HT) from the olive oil industry, has been reported to exhibit virucidal activity against extracellular SARS-CoV-2 in a time and dose-dependent manner by altering the structure of the S protein. Interestingly, HIDROX-containing cream also displayed virucidal activity against SARS-CoV-2, suggesting its potential application for skin protection to reduce COVID-19 transmission (Takeda et al., 2021).

The water extract of *Prunella vulgaris* L. (Lamiaceae) has been found to hinder the entry of SARS-CoV-2 pseudotyped HIV carrying the full-length S protein or the D614 mutated S protein, which enhances virus infectivity. This effect is further enhanced at lower concentrations when combined with anti-SARS-CoV-2 neutralizing antibody (Ao et al., 2021).

A combination of *Agrimonia pilosa* Ledeb. (Rosaceae) and *Galla rhois* (gall caused by the Chinese aphid, *Schlechtendalia chinensis* (Bell), on the leaves of *Rhus chinensis*) in a 6:4 ratio (APRG64) has been shown to block the entry of SARS-CoV-2 into host cells and inhibit the formation of SARS-CoV-2 plaques. The antiviral effects of APRG64 are on par with those of remdesivir and chloroquine phosphate. The active compounds responsible for APRG64's anti-SARS-CoV-2 activity include ursolic acid, quercetin, and 1,2,3,4,6-penta-*O*-galloyl-β-D-glucose. These compounds reduce the presence of the S protein in cell supernatants and prevent the propagation of SARS-CoV-2 (Y.-G. Lee et al., 2021).

2.5.2. Immunomodulatory therapies

Immunomodulatory therapies refer to antiviral drugs that function after a person has already been infected with the virus. These drugs have the potential to reduce the severity and duration of symptoms and may also lower the risk of complications resulting from the infection.

Molecules and extracts currently in clinical trials

An extract derived from *Andrographis paniculata* (Burm. f.) Nees. (Acanthaceae) and its major labdane diterpenoid, andrographolide, have been shown to reduce the production of viral progeny *in vitro*. Computational molecular docking studies suggested that andrographolide may have the potential to target the primary protease of SARS-CoV-2, Mpro (Enmozhi et al., 2021). Currently, a phase 3 clinical trial (NCT05019326) has enrolled 3060 participants to assess the effectiveness of *Andrographis paniculata* in asymptomatic COVID-19 cases, with the primary endpoint defined as the requirement of hospitalization. The results are not published yet.

Xanthohumol, a chalcone undergoing clinical trials (NCT05463393) derived from hops (*Humulus lupulus* L.), has demonstrated strong inhibitory effects against multiple coronaviruses by targeting the Mpro proteins of betacoronavirus SARS-CoV-2 and alphacoronavirus PEDV (Lin et al., 2021). The completion of these clinical trials is anticipated by the end of 2023. The stilbenoids, resveratrol and pterostilbene, have demonstrated the ability to inhibit the production of SARS-CoV-2 progeny *in vitro*. A randomized, double-blind, placebo-controlled trial (NCT04400890) found that resveratrol could reduce the incidence of hospitalization, emergency visits, and pneumonia in mild COVID-19 outpatients (She et al., 2010). However, this trial had limitations due to a small sample size. A larger trial is currently underway to investigate the benefits of resveratrol in COVID-19 and its potential long-term effects on patients post-COVID-19. In a retrospective study (NCT04666753), resveratrol was combined with other natural compounds, including selenium yeast, cholecalciferol, ascorbic acid, ferulic acid, spirulina, N-acetylcysteine, and more, to evaluate its effects on SARS-CoV-2 by measuring the duration of clinical symptoms (primary endpoint). Given resveratrol's potential in preventing liver fibrosis by inhibiting the Akt/NF-κB pathways, and considering the lung fibrotic damage caused by COVID-19, a randomized clinical trial (NCT04799743) was registered to assess resveratrol's anti-fibrotic therapeutic effects on discharged COVID-19 patients (Sönmez et al., 2010). However, none of these clinical trials allowed for the identification of novel active compounds effective against SARS-CoV-2.

In vitro antiviral molecules and extracts

Shuanghuanglian preparation is a traditional Chinese medicine (TCM) made of extracts obtained from *Lonicera japonica* Thunb. (Caprifoliaceae), *Scutellaria baicalensis* Georgi (Lamiaceae), and *Forsythia suspense* (Thunb.) Vahl. (Oleaceae), commonly used to treat respiratory tract infections. *Shuanghuanglian* preparation, along with its active flavonoids, baicalin and baicalein, have demonstrated significant antiviral activity against SARS-CoV-2. They achieved this by inhibiting the activity of 3CLpro, PLpro, and RdRp enzymes (Su et al., 2020; Zandi et al., 2021). Baicalin and baicalein both exhibited strong binding affinity with the SARS-CoV-2 PLpro. Baicalein serves as a protective shield by interacting with S1/S2 site and the oxyanion loop, thereby preventing the substrate from binding to the catalytic site of SARS-CoV-2 PLpro. Additionally, both baicalein and baicalin are effective inhibitors of SARS-CoV-2 RdRp (Zandi et al., 2021). Naringenin, a flavanone present in various Citrus plants, possessing diverse biological functions, including antiviral, antibacterial, and anticancer properties, has recently emerged as a potent antiviral agent against SARS-CoV-2 MPro (Abdallah et al., 2021).

Part 2

1. Extremophiles as source of novel bioactive compounds

Plants adapted to extreme conditions, known as extremophile plants, have the ability to thrive and flourish in challenging environments characterized by severe abiotic stress factors. These environments include extremes of temperature, pH, salinity, radiation, pressure, and metal concentrations. Extremophile plants, including halophytes (growing in soils with high salinity), xerophytes (growing in dry and arid environments), resurrection plants (survive almost complete dehydration or desiccation even over years), metal hyperaccumulators (growing in soils or waters with extreme levels of metals and concentrate these metals in their living tissues), etc. have undergone evolutionary adaptations and developed numerous mechanisms to successfully carry out their life cycles and adapt to fluctuations in their growth conditions in challenging environments. They have developed a range of mechanisms to manage these stresses at anatomical, physiological, biochemical, and molecular levels. The synthesis of plant specialized metabolites (PSMs) is regarded an adaptive capacity for dealing with stressful environmental conditions that can challenge the plant growth (Isah, 2019). This adaptation involves the production of different chemical compounds and their interactions to support structural and functional stability through signaling processes and pathways. Environmental responses are coordinated by interactions and communication between various signaling and stress-response networks.

The word halophyte, derives from Ancient Greek ἅλας (halas) 'salt' and φυτόν (phyton) 'plant', was introduced in 1809 by Peter Simon Pallas. Salt-tolerant plant species or halophytes are plants that exhibit resistance or tolerance to high salt levels and possess a remarkable ability to go complete their entire life cycle in in a salt concentration of at least 200 mM NaCl (Flowers & Colmer, 2008). They do not form a systematical group and, phylogenetically, they are not related to each other. Halophytes are found to live and grow in a wide variety of saline habitats as mangrove forests, inlands deserts, salt marshes. mudflats, steppes, and coastal regions such as coastal salt marshes, and coastal fringe forests. Even though these plants thrive in regions with water saturation, they cannot utilize this water due to saline stress. Therefore, halophytes are plants found in environments that are physically wet but physiologically dry. Due to high salinity

environment, these plants have evolved a range of adaptations to harsh environmental conditions by evolving morphologically, physiologically, and biochemically. Salinity avoidance is accomplished by modifications of their internal water balance by compartmentalizing ions within cell vacuoles, accumulating compatible organic solutes, developing succulence, and forming salt-secreting glands and bladders (Colmer et al., 2005; Flowers et al., 2010; Flowers & Colmer, 2008). Ecologists have suggested a limit of 200 mM NaCl in order to separate true halophytes (euhalophytes) from relatively tolerant species. Some species, such as *Tecticornia* spp., are capable of withstanding NaCl concentrations of 10 mM to 2 M (Chapman, 1942; Cheeseman, 2015; Santos et al., 2016). A plethora of definitions have been attributed to halophytes due to their taxonomical and ecological complexity, and the definition remains debated. Halophytes share certain structural adaptations seen in xerophytes, such as being succulent in nature. The majority of halophytes found in tropical and subtropical regions are shrubs, although there are a few herbaceous varieties among them. In temperate zones, halophytic vegetation is purely herbaceous.

1.1.1. Morphological characteristics of halophytes

Roots

Halophytes typically produce numerous shallow primary roots. In addition to these primary roots, many stilt or prop roots develop from the above-ground branches of the stem to provide effective anchorage in soft, muddy, or loose sandy soil. These specialized roots extend downward and penetrate into the deeper and more compact soil layers. the stilt roots may be strong and extensively developed, but in others they may be poorly developed. Others may not develop stilt roots. Some halophytes develop adventitious root buttresses originating from the lower sections of tree trunks, offering adequate support to the plants (Plantlet, 2021). Besides, in coastal regions, where soil is poorly aerated, hydro halophytes develop special type of negatively geotropic roots, called pneumatophores or breathing roots (eHALOPH, 2022; Plantlet, 2021). Pneumatophores typically emerge from the underground roots and extend into the air well beyond the water surface **(Figure 16)**. The appearance and structures that define specific plant groups sum up their ecological and physiological adaptations.

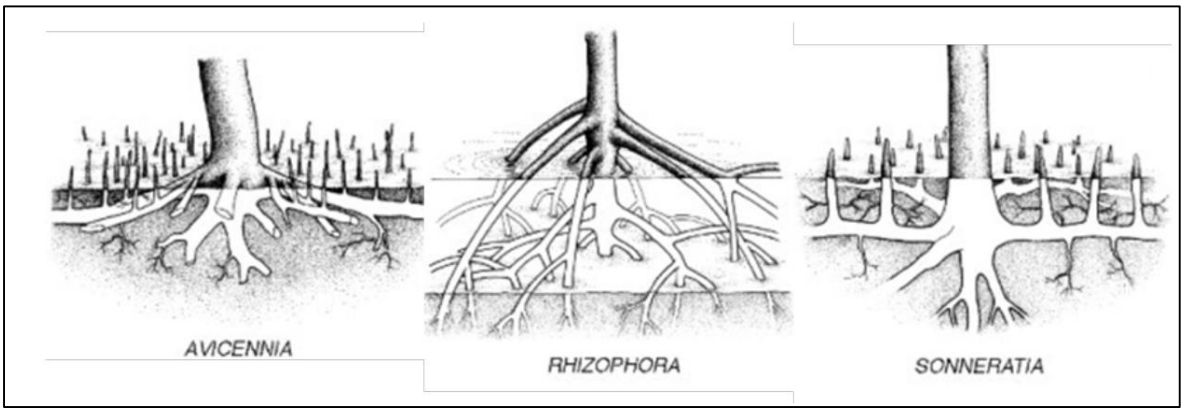

Figure 16. Pneumatophores of mangrove plants *(Takarina, 2020)*.

Stem

Stems in several halophytes develop succulence, an example is *Suaeda maritima* **(Figure 17)**. As per Pokrovskaya's research in 1954 and 1957, high salinity suppresses cell division while promoting cell elongation. Repp et al 1959 noted that this effect results in a reduction in the number of cells and an enlargement of individual cell sizes, which is characteristic of succulent plants. The extent of their succulence development can serve as an indicator of a plant's capacity to thrive in extremely saline environments (eHALOPH, 2022; Plantlet, 2021).

Figure 17. *Suaeda maritima* (L.) Dumort. (Wikipedia)

Leaves

In the majority of halophytes, the leaves tend to be dense, undivided, fleshy, typically small, and frequently have a shiny or translucent quality, however some species are aphyllous. The stems and leaves of coastal aerohalophytes have evolved an additional adaptation to their surroundings, featuring a dense covering of trichomes on their surfaces (eHALOPH, 2022; Plantlet, 2021). The leaves of submerged marine halophytes are typically thin and possess an underdeveloped vascular system, often having a green epidermis. These adaptations enable them to efficiently absorb water and nutrients directly from their surrounding environment.

1.2. *Hippophae rhamnoides* L.

1.2.1. Taxonomical Classification

Seabuckthorn (*Hippophae* L.) is classified within the Elaeagnaceae family, the Elaeagnales order, the Rosidae subclass. However, the classification is still controversial. Sea buckthorn is a hardy, deciduous shrub with yellow or orange berries, which has been used for centuries. In ancient Greece, it was believed that adding sea buckthorn leaves to the diet of horses could lead to increased weight and shiny hair. This association is reflected in the Latin name "*Hippophae*" which means "shining horse." This plant was first recorded by Carl Linnaeus in 1753, and thus the genus *Hippophae* was established, including species *H. rhamnoides* L. Subsequently, various taxonomists identified and named several additional species and their subspecies based on their morphological descriptors like phyllotaxy, position of scales, characteristics of bark, fruit, and seed. Over time, the classification and naming of *Hippophae* species have evolved based on morphological traits. Initially, Rousi (1971) divided *Hippophae* into three species: *H. rhamnoides*, *H. salicifolia*, and *H. tibetana*. Later, Liu and He (1978) added a fourth species, *H. neurocarpa*. Subsequent taxonomists introduced further variations, such as *H. rhamnoides* subsp. *gyantsensis* by Lian (1988), *H. goniacarpa*, H. *litangensis*, and *H. stellatopilosa* by Lian et al. (1995), and *H. litangensis* elevated to species level by Lian and Chen (2002). Swenson and Bartish (2002) proposed seven species, with *H. rhamnoides* having eight subspecies, whereas the recognized international botanical website (World Flora Online, 2023) identifies nine accepted species and five recognized subspecies for *H. rhamnoides* This classification is constantly changing and adjustments

are regularly made (Yongshan et al., 2003). Nevertheless, *H. rhamnoides* is the most significant and widely distributed species in the Eurasian region, with *Hippophae salicifolia* and *Hippophae tibetana* following as important species.

1.2.2. Ecological and geographical distribution of *Hippophae* species and *Hippophae rhamnoides*

Hippophae species are widely distributed but are relatively sparse in Asia and Europe. Sea buckthorn is naturally found across temperate regions, including China, Mongolia, Russia, Great Britain, France, Denmark, Netherlands, Germany, Poland, Finland, Sweden, and Norway, within the geographical coordinates of 27° to 69° N latitude and 7° W to 122° E longitude **(Figure 18)** (T. S. C. Li & Schroeder, 1996). It can also thrive at higher altitudes in the sub-tropical regions of Asia, although fruit setting fails to occur at altitudes of 3900 meters. In Russia, substantial native populations exist at elevations ranging from 1200 to 2000 meters above sea level (Eliseev IP, Fefelov VA, 1977). Sea buckthorn exhibits remarkable temperature tolerance, enduring temperatures ranging from -43 to 40°C. Furthermore, it is recognized for its drought and salinity resistance (W. Chen et al., 2009; Heinze, M. and H.J. Fiedler, 1981). The current total acreage of *H. rhamnoides* is about 3.0 million ha worldwide, including wild and cultivated plants. China leads the world in terms of the total area covered by *Hippophae*, with approximately 920,000 hectares, and it also possesses the greatest diversity of *Hippophae* species, particularly in Qinghai Plateau (Lian Yong-Shan, 1988). Each year, China adds roughly 10,000 acres of sea buckthorn plantations primarily for the purpose of berry production and environmental enhancement. Mongolia has 20, 000 hectars of HR, India has 12,000, and Pakistan has around 3 000 hectars of *H. rhamnoides* (Unasylva, 1993). Russia has around 200,000 hectares of natural *Hippophae* forests, in addition to over 6,000 hectares in plantations. By 2003, Canada was annually planting around 100 kilometers of field shelterbelts, and they had over 250,000 mature fruit-bearing sea buckthorn plants on the Canadian prairies, yielding an estimated annual fruit harvest of 750,000 kilograms. Other nations cultivating *H. rhamnoides* for agricultural purposes include Germany (Höhne F & Kuhnke KH, 2015) and France, among others. *H. rhamnoides* is part of the vegetation of shrubby thickets of fixed coastal dunes, more

rarely at the top of cliffs swept by salt spray **(Figure 19)**. This species is frequent and became invasive in the dunes of the North of France (Digitale2, 2023a).

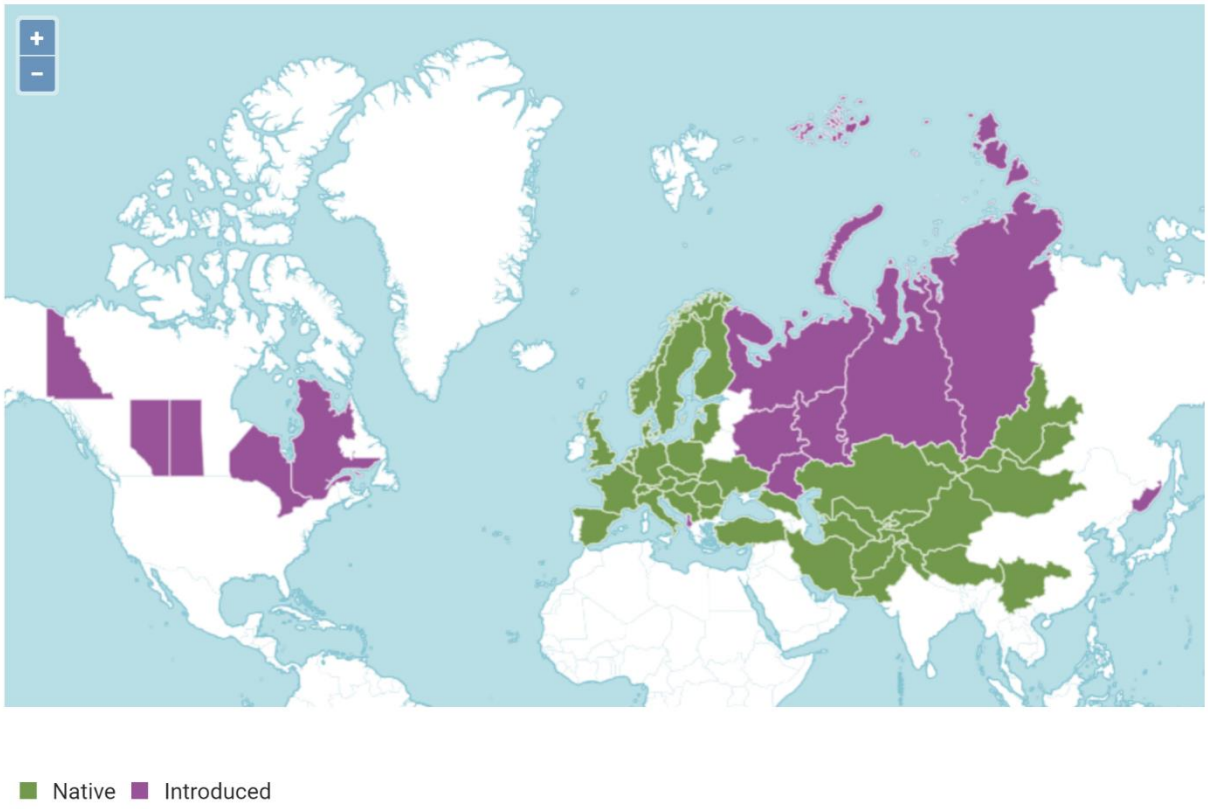

Figure 18. Distribution of *H. rhamnoides*. Green: native, purple, introduced (powo.science.kew, 2023)

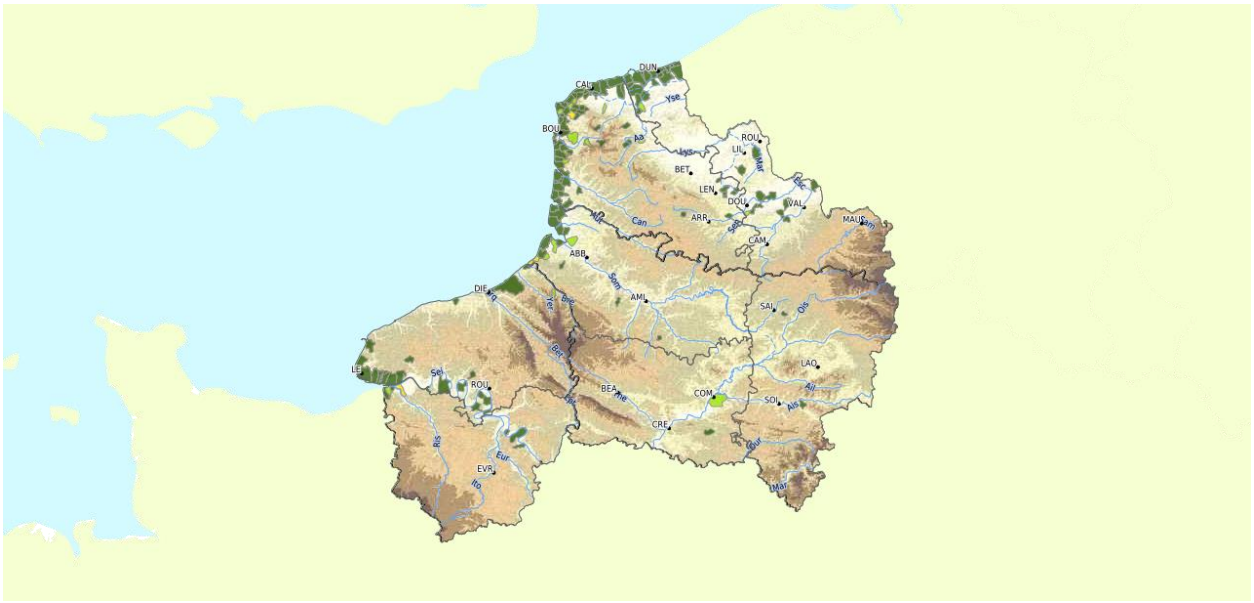

Figure 19. Distribution of *H. rhamnoides* in the North of France (Digitale2, 2023a).

1.2.3. Botany

H. rhamnoides is a tough, deciduous shrub that typically reaches a height of 2 to 4 meters (Li & Schroeder, 1996). It has a spiny and branched structure with an irregularly shaped grayish-green crown and rough brown or black bark **(Figure 20)**. The branches are covered in spines. The leaves are narrow and lanceolate, measuring 2-6 cm in length, with silver-green scales on both sides and brown dots underneath (A. Gupta & Upadhyay, 2011).

This shrub is dioecious, meaning that male and female flowers grow on separate plants. The gender of seedlings can only be determined when they first bloom, typically around three years of age (T. S. C. Li & Schroeder, 1996). Male buds have four to six apetalous flowers, while female buds usually have a single apetalous flower with one ovary and one ovule. Fertilization occurs through wind pollination, so it is essential for male plants to be close to female ones for successful fruit production.

The flowers are inconspicuous and yellow, appearing before the leaves. The ripe fruits are oval or slightly roundish and have a drupe-like structure, with an orange/red color. Each fruit contains a single seed surrounded by a soft, fleshy outer tissue. These fruits weigh between 270 and 480 mg and are rich in vitamin C, vitamin E, carotenoids, flavonoids, health-beneficial fatty acids, and even higher amounts of vitamin B12 compared to other fruits (Kallio et al., 2002). The seeds are dark brown, glossy, ovoid to elliptical in shape, and contain 8–18% oil (Bartish et al., 2002).

Sea buckthorn has an extensive root system with nitrogen-fixing nodules, forming a symbiotic relationship with nitrogen-fixing Frankia bacteria (Mohr et al., 2020). This makes it an excellent pioneer plant for conserving water and soil in eroded areas. The roots also play a role in converting insoluble organic and mineral substances in the soil into more soluble forms. Additionally, the plant can rapidly reproduce vegetatively through root suckers (T. S. C. Li & Schroeder, 1996).

Figure 20. *H. rhamnoides* collected on the coastline on northern France, Dannes (Lefèvre and Rivière, 2019).

1.2.4. Traditional use

H. rhamnoides has a rich history of use in traditional folk medicine, particularly in Russia and China. In China, the berries have served as a primary ingredient in functional foods and medicinal preparations for the treatment of cough and for improving blood circulation and digestion for many decades, while in Russsia the fruit oil was tested as a treatment for eye disorders showing beneficial effects on lesions of the cornea, dark adaptations, and visual acuity (Larmo et al., 2014). Historical records indicate its therapeutic benefits dating back to the eighth century A.D., and even as far back as the 4th century BC (Dwight Baker, 1993).

References to its use can also be found in both Tibetan traditional medicine and Chinese medicine (Lu, R., 1992). The Tibetan medical classic known as the "Four Books of Pharmacopeia" contains 84 prescriptions for preparing sea buckthorn-based medicines (Dwight Baker, 1993). Notably, a Tibetan lama regarded this plant as a universal remedy and made extensive use of its roots, stems, leaves, flowers, fruits, and seeds. Additionally, historical accounts suggest that during the 13th century, Jenkins Khan incorporated sea buckthorn into his campaigns (Zakynthinos & Varzakas, 2015). There is even historical evidence that sea buckthorn was part of the diet of Alexander the Great's army, where both patients and injured horses were treated using the leaves and fruits of this plant.

In 1929, the first biochemical analysis of *Hippophae* fruits was conducted (Guliyev et al., 2004). Over the past few years, our understanding of its nutritional significance and health benefits has grown, leading to increased recognition in Europe and North America.

1.2.5. Nutrient and bioactive compounds of *H. rhamnoides*

H. rhamnoides fruits are recognized for their substantial content of various nutrients, including carbohydrates including monosaccharides, proteins, amino acids, organic acids, significant quantities of carotenoids (provitamine A), vitamin C and vitamin E, alpha-tocopherol, minerals like potassium, sodium, magnesium, calcium, iron, zinc, and selenium, as well as fatty acids, glycerophospholipids, phytosterols, zeaxanthin esters, triterpenoids and polyphenolic compounds (flavonoids, tannins, phenolic acids) (Chen et al., 2023). The specific composition of these constituents can vary depending on factors such as the plant's origin, climate conditions, and the method of extraction employed.

Notably, vitamin C is among the prominent vitamins present in *H. rhamnoides*. The fruit of this plant typically contains approximately 400-600 mg of vitamin C per 100 grams (Guliyev et al., 2004). Variations in the chemical composition, including carbohydrates, moisture content, lipids, organic acids, and vitamins A and C, have been observed between large and small fruits (Zielińska & Nowak, 2017), as well as among different subspecies (Zheng et al., 2009) and geographic regions (Shouzong, 2012). It is worth noting that biologically active substances like ascorbic acid and β-carotene tend to be more abundant in tree-like forms of the plant compared to bush forms.

1.2.6. Phytochemical characterization of *H. rhamnoides*

H. rhamnoides L. has wide range of biological activities due to some primary and specialized metabolites including carotenoids, tocopherols, sterols, flavonoids, lipids, ascorbic acid, tannins, etc (Tiitinen et al., 2005). These compounds are of interest because they possess biological and pharmacological activities including antioxidant, antimicrobial, antitumoral, hepato-protective and immunomodulatory properties (Ji et al., 2020; Jiang et al., 2017; Olas, 2018), allowing the plant to be excessively used in traditional medicine.

Terpenes

Terpenes have as basic formula $(C_5H_8)_n$. They are formed from isopentenyl-pyrophosphate (IPP) which reacts with a starter molecule such as dimethylallyl-pyrophosphate (DMAPP), geranyl-pyrophosphate (GPP), geranylgeranyl-pyrophosphate (GGPP), etc. They are categorized based on the number of carbon atoms they contain, leading to divisions such as monoterpenes (n=2), sesquiterpenes (n=3), diterpenes (n=4), triterpenes (n=6), until n>8.

Investigations into the phytochemical composition of *H. rhamnoides* unveiled a prevalence of pentacyclic triterpenoids, predominantly oleanane- and ursane-types, found abundantly in the fruit, branches, and leaves (Żuchowski, 2023). Among these triterpenoids, oleanolic acid and ursolic acid was the most abundantly isolated compounds from *H. rhamnoides* (Z.-G. Yang et al., 2007, 2013). Additionally, other triterpenoids such as pomolic acid, dulcioic acid, corosolic acid, 23-hydroxyursolic acid, oleanolic aldehyde, ursolic aldehyde, uvaol, and a nortriterpenoid 28-nor-urs-12-ene-3β,17β-diol were purified from *H. rhamnoides* (Z.-G. Yang et al., 2013; R.-X. Zheng et al., 2009). Major triterpenoids identified in *H. rhamnoides* included maslinic acid, arjunolic acid, betulinic acid, 23-hydroxybetulinic acid, betulin, and 1,2,3,19-tetrahydroxy-12-ursen-28-oic acid **(Figure 21)** (Sun et al., 2019; Tkacz et al., 2021).

Furthermore, the branch bark of this plant served as a source for 3-*O*-*E*-*p*-coumaroyl oleanolic acid, 3-*O*-*E*-caffeoyl oleanolic acid, 2-*O*-*E*-*p*-coumaroyl maslinic acid, and 2-*O*-*E*-caffeoyl maslinic acid (Z.-G. Yang et al., 2007). Besides, branches contain high contents of corosolic acid and betulinic acid (Tkacz et al., 2021). Additionally, 3-*O*-*E*-*p*-coumaroyl 2,23-dihydroxyoleanolic acid (3-*O*-*E*-*p*-coumaroyl arjunolic acid) was isolated from the fruit. Notably, triterpenoids were found to be five times more abundant in the fruit flesh compared to the leaves, with ursolic acid constituting 46% of these triterpenes (Tkacz et al., 2021).

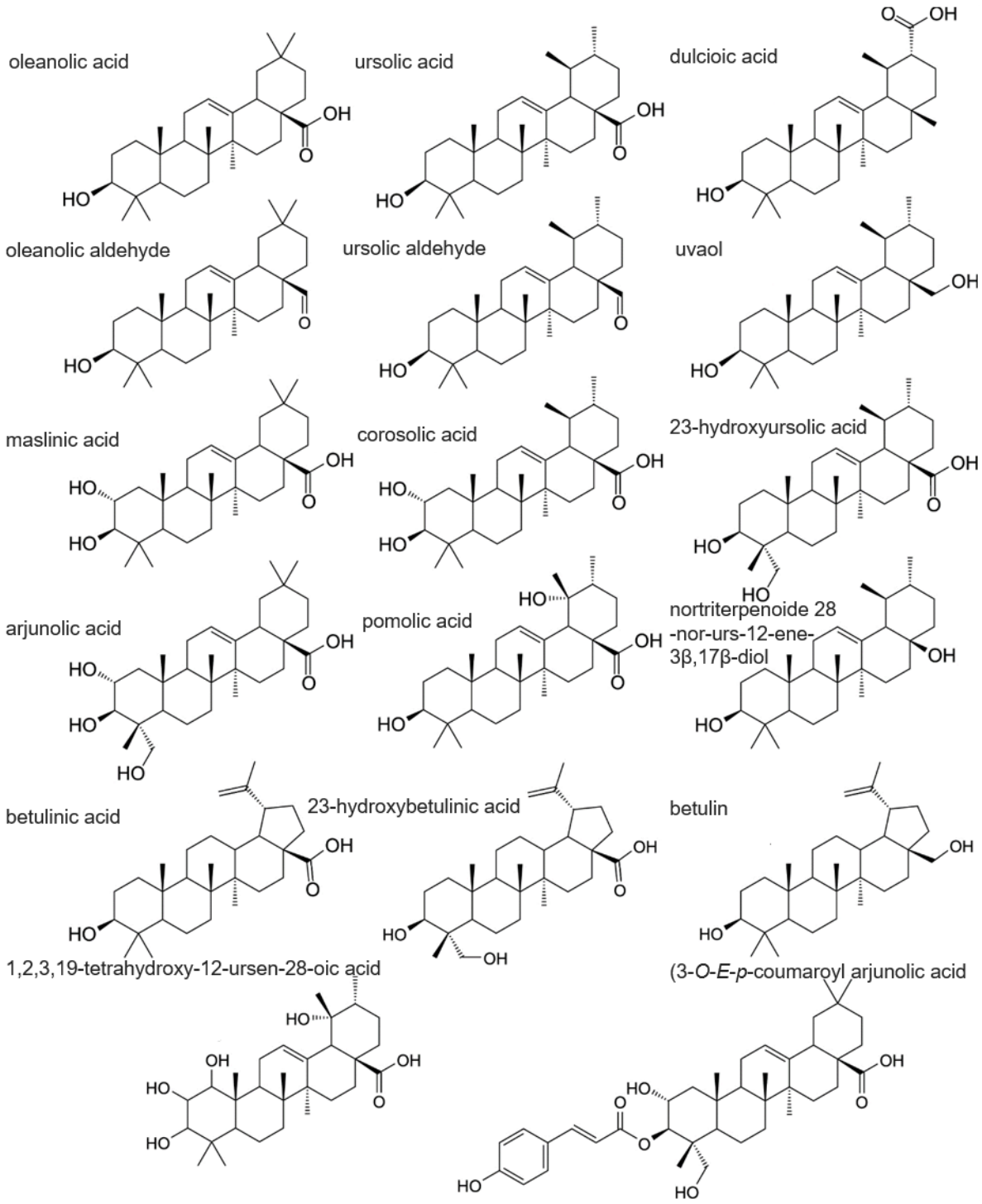

Figure 21. Triterpenoids isolated from *Hippophae rhamnoides* (Żuchowski, 2023) (Edited).

Carotenoids

Carotenoids are a group of natural pigments widely found in nature, with more than 600 different compounds identified so far, with β-carotene being the most predominant among them. One of the primary functions of carotenoids is serving as a source of vitamin A. Numerous studies have shown that these plant pigments play significant roles in promoting health, primarily attributed to their antioxidant properties, which help protect cells and tissues against oxidative harm (Schoefs, 2002; Stahl & Sies, 2003).

H. rhamnoides are known for their high carotenoid content, which give the characteristic orange-yellow color to sea buckthorn. The concentration of carotenoids in sea buckthorn can vary significantly among different species and parts of the plant. For instance, a study found an average of 11 mg/100 g fresh weight of total carotenoids in eight species of Russian sea buckthorn (Teleszko et al., 2015). In another study involving six Romanian sea buckthorn varieties (*H. rhamnoides* ssp. *carpatica*), the total carotenoid content ranged from 53 to 97 mg/100 g dry weight in berries and from 3.5 to 4.2 mg/100 g dry weight in leaves (Pop et al., 2014). The main carotenoid in sea buckthorn is β-carotene, constituting 15–55% of carotenoids in berries and 26–34% in the peel, pulp, and seed oil (Teleszko et al., 2015). Additionally, sea buckthorn contains other carotenoids such as γ-carotene, cis-lycopene, lycopene, cis-γ-carotene, β-cryptoxanthin, α-carotene, and more.

Phenolic compounds

Phenolic acids

Phenolic acids are a significant category of organic acids characterized by the presence of an aromatic ring. They can exist in different forms: free molecules, bound to sugars, or oligomers. Within the *Hippophae* species, phenolic acids are notably abundant, occurring both in their free state and as esters and glycosides (M. S. Y. Kumar et al., 2011). The seeds of *Hippophae* species contain a higher total phenolic acid content compared to the fruits and seed coat (R. K. Shah et al., 2021). These phenolic acids are categorized into hydroxybenzoic acids, hydroxycinnamic acids, and their derivatives, based on the number and position of hydroxyl and methoxy groups on their aromatic ring.

The phenolic acids found in *Hippophae* species encompass a range of compounds, including gallic acid, syringic acid, protocatechuic acid, salicylic acid, vanillic acid, gentisic acid, caffeic acid, sinapic acid, ferulic acid, cinnamic acid, 1-feruloyl-*β*-D-glucopyranoside, and chlorogenic acid. Earlier studies pointed to salicylic acid as the primary phenolic acid in berries, constituting 55-73% of the total phenolic acids followed by gallic acid and vanillic acid (Zadernowski et al., 2005; Mu et al., 2022); however, other research indicates that gallic acid serves as the principal phenolic acid in *H. rhamnoides* leaves and fruits.Other phenolic acids, such as caffeic acid, *p*-coumaric acid, and ferulic acid, are present in lower concentrations (Bittová et al., 2014).

Flavonoids

Flavonoids, which are polyphenolic compounds characterized by the diphenyl propane (C6-C3-C6) structure (Karakaya, 2004), are predominantly present in the fruits and leaves of *H. rhamnoides*. Within the *Hippophae* species, flavonoids are further categorized into flavonols, flavanols and flavanones. Sea buckthorn berries exhibit a total flavonoid concentration ranging from 1680 to 8590 mg/kg FW, which is notably higher than the levels found in other plants recognized for their high flavonoid content, such as hawthorn, cornelian cherry, european blackberry, blackthorn or dog rose (Cosmulescu et al., 2017; Heinäaho & Julkunen-Tiitto, 2011).

When examining various parts of *Hippophae* species, the total flavonoid content in leaves, pulp, pericarp, and seeds was found to be 2.24%, 0.95%, 0.51%, and 0.31%, respectively, with leaves containing the highest total flavonoid content (Ji et al., 2020). A comparative analysis of total flavonoid content in the leaves of different *Hippophae* species revealed that *H. rhamnoides* L. subsp. *sinensis* and *H. gyantsensis* had the highest levels at 0.7392% and 0.7814%, respectively, followed by *H. tibetana* S. and *H. rhamnoides* L. subsp. *yunnanensis* at 0.5879% and 0.4980%, respectively (Fu, 1997).
Researchers have identified a total of 95 different flavonoids in sea buckthorn, including 75 flavonols, 2 dihydroflavones, 6 catechins, 1 leucocyanidin, 9 anthocyanidins, 1 proanthocyanidin, and 1 chalcone (S. Liu et al., 2021). The content of flavonols in sea buckthorn varies, ranging from 463.14 mg to 893.92 mg/100 g DM and accounts for approximately 99% of the total phenolic compounds (Arimboor & Arumughan, 2012; Tkacz et al., 2019).

Among these flavonols, the most prevalent are typically glycosylated forms of myricetin, quercetin (Q), isorhamnetin (I), and kaempferol (K) **(Figure 22)** (Liu et al., 2021; Teleszko et al., 2015). Isorhamnetin glycosides, followed by quercetin glycosides, are typically the predominant flavonols found in sea buckthorn berries and leaves (Pop et al., 2013). Generally, berries are rich in flavonoid glycosides such as I-3-*O*-rutinoside, I-3-*O*-glucoside, Q-3-*O*-rutinoside, Q-3-*O*-glucoside, I-3-glucoside-7-rhamnoside, K-3-sorphoroside-7-*O*-rhamnoside, I-3-*O*-sorphoroside-7-*O*-rhamnoside, and rutin (Guo et al., 2017; Teleszko et al., 2015). The major aglycons present in berries include kaempferol (32–72 mg/kg FW), quercetin (67–175 mg/kg FW), myricetin (36–172 mg/kg FW), and isorhamnetin (45–106 mg/kg FW) (Guo et al., 2017).

In contrast, the concentration of flavonol glycosides in leaves is approximately 15 times higher than in berries (Pop et al., 2013). Major flavonoids identified in sea buckthorn leaves consist of rutin, Q-3-*O*-galactoside, I-3-*O*-glucoside, quercetin, K-3-*O*-glucoside, and kaempferol (Morgenstern et al., 2014). Additionally, another study indicated that I-3-rhamnosylglucoside, I-3-neohesperidoside, I-3-glucoside, quercetin-3-pentoside, kaempferol-3-rutinoside, and quercetin-3-glucoside were prevalent in leaves (Pop et al., 2013). It is worth noting that the concentration of flavonoids is influenced by the developmental stage of the leaves (Morgenstern et al., 2014).

As for sea buckthorn seeds, the major flavonoid glycosides found include Q-3-rutinoside, I-3-O-rutinoside, I-3-*O*-glucosides, 3-*O*-sophroside-7-*O*-rhamnosides of quercetin and kaempferol, and 3-*O*-glucoside-7-*O*-rhamnosides of quercetin and isorhamnetin, although significant amounts of isorhamnetin, quercetin, and kaempferol are also present in the seed fraction (Arimboor & Arumughan, 2012).

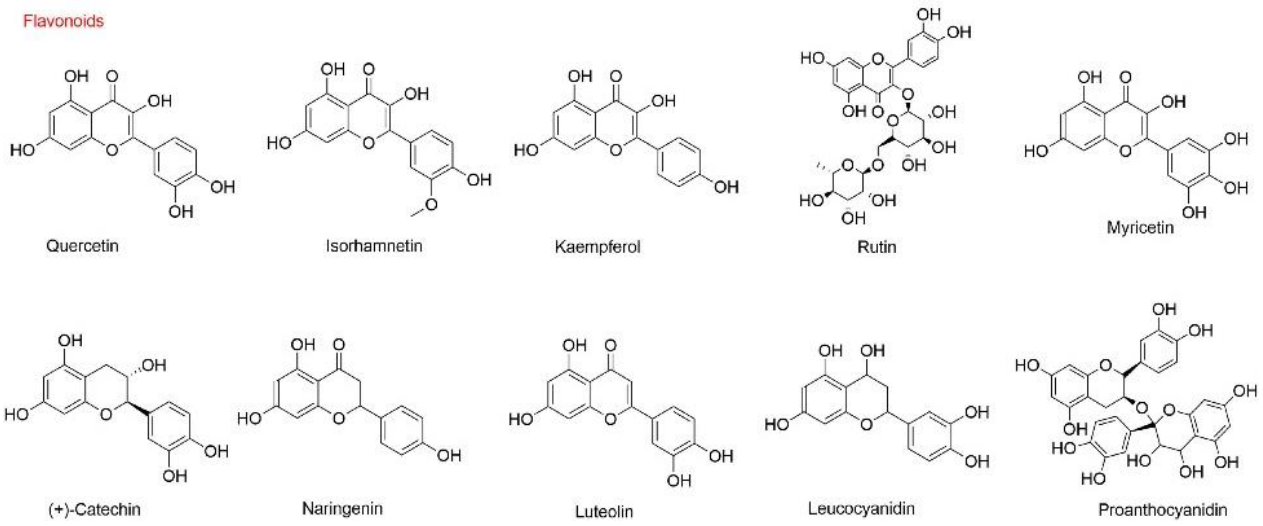

Figure 22. Structure of the main flavonoids in sea buckthorn (Z. Wang et al., 2022).

Tannins

Tannins are polyphenolic compounds that are soluble in water and can be found with alkaloids, polysaccharides, and proteins with relatively high molecular weights. They are categorized into two main groups: hydrolysable tannins and condensed tannins. Hydrolysable tannins or ellagitanins, primarily comprised of gallic acid esters, include compounds such as stachyurin, casuarinin, casuarictin, hippophaenin B, strictinin, and isostrictinin. These tannins contain ester and glycosidic bonds, which can be broken down into smaller molecule compounds along with sugars or polyols (Fatima, 2018). These tannins are found in higher concentrations in various parts of sea buckthorn, including seeds, roots, flowers, green berries, and stems.

On the other hand, condensed tannins, also known as proanthocyanidins, are polymers formed from monomeric catechin or (-)-epicatechin units (procyanidins) and can also consist of (+)-gallocatechin or (-)-epigallocatechin units (prodelphinidins). These basic structures are created through the condensation of two or more of these monomeric units (Salminen & Karonen, 2011) (Singh et al., 2017).

1.2.7. Antimicrobial and antiviral activities of *H. rhamnoides*

Antiviral activity

H. rhamnoides have been proven to exhibit antioxidant, immunomodulatory, antitumor, and antibacterial effects; however, limited research has been conducted to investigate its antiviral properties.

An *in vitro* study has investigated the antiviral activity of methanolic and ethyl acetate extracts of *H. rhamnoides* leaves against the influenza virus with IC_{50} value of 7.2 μg/ml and 10.3 μg/ml, respectively. Some compounds such as aglycones and mono-glycoside flavonols isolated from these two extracts exhibited a strong anti-influenza A activity (Enkhtaivan et al., 2017). Furthermore, the EtOAc extract exhibited IC_{50} values of 2.87 μg/ml and 4.5 μg/ml against two influenza B strains, significantly lower than those of the known drug oseltamivir. Similarly, *in vivo* research revealed that specific flavonoids, particularly quercetin derivatives, displayed superior inhibition activity against influenza A virus upon treatment with 6.25 mg/kg per dose at when compared to oseltamivir, a commonly used anti-influenza drug, in mice (Choi et al., 2012).

Furthermore, a study identified two 14-noreudesmanes, a phenylpropane heterodimer, and uvaol in the 70% methanolic extract of sea buckthorn fruit. These compounds demonstrated their ability to inhibit the replication of the herpes simplex type 2 (HSV-2) virus. Specifically, 6,9-dihydroxy-1-oxo-14-noreudesm-5,7,9-triene and phenylpropane dimer, along with musizin, were found to cause a reduction in HSV-2 yield by 2 $\log_{10}$, 3.49 $\log_{10}$, and 2.33 $\log_{10}$, respectively, at a concentration of 12.5 μM. On the other hand, 2-hydroxy-7-isopropyl-1-methoxy-4-methyl-1,4-naphthoquinone exhibited antiviral activity only at concentrations of 50 μM or higher. This suggests that sea buckthorn may serve as a promising potential source of antiviral agents effective against HSV-2 (Rédei et al., 2019).

In addition to its potential against influenza and HSV-2, sea buckthorn has shown promise in the context of immunization. Immunization with sea buckthorn leaf extract and inactivated rabies virus antigens has been shown to increase the levels of rabies virus neutralizing antibodies (RVNA) and stimulate the cytotoxic T lymphocytes (CTLs) response at a dose of 100 mg/kg. This immunomodulatory effect is attributed to

components of sea buckthorn leaf extract, such as isorhamnetin and other flavonoids (D. Singh et al., 2018).

Additionally, extracts obtained from sea buckthorn, including ethyl acetate, butanolic, and aqueous extracts, have shown significant inhibitory effects on the expression levels of hepatitis B surface antigens (HBsAg) and hepatitis B e-antigen (HBeAg) at 50 μg/ml. These findings suggest that sea buckthorn extracts possess potential antiviral activity against the hepatitis B virus. Among the compounds tested, quercetin and kaempferol, displayed potent inhibitory effects on HBsAg and HBeAg synthesis at 10 μg/ml compared to isorhamnetin (Parvez et al., 2022).

Finally, another study found that isorhamnetin isolated from berries may interact with ACE2, the functional receptor for SARS-CoV-2, potentially inhibiting the entry and infection of human cells expressing ACE2 at concentration of 2.51 ± 0.68 μM. This suggests that isorhamnetin could be explored as a blocker of ACE2-spike protein interactions, with potential relevance in combating SARS-CoV-2 infection (Zhan et al., 2021).

Antibacterial activity

Sea buckthorn has demonstrated antimicrobial activities *in vitro*, with its phenolic compounds exhibiting inhibitory effects against various microorganisms. The phenolic compounds found in *H. rhamnoides* L. berries have been shown to inhibit the growth of Gram-negative bacteria. Myricetin, a flavonol of sea buckthorn, was found to inhibit the growth of lactic acid bacteria commonly found in the human gastrointestinal tract flora at 0.5 mg/ml (Puupponen-Pimiä et al., 2001). Additionally, the aqueous extract of sea buckthorn seeds displayed antibacterial activity against *Listeria monocytogenes* and *Yersinia enterocolitica* with MIC value of 750 and 1000 ppm, respectively (Chauhan et al., 2007). Ethanolic extracts of *H. rhamnoides* seeds were effective at a concentration of 100 μg/ml against both Gram-positive and Gram-negative bacteria, attributed to the higher concentration of condensed tannins in this part of the plant (Michel et al., 2012; Negi et al., 2005).

The aqueous and the hydroalcoholic extracts of sea buckthorn leaves exhibited significant antibacterial activity at 5 mg/mL against several bacteria, including *Bacillus*

cereus, *Pseudomonas aeruginosa*, *Staphylococcus aureus,* and *Enterococcus faecalis*, with quercetin derivatives in the leaf extracts being implicated in this activity (Upadhyay et al., 2010).

Another research investigation assessed the antimicrobial efficacy of leaf extracts from four Romanian species of *H. rhamnoides* in comparison to extracts from berries. This evaluation targeted Gram-positive bacteria such as *S. aureus* and *B. cereus*, alongside the Gram-negative bacteria *P. aeruginosa*. The leaf extract exhibited the lowest MIC value compared to the berries extract: 6.2 mg/mL versus 12.5 mg/mL for *S. aureus*, 12.5 mg/mL versus 25.0 mg/mL for *B. cereus*, and 6.2 mg/mL versus 12.5 mg/mL for *P. aeruginosa* (Criste et al., 2020). These finding are in agreement with the study of Upadhyay et al. (Upadhyay et al., 2010). The higher antimicrobial potential of leaf extracts may be attributed to the levels of polyphenol compounds, especially quercetin derivatives and gallic acid.

Furthermore, extracts obtained from sea buckthorn leaves and shoots using 20% ethanol displayed notable antimicrobial activity at 100 μg/ml, against both Gram-positive and Gram-negative pathogenic bacteria, such as *Bacillu*s spp., *Salmonella* spp., *Escherichia coli*, *Yersinia pestis*, *Klebsiella,* and *Shigella* (Radenkovs et al., 2018).
Ethanolic extracts from different parts of *H. rhamnoides*, including leaves, stems, roots, and seeds, as well as their fractions (water, ethyl acetate, and hexane), exhibited antimicrobial activity at a concentration of 100 μg/ml, against various bacteria, including *Bacillus cereus*, *Pseudomonas aeruginosa*, *Escherichia coli*, *Staphylococcus aureus*, and *Enterococcus durans* (Michel et al., 2012). Additionally, non-polar fractions (n-hexane) of sea buckthorn demonstrated strong antibacterial activity at 2 mg/ml, 4 mg/ml and 6 mg/ml against methicillin-resistant *Staphylococcus aureus* (Qadir et al., 2016).

In a study evaluating extracts from sea buckthorn seeds, including chloroform, ethyl acetate, acetone, and methanol extracts, their antibacterial activity against different bacterial species was examined. The methanolic extract displayed the highest antimicrobial activity of 200, 300, 300, 300, and 350 ppm against *Bacillus cereus*, *Bacillus coagulans*, *Bacillus subtilis*, *Listeria monocytogenes*, *Yersinia enterocolitica*, respectively (Negi et al., 2005).

Furthermore, one study found that sea buckthorn leaf extract was significantly effective against 67 gram-positive bacteria recovered from clinical samples (Harshit et al., 2011). At a 5% concentration, sea buckthorn leaf extract inhibited the growth of *S. aureus*, *S. epidermidis*, *S. intermedius*, and *S. pyogenes* by nearly 50%. Additionally, sea buckthorn extract may have a positive impact on human keratinocytes by down-regulating various pro-inflammatory cytokines and apoptotic pathways, which could be beneficial in addressing skin-related issues (H. Shah et al., 2021).

Many of the microorganisms targeted in these studies are also known to be involved in various dermatological issues. Therefore, sea buckthorn could potentially be utilized to address skin-related problems associated with these microorganisms as causative agents.

Antioxidative and other properties

Antioxidative properties

Polyphenols are the primary constituents of *Hippophae* plants known for their antioxidant properties. Numerous *in vitro* and *in vivo* studies provide clear evidence of the antioxidant activity of *H. rhamnoides*. One study involving finishing lambs found that the plasma superoxide dismutase activity, a vital antioxidant enzyme, was significantly higher in lambs fed diets containing moderate and high levels of sea buckthorn leaves compared to control and low seabuckthorn groups (Hao et al., 2023). Another study on male albino rats demonstrated that leaf extract from this plant protected against chromium-induced oxidative damage in serum (Geetha et al., 2003). Moreover, aqueous and hydroalcoholic extracts of *H. rhamnoides* L. leaves demonstrated free radical scavenging activity against 2,2′-Azino-bis(3-ethylbenzthiazoline-6-sulfonic acid (ABTS) and 2,2-Diphenyl-1-picrylhydrazyl (DPPH) radicals *in vitro* (Upadhyay et al., 2010). The phenolic fraction, rich in flavonoids, from *H. rhamnoides* L. was reported to exhibit antioxidant and hepatoprotective activities in rats with CCl4-induced oxidative stress (Maheshwari et al., 2011). Furthermore, alcoholic extracts of both leaves and fruits of this plant were shown to inhibit chromium (VI)-induced free radical production, apoptosis, DNA fragmentation, restore antioxidant status in cells, and counteract the inhibition of lymphocyte proliferation caused by chromium exposure (Geetha et al., 2002).

Additionally, *H. rhamnoides* L. leaf extract dose-dependently reduced intracellular oxidative stress, enhancing neuronal PC-12 cell viability and membrane integrity (Cho et al., 2017). Collectively, these studies indicate that sea buckthorn can serve as a natural source of antioxidants to prevent and treat diseases associated with oxidative stress.

Other properties

H. rhamnoides exhibits a wide array of pharmacological properties and potential health benefits. These include anti-inflammatory, antifungal, anti-sebum, anti-atherogenic, antitumor, anti-diabetic, anti-psoriasis, anti-atopic dermatitis, wound healing and tissue regeneration, hepatoprotective, cardioprotective, UV-protective, radio-protective, along with its various uses in cosmeceuticals (Pundir et al., 2021).

2. Invasive plants

An invasive alien species (IAS) refers to a non-native plant that, after being introduced to a new location, starts to expand and extend beyond its initial introduction point. One crucial aspect of biological invasions involves the ways in which human actions influence the introduction and propagation of non-native species. Numerous human activities have been pinpointed as supporting the dissemination of alien plant species (Richardson et al., 2000) . In addition to disruptions caused by human activity, natural disturbances are on the rise due to climate change. Incidents like storms, floods, and forest fires create openings for alien plants to invade new areas (Brooks et al., 2004; Hobbs & Huenneke, 1992). IAS has the potential to inflict damage on the environment, economy, or human health. Invasive plants pose a significant menace to biodiversity since they establish themselves and outcompete native species, often resulting in the extinction of the native species. Interactions of invasive plants within the ecosystem involve changing either the non-living (abiotic) or living (biotic) factors, including nutrient and water availability, and disrupting bacterial and fungal communities, as well as interactions between plants and herbivores.

2.1. *Senecio inaequidens* DC.

2.1.1.Taxonomy

Senecio inaequidens DC., commonly known as Narrow Leaved Ragwort or South African ragwort, is a perennial plant belonging to the Asteraceae family, order Asterales and genus *Senecio*. The *Senecio* genus represents the largest genus of the Asteraceae family and includes more than 1500 species of herbs and trees (Faraone et al., 2018). The morphological variation within *S. inaequidens* has led to a complex and confusing taxonomy for the species, particularly for the identity of the introduced taxon. This is due to the superficial similarity between two disjunct groups of species, one in South Africa and Madagascar (*S. madagascariensis* Poiret complex; (Hilliard, 1977) and the other in Australia (*S. lautus* Forster f. ex Willd. complex; (S. I. Ali, 1969). *S. inaequidens* belongs to the latter complex. The name "*Senecio*" (from "sen-" or "senic-") originates from the Latin word for "old man," referencing the hoary pappus of hairs. The term "*inaequidens*" is derived from Latin and means 'irregular teeth,' likely alluding to the varying patterns of leaf margin dentition that can be observed, even within a single plant.

2.1.2. Geographical distribution

It is native to South Africa and has become widely established in Europe. Its unintentional introduction to Europe occurred at the end of the 19th century, often accompanying shipments of wool. Some classify it as an 'invasive alien' species. The initial European sightings were in proximity to wool-processing facilities in Germany (Kuhbier, 1977). Other notable introductions occurred at locations connected to the wool trade, including Mazamet in southern France (Guillerm et al., 1990), Calais in northern France **(Figure 23)** (Jovet, & Bosserdet, 1962), Verona in northern Italy (Kiem, J., 1975), Lüttich in eastern Belgium (Lambinon, 1957), and Bremen in northern Germany (Kuhbier, 1977). *S. inaequidens* is very abundant on the coastline and in the towns of Calais (where the plant has been reported for at least half a century), Dunkirk and Lille. This species is invasive in the dunes, especially in the most frequented or ruderalized areas. It is spreading elsewhere, along roads and railways in particular (Digitale2, 2023b). Cape Ragwort can produce seeds year-round, with spring and autumn being the most favorable periods (Dimande et al., 2007. A single plant can produce between 10,000 to 30,000 seeds annually, and its achenes can survive two years in dry storage conditions (Ernst,

1998). Wind disperses the fruits over considerable distances, and germination occurs across a broad temperature range, spanning from 14 to 30°C (ISSG, 2017). In some instances, invasive populations of *S. madagascariensis* reported in Australia are regarded as part of *S. inaequidens* (Lafuma & Maurice, 2007).

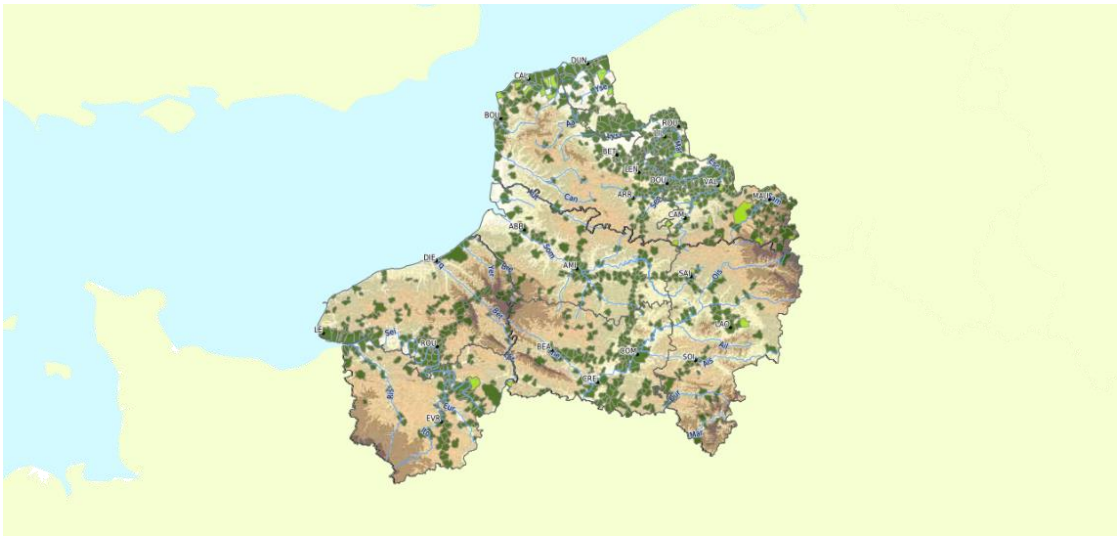

Figure 23. Distribution of *S. inaequidens* in the North of France (Digitale2, 2023b).

2.1.3. Botany

It is a shrubby herb that reach approximately 60 cm in height. It features a heavily branched stem that becomes woody near the base, accompanied by numerous mostly slender, linear leaves measuring between 1 to 7 mm in width. Additionally, it has yellow flower heads that can reach up to 25 mm in diameter **(Figure 24)**. Notably, this species exhibits a significant degree of diversity in leaf shape and width (Hilliard, 1977).

Figure 24. *Senecio inaequidens* (Wikipedia)

2.1.4. Traditional use of other of *Senecio* plant species

Traditionally, *Senecio* species have found applications in folk medicine for a variety of conditions, including the treatment of coughs, wound healing acceleration, asthma and eczema remedies, as well as anti-emetic, anti-inflammatory, and vasodilator preparations. These plants have been employed in the treatment of diverse ailments across different regions (Oladipupo & Adebola, 2009). *Senecio graveolens,* is used in Argentina for its emmenagogue, digestive aid and cough suppressant properties. The leaves of *Senecio latifolius* (=*Brachyglottis laxifolia* (Buchanan) B.Nord.) are historically used by the Zulu people as an emetic and as a treatment for chest-related problems (Pérez et al., 1999). In China, *Senecio cannabifolius* (=*Jacobaea cannabifolia* (Less.) E.Wiebe), is a traditional remedy for addressing conditions such as viral influenza, enteritis, and pneumonia. *Senecio scandens* is utilized in traditional and folk medicine in China for its anti-inflammatory, antipyretic, and detoxification effects (B. Wu et al., 2006). *Senecio vulgaris* has been applied as an emmenagogue and in cases of functional amenorrhea in Europe (X. Yang et al., 2011). These diverse uses underscore the wide range of potential medicinal applications associated with *Senecio* plants in various regions and cultures around the world.

2.1.5. Phytochemical characterization of Senecio plant species

Terpenes

The most common classes of compound identified and published from African *Senecio* include pyrrolizidine alkaloids, flavonoids as well as sesquiterpenoid derivatives including eremophilanes, bisabolols, cacalols. Derivatives of these include furans, oxides, *O*-linked moieties, and stereoisomers.

Specifically, sesquiterpenes represent a specific class of terpenes. Their structural hallmark lies in their fifteen carbon atoms, which aligns with the "sesqui" prefix. They have as basic formula $C_{15}H_{24}$. Sesquiterpenes and sesquiterpenoids that contain additional functional groups exhibit diverse structural variations and are renowned for their aromatic and medicinal properties.

In a chemotaxonomic analysis of the *Senecio* genus, it has been segmented into different sections, each corresponding to various types of sesquiterpenes. These sections include

bisabolenes, cacalols, eremophilanes, furanoeremophilanes, eremophilanolides, and germacranes **(Figure 25)** (Zhao et al., 2015). Notably, a study has documented the isolation of three previously unreported sesquiterpenes from *Senecio digitalifolius* (Bohlmann & Zdero, 1978). Besides, phytochemical investigation on the aerial parts of *Senecio hadiensis* grown in Saudi Arabia led to the discovery of two sesquiterpene alcohols with furanoeremophilane skeleton belong to presilphiperfolanol group which serves as an important branch point for the biosynthesis of many sesquiterpenoids (Ahmed et al., 2017). Other groups of compounds that are less frequently reported include phenylpropanes, monoterpenes, other sesquiterpenes such oxyeuryopsin derivatives and dimers of sesquiterpenes, diterpenes, triterpenes, sterols, fatty acid derivatives, and polyunsaturated alkynes and alkenes (Sadgrove, 2022).

These metabolites have several important properties as insect antifeedant, antifungal, cytotoxic, antioxidant, anti-inflammatory, and antimicrobial agents. Some furanoeremophilanes, such as cacalone, have a radical scavenging and antioxidant activity (Krasovskaya et al., 1989). Cacalol, 9-hydroxy-3,4,5-trimethyl-5,6,7,8-tetrahydronaphto (2,3-b) furan, named after its first isolation from *Cacalia decomposita* (=*Psacalium decompositum* (A.Gray) H.Rob. & Brettell) has been considered as natural anti-oxidants (Krasovskaya et al., 1989), with anti-microbial , hypoglycemic (Wd et al., 1999), and anti-inflammatory activities (Jimenez-Estrada et al., 2006). A previously published study has isolated other cacalol families such as 14-oxocacalol methyl ether, 14-oxo-1,2-dehydrocacalol methyl ether, 14-hydroxy-1,2-dehydrocacalol methyl ether, and 14-nordehydrocacalohastine from *Senecio* species that might also be expected to possess antimicrobial and antihyperglycemic activities (Hirai et al., 2004).

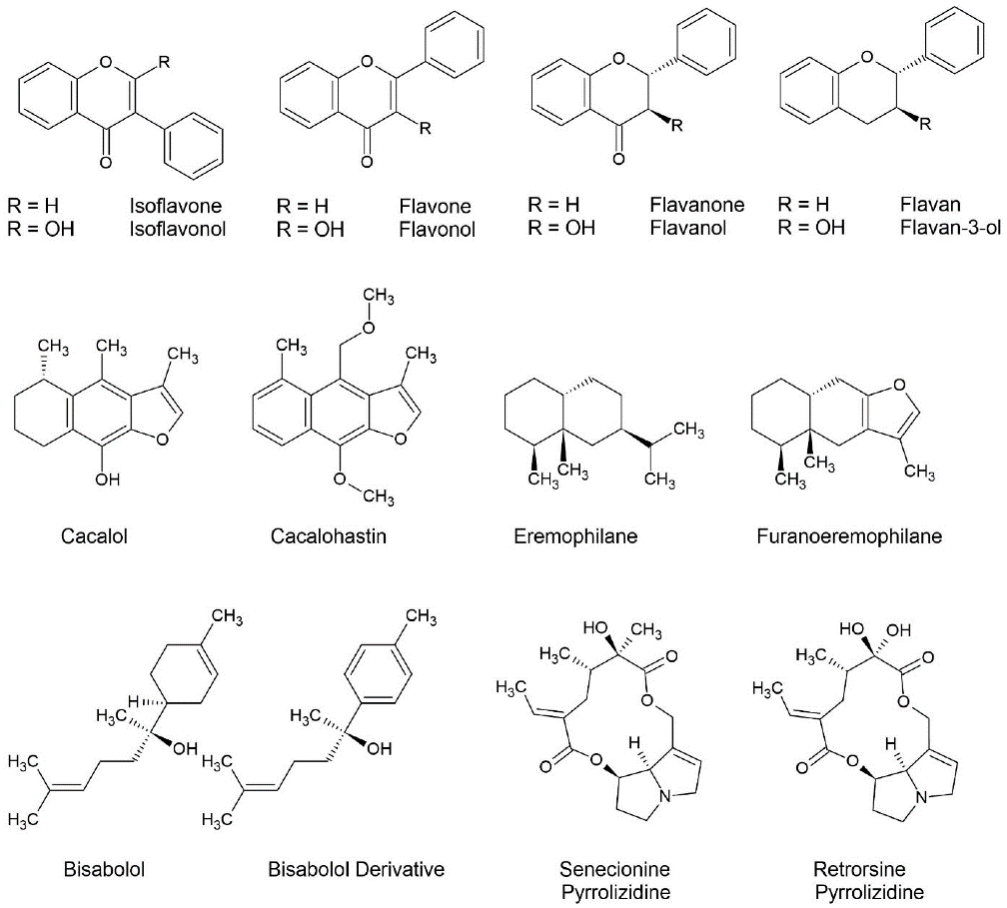

Figure 25. Common classes of compound in African species of *Senecio* (Sadgrove, 2022).

Pyrrolizidine alkaloids

Pyrrolizidine alkaloids are composed of a necine base, which is esterified with a necic acid. The necine base typically consists of pyrrolizidine, a bicyclic aliphatic hydrocarbon consisting of two fused five-membered rings with a nitrogen at the bridgehead (Schramm et al., 2019). There are more than 500 known variations of pyrrolizidine alkaloids, senecionine, retrorsin and integerrimine the most known. These compounds are found in several species of *Senecio* and in Boraginaceae genus and are responsible for poisonings in both ruminants (Cortinovis & Caloni, 2015) and humans. Poisoning can lead to conditions such as hepatomegaly (enlarged liver), ascites (abdominal fluid buildup), and cirrhosis (Steenkamp et al., 2000).

Human toxicosis can occur through accidental contamination of medicinal plants (Van Schalkwyk et al., 2021), honey contamination by bees (Valese et al., 2021) lateral transfer of toxic alkaloids in tea plantations (Van Wyk et al., 2017), and water

contamination (Hama & Strobel, 2021). The presence of pyrrolizidine alkaloids in honey has been reported in Europe (Gottschalk et al., 2020). Bees collect pollen from *Senecio* species, which can lead to honey contamination. This issue prompted the European Food and Safety Authority to assess the health risks associated with consuming honey or plant products known to contain or be contaminated by pyrrolizidine alkaloids (Bassignana, M. et al., 2018).

The toxicity mechanism of pyrrolizidine alkaloids involves metabolic activation. First, PAs are metabolized by P450 enzymes to generate dehydropyrrolizidine (DHP). DHP, with its strong electrophilic properties, then attacks proteins or DNA molecules to form adducts, ultimately leading to various signs of toxicity. These compounds result from the esterification of a carboxylic acid known as necic acid with a double pyrrole ring referred to as necine. They are categorized into two types, retronecine and otonecine, with the presence of a 1,2-double bond being a key structural feature responsible for their toxicity (Schramm et al., 2019).

2.1.6. Antimicrobial activities of *Senecio* species

Antiviral activity of Senecio *species*

Limited studies have tackled the antiviral activity of *Senecio* species. Screening of the extracts of *S. tsoongianus* Ling (= *Synotis cappa* (Buch.-Ham. ex D. Don) C.Jeffrey & Y.L.Chen and *S. saluenensis* (= *Synotis saluenensis* (Diels) C.Jeffrey & Y.L.Chen) revealed that a solution of 10 mg/ml of petroleum ether extracts of these two plants have activities on suppressing the secretion levels of HBV surface antigen (HBsAg) by 45 and 56%, respectively. A further bioguided purification of *S. tsoongianus* led to the isolation of three enantiomeric sesquiterpene lactones that are the main components performing the anti-HBV activity (H. Li et al., 2005). Another study showed that the methanolic extract of *Senecio ambavilla* (=*Hubertia ambavilla* Bory) collected from Reunion Island has an antiviral activity against herpes simplex type 1 (HSV-1) and poliovirus type 2 (PV) at concentrations of 170 µg/ml and 380 µg/ml, respectively due to the presence of a high level of flavonoids and condensed tannins (Fortin et al., 2002).

Antibacterial and antifungal activities of *Senecio* species

Few studies are available on the antimicrobial activities of Senecio *inaequidens*, but several other *Senecio* species have exhibited antibacterial and antifungal activities.

S. vulgaris L. and *S. inaequidens* DC.

One investigation into the antibacterial properties of *S. inaequidens* was conducted in the same time than another species, *S. vulgaris*. *S. inaequidens* had no effect on both Gram-positive and Gram-negative bacteria while *S. vulgaris* showed antimicrobial activity against the Gram-positive bacteria, i.e. 0.5 mg/ml for *Bacillus subtilis* and 0.125 mg/ml for *Staphylococcus aureus*. However, the methanolic extract of both *Senecio* species exhibited limited effectiveness against dermatophytes with values of MIC between 0.5 to 0.125 mg/ml. Notably, the n-hexane and chloroform fractions showed activity against *Trichophyton* sp. and *Microsporum gypseum*, particularly at higher concentrations with MIC value of the hexane fraction between 0.031 mg/ml for *S. vulgaris* and 0.125 mg/ml for *S. inaequidens* and that of the chloroform fractions between 0.125 mg/ml for *S. vulgaris* and 0.25 mg/ml for S. *inaequidens*. Concerning the yeast *Candida albicans*, only the ethyl acetate fraction from both *Senecio* species exhibited any notable activity at MIC, 0.125 mg/ml (Loizzo et al., 2004).

S. sandrasicus P.H. Davis (= *Jacobaea sandrasica* (P.H. Davis) B. Nord. & Greuter)

In a separate study, the hexanic extract of *S. sandrasicus* from Turkey demonstrated antimicrobial activity against various microorganisms, including multidrug-resistant staphylococci (Ugur et al., 2009). Conversely, chloroformic, ethanolic, and ethyl acetate extracts of *Senecio sandrasicus*, except for hexanic extracts, exhibited an inhibitory effect using 0.4 and 3.6 µg/disc on multidrug-resistant *Stenotrophomonas maltophilia* bacteria. These bacteria are known to be resistant to a range of antibiotics. However, the hexanic extracts did not display an inhibitory effect on two strains of *S. maltophilia* (Uğur et al., 2006).

S. graveolens Wedd. (*Senecio nutans* Sch.Bip.)

Furthermore, research on the antimicrobial activity of *Senecio graveolens* essential oil revealed its bacteriostatic effect on *Micrococcus luteus* ATCC 9341, oxacillin-sensitive and oxacillin-resistant *Staphylococcus aureus*, as well as antifungal effects against clinically

isolated *Candida albicans* with MIC value of 8.73, 10.91 and 2.13 x 10^{-2} mg/ml, respectively (Pérez et al., 1999).

S. *leucanthemifolius* Poir.

Another study documented that the extracts from *S. leucanthemifolius* displayed antimicrobial and antifungal properties against seven different pathogenic microorganisms. Notably, the ethyl acetate extract exhibited robust antibacterial activity against *Staphylococcus aureus*, with a MIC value of 31.25 mg/ml, while the hexanic extract demonstrated significant activity against dermatophytic fungi (Tundis et al., 2007).

S. cannabifolius Less. (= *Jacobaea cannabifolia* (Less.) E.Wiebe)

In the case of *S. cannabifolius*, a different study found that 4 isolated compounds possess notable antimicrobial activity against Gram-positive bacteria with MIC values between *31.2* µg*/ml* and *125* µg/ml as *Staphylococcus aureus* and between *7.8* µg/ml - *62.5* µg/ml for *Bacillus subtilis*. However, they did not exhibit activity against Gram-negative bacteria *E. coli* (B. Wu et al., 2006).

S. lyratus DC. (= *Senecio anapetes* C. Jeffrey)

Furthermore, an antibacterial test involving methanolic extracts from dried and ground aerial parts of *Senecio lyratus* revealed activity against *Salmonella typhii* and *Corynebacterium diphtheria*. While its activity against *Vibrio cholerae* was relatively modest, the fact that it exhibited any activity against this highly resistant strain is a noteworthy indicator of its potency (Kiprono et al., 2000).

Notably, anti-fungal testing revealed the significant effectiveness of ß-sitosterol at 12 mM, which was isolated from *Senecio lyratus*, against *Fusarium* spp. (Kiprono et al., 2000).

III. Materials & Methods

1. Plant Material

Hippophae rhamnoides and other salt tolerant species

Plant species, mainly halophytes, were selected and collected between July 2020 and November 2020 from five different locations (Étaples, Dannes, Le Portel, Gravelines, Zuydcoote) distributed across the coastline region of northern France (Hauts-de-France region) in conjunction with the managers of the natural sites (Table 2). Plants were mainly collected from schorres; coastal cliffs; and incipient, established, and relict dunes. All these operations, followed by the identification of plant materials, were conducted by Prof. Céline Rivière and Dr. Gabriel Lefèvre from the Faculty of Pharmacy in Lille (UMRt BioEcoAgro). These samples were collected in accordance with the rules of the Nagoya Protocol and the French biodiversity law of 2017 (decision of 23 September 2020 issued by the Ministry of Ecological and Inclusive Transition; NOR: TREL2002508 S/342 and ABSCH-IRCC-FR-252501-1). Specific authorizations were also granted by the "Direction Interrégionale de la Mer Manche Est-Mer du Nord" (Decision n°778/2020) and by the prefect of the region of Normandy (regulation service for maritime activities). Harvested plant species were dried at 30 °C in an oven for a maximum of one week and protected from light. Different parts of these plants (leaves, stems, roots) were pulverized separately using a crushed Retsh Cutting Mill SM200. This gathered material was utilized for an initial evaluation to identify potential active compounds. Another gathering of *Hippophae rhamnoides* took place in Wissant in 2022.

Table 2. List of plant species used in this study.

Botanical Family	Plant Species	Parts	Place of Collection	Voucher Code
Amaranthaceae	*Atriplex prostrata* Boucher ex DC.	Whole plant	Dannes (at the base of an incipient dune)	LIP007584
	Salicornia procumbens Sm.	Whole plant	Etaples (in the schorre)	LIP007585
	Salsola kali L.	Whole plant	Dannes (at the base of an incipient dune)	LIP007586
	Suaeda maritima (L.) Dumort.	Whole plant	Etaples (in the schorre)	LIP007587
Apiaceae	*Crithmum maritimum* L.	Aerial parts	Le Portel (on a coastal cliff)	LIP007588
	Baccharis halimifolia L.	Leaves (L), stems (S)	Gravelines (planted in a roadside hedge)	LIP007589
Asteraceae	*Centaurea aspera* L.	Whole plant	Zuydcoote (on a relict foredune)	LIP007590
	Tripleurospermum maritimum (L.) W. D. J. Koch	Whole plant	Le Portel (on a coastal cliff)	LIP007591
	Tripolium pannonicum (Jacq.) Dobroc.	Whole plant	Dannes (in the schorre)	LIP007592
Berberidaceae	*Berberis aquifolium* Pursh	Leaves (L), roots (R)	Zuydcoote (on a relict foredune)	LIP007593
Brassicaceae	*Cakile maritima* Scop. subsp. *integrifolia* (Hornem.) Greuter and Burdet	Whole plant	Dannes (at the base of an incipient dune)	LIP007594
Convolvulaceae	*Convolvulus soldanella* L.	Whole plant	Dannes (on an incipient dune)	LIP007595
Cyperaceae	*Bolboschoenus maritimus* (L.) Palla	Whole plant	Dannes (in the schorre)	LIP007596
	Carex arenaria L.	Whole plant	Dannes (in the schorre)	LIP007597

Elaeagnaceae	*Hippophae rhamnoides* L.	Whole plant	Dannes (on an established foredune)	LIP007598
Euphorbiaceae	*Euphorbia paralias* L.	Whole plant	Dannes (on an incipient foredune)	LIP007599
Onagraceae	*Oenothera biennis* L.	Whole plant	Zuydcoote (on a relict foredune)	LIP007600
Poaceae	*Ammophila arenaria* subsp. *arenaria* (L.) Link	Whole plant	Dannes (on an established foredune)	LIP007601
	Elytrigia acuta (DC.) Tzvelev	Whole plant	Zuydcoote (on an incipient foredune)	LIP007602
Primulaceae	*Lysimachia maritima* (L.) Galasso, Banfi, and Soldano	Whole plant	Dannes (in the schorre)	LIP007603
Rosaceae	*Rosa rugosa* Thumb.	Aerial parts	Dannes (on an established foredune)	LIP007604
Salicaceae	*Salix repens* subsp. *dunensis* Rouy	Stems (S), roots (R)	Zuydcoote (on a relict foredune)	LIP007605

Senecio inaequidens

Senecio inaequidens DC. was collected two times, in 2020 for preliminary screening at the same time as the halophytes, and a second time in May 2022 for purification of bioactive compounds, in Zuydcoote in northern France by Dr Gabriel Lefèvre. During collection, the plant had not fully blossomed and was predominantly obtained from dunes along the coastline. The harvested plant species was dried at 30°C in an oven for a maximum of one week, shielded from light. The aerial parts of the plant were individually pulverized using a Retsh Cutting Mill SM200.

2. Solid/Liquid Extraction

Crude methanolic extracts were prepared by maceration by soaking the powder in 10 mL/g of methanol for 24 h, and the mixtures were then filtered through Whatman filter paper (11 µm pore size). The process was repeated three times. The resulting extracts were then dried in vacuum at 35 °C using a rotary evaporator and stored at −20 °C until tested. For cytotoxicity and antiviral assays, extracts were re-suspended in DMSO at 25 mg/mL, aliquoted, and stored at −20 °C.

3. Liquid/Liquid Extraction

The active crude methanolic extracts were subjected to fractionation using first liquid–liquid partitioning.

Hippophae rhamnoides

An amount of 3 g then 500 g of crude methanolic extract was dissolved in water and then partitioned with DCM and EtOAc (3 x 300 mL) to obtain three solvent partitions. The partitions were evaporated using a rotary evaporator and transferred to vials for storage. The apolar partitions (DCM and EtOAc) were evaporated at ambient temperature and then desiccated under vacuum in a desiccator; the polar (Aq) partitions were dried by lyophilization (freeze-drying).

Senecio inaequidens

An amount of 50 g then 900 g of crude methanolic extract was dissolved in water (Aq, 1x1L) and then partitioned with dichloromethane (DCM, 3x1L) and ethyl acetate (EtOAc, 2x1L) to obtain three solvent partitions **(Table 3)**. The partitions were evaporated using a rotary evaporator and transferred to vials for storage. The apolar partitions (DCM and EtOAc) were evaporated at an ambient temperature and then desiccated under vacuum (desiccator); the polar (Aq) partitions were dried by lyophilization (freeze-drying).

Table 3. The yield (%) of the partitions obtained after successive extraction.

	Crude methanolic extract (g)	**Sub-extract (%)**		
		DCM	EtOAc	Aq
Hippophae rhamnoides	8.02	9.2	3.33	70.33
Senecio inaequidens	12.3	29.3	5.06	14.86

4. Fractionation of the DCM Sub-Extract of *Hippophae rhamnoides* and *Senecio inaequidens by Centrifugal Partition Chromatography (CPC)*

Centrifugal partition chromatography (CPC) is a liquid–liquid preparative chromatographic technique, where both the stationary and mobile phases are liquids **(Figure 26)**. The separation is based on the partitioning of the solutes between these immiscible liquid phases and the determination of a Kd. Before CPC, it is necessary to find the appropriate ternary or quaternary biphasic system allowing a Kd closest to 1 for the compound that we wish to purify. The Arizona systems, the most common in CPC, consists of four solvents, heptane, ethyl acetate, methanol, water with different volume ratios (Berthod et al., 2005).

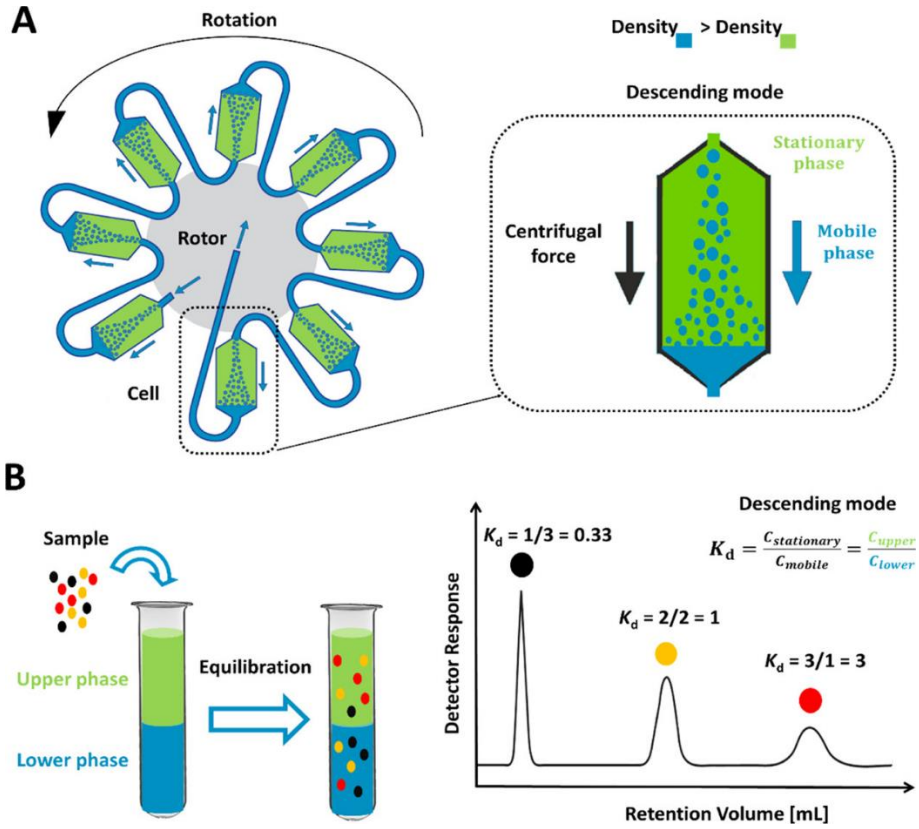

Figure 26. Working principles od CPC *(Lorántfy et al., 2020)*.

The DCM extracts of *Hippophae rhamnoides* (HR DCM SE) and *Senecio inaequidens* (SI DCM SE) were fractionated by centrifugal partition chromatography (Armen instruments®, Saint-Avé, France) with a rotor of a capacity of 1 L, after determination of the most effective quaternary system and optimization on a rotor of 250 mL. The liquid phases were pumped with a Shimazu® pump (LC-20AP, Kyoto, Japan). The column was coupled online with a DAD detector (SPD-M20A). Fractions were collected with an automated fraction collector (Gilson® FC 204, Villiers-le-Bel, France). The elution profile was recorded using LabSolutions™ software version 1.25.

HR DCM SE

The CPC rotor was first filled with the stationary phase (upper phase) at a flow rate of 50 mL.min^{-1} (500 rpm) in descending mode. Equilibrium was reached by introducing the mobile phase (lower phase) at 1200 rpm and a flow rate of 30 mL.min^{-1}. Six systems

(P—> U) were tested. The solvent system was composed of heptane, EtOAc, methanol, and water with ratio (2:1:2:1) (Arizona R system). An amount of 5.9 g of the HR DCM SE (obtained from the whole plant) was dissolved in 46 mL of the organic/aqueous phase mixture (1:1, v/v) and filtered through a Millipore syringe filter (0.45 µm). The filtered solution was injected immediately after displacement of the stationary phase (170 mL). The elution was carried out at 30 mL.min^{-1}. for 60 min and monitored at λ = 254 nm. After that, extrusion mode was performed to allow for the recovery of highly retained molecules in the stationary phase 30 mL.min $^{-1}$ for 15 min. At the end of the CPC cycle, the 193 tubes obtained were characterized by UHPLC-UV-MS and then grouped into 10 fractions according to their phytochemical profiles. The 10 fractions for HR were then concentrated by a centrifugal concentrator (Genevac™, Fisher Scientific, Illkirch, France).

SI DCM SE

The CPC rotor was first filled with the stationary phase (upper phase) at a flow rate of 50 mL.min^{-1} (500 rpm) in ascending mode. Equilibrium was reached by introducing the mobile phase (lower phase) at 1200 rpm and a flow rate of 30 mL.min^{-1}. 14 different Arizona systems (L → Z) were tested. The selected solvent system was composed of heptane, EtOAc, methanol, and water with ratio (3:2:3:2) (Arizona Q system) for *Senecio inaequidens*. An amount of 6.03 g of SI DCM SE were injected in the sample loop. The elution was carried out at 30 mL.min^{-1} for 60 min and monitored at λ = 254 nm. After that, extrusion mode was performed to allow for the recovery of highly retained molecules in the stationary phase at 50 mL.min $^{-1}$ for 20 min. At the end of the CPC cycle, the 121 tubes obtained were characterized by UHPLC-UV-MS and then grouped into 12 fractions according to their phytochemical profiles. The 12 fractions for SI were then concentrated by a centrifugal concentrator (Genevac™, Fisher Scientific, Illkirch, France).

5. UHPLC-UV-MS Analysis

The Acquity UPLC H-Class Waters® System (Guyancourt, France) apparatus was equipped with two independent pumps, a controller, a diode array detector (DAD), and a QDa electrospray quadrupole mass spectrometer. The stationary phase was a C18 BEH

(2.1 × 50 mm, 1.7 µm) reverse column. The mobile phase was composed of two solvents: (A) ultrapure water + 0.1% formic acid (Carlo Erba Reagents®, Val de Reuil, France) and (B) acetonitrile (Carlo Erba Reagents®, Val de Reuil, France) + 0.1% formic acid. The flow rate and column temperature were set at 0.3 mL.min^{-1} and 30°C, respectively. The wavelength range was fixed at 200–790 nm with a resolution of 1.2 nm. Ionization was carried out in both negative and positive modes, with the mass ranging from 50 to 1250 Da. The cone voltage and capillary voltage values were 15 V and 0.8 kV, respectively. The injection volume was set at 2 µL. UHPLC-UV-MS analysis was executed following the elution program 10%→100% B (0–9 min), 100% B (9–11.5 min), and 10% B (11.5–14 min) in case of *Hippophae rhamnoides,* and 10% B (0-1 min), 10-100% B (1-9 min), 100% B (9-11 min) at 0.3 ml/min in case of *Senecio inaequidens*.

All samples were prepared at 1 mg·mL^{-1} in analytical grade MeOH and filtered through a PTFE 0.4 µm membrane before injection.

6. Purification of pure compounds by Preparative HPLC

The equipment consisted of Shimadzu® LC-20AP binary high-pressure pumps, an SPD-M20A photodiode array detector, and a CBM-20A controller. The mobile phase was composed of ultra-pure water (Millipore Integral 5 Milli-Q, Merck™, Trosly-Breuil, France) + 0.1% formic acid (Merck™, Darmstadt, Germany) (solvent A) and acetonitrile (Carlo Erba Reagents®, Val de Reuil, France) (solvent B). The flow rate was set at 15 mL·min^{-1}. The purification monitoring was carried out wavelengths 247 nm and 254 nm for *Hippophae rhamnoides* and 254 nm for *Senecio inaequidens*. The elution program was first optimized on analytical HPLC.

Hippophae rhamnoides

Preparative HPLC was performed on fractions F2, F4, and F7 obtained from HR DCM SE after CPC. A column Interchim US5C18HQ-250/212 Uptisphere Strategy C18-HQ 5µm (250 × 21.2 mm) prep-LC was used in this experiment as the stationary phase. The gradients used were 60% B (0.01 min), 60% to 100% B (0.01-25 min), 100% B (25.01–28.99 min), and 60% B (29–30 min) for fraction 2; and 80% B (0.01 min), 80% to 100%

B (0.01–25 min), 100% B (25.01–28.99 min), and 80% B (29–30 min) for fractions 4 and 7.

Senecio inaequidens

Preparative HPLC was performed using Kinetex F5 column, (5 µm, 250 × 21.2 mm) on fractions F4 and F7 obtained from SI-DCM SE after CPC. The gradient used was 10% B (0.01 min), 10% to 55% B (0.01-5 min), 55% to 65% B (5 min-18 min), 65% to 80% B (18-25 min), 80% to 100% B (25-27 min), 100% B (27-30 min).

Preparative HPLC was performed on F11 using a VisionHT Basic C18 (5 µm, 250 x 22 mm) column. The gradient used was 10% B (0.01 min), 10-50% B (0.01-3 min), 50% B (3-14 min), 50-100% B (14-20 min), 100% B (20-30 min).

7. NMR and HRMS

The structures of the purified compounds were determined using NMR and HR-MS by Professor Céline Rivière, with the support of Dr. Evariste Akissi and Mrs. Jennifer Samaillie. NMR spectra (mono- and bi-dimensional) were recorded on a Bruker ® DPX-500 spectrometer (^{1}H- and ^{13}C-NMR at 500 and 125 MHz) (Bruker, Bremen, Germany). The pure compounds were analyzed in deuterated methanol MeOD or in deutered chloroform CDCL3 (Euriso-Top®, Gif-sur-Yvette, France). High-Resolution Mass Spectrometry (HR-MS) analyses were carried out using a Thermo Fisher Scientific® Exactive Orbitrap Mass Spectrometer *(*Thermo Fisher Scientific, Waltham, MA USA) equipped with an electrospray ion source. HR-MS analyses were carried out in negative mode with a range of *m/z* 100–1000 amu. Products were solubilized in methanol.

8. Virus and Cell Lines

The human hepatoma cell line (Huh-7), whether expressing the TMPRSS2 protease or not (Belouzard et al., 2012), the African green monkey kidney Vero-81 cells, and the rhesus monkey kidney epithelial cells (LLC-MK2) were grown in DMEM supplemented with GlutaMax-I and 10% fetal bovine serum and cultured at 37°C in 5% CO_2 in a humidified incubator. All cell lines used in this study were regularly screened for mycoplasma contamination using the MycoAlert™ Mycoplasma Detection Kit (Lonza Bioscience, Basel, Switzerland). The viruses used were HCoV-229E strain VR-740 (ATCC), a recombinant HCoV-229E-Luc (kind gift of Volker Thiel), SARS-CoV-2 (isolate

SARS-CoV- 536 2/human/FRA/Lille_Vero-81-TMPRSS2/2020, NCBI MW575140), and HPIV-3-GFP (based on the JS strain) in which the GFP had been inserted between the P/C/D/V and M genes. The isolate was plaque purified and passaged in LLC-MK2 cells. Virus titer >8.0 log10 TCID50 per ml.

9. Cell Viability Assay

Huh-7 cells, Vero-81, and LLC-MK2 cells were seeded in 96-well plates and incubated with 100 µl of culture medium containing increasing concentrations of our compounds for 24 h and 72 h for LLC-MK2 cells. An MTS based viability assay (CellTiter 96 aqueous nonradioactive cell proliferation assay, Promega, Madison WI, USA) was performed, as recommended by the manufacturer. The absorbance of formazan at 490 nm was detected using ELx808 plate reader (BioTek Instruments Inc., Winooski, VT, USA). Each measurement was performed in triplicate.

10. Virus Infection Assay

HCoV-229E

Huh-7 and Huh-7/TMPRSS2 cells, were seeded in 96-well plates and inoculated with HCoV-229E-Luc at an MOI of 0.3 simultaneously with the compounds for 7 h and then lysed in 20 µL of 1× luciferase lysis buffer (Promega) as described (Belouzard et al., 2022). The luciferase activity was quantified in a TriStar LB 941 luminometer (Berthold Technologies, Bad Wildbad, Germany) using the Renilla luciferase assay system (Promega), as recommended by the manufacturer.

SARS-CoV-2

Vero-81 cells were seeded in 24-well plates, inoculated with SARS-CoV-2, and incubated simultaneously with the different compounds for 16 h (Meunier et al., 2022). Cells were lysed in ice-cold lysis buffer (Tris HCl, 50 mM; NaCl, 100 mM; EDTA, 2 mM; Triton X-100, 1%; SDS, 0.1%) on ice for 20 min. Lysates were collected and analyzed by Western blotting using rabbit polyclonal anti-SARS-CoV-2 nucleocapsid antibodies (Novus Biologicals, Littleton, CO, USA) and mouse anti-®-tubulin monoclonal antibody

(TUB 2.1) from Sigma. Horse-radish peroxidase-conjugated goat anti-rabbit and anti-mouse secondary antibodies (Jackson ImmunoResearch, West Grove, PA, USA) were used for the revelation using an enhanced chemiluminescence (ECL) Western blotting substrate (Thermo Fisher Scientific). The intensity of the bands was quantified using ImageJ software version 1.53i.

HPIV-3

LLC-MK2 cells were plated in 96-well plates and exposed to HPIV-3 at a multiplicity of infection (MOI) of 1, along with the presence of compounds, for a duration of 72 hours. The measurement of GFP was conducted using SPARK with excitation and emission maxima at 485 and 535 nm, respectively.

11. Statistical Analysis

The results were presented as the means ± SEM of three independent experiments performed in triplicate. The data were analyzed using GraphPad Prism software version 10.0.3 (Boston, MA, USA) by comparing each treated group and untreated group (DMSO control). Differences between means were assessed by ANOVA unpaired t-test or Mann-Whitney U test as deemed appropriate.

IV. Results and Discussions

Part I: Discovery of Anti-Coronavirus Cinnamoyl Triterpenoids Isolated from *Hippophae rhamnoides* during a Screening of Halophytes from the North Sea and Channel Coasts in Northern France

Abstract

The limited availability of antiviral therapy for severe acute respiratory syndrome coronavirus 2 (SARS-CoV-2) has spurred the search for novel antiviral drugs. Here, we investigated the potential antiviral properties of plants adapted to high-salt environments collected in the north of France. Twenty-five crude methanolic extracts obtained from twenty-two plant species were evaluated for their cytotoxicity and antiviral effectiveness against coronaviruses HCoV-229E and SARS-CoV-2. Then, a bioguided fractionation approach was employed. The most active crude methanolic extracts were partitioned into three different sub-extracts. Notably, the dichloromethane sub-extract of the whole plant *Hippophae rhamnoides* L. demonstrated the highest antiviral activity against both viruses. Its chemical composition was evaluated by ultra-high performance liquid chromatography (UHPLC) coupled with mass spectrometry (MS) and then it was fractionated by centrifugal partition chromatography (CPC). Six cinnamoyl triterpenoid compounds were isolated from the three most active fractions by preparative high-performance liquid chromatography (HPLC) and identified by high resolution MS (HR-MS) and mono- and bi-dimensional nuclear magnetic resonance (NMR). pecifically, these compounds were identified as 2-*O*-*trans*-*p*-coumaroyl-maslinic acid, 3β-hydroxy-2α-*trans*-*p*-coumaryloxy-urs-12-en-28-oic acid, 3β-hydroxy-2α-*cis*-*p*-coumaryloxy-urs-12-en-28-oic acid, 3-*O*-*trans*-caffeoyl oleanolic acid, a mixture of 3-*O*-*trans*-caffeoyl oleanolic acid/3-*O*-*cis*-caffeoyl oleanolic acid (70/30), and 3-*O*-*trans*-*p*-coumaroyl oleanolic acid. Infection tests demonstrated a dose-dependent inhibition of these triterpenes against HCoV-229E and SARS-CoV-2. Notably, cinnamoyl oleanolic acids displayed activity against both SARS-CoV-2 and HCoV-229E. Our findings suggest that *Hippophae rhamnoides* could represent a source of potential antiviral agents against coronaviruses.

Keywords: SARS-CoV-2; HCoV-229E; antiviral agents; halophytes; *Hippophae rhamnoides*; triterpenoids.

Results

1. Sampling and Classification of the Collected Plant Species

Twenty-two plant species, including strictly halophytes and relatively salt-tolerant species, were selected and collected from five different locations (Étaples, Dannes, Le Portel, Gravelines, Zuydcoote) distributed across the coastline of the North Sea and the English Channel in northern France (Hauts-de-France region). The whole plant or, in some cases, different parts of the plants (leaves (L), stems (S), roots (R)) were powdered to produce twenty-five crude methanolic extracts. The majority of these plants are representative of the botanical families of salt-tolerant plants distributed on the coasts of the North Sea and the English Channel. Some of them are considered strictly halophytes and were found in a schorre or at the base of an incipient dune, such as the Amaranthaceae species, *Cakile maritima* Scop. subsp. i*ntegrifolia* (Brassicaceae), and *Lysimachia maritima* (Primulaceae). The majority of the collected plants belong to the families of Asteraceae and Amaranthaceae, each representing 18% (n = 4) of all the plants collected. This repartition is logical with regard to Amaranthaceae since they are the most representative family of halophytes from the coast in the region (Lefèvre & Rivière, 2019). Cyperaceae and Poaceae each represent 9% (n = 2). The remaining families (Apiaceae, Berberidaceae, Convolvulaceae, Brassicaceae, Elaeagnaceae, Euphorbiaceae, Onagraceae, Primulaceae, Rosaceae, and Salicaceae) each represent 4.5% (n = 1) of the collected plants (**Figures 27, and 28).**

Figure 27. Pictures of some collected plant species: (**A**) *Salicornia procumbens* Sm. and *Suaeda maritima* (L.) Dumort. (Etaples), (**B**) *Salsola kali L.* (Dannes), (**C**) *Tripleurospermum maritimum* (L.) W. D. J. Koch (Le Portel), (**D**) *Crithmum maritimum* L. (Le Portel), (**E**) *Cakile maritima* Scop. subsp. *integrifolia* (Hornem.) Greuter and Burdet (Dannes), (**F**) *Ammophila arenaria* subsp. *arenaria* (L.) Link (Dannes), (**G**) *Convolvulus soldanella* L. (Dannes), and (**H**) *Hippophae rhamnoides* L. (Dannes) (Lefèvre & Rivière, 2019).

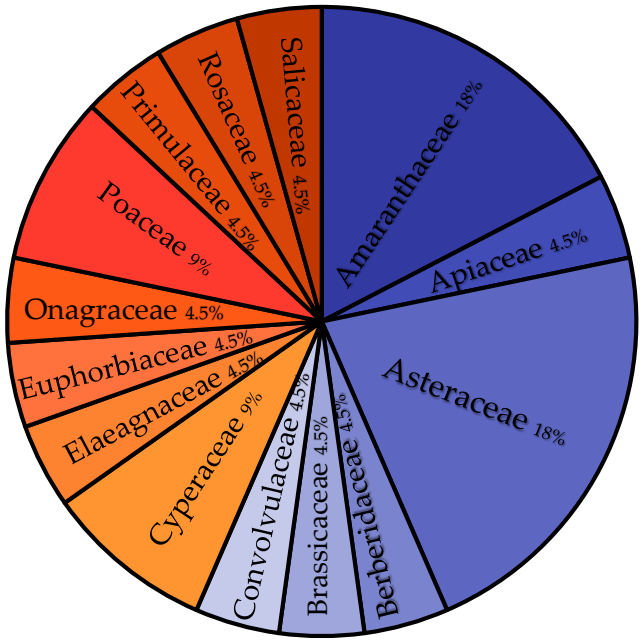

Figure 28. Chart representing the percentage of the collected plants botanical families.

2. Cytotoxicity and Antiviral Activity of Plant Crude Methanolic Extracts

2.1. Effect of Crude Methanolic Extracts on Cell Viability

The cytotoxicity of 25 crude methanolic extracts was tested on Huh-7 cells using an [3-(4,5-dimethylthiazol-2-yl)-5-(3-carboxymethoxyphenyl)-2-(4-sulfophenyl)-2H-tetrazolium]- based (MTS) viability assay. Huh-7 cells were treated with two different concentrations of the crude methanolic extracts (25 and 100 µg/mL) for 24 h. Non-treated control cells were incubated with 0.1% dimethyl sulfoxide (DMSO) in the media. The concentration of 25 µg/mL of all crude methanolic extracts was tolerated by Huh-7 cells after 24 h treatment. Similarly, no cellular cytotoxicity was observed using a concentration of 100 µg/mL of the crude methanolic extracts on Huh-7 cells, except for *Convolvulus soldanella*, *Berberis aquifolium* (R), and *Lysimachia maritima*, causing a decrease in cell viability by 53%, 60%, and 72.6%, respectively **(Figure 29).**

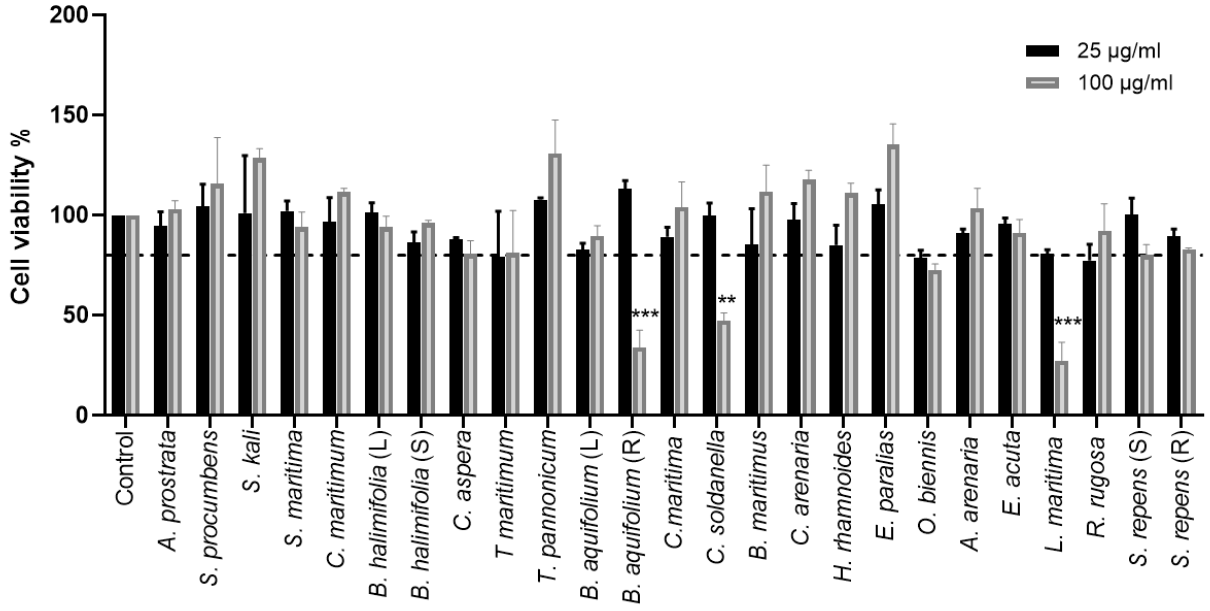

Figure 29. Cytotoxicity of the methanolic crude extracts on Huh-7 cells. Huh-7 cells were treated with two concentrations, 25 and 100 µg/mL, of crude extracts. Control cells were treated with 0.1% DMSO only. The cells were incubated for 24 h, and an MTS assay was then performed to determine the cell viability. The data bars represent the mean ± standard error of the mean (SEM) of three experiments performed in triplicate. The asterisk indicates a statistical difference compared to the control. (**, $p < 0.01$; ***, $p < 0.001$). (L) = Leaves, (S) = Stem, (R) = Roots.

2.2. Antiviral Screening of the Plant Crude Methanolic Extracts on HCoV-229E

Following the identification of the toxicity, we studied the antiviral activity of the extract on HCoV-229E infection. A coronavirus enters the cells through one of two pathways: by endocytosis or by direct fusion with the plasma membrane. The host-cell protease transmembrane serine protease 2 (TMPRSS2) is necessary for the plasma membrane fusion of many coronaviruses, including HCoV-229E, whereas cathepsins are often involved in fusion processes at endosomal membranes (Belouzard et al., 2012). We screened the antiviral activity of the crude methanolic extracts at a concentration of 25 µg/mL by quantifying the infection of HCoV-229E-Luc in Huh-7 cells, whether they expressed the TMPRSS2 protease or not. A significant decrease in the luciferase activity representing an antiviral effect was observed using *Hippophae rhamnoides*, *Salix repens* (R), *Salix repens* (S), *Berberis aquifolium* (R), and *Baccharis halimifolia* (L) in Huh-7/TMPRSS2 cells. Similarly, an antiviral effect was observed with *Hippophae*

rhamnoides, *Salix repens* (R), *Salix repens* (S), *Berberis aquifolium* (R), and *Baccharis halimifolia* (L) in Huh-7 cells **(Figure 30)**. Since *Berberis aquifolium* (R) crude methanolic extracts showed cytotoxicity at 100 µg/mL, we decided not to study it further.

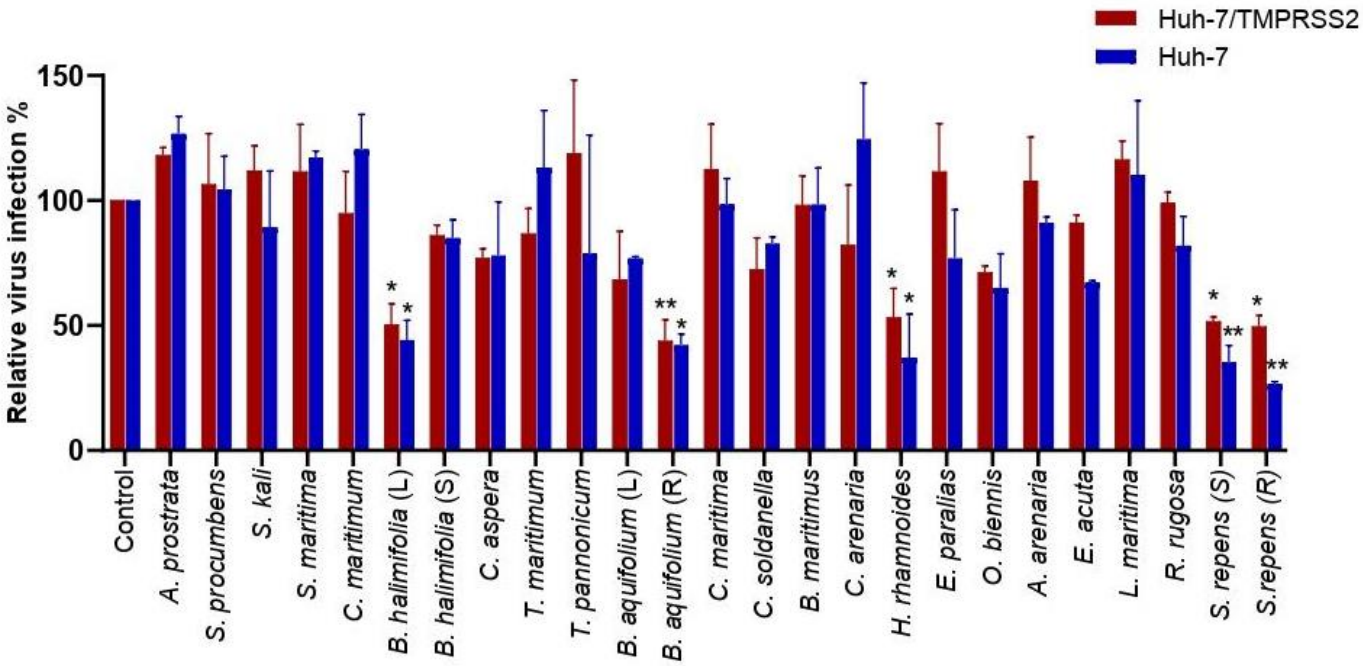

Figure 30. Screening of the antiviral activity of crude methanolic extracts on HCoV-229E-Luc. Huh-7 or Huh-7/TMPRSS2 cells were inoculated with HCoV-229E-Luc in the presence of various plant extracts at 25 µg/mL. Cells were lysed 7 h post-inoculation, and luciferase activity was quantified. Experiments were performed in triplicate, with each experiment being repeated thrice. The data bars represent the mean ± SEM. The asterisk indicates a statistical difference compared to the control (*, $p < 0.05$; **, $p < 0.01$).

3. Dose-Response Antiviral Activity of Plant Extracts

In order to confirm the antiviral activity of *Hippophae rhamnoides*, *Salix repens* (R), *Salix repens* (S), and *Baccharis halimifolia* (L) extracts on HCoV-229E, dose-response experiments were conducted. Antiviral assays were conducted in Huh-7 and Huh-7/TMPRSS2 cells to cover the two entry pathways. Cytotoxicity was also evaluated in parallel. The results presented in **(Figure 31)** show that the four selected extracts were able to decrease HCoV-229E infection in a dose-dependent manner, confirming their antiviral capacity. These results allowed us to determine the 50% cytotoxic concentration

(CC_{50}) and the 50% inhibitory concentration (IC_{50}) of each extract and calculate their selectivity index (SI), which is the ratio between CC_{50} and IC_{50} **(Table 4)**.

Hippophae rhamnoides showed the highest CC_{50} in Huh-7 cells (621 µg/mL), whereas *Salix repens* (R) showed the lowest CC_{50} of 149 µg/mL. For antiviral activity, *Salix repens* (S) demonstrated the lowest IC_{50} in both Huh-7 and Huh-7/TMPRSS2 cells (15.1 and 14.7 µg/mL, respectively). However, *Baccharis halimifolia* (L) extract was the most active among the extracts but only in Huh-7/TMPRSS2 cells, with an IC_{50} of 11.2 µg/mL, showing that it might inhibit the TMPRSS2 entry pathway. Finally, for the four extracts, antiviral activity was not due to cytotoxicity, with the calculated SIs ranging from 5 to 35.

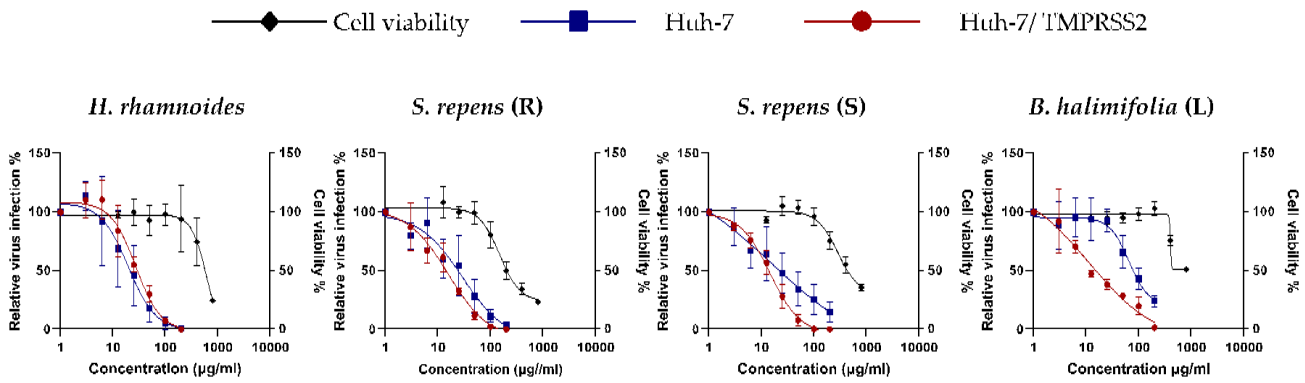

Figure 31. Cytotoxicity and antiviral activity on HCoV-229E of crude methanolic extracts of *Hippophae rhamnoides*, *Salix repens* (R), *Salix repens* (S), and *Baccharis halimifolia* (L). For infection assays, Huh-7 cells were inoculated with HCoV-229E in presence of various concentrations of each crude methanolic extract up to 200 µg/ml for 7 h. Cells were lysed 7 h post-inoculation and luciferase activity quantified. For cytotoxicity assays, cells were incubated with the different crude methanolic extracts at different concentrations, up to 800 µg/ml for 24 h. MTS assay was performed to monitor cell viability. Results are expressed as mean ± SEM of 3 independent experiments.

hTable 4. Cytotoxicity, antiviral activity, and SI of each of the crude methanolic extracts against HCoV-229E.

Crude extract	CC_{50} (µg/mL) Vero-81	CC_{50} (µg/mL) Huh-7	Huh-7		Huh-7/TMPRSS2	
			IC_{50} (µg/mL)	SI	IC_{50} (µg/mL)	SI
H. rhamnoides	499	621	19.7	31.5	27.2	22
S. repens (R)	441	149	29.1	5.1	15.5	9
S. repens (S)	438	285	15.1	28.9	14.7	19
B halimifolia (L)	820	>1000	65.3	>15	11.2	>89

As a next step, we wondered if the extracts could have antiviral activity against other HCoVs and examined their antiviral capacity against SARS-CoV-2 in Vero-81 cells. Cytotoxicity was first evaluated **(Table 4, Figure 32)**. Vero-81 cells showed higher tolerance to the crude methanolic extracts compared to Huh-7 cells due to the presence of a P-glycoprotein efflux pump (Y. Zhu et al., 2022). Vero-81 cells infected with the SARS-CoV-2 were treated with two concentrations, 25 and 50 µg/mL, of the crude methanolic extracts, and chloroquine, an inhibitor of the endocytic entry pathway, was added as control. Western blot analyses showed a dose-dependent decrease in the SARS-CoV-2 N protein expression levels for the four extracts, indicating an antiviral effect **(Table 4)**. Three crude methanolic extracts, *Hippophae rhamnoides*, *Salix repens* (R), and *Baccharis halimifolia* (L), showed a high antiviral effect at both concentrations. Even though *Salix repens* (S) showed an antiviral effect at 50 µg/mL, the antiviral activity at 25 µg/mL was weaker **(Figure 33)**.

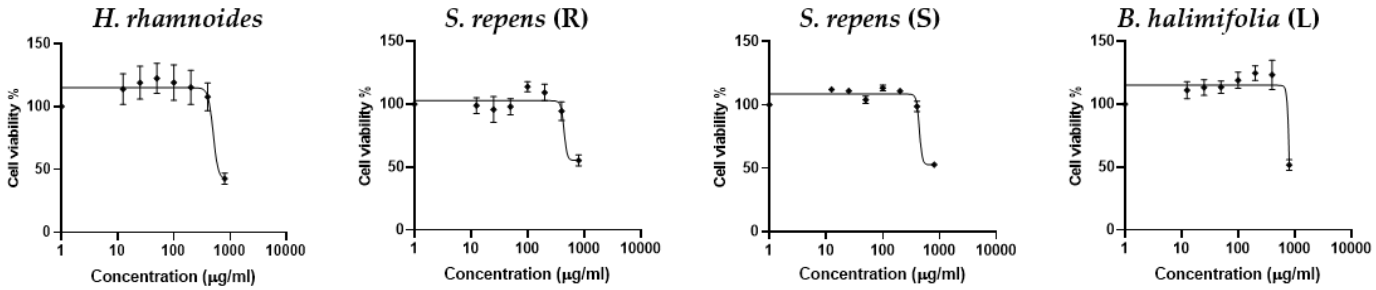

Figure 32. Cytotoxicity of crude methanolic extracts of *Hippophae rhamnoides*, *Salix repens* (R), *Salix repens* (S), and *Baccharis halimifolia* (L). Vero-81 cells were incubated with the different crude methanolic extracts at different concentrations, up to 800 µg/ml for 24 h. MTS assay was performed to monitor cell viability. Results are expressed as mean ± SEM of 3 independent experiments.

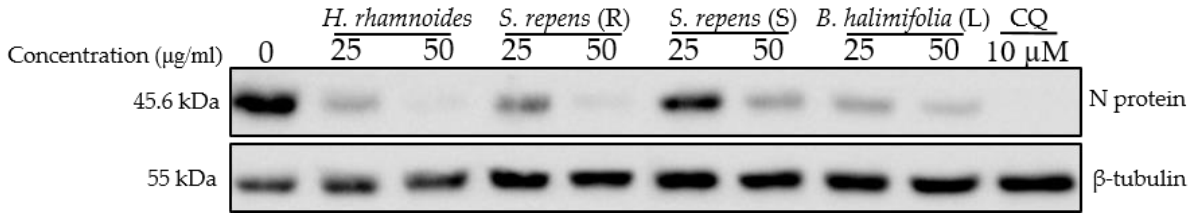

Figure 33. Antiviral activity on SARS-CoV-2 of crude methanolic extract of *Hippophae rhamnoides*, *Salix repens* (R), *Salix repens* (S), and *Baccharis halimifolia* (L). Vero-81 cells were infected with SARS-CoV-2 in the presence of different plant extracts at 25 and 50 µg/mL, or 10 µM chloroquine (CQ). Cell lysates were collected after 16 h and subjected to immunoblotting analysis using an anti-SARS-CoV-2 N antibody and an anti-ß-tubulin antibody to show an equal amount of cellular protein in each lane. This immunoblot is representative of two independent experiments.

Taken together, these results show that the four crude methanolic extracts of salt-tolerant species might be a source of antiviral compounds against human coronaviruses HCoV-229E and SARS-CoV-2.

4. Bioguided Fractionation Assay to Determine the Active Sub-Extracts

A bioguided fractionation assay was conducted in order to isolate the active compounds present in the active crude methanolic extracts. The four extracts were partitioned using three solvents of different polarities, yielding DCM, EtOAc, and Aq sub-extracts. The different partitions obtained were tested for cytotoxicity at 25 and 100 µg/mL through the MTS assay. None of the tested sub-extracts appeared to be cytotoxic at 25 µg/mL **(Figure 34)**.

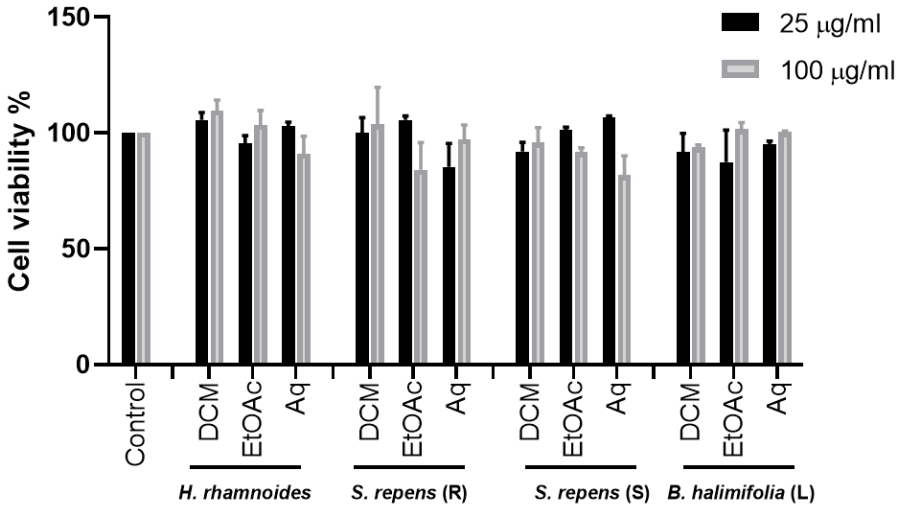

Figure 34. Effect of the different sub-extracts on Huh-7 cell viability. Cells were treated with the different sub-extracts for 24 h at 25 and 100 µg/ml or with 0.1% DMSO (control). No significant difference between the sub-extracts and control ($P < 0.05$). Data are represented as mean ± SEM of three independent experiments.

Then, the antiviral activity of each sub-extract at 25 µg/mL was tested against HCoV-229E **(Figure 35)**. The DCM sub-extract was the most active for *Hippophae rhamnoides* in both Huh-7 and Huh-7/TMPRSS2 cells. The Aq sub-extract was the most active in *Salix repens* (S) in both Huh-7 and Huh-7/TMPRSS2 cells. All sub-extracts of *Salix repens* (R) showed an antiviral effect against HCoV-229E. Surprisingly, for *Baccharis halimifolia* (L), fractionation did not permit the identification of a very active sub-extract. We selected *H. rhamnoides* DCM, *S. repens* (R) EtOAc, *S. repens* (S) Aq, and *B. halimifolia* DCM for further investigations.

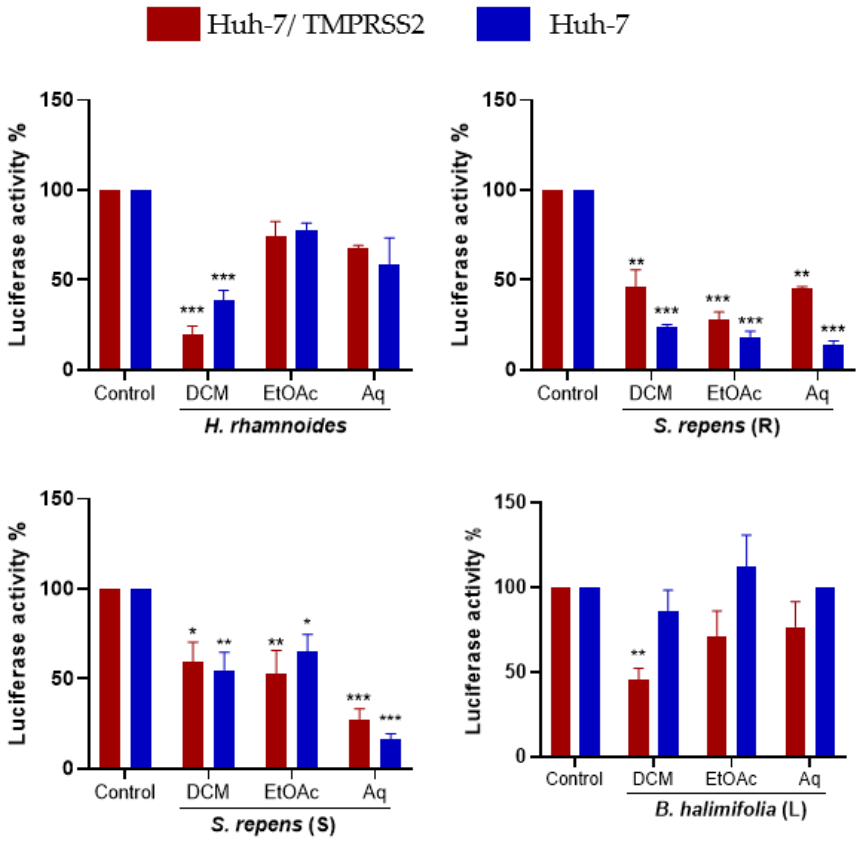

Figure 35. Inhibitory activity of the three partitions obtained from each plant's crude methanolic extract on HCoV-229E-Luc infection. Experiments were conducted as described earlier. Data are represented as the mean ± SEM of three independent experiments. (*, $p < 0.05$; **, $p < 0.01$; ***, $p < 0.001$).

In order to confirm the antiviral activity of the selected sub-extracts and determine their cytotoxicity, dose-response experiments were performed as described. This allowed us to calculate the CC_{50}, IC_{50}, and SI values **(Table 5, Figure 36)**. All the tested sub-extracts showed a dose-dependent reduction in infection with a high SI (SI > 10). The EtOAc sub-extract of *Salix repens* (R) displayed the lowest IC_{50} in Huh-7/TMPRSS2 cells (IC_{50} = 28.8 µg/mL), whereas the Aq sub-extract of *Salix repens* (S) showed the lowest IC_{50} value in Huh-7 cells (IC_{50} = 7.6 µg/mL). On the other hand, the DCM sub-extract of *Baccharis halimifolia* showed the highest IC_{50} values of 38.3 µg/mL and 31.1 µg/mL in Huh-7/TMPRSS2 and Huh-7 cells, respectively.

Table 5. Cytotoxicity, activity, and SI of each of the sub-extracts against HCoV-229E.

Sub-extract	Vero-81 CC_{50} (µg/mL)	Huh-7 CC_{50} (µg/mL)	Huh-7		Huh-7/TMPRSS2	
			IC_{50} (µg/mL)	SI	IC_{50} (µg/mL)	SI
H. rhamnoides DCM	264	410	18.7	21	36.	11
S. repens (R) EtOAc	344	500	15.8	31	28.87	17
S. repens (S) Aq	262	550	7.6	71	30.5	18
B. halimifolia (L) DCM	347	368	31.1	11	38.3	9

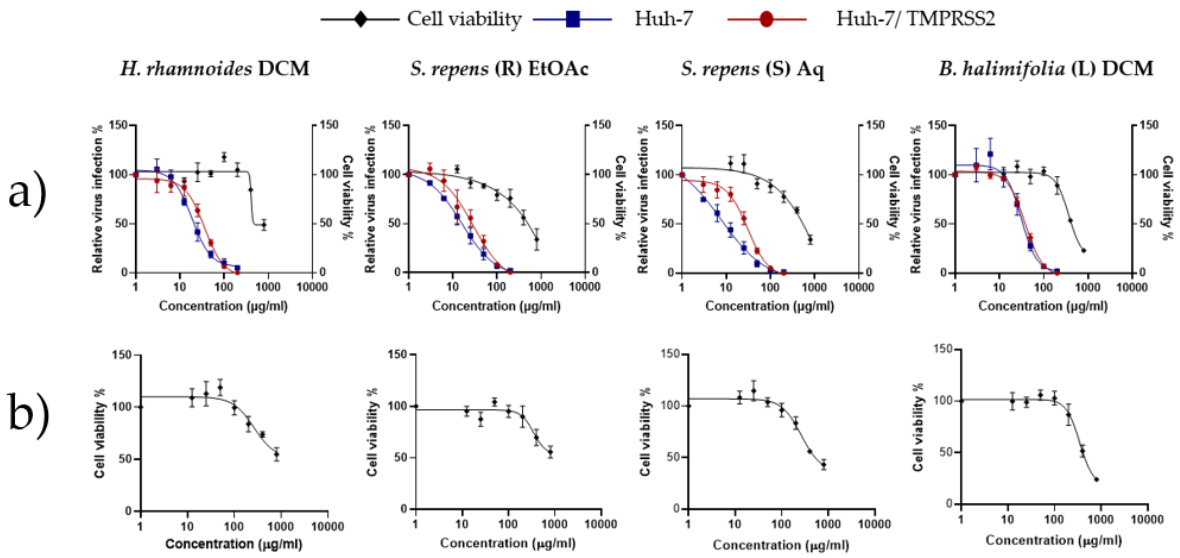

Figure 36. Cytotoxicity and antiviral activity on HCoV-229E of sub extracts of *Hippophae rhamnoides* DCM, *Salix repens* (R) EtOAc, *Salix repens* (S) Aq, and *Baccharis halimifolia* (L) DCM. **a)** Cell viability and inhibition of HCoV-229E infection of Huh-7 cells in the presence of increasing concentrations of the sub-extracts. The infection was quantified by measuring luciferase activity **b)** Dose-response curves showing cell viability as a function of sub-extracts concentration, measured with the MTS assay in Vero-81 cells, after 24 h. Data points are mean ± SEM.

We then tested the antiviral activity of the sub-extracts on SARS-CoV-2. A dose-dependent inhibitory effect was observed for all extracts **(Figure 37)**. Treatment with the DCM sub-extract of *Hippophae rhamnoides* (HR DCM SE) at a concentration of 50

µg/mL led to a strong reduction in SARS-CoV-2 infection by showing a complete decrease in N protein expression levels in the cell lysate. The DCM sub-extract of *Baccharis halimifolia* showed the lowest inhibitory activity against SARS-CoV-2 at both concentrations. Both the EtOAc sub-extract of *Salix repens* (R) and the Aq sub-extract of *Salix repens* (S) showed similar inhibitory effects against SARS-CoV-2; however, it was lower than that of HR DCM SE.

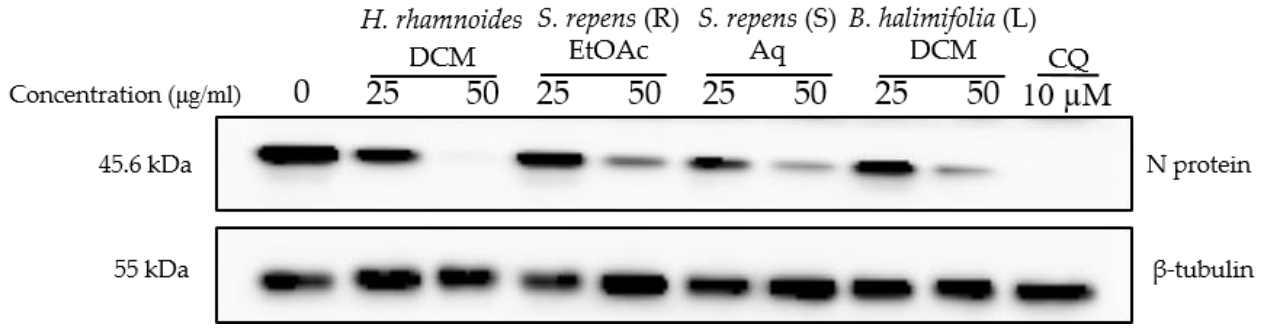

Figure 37. Antiviral activity on SARS-CoV-2 of sub-extracts. Vero-81 cells were infected with SARS-CoV-2 in the presence and absence of different plant sub-extracts at 25 and 50 µg/mL, or 10 µM chloroquine. Cell lysates were collected after 16 h and subjected to immunoblotting as described. This blot is representative of two independent experiments.

Since the HR DCM SE showed a strong antiviral effect against both HCoV-229E and SARS-CoV-2, we decided to study this plant in depth to determine the major bioactive compounds responsible for the anti-coronavirus effect.

5. Characterization of HR DCM SE by UHPLC UV-MS

The analysis of HR DCM SE by UHPLC-UV-MS showed different compounds with different levels and polarities. HR DCM SE was fractionated by CPC with the Arizona R system in descending mode. The collected fractions were dried and analyzed by UHPLC-UV-MS. The fractions that showed the same chromatographic profile were pooled together. Thus, we ended up with 10 fractions **(Figure 38)**.

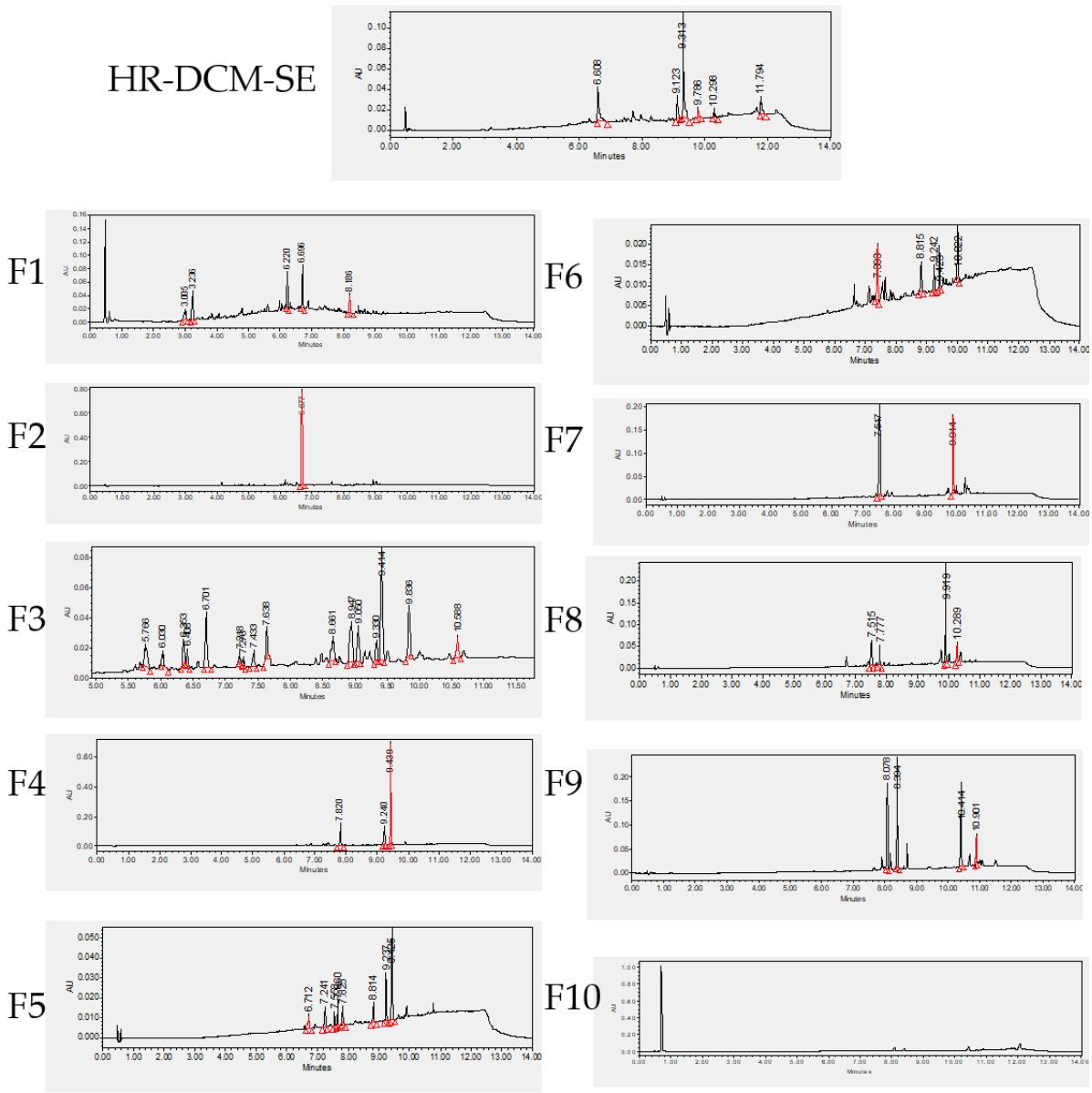

Figure 38. Chromatograms obtained by UHPLC-UV-MS at λ = 254 nm of different fractions resulting from CPC fractionation of the DCM sub-extract of *Hippophae rhamnoides*.

6. Cytotoxicity of Ten Fractions Prepared from HR DCM SE

The cytotoxicity of the ten fractions of HR DCM SE obtained through CPC was assessed in Huh-7 cells and Vero-81 cells at 25 and 100 µg/mL. Generally, a dose-dependent decrease in cell viability was observed upon testing the fractions at increasing concentrations. However, at 25 µg/mL, all fractions showed no cytotoxicity on Huh-7 cells. At 100 µg/mL, fractions F2, F3, F4, F6, and F7 were considered cytotoxic upon treating the cells, causing a decrease in cell viability by 41.7%, 44.2%,

61.4%, 30.9%, and 70.4%, respectively. However, fractions F1, F2, F9, and F10, did not show cellular toxicity. Similar to Huh-7, these fractions were not cytotoxic on Vero-81 cells when tested at 25 µg/mL. Fractions F2, F4, F6, and F7, which showed cytotoxicity on Huh-7 cells, were also toxic on Vero-81 cells at 100 µg/mL, decreasing the viability by 55.7%, 75.7%, 81.7%, and 66.4%, respectively **(Figure 39)**.

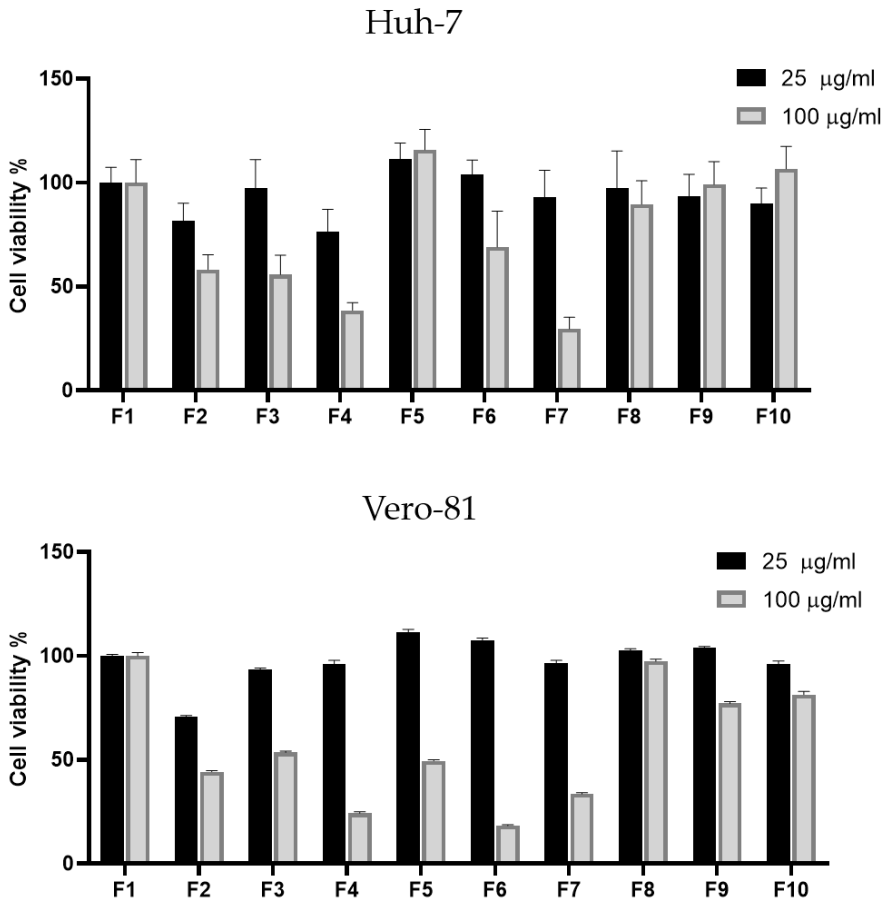

Figure 39. Cytotoxicity of fractions resulting from CPC fractionation of the DCM sub-extract of *Hippophae rhamnoides*. Effect of the different fractions on Huh-7 and Vero-81 cell viability when treated for 24 h at 25 and 100 µg/ml. Data are represented as mean ± SEM of three independent experiments.

7. Antiviral Screening of Ten Fractions Obtained from HR DCM SE against HCoV-229E and SARS-CoV-2

After identifying a concentration that could be tolerated by Huh-7 cells, the antiviral activity on HCoV-229E-Luc in Huh-7 and Huh-7/TMPRSS2 cells was monitored. Huh-7 cells were infected with the virus and treated simultaneously with the different fractions

at 10 and 25 µg/mL. Three fractions (F3, F4, and F7) showed a 10-fold decrease in virus infection levels compared to the control, indicating an antiviral effect against HCoV-229E **(Figure 40A)**.

Similarly, the ten fractions were tested for antiviral activity against SARS-CoV-2. The results presented in **(Figure 40B)** show that, interestingly, fractions F2 and F6, which were not active on HCoV-229E, were able to inhibit the expression of the SARS-CoV-2 N protein. Similar to HCoV-229E, fractions F3, F4, and F7 were able to inhibit SARS-CoV-2 replication, showing a dose-dependent decrease in antiviral activity **(Figure 40B)**.

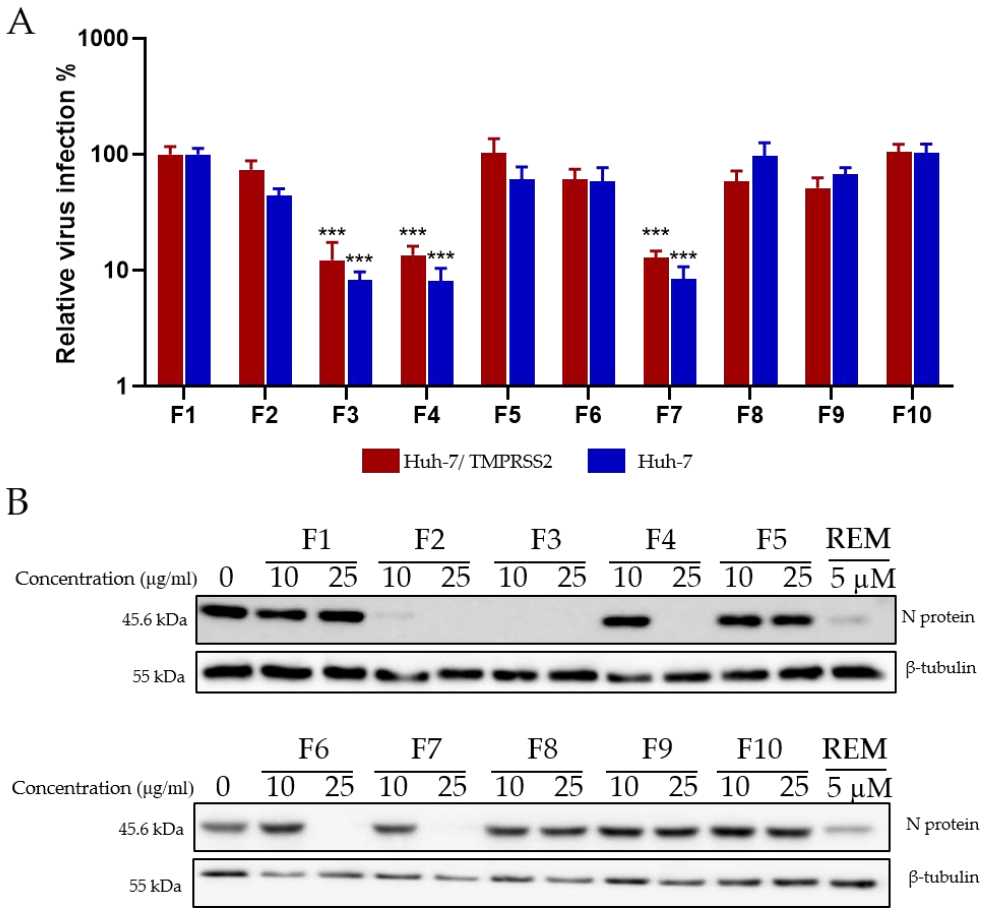

Figure 40. Antiviral activity of *Hippophae rhamnoides* fractions. **(A)** Screening of the antiviral activity of the fractions of *Hippophae rhamnoides* with HCoV-229E-Luc. The different fractions were tested at 25 µg/mL. **(B)** Western blotting analysis showing the effects of the different fractions of *Hippophae rhamnoides* on N protein expression in Vero-81 cells. Vero-81 cells were infected with SARS-CoV-2 in the presence of the different fractions at 10 and 25 µg/mL. Cell lysates were collected after 16 h and subjected to Western blotting. (***, $p < 0.001$).

8. Isolation of Compounds by Preparative HPLC and Identification by HRMS and NMR

To isolate the active compounds responsible for an antiviral effect against both viruses, a preparative HPLC was performed. Fractions F2, F4, and F7 were first analyzed by analytical HPLC to find the best purification method. We chose not to purify compounds from F3 due to their high complexity and because the compounds of interest were also found in the less complex fractions, F2 and F4. Then, the major compounds were purified by preparative HPLC using the same stationary phase. Fraction 2 was purified with a gradient system (60–100% CH3CN, 30 min), providing compounds F2-1 (tr = 23.00 min, 2.41 mg), F2-2 (tr = 23.55 min, 2 mg), F2-3 (tr = 26.00 min, 2 mg), and F2-4 (tr = 9.830 min, 3 mg) **(Figure 41)**. F2-1, F2-2, and F2-3 have a molecular mass of 618 g.mol−1. Two compounds, F4-1 (tr = 16.507 min, 3 mg) and F4-2 (tr = 18.946 min, 8 mg), with a molecular mass of 618 g.mol−1, were purified from F4 with a gradient system (80–100% CH3CN, 30 min) **(Figure 41)**. Compound F4-1 was isolated as a mixture (30:70) with compound F4-2. F7 was fractionated with a gradient system (80–100% CH3CN, 30 min) to give compound F7-1 (tr = 19.030 min, 3.4 mg) with a molecular mass of 602 g.mol−1 **(Figure 41)**.

Taken together, F2-1, F2-2, F3-2, F4-1, F4-2, and F7-1 were identified as six cinnamoyl triterpenoids. Their purities were, respectively, estimated at 98.8, 88.6, 97.1, 90.7, 96.4, and 91.7% on the basis of PDA chromatograms (**Figure S1**). Their structures were established through a comparison of their physical and spectral data, including HRMS and extensive 1D- and 2D-NMR data, with reported values of 2-*O*-*trans*-*p*-coumaroyl-maslinic acid (F2-1) (Z.-G. Yang et al., 2007), 3β-hydroxy-2α-*trans*-*p*-coumaryloxy-urs-12-en-28-oic acid (F2-2) (Siddiqui et al., 1987), 3β-hydroxy-2α-*cis*-*p*-coumaryloxy-urs-12-en-28-oic acid (F2-3) (Siddiqui et al., 1987), 3-*O*-*cis*-caffeoyl-oleanolic acid (F4-1), 3-*O*-*trans*-caffeoyl-oleanolic acid (F4-2) (Fuchino et al., 1996), and 3-*O*-*trans*-*p*-coumaroyl-oleanolic acid (F7-1) (H. Takahashi et al., 1999) (**Figures 42** and **S2**).

Unfortunately, F2-4 could not be precisely identified due to the lack of a mass response and poor NMR resolution. It was not a triterpenoid and seemed to be a flavonoid due to a positive response to Neu's reagent.

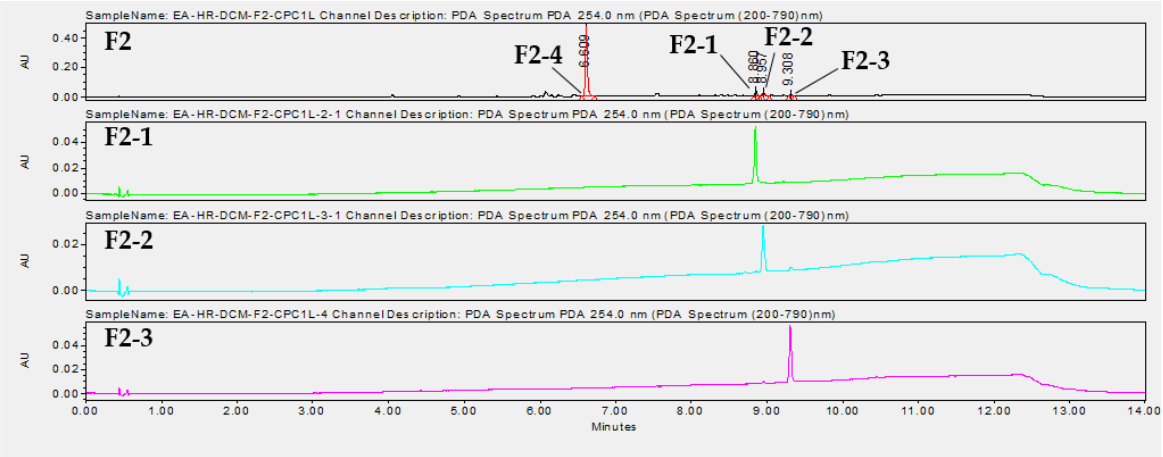

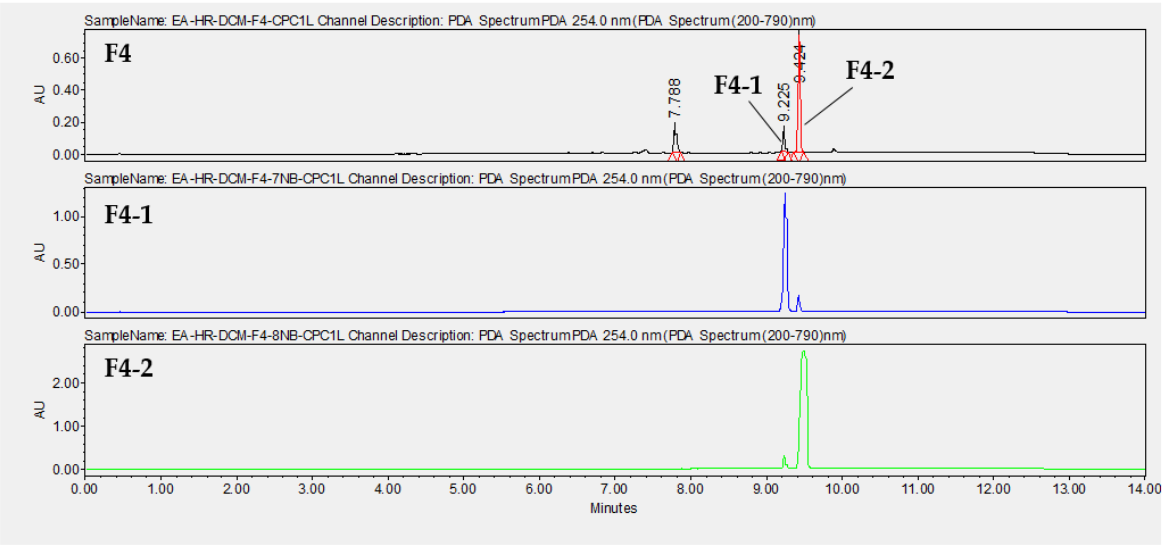

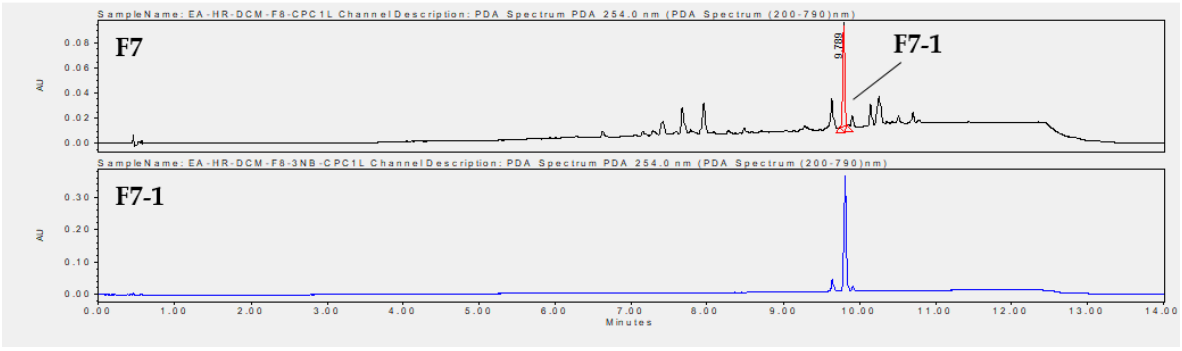

Figure 41. Chromatograms at λ = 254 nm obtained by UHPLC-UV-MS of F2, F4, and F7, as well as purified compounds obtained by preparative HPLC.

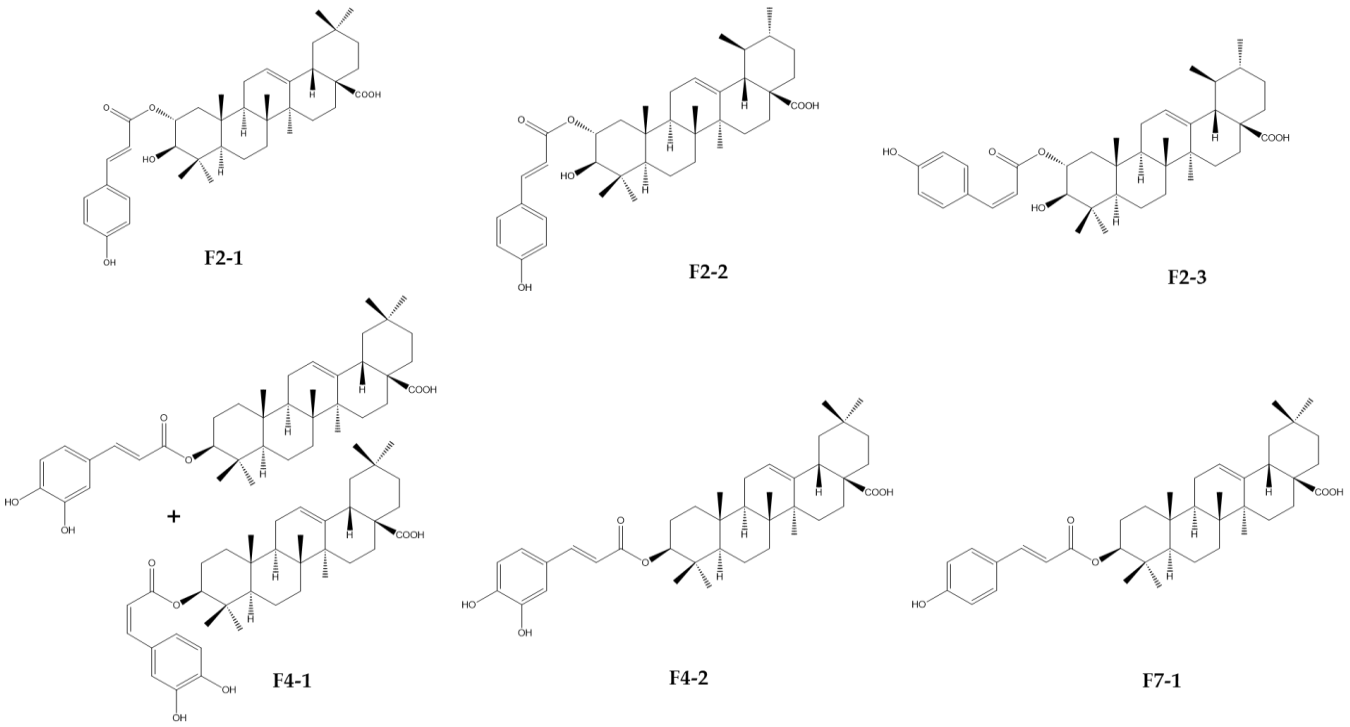

Figure 42. Chemical structures of cinnamoyl triterpenoids purified from fractions F2, F4, and F7 resulting from CPC fractionation of the DCM sub-extract of *Hippophae rhamnoides*.

9. Cytotoxicity and Antiviral Activity of the Purified Compounds on HCoV-229E and SARS-CoV-2

To determine whether the purified compounds were responsible for the antiviral effects on both coronaviruses, we conducted cytotoxicity and antiviral dose-response experiments. Huh-7 cells were treated with the various compounds at different concentrations of up to 100 µM for 24 h, and the cytotoxicity was quantified using an MTS assay. Among the compounds, F4-2 displayed the highest CC_{50} value of 81.4 µM. Conversely, the mixture F4-1 exhibited the lowest CC_{50} value of 21 µM. The CC_{50} values for F2-2 and F2-3 were found to be 44.4 and 52.1 µM, respectively. Both F2-1 and F7-1 demonstrated similar CC_{50} values of 39.9 µM and 39.3 µM, respectively **(Figure 43, Table 6)**.

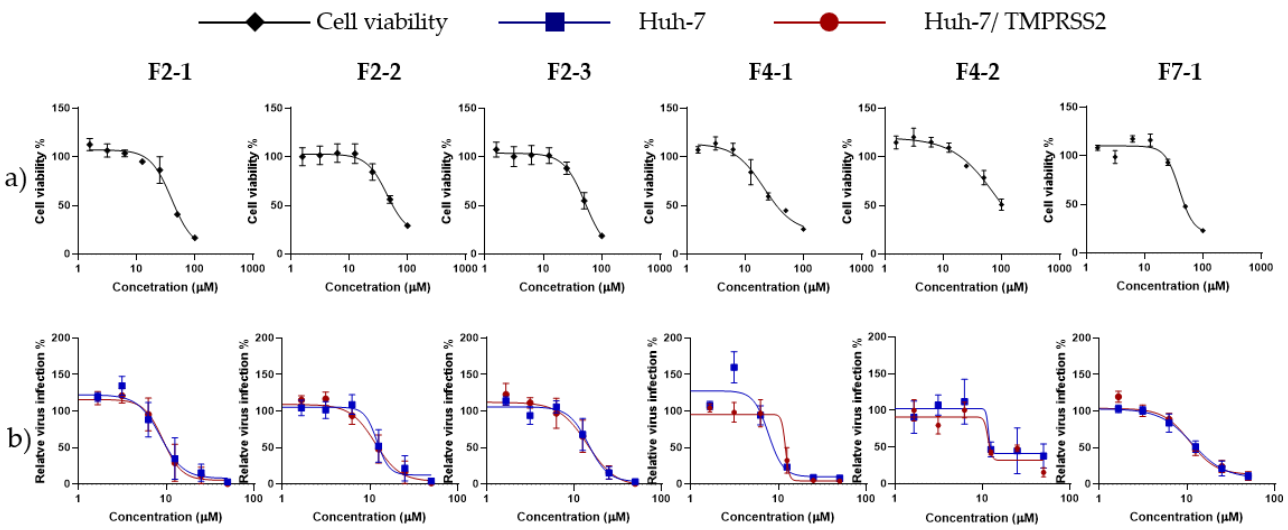

Figure 43. Cytotoxicity and antiviral activity on HCoV-229E of different pure compounds. **a)** Dose-response curves showing cell viability as a function of pure compounds concentrations, measured with the MTS assay in Huh-7 cells, after 24 h. Data points are mean ± SEM. **b)** Inhibition of HCoV-229E infection of Huh-7 cells in the presence of increasing concentrations of different pure compounds. The infection was quantified by measuring luciferase activity.

Table 6. Cytotoxicity, antiviral activity, and SI of each purified compound against HCoV-229E.

Sub-Extract	Huh-7 CC_{50} (µM)	Huh-7		Huh-7/TMPRSS2	
		IC_{50} (µM)	SI	IC_{50} (µM)	SI
F2-1 (2-*O*-*trans*-*p*-coumaroyl-maslinic acid)	39.9	8.6	4	9.1	4
F2-2 (3β-hydroxy-2α-*trans*-*p*-coumaryloxy-urs-12-en-28-oic acid)	44.4	12.0	3	11.4	3
F2-3 (3β-hydroxy-2α-*cis*-*p*-coumaryloxy-urs-12-en-28-oic acid)	52.1	14.5	3	14.1	3
F4-1 Mixture 3-*O*-*trans*-caffeoyl oleanolic acid / 3-*O*-*cis*-caffeoyl oleanolic acid (70/30)	21.0	7.6	2	12.0	1
F4-2 (3-*O*-*trans*-caffeoyl-oleanolic acid)	81.4	11.6	6	11.5	7
F7-1 (3-*O*-*trans*-*p*-coumaroyl-oleanolic acid)	39.3	11.4	3	10.7	3

Antiviral testing against HCoV-229E showed that the six compounds isolated from the three fractions (F2, F4, and F7) demonstrated a dose-dependent antiviral activity in

both Huh-7 and Huh-7/TMPRSS2 cells **(Table 6 , Figure 43).** F2-1 displayed the most promising performance, showing IC_{50} values of 8.6 and 9.1 µM in Huh-7 and Huh-7/TMPRSS2 cells, respectively, with an SI of approximately 4. It is noteworthy that the major compound F2-4 of fraction 2, which was not chemically characterized, did not exhibit either cytotoxicity or antiviral effects on HCoV-229E **(Figure 44)**. F4-2 also displayed interesting antiviral activities and the highest SI of 7. F4-1 was the most active but only in Huh-7 cells with an IC_{50} value of 7.6 µM.

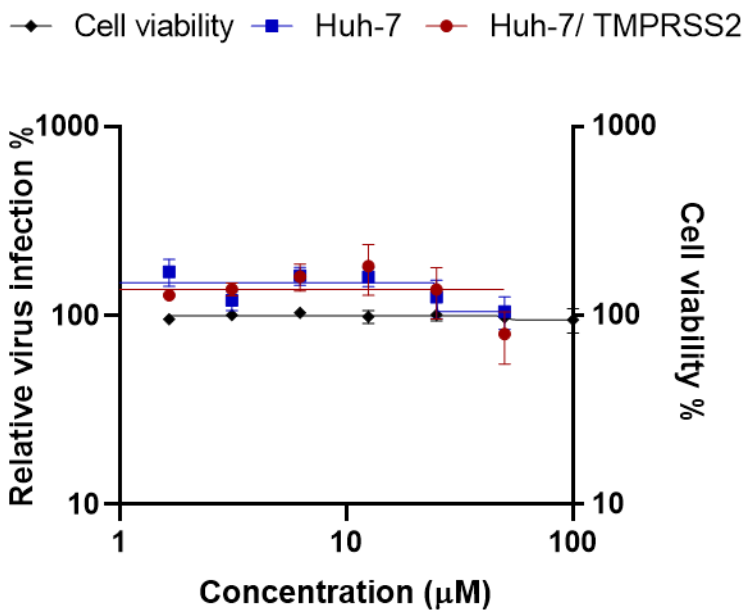

Figure 44. Cytotoxicity and HCoV-229E infectivity assays of F2-4 isolated from F2 of *Hippophae rhamnoides* DCM SE. For infection assays, Huh-7 cells were inoculated with HCoV-229E in presence of various concentrations of each crude methanolic extract up to 50 µM for 7 h. Cells were lysed 7 h post-inoculation and luciferase activity quantified. For toxicity assays, cells were incubated with the different concentrations, up to 800 µM for 24 h. MTS assay was performed to monitor cell viability. Results are expressed as mean ± SEM of 3 independent experiments.

Finally, we explored the antiviral impact of the three cinnamoyl oleanolic acids, F4-1, F4-2, and F7-1, on SARS-CoV-2 at various concentrations. The inhibitory activity was assessed by quantifying the levels of N protein expression **(Figure 45)**. A noticeable, dose-dependent reduction in N protein levels, indicative of an antiviral effect, was observed for all three compounds. Specifically, F4-1 exhibited the highest antiviral activity, significantly inhibiting SARS-CoV-2 by 54% at 12.5 µM, 68% at 25 µM, and 93.3% at 50 µM. In contrast, both F4-2 and F7-1 demonstrated significant inhibitory effects,

reaching 54% and 55.5%, respectively, but only at the concentration of 50 µM **(Figure 45)**. The difference in activity observed between F4-1 and F4-2 could suggest better activity for 3-*O*-*cis*-caffeoyl oleanolic acid. Unfortunately, this compound could not be obtained in pure form due to a spontaneous conversion to the *trans* isomer during the purification process.

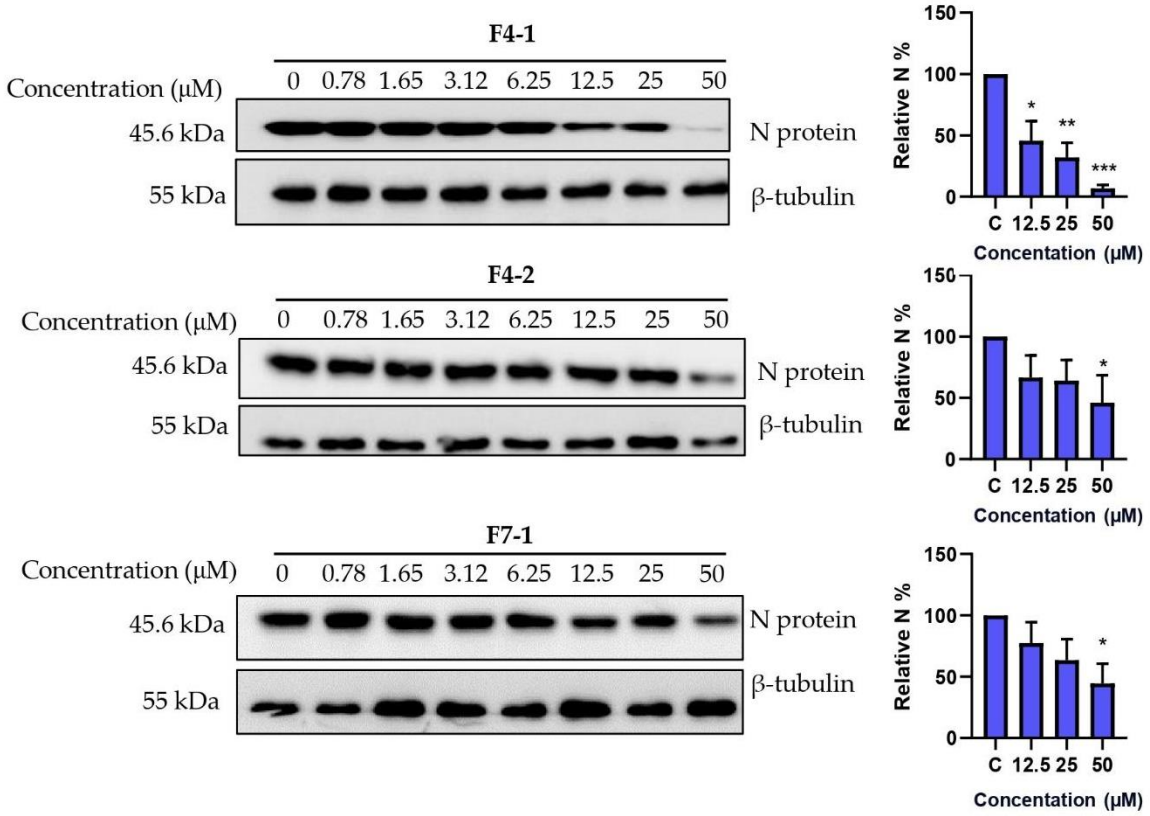

Figure 45. Antiviral activity of cinnamoyl oleanolic acids against SARS-CoV-2. The antiviral effect of F4-1 (3-O-cis-caffeoyl-oleanolic acid), F4-2 (3-O-trans-caffeoyl-oleanolic), and F7-1 (3-O-trans-p-coumaroyl-oleanolic acid) against SARS-CoV-2 was determined by Western blot. Vero-81 cells were treated with the different compounds at different concentrations for 16 h. Cell lysates were collected after 16 h and subjected to Western blotting. Data values represent the mean ± SD from 3 independent experiments, (*, $p < 0.05$; **, $p < 0.01$; ***, $p < 0.001$).

Taken together, the results show that several cinnamoyl triterpenoids, isolated from three different fractions of HR DCM SE, have antiviral activities against both HCoV-229E and SARS-CoV-2.

10. Antiviral activity of *Hippophae rhamnoides* on Parainfluenza Virus

To determine if HR DCM SE fractions exhibit an antiviral effect against other enveloped respiratory tract viruses, LLC-MK2 cells were infected with an engineered human parainfluenza virus-3, HPIV-3-GFP, and treated with the different fractions. The inhibitory effect of *H. rhamnoides* DCM fractions on infection was evaluated for HPIV-3-GFP. Cytotoxicity assay showed that *H. rhamnoides* fractions have no effect on cell viability at 25 µg/ml except for F2, and F4. However, F2, F4, F6, and F7 showed cellular toxicity at 50 µg/ml **(Figure 46a).** Antiviral testing revealed that different fractions were able to inhibit infection at 25 µg/ml, with F4 and F7 showing the highest level of inhibition (98%) **(Figure 46b).** This result suggests that HR DCM SE fractions could potentially have an antiviral effect against other enveloped RNA viruses. Interestingly, F4 and F7 are also active against HCoVs. Unfortunately, the limited quantity of pure compounds isolated from F4 and F7 did not allow us to test them against HPIV-3.

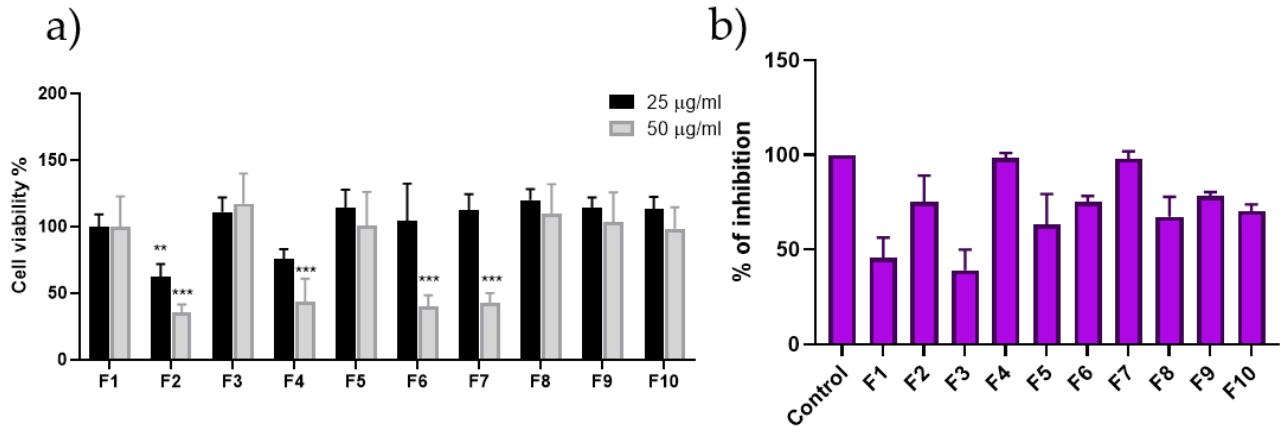

Figure 46. Toxicity and antiviral testing of *H. rhamnoides* DCM Fractions against human parainfluenza virus. a) LLC-MK2 cells were treated with 25 and 50 µg/ml for 72 h. b) Percentage of viral inhibition against HPIV-3 at 25 µg/ml after 72 h. (*, $P < 0.05$; **, $P < 0.01$; ***, $P < 0.001$).

Graphical Abstract: Discovery of Anti-Coronavirus Cinnamoyl Triterpenoids Isolated from *Hippophae rhamnoides* during a Screening of Halophytes from the North Sea and Channel Coasts in Northern France

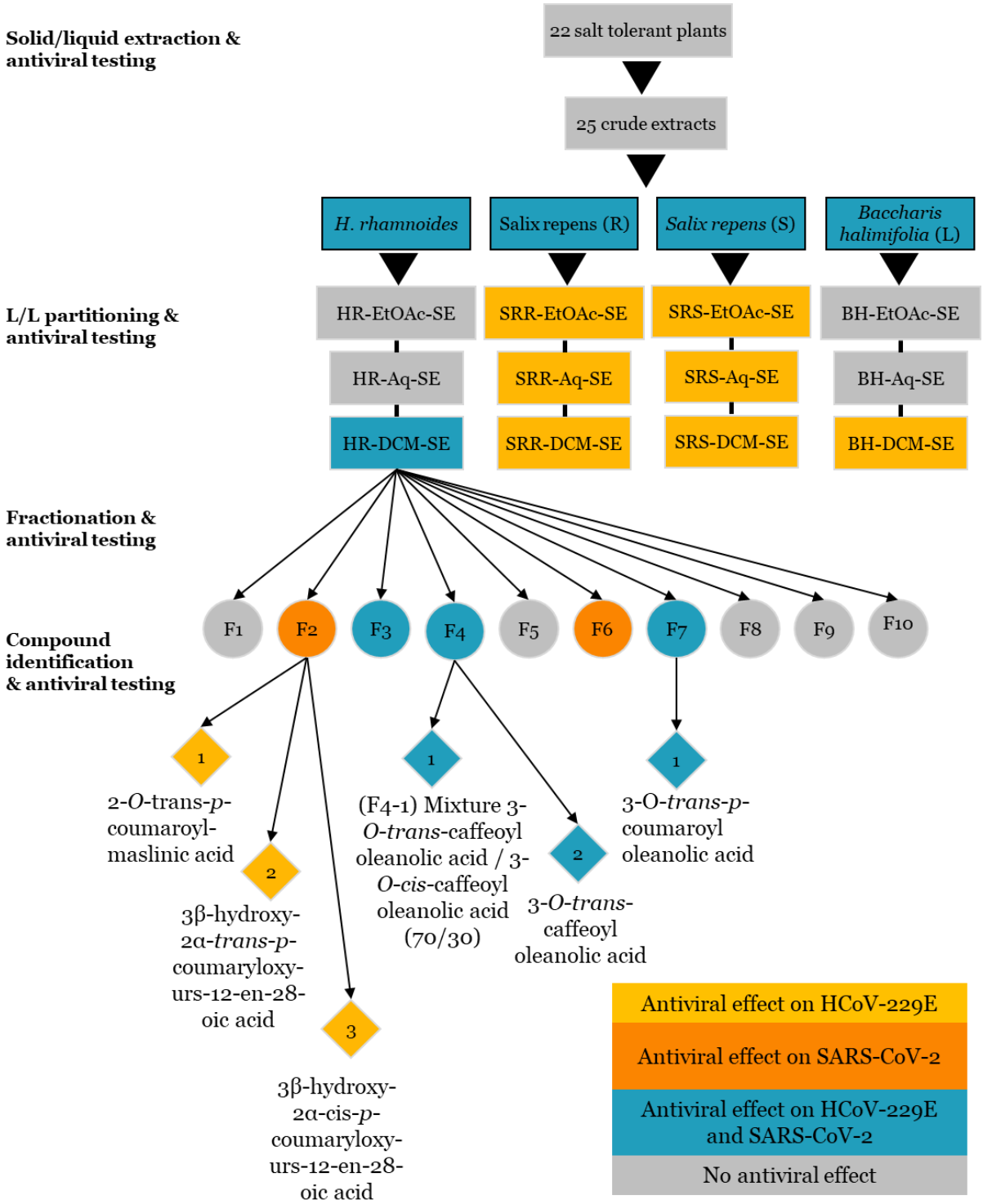

Discussion

In light of the emergence of coronavirus outbreaks and the predictability of future epidemics and pandemics, it has become imperative to discover effective antiviral solutions. Despite the development of vaccines and antiviral drugs, several significant challenges hinder progress, such as unequal access to treatments and vaccines, the emergence of variant strains, and more. Therefore, there is a critical need for effective, accessible, and cost-effective antiviral treatments targeting SARS-CoV-2, especially in low-income countries. Natural products have played a crucial role in the field of drug discovery, particularly in the discovery of antibacterial and anti-tumoral agents. Halophytes and salt-tolerant plants are recognized as abundant sources of specialized metabolites that exhibit a wide range of biological functions, including survival under challenging environmental conditions and defense mechanisms against microorganisms.

In our study, we explored the antiviral potential of halophytes and salt-tolerant plants collected from the North Sea and English Channel coasts in northern France against various coronaviruses. The crude-methanolic extracts of *Hippophae rhamnoides*, *Salix repens* (S and R), and *Baccharis halimifolia* exhibited significant antiviral effects against HCoV-229E and SARS-CoV-2. A recent paper demonstrated the antiviral activity of Salix spp against both seasonal and pandemic coronaviruses (Dhanik Reshamwala et al., 2023). Furthermore, a flavonoid compound, isorhamnetin, isolated from *Hippophae rhamnoides* fruits, displayed antiviral activity against the SARS-CoV-2 spike pseudotyped virus *in vitro* (Zhan et al., 2021). However, no prior research has investigated the antiviral activity of these plants against HCoV-229E.

Hippophae rhamnoides belongs to the Elaeagnaceae family and is native to the cold-temperate regions of Europe and Asia (Rousi, 1971). Sea buckthorn berries are known for their rich nutritional content, including vitamins and specialized metabolites like tocopherols, phenolic acids, carotenoids, flavonoids, tocopherols, and phytosterols (Zakynthinos & Varzakas, 2015; Żuchowski, 2023). Traditional medicine in China and Russia has previously employed this plant to treat dermatological diseases. Additionally, numerous studies have highlighted the pharmacological effects of *Hippophae rhamnoides*, including its antioxidant (S.-J. Kim et al., 2017), antimicrobial (Upadhyay et al., 2010), anti-atherogenic (Basu et al., 2007), cardioprotective (Basu et al., 2007), hepatoprotective (Solcan et al., 2013), radioprotective (Goel et al., 2003), and tissue

regeneration properties (Upadhyay et al., 2011). Nonetheless, research on the antiviral activity of *Hippophae rhamnoides* remains limited.

Liquid–liquid partitioning, combined with simultaneous biological testing, revealed that the HR DCM SE exhibited the most substantial antiviral effect against coronaviruses. Consequently, we decided to narrow our investigation to this specific sub-extract to pinpoint the active fraction and subsequently isolate the bioactive compounds responsible for the antiviral effect against coronaviruses. The nonpolar nature of this sub-extract suggests that the active compounds are rather lipophilic.

Using a bio-guided fractionation approach combining fractionation by CPC and antiviral testing, we identified F3, F4, and F7 as the most potent fractions against HCoV-229E, whereas F2, F3, F4, and F7 were the most effective against SARS-CoV-2. UHPLC-UV-MS analysis revealed the presence of compounds, with a similar absorbance and molecular mass of around 600 $g.mol^{-1}$ found in several fractions, suggesting that analogs contribute to the antiviral activity in different fractions.

Six compounds were isolated from HR DCM SE and identified through NMR and HR-MS analysis as cinnamoyl triterpenoids. Among these, three compounds—2-*O-trans-p*-coumaroyl-maslinic acid, 3β-hydroxy-2α-*trans-p*-coumaryloxy-urs-12-en-28-oic acid, and 3β-hydroxy-2α-*cis-p*-coumaryloxy-urs-12-en-28-oic acid—were isolated from F2 and are derivatives of maslinic acid (MA) and ursolic acid (UA), respectively. The remaining compounds were cinnamoyl derivatives of oleanolic acid (OA), obtained from F4 (mixture of 3-*O-trans*-caffeoyl oleanolic acid/3-*O-cis*-caffeoyl oleanolic acid (70/30) and 3-*O-trans*-caffeoyl oleanolic acid) and F7 (3-*O-trans-p*-coumaroyl oleanolic acid). MA, UA, and OA are common triterpenoids and are known to be abundant in *Hippophae rhamnoides* (Żuchowski, 2023). Despite F2 not demonstrating an antiviral effect against HCoV-229E, the UHPLC-UVMS analysis indicated the presence of a major compound, seemingly a flavonoid, which also proved to be inactive when tested at different doses. However, the antiviral impact of F2 on SARS-CoV-2 prompted us to isolate three other compounds, which are cinnamoyl derivatives of MA and UA. Unexpectedly, these compounds exhibited inhibitory activity against HCoV-229E following separation and isolation, whereas F2 was inactive. This might be due to the fact that these three compounds were present at low levels in F2.

Triterpenoids represent the most widely distributed category of natural compounds, typically originating from the C30 molecular structure, which is synthesized by rearranging six isoprene units following the isoprene rule. They are found in plants either in their free form or as glycosides (saponins). Some of these triterpenoids can, in some cases, be acylated. Among triterpenoids, the tricyclic and pentacyclic varieties are the most abundant (Goel et al., 2003; Solcan et al., 2013). Previous phytochemical studies conducted on different parts of *Hippophae rhamnoides* highlighted the presence of pentacyclic triterpenoids, mostly the oleanane and ursane types, with different biological activities (Żuchowski, 2023). Some cinnamoyl triterpenoids, including 2-*O*-trans-*p*-coumaroyl maslinic acid, 2-*O*-trans-caffeoyl maslinic acid, 3-*O*-trans-*p*-coumaroyl oleanolic acid, and 3-*O*-trans-caffeoyl oleanolic acid have already been isolated from the branch bark of this plant (Z.-G. Yang et al., 2007). Some other derivatives have been tentatively identified in different parts of *Hippophae rhamnoides* by LC-HRMS (Marciniak et al., 2021). Pentacyclic triterpenes, such as analogs or derivatives of OA, have demonstrated various inhibitory activities against viruses, primarily linked to their structures. They have been found to be effective against the influenza virus and hepatitis C virus (HCV) infections. These triterpenes work by binding to viral fusion proteins like hemagglutinin (HA2) of influenza (M. Yu et al., 2014), E2 of HCV (F. Yu et al., 2013), and GP41 of human immunodeficiency virus-1, thus disrupting the entry of the virus into host cells. Further exploration of OA revealed that it can interact with heptad repeat-2 and hinder Ebola virus–cell fusion (Si et al., 2018), shedding light on its mechanism of action against SARS-CoV-2. Additionally, research suggests that OA may act as an inhibitor of viral replication by blocking the activity of SARS-CoV 3CLpro (Ryu et al., 2010). Moreover, friedlane-type triterpenoids isolated from *Euphorbia neriifolia* L. leaves, a drought-tolerant plant, exhibited potent antiviral activity against HCoV-229E cultured in MRC-5 cells (Darshani et al., 2022). The friedelane skeleton could act on multiple targets simultaneously, making it a potential candidate for exerting an antiviral effect against various human coronaviruses. MA is a commonly occurring triterpenoid abundant in the fruits of *Hippophae rhamnoides* (Tkacz et al., 2021). MA has demonstrated a wide spectrum of biological activities, including antibacterial, anti-inflammatory, and antitumor properties. Moreover, in another study, a cinnamoyl maslinic acid named 3-β-O-(trans-p-coumaroyl)-maslinic acid, demonstrated broad antimicrobial activity against

Gram-positive bacteria and yeasts, with a minimum inhibitory concentration of 12.5 μg/mL against *Staphylococcus capitis* and *Candida* albicans (Braca et al., 2000).

UA and OA share similar chemical structures but differ in the position of one methyl group on ring E. UA has been recognized for its anti-inflammatory, antibacterial, antioxidant, anti-diabetic, and anticancer properties. While there are limited data regarding the antiviral activity of UA against HCoV-229E, there are several reports related to its potential against SARS-CoV-2, given their similar morphologies, replication cycles, and symptoms. It has been tested against the SARS-CoV-2 Mpro enzyme and successfully inhibited its activity (S. Ali et al., 2022). Additionally, molecular docking (MD) and molecular dynamic simulation studies have confirmed the ability of UA and its derivatives to interact with SARS-CoV-2 protease during 50 nanoseconds of MD simulation (A. Kumar et al., 2021). UA exhibits high binding affinity, forming a hydrogen bond with the amino group of Asp 108 in the PLpro protease enzyme and engaging in hydrophobic interactions with Ala 107, Pro 248, and Tyr 264 of the same enzyme (Mitra et al., 2022). *In silico* studies suggest that UA could inhibit the interaction between SARS-CoV-2 spike proteins and the receptor ACE-2 (Anbazhagan et al., 2020). However, further confirmation is needed through *in vitro* or *in vivo* studies. In this study, we showed that the antiviral activity of cinnamoyl terpenoids on human coronaviruses is promising. However, they display relatively low SIs (between 1 and 7) due to their cytotoxicity. The toxicity and antiviral assays were performed in Huh-7 cells, which is a hepatoma cell line. It would be interesting to evaluate the cytotoxicity of the compounds in respiratory cell lines or in animal models (*in vivo*). Few studies exist on this type of compound. Furthermore, if the cytotoxicity is high in other cell lines, one could envisage administrating the compound via aerosols (orally or nasally), limiting any toxic side effects. This mode of administration would reach the nasal or bronchial epithelial cells, the sites of viral replication.

Additional work is necessary to determine the mechanism of action of the active isolated compounds against SARS-CoV-2 and HCoV-229E. It would be necessary to determine if they act in the entry or replication step. It is unlikely that one compound could act in both steps; however, it would be very interesting to show that *Hippophae rhamnoides* extract contains a mixture of compounds, with some active on entry and others on replication. It would also be interesting to perform combination assays with the

different compounds to determine if the mixture of all these compounds is more active than each isolated molecule.

Considering all the aforementioned information, it is evident that pentacyclic triterpenoids exhibit anti-coronavirus activity, perhaps due to their structural properties. The presence of cinnamoyl triterpenoid derivatives like MA, UA, and OA, which share structural similarities, in plants like *Hippophae rhamnoides* points to potential antiviral activity, particularly against SARS-CoV-2. Further in-depth investigations are necessary to gain a deeper understanding of their specific targets and mechanisms of action, facilitating their development and ensuring safety, and fully exploring their therapeutic efficacy.

Part II: Exploring the Antiviral Potential of the Invasive Plant *Senecio inaequidens* Against Coronaviruses

Abstract

Senecio inequidens, an invasive plant species in Europe, known for its negative impact on biodiversity, harbors a diverse array of bioactive compounds recognized in traditional medicine. Few studies have explored the antiviral properties of *Senecio inaequidens* and none have specifically investigated its effects on human coronaviruses. Hence, this study aimed to evaluate the *in vitro* activity of *Senecio inaequidens* against coronaviruses. The antiviral effect against HCoV-229E and SARS-CoV-2 was assessed using Huh-7 and Vero-81 cell lines. The crude methanolic extract of *Senecio inaequidens* exhibited a dose-dependent antiviral effect against both viruses, displaying an IC50 ranging between 18.81 µg/ml and 21.17 µg/ml for HCoV-229E and a notable inhibition of SARS-CoV-2. Further partitioning of the active crude extract into three sub-extracts revealed that the dichloromethane sub-extract (SI DCM SE) demonstrated the most potent antiviral activity against both viruses, with IC50 ranges between 23.24 µg/ml and 28.41 µg/ml. The analysis of the chemical composition of SI DCM SE involved ultra-high performance liquid chromatography (UHPLC) coupled with mass spectrometry (MS), followed by fractionation via centrifugal partition chromatography (CPC). Some compounds were isolated from the three most active fractions (F4, F7, and F11) by preparative high-performance liquid chromatography (HPLC) and were identified as cacalolides and one furoeremophilane sesquiterpenoid by high-resolution MS (HR-MS) and nuclear magnetic resonance (NMR). Infection tests revealed varying inhibitory activities of these sesquiterpenoids against HCoV-229E and SARS-CoV-2, with some compounds isolated from F4 displaying activity against both viruses. These findings suggest that *Senecio inaequidens* could potentially serve as a source of antiviral agents against coronaviruses.

Keyword: *Senecio inaequidens*; invasive plant; sesquiterpenes; SARS-CoV-2; HCoV-229E

Results

1. Cytotoxicity and antiviral activity of *S. inaequidens* crude methanolic extract

The cytotoxicity of the crude methanolic extracts of *Senecio inaequidens* was assessed on Huh-7 cells through the MTS assay. Huh-7 cells were treated with two different concentrations of the crude extracts, 25 µg/ml and 100 µg/ml, for 24 h and compared with control cells treated 0.1% DMSO. As shown in **(Figure 47A)**, Huh-7 cells tolerated both concentrations after 24 h of treatment.

In parallel, we investigated the antiviral activity against HCoV-229E infection at a concentration of 25 µg/ml and measured the infection of HCoV-229E-Luc in Huh-7 cells, that express TMPRSS2 protease or not **(Figure 47B)**. A 57.42% and 54.8% reduction in luciferase activity, indicating an antiviral effect against HCoV-229E, was observed with *Senecio inaequidens* crude methanolic extract in Huh-7 cells with or without TMPRSS2, respectively.

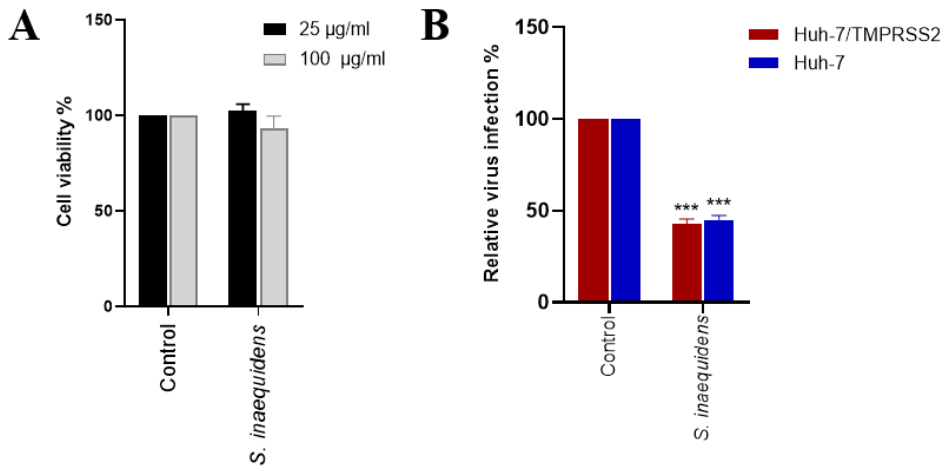

Figure 47. Cytotoxicity of *S. inaequidens* crude methanolic extract. Huh-7 cells were treated with two concentrations, 25 and 100 µg/mL, of the crude extract. Control cells were treated with 0.1% DMSO only. The cells were incubated for 24 h, and an MTS assay was then performed to determine the cell viability (A). Screening of the antiviral activity of *S. inaequidens* crude extract on HCoV-229E-Luc. Huh-7 or Huh-7/TMPRSS2 cells were inoculated with HCoV-229E-Luc in the presence of various plant extracts at 25 µg/mL. Cells were lysed 7 h post-inoculation, and luciferase activity was quantified (B). Experiments were performed in triplicate, with each experiment being repeated thrice. The data bars represent the mean ± SEM. The asterisk indicates a statistical difference compared to the control (***, $p < 0.001$).

2. Dose-response antiviral activity of *S. inaequidens* crude methanolic activity

After identifying the antiviral activity of the *S. inaequidens* crude methanolic extract, we conducted a dose-response antiviral testing experiment on HCoV-229E and SARS-CoV-2. Antiviral assays were performed in Huh-7 and Huh-7/TMPRSS2 cells to cover the two entry pathways, as well as in Vero-81 cells. Simultaneously, the CC_{50} was evaluated, resulting in values of 205 µg/ml in Huh-7 cells **(Figure 48A)**. As shown in **(Figure 48A)**, *S. inaequidens* crude methanolic extract demonstrated a dose-dependent reduction in HCoV-229E infection, confirming its antiviral capacity, with IC50 values of 21.17 µg/ml and 18.81 µg/ml in Huh-7 cells with or without TMPRSS2, respectively. These values allowed the identification of a selectivity index (SI) between 9 and 11.

Similarly, the *S. inaequidens* crude methanolic extract exhibited a high CC_{50} on Vero-81 cells of 362.6 µg/ml **(Figure 48B)**. We further evaluated its inhibitory effect against SARS-CoV-2, and as shown in (**Figure 48C**), the *S. inaequidens* crude extract demonstrated a dose-dependent inhibition of infection, confirming its antiviral activity against SARS-CoV-2.

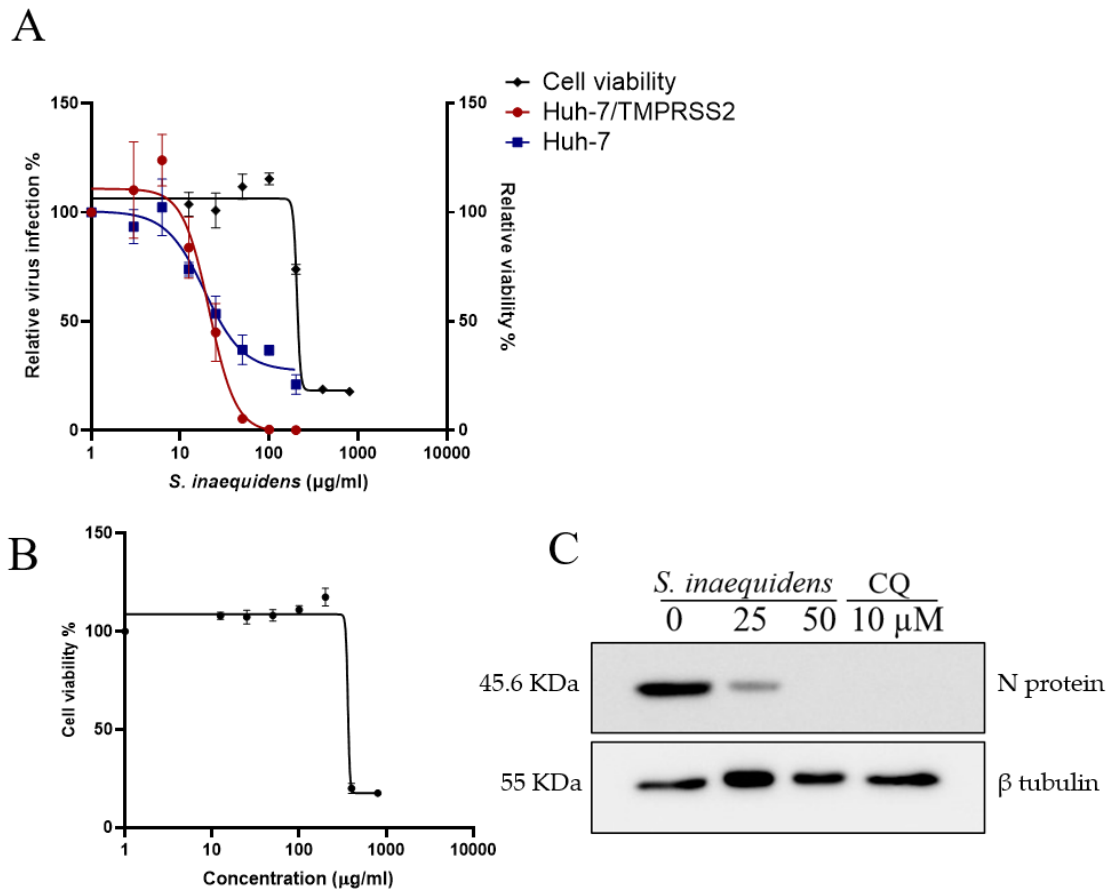

Figure 48. Cytotoxicity and antiviral activity of *S. inaequidens* crude methanolic extract. (A) Assessment of cell viability and inhibition of HCoV-229E infection in Huh-7 and Huh-7/TMPRSS2 cells with increasing concentrations of *S. inaequidens* crude methanolic extract. Infection levels were quantified via luciferase activity measurement. (B) Dose-response curves illustrating the relationship between *S. inaequidens* crude methanolic extract concentration and cell viability, evaluated using the MTS assay in Vero-81 cells after a 24-hour duration. (C) *S. inaequidens* antiviral activity on SARS-CoV-2.

3. Antiviral screening of *S. inaequidens* sub-extracts

A bioguided fractionation assay was performed in order to identify *S. inaequidens* active compounds. First, the crude methanolic extract was subjected to a liquid-liquid partitioning using solvents with increasing polarity yielding a DCM, EtOAc, and Aq sub-extracts. These extracts showed no cytotoxicity when tested at 25 µg/ml and 100 µg/ml on Huh-7 cells **(Figure 49A)**.

Using a well-tolerated cellular concentration of 25 µg/ml, we conducted antiviral testing against HCoV-229E in Huh-7 cells. As illustrated in **(Figure 49B)**, the DCM sub-extracts exhibited the highest infection inhibition compared to EtOAc and Aq sub-extracts, with inhibitory activities of 91.2% and 84.5% in Huh-7 cells with and without TMPRSS2, respectively. Subsequently, we conducted a dose-dependent antiviral test on HCoV-229E. The DCM sub-extract (SI DCM SE) exhibited a dose-dependent inhibitory activity on HCoV-229E with IC_{50} values of 28.41 and 23.4 µg/ml and a selectivity index (SI) ranging between 6 and 8 **(Figure 49C)**.

Likewise, the SI DCM SE showed the highest activity among all sub-extracts against SARS-CoV-2 at 50 µg/ml, significantly reducing N protein expression levels and inhibiting viral replication **(Figure 49D)**. Importantly, this concentration was non-toxic when tested on Vero-81 cells, indicating that the inhibition is attributable to antiviral activity rather than cytotoxicity **(Figure 49E)**.

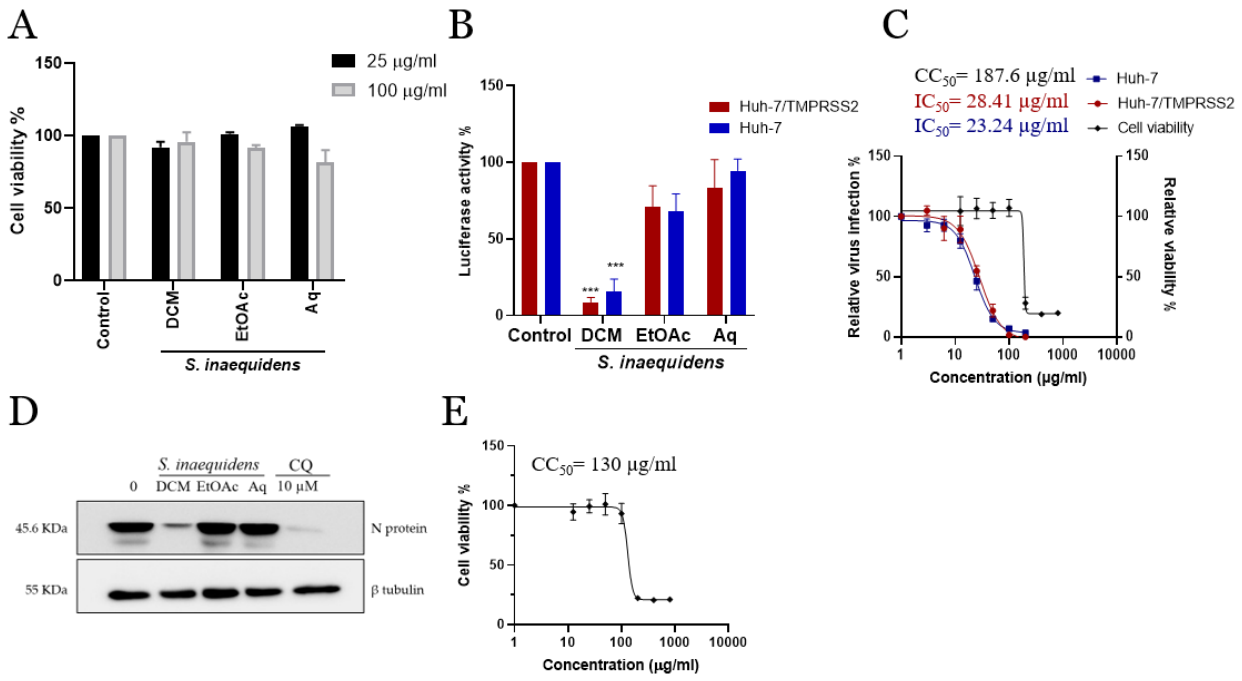

Figure 49. Antiviral activity of *S. inaequidens* sub-extracts on HCoV-229E and SARS-CoV-2. Cytotoxicity on Huh-7 cells (A) and antiviral activity on HCoV-229E (B) of *S. inaequidens* DCM, EtOAc, and Aq sub-extracts. Dose-dependent cytotoxicity on Huh-7 cells and antiviral activity on HCoV-229E of *S. inaequidens* DCM (C). Antiviral activities on SARS-CoV-2 of different *S. inaequidens* DCM, EtOAc, and Aq sub-extracts (D). Dose-dependent cytotoxicity of *S. inaequidens* SI DCM SE on Vero-81 cells at 24 h post-treatment was measured using the MTS assay (E).

4. Purification of the different compounds detected in *S. inaequidens* DCM sub-extract by Centrifugal Partition Chromatography

The SI DCM SE demonstrated potent inhibitory activity against HCoV-229E and SARS-CoV-2 without causing cellular toxicity in Huh-7 and Vero-81 cells. Consequently, we continued the bioguided fractionation on this sub-extract. Analysis of the SI DCM SE by UHPLC-MS revealed the presence of various molecules with different levels of polarity. For the first fractionation of SI DCM SE, we opted for CPC and selected the Arizona system Q as the most convenient choice among 14 different Arizona systems.

Following CPC, we collected 121 fractions, which were subsequently dried and analyzed by UHPLC-UV-MS. Fractions exhibiting similar chromatographic profiles were pooled together, resulting in the consolidation of 12 fractions **(Figure 50)**.

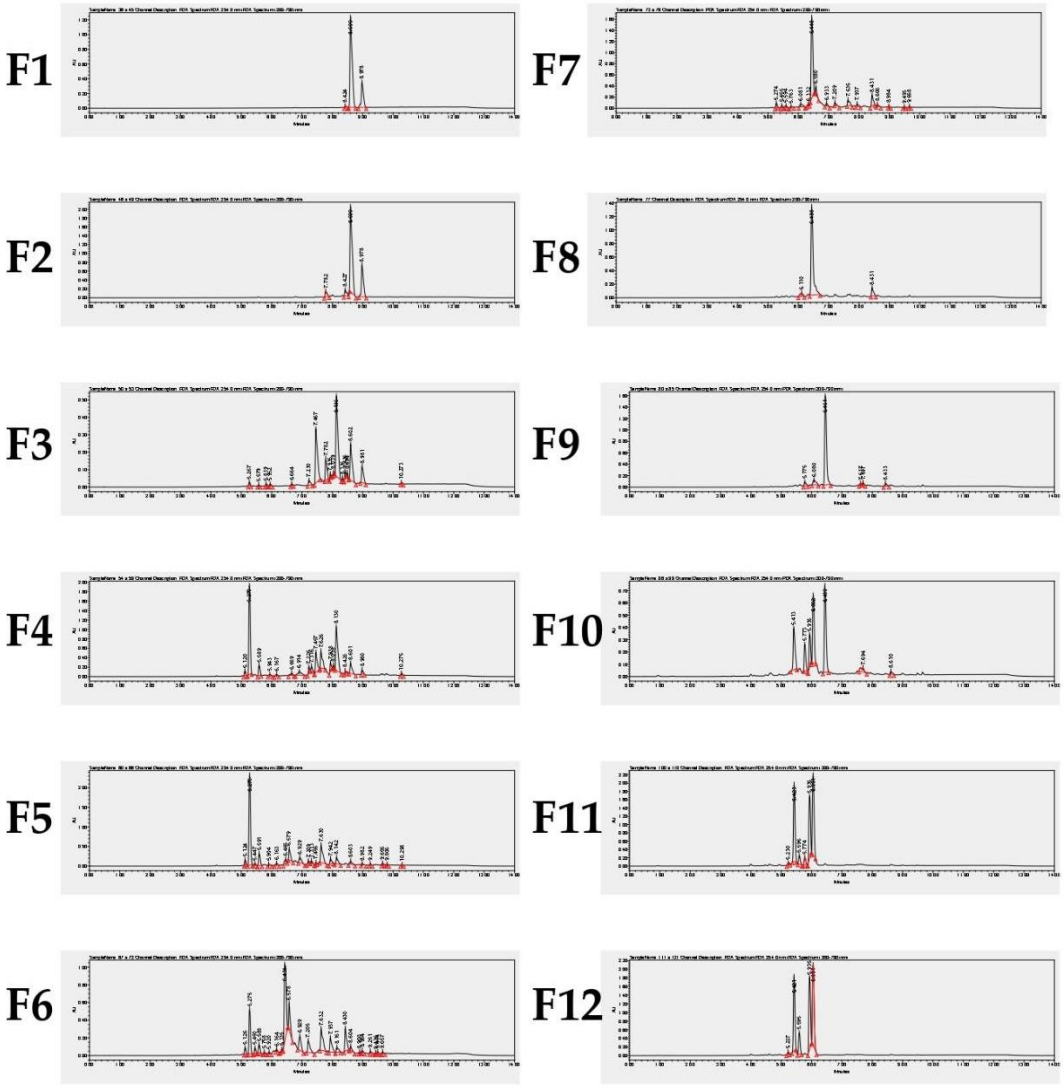

Figure 50. Chromatograms of the twelve fractions obtained from *S. inaequidens* DCM sub-extract after CPC using Arizona system Q. UV chromatogram at 254 nm.

5. Cytotoxic and antiviral screening of the twelve fractions of *S. inaequidens* DCM sub-extract

The MTS assay was employed to evaluate the cytotoxicity of the twelve fractions derived from the *S. inaequidens* DCM sub-extract, obtained through CPC, in both Huh-7 and Vero-81 cells. Each fraction was tested at a concentration of 25 µg/ml, and the cells were incubated for 24 h. Notably, a variability in the susceptibility of the two cell lines to some fractions was observed. Fractions 3, 9, 10, and 11 demonstrated a cytotoxic effect on Huh-7 cells at the concentration of 25 µg/ml, unlike the remaining fractions, which exhibited no cytotoxicity. In contrast, Vero-81 cells displayed higher tolerance to the fractions, showing no cytotoxic effects when tested at the same concentration of 25 µg/ml. **(Figure 51)**.

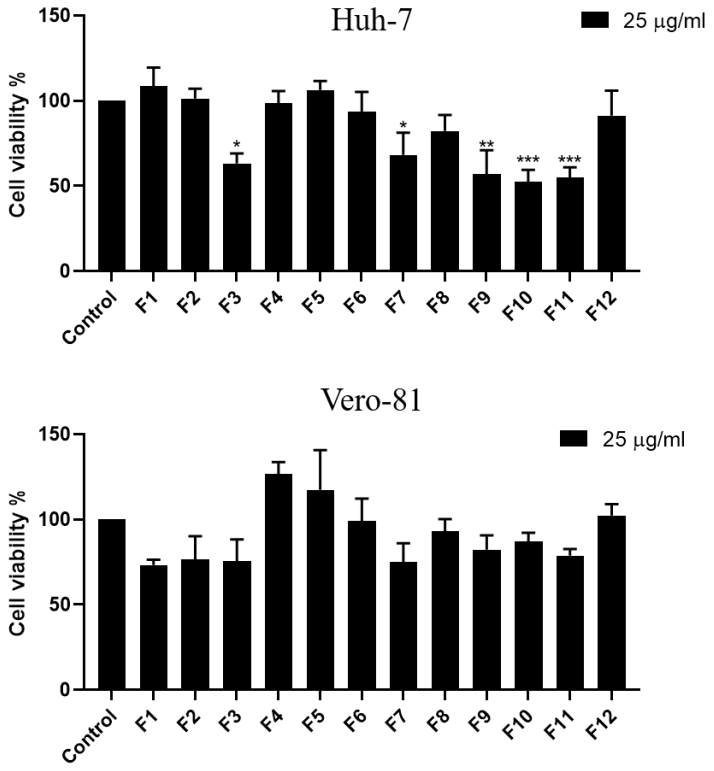

Figure 51. Cytotoxicity of the fractions obtained by CPC. Huh-7 and Vero-81 cells were incubated for 24 h with fractions at 25µg/ml. The fractions showed variation in toxicity on Huh-7 cells but no toxicity on Vero-81 cells. Data are represented as mean ± SEM of three independent experiments (*, $p < 0.05$**, $p < 0.01$; ***, $p < 0.001$).

Simultaneously, we evaluated the antiviral efficacy of the various fractions against HCoV-229E-Luc in Huh-7 cells, irrespective of TMPRSS2 protease expression. Huh-7

cells were infected with the virus and treated with each fraction at 25 μg/ml for 7 h. Infection levels were quantified using a luciferase assay. All fractions exhibited a reduction in virus infection levels, except for fraction F1 when compared to the negative control. However, the level of inhibition varied among the different fractions. F3, F4, F7, F8, and F9 demonstrated the highest antiviral activity, resulting in a one-log decrease in HCoV-229E infection in both Huh-7 and Huh-7/TMPRSS2 cells **(Figure 52A)**. It is important to note that some active fractions were also cytotoxic.

Similarly, the antiviral activity of the fractions was tested against SARS-CoV-2 at 10 and 25 μg/ml. All fractions displayed a dose-dependent antiviral activity against SARS-CoV-2. Consistent with HCoV-229E, all fractions exhibited a significant antiviral effect at 25 μg/ml, except for F1, F2, and F12. F4 and F5 were the most active, showing a 96% decrease in infection levels, and fractions F3, F7, F8, F9, and F11, displaying over 80% inhibition **(Figure 52B)**. The observed inhibitory activity in different samples may be attributed to the repetitive presence of the same class of specialized metabolites in the various fractions. Thus, active fractions against SARS-CoV-2 or both, with relatively simpler chromatograms, in particular F4, F7 and F11, were selected for further compound isolation and characterization.

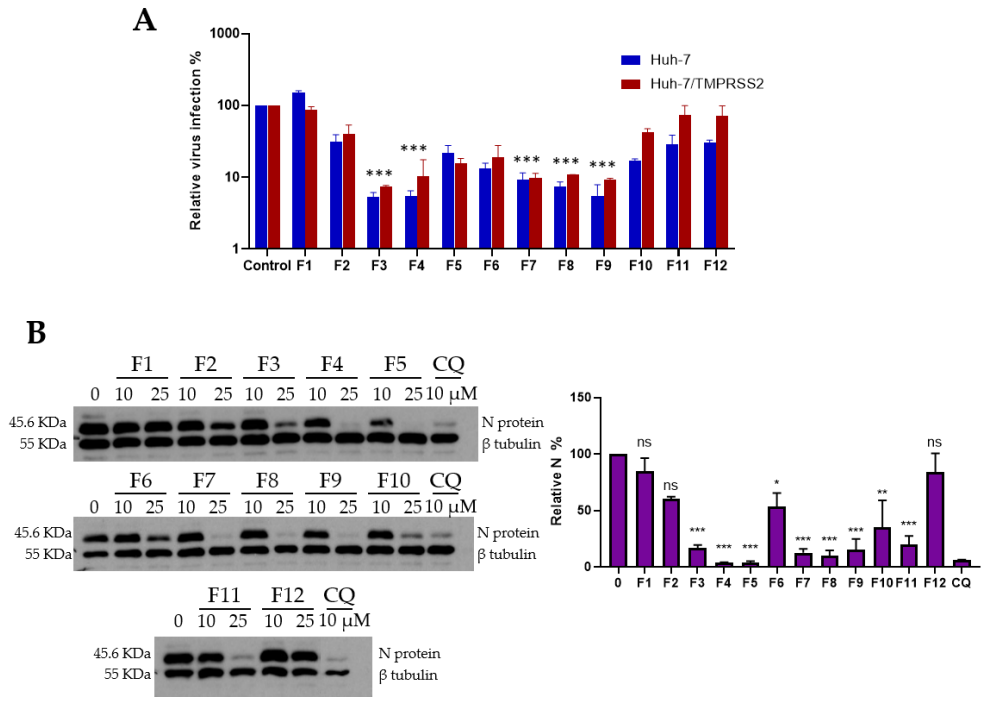

Figure 52. *S. inaequidens* DCM fractions antiviral activity. (A) Antiviral effect of *S. inaequidens* fractions obtained from the DCM sub-extract on HCoV-229E. (B) *S. inaequidens* DCM fractions treatment inhibited SARS-CoV-2 infection. LC3-II and N protein expression was evaluated in Vero-81 cells by Western blotting and normalized to the tubulin signal. Data values represent the mean ± SD. *, $p \leq 0.05$; **, $p \leq 0.01$; ***, $p \leq 0.001$.

6. Isolation of compounds by preparative HPLC and identification by HRMS and NMR

To identify the active compounds responsible for the antiviral effect against both viruses, a preparative HPLC procedure was conducted. First, fractions underwent analysis using analytical HPLC to determine the most effective purification method by preparative HPLC. We chose to purify the compounds with sufficiently high contents in the different active fractions, then allowing them to be obtained in sufficient quantities to test them; some fractions being sometimes relatively complex. These compounds were then purified through preparative HPLC using the same stationary phase. The same gradient was applied for F4 and F7; it was different for F11. Fraction F4 underwent purification using a gradient system resulting in the isolation of compounds **F4-1** (tr = 16.8 min, 11.8 mg, MW = 302 g/mol), **F4-2** (tr = 19.7 min, 2.1 mg, MW= 288 g/mol), **F4-3** (tr = 17.3 min, 2.1 mg, MW = 230 g/mol), **F4-4** (tr = 17.8 min, 6.5 mg, MW = 326+ 366 g/mol), and **F4-5** (tr = 18.8 min, 17.4 mg, MW = 330 g/mol). The primary compound,

F7-1 (tr = 20 min, 7.5 mg, MW = 272 g/mol), was purified from fraction F7 using a gradient system. Fraction F11 was subjected to fractionation, yielding compounds **F11-1** (tr = 12.9 min, 6 mg, MW = 288 g/mol), **F11-2** (tr = 13.6 min, 3.75 mg, MW = 288 g/mol), **F11-3** (tr = 14.6 min, 3.6 mg, MW = 286 g/mol), and **F11-4** (tr = 17.4 min, 10.1 mg, MW = 286 g/mol). **(Figure 53 and S3)**. Taken together, **F4-1**, **F4-2**, **F4-3**, **F4-5**, **F7-1**, **F11-1**, **F11-2**, **F11-3**, **F11-4** were identified as eight sesquiterpenoid derivatives. Their purities were, respectively, estimated at 99,71, 99.17, 90.56, 94.31, 90.87, 98.89, 96.74, 91.4 and 99.95% on the basis of PDA chromatograms. **F4-4** was not obtained pure despite several tentatives and it obtained as a mixture of two products with respective purity of 60.48 and 32.18%. The pure compounds were identified as: 2-methoxy-*O*-methyl-1-oxo-2,3-dehydrocacalol (**F4-1)**, (6*R*) 1-hydroxy-2-methoxy-1,2,3,4-dehydrocacalone (**F4-2 = F11-2)**, cacalol (**F4-3)**, butanoic acid, 3-methyl-, 4,4a,5,6,7,9-hexahydro-3,4a,5-trimethyl-9-oxonaphtho[2,3-*b*]furan-4-yl ester, [4*S*-(4α,4aα,5α)]- (9CI) (**F4-5)**, 1-hydroxy-2-methoxy-1,2,3,4-dehydro-6-dehydroxycacalone (**F7-1)**, (6*S*) 1-hydroxy-2-methoxy-1,2,3,4-dehydrocacalone (**F11-1)**, (6*R*) 1-hydroxy-2-methoxy-1,2,3,4-dehydrocacalone (**F11-2 = F4-2)**, 1,2-dimethoxy-1,2,3,4-dehydro-6-dehydroxycacalone (**F11-3)**, and 2,3-dehydro-2-methoxy-1-oxocacalol methyl ether (**F11-4) (Figure 54 and S4)**. Their structures were established through a comparison of their physical and spectral data, including HRMS and extensive 1D- and 2D-NMR data, with reported values (Bohlmann et al., 1977; Burgueño-Tapia et al., 2001; Dupré et al., 1991). The structures were also checked on SciFinder in order to find their CAS number. On SciFinder, usually only one configuration was found. Some publications on these compounds are in general old. Their structural elucidation must be comforted. Measuring their rotating power or studies of circular dichroism would also be necessary. Also, we obtained certain discrepancies between HRMS and NMR data for F4-1, F4-2, F11-3 and F11-4 which need to be resolved.

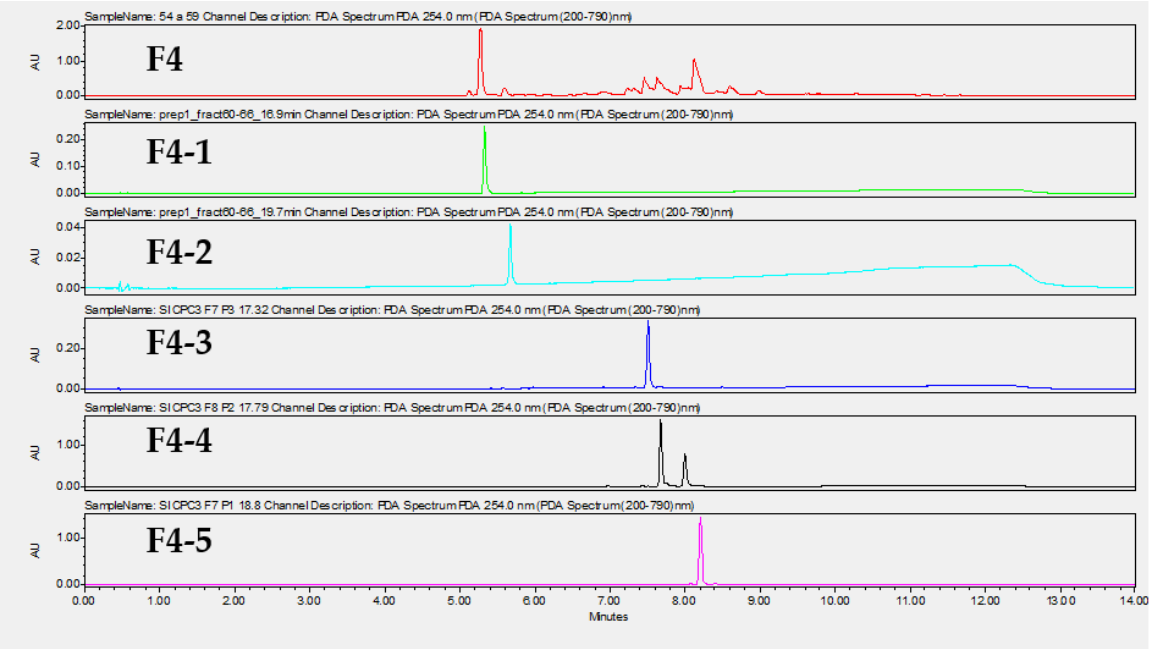

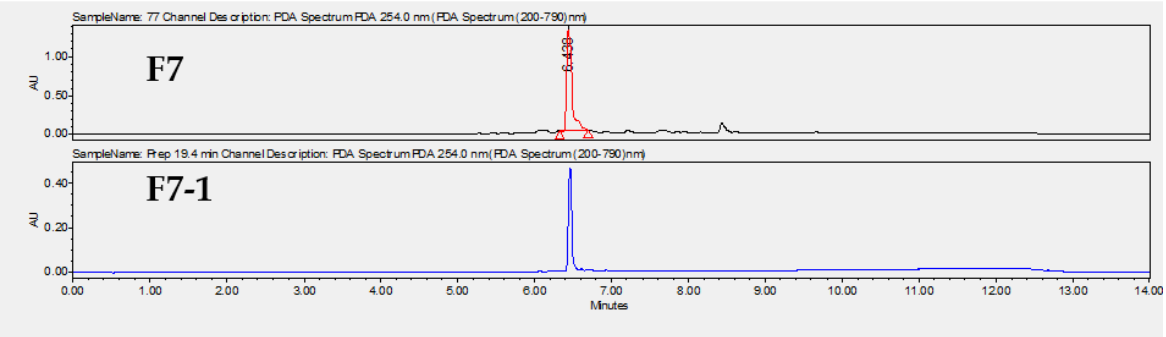

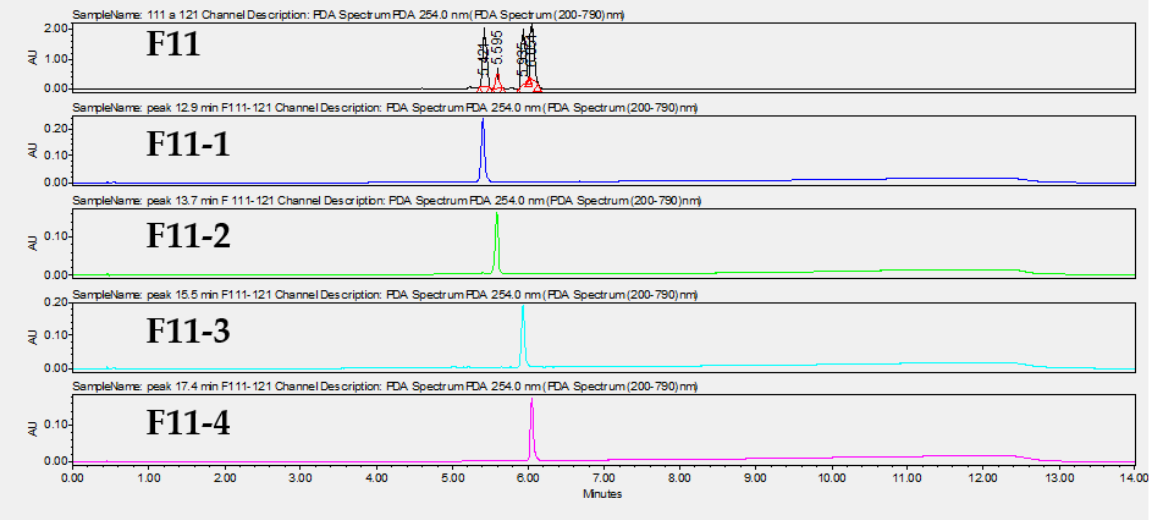

Figure 53. Chromatograms at λ = 254 nm obtained by UHPLC-UV-MS of F4, F7 and F11, as well as purified compounds obtained by preparative HPLC. Retention times in minutes for F11-1=5.405, F11-2=5.587, F11-3= 5.935, F11-4= 6.051, F7-1=6.459, F4-1= 5.334, F4-2= 5.672, F4-3= 7.511, F4-4= 7.680 and 8.002, F4-5= 8.201.

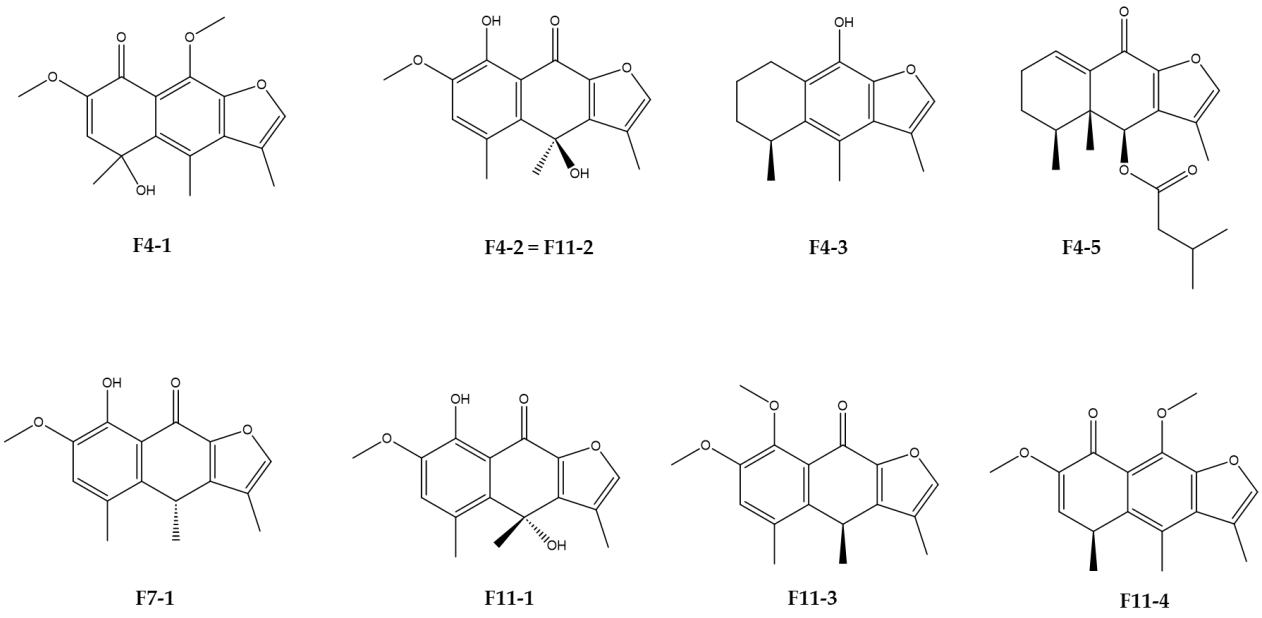

Figure 54. Chemical structures of the sesquiterpenoids purified from fractions F4, F7, and F11 resulting from CPC fractionation of the DCM sub-extract of *S. inaequidens*.

7. Cytotoxicity and antiviral activity of the purified compounds on HCoV-229E and SARS-CoV-2

To ascertain if the purified compounds are accountable for the antiviral impact on both types of coronaviruses, we performed toxicity assays and the dose-response antiviral assays. First, Huh-7 cells and Vero-81 cells were incubated with the various compounds across a range of concentrations up to 100 µM for a duration of 24 h, and toxicity was measured. At the maximum concentration tested, none of the purified compounds displayed any harmful effects except for **F4-5**, which demonstrated CC50 values of 14.5 µM and 9.7 µM, in Huh-7 and Vero-81 cells respectively, indicating some cytotoxicity **(Figure 55 and 56)**.

Huh-7

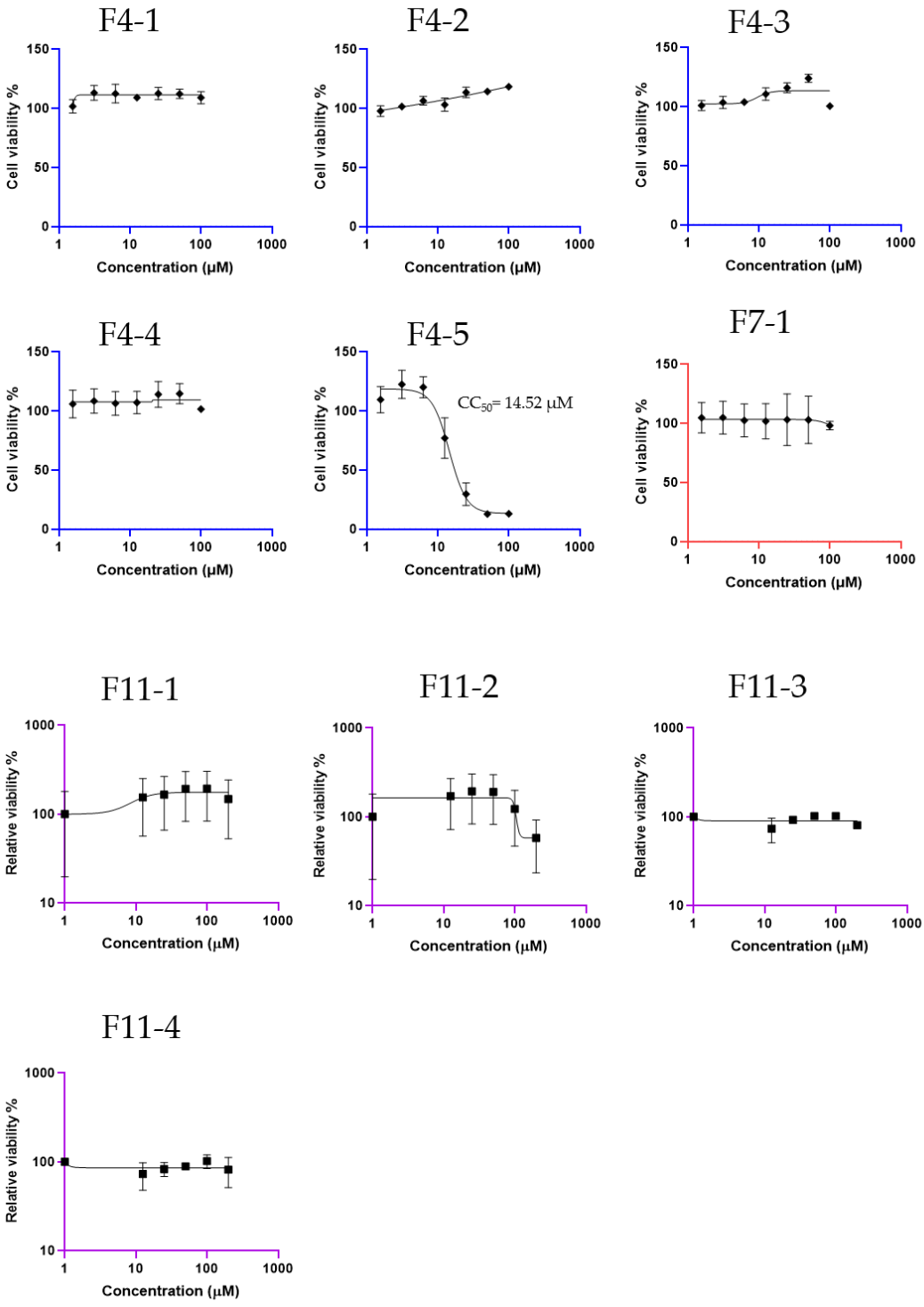

Figure 55. Dose-response curves showing cell viability as a function of purified compounds concentration, measured with the MTS assay in Huh-7 cells, after 24 h. Data points are mean ± SD.

Vero-81

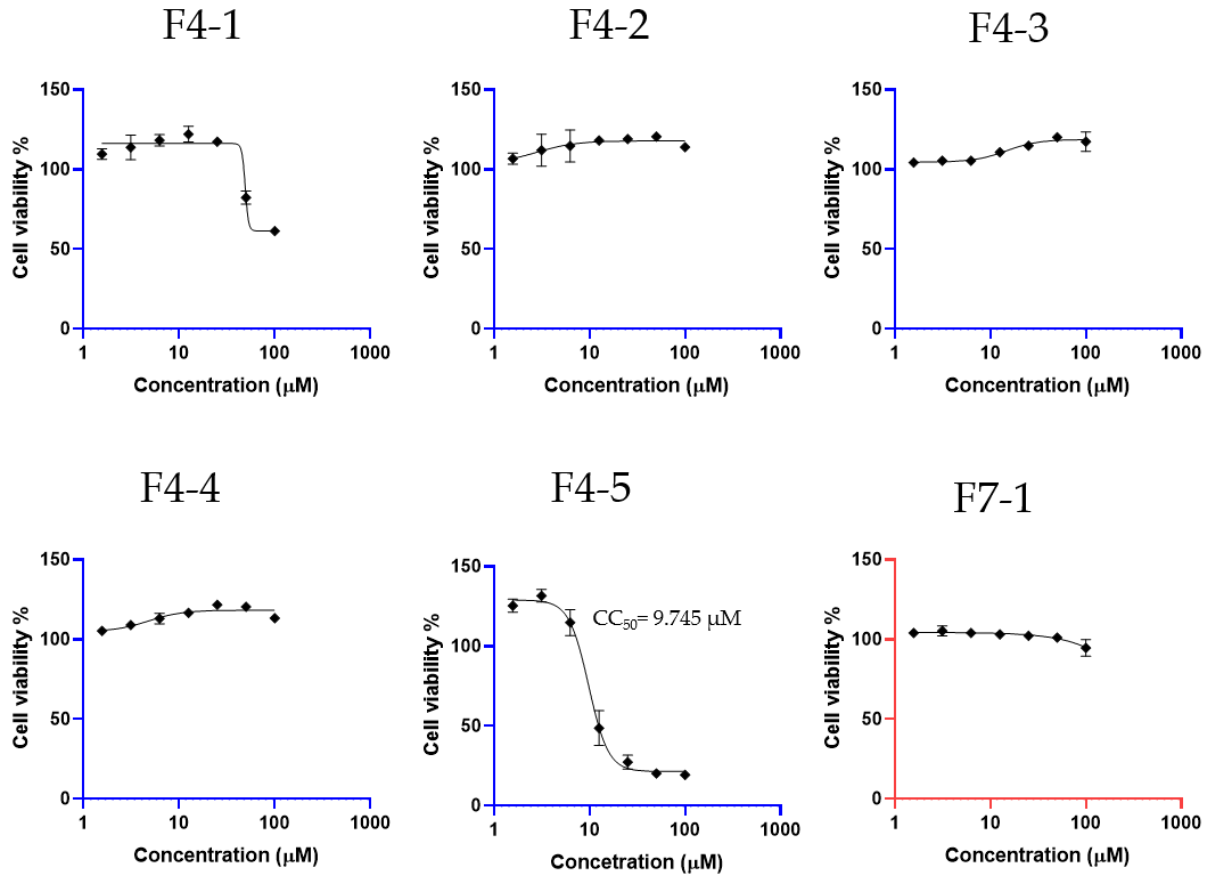

Figure 56. Dose-response curves showing cell viability as a function of purified compounds concentration, measured with the MTS assay in Vero-81 cells, after 24 h. Data points are mean ± SD.

Antiviral testing against HCoV-229E revealed that six compounds from F7 and F4 demonstrated a dose-dependent antiviral effect in both Huh-7 and Huh-7/TMPRSS2 cells **(Figure 57)**. Conversely, the four compounds derived from F11 did not display any antiviral potential (data not shown). Notably, F4-4 exhibited the most promising performance, indicating IC50 values of 10.77 μM and 14.79 μM in Huh-7 and Huh-7/TMPRSS2 cells, respectively, with an SI index exceeding 6. Despite F4-5 demonstrating the lowest IC50 value, this compound exhibited toxicity at low concentrations, resulting in a relatively lower SI (< 4) **(Table 7)**.

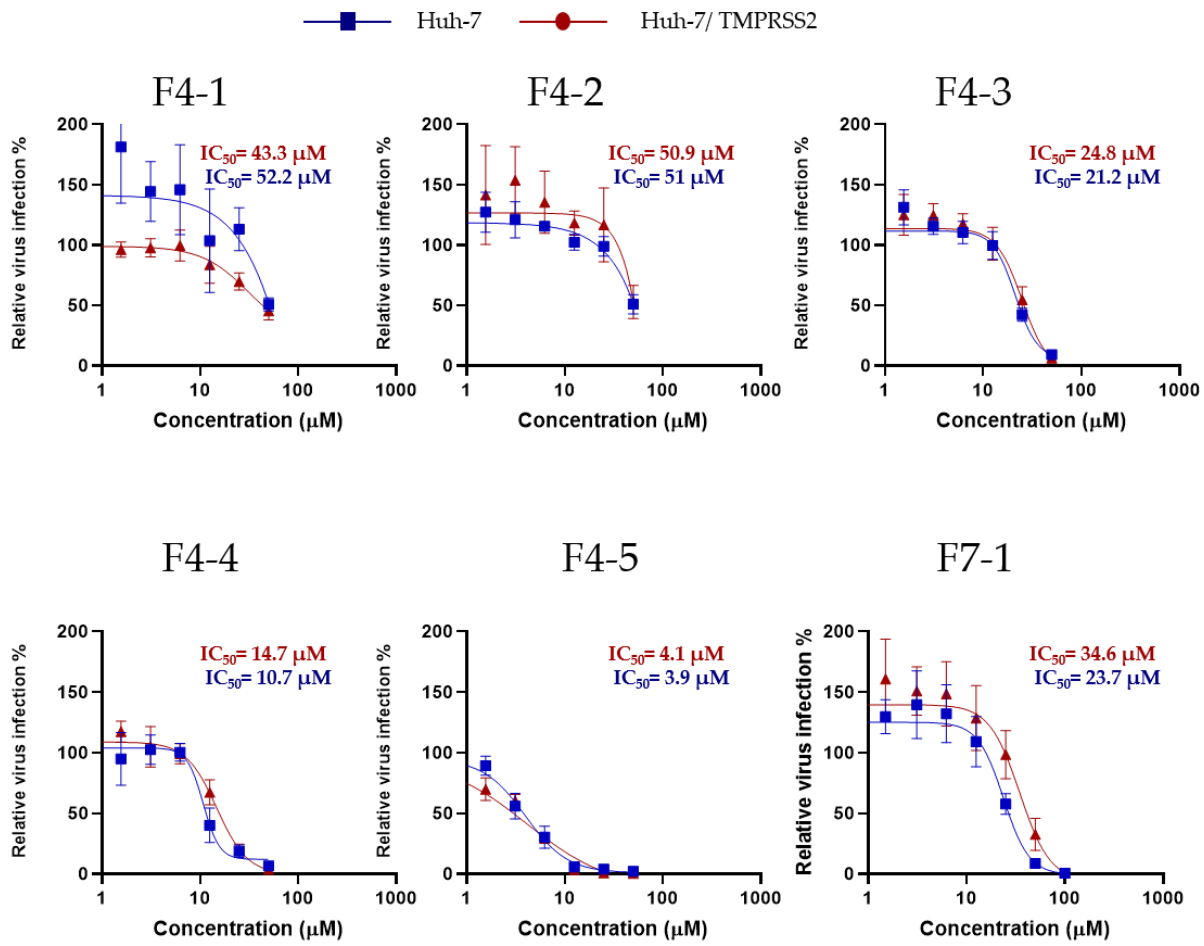

Figure 57. Inhibition of HCoV-229E infection of Huh-7 cells in the presence of increasing concentrations of the purified compounds. The infection was quantified by measuring luciferase activity.

Table 7. Toxicity, activity, and SI selectivity index of each of the isolated compounds against HCoV-229E.

Purified compounds	Huh-7 CC50 (µM)	Huh-7		Huh-7/ TMPRSS2	
		IC50 (µM)	SI	IC50 (µM)	SI
F4-1 2-methoxy-*O*-methyl-1-oxo-2,3-dehydrocacalol	>100	52.2	>1.9	43.3	>2.3
F4-2 (6*R*) 1-hydroxy-2-methoxy-1,2,3,4-dehydrocacalone	>100	51	>1.9	50.9	>1.9
F4-3 Cacalol	>100	21.2	>4.7	24.8	>4
F4-4 unidentified mixture	>100	10.7	>9.3	14.7	>6.8
F4-5 Butanoic acid, 3-methyl-, 4,4a,5,6,7,9-hexahydro-3,4a,5-trimethyl-9-oxonaphtho[2,3-*b*]furan-4-yl ester, [4*S*-(4α,4aα,5α)]- (9CI)	14.52	3.9	3.7	4.1	3.5
F7-1 1-hydroxy-2-methoxy-1,2,3,4-dehydro-6-dehydroxycacalone	>100	23.7	4.2	34.6	>2.8

Ultimately, we investigated the antiviral impact of six compounds— **F4-1**, **F4-2**, **F4-3**, **F4-4**, **F4-5**, and **F7-1** —on SARS-CoV-2 at varying concentrations. Four compounds exhibited a noticeable, dose-dependent reduction in N protein levels in SARS-CoV-2 infected cells, indicating their potential antiviral effects. Specifically, **F4-4** and **F4-5** showcased the highest antiviral activity. The mixture **F4-4** notably inhibited SARS-CoV-2 by 75.1% and 99.14% at 25 µM and 50 µM, respectively, whereas **F4-5** demonstrated a significant reduction in infection by 51% at 3.1 µM, 68% at 6.2 µM, and 93.3% at 12.5 µM. However, **F4-5** exhibited high antiviral efficacy at 50 µM but also showed toxicity at this concentration **(Figure 58)**.

On the other hand, both **F4-1** and **F4-3** displayed substantial inhibitory effects, reaching 52% and 56.1%, respectively, but only at a concentration of 50 µM. Surprisingly, even though F7 showed an antiviral effect on SARS-CoV-2, the purified compound, **F7-1,** did not exert an antiviral effect on SARS-CoV-2 **(Figure 58)**. Collectively, these results

demonstrate that several compounds isolated from *S. inaequidens* DCM sub-extract possess antiviral activities against both HCoV-229E and SARS-CoV-2.

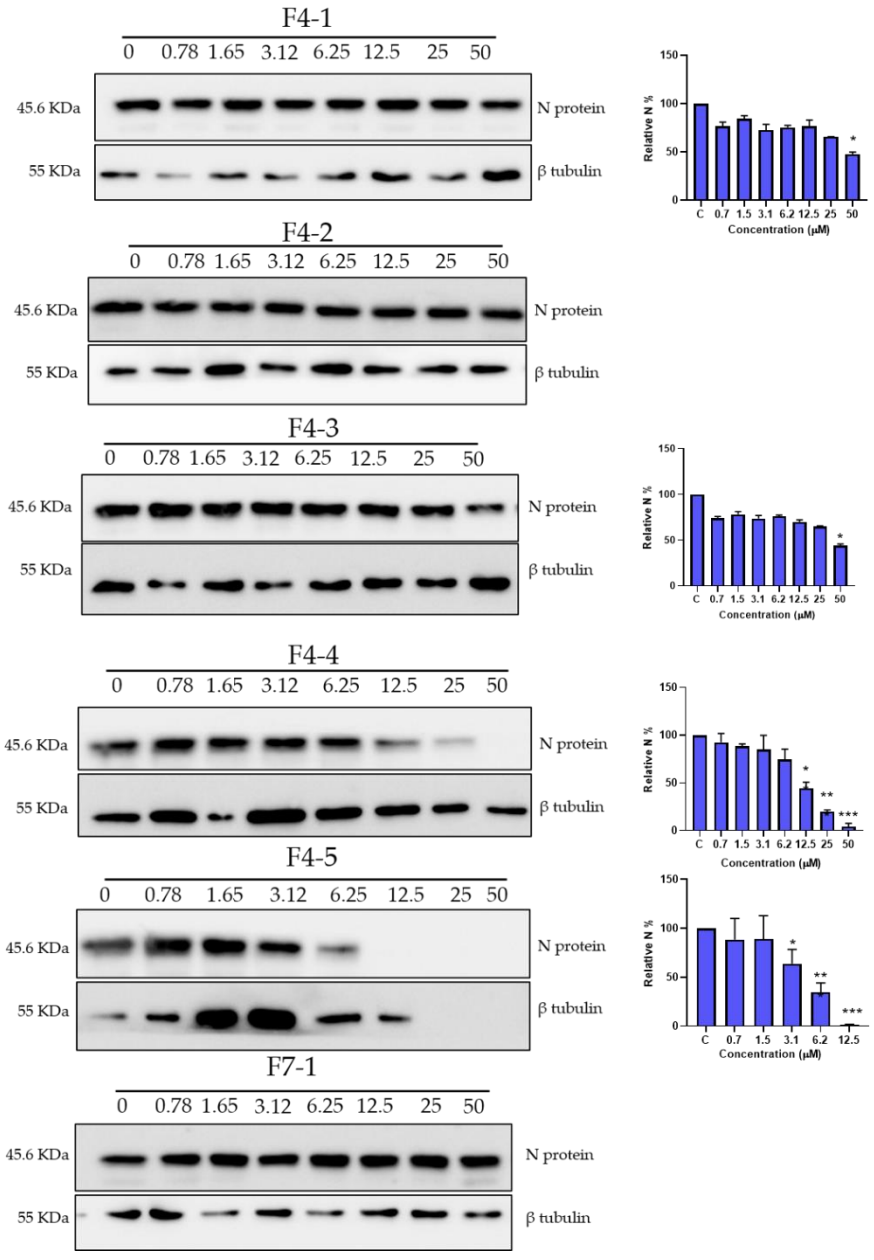

Figure 58. The antiviral impact of F4-1, F4-2, F4-3, F4-4, F4-5 and F7-1 against SARS-CoV-2 was assessed through western blot analysis. Vero-81 cells were exposed to varying concentrations of the different compounds for 16 h. Cell lysates were collected and underwent western blot analysis. The data values presented represent the mean ± SD from three independent experiments; significance levels were denoted as (* for $P < 0.05$, ** for $P < 0.01$, and *** for $P < 0.001$).

Graphical Abstract: Exploring the Antiviral Potential of Invasive Plant *Senecio inaequidens* Against Coronaviruses

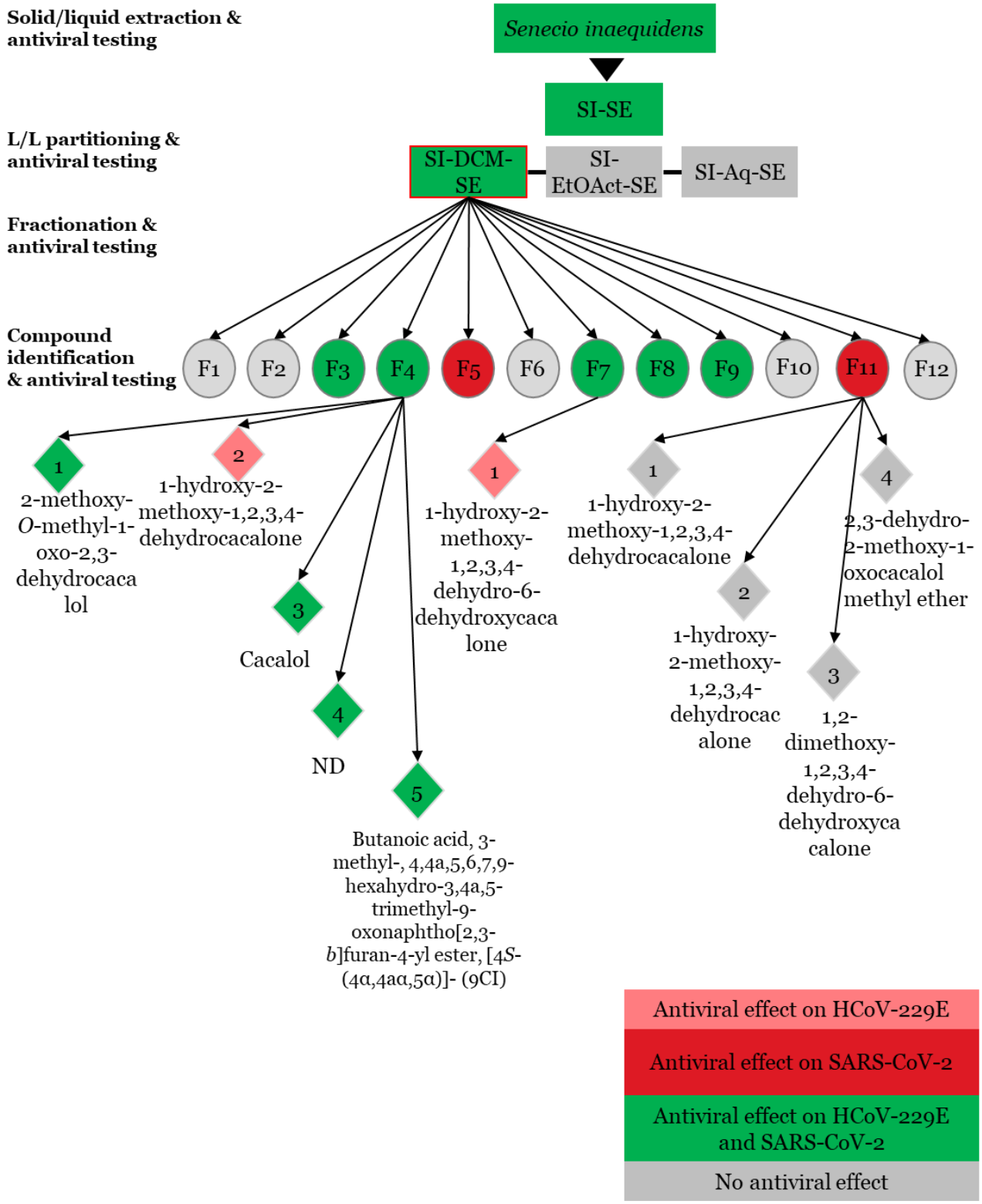

Discussion

The rise of coronavirus outbreaks, including pandemics, has posed a significant threat to global public health. The SARS-CoV-2 outbreak has persisted for four years and is anticipated to continue spreading in the future. Despite extensive efforts to create effective treatments for COVID-19, only two drugs, paxlovid, and remdesivir, have been authorized for treating COVID-19. This highlights the urgent need for developing more effective agents against SARS-CoV-2 (CDC, 2020b). Plant-based natural compounds offer a valuable source for designing new antiviral drugs. Several natural products have exhibited strong antiviral effects against viruses like SARS- CoV, MERS-CoV, HCoV-229 E, and HCoV-OC43 (Cheng et al., 2006; D. E. Kim et al., 2019; J. Y. Kim et al., 2018; S.-Y. Li et al., 2005; Meunier et al., 2022; C.-Y. Wu et al., 2004). Invasive plants, although they are rich in phytochemical components that can contribute to their harmful environmental impact due to their invasive nature, paradoxically possess an underestimated biological potential allowing the identification of pharmacologically active ingredients. The study was conducted on several invasive plants but we focused on the potential of *Senecio inaequidens* in order to extract and identify the specialized metabolites involved in its anti-coronavirus potential.

S. inaequidens, a member of the Senecioneae tribe within the Asteraceae family, holds a significant historical presence in chinese traditional medicine. *Senecio species* has been used either solely or in conjunction with other ingredients in more than 100 chinese medicinal plant preparations, such as *Qianbai Biyan Pian*, *Qian Li Guang Pian*, and *Qingre Sanjie Pian*. It has been utilized as a remedy for various conditions like bacterial diarrhea, enteritis, conjunctivitis, respiratory tract infections, hepatitis B, dermatosis, and inflammation (S.-Y. Li et al., 2005; Roeder, 2000). Originally native to South Africa, *S. inaequidens* has considerably expanded its distribution in Europe and around the world. Its presence has become widespread and it has become invasive in northern and central Europe due to accidental introduction via wool imported from South Africa in the late 1800s. This plant demonstrates extensive ecological adaptability, thriving in a wide range of environments, including both dry and moist conditions, various soil types from stone to clay, and locations ranging from sunny to shady (Scher et al., 2015).

In our study, *S. inaequidens* was collected from the coastline in a sand dune area in Zuydcoote, France and was frequently exposed to high soil salinity, high temperature, low nutrients, and limited water availability. A previous report published by the European Public Prosecutor's Office demonstrated that *S. inaequidens* colonizes open and disturbed lands such as wastelands, fallows, railways and roadsides, crops (mainly vineyards), burnt lands and pastures (EPPO Global Database, 2006). Furthermore, this plant species is also found in natural environments such as dunes and cliffs in littoral areas, and temporary ponds in France (Brunel S, 2003).

Methanol was chosen as the preferred solvent to perform initial solid/liquid extraction in our study. Methanol is recognized for its excellent solvent properties and is commonly employed in biological processes due to its polarity (Sultana et al., 2009). Its efficacy in extraction surpasses that of ethanol and other solvents, enabling the retrieval of both lipophilic and hydrophilic molecules or compounds. Additionally, its low boiling point facilitates easy removal at room temperature owing to its higher volatility, presenting another advantage in the extraction process (Truong et al., 2019).

The crude methanolic extract obtained from *S. inaequidens* exhibited antiviral effects against human coronaviruses. A previously published study demonstrated that through docking studies performed on *Senecio massaicus*, certain compounds exhibited robust interactions with both the SARS-CoV-2 main protease and Nsp15 endoribonuclease. This suggests that Senecio species harbor potential bioactive compounds as candidates for combating coronaviruses (Kebbi et al., 2021). However, no *in vitro* studies were carried out to confirm this hypothesis.

The secondary metabolites of *Senecio* species have been extensively studied, encompassing alkaloids including pyrrolizidine alkaloids (PAs) (Bohlmann et al., 1986), monoterpenoids (Bohlmann et al., 1985) and sesquiterpenoids (Bohlmann & Ziesche, 1981) found in essential oils (X. Yang et al., 2011), as well as diterpenoids (Mohamed et al., 2022), triterpenoids (Torres et al., 1998), and phenolic compounds (Díaz et al., 2015). Senecio plants are known to produce PAs, recognized as hepatotoxins and carcinogens affecting numerous animal species, including most livestock (G. M. Williams et al., 1980). Cases of liver tumors and pulmonary lesions observed in experimental animals raised

concerns, particularly regarding hepatotoxicity, carcinogenicity, and the presence of PAs in the human diet. Human toxicosis cases have been documented due to accidental contamination with medicinal species (Van Schalkwyk et al., 2021), honey contamination by bees (Valese et al., 2021), lateral transfer of toxic alkaloids in tea plantations (Van Wyk et al., 2017), and water contamination (Hama & Strobel, 2021; Kisielius et al., 2020). Although the chemical profile of *Senecio* species is recognized for the presence of pyrrolizidine alkaloids and the genus exhibits considerable chemical diversity, certain Senecio taxa are richer in terpenoids (Bisht et al., 2023; Sadgrove, 2022).

To further characterize the bioactive compounds present in the crude methanolic extract of *S. inaequidens*, we carried out a liquid-liquid partitioning using 3 different solvents of increasing polarities. The DCM sub-extract showed the highest antiviral activity against both viruses indicating that the antiviral compounds are relatively apolar. The fractionation of *S. inaequidens* DCM sub-extract, produces 12 fractions, 4 of them where highly active against HCoV-229E and SARS-CoV-2. The presence of antiviral activity in different fractions could be attributed to the presence of the same class of compounds in the different fractions. The identified compounds are: 2-methoxy-*O*-methyl-1-oxo-2,3-dehydrocacalol (**F4-1)**, (6*R*) 1-hydroxy-2-methoxy-1,2,3,4-dehydrocacalone (**F4-2 = F11-2)**, cacalol (**F4-3)**, butanoic acid, 3-methyl-, 4,4a,5,6,7,9-hexahydro-3,4a,5-trimethyl-9-oxonaphtho[2,3-*b*]furan-4-yl ester, [4*S*-(4α,4aα,5α)]-(9CI) (**F4-5)**, 1-hydroxy-2-methoxy-1,2,3,4-dehydro-6-dehydroxycacalone (**F7-1)**, (6*S*) 1-hydroxy-2-methoxy-1,2,3,4-dehydrocacalone (**F11-1)**, (6*R*) 1-hydroxy-2-methoxy-1,2,3,4-dehydrocacalone (**F11-2 = F4-2)**, 1,2-dimethoxy-1,2,3,4-dehydro-6-dehydroxycacalone (**F11-3)**, and 2,3-dehydro-2-methoxy-1-oxocacalol methyl ether (**F11-4)**. Some of these compounds have been previously isolated from *S. madagascariensis* found in South America (Burgueño-Tapia et al., 2001).

These compounds were identified as cacalolides and one furoeremophilane. But their structural identification is still in progress and need to be comforted, in particular their configuration. These compounds fall under the category of sesquiterpenes. Sesquiterpenes, composed of three isoprene units forming C15-terpenoids, occur naturally as hydrocarbons or in various oxygenated forms such as lactones, alcohols, carboxylic acids, aldehydes, and ketones (Awouafack et al., 2013). Typically, most

sesquiterpenes possess cyclic structures and encompass aromatic constituents displaying diverse pharmacological activities. These compounds and their derivatives have gained attention in drug discovery due to their important biological properties (Bartikova et al., 2014; Chopra & Dhingra, 2021; Moujir et al., 2020). Recent efforts in the development of new medications derived from natural products have unveiled various pharmacological activities exhibited by sesquiterpenes. These include antimalarial (Chaturvedi et al., 2010; Toyang et al., 2013), anti-leishmanial (Cortés-Selva et al., 2005), antifungal (Duraipandiyan et al., 2012; Feng et al., 2010), antibacterial (Cantrell et al., 1999; Sotanaphun et al., 1999), antiviral (Sotanaphun et al., 1999), antifeedant, cytotoxic (Cerda-García-Rojas et al., 2010; David et al., 1999), anti-inflammatory ones (Lyß et al., 1998; H. R. Wong & Menendez, 1999), anti-nociceptive (Trentin et al., 1999), as well as inhibition of nitric oxide production (H. R. Wong & Menendez, 1999), lipid peroxidation effect (Jodynis-Liebert et al., 1999), lymphocyte proliferation, and hydroxyl radical scavenging. Furthermore, recent research highlighted the COVID-19 Mpro inhibitory activity exhibited by sesquiterpenes isolated from *Carpesium abrotanoides* L. (Y.-W. Fan et al., 2023).

Cacalolides, derived from furoeremophilanes through the biogenetic Wagner–Meerwein rearrangement. The name of which is derived from cacalol, initially isolated from the antihyperglycemic plant species *Cacalia* decomposita A. Gray (=*Psacalium decompositum* (Gray) H.E. Robins. & Brett.) (Burgueño-Tapia & Joseph-Nathan, 2003). Cacalolide compounds, categorized as sesquiterpenoids, are naturally synthesized by *Senecio* species. Previous studies have detected cacalol derivatives in the *Senecio* genus (Bohlmann & Bapuji, 1982; Burgueño-Tapia et al., 2001; X. Yang et al., 2011). Although cacalolides such as cacalol, cacalone, or maturine have exhibited antioxidant and hypoglycemic effects, their impact on antiviral activities remains relatively unclear (Castillo-Arellano et al., 2018). For instance, cacalol, a potent antioxidative sesquiterpene, has shown significant antioxidative activity against lipid peroxidation induced by free radicals in a rat brain homogenate model (with an IC50 of 40 nM) and has demonstrated notable neuroprotective properties (SHINDO et al., 2004). Moreover, research has indicated that cacalol acetate regulates the NF-κB signaling pathway, suggesting its potential anti-inflammatory effect. Interestingly, cacalol can be synthesized through a seven-step process (Kedrowski & Hoppe, 2008). It would be interesting to

determine the mechanism of action of the different molecules and elucidate, at first, the viral infection step inhibited by each compound.

V. Conclusion & Perspectives

The recent coronavirus pandemic, along with recurrent epidemics and the potential for future outbreaks, is concerning considering the ability of the virus to easily cross species barriers and infect a wide range of hosts. Additionally, animal coronaviruses continue to pose challenges to the global pork and poultry industries, with ongoing emergence of new avian and swine coronavirus variants leading to new outbreaks. Consequently, coronaviruses have garnered significant attention in both human and veterinary medicine. Despite the development of multiple vaccines against SARS-CoV-2, the effectiveness of these vaccines has been impacted by the emergence of virus variants. Moreover, despite substantial efforts to create specific inhibitors for SARS-CoV-2, only two antiviral agents authorized by the FDA have shown efficacy in treating COVID-19 patients.

In the quest for additional treatment options, natural products have proven to be an invaluable source of structurally diverse compounds for discovering new antivirals against human coronaviruses, including SARS-CoV-2. Our study underlined the antiviral potential of some salt tolerant and invasive plants. Our findings indicate that *H. rhamnoides*, an extensively studied plant with a broad range of biological activities, has been confirmed to possess antiviral properties, especially against enveloped viruses. Similarly, the invasive plant *Senecio inaequidens* demonstrated the ability to inhibit human coronaviruses.-The discovery of triterpenoids and sesquiterpenoids from these distinct plant species, both capable of inhibiting human coronaviruses, suggests that terpenes could be promising sources for discovering effective agents against CoV infections, suitable for use as treatments or supplements to conventional COVID-19 therapies.

While research in this field is in its early stages, further studies are warranted to characterize bioactive compounds by determining their chemical and physical properties. This entails identifying and understanding their structure, composition, and behavior to gain a thorough understanding of their chemical, physical, and biological properties. Additionally, investigating the mechanism of action of a compound involves elucidating specific biochemical, physiological, or molecular pathways through which it exerts its effects using a multidisciplinary approach that combines experimental and computational methods. Furthermore, evaluating the toxicity and efficacy of these compounds in vivo is essential to assess their safety and potential therapeutic benefits,

facilitating the development of effective antiviral treatments. This process typically involves a series of preclinical studies aimed at characterizing the compound's pharmacokinetic profile, toxicity profile, and therapeutic efficacy in relevant animal models. Moreover, investigating the solubility and stability of a compound is crucial for assessing its suitability and gaining valuable insights into its behavior. This information is essential for making informed decisions regarding its formulation, storage, and potential applications. Finally, exploring potential combination therapies involving other natural agents or standard therapeutics as a multi-target approach may help mitigate the risk of generating drug-resistant viruses. Natural products are expected to remain pivotal and contribute significantly to the development of antiviral drugs.

VI. Bibliography

Abdallah, H. M., El-Halawany, A. M., Sirwi, A., El-Araby, A. M., Mohamed, G. A., Ibrahim, S. R. M., Koshak, A. E., Asfour, H. Z., Awan, Z. A., & A Elfaky, M. (2021). Repurposing of Some Natural Product Isolates as SARS-COV-2 Main Protease Inhibitors via In Vitro Cell Free and Cell-Based Antiviral Assessments and Molecular Modeling Approaches. *Pharmaceuticals (Basel, Switzerland)*, *14*(3), 213. https://doi.org/10.3390/ph14030213

Ahmed, S., Ahmad, M. S., Yousaf, M., Nur-e-Alam, M., & Al-Rehaily, A. J. (2017). Two New Sesquiterpene Alcohols Isolated from Senecio hadiensis Forssk. Grown in Saudi Arabia. *Chemistry & Biodiversity*, *14*(9), e1700144. https://doi.org/10.1002/cbdv.201700144

Akimkin, V., Beer, M., Blome, S., Hanke, D., Höper, D., Jenckel, M., & Pohlmann, A. (2016). New Chimeric Porcine Coronavirus in Swine Feces, Germany, 2012. *Emerging Infectious Diseases*, *22*(7), 1314–1315. https://doi.org/10.3201/eid2207.160179

Ali, S., Alam, M., Khatoon, F., Fatima, U., Elasbali, A. M., Adnan, M., Islam, A., Hassan, Md. I., Snoussi, M., & De Feo, V. (2022). Natural products can be used in therapeutic management of COVID-19: Probable mechanistic insights. *Biomedicine & Pharmacotherapy*, *147*, 112658. https://doi.org/10.1016/j.biopha.2022.112658

Ali, S. I. (1969). Senecio lautus complex in Australia. V. Taxonomic interpretations. *Australian Journal of Botany*, *17*(1), 161–176. https://doi.org/10.1071/bt9690161

Almeida, M. S., Johnson, M. A., Herrmann, T., Geralt, M., & Wüthrich, K. (2007). Novel β-Barrel Fold in the Nuclear Magnetic Resonance Structure of the Replicase Nonstructural Protein 1 from the Severe Acute Respiratory Syndrome Coronavirus. *Journal of Virology*, *81*(7), 3151–3161. https://doi.org/10.1128/jvi.01939-06

Alotaibi, M. H., & Bahammam, S. A. (2021). Determining the correlation between comorbidities and MERS-CoV mortality in Saudi Arabia. *Journal of Taibah University Medical Sciences*, *16*(4), 591–595. https://doi.org/10.1016/j.jtumed.2021.02.003

Al-Tawfiq, J. A., Momattin, H., Dib, J., & Memish, Z. A. (2014). Ribavirin and interferon therapy in patients infected with the Middle East respiratory syndrome coronavirus: An observational study. *International Journal of Infectious Diseases*, *20*, 42–46. https://doi.org/10.1016/j.ijid.2013.12.003

Aly, M., Elrobh, M., Alzayer, M., Aljuhani, S., & Balkhy, H. (2017). Occurrence of the Middle East Respiratory Syndrome Coronavirus (MERS-CoV) across the Gulf Corporation Council countries: Four years update. *PloS One*, *12*(10), e0183850. https://doi.org/10.1371/journal.pone.0183850

Anbazhagan, S., Muthu, S., Singh, R. K., & Pallab, C. (2020). In silico molecular docking analysis targeting SARS-CoV-2 spike protein and selected herbal constituents. (Special Issue: Coronaviruses and COVID-19- Past, Present, and Future.). *Journal of Pure and Applied Microbiology*, 989–998.

Andersen, R. J., Ntie-Kang, F., & Tietjen, I. (2018). Natural product-derived compounds in HIV suppression, remission, and eradication strategies. *Antiviral Research*, *158*, 63–77. https://doi.org/10.1016/j.antiviral.2018.07.016

Anderson-Daniels, J., Gribble, J., & Denison, M. (2022). Proteolytic Processing of the Coronavirus Replicase Nonstructural Protein 14 Exonuclease Is Not Required for Virus Replication but Alters RNA Synthesis and Viral Fitness. *Journal of Virology*, *96*(16), e00841-22. https://doi.org/10.1128/jvi.00841-22

Ao, Z., Chan, M., Ouyang, M. J., Olukitibi, T. A., Mahmoudi, M., Kobasa, D., & Yao, X. (2021). Identification and evaluation of the inhibitory effect of Prunella vulgaris extract on SARS-coronavirus 2 virus entry. *PLOS ONE*, *16*(6), e0251649. https://doi.org/10.1371/journal.pone.0251649

Arimboor, R., & Arumughan, C. (2012). HPLC-DAD-MS/MS profiling of antioxidant flavonoid glycosides in sea buckthorn (Hippophae rhamnoides L.) seeds. *International Journal of Food Sciences and Nutrition*, *63*(6), 730–738. https://doi.org/10.3109/09637486.2011.652075

Arndt, A. L., Larson, B. J., & Hogue, B. G. (2010). A Conserved Domain in the Coronavirus Membrane Protein Tail Is Important for Virus Assembly. *Journal of Virology*, *84*(21), 11418–11428. https://doi.org/10.1128/JVI.01131-10

Awouafack, M. D., Tane, P., Kuete, V., & Eloff, J. N. (2013). 2—Sesquiterpenes from the Medicinal Plants of Africa. In V. Kuete (Ed.), *Medicinal Plant Research in Africa* (pp. 33–103). Elsevier. https://doi.org/10.1016/B978-0-12-405927-6.00002-3

Baczenas, J. J., Andersen, H., Rashid, S., Yarmosh, D., Puthuveetil, N., Parker, M., Bradford, R., Florence, C., Stemple, K. J., Lewis, M. G., & O'Connor, S. L. (2021). Propagation of SARS-CoV-2

in Calu-3 Cells to Eliminate Mutations in the Furin Cleavage Site of Spike. *Viruses*, *13*(12), 2434. https://doi.org/10.3390/v13122434

Baden, L. R., El Sahly, H. M., Essink, B., Kotloff, K., Frey, S., Novak, R., Diemert, D., Spector, S. A., Rouphael, N., Creech, C. B., McGettigan, J., Khetan, S., Segall, N., Solis, J., Brosz, A., Fierro, C., Schwartz, H., Neuzil, K., Corey, L., … Zaks, T. (2021). Efficacy and Safety of the mRNA-1273 SARS-CoV-2 Vaccine. *New England Journal of Medicine*, *384*(5), 403–416. https://doi.org/10.1056/NEJMoa2035389

Baram, A., Kakamad, F. H., Abdullah, H. M., Mohammed-Saeed, D. H., Hussein, D. A., Mohammed, S. H., Abdulrahman, B. B., Mirza, A. J., Abdulla, B. A., Rahim, H. M., Rashid, M. J., Mohammed-Al, F. F., Othman, Y. N., & Salih, A. M. (2020). Large vessel thrombosis in patient with COVID-19, a case series. *Annals of Medicine and Surgery*, *60*, 526–530. https://doi.org/10.1016/j.amsu.2020.11.030

Bartikova, H., Hanusova, V., Skalova, L., Ambroz, M., & Bousova, I. (2014). Antioxidant, Pro-Oxidant and Other Biological Activities of Sesquiterpenes. *Current Topics in Medicinal Chemistry*, *14*(22), 2478–2494. https://doi.org/10.2174/1568026614666141203120833

Bartish, I. V., Jeppsson, N., Nybom, H., & Swenson, U. (2002). Phylogeny of Hippophae (Elaeagnaceae) Inferred from Parsimony Analysis of Chloroplast DNA and Morphology. *Systematic Botany*, *27*(1), 41–54.

Bassignana, M., Mainetti, A., & Madormo, F. (2018). *Invasion of Senecio inaequidens and risks for honey and bee pollen in Aosta Valley*. 113.

Basu, M., Prasad, R., Jayamurthy, P., Pal, K., Arumughan, C., & Sawhney, R. C. (2007). Anti-atherogenic effects of seabuckthorn (Hippophaea rhamnoides) seed oil. *Phytomedicine: International Journal of Phytotherapy and Phytopharmacology*, *14*(11), 770–777. https://doi.org/10.1016/j.phymed.2007.03.018

Bayati, A., Kumar, R., Francis, V., & McPherson, P. S. (2021). SARS-CoV-2 infects cells after viral entry via clathrin-mediated endocytosis. *The Journal of Biological Chemistry*, *296*, 100306. https://doi.org/10.1016/j.jbc.2021.100306

Bayati, M., Noroozi, R., Ghanbari-Jahromi, M., & Jalali, F. S. (2022). Inequality in the distribution of Covid-19 vaccine: A systematic review. *International Journal for Equity in Health*, *21*(1), 122. https://doi.org/10.1186/s12939-022-01729-x

Belouzard, S., Chu, V. C., & Whittaker, G. R. (2009). Activation of the SARS coronavirus spike protein via sequential proteolytic cleavage at two distinct sites. *Proceedings of the National Academy of Sciences of the United States of America*, *106*(14), 5871–5876. https://doi.org/10.1073/pnas.0809524106

Bergmann, C. C., & Silverman, R. H. (2020). COVID-19: Coronavirus replication, pathogenesis, and therapeutic strategies. *Cleveland Clinic Journal of Medicine*, *87*(6), 321–327. https://doi.org/10.3949/ccjm.87a.20047

Berthod, A., Hassoun, M., & Ruiz-Angel, M. J. (2005). Alkane effect in the Arizona liquid systems used in countercurrent chromatography. *Analytical and Bioanalytical Chemistry*, *383*(2), 327–340. https://doi.org/10.1007/s00216-005-0016-7

Bertram, S., Dijkman, R., Habjan, M., Heurich, A., Gierer, S., Glowacka, I., Welsch, K., Winkler, M., Schneider, H., Hofmann-Winkler, H., Thiel, V., & Pöhlmann, S. (2013). TMPRSS2 Activates the Human Coronavirus 229E for Cathepsin-Independent Host Cell Entry and Is Expressed in Viral Target Cells in the Respiratory Epithelium. *Journal of Virology*, *87*(11), 6150–6160. https://doi.org/10.1128/JVI.03372-12

Bhogadi, M., Suen, I. H., Gupta, A. R., & Khanna, A. (2022). A case series of conduction abnormalities in covid patients. *Journal of the American College of Cardiology*, *79*(9), 2196. https://doi.org/10.1016/S0735-1097(22)03187-4

Bisht, B. S., Singh, D., & Mathela, C. S. (2023). Terpenoid diversity and antimicrobial activity of five Himalayan Senecio species. *Journal of Essential Oil Bearing Plants*, *26*(4), 946–957. https://doi.org/10.1080/0972060X.2023.2247017

Bittová, M., Krejzová, E., Roblová, V., Kubáň, P., & Kubáň, V. (2014). Monitoring of HPLC profiles of selected polyphenolic compounds in sea buckthorn (Hippophaë rhamnoides L.) plant parts during annual growth cycle and estimation of their antioxidant potential. *Open Chemistry*, *12*(11), 1152–1161. https://doi.org/10.2478/s11532-014-0562-y

Boda, B., Benaoudia, S., Huang, S., Bonfante, R., Wiszniewski, L., Tseligka, E. D., Tapparel, C., & Constant, S. (2018). Antiviral drug screening by assessing epithelial functions and innate immune responses in human 3D airway epithelium model. *Antiviral Research*, *156*, 72–79. https://doi.org/10.1016/j.antiviral.2018.06.007

Bohlmann, F., & Bapuji, M. (1982). Cacalol derivatives from Senecio lydenburgensis. *Phytochemistry*, *21*(3), 681–683. https://doi.org/10.1016/0031-9422(82)83165-8

Bohlmann, F., Knoll, K.-H., Zdero, C., Mahanta, P. K., Grenz, M., Suwita, A., Ehlers, D., Van, N. L., Abraham, W.-R., & Natu, A. A. (1977). Terpen-derivate aus Senecio-arten. *Phytochemistry*, *16*(7), 965–985. https://doi.org/10.1016/S0031-9422(00)86705-9

Bohlmann, F., & Zdero, C. (1978). New norsesquiterpenes from Senecio digitalifolius. *Phytochemistry*, *17*(4), 759–761. https://doi.org/10.1016/S0031-9422(00)94221-3

Bohlmann, F., Zdero, C., Jakupovic, J., Grenz, M., Castro, V., Kino, R. M., Robinson, H., & Vincent, L. P. D. (1986). Further pyrrolizidine alkaloids and furoeremophilanes from Senecio species. *Phytochemistry*, *25*(5), 1151–1159. https://doi.org/10.1016/S0031-9422(00)81571-X

Bohlmann, F., Zdero, C., Jakupovic, J., Misra, L. N., Banerjee, S., Singh, P., Baruah, R. N., Metwally, M. A., Schmeda-Hirschmann, G., Vincent, L. P. D., King, R. M., & Robinson, H. (1985). Eremophilane derivatives and other constituents from Senecio species. *Phytochemistry*, *24*(6), 1249–1261. https://doi.org/10.1016/S0031-9422(00)81111-5

Bohlmann, F., & Ziesche, J. (1981). Sesquiterpenes from three Senecio species. *Phytochemistry*, *20*(3), 469–472. https://doi.org/10.1016/S0031-9422(00)84168-0

Boniotti, M. B., Papetti, A., Lavazza, A., Alborali, G., Sozzi, E., Chiapponi, C., Faccini, S., Bonilauri, P., Cordioli, P., & Marthaler, D. (2016). Porcine Epidemic Diarrhea Virus and Discovery of a Recombinant Swine Enteric Coronavirus, Italy. *Emerging Infectious Diseases*, *22*(1), 83–87. https://doi.org/10.3201/eid2201.150544

Bonny, T. S., Yezli, S., & Lednicky, J. A. (2018). Isolation and identification of human coronavirus 229E from frequently touched environmental surfaces of a university classroom that is cleaned daily. *American Journal of Infection Control*, *46*(1), 105–107. https://doi.org/10.1016/j.ajic.2017.07.014

Bosch, B. J., van der Zee, R., de Haan, C. A. M., & Rottier, P. J. M. (2003). The coronavirus spike protein is a class I virus fusion protein: Structural and functional characterization of the fusion core complex. *Journal of Virology*, *77*(16), 8801–8811. https://doi.org/10.1128/jvi.77.16.8801-8811.2003

Bouhaddou, M., Memon, D., Meyer, B., White, K. M., Rezelj, V. V., Correa Marrero, M., Polacco, B. J., Melnyk, J. E., Ulferts, S., Kaake, R. M., Batra, J., Richards, A. L., Stevenson, E., Gordon, D. E., Rojc, A., Obernier, K., Fabius, J. M., Soucheray, M., Miorin, L., … Krogan, N. J. (2020). The Global Phosphorylation Landscape of SARS-CoV-2 Infection. *Cell*, *182*(3), 685-712.e19. https://doi.org/10.1016/j.cell.2020.06.034

Braca, A., Morelli, I., Mendez, J., Battinelli, L., Braghiroli, L., & Mazzanti, G. (2000). Antimicrobial triterpenoids from Licania heteromorpha. *Planta Medica*, *66*(8), 768–769. https://doi.org/10.1055/s-2000-9601

Brooks, M. L., D'Antonio, C. M., Richardson, D. M., Grace, J. B., Keeley, J. E., DiTomaso, J. M., Hobbs, R. J., Pellant, M., & Pyke, D. (2004). Effects of Invasive Alien Plants on Fire Regimes. *BioScience*, *54*(7), 677–688. https://doi.org/10.1641/0006-3568(2004)054[0677:EOIAPO]2.0.CO;2

Brunel S. (2003). *Plantes envahissantes de la région méditerranéenne, Fiche No. 15. Agence Méditerranéenne de l'environnement Languedoc-Roussillon, Agence Régionale Pour l'Environnement Provence-Alpes-Côte d'Azur. Montpellier. Agence Méditerranéenne de l'Environnement*. https://www.yumpu.com/fr/document/view/12287271/plantes-envahissantes-de-la-region-mediterraneenne-tela-botanica

Burgueño-Tapia, E., Bucio, M. A., Rivera, A., & Joseph-Nathan, P. (2001). Cacalolides from Senecio madagascariensis. *Journal of Natural Products*, *64*(4), 518–521. https://doi.org/10.1021/np000257a

Burgueño-Tapia, E., & Joseph-Nathan, P. (2003). Cacalolides from Senecio barba-johannis. *Magnetic Resonance in Chemistry*, *41*(5), 386–390. https://doi.org/10.1002/mrc.1179

Cantoni, D., Mayora-Neto, M., Thakur, N., Elrefaey, A. M. E., Newman, J., Vishwanath, S., Nadesalingam, A., Chan, A., Smith, P., Castillo-Olivares, J., Baxendale, H., Charleston, B., Heeney, J., Bailey, D., & Temperton, N. (2022). Pseudotyped Bat Coronavirus RaTG13 is efficiently neutralised by convalescent sera from SARS-CoV-2 infected patients. *Communications Biology*, *5*(1), Article 1. https://doi.org/10.1038/s42003-022-03325-9

Cantrell, C. L., Abate, L., Fronczek, F. R., Franzblau, S. G., Quijano, L., & Fischer, N. H. (1999). Antimycobacterial eudesmanolides from Inula helenium and Rudbeckia subtomentosa. *Planta Medica*, *65*(4), 351–355. https://doi.org/10.1055/s-1999-14001

Cappell, M. S., & Friedel, D. M. (2023). Gastrointestinal Bleeding in COVID-19-Infected Patients. *Gastroenterology Clinics of North America*, *52*(1), 77–102. https://doi.org/10.1016/j.gtc.2022.10.004

Castillo-Arellano, J. I., Gómez-Verjan, J. C., Rojano-Vilchis, N. A., Mendoza-Cruz, M., Jiménez-Estrada, M., López-Valdés, H. E., Martínez-Coria, H., Gutiérrez-Juárez, R., González-Espinosa, C., Reyes-Chilpa, R., & Arrieta-Cruz, I. (2018). Chemoinformatic Analysis of Selected Cacalolides from Psacalium decompositum (A. Gray) H. Rob. & Brettell and Psacalium peltatum (Kunth) Cass. And Their Effects on FcεRI-Dependent Degranulation in Mast Cells. *Molecules*, *23*(12), 3367. https://doi.org/10.3390/molecules23123367

Cavanagh, D. (2007). Coronavirus avian infectious bronchitis virus. *Veterinary Research*, *38*(2), 281–297. https://doi.org/10.1051/vetres:2006055

CDC. (2003). Severe acute respiratory syndrome—Singapore, 2003. *MMWR. Morbidity and Mortality Weekly Report*, *52*(18), 405–411.

CDC. (2020a, February 11). *Coronavirus Disease 2019 (COVID-19)*. Centers for Disease Control and Prevention. https://www.cdc.gov/coronavirus/2019-ncov/variants/variant-classifications.html

CDC. (2020b, February 11). *COVID-19 and Your Health*. Centers for Disease Control and Prevention. https://www.cdc.gov/coronavirus/2019-ncov/your-health/treatments-for-severe-illness.html

Center for Disease Control and Prevention. (2005, May 3). *SARS | Frequently Asked Questions | CDC*. https://www.cdc.gov/sars/about/faq.html

Cerda-García-Rojas, C. M., Burgueño-Tapia, E., Román-Marín, L. U., Hernández-Hernández, J. D., Agulló-Ortuño, T., González-Coloma, A., & Joseph-Nathan, P. (2010). Antifeedant and cytotoxic activity of longipinane derivatives. *Planta Medica*, *76*(3), 297–302. https://doi.org/10.1055/s-0029-1186080

Chan, K. H., Poon, L. L. L. M., Cheng, V. C. C., Guan, Y., Hung, I. F. N., Kong, J., Yam, L. Y. C., Seto, W. H., Yuen, K. Y., & Peiris, J. S. M. (2004). Detection of SARS Coronavirus in Patients with Suspected SARS. *Emerging Infectious Diseases*, *10*(2), 294–299. https://doi.org/10.3201/eid1002.030610

Chapman, V. J. (1942). The New Perspective in the Halophytes. *The Quarterly Review of Biology*, *17*(4), 291–311.

Chaturvedi, D., Goswami, A., Saikia, P. P., Barua, N. C., & Rao, P. G. (2010). Artemisinin and its derivatives: A novel class of anti-malarial and anti-cancer agents. *Chemical Society Reviews*, *39*(2), 435–454. https://doi.org/10.1039/b816679j

Chatzis, D. G., Magounaki, K., Pantazopoulos, I., & Bhaskar, S. M. M. (2022). COVID-19 and the cardiovascular system-current knowledge and future perspectives. *World Journal of Clinical Cases*, *10*(27), 9602–9610. https://doi.org/10.12998/wjcc.v10.i27.9602

Chauhan, A. S., Negi, P. S., & Ramteke, R. S. (2007). Antioxidant and antibacterial activities of aqueous extract of Seabuckthorn (Hippophae rhamnoides) seeds. *Fitoterapia*, *78*(7–8), 590–592. https://doi.org/10.1016/j.fitote.2007.06.004

Cheeseman, J. M. (2015). The evolution of halophytes, glycophytes and crops, and its implications for food security under saline conditions. *The New Phytologist*, *206*(2), 557–570. https://doi.org/10.1111/nph.13217

Chen, A., Feng, X., Dorjsuren, B., Chimedtseren, C., Damda, T.-A., & Zhang, C. (2023). Traditional food, modern food and nutritional value of Sea buckthorn (Hippophae rhamnoides L.): A review. *Journal of Future Foods*, *3*(3), 191–205. https://doi.org/10.1016/j.jfutfo.2023.02.001

Chen, H., & Du, Q. (2020). *Potential Natural Compounds for Preventing SARS-CoV-2 (2019-nCoV) Infection* (2020010358). Preprints. https://doi.org/10.20944/preprints202001.0358.v3

Chen, W., Cui, P., Sun, H., Guo, W., Yang, C., Jin, H., Fang, B., & Shi, D. (2009). Comparative effects of salt and alkali stresses on organic acid accumulation and ionic balance of seabuckthorn (Hippophae rhamnoides L.). *Industrial Crops and Products*, *30*(3), 351–358. https://doi.org/10.1016/j.indcrop.2009.06.007

Cheng, P.-W., Ng, L.-T., Chiang, L.-C., & Lin, C.-C. (2006). Antiviral effects of saikosaponins on human coronavirus 229E in vitro. *Clinical and Experimental Pharmacology & Physiology*, *33*(7), 612–616. https://doi.org/10.1111/j.1440-1681.2006.04415.x

Chibo, D., & Birch, C. (2006). Analysis of human coronavirus 229E spike and nucleoprotein genes demonstrates genetic drift between chronologically distinct strains. *Journal of General Virology*, *87*(5), 1203–1208. https://doi.org/10.1099/vir.0.81662-0

Cho, C. H., Jang, H., Lee, M., Kang, H., Heo, H. J., & Kim, D.-O. (2017). Sea Buckthorn (Hippophae rhamnoides L.) Leaf Extracts Protect Neuronal PC-12 Cells from Oxidative Stress. *Journal of Microbiology and Biotechnology*, *27*(7), 1257–1265. https://doi.org/10.4014/jmb.1704.04033

Choi, H. J., Song, J. H., & Kwon, D. H. (2012). Quercetin 3-rhamnoside exerts antiinfluenza A virus activity in mice. *Phytotherapy Research: PTR*, *26*(3), 462–464. https://doi.org/10.1002/ptr.3529

Chopra, B., & Dhingra, A. K. (2021). Natural products: A lead for drug discovery and development. *Phytotherapy Research: PTR*, *35*(9), 4660–4702. https://doi.org/10.1002/ptr.7099

Chu, H., Chan, J. F.-W., Yuen, T. T.-T., Shuai, H., Yuan, S., Wang, Y., Hu, B., Yip, C. C.-Y., Tsang, J. O.-L., Huang, X., Chai, Y., Yang, D., Hou, Y., Chik, K. K.-H., Zhang, X., Fung, A. Y.-F., Tsoi, H.-W., Cai, J.-P., Chan, W.-M., … Yuen, K.-Y. (2020). Comparative tropism, replication kinetics, and cell damage profiling of SARS-CoV-2 and SARS-CoV with implications for clinical manifestations, transmissibility, and laboratory studies of COVID-19: An observational study. *The Lancet. Microbe*, *1*(1), e14–e23. https://doi.org/10.1016/S2666-5247(20)30004-5

Circella, E., Camarda, A., Martella, V., Bruni, G., Lavazza, A., & Buonavoglia, C. (2007). Coronavirus associated with an enteric syndrome on a quail farm. *Avian Pathology: Journal of the W.V.P.A*, *36*(3), 251–258. https://doi.org/10.1080/03079450701344738

Colmer, T. D., Munns, R., Flowers, T. J., Colmer, T. D., Munns, R., & Flowers, T. J. (2005). Improving salt tolerance of wheat and barley: Future prospects. *Australian Journal of Experimental Agriculture*, *45*(11), 1425–1443. https://doi.org/10.1071/EA04162

Comber, L., O Murchu, E., Drummond, L., Carty, P. G., Walsh, K. A., De Gascun, C. F., Connolly, M. A., Smith, S. M., O'Neill, M., Ryan, M., & Harrington, P. (2021). Airborne transmission of SARS-CoV-2 via aerosols. *Reviews in Medical Virology*, *31*(3), e2184. https://doi.org/10.1002/rmv.2184

Corman, V. M., Muth, D., Niemeyer, D., & Drosten, C. (2018). Hosts and Sources of Endemic Human Coronaviruses. *Advances in Virus Research*, *100*, 163–188. https://doi.org/10.1016/bs.aivir.2018.01.001

Cortés-Selva, F., Jiménez, I. A., Munoz-Martínez, F., Campillo, M., Bazzocchi, I. L., Pardo, L., Ravelo, A. G., Castanys, S., & Gamarro, F. (2005). Dihydro-beta-agarofuran sesquiterpenes: A

new class of reversal agents of the multidrug resistance phenotype mediated by P-glycoprotein in the protozoan parasite Leishmania. *Current Pharmaceutical Design*, *11*(24), 3125–3139. https://doi.org/10.2174/1381612054864920

Cortinovis, C., & Caloni, F. (2015). Alkaloid-Containing Plants Poisonous to Cattle and Horses in Europe. *Toxins*, *7*(12), 5301–5307. https://doi.org/10.3390/toxins7124884

Cosmulescu, S., Trandafir, I., & Nour, V. (2017). Phenolic acids and flavonoids profiles of extracts from edible wild fruits and their antioxidant properties. *International Journal of Food Properties*, *20*(12), 3124–3134. https://doi.org/10.1080/10942912.2016.1274906

Costello, S. M., Shoemaker, S. R., Hobbs, H. T., Nguyen, A. W., Hsieh, C.-L., Maynard, J. A., McLellan, J. S., Pak, J. E., & Marqusee, S. (2022). The SARS-CoV-2 spike reversibly samples an open-trimer conformation exposing novel epitopes. *Nature Structural & Molecular Biology*, *29*(3), Article 3. https://doi.org/10.1038/s41594-022-00735-5

Criste, A., Urcan, A. C., Bunea, A., Pripon Furtuna, F. R., Olah, N. K., Madden, R. H., & Corcionivoschi, N. (2020). Phytochemical Composition and Biological Activity of Berries and Leaves from Four Romanian Sea Buckthorn (Hippophae Rhamnoides L.) Varieties. *Molecules*, *25*(5), Article 5. https://doi.org/10.3390/molecules25051170

da Costa e Silva, G. R., Moura, W. É. A., dos Santos, K. C., Gomes, D. O., Bandeira, G. N., Guimarães, R. A., Rosso, C. F. W., Bazilio, G. S., Leite, V. R. M. C., Caetano, K. A. A., Carneiro, M. A. dos S., & Teles, S. A. (2023). Long-Term Symptoms after Mild Coronavirus Disease in Healthy Healthcare Professionals: A 12-Month Prospective Cohort Study. *International Journal of Environmental Research and Public Health*, *20*(2), 1483. https://doi.org/10.3390/ijerph20021483

Darshani, P., Sen Sarma, S., Srivastava, A. K., Baishya, R., & Kumar, D. (2022). Anti-viral triterpenes: A review. *Phytochemistry Reviews*, *21*(6), 1761–1842. https://doi.org/10.1007/s11101-022-09808-1

David, J. P., De O. Santos, A. J., Da S. Guedes, M. L., David, J. M., Chai, H.-B., Pezzuto, J. M., Angerhofer, C. K., & Cordell, G. A. (1999). Sesquiterpene Lactones from Ambrosia artemisiaefolia (Asteraceae). *Pharmaceutical Biology*, *37*(2), 165–168. https://doi.org/10.1076/phbi.37.2.165.6077

de Nova, P. J. G., Cortey, M., Díaz, I., Puente, H., Rubio, P., Martín, M., & Carvajal, A. (2020). A retrospective study of porcine epidemic diarrhoea virus (PEDV) reveals the presence of swine enteric coronavirus (SeCoV) since 1993 and the recent introduction of a recombinant PEDV-SeCoV in Spain. *Transboundary and Emerging Diseases*, *67*(6), 2911–2922. https://doi.org/10.1111/tbed.13666

de Wilde, A. H., Raj, V. S., Oudshoorn, D., Bestebroer, T. M., van Nieuwkoop, S., Limpens, R. W. A. L., Posthuma, C. C., van der Meer, Y., Bárcena, M., Haagmans, B. L., Snijder, E. J., & van den Hoogen, B. G. (2013). MERS-coronavirus replication induces severe in vitro cytopathology and is strongly inhibited by cyclosporin A or interferon-α treatment. *The Journal of General Virology*, *94*(Pt 8), 1749–1760. https://doi.org/10.1099/vir.0.052910-0

Dea, S., & Tijssen, P. (1989). Detection of turkey enteric coronavirus by enzyme-linked immunosorbent assay and differentiation from other coronaviruses. *American Journal of Veterinary Research*, *50*(2), 226–231.

Desmarets, L., Danneels, A., Burlaud-Gaillard, J., Blanchard, E., Dubuisson, J., & Belouzard, S. (2023). The KxGxYR and DxE motifs in the C-tail of the Middle East respiratory syndrome coronavirus membrane protein are crucial for infectious virus assembly. *Cellular and Molecular Life Sciences: CMLS*, *80*(12), 353. https://doi.org/10.1007/s00018-023-05008-y

Díaz, O., Alarcón, R., Gutiérrez, D., Pacciaroni, A., Cayo, F., & Sosa, V. (2015). 6-Methoxyflavonoids and Other Constituents from Microliabum polymnioides (Asteraceae). *Natural Product Communications*, *10*(7), 1934578X1501000712. https://doi.org/10.1177/1934578X1501000712

Digitale2. (2023a). *Hippophae rhamnoides*. https://digitale.cbnbl.org/digitale-rft/Consultation/Taxon_accueil.do?codeMetier=7691

Digitale2. (2023b). *Senecio inaequidens*. https://digitale.cbnbl.org/digitale-rft/Consultation/Taxon_accueil.do?codeMetier=10458

Dijkman, R., Jebbink, M. F., Gaunt, E., Rossen, J. W. A., Templeton, K. E., Kuijpers, T. W., & van der Hoek, L. (2012). The dominance of human coronavirus OC43 and NL63 infections in infants. *Journal of Clinical Virology: The Official Publication of the Pan American Society for Clinical Virology*, *53*(2), 135–139. https://doi.org/10.1016/j.jcv.2011.11.011

Dolan, K. A., Dutta, M., Kern, D. M., Kotecha, A., Voth, G. A., & Brohawn, S. G. (2022). Structure of SARS-CoV-2 M protein in lipid nanodiscs. *eLife*, *11*, e81702. https://doi.org/10.7554/eLife.81702

Donnelly, C. A., Ghani, A. C., Leung, G. M., Hedley, A. J., Fraser, C., Riley, S., Abu-Raddad, L. J., Ho, L.-M., Thach, T.-Q., Chau, P., Chan, K.-P., Lam, T.-H., Tse, L.-Y., Tsang, T., Liu, S.-H., Kong, J. H., Lau, E. M., Ferguson, N. M., & Anderson, R. M. (2003). Epidemiological determinants of spread of causal agent of severe acute respiratory syndrome in Hong Kong. *Lancet (London, England)*, *361*(9371), 1761–1766. https://doi.org/10.1016/S0140-6736(03)13410-1

Doyle, L. P., & Hutchings, L. M. (1946). A transmissible gastroenteritis in pigs. *Journal of the American Veterinary Medical Association*, *108*, 257–259.

Dupré, S., Grenz, M., Jakupovic, J., Bohlmann, F., & Niemeyer, H. M. (1991). Eremophilane, germacrane and shikimic acid derivatives from chilean Senecio species. *Phytochemistry*. https://doi.org/10.1016/S0031-9422(00)95204-X

Duraipandiyan, V., Al-Harbi, N. A., Ignacimuthu, S., & Muthukumar, C. (2012). Antimicrobial activity of sesquiterpene lactones isolated from traditional medicinal plant, Costus speciosus (Koen ex.Retz.) Sm. *BMC Complementary and Alternative Medicine*, *12*, 13. https://doi.org/10.1186/1472-6882-12-13

Dwight Baker. (1993, June). *Winrock International - Hippophaë rhamnoides: An NFT valued for centuries*. https://winrock.org/factnet-a-lasting-impact/fact-net-resources/nitrogen-fixing-trees-and-shrubs-for-acid-soils/hippophae-rhamnoides-an-nft-valued-for-centuries/

eHALOPH. (2022). *eHALOPH*. https://ehaloph.uc.pt/

Eichberg, J., Maiworm, E., Oberpaul, M., Czudai-Matwich, V., Lüddecke, T., Vilcinskas, A., & Hardes, K. (2022). Antiviral Potential of Natural Resources against Influenza Virus Infections. *Viruses*, *14*(11), 2452. https://doi.org/10.3390/v14112452

Eliseev IP, Fefelov VA. (1977). *"Material for studying Hippophae rhamnoides in Kabardino – Balkaria*. Tr. Gor'k. S-Kh Inst. 105: 3-7.

EMA. (2022, January 24). *Paxlovid* [Text]. European Medicines Agency. https://www.ema.europa.eu/en/medicines/human/EPAR/paxlovid

EMA. (2023, June 27). *Lagevrio: Withdrawn application* [Text]. European Medicines Agency. https://www.ema.europa.eu/en/medicines/human/withdrawn-applications/lagevrio

Enjuanes, L., & van der Zeijst, B. A. M. (1995). Molecular Basis of Transmissible Gastroenteritis Virus Epidemiology. In S. G. Siddell (Ed.), *The Coronaviridae* (pp. 337–376). Springer US. https://doi.org/10.1007/978-1-4899-1531-3_16

Enkhtaivan, G., Maria John, K. M., Pandurangan, M., Hur, J. H., Leutou, A. S., & Kim, D. H. (2017). Extreme effects of Seabuckthorn extracts on influenza viruses and human cancer cells and correlation between flavonol glycosides and biological activities of extracts. *Saudi Journal of Biological Sciences*, *24*(7), 1646–1656. https://doi.org/10.1016/j.sjbs.2016.01.004

Enmozhi, S. K., Raja, K., Sebastine, I., & Joseph, J. (2021). Andrographolide as a potential inhibitor of SARS-CoV-2 main protease: An in silico approach. *Journal of Biomolecular Structure & Dynamics*, *39*(9), 3092–3098. https://doi.org/10.1080/07391102.2020.1760136

EPPO Global Database. (2006, February 1). *Senecio inaequidens (SENIQ)[Documents]| EPPO Global Database*. https://gd.eppo.int/taxon/SENIQ/documents

Ernst, W. H. O. (1998). Invasion, dispersal and ecology of the South African neophyte Senecio inaequidens in The Netherlands: From wool alien to railway and road alien. *Acta Botanica Neerlandica*, *47*(1), 131–151.

European Centre for Disease Prevention and Control. (2021, April 30). *SARS-CoV-2 variants of concern as of 21 September 2023*. https://www.ecdc.europa.eu/en/covid-19/variants-concern

European Centre for Disease Prevention and Control. (2023, July 31). *MERS-CoV worldwide overview*. https://www.ecdc.europa.eu/en/middle-east-respiratory-syndrome-coronavirus-mers-cov-situation-update

Fan, H., Zhang, J., Ye, Y., Tong, T., Xie, K., & Liao, M. (2012). Complete Genome Sequence of a Novel Porcine Epidemic Diarrhea Virus in South China. *Journal of Virology*, *86*(18), 10248–10249. https://doi.org/10.1128/jvi.01589-12

Fan, Y.-W., Ao, Z.-Y., Zhang, W.-J., Chen, J.-Y., Lian, X., Chen Pan, Y.-, Chen, L.-P., Wu, J.-W., & Yuan, J. (2023). The sesquiterpenes with the COVID-19 Mpro inhibitory activity from the Carpesium abrotanoides L. *Natural Product Research*, *0*(0), 1–9. https://doi.org/10.1080/14786419.2023.2230609

Faraone, I., Rai, D. K., Chiummiento, L., Fernandez, E., Choudhary, A., Prinzo, F., & Milella, L. (2018). Antioxidant Activity and Phytochemical Characterization of Senecio clivicolus Wedd. *Molecules*, *23*(10), Article 10. https://doi.org/10.3390/molecules23102497

Farkaš, B., Minneci, M., Misevicius, M., & Rozas, I. (2023). A Tale of Two Proteases: MPro and TMPRSS2 as Targets for COVID-19 Therapies. *Pharmaceuticals*, *16*(6), Article 6. https://doi.org/10.3390/ph16060834

Fatima, T. (2018). *Seabuckthorn (Hippophae rhamnoides): A repository of phytochemicals*. https://www.academia.edu/98919248/Seabuckthorn_Hippophae_rhamnoides_A_repository_of_phytochemicals

Feng, J.-T., Ma, Z.-Q., Li, J.-H., He, J., Xu, H., & Zhang, X. (2010). Synthesis and antifungal activity of carabrone derivatives. *Molecules (Basel, Switzerland)*, *15*(9), 6485–6492. https://doi.org/10.3390/molecules15096485

Finkel, Y., Gluck, A., Nachshon, A., Winkler, R., Fisher, T., Rozman, B., Mizrahi, O., Lubelsky, Y., Zuckerman, B., Slobodin, B., Yahalom-Ronen, Y., Tamir, H., Ulitsky, I., Israely, T., Paran, N., Schwartz, M., & Stern-Ginossar, N. (2021). SARS-CoV-2 uses a multipronged strategy to impede host protein synthesis. *Nature*, *594*(7862), Article 7862. https://doi.org/10.1038/s41586-021-03610-3

Flowers, T. J., & Colmer, T. D. (2008). Salinity tolerance in halophytes. *The New Phytologist*, *179*(4), 945–963. https://doi.org/10.1111/j.1469-8137.2008.02531.x

Flowers, T. J., Galal, H. K., Bromham, L., Flowers, T. J., Galal, H. K., & Bromham, L. (2010). Evolution of halophytes: Multiple origins of salt tolerance in land plants. *Functional Plant Biology*, *37*(7), 604–612. https://doi.org/10.1071/FP09269

Fortin, H., Vigor, C., Lohézic-Le Dévéhat, F., Robin, V., Le Bossé, B., Boustie, J., & Amoros, M. (2002). In vitro antiviral activity of thirty-six plants from La Réunion Island. *Fitoterapia*, *73*(4), 346–350. https://doi.org/10.1016/S0367-326X(02)00080-1

Freymuth, F., Vabret, A., Rozenberg, F., Dina, J., Petitjean, J., Gouarin, S., Legrand, L., Corbet, S., Brouard, J., & Lebon, P. (2005). Replication of respiratory viruses, particularly influenza virus, rhinovirus, and coronavirus in HuH7 hepatocarcinoma cell line. *Journal of Medical Virology*, *77*(2), 295–301. https://doi.org/10.1002/jmv.20449

Fu, G. X. ; F., R. Z. ;. Xiao, P. G. (1997). *Determination and Comparison of Total Flavonoids in Seabuckthorn Leaves of Different Species and Different Harvesting Times*. *22*, 147–148.

Fujioka, Y., Kashiwagi, S., Yoshida, A., Satoh, A. O., Fujioka, M., Amano, M., Yamauchi, Y., & Ohba, Y. (2022). A method for the generation of pseudovirus particles bearing SARS coronavirus spike protein in high yields. *Cell Structure and Function*, *47*(1), 43–53. https://doi.org/10.1247/csf.21047

Galmiche, S., Cortier, T., Charmet, T., Schaeffer, L., Chény, O., Platen, C. von, Lévy, A., Martin, S., Omar, F., David, C., Mailles, A., Carrat, F., Cauchemez, S., & Fontanet, A. (2023). SARS-CoV-2 incubation period across variants of concern, individual factors, and circumstances of infection in France: A case series analysis from the ComCor study. *The Lancet Microbe*, *4*(6), e409–e417. https://doi.org/10.1016/S2666-5247(23)00005-8

Gaunt, E. R., Hardie, A., Claas, E. C. J., Simmonds, P., & Templeton, K. E. (2010). Epidemiology and Clinical Presentations of the Four Human Coronaviruses 229E, HKU1, NL63, and OC43 Detected over 3 Years Using a Novel Multiplex Real-Time PCR Method. *Journal of Clinical Microbiology*, *48*(8), 2940–2947. https://doi.org/10.1128/JCM.00636-10

Ge, X.-Y., Li, J.-L., Yang, X.-L., Chmura, A. A., Zhu, G., Epstein, J. H., Mazet, J. K., Hu, B., Zhang, W., Peng, C., Zhang, Y.-J., Luo, C.-M., Tan, B., Wang, N., Zhu, Y., Crameri, G., Zhang, S.-Y., Wang, L.-F., Daszak, P., & Shi, Z.-L. (2013). Isolation and characterization of a bat SARS-like coronavirus that uses the ACE2 receptor. *Nature*, *503*(7477), Article 7477. https://doi.org/10.1038/nature12711

Geetha, S., Sai Ram, M., Mongia, S. S., Singh, V., Ilavazhagan, G., & Sawhney, R. C. (2003). Evaluation of antioxidant activity of leaf extract of Seabuckthorn (Hippophae rhamnoides L.) on chromium(VI) induced oxidative stress in albino rats. *Journal of Ethnopharmacology*, *87*(2), 247–251. https://doi.org/10.1016/S0378-8741(03)00154-5

Geetha, S., Sai Ram, M., Singh, V., Ilavazhagan, G., & Sawhney, R. C. (2002). Anti-oxidant and immunomodulatory properties of seabuckthorn (Hippophae rhamnoides)—An in vitro study. *Journal of Ethnopharmacology*, *79*(3), 373–378. https://doi.org/10.1016/S0378-8741(01)00406-8

Ghasemzadeh, M., Ghasemzadeh, A., & Hosseini, E. (2022). Exhausted NK cells and cytokine storms in COVID-19: Whether NK cell therapy could be a therapeutic choice. *Human Immunology*, *83*(1), 86. https://doi.org/10.1016/j.humimm.2021.09.004

Glowacka, I., Bertram, S., Müller, M. A., Allen, P., Soilleux, E., Pfefferle, S., Steffen, I., Tsegaye, T. S., He, Y., Gnirss, K., Niemeyer, D., Schneider, H., Drosten, C., & Pöhlmann, S. (2011). Evidence that TMPRSS2 activates the severe acute respiratory syndrome coronavirus spike protein for membrane fusion and reduces viral control by the humoral immune response. *Journal of Virology*, *85*(9), 4122–4134. https://doi.org/10.1128/JVI.02232-10

Goel, H. C., Kumar, I. P., Samanta, N., & Rana, S. V. S. (2003). Induction of DNA-protein cross-links by Hippophae rhamnoides: Implications in radioprotection and cytotoxicity. *Molecular and Cellular Biochemistry*, *245*(1–2), 57–67. https://doi.org/10.1023/a:1022809625826

Gonçalves, J. J., da Mata, C. P. S. M., Lourenço, A. A., Ribeiro, Á. L., Ferreira, G. M., Fraga-Silva, T. F. de C., de Souza, F. M., Almeida, V. E. S., Batista, I. A., D`Avila-Mesquita, C., Couto, A. E. S., Campos, L. C. B., Paim, A. A. O., Ferreira, L. L., de Melo Oliveira, P., de Almeida Teixeira, L., Priscila de Almeida Marques, D., Retes de Moraes, H., Pereira, S. H., … Martins-Filho, O. A. (2022). Timeline Kinetics of Systemic and Airway Immune Mediator Storm for Comprehensive Analysis of Disease Outcome in Critically Ill COVID-19 Patients. *Frontiers in Immunology*, *13*, 903903. https://doi.org/10.3389/fimmu.2022.903903

Gong, L., Li, J., Zhou, Q., Xu, Z., Chen, L., Zhang, Y., Xue, C., Wen, Z., & Cao, Y. (2017). A New Bat-HKU2–like Coronavirus in Swine, China, 2017. *Emerging Infectious Diseases*, *23*(9), 1607–1609. https://doi.org/10.3201/eid2309.170915

González-Vázquez, L. D., & Arenas, M. (2023). Molecular Evolution of SARS-CoV-2 during the COVID-19 Pandemic. *Genes*, *14*(2), 407. https://doi.org/10.3390/genes14020407

Gordon, C. J., Tchesnokov, E. P., Woolner, E., Perry, J. K., Feng, J. Y., Porter, D. P., & Götte, M. (2020). Remdesivir is a direct-acting antiviral that inhibits RNA-dependent RNA polymerase from severe acute respiratory syndrome coronavirus 2 with high potency. *The Journal of Biological Chemistry*, *295*(20), 6785–6797. https://doi.org/10.1074/jbc.RA120.013679

Gorkhali, R., Koirala, P., Rijal, S., Mainali, A., Baral, A., & Bhattarai, H. K. (2021). Structure and Function of Major SARS-CoV-2 and SARS-CoV Proteins. *Bioinformatics and Biology Insights*, *15*, 11779322211025876. https://doi.org/10.1177/11779322211025876

Gottlieb, R. L., Vaca, C. E., Paredes, R., Mera, J., Webb, B. J., Perez, G., Oguchi, G., Ryan, P., Nielsen, B. U., Brown, M., Hidalgo, A., Sachdeva, Y., Mittal, S., Osiyemi, O., Skarbinski, J., Juneja, K., Hyland, R. H., Osinusi, A., Chen, S., … Hill, J. A. (2022). Early Remdesivir to Prevent

Progression to Severe Covid-19 in Outpatients. *New England Journal of Medicine*, *386*(4), 305–315. https://doi.org/10.1056/NEJMoa2116846

Gottschalk, C., Kaltner, F., Zimmermann, M., Korten, R., Morris, O., Schwaiger, K., & Gareis, M. (2020). Spread of Jacobaea vulgaris and Occurrence of Pyrrolizidine Alkaloids in Regionally Produced Honeys from Northern Germany: Inter- and Intra-Site Variations and Risk Assessment for Special Consumer Groups. *Toxins*, *12*(7), 441. https://doi.org/10.3390/toxins12070441

Greig, A. S., Mitchell, D., Corner, A. H., Bannister, G. L., Meads, E. B., & Julian, R. J. (1962). A Hemagglutinating Virus Producing Encephalomyelitis in Baby Pigs. *Canadian Journal of Comparative Medicine and Veterinary Science*, *26*(3), 49–56.

Guillerm, J. L., Le Floc'h, E., Maillet, J., & Boulet, C. (1990). The invading weeds within the Western Mediterranean Basin. In F. di Castri, A. J. Hansen, & M. Debussche (Eds.), *Biological Invasions in Europe and the Mediterranean Basin* (pp. 61–84). Springer Netherlands. https://doi.org/10.1007/978-94-009-1876-4_5

Guliyev, V. B., Gul, M., & Yildirim, A. (2004). Hippophae rhamnoides L.: Chromatographic methods to determine chemical composition, use in traditional medicine and pharmacological effects. *Journal of Chromatography. B, Analytical Technologies in the Biomedical and Life Sciences*, *812*(1–2), 291–307. https://doi.org/10.1016/j.jchromb.2004.08.047

Guo, R., Guo, X., Li, T., Fu, X., & Liu, R. H. (2017). Comparative assessment of phytochemical profiles, antioxidant and antiproliferative activities of Sea buckthorn (Hippophaë rhamnoides L.) berries. *Food Chemistry*, *221*, 997–1003. https://doi.org/10.1016/j.foodchem.2016.11.063

Gupta, A., & Upadhyay, N. K. (2011). Chapter 120 - Sea Buckthorn (Hippophae rhamnoides L.) Seed Oil: Usage in Burns, Ulcers, and Mucosal Injuries. In V. R. Preedy, R. R. Watson, & V. B. Patel (Eds.), *Nuts and Seeds in Health and Disease Prevention* (pp. 1011–1018). Academic Press. https://doi.org/10.1016/B978-0-12-375688-6.10120-3

Gupta, S. K., Minocha, R., Thapa, P. J., Srivastava, M., & Dandekar, T. (2022). Role of the Pangolin in Origin of SARS-CoV-2: An Evolutionary Perspective. *International Journal of Molecular Sciences*, *23*(16), 9115. https://doi.org/10.3390/ijms23169115

Hama, J. R., & Strobel, B. W. (2021). Occurrence of pyrrolizidine alkaloids in ragwort plants, soils and surface waters at the field scale in grassland. *Science of The Total Environment*, *755*, 142822. https://doi.org/10.1016/j.scitotenv.2020.142822

Hammond, J., Leister-Tebbe, H., Gardner, A., Abreu, P., Bao, W., Wisemandle, W., Baniecki, M., Hendrick, V. M., Damle, B., Simón-Campos, A., Pypstra, R., & Rusnak, J. M. (2022). Oral Nirmatrelvir for High-Risk, Nonhospitalized Adults with Covid-19. *New England Journal of Medicine*, *386*(15), 1397–1408. https://doi.org/10.1056/NEJMoa2118542

Hamre, D., & Procknow, J. J. (1966). A new virus isolated from the human respiratory tract. *Proceedings of the Society for Experimental Biology and Medicine. Society for Experimental Biology and Medicine (New York, N.Y.)*, *121*(1), 190–193. https://doi.org/10.3181/00379727-121-30734

Hao, X., Zhang, X., Yang, D., Xie, Y., Mu, C., & Zhang, J. (2023). Effects of sea-buckthorn flavonoids on growth performance, nutrient digestibility, microbial protein synthesis, and plasma antioxidant capacity of finishing lambs. *Animal Feed Science and Technology*, *305*, 115783. https://doi.org/10.1016/j.anifeedsci.2023.115783

Hardenbrook, N. J., & Zhang, P. (2022). A structural view of the SARS-CoV-2 virus and its assembly. *Current Opinion in Virology*, *52*, 123–134. https://doi.org/10.1016/j.coviro.2021.11.011

Harris, D. A., Hayes, K. N., Zullo, A. R., Mor, V., Chachlani, P., Deng, Y., McCarthy, E. P., Djibo, D. A., McMahill-Walraven, C. N., & Gravenstein, S. (2023). Comparative Risks of Potential Adverse Events Following COVID-19 mRNA Vaccination Among Older US Adults. *JAMA Network Open*, *6*(8), e2326852. https://doi.org/10.1001/jamanetworkopen.2023.26852

Harshit, V., Chahota Rajesh, Palial Akansha, & Sharma Mandeep. (2011, September 17). *Antibacterial properties of seabuckthorn (Hippophae rhamnoides L.) leaf extracts against common skind and wound bacteria*. https://www.indianjournals.com/ijor.aspx?target=ijor:ijvr&volume=20&issue=1&article=008

Hashemian, S. M. R., Pourhanifeh, M. H., Hamblin, M. R., Shahrzad, M. K., & Mirzaei, H. (2022). RdRp inhibitors and COVID-19: Is molnupiravir a good option? *Biomedicine & Pharmacotherapy = Biomedecine & Pharmacotherapie*, *146*, 112517. https://doi.org/10.1016/j.biopha.2021.112517

Hayashi, T., Goto, N., Takahashi, R., & Fujiwara, K. (1977). Systemic vascular lesions in feline infectious peritonitis. *Nihon Juigaku Zasshi. The Japanese Journal of Veterinary Science*, *39*(4), 365–377. https://doi.org/10.1292/jvms1939.39.365

Heinäaho, M., & Julkunen-Tiitto, R. (2011). Efficient extraction of flavonoids of sea buckthorn berries. *BioChemistry: An Indian Journal*. https://www.semanticscholar.org/paper/Efficient-extraction-of-flavonoids-of-sea-buckthorn-Hein%C3%A4aho-Julkunen-Tiitto/41608a95f09950921f3f238ab33134800e4e395a

Heinze, M. and H.J. Fiedler. (1981). *Experi-mental planting of potash waste dumps. I.Communication: Pot experiments withtrees and shrubs under various water andnutrient conditions. Archiv fur Acker- undPflanzenbau und Bodenkunde. 25*, 315–322.

Hendley, J. O., Fishburne, H. B., & Gwaltney, J. M. (1972). Coronavirus infections in working adults. Eight-year study with 229 E and OC 43. *The American Review of Respiratory Disease*, *105*(5), 805–811. https://doi.org/10.1164/arrd.1972.105.5.805

Henss, L., Auste, A., Schürmann, C., Schmidt, C., Rhein, C. von, Mühlebach, M. D., & Schnierle, B. S. (2021). The green tea catechin epigallocatechin gallate inhibits SARS-CoV-2 infection. *The Journal of General Virology*, *102*(4). https://doi.org/10.1099/jgv.0.001574

Hilliard, O. M. (1977). *Compositae in Natal*. University of Natal Press.

Hirai, Y., Doe, M., Kinoshita, T., & Morimoto, Y. (2004). Total Synthesis of Five Cacalol Families at Different Oxidation Stages, Modified Furanoeremophilane Sesquiterpenes from *Cacalia* and *Senecio* Species. *Chemistry Letters*, *33*(2), 136–137. https://doi.org/10.1246/cl.2004.136

Hobbs, R. J., & Huenneke, L. F. (1992). Disturbance, Diversity, and Invasion: Implications for Conservation. *Conservation Biology*, *6*(3), 324–337.

Hoffmann, M., Hofmann-Winkler, H., Smith, J. C., Krüger, N., Sørensen, L. K., Søgaard, O. S., Hasselstrøm, J. B., Winkler, M., Hempel, T., Raich, L., Olsson, S., Yamazoe, T., Yamatsuta, K., Mizuno, H., Ludwig, S., Noé, F., Sheltzer, J. M., Kjolby, M., & Pöhlmann, S. (2020). Camostat mesylate inhibits SARS-CoV-2 activation by TMPRSS2-related proteases and its metabolite GBPA exerts antiviral activity. *bioRxiv*, 2020.08.05.237651. https://doi.org/10.1101/2020.08.05.237651

Hoffmann, M., Krüger, N., Schulz, S., Cossmann, A., Rocha, C., Kempf, A., Nehlmeier, I., Graichen, L., Moldenhauer, A.-S., Winkler, M. S., Lier, M., Dopfer-Jablonka, A., Jäck, H.-M., Behrens, G. M. N., & Pöhlmann, S. (2022). The Omicron variant is highly resistant against antibody-mediated neutralization: Implications for control of the COVID-19 pandemic. *Cell*, *185*(3), 447-456.e11. https://doi.org/10.1016/j.cell.2021.12.032

Höhne F & Kuhnke KH. (2015). *Die Sanddornfruchtfliege (Rhagoletis batava): Untersuchungen zur Biologie und zum Auftreten 2014 in Gülzow*. https://bladmineerders.nl/reference/hohne-f-kuhnke-kh-2015a/

Hu, B., Ge, X., Wang, L.-F., & Shi, Z. (2015). Bat origin of human coronaviruses. *Virology Journal*, *12*, 221. https://doi.org/10.1186/s12985-015-0422-1

Huang, X., Dong, W., Milewska, A., Golda, A., Qi, Y., Zhu, Q. K., Marasco, W. A., Baric, R. S., Sims, A. C., Pyrc, K., Li, W., & Sui, J. (2015). Human Coronavirus HKU1 Spike Protein Uses O-Acetylated Sialic Acid as an Attachment Receptor Determinant and Employs Hemagglutinin-Esterase Protein as a Receptor-Destroying Enzyme. *Journal of Virology*, *89*(14), 7202–7213. https://doi.org/10.1128/JVI.00854-15

Hui, D. S. (2016). Super-spreading events of MERS-CoV infection. *Lancet (London, England)*, *388*(10048), 942–943. https://doi.org/10.1016/S0140-6736(16)30828-5

Hurdiss, D. L., Drulyte, I., Lang, Y., Shamorkina, T. M., Pronker, M. F., van Kuppeveld, F. J. M., Snijder, J., & de Groot, R. J. (2020). Cryo-EM structure of coronavirus-HKU1 haemagglutinin esterase reveals architectural changes arising from prolonged circulation in humans. *Nature Communications*, *11*(1), Article 1. https://doi.org/10.1038/s41467-020-18440-6

Huynh, J., Li, S., Yount, B., Smith, A., Sturges, L., Olsen, J. C., Nagel, J., Johnson, J. B., Agnihothram, S., Gates, J. E., Frieman, M. B., Baric, R. S., & Donaldson, E. F. (2012). Evidence Supporting a Zoonotic Origin of Human Coronavirus Strain NL63. *Journal of Virology*, *86*(23), 12816–12825. https://doi.org/10.1128/jvi.00906-12

Imam, M. S., Abdelazim, A. H., Batubara, A. S., Gamal, M., Almrasy, A. A., Ramzy, S., Khojah, H., & Hasanin, T. H. A. (2023). Simultaneous green TLC determination of nirmatrelvir and ritonavir in the pharmaceutical dosage form and spiked human plasma. *Scientific Reports*, *13*(1), Article 1. https://doi.org/10.1038/s41598-023-32904-x

Isah, T. (2019). Stress and defense responses in plant secondary metabolites production. *Biological Research*, *52*, 39. https://doi.org/10.1186/s40659-019-0246-3

ISSG. (2017). *Global invasive species database*. http://www.iucngisd.org/gisd/species.php?sc=1458

Jackson, C. B., Farzan, M., Chen, B., & Choe, H. (2022). Mechanisms of SARS-CoV-2 entry into cells. *Nature Reviews Molecular Cell Biology*, *23*(1), Article 1. https://doi.org/10.1038/s41580-021-00418-x

Jamison, D. A., Anand Narayanan, S., Trovão, N. S., Guarnieri, J. W., Topper, M. J., Moraes-Vieira, P. M., Zaksas, V., Singh, K. K., Wurtele, E. S., & Beheshti, A. (2022). A comprehensive SARS-CoV-2 and COVID-19 review, Part 1: Intracellular overdrive for SARS-CoV-2 infection. *European Journal of Human Genetics*, *30*(8), Article 8. https://doi.org/10.1038/s41431-022-01108-8

Ji, M., Gong, X., Li, X., Wang, C., & Li, M. (2020). Advanced Research on the Antioxidant Activity and Mechanism of Polyphenols from Hippophae Species—A Review. *Molecules*, *25*(4), 917. https://doi.org/10.3390/molecules25040917

Jiang, F., Guan, H., Liu, D., Wu, X., Fan, M., & Han, J. (2017). Flavonoids from sea buckthorn inhibit the lipopolysaccharide-induced inflammatory response in RAW264.7 macrophages through the MAPK and NF-κB pathways. *Food & Function*, *8*(3), 1313–1322. https://doi.org/10.1039/c6fo01873d

Jiang, H., Zhang, H., Meng, Q., Xie, J., Li, Y., Chen, H., Zheng, Y., Wang, X., Qi, H., Zhang, J., Wang, P.-H., Han, Z.-G., & Tao, S. (2020). SARS-CoV-2 Orf9b suppresses type I interferon responses by targeting TOM70. *Cellular & Molecular Immunology*, *17*(9), Article 9. https://doi.org/10.1038/s41423-020-0514-8

Jimenez-Estrada, M., Chilpa, R. R., Apan, T. R., Lledias, F., Hansberg, W., Arrieta, D., & Aguilar, F. J. A. (2006). Anti-inflammatory activity of cacalol and cacalone sesquiterpenes isolated from Psacalium decompositum. *Journal of Ethnopharmacology*, *105*(1), 34–38. https://doi.org/10.1016/j.jep.2005.09.039

Jiménez-Estrada, M, Lozano, R.C, Valdés, M.J, & León, C.J.R. (1992). *Actividad antimicrobiana del cacalol y sus derivados*. *Revista Latinoamericana de Química*.

Jindal, N., Mor, S. K., & Goyal, S. M. (2014). Enteric viruses in turkey enteritis. *VirusDisease*, *25*(2), 173–185. https://doi.org/10.1007/s13337-014-0198-8

Jing, S., Milne, R., Wang, H., & Xue, L. (2023). Vaccine hesitancy promotes emergence of new SARS-CoV-2 variants. *Journal of Theoretical Biology*, *570*, 111522. https://doi.org/10.1016/j.jtbi.2023.111522

Jodynis-Liebert, J., Murias, M., & Błoszyk, E. (1999). Effect of several sesquiterpene lactones on lipid peroxidation and glutathione level. *Planta Medica*, *65*(4), 320–324. https://doi.org/10.1055/s-1999-13994

Jovet, P. & Bosserdet, P. (1962). *Senecio harveianus MacOwan relevé chronologique des observations en France. Bulletin de la Centre Etudes Recherches. 7*, 417-420.

Jung, K., & Saif, L. J. (2015). Porcine epidemic diarrhea virus infection: Etiology, epidemiology, pathogenesis and immunoprophylaxis. *Veterinary Journal (London, England: 1997)*, *204*(2), 134–143. https://doi.org/10.1016/j.tvjl.2015.02.017

Kakavandi, S., Zare, I., VaezJalali, M., Dadashi, M., Azarian, M., Akbari, A., Ramezani Farani, M., Zalpoor, H., & Hajikhani, B. (2023). Structural and non-structural proteins in SARS-CoV-2: Potential aspects to COVID-19 treatment or prevention of progression of related diseases. *Cell Communication and Signaling*, *21*(1), 110. https://doi.org/10.1186/s12964-023-01104-5

Kalil, A. C., Patterson, T. F., Mehta, A. K., Tomashek, K. M., Wolfe, C. R., Ghazaryan, V., Marconi, V. C., Ruiz-Palacios, G. M., Hsieh, L., Kline, S., Tapson, V., Iovine, N. M., Jain, M. K., Sweeney, D. A., El Sahly, H. M., Branche, A. R., Regalado Pineda, J., Lye, D. C., Sandkovsky, U., … Beigel, J. H. (2021). Baricitinib plus Remdesivir for Hospitalized Adults with Covid-19. *New England Journal of Medicine*, *384*(9), 795–807. https://doi.org/10.1056/NEJMoa2031994

Kallio, H., Yang, B., Peippo, P., Tahvonen, R., & Pan, R. (2002). Triacylglycerols, glycerophospholipids, tocopherols, and tocotrienols in berries and seeds of two subspecies (ssp. Sinensis and mongolica) of Sea Buckthorn (Hippophaë rhamnoides). *Journal of Agricultural and Food Chemistry*, *50*(10), 3004–3009. https://doi.org/10.1021/jf0115560

Kana, B. D., Arbuthnot, P., Botwe, B. K., Choonara, Y. E., Hassan, F., Louzir, H., Matsoso, P., Moore, P. L., Muhairwe, A., Naidoo, K., Ndomondo-Sigonda, M., & Madhi, S. A. (2023). Opportunities and challenges of leveraging COVID-19 vaccine innovation and technologies for developing sustainable vaccine manufacturing capabilities in Africa. *The Lancet Infectious Diseases*, *23*(8), e288–e300. https://doi.org/10.1016/S1473-3099(22)00878-7

Karakaya, S. (2004). Bioavailability of phenolic compounds. *Critical Reviews in Food Science and Nutrition*, *44*(6), 453–464. https://doi.org/10.1080/10408690490886683

Karesh, W. B., Uhart, M. M., Frere, E., Gandini, P., Braselton, W. E., Puche, H., & Cook, R. A. (1999). Health Evaluation of Free-Ranging Rockhopper Penguins (Eudyptes chrysocomes) in Argentina. *Journal of Zoo and Wildlife Medicine*, *30*(1), 25–31.

Kebbi, S., Noman, L., Demirtas, I., Bensouici, C., Adem, S., Benayache, S., Benayache, F., Seghiri, R., & Gok, M. (2021). In vitro Antioxidant and Anticholinesterase Activities of Senecio massaicus Essential Oil and Its Molecular Docking Studies as a Potential Inhibitor of Covid-19 and Alzheimer's Diseases. *Journal of Biologically Active Products from Nature*, *11*(4), 380–394. https://doi.org/10.1080/22311866.2021.1955006

Kedrowski, B. L., & Hoppe, R. W. (2008). A Concise Synthesis of (±)-Cacalol. *The Journal of Organic Chemistry*, *73*(13), 5177–5179. https://doi.org/10.1021/jo800324c

Keh, D., Boehnke, T., Weber-Cartens, S., Schulz, C., Ahlers, O., Bercker, S., Volk, H.-D., Doecke, W.-D., Falke, K. J., & Gerlach, H. (2003). Immunologic and hemodynamic effects of "low-dose" hydrocortisone in septic shock: A double-blind, randomized, placebo-controlled, crossover study. *American Journal of Respiratory and Critical Care Medicine*, *167*(4), 512–520. https://doi.org/10.1164/rccm.200205-446OC

Kemeny, L. J., & Woods, R. D. (1977). Quantitative transmissible gastroenteritis virus shedding patterns in lactating sows. *American Journal of Veterinary Research*, *38*(3), 307–310.

Kern, D. M., Sorum, B., Mali, S. S., Hoel, C. M., Sridharan, S., Remis, J. P., Toso, D. B., Kotecha, A., Bautista, D. M., & Brohawn, S. G. (2021). Cryo-EM structure of the SARS-CoV-2 3a ion channel in lipid nanodiscs. *bioRxiv*, 2020.06.17.156554. https://doi.org/10.1101/2020.06.17.156554

Keyaerts, E., Vijgen, L., Maes, P., Neyts, J., & Ranst, M. V. (2005). Growth kinetics of SARS-coronavirus in Vero E6 cells. *Biochemical and Biophysical Research Communications*, *329*(3), 1147–1151. https://doi.org/10.1016/j.bbrc.2005.02.085

Kiem, J. (1975). *Ein afrikanischer Korbblütler im südlichen Etschtal (Senecio inaequidens)*. *,49*, 238-239.

Kim, D. E., Min, J. S., Jang, M. S., Lee, J. Y., Shin, Y. S., Song, J. H., Kim, H. R., Kim, S., Jin, Y.-H., & Kwon, S. (2019). Natural Bis-Benzylisoquinoline Alkaloids-Tetrandrine, Fangchinoline, and Cepharanthine, Inhibit Human Coronavirus OC43 Infection of MRC-5 Human Lung Cells. *Biomolecules*, *9*(11), 696. https://doi.org/10.3390/biom9110696

Kim, J. Y., Kim, Y. I., Park, S. J., Kim, I. K., Choi, Y. K., & Kim, S.-H. (2018). Safe, high-throughput screening of natural compounds of MERS-CoV entry inhibitors using a pseudovirus expressing MERS-CoV spike protein. *International Journal of Antimicrobial Agents*, *52*(5), 730–732. https://doi.org/10.1016/j.ijantimicag.2018.05.003

Kim, S.-J., Hwang, E., Yi, S. S., Song, K. D., Lee, H.-K., Heo, T.-H., Park, S.-K., Jung, Y. J., & Jun, H. S. (2017). Sea Buckthorn Leaf Extract Inhibits Glioma Cell Growth by Reducing Reactive Oxygen Species and Promoting Apoptosis. *Applied Biochemistry and Biotechnology*, *182*(4), 1663–1674. https://doi.org/10.1007/s12010-017-2425-4

King, B., & Brian, D. A. (1982). Bovine coronavirus structural proteins. *Journal of Virology*, *42*(2), 700–707. https://doi.org/10.1128/JVI.42.2.700-707.1982

Kiprono, P. C., Kaberia, F., Keriko, J. M., & Karanja, J. N. (2000). The in vitro anti-fungal and anti-bacterial activities of beta-sitosterol from Senecio lyratus (Asteraceae). *Zeitschrift Fur Naturforschung. C, Journal of Biosciences*, *55*(5–6), 485–488. https://doi.org/10.1515/znc-2000-5-629

Kisielius, V., Hama, J. R., Skrbic, N., Hansen, H. C. B., Strobel, B. W., & Rasmussen, L. H. (2020). The invasive butterbur contaminates stream and seepage water in groundwater wells with toxic pyrrolizidine alkaloids. *Scientific Reports*, *10*(1), Article 1. https://doi.org/10.1038/s41598-020-76586-1

Klompas, M., Baker, M. A., Rhee, C., Tucker, R., Fiumara, K., Griesbach, D., Bennett-Rizzo, C., Salmasian, H., Wang, R., Wheeler, N., Gallagher, G. R., Lang, A. S., Fink, T., Baez, S., Smole, S., Madoff, L., Goralnick, E., Resnick, A., Pearson, M., … Morris, C. A. (2021). A SARS-CoV-2 Cluster in an Acute Care Hospital. *Annals of Internal Medicine*, M20-7567. https://doi.org/10.7326/M20-7567

Knowles, S. R., Phillips, E. J., Dresser, L., & Matukas, L. (2003). Common Adverse Events Associated with the Use of Ribavirin for Severe Acute Respiratory Syndrome in Canada. *Clinical Infectious Diseases: An Official Publication of the Infectious Diseases Society of America*, *37*(8), 1139–1142. https://doi.org/10.1086/378304

Kokic, G., Hillen, H. S., Tegunov, D., Dienemann, C., Seitz, F., Schmitzova, J., Farnung, L., Siewert, A., Höbartner, C., & Cramer, P. (2021). Mechanism of SARS-CoV-2 polymerase stalling by remdesivir. *Nature Communications*, *12*(1), Article 1. https://doi.org/10.1038/s41467-020-20542-0

Konno, Y., Kimura, I., Uriu, K., Fukushi, M., Irie, T., Koyanagi, Y., Sauter, D., Gifford, R. J., USFQ-COVID19 Consortium, Nakagawa, S., & Sato, K. (2020). SARS-CoV-2 ORF3b Is a Potent Interferon Antagonist Whose Activity Is Increased by a Naturally Occurring Elongation Variant. *Cell Reports*, *32*(12), 108185. https://doi.org/10.1016/j.celrep.2020.108185

Krasovskaya, N. P., Kulesh, N. I., & Denisenko, V. A. (1989). Natural antioxidants. Furanoeremophilanes from Cacalia roots. *Chemistry of Natural Compounds*, *25*(5), 545–548. https://doi.org/10.1007/BF00598072

Kuhbier, H. (1977). *Senecio inaequidens DC -A new resident of the northwest German flora*. Antiquarische, Gebrauchte Und Neue Bücher. https://www.buchfreund.de/de/d/p/115427938/senecio-inaequidens-dc-ein-neubuerger-der

Kumar, A., Choudhir, G., Shukla, S. K., Sharma, M., Tyagi, P., Bhushan, A., & Rathore, M. (2021). Identification of phytochemical inhibitors against main protease of COVID-19 using molecular modeling approaches. *Journal of Biomolecular Structure & Dynamics*, *39*(10), 3760–3770. https://doi.org/10.1080/07391102.2020.1772112

Kumar, M. S. Y., Dutta, R., Prasad, D., & Misra, K. (2011). Subcritical water extraction of antioxidant compounds from Seabuckthorn (Hippophae rhamnoides) leaves for the comparative evaluation of antioxidant activity. *Food Chemistry*, *127*(3), 1309–1316. https://doi.org/10.1016/j.foodchem.2011.01.088

Kung, S., Doppen, M., Black, M., Braithwaite, I., Kearns, C., Weatherall, M., Beasley, R., & Kearns, N. (2021). Underestimation of COVID-19 mortality during the pandemic. *ERJ Open Research*, *7*(1). https://doi.org/10.1183/23120541.00766-2020

Kwon, P. S., Oh, H., Kwon, S.-J., Jin, W., Zhang, F., Fraser, K., Hong, J. J., Linhardt, R. J., & Dordick, J. S. (2020). Sulfated polysaccharides effectively inhibit SARS-CoV-2 in vitro. *Cell Discovery*, *6*(1), Article 1. https://doi.org/10.1038/s41421-020-00192-8

La Monica, G., Bono, A., Lauria, A., & Martorana, A. (2022). Targeting SARS-CoV-2 Main Protease for Treatment of COVID-19: Covalent Inhibitors Structure-Activity Relationship Insights and Evolution Perspectives. *Journal of Medicinal Chemistry*, *65*(19), 12500–12534. https://doi.org/10.1021/acs.jmedchem.2c01005

Lamb, Y. N. (2020). Remdesivir: First Approval. *Drugs*, *80*(13), 1355–1363. https://doi.org/10.1007/s40265-020-01378-w

Lambinon, J. (1957). Contribution a L'étude De La Flore Adventice De La Belgique: Adventices Rares Ou Nouvelles Pour La Belgique. *Bulletin de La Société Royale de Botanique de Belgique / Bulletin van de Koninklijke Belgische Botanische Vereniging*, *89*, 85–100.

Larmo, P. S., Järvinen, R. L., Yang, B., & Kallio, H. P. (2014). Sea Buckthorn, Dry Eye, and Vision. In *Handbook of Nutrition, Diet and the Eye* (pp. 473–480). Elsevier. https://doi.org/10.1016/B978-0-12-401717-7.00048-4

Lau, S. K. P., Li, K. S. M., Tsang, A. K. L., Lam, C. S. F., Ahmed, S., Chen, H., Chan, K.-H., Woo, P. C. Y., & Yuen, K.-Y. (2013). Genetic Characterization of Betacoronavirus Lineage C Viruses in Bats Reveals Marked Sequence Divergence in the Spike Protein of Pipistrellus Bat Coronavirus HKU5 in Japanese Pipistrelle: Implications for the Origin of the Novel Middle East Respiratory Syndrome Coronavirus. *Journal of Virology*, *87*(15), 8638–8650. https://doi.org/10.1128/JVI.01055-13

Lau, S. K. P., Woo, P. C. Y., Yip, C. C. Y., Tse, H., Tsoi, H., Cheng, V. C. C., Lee, P., Tang, B. S. F., Cheung, C. H. Y., Lee, R. A., So, L., Lau, Y., Chan, K., & Yuen, K. (2006). Coronavirus HKU1 and Other Coronavirus Infections in Hong Kong. *Journal of Clinical Microbiology*, *44*(6), 2063–2071. https://doi.org/10.1128/JCM.02614-05

Lee, T. C., Murthy, S., Del Corpo, O., Senécal, J., Butler-Laporte, G., Sohani, Z. N., Brophy, J. M., & McDonald, E. G. (2022). Remdesivir for the treatment of COVID-19: A systematic review and meta-analysis. *Clinical Microbiology and Infection*, *28*(9), 1203–1210. https://doi.org/10.1016/j.cmi.2022.04.018

Lee, Y.-G., Kang, K. W., Hong, W., Kim, Y. H., Oh, J. T., Park, D. W., Ko, M., Bai, Y.-F., Seo, Y.-J., Lee, S.-M., Kim, H., & Kang, S. C. (2021). Potent antiviral activity of Agrimonia pilosa, Galla rhois, and their components against SARS-CoV-2. *Bioorganic & Medicinal Chemistry*, *45*, 116329. https://doi.org/10.1016/j.bmc.2021.116329

Lefèvre, G., & Rivière, C. (2019). Amaranthaceae halophytes from the French Flanders coast of the North Sea: A review of their phytochemistry and biological activities. *Phytochemistry Reviews*, *19*(5), 1263–1302. https://doi.org/10.1007/s11101-019-09636-w

Lei, J., Kusov, Y., & Hilgenfeld, R. (2018). Nsp3 of coronaviruses: Structures and functions of a large multi-domain protein. *Antiviral Research*, *149*, 58–74. https://doi.org/10.1016/j.antiviral.2017.11.001

Letko, M., Marzi, A., & Munster, V. (2020). Functional assessment of cell entry and receptor usage for SARS-CoV-2 and other lineage B betacoronaviruses. *Nature Microbiology*, *5*(4), Article 4. https://doi.org/10.1038/s41564-020-0688-y

Li, H., Zhou, C., Zhou, L., Chen, Z., Yang, L., Bai, H., Wu, X., Peng, H., & Zhao, Y. (2005). In vitro antiviral activity of three enantiomeric sesquiterpene lactones from Senecio species against hepatitis B virus. *Antiviral Chemistry and Chemotherapy*, *16*(4), 277–282. https://doi.org/10.1177/095632020501600407

Li, S.-Y., Chen, C., Zhang, H.-Q., Guo, H.-Y., Wang, H., Wang, L., Zhang, X., Hua, S.-N., Yu, J., Xiao, P.-G., Li, R.-S., & Tan, X. (2005). Identification of natural compounds with antiviral activities against SARS-associated coronavirus. *Antiviral Research*, *67*(1), 18–23. https://doi.org/10.1016/j.antiviral.2005.02.007

Li, T. S. C., & Schroeder, W. R. (1996). Sea Buckthorn (Hippophae rhamnoides L.): A Multipurpose Plant. *HortTechnology*, *6*(4), 370–380. https://doi.org/10.21273/HORTTECH.6.4.370

Li, W., Moore, M. J., Vasilieva, N., Sui, J., Wong, S. K., Berne, M. A., Somasundaran, M., Sullivan, J. L., Luzuriaga, K., Greenough, T. C., Choe, H., & Farzan, M. (2003). Angiotensin-converting enzyme 2 is a functional receptor for the SARS coronavirus. *Nature*, *426*(6965), Article 6965. https://doi.org/10.1038/nature02145

Li, W., Shi, Z., Yu, M., Ren, W., Smith, C., Epstein, J. H., Wang, H., Crameri, G., Hu, Z., Zhang, H., Zhang, J., McEachern, J., Field, H., Daszak, P., Eaton, B. T., Zhang, S., & Wang, L.-F. (2005). Bats are natural reservoirs of SARS-like coronaviruses. *Science (New York, N.Y.)*, *310*(5748), 676–679. https://doi.org/10.1126/science.1118391

Lian Yong-Shan. (1988). *New Discoveries of the Genus Hippophae L. (Elaeagnaceae)*. https://www.jse.ac.cn/EN/Y1988/V26/I3/235

Lin, H., Singla, B., Ghoshal, P., Faulkner, J. L., Cherian-Shaw, M., O'Connor, P. M., She, J., Belin de Chantemele, E. J., & Csányi, G. (2018). Identification of novel macropinocytosis inhibitors using a rational screen of Food and Drug Administration-approved drugs. *British Journal of Pharmacology*, *175*(18), 3640–3655. https://doi.org/10.1111/bph.14429

Lin, Y., Zang, R., Ma, Y., Wang, Z., Li, L., Ding, S., Zhang, R., Wei, Z., Yang, J., & Wang, X. (2021). Xanthohumol Is a Potent Pan-Inhibitor of Coronaviruses Targeting Main Protease. *International Journal of Molecular Sciences*, *22*(22), 12134. https://doi.org/10.3390/ijms222212134

Liu, J., Cao, R., Xu, M., Wang, X., Zhang, H., Hu, H., Li, Y., Hu, Z., Zhong, W., & Wang, M. (2020). Hydroxychloroquine, a less toxic derivative of chloroquine, is effective in inhibiting SARS-CoV-2 infection in vitro. *Cell Discovery*, *6*, 16. https://doi.org/10.1038/s41421-020-0156-0

Liu, S., Xiao, G., Chen, Y., He, Y., Niu, J., Escalante, C. R., Xiong, H., Farmar, J., Debnath, A. K., Tien, P., & Jiang, S. (2004). Interaction between heptad repeat 1 and 2 regions in spike protein of SARS-associated coronavirus: Implications for virus fusogenic mechanism and identification of fusion inhibitors. *Lancet (London, England)*, *363*(9413), 938–947. https://doi.org/10.1016/S0140-6736(04)15788-7

Liu, S., Xiao, P., Kuang, Y., Hao, J., Huang, T., & Liu, E. (2021). Flavonoids from sea buckthorn: A review on phytochemistry, pharmacokinetics and role in metabolic diseases. *Journal of Food Biochemistry*, *45*(5), e13724. https://doi.org/10.1111/jfbc.13724

Loizzo, M. R., Statti, G. A., Tundis, R., Conforti, F., Bonesi, M., Autelitano, G., Houghton, P. J., Miljkovic-Brake, A., & Menichini, F. (2004). Antibacterial and antifungal activity ofSenecio inaequidens DC. andSenecio vulgaris L. *Phytotherapy Research*, *18*(9), 777–779. https://doi.org/10.1002/ptr.1562

Long, S. (2021). SARS-CoV-2 Subgenomic RNAs: Characterization, Utility, and Perspectives. *Viruses*, *13*(10), 1923. https://doi.org/10.3390/v13101923

Loo, S.-L., Wark, P. A. B., Esneau, C., Nichol, K. S., Hsu, A. C.-Y., & Bartlett, N. W. (2020). Human coronaviruses 229E and OC43 replicate and induce distinct antiviral responses in differentiated primary human bronchial epithelial cells. *American Journal of Physiology. Lung Cellular and Molecular Physiology*, *319*(6), L926–L931. https://doi.org/10.1152/ajplung.00374.2020

Lorántfy, L., Rutterschmid, D., Örkényi, R., Bakonyi, D., Faragó, J., Dargó, G., & Könczöl, Á. (2020). Continuous Industrial-Scale Centrifugal Partition Chromatography with Automatic Solvent System Handling: Concept and Instrumentation. *Organic Process Research & Development*, *24*(11), 2676–2688. https://doi.org/10.1021/acs.oprd.0c00338

Loutfy, M. R., Blatt, L. M., Siminovitch, K. A., Ward, S., Wolff, B., Lho, H., Pham, D. H., Deif, H., LaMere, E. A., Chang, M., Kain, K. C., Farcas, G. A., Ferguson, P., Latchford, M., Levy, G., Dennis,

J. W., Lai, E. K. Y., & Fish, E. N. (2003). Interferon alfacon-1 plus corticosteroids in severe acute respiratory syndrome: A preliminary study. *JAMA*, *290*(24), 3222–3228. https://doi.org/10.1001/jama.290.24.3222

Lu, R. (1992). *Seabuckthorn–a multipurpose plant for fragile mountains*. occasional paper, 20.

Lundin, A., Dijkman, R., Bergström, T., Kann, N., Adamiak, B., Hannoun, C., Kindler, E., Jónsdóttir, H. R., Muth, D., Kint, J., Forlenza, M., Müller, M. A., Drosten, C., Thiel, V., & Trybala, E. (2014). Targeting Membrane-Bound Viral RNA Synthesis Reveals Potent Inhibition of Diverse Coronaviruses Including the Middle East Respiratory Syndrome Virus. *PLOS Pathogens*, *10*(5), e1004166. https://doi.org/10.1371/journal.ppat.1004166

Luo, Y., Zhang, J., Deng, X., Ye, Y., Liao, M., & Fan, H. (2012). Complete genome sequence of a highly prevalent isolate of porcine epidemic diarrhea virus in South China. *Journal of Virology*, *86*(17), 9551. https://doi.org/10.1128/JVI.01455-12

Lyß, G., Knorre, A., Schmidt, T. J., Pahl, H. L., & Merfort, I. (1998). The Anti-inflammatory Sesquiterpene Lactone Helenalin Inhibits the Transcription Factor NF-κB by Directly Targeting p65*. *Journal of Biological Chemistry*, *273*(50), 33508–33516. https://doi.org/10.1074/jbc.273.50.33508

MacLachlan, N. J., & Dubovi, E. J. (Eds.). (2017). Chapter 24—Coronaviridae. In *Fenner's Veterinary Virology (Fifth Edition)* (pp. 435–461). Academic Press. https://doi.org/10.1016/B978-0-12-800946-8.00024-6

Maheshwari, D. T., Yogendra Kumar, M. S., Verma, S. K., Singh, V. K., & Singh, S. N. (2011). Antioxidant and hepatoprotective activities of phenolic rich fraction of Seabuckthorn (Hippophae rhamnoides L.) leaves. *Food and Chemical Toxicology: An International Journal Published for the British Industrial Biological Research Association*, *49*(9), 2422–2428. https://doi.org/10.1016/j.fct.2011.06.061

Malone, B., Urakova, N., Snijder, E. J., & Campbell, E. A. (2022). Structures and functions of coronavirus replication–transcription complexes and their relevance for SARS-CoV-2 drug design. *Nature Reviews Molecular Cell Biology*, *23*(1), Article 1. https://doi.org/10.1038/s41580-021-00432-z

Mandelik, R., Sarvas, M., Jackova, A., Salamunova, S., Novotny, J., & Vilcek, S. (2018). First outbreak with chimeric swine enteric coronavirus (SeCoV) on pig farms in Slovakia—Lessons to learn. *Acta Veterinaria Hungarica*, *66*(3), 488–492. https://doi.org/10.1556/004.2018.043

Marciniak, B., Kontek, R., Żuchowski, J., & Stochmal, A. (2021). Novel bioactive properties of low-polarity fractions from sea-buckthorn extracts (Elaeagnus rhamnoides (L.) A. Nelson) – (in vitro). *Biomedicine & Pharmacotherapy*, *135*, 111141. https://doi.org/10.1016/j.biopha.2020.111141

Markov, P. V., Ghafari, M., Beer, M., Lythgoe, K., Simmonds, P., Stilianakis, N. I., & Katzourakis, A. (2023). The evolution of SARS-CoV-2. *Nature Reviews Microbiology*, *21*(6), Article 6. https://doi.org/10.1038/s41579-023-00878-2

Marthaler, D., Raymond, L., Jiang, Y., Collins, J., Rossow, K., & Rovira, A. (2014). Rapid Detection, Complete Genome Sequencing, and Phylogenetic Analysis of Porcine Deltacoronavirus. *Emerging Infectious Diseases*, *20*(8), 1347–1350. https://doi.org/10.3201/eid2008.140526

Martono, Fatmawati, F., & Mulyanti, S. (2023). Risk Factors Associated with the Severity of COVID-19. *The Malaysian Journal of Medical Sciences : MJMS*, *30*(3), 84–92. https://doi.org/10.21315/mjms2023.30.3.7

Masters, P. S. (2006). The Molecular Biology of Coronaviruses. In *Advances in Virus Research* (Vol. 66, pp. 193–292). Academic Press. https://doi.org/10.1016/S0065-3527(06)66005-3

McIntosh, K., Becker, W. B., & Chanock, R. M. (1967). Growth in suckling-mouse brain of "IBV-like" viruses from patients with upper respiratory tract disease. *Proceedings of the National Academy of Sciences of the United States of America*, *58*(6), 2268–2273. https://doi.org/10.1073/pnas.58.6.2268

Meduri, G. U., Headley, A. S., Golden, E., Carson, S. J., Umberger, R. A., Kelso, T., & Tolley, E. A. (1998). Effect of prolonged methylprednisolone therapy in unresolving acute respiratory distress syndrome: A randomized controlled trial. *JAMA*, *280*(2), 159–165. https://doi.org/10.1001/jama.280.2.159

Menter, T., Haslbauer, J. D., Nienhold, R., Savic, S., Hopfer, H., Deigendesch, N., Frank, S., Turek, D., Willi, N., Pargger, H., Bassetti, S., Leuppi, J. D., Cathomas, G., Tolnay, M., Mertz, K. D., & Tzankov, A. (2020). Postmortem examination of COVID-19 patients reveals diffuse alveolar damage with severe capillary congestion and variegated findings in lungs and other organs

suggesting vascular dysfunction. *Histopathology*, *77*(2), 198–209. https://doi.org/10.1111/his.14134

Meunier, T., L, D., S, B., M, B., K, H., Y, R., N, F., M, D., V, S., F, T., Fh, T. B., O, L., J, D., S, B., S, S., & K, S. (2022). A Photoactivable Natural Product with Broad Antiviral Activity against Enveloped Viruses, Including Highly Pathogenic Coronaviruses. *Antimicrobial Agents and Chemotherapy*, *66*(2). https://doi.org/10.1128/AAC.01581-21

Michel, T., Destandau, E., Le Floch, G., Lucchesi, M. E., & Elfakir, C. (2012). *Food Chemistry*, *131*(3), 754–760. https://doi.org/10.1016/j.foodchem.2011.09.029

Millet, J. K., & Whittaker, G. R. (2016). Murine Leukemia Virus (MLV)-based Coronavirus Spike-pseudotyped Particle Production and Infection. *Bio-Protocol*, *6*(23), e2035. https://doi.org/10.21769/BioProtoc.2035

Miorin, L., Kehrer, T., Sanchez-Aparicio, M. T., Zhang, K., Cohen, P., Patel, R. S., Cupic, A., Makio, T., Mei, M., Moreno, E., Danziger, O., White, K. M., Rathnasinghe, R., Uccellini, M., Gao, S., Aydillo, T., Mena, I., Yin, X., Martin-Sancho, L., … García-Sastre, A. (2020). SARS-CoV-2 Orf6 hijacks Nup98 to block STAT nuclear import and antagonize interferon signaling. *Proceedings of the National Academy of Sciences*, *117*(45), 28344–28354. https://doi.org/10.1073/pnas.2016650117

Mitra, D., Verma, D., Mahakur, B., Kamboj, A., Srivastava, R., Gupta, S., Pandey, A., Arora, B., Pant, K., Panneerselvam, P., Ghosh, A., Barik, D. P., & Mohapatra, P. K. D. (2022). Molecular docking and simulation studies of natural compounds of Vitex negundo L. against papain-like protease (PLpro) of SARS CoV-2 (coronavirus) to conquer the pandemic situation in the world. *Journal of Biomolecular Structure & Dynamics*, *40*(12), 5665–5686. https://doi.org/10.1080/07391102.2021.1873185

Moës, E., Vijgen, L., Keyaerts, E., Zlateva, K., Li, S., Maes, P., Pyrc, K., Berkhout, B., van der Hoek, L., & Van Ranst, M. (2005). A novel pancoronavirus RT-PCR assay: Frequent detection of human coronavirus NL63 in children hospitalized with respiratory tract infections in Belgium. *BMC Infectious Diseases*, *5*, 6. https://doi.org/10.1186/1471-2334-5-6

Mohamed, A. E.-H. H., El-Amir, D. A., Radwan, U. A. A., & El-Sayed, M. A. (2022). Phytochemical and Biological Studies of Senecio glaucus subsp. Coronopifolius. *European Journal of Biology and Biotechnology*, *3*(1), Article 1. https://doi.org/10.24018/ejbio.2022.3.1.330

Mohammadi-Dehcheshmeh, M., Moghbeli, S. M., Rahimirad, S., Alanazi, I. O., Shehri, Z. S. A., & Ebrahimie, E. (2021). A Transcription Regulatory Sequence in the 5′ Untranslated Region of SARS-CoV-2 Is Vital for Virus Replication with an Altered Evolutionary Pattern against Human Inhibitory MicroRNAs. *Cells*, *10*(2), 319. https://doi.org/10.3390/cells10020319

Mohd, H. A., Al-Tawfiq, J. A., & Memish, Z. A. (2016). Middle East Respiratory Syndrome Coronavirus (MERS-CoV) origin and animal reservoir. *Virology Journal*, *13*(1), 87. https://doi.org/10.1186/s12985-016-0544-0

Mohr, J. F., Weiss, A., Roy, S., & Wichard, T. (2020). Genome Sequence of Frankia sp. Strain CH37, a Metallophore-Producing, Nitrogen-Fixing Actinobacterium Isolated from the Sea Buckthorn, Hippophae rhamnoides (Elaeagnaceae). *Microbiology Resource Announcements*, *9*(50), 10.1128/mra.01184-20. https://doi.org/10.1128/mra.01184-20

Montazersaheb, S., Hosseiniyan Khatibi, S. M., Hejazi, M. S., Tarhriz, V., Farjami, A., Ghasemian Sorbeni, F., Farahzadi, R., & Ghasemnejad, T. (2022). COVID-19 infection: An overview on cytokine storm and related interventions. *Virology Journal*, *19*(1), 92. https://doi.org/10.1186/s12985-022-01814-1

Mora-Díaz, J. C., Piñeyro, P. E., Rauh, R., Nelson, W., Sankoh, Z., Gregg, E., Carrillo-Ávila, J. A., Shen, H., Nelli, R. K., Zimmerman, J. J., & Giménez-Lirola, L. G. (2021). Porcine Hemagglutinating Encephalomyelitis Virus Infection In Vivo and Ex Vivo. *Journal of Virology*, *95*(12), e02335-20. https://doi.org/10.1128/JVI.02335-20

Morfopoulou, S., Brown, J. R., Davies, E. G., Anderson, G., Virasami, A., Qasim, W., Chong, W. K., Hubank, M., Plagnol, V., Desforges, M., Jacques, T. S., Talbot, P. J., & Breuer, J. (2016). Human Coronavirus OC43 Associated with Fatal Encephalitis. *The New England Journal of Medicine*, *375*(5), 497–498. https://doi.org/10.1056/NEJMc1509458

Morgenstern, A., Ekholm, A., Scheewe, P., & Rumpunen, K. (2014). Changes in content of major phenolic compounds during leaf development of sea buckthorn (Hippophaë rhamnoides L.). *Agricultural and Food Science*, *23*(3), Article 3. https://doi.org/10.23986/afsci.9489

Morris, S. B., Schwartz, N. G., Patel, P., Abbo, L., Beauchamps, L., Balan, S., Lee, E. H., Paneth-Pollak, R., Geevarughese, A., Lash, M. K., Dorsinville, M. S., Ballen, V., Eiras, D. P., Newton-Cheh, C., Smith, E., Robinson, S., Stogsdill, P., Lim, S., Fox, S. E., … Godfred-Cato, S. (2020). Case Series of Multisystem Inflammatory Syndrome in Adults Associated with SARS-CoV-2 Infection—

United Kingdom and United States, March-August 2020. *MMWR. Morbidity and Mortality Weekly Report*, *69*(40), 1450–1456. https://doi.org/10.15585/mmwr.mm6940e1

Moujir, L., Callies, O., Sousa, P. M. C., Sharopov, F., & Seca, A. M. L. (2020). Applications of Sesquiterpene Lactones: A Review of Some Potential Success Cases. *Applied Sciences*, *10*(9), Article 9. https://doi.org/10.3390/app10093001

Mu, J., Wang, L., Lv, J., Chen, Z., Brennan, M., Ma, Q., Wang, W., Liu, W., Wang, J., & Brennan, C. (2022). Phenolics from sea buckthorn (Hippophae rhamnoides L.) modulate starch digestibility through physicochemical modifications brought about by starch – Phenolic molecular interactions. *LWT*, *165*, 113682. https://doi.org/10.1016/j.lwt.2022.113682

Munblit, D., Bobkova, P., Spiridonova, E., Shikhaleva, A., Gamirova, A., Blyuss, O., Nekliudov, N., Bugaeva, P., Andreeva, M., DunnGalvin, A., Comberiati, P., Apfelbacher, C., Genuneit, J., Avdeev, S., Kapustina, V., Guekht, A., Fomin, V., Svistunov, A. A., Timashev, P., … Sechenov StopCOVID Research Team. (2021). Incidence and risk factors for persistent symptoms in adults previously hospitalized for COVID-19. *Clinical and Experimental Allergy: Journal of the British Society for Allergy and Clinical Immunology*, *51*(9), 1107–1120. https://doi.org/10.1111/cea.13997

Narayanan, A., Narwal, M., Majowicz, S. A., Varricchio, C., Toner, S. A., Ballatore, C., Brancale, A., Murakami, K. S., & Jose, J. (2022). Identification of SARS-CoV-2 inhibitors targeting Mpro and PLpro using in-cell-protease assay. *Communications Biology*, *5*(1), Article 1. https://doi.org/10.1038/s42003-022-03090-9

National Institutes of Health. (2023, March 6). *Anti-SARS-CoV-2 Monoclonal Antibodies*. COVID-19 Treatment Guidelines. https://www.covid19treatmentguidelines.nih.gov/therapies/antivirals-including-antibody-products/anti-sars-cov-2-monoclonal-antibodies/

Negi, P. S., Chauhan, A. S., Sadia, G. A., Rohinishree, Y. S., & Ramteke, R. S. (2005). Antioxidant and antibacterial activities of various seabuckthorn (Hippophae rhamnoides L.) seed extracts. *Food Chemistry*, *92*(1), 119–124. https://doi.org/10.1016/j.foodchem.2004.07.009

Neuman, B. W., Adair, B. D., Yoshioka, C., Quispe, J. D., Orca, G., Kuhn, P., Milligan, R. A., Yeager, M., & Buchmeier, M. J. (2006). Supramolecular Architecture of Severe Acute Respiratory Syndrome Coronavirus Revealed by Electron Cryomicroscopy. *Journal of Virology*, *80*(16), 7918–7928. https://doi.org/10.1128/JVI.00645-06

Newman, J. A., Douangamath, A., Yadzani, S., Yosaatmadja, Y., Aimon, A., Brandão-Neto, J., Dunnett, L., Gorrie-stone, T., Skyner, R., Fearon, D., Schapira, M., von Delft, F., & Gileadi, O. (2021). Structure, mechanism and crystallographic fragment screening of the SARS-CoV-2 NSP13 helicase. *Nature Communications*, *12*(1), Article 1. https://doi.org/10.1038/s41467-021-25166-6

Ni, W., Yang, X., Yang, D., Bao, J., Li, R., Xiao, Y., Hou, C., Wang, H., Liu, J., Yang, D., Xu, Y., Cao, Z., & Gao, Z. (2020). Role of angiotensin-converting enzyme 2 (ACE2) in COVID-19. *Critical Care*, *24*(1), 422. https://doi.org/10.1186/s13054-020-03120-0

Nie, Y., Wang, P., Shi, X., Wang, G., Chen, J., Zheng, A., Wang, W., Wang, Z., Qu, X., Luo, M., Tan, L., Song, X., Yin, X., Chen, J., Ding, M., & Deng, H. (2004). Highly infectious SARS-CoV pseudotyped virus reveals the cell tropism and its correlation with receptor expression. *Biochemical and Biophysical Research Communications*, *321*(4), 994–1000. https://doi.org/10.1016/j.bbrc.2004.07.060

Niederwerder, M. C., Nietfeld, J. C., Bai, J., Peddireddi, L., Breazeale, B., Anderson, J., Kerrigan, M. A., An, B., Oberst, R. D., Crawford, K., Lager, K. M., Madson, D. M., Rowland, R. R. R., Anderson, G. A., & Hesse, R. A. (2016). Tissue localization, shedding, virus carriage, antibody response, and aerosol transmission of Porcine epidemic diarrhea virus following inoculation of 4-week-old feeder pigs. *Journal of Veterinary Diagnostic Investigation: Official Publication of the American Association of Veterinary Laboratory Diagnosticians, Inc*, *28*(6), 671–678. https://doi.org/10.1177/1040638716663251

Olas, B. (2018). The beneficial health aspects of sea buckthorn (Elaeagnus rhamnoides (L.) A.Nelson) oil. *Journal of Ethnopharmacology*, *213*, 183–190. https://doi.org/10.1016/j.jep.2017.11.022

Osipiuk, J., Azizi, S.-A., Dvorkin, S., Endres, M., Jedrzejczak, R., Jones, K. A., Kang, S., Kathayat, R. S., Kim, Y., Lisnyak, V. G., Maki, S. L., Nicolaescu, V., Taylor, C. A., Tesar, C., Zhang, Y.-A., Zhou, Z., Randall, G., Michalska, K., Snyder, S. A., … Joachimiak, A. (2021). Structure of papain-like protease from SARS-CoV-2 and its complexes with non-covalent inhibitors. *Nature Communications*, *12*(1), Article 1. https://doi.org/10.1038/s41467-021-21060-3

Otomo, M., Takahashi, K., Miyoshi, H., Osada, K., Nakashima, H., & Yamaguchi, N. (2008). Some selective serotonin reuptake inhibitors inhibit dynamin I guanosine triphosphatase (GTPase). *Biological & Pharmaceutical Bulletin*, *31*(8), 1489–1495. https://doi.org/10.1248/bpb.31.1489

Ousseiran, Z. H., Fares, Y., & Chamoun, W. T. (2023). Neurological manifestations of COVID-19: A systematic review and detailed comprehension. *The International Journal of Neuroscience*, *133*(7), 754–769. https://doi.org/10.1080/00207454.2021.1973000

Oziminski, W. P., & Bycul, A. (2023). Thermodynamic and Kinetic Characteristics of Molnupiravir Tautomers and Its Complexes with RNA Purine Bases as an Explanation of the Possible Mechanism of Action of This Novel Antiviral Medicine: A Quantum-Chemical Study. *The Journal of Organic Chemistry*, *88*(19), 14048–14064. https://doi.org/10.1021/acs.joc.3c01580

Parvez, M. K., Al-dosari, M. S., Basudan, O. A., & Herqash, R. N. (2022). The anti-hepatitis B virus activity of sea buckthorn is attributed to quercetin, kaempferol and isorhamnetin. *Biomedical Reports*, *17*(5), 1–7. https://doi.org/10.3892/br.2022.1573

Payne, S. (2017). Family Coronaviridae. *Viruses*, 149–158. https://doi.org/10.1016/B978-0-12-803109-4.00017-9

Peacock, T. P., Goldhill, D. H., Zhou, J., Baillon, L., Frise, R., Swann, O. C., Kugathasan, R., Penn, R., Brown, J. C., Sanchez-David, R. Y., Braga, L., Williamson, M. K., Hassard, J. A., Staller, E., Hanley, B., Osborn, M., Giacca, M., Davidson, A. D., Matthews, D. A., & Barclay, W. S. (2021). The furin cleavage site in the SARS-CoV-2 spike protein is required for transmission in ferrets. *Nature Microbiology*, *6*(7), Article 7. https://doi.org/10.1038/s41564-021-00908-w

Pedersen, N. C. (2009). A review of feline infectious peritonitis virus infection: 1963–2008. *Journal of Feline Medicine and Surgery*, *11*(4), 225–258. https://doi.org/10.1016/j.jfms.2008.09.008

Pedersen, N. C., Black, J. W., Boyle, J. F., Evermann, J. F., McKeirnan, A. J., & Ott, R. L. (1984). Pathogenic differences between various feline coronavirus isolates. *Advances in Experimental Medicine and Biology*, *173*, 365–380. https://doi.org/10.1007/978-1-4615-9373-7_36

Peiris, J. S. M., Lai, S. T., Poon, L. L. M., Guan, Y., Yam, L. Y. C., Lim, W., Nicholls, J., Yee, W. K. S., Yan, W. W., Cheung, M. T., Cheng, V. C. C., Chan, K. H., Tsang, D. N. C., Yung, R. W. H., Ng, T. K., Yuen, K. Y., & SARS study group. (2003). Coronavirus as a possible cause of severe acute respiratory syndrome. *Lancet (London, England)*, *361*(9366), 1319–1325. https://doi.org/10.1016/s0140-6736(03)13077-2

Pekosz, A., Schaecher, S. R., Diamond, M. S., Fremont, D. H., Sims, A. C., & Baric, R. S. (2006). Structure, Expression, and Intracellular Localization of the SARS-CoV Accessory Proteins 7a and 7b. *The Nidoviruses*, *581*, 115–120. https://doi.org/10.1007/978-0-387-33012-9_20

Pene, F., Merlat, A., Vabret, A., Rozenberg, F., Buzyn, A., Dreyfus, F., Cariou, A., Freymuth, F., & Lebon, P. (2003). Coronavirus 229E-related pneumonia in immunocompromised patients. *Clinical Infectious Diseases: An Official Publication of the Infectious Diseases Society of America*, *37*(7), 929–932. https://doi.org/10.1086/377612

Pérez, C., Agnese, A. M., & Cabrera, J. L. (1999). The essential oil of Senecio graveolens (Compositae): Chemical composition and antimicrobial activity tests. *Journal of Ethnopharmacology*, *66*(1), 91–96. https://doi.org/10.1016/s0378-8741(98)00204-9

Perrier, A., Bonnin, A., Desmarets, L., Danneels, A., Goffard, A., Rouillé, Y., Dubuisson, J., & Belouzard, S. (2019). The C-terminal domain of the MERS coronavirus M protein contains a trans-Golgi network localization signal. *The Journal of Biological Chemistry*, *294*(39), 14406–14421. https://doi.org/10.1074/jbc.RA119.008964

Petersen, E., Koopmans, M., Go, U., Hamer, D. H., Petrosillo, N., Castelli, F., Storgaard, M., Al Khalili, S., & Simonsen, L. (2020). Comparing SARS-CoV-2 with SARS-CoV and influenza pandemics. *The Lancet. Infectious Diseases*, *20*(9), e238–e244. https://doi.org/10.1016/S1473-3099(20)30484-9

Pfizer, BioNTech. (2021, April 1). *Pfizer and BioNTech Confirm High Efficacy and No Serious Safety Concerns Through Up to Six Months Following Second Dose in Updated Topline Analysis of Landmark COVID-19 Vaccine Study*. https://www.businesswire.com/news/home/20210401005365/en/Pfizer-and-BioNTech-Confirm-High-Efficacy-and-No-Serious-Safety-Concerns-Through-Up-to-Six-Months-Following-Second-Dose-in-Updated-Topline-Analysis-of-Landmark-COVID-19-Vaccine-Study

Plantlet. (2021, August 20). Halophytes: Salient Features, Adaptations & Classification. *Plantlet*. https://plantlet.org/halophytes-salient-features-adaptations-classification/

Polack, F. P., Thomas, S. J., Kitchin, N., Absalon, J., Gurtman, A., Lockhart, S., Perez, J. L., Pérez Marc, G., Moreira, E. D., Zerbini, C., Bailey, R., Swanson, K. A., Roychoudhury, S., Koury, K., Li, P., Kalina, W. V., Cooper, D., Frenck, R. W., Hammitt, L. L., … Gruber, W. C. (2020). Safety and Efficacy of the BNT162b2 mRNA Covid-19 Vaccine. *New England Journal of Medicine*, *383*(27), 2603–2615. https://doi.org/10.1056/NEJMoa2034577

Pop, R. M., Socaciu, C., Pintea, A., Buzoianu, A. D., Sanders, M. G., Gruppen, H., & Vincken, J.-P. (2013). UHPLC/PDA-ESI/MS analysis of the main berry and leaf flavonol glycosides from different Carpathian Hippophaë rhamnoides L. varieties. *Phytochemical Analysis: PCA*, *24*(5), 484–492. https://doi.org/10.1002/pca.2460

Pop, R. M., Weesepoel, Y., Socaciu, C., Pintea, A., Vincken, J.-P., & Gruppen, H. (2014). Carotenoid composition of berries and leaves from six Romanian sea buckthorn (Hippophae rhamnoides L.) varieties. *Food Chemistry*, *147*, 1–9. https://doi.org/10.1016/j.foodchem.2013.09.083

Poutanen, S. M. (2018). Human Coronaviruses. In *Principles and Practice of Pediatric Infectious Diseases* (pp. 1148-1152.e3). Elsevier. https://doi.org/10.1016/B978-0-323-40181-4.00222-X

Poutanen, S. M., Low, D. E., Henry, B., Finkelstein, S., Rose, D., Green, K., Tellier, R., Draker, R., Adachi, D., Ayers, M., Chan, A. K., Skowronski, D. M., Salit, I., Simor, A. E., Slutsky, A. S., Doyle, P. W., Krajden, M., Petric, M., Brunham, R. C., & McGeer, A. J. (2003). Identification of Severe Acute Respiratory Syndrome in Canada. *New England Journal of Medicine*, *348*(20), 1995–2005. https://doi.org/10.1056/NEJMoa030634

powo.science.kew. (2023). *Plants of the World Online | Kew Science*. Plants of the World Online. https://powo.science.kew.org/

Pratelli, A., Martella, V., Decaro, N., Tinelli, A., Camero, M., Cirone, F., Elia, G., Cavalli, A., Corrente, M., Greco, G., Buonavoglia, D., Gentile, M., Tempesta, M., & Buonavoglia, C. (2003). Genetic diversity of a canine coronavirus detected in pups with diarrhoea in Italy. *Journal of Virological Methods*, *110*(1), 9–17. https://doi.org/10.1016/s0166-0934(03)00081-8

Pritchard, G. C. (1987). Transmissible gastroenteritis in endemically infected breeding herds of pigs in East Anglia, 1981-85. *The Veterinary Record*, *120*(10), 226–230. https://doi.org/10.1136/vr.120.10.226

Pundir, S., Garg, P., Dviwedi, A., Ali, A., Kapoor, V. K., Kapoor, D., Kulshrestha, S., Lal, U. R., & Negi, P. (2021). Ethnomedicinal uses, phytochemistry and dermatological effects of Hippophae rhamnoides L.: A review. *Journal of Ethnopharmacology*, *266*, 113434. https://doi.org/10.1016/j.jep.2020.113434

Puupponen-Pimiä, R., Nohynek, L., Meier, C., Kähkönen, M., Heinonen, M., Hopia, A., & Oksman-Caldentey, K.-M. (2001). Antimicrobial properties of phenolic compounds from berries.

Journal of Applied Microbiology, *90*(4), 494–507. https://doi.org/10.1046/j.1365-2672.2001.01271.x

Qadir, M. I., Abbas, K., Younus, A., & Shaikh, R. S. (2016). Negi. *Pakistan Journal of Pharmaceutical Sciences*, *29*(5), 1711–1713.

Rabaan, A. A., Al-Ahmed, S. H., Muhammad, J., Khan, A., Sule, A. A., Tirupathi, R., Mutair, A. A., Alhumaid, S., Al-Omari, A., Dhawan, M., Tiwari, R., Sharun, K., Mohapatra, R. K., Mitra, S., Bilal, M., Alyami, S. A., Emran, T. B., Moni, M. A., & Dhama, K. (2021). Role of Inflammatory Cytokines in COVID-19 Patients: A Review on Molecular Mechanisms, Immune Functions, Immunopathology and Immunomodulatory Drugs to Counter Cytokine Storm. *Vaccines*, *9*(5), 436. https://doi.org/10.3390/vaccines9050436

Radenkovs, V., Püssa, T., Juhnevica-Radenkova, K., Anton, D., & Seglina, D. (2018). Michel. *Food Bioscience*, *24*, 56–66. https://doi.org/10.1016/j.fbio.2018.05.010

Raj, V. S., Mou, H., Smits, S. L., Dekkers, D. H. W., Müller, M. A., Dijkman, R., Muth, D., Demmers, J. A. A., Zaki, A., Fouchier, R. A. M., Thiel, V., Drosten, C., Rottier, P. J. M., Osterhaus, A. D. M. E., Bosch, B. J., & Haagmans, B. L. (2013). Dipeptidyl peptidase 4 is a functional receptor for the emerging human coronavirus-EMC. *Nature*, *495*(7440), 251–254. https://doi.org/10.1038/nature12005

Rédei, D., Kúsz, N., Rafai, T., Bogdanov, A., Burián, K., Csorba, A., Mándi, A., Kurtán, T., Vasas, A., & Hohmann, J. (2019). 14-Noreudesmanes and a phenylpropane heterodimer from sea buckthorn berry inhibit Herpes simplex type 2 virus replication. *Tetrahedron*, *75*(10), 1364–1370. https://doi.org/10.1016/j.tet.2019.01.050

Rehfeld, F., Eitson, J. L., Ohlson, M. B., Chang, T.-C., Schoggins, J. W., & Mendell, J. T. (2023). CRISPR screening reveals a dependency on ribosome recycling for efficient SARS-CoV-2 programmed ribosomal frameshifting and viral replication. *Cell Reports*, *42*(2), 112076. https://doi.org/10.1016/j.celrep.2023.112076

Ren, Y., Shu, T., Wu, D., Mu, J., Wang, C., Huang, M., Han, Y., Zhang, X.-Y., Zhou, W., Qiu, Y., & Zhou, X. (2020). The ORF3a protein of SARS-CoV-2 induces apoptosis in cells. *Cellular & Molecular Immunology*, *17*(8), Article 8. https://doi.org/10.1038/s41423-020-0485-9

Reyna, R. A., Kishimoto-Urata, M., Urata, S., Makishima, T., Paessler, S., & Maruyama, J. (2022). Recovery of anosmia in hamsters infected with SARS-CoV-2 is correlated with repair of the

olfactory epithelium. *Scientific Reports*, *12*(1), Article 1. https://doi.org/10.1038/s41598-021-04622-9

Richardson, D. M., Pysek, P., Rejmanek, M., Barbour, M. G., Panetta, F. D., & West, C. J. (2000). Naturalization and Invasion of Alien Plants: Concepts and Definitions. *Diversity and Distributions*, *6*(2), 93–107.

Risku, M., Lappalainen, S., Räsänen, S., & Vesikari, T. (2010). Detection of human coronaviruses in children with acute gastroenteritis. *Journal of Clinical Virology*, *48*(1), 27–30. https://doi.org/10.1016/j.jcv.2010.02.013

Roe, C. K., & Alexander, T. J. (1958). A Disease of Nursing Pigs Previously Unreported in Ontario. *Canadian Journal of Comparative Medicine and Veterinary Science*, *22*(9), 305–307.

Roeder, E. (2000). Medicinal plants in China containing pyrrolizidine alkaloids. *Die Pharmazie*, *55*(10), 711–726.

Rosa, R. B., Dantas, W. M., do Nascimento, J. C. F., da Silva, M. V., de Oliveira, R. N., & Pena, L. J. (2021). In Vitro and In Vivo Models for Studying SARS-CoV-2, the Etiological Agent Responsible for COVID-19 Pandemic. *Viruses*, *13*(3), 379. https://doi.org/10.3390/v13030379

Rousi, A. (1971). The genus Hippophaë L. A taxonomic study. *Annales Botanici Fennici*, *8*(3), 177–227.

Ryu, Y. B., Park, S.-J., Kim, Y. M., Lee, J.-Y., Seo, W. D., Chang, J. S., Park, K. H., Rho, M.-C., & Lee, W. S. (2010). SARS-CoV 3CLpro inhibitory effects of quinone-methide triterpenes from Tripterygium regelii. *Bioorganic & Medicinal Chemistry Letters*, *20*(6), 1873–1876. https://doi.org/10.1016/j.bmcl.2010.01.152

Sadgrove, N. J. (2022). Comment on Pyrrolizidine Alkaloids and Terpenes from Senecio (Asteraceae): Chemistry and Research Gaps in Africa. *Molecules*, *27*(24), 8868. https://doi.org/10.3390/molecules27248868

Sahuc, M.-E., Sahli, R., Rivière, C., Pène, V., Lavie, M., Vandeputte, A., Brodin, P., Rosenberg, A. R., Dubuisson, J., Ksouri, R., Rouillé, Y., Sahpaz, S., & Séron, K. (2019). Dehydrojuncusol, a Natural Phenanthrene Compound Extracted from Juncus maritimus, Is a New Inhibitor of Hepatitis C Virus RNA Replication. *Journal of Virology*, *93*(10), e02009-18. https://doi.org/10.1128/JVI.02009-18

Sakai, Y., Kawachi, K., Terada, Y., Omori, H., Matsuura, Y., & Kamitani, W. (2017). Two-amino acids change in the nsp4 of SARS coronavirus abolishes viral replication. *Virology*, *510*, 165–174. https://doi.org/10.1016/j.virol.2017.07.019

Salminen, J.-P., & Karonen, M. (2011). Chemical ecology of tannins and other phenolics: We need a change in approach. *Functional Ecology*, *25*(2), 325–338. https://doi.org/10.1111/j.1365-2435.2010.01826.x

Sanche, S., Lin, Y. T., Xu, C., Romero-Severson, E., Hengartner, N., & Ke, R. (2020). High Contagiousness and Rapid Spread of Severe Acute Respiratory Syndrome Coronavirus 2. *Emerging Infectious Diseases*, *26*(7), 1470–1477. https://doi.org/10.3201/eid2607.200282

Sanderson, T., Hisner, R., Donovan-Banfield, I., Hartman, H., Løchen, A., Peacock, T. P., & Ruis, C. (2023). A molnupiravir-associated mutational signature in global SARS-CoV-2 genomes. *Nature*, *623*(7987), Article 7987. https://doi.org/10.1038/s41586-023-06649-6

Santos, J., Al-Azzawi, M., Aronson, J., & Flowers, T. J. (2016). eHALOPH a Database of Salt-Tolerant Plants: Helping put Halophytes to Work. *Plant & Cell Physiology*, *57*(1), e10. https://doi.org/10.1093/pcp/pcv155

Saramago, M., Costa, V. G., Souza, C. S., Bárria, C., Domingues, S., Viegas, S. C., Lousa, D., Soares, C. M., Arraiano, C. M., & Matos, R. G. (2022). The nsp15 Nuclease as a Good Target to Combat SARS-CoV-2: Mechanism of Action and Its Inactivation with FDA-Approved Drugs. *Microorganisms*, *10*(2), 342. https://doi.org/10.3390/microorganisms10020342

Scher, J. L., Walters, D. S., & Redford, A. J. (2015, April). *Senecio inaequidens*. https://idtools.org/id/fnw/factsheet.php?name=14706

Schoefs, B. (2002). Chlorophyll and carotenoid analysis in food products. Properties of the pigments and methods of analysis. *Trends in Food Science & Technology*, *13*(11), 361–371. https://doi.org/10.1016/S0924-2244(02)00182-6

Schramm, S., Köhler, N., & Rozhon, W. (2019). Pyrrolizidine Alkaloids: Biosynthesis, Biological Activities and Occurrence in Crop Plants. *Molecules*, *24*(3), 498. https://doi.org/10.3390/molecules24030498

Scovino, A. M., Dahab, E. C., Vieira, G. F., Freire-de-Lima, L., Freire-de-Lima, C. G., & Morrot, A. (2022). SARS-CoV-2's Variants of Concern: A Brief Characterization. *Frontiers in Immunology*, *13*. https://www.frontiersin.org/articles/10.3389/fimmu.2022.834098

Shah, H., Shakir, H. A., Safi, S. Z., & Ali, A. (2021). Hippophae rhamnoides mediate gene expression profiles against keratinocytes infection of Staphylococcus aureus. *Molecular Biology Reports*, *48*(2), 1409–1422. https://doi.org/10.1007/s11033-021-06221-3

Shah, M. M., Winn, A., Dahl, R. M., Kniss, K. L., Silk, B. J., & Killerby, M. E. (2022). *Seasonality of Common Human Coronaviruses, United States, 2014–2021—Volume 28, Number 10—October 2022—Emerging Infectious Diseases journal—CDC*. https://doi.org/10.3201/eid2810.220396

Shah, R. K., Idate, A., Ugale, V., & Poorva. (2021). Comprehensive review on sea buckthorn: Biological activity and its potential uses. *The Pharma Innovation Journal*, *10*(5), 942–953. https://doi.org/10.22271/tpi.2021.v10.i5l.6325

Shalhoub, S., Farahat, F., Al-Jiffri, A., Simhairi, R., Shamma, O., Siddiqi, N., & Mushtaq, A. (2015). IFN-α2a or IFN-β1a in combination with ribavirin to treat Middle East respiratory syndrome coronavirus pneumonia: A retrospective study. *The Journal of Antimicrobial Chemotherapy*, *70*(7), 2129–2132. https://doi.org/10.1093/jac/dkv085

Sharma, R. K., Sehgal, S., Sachdeva, N., Kumar, R., & Gupta, A. (2019). Direct Engagement of TLR9 Ligand with T Helper Cells Leads to Cell Proliferation & Up-regulation of Cytokines. *Immunological Investigations*, *48*(1), 79–95. https://doi.org/10.1080/08820139.2018.1515223

Sharun, K., Sircar, S., Malik, Y. S., Singh, R. K., & Dhama, K. (2020). How close is SARS-CoV-2 to canine and feline coronaviruses? *Journal of Small Animal Practice*, *61*(8), 523–526. https://doi.org/10.1111/jsap.13207

She, G.-M., Xu, C., Liu, B., & Shi, R.-B. (2010). Polyphenolic acids from mint (the aerial of Mentha haplocalyx Briq.) with DPPH radical scavenging activity. *Journal of Food Science*, *75*(4), C359-362. https://doi.org/10.1111/j.1750-3841.2010.01603.x

SHINDO, K., KIMURA, M., & IGA, M. (2004). Potent Antioxidative Activity of Cacalol, a Sesquiterpene Contained in Cacalia delphiniifolia Sleb et Zucc. *Bioscience, Biotechnology, and Biochemistry*, *68*(6), 1393–1394. https://doi.org/10.1271/bbb.68.1393

Shionogi & Co. (2023, September 19). *Shionogi Presents New Ensitrelvir Clinical and Real-World Data Reinforcing Potential Across COVID-19 Populations at ESWI 2023*. https://www.shionogi.com/global/en/news/2023/9/20230919.html

Shionogi Inc. (2023, October 11). *Shionogi Presents New Ensitrelvir COVID-19 Data Supporting Effectiveness in Real-World and Clinical Settings at IDWeek 2023*. https://www.shionogi.com/us/en/news/2023/10/shionogi-presents-new-ensitrelvir-covid-19-data-supporting-effectiveness-in-real-world-and-clinical-settings-at-idweek-2023.html

Shirato, K., Imada, Y., Kawase, M., Nakagaki, K., Matsuyama, S., & Taguchi, F. (2014). Possible involvement of infection with human coronavirus 229E, but not NL63, in Kawasaki disease. *Journal of Medical Virology*, *86*(12), 2146–2153. https://doi.org/10.1002/jmv.23950

Shirato, K., Kawase, M., & Matsuyama, S. (2013). Middle East respiratory syndrome coronavirus infection mediated by the transmembrane serine protease TMPRSS2. *Journal of Virology*, *87*(23), 12552–12561. https://doi.org/10.1128/JVI.01890-13

Shouzong, W. (2012). Studies on the chemical components in fruits of h. Rhamnoides. *Forestry Science Research*, *3*(1), 98–102.

Si, L., Meng, K., Tian, Z., Sun, J., Li, H., Zhang, Z., Soloveva, V., Li, H., Fu, G., Xia, Q., Xiao, S., Zhang, L., & Zhou, D. (2018). Triterpenoids manipulate a broad range of virus-host fusion via wrapping the HR2 domain prevalent in viral envelopes. *Science Advances*, *4*(11), eaau8408. https://doi.org/10.1126/sciadv.aau8408

Signer, J., Jonsdottir, H. R., Albrich, W. C., Strasser, M., Züst, R., Ryter, S., Ackermann-Gäumann, R., Lenz, N., Siegrist, D., Suter, A., Schoop, R., & Engler, O. B. (2020). In vitro virucidal activity of Echinaforce®, an Echinacea purpurea preparation, against coronaviruses, including common cold coronavirus 229E and SARS-CoV-2. *Virology Journal*, *17*(1), 136. https://doi.org/10.1186/s12985-020-01401-2

Singh, B., Singh, J. P., Kaur, A., & Singh, N. (2017). Phenolic composition and antioxidant potential of grain legume seeds: A review. *Food Research International (Ottawa, Ont.)*, *101*, 1–16. https://doi.org/10.1016/j.foodres.2017.09.026

Singh, D., Jayashankar, B., Mishra, K. P., Tanwar, H., Madhusudana, S. N., Belludi, A. Y., Tulsawani, R., Singh, S. B., & Ganju, L. (2018). Adjuvant activity of ethanol extract of Hippophae

rhamnoides leaves with inactivated rabies virus antigen. *Pharmaceutical Biology*, *56*(1), 25–31. https://doi.org/10.1080/13880209.2017.1413662

So, W. K. W., Chan, S. S. C., Lee, A. C. K., & Tiwari, A. F. Y. (2004). The knowledge level and precautionary measures taken by older adults during the SARS outbreak in Hong Kong. *International Journal of Nursing Studies*, *41*(8), 901–909. https://doi.org/10.1016/j.ijnurstu.2004.04.004

Sola, I., Almazán, F., Zúñiga, S., & Enjuanes, L. (2015). Continuous and Discontinuous RNA Synthesis in Coronaviruses. *Annual Review of Virology*, *2*(1), 265–288. https://doi.org/10.1146/annurev-virology-100114-055218

Solcan, C., Gogu, M., Floristean, V., Oprisan, B., & Solcan, G. (2013). The hepatoprotective effect of sea buckthorn (Hippophae rhamnoides) berries on induced aflatoxin B1 poisoning in chickens 1. *Poultry Science*, *92*(4), 966–974. https://doi.org/10.3382/ps.2012-02572

Song, D., & Park, B. (2012). Porcine epidemic diarrhoea virus: A comprehensive review of molecular epidemiology, diagnosis, and vaccines. *Virus Genes*, *44*(2), 167–175. https://doi.org/10.1007/s11262-012-0713-1

Sönmez, G., Çolak, M., Sönmez, S., & Schoenfeld, B. (2010). Effects of oral supplementation of mint extract on muscle pain and blood lactate. *Biomedical Human Kinetics*, *2*(2010), 66–69. https://doi.org/10.2478/v10101-0016-8

Sotanaphun, U., Lipipun, V., Suttisri, R., & Bavovada, R. (1999). A New Antiviral and Antimicrobial Sesquiterpene from Glyptopetalum sclerocarpum. *Planta Medica*, *65*(3), 257–258. https://doi.org/10.1055/s-2006-960472

Stahl, W., & Sies, H. (2003). Antioxidant activity of carotenoids. *Molecular Aspects of Medicine*, *24*(6), 345–351. https://doi.org/10.1016/s0098-2997(03)00030-x

Steenkamp, V., Stewart, M. J., & Zuckerman, M. (2000). Clinical and analytical aspects of pyrrolizidine poisoning caused by South African traditional medicines. *Therapeutic Drug Monitoring*, *22*(3), 302–306. https://doi.org/10.1097/00007691-200006000-00011

Stevenson, G. W., Hoang, H., Schwartz, K. J., Burrough, E. R., Sun, D., Madson, D., Cooper, V. L., Pillatzki, A., Gauger, P., Schmitt, B. J., Koster, L. G., Killian, M. L., & Yoon, K. J. (2013). Emergence of Porcine epidemic diarrhea virus in the United States: Clinical signs, lesions, and

viral genomic sequences. *Journal of Veterinary Diagnostic Investigation: Official Publication of the American Association of Veterinary Laboratory Diagnosticians, Inc*, *25*(5), 649–654. https://doi.org/10.1177/1040638713501675

Storz, J., Lin, X., Purdy, C. W., Chouljenko, V. N., Kousoulas, K. G., Enright, F. M., Gilmore, W. C., Briggs, R. E., & Loan, R. W. (2000). Coronavirus and Pasteurella infections in bovine shipping fever pneumonia and Evans' criteria for causation. *Journal of Clinical Microbiology*, *38*(9), 3291–3298. https://doi.org/10.1128/JCM.38.9.3291-3298.2000

Su, H., Yao, S., Zhao, W., Li, M., Liu, J., Shang, W., Xie, H., Ke, C., Hu, H., Gao, M., Yu, K., Liu, H., Shen, J., Tang, W., Zhang, L., Xiao, G., Ni, L., Wang, D., Zuo, J., … Xu, Y. (2020). Anti-SARS-CoV-2 activities in vitro of Shuanghuanglian preparations and bioactive ingredients. *Acta Pharmacologica Sinica*, *41*(9), Article 9. https://doi.org/10.1038/s41401-020-0483-6

Sultana, B., Anwar, F., & Ashraf, M. (2009). Effect of extraction solvent/technique on the antioxidant activity of selected medicinal plant extracts. *Molecules (Basel, Switzerland)*, *14*(6), 2167–2180. https://doi.org/10.3390/molecules14062167

Sun, Y., Feng, F., Nie, B., Cao, J., & Zhang, F. (2019). High throughput identification of pentacyclic triterpenes in Hippophae rhamnoides using multiple neutral loss markers scanning combined with substructure recognition (MNLSR). *Talanta*, *205*, 120011. https://doi.org/10.1016/j.talanta.2019.06.011

Takahashi, K., Miyoshi, H., Otomo, M., Osada, K., Yamaguchi, N., & Nakashima, H. (2010). Suppression of dynamin GTPase activity by sertraline leads to inhibition of dynamin-dependent endocytosis. *Biochemical and Biophysical Research Communications*, *391*(1), 382–387. https://doi.org/10.1016/j.bbrc.2009.11.067

Takarina, N. D. (2020). Mangrove Root Diversity and Structure (cone, pencil, prop) Effectiveness in Accumulating Cu and Zn in Sediments and Water in River Blanakan. *IOP Conference Series: Earth and Environmental Science*, *550*(1), 012009. https://doi.org/10.1088/1755-1315/550/1/012009

Takeda, Y., Jamsransuren, D., Matsuda, S., Crea, R., & Ogawa, H. (2021). The SARS-CoV-2-Inactivating Activity of Hydroxytyrosol-Rich Aqueous Olive Pulp Extract (HIDROX®) and Its Use as a Virucidal Cream for Topical Application. *Viruses*, *13*(2), 232. https://doi.org/10.3390/v13020232

Teleszko, M., Wojdyło, A., Rudzińska, M., Oszmiański, J., & Golis, T. (2015). Analysis of Lipophilic and Hydrophilic Bioactive Compounds Content in Sea Buckthorn (Hippophaë rhamnoides L.) Berries. *Journal of Agricultural and Food Chemistry*, *63*(16), 4120–4129. https://doi.org/10.1021/acs.jafc.5b00564

Teli, D., Balar, P., Patel, K., Sharma, A., Chavda, V., & Vora, L. (2023). Molnupiravir: A Versatile Prodrug against SARS-CoV-2 Variants. *Metabolites*, *13*(2), 309. https://doi.org/10.3390/metabo13020309

Thiel, V., Herold, J., Schelle, B., & Siddell, S. G. (2001). Infectious RNA transcribed in vitro from a cDNA copy of the human coronavirus genome cloned in vaccinia virus. *The Journal of General Virology*, *82*(Pt 6), 1273–1281. https://doi.org/10.1099/0022-1317-82-6-1273

Tiitinen, K. M., Hakala, M. A., & Kallio, H. P. (2005). Quality Components of Sea Buckthorn (Hippophaë rhamnoides) Varieties. *Journal of Agricultural and Food Chemistry*, *53*(5), 1692–1699. https://doi.org/10.1021/jf0484125

Tkacz, K., Wojdyło, A., Turkiewicz, I. P., Bobak, Ł., & Nowicka, P. (2019). Anti-Oxidant and Anti-Enzymatic Activities of Sea Buckthorn (Hippophaë rhamnoides L.) Fruits Modulated by Chemical Components. *Antioxidants (Basel, Switzerland)*, *8*(12), 618. https://doi.org/10.3390/antiox8120618

Tkacz, K., Wojdyło, A., Turkiewicz, I. P., & Nowicka, P. (2021). Triterpenoids, phenolic compounds, macro- and microelements in anatomical parts of sea buckthorn (Hippophaë rhamnoides L.) berries, branches and leaves. *Journal of Food Composition and Analysis*, *103*, 104107. https://doi.org/10.1016/j.jfca.2021.104107

Tomkiewicz, R. P., App, E. M., Zayas, J. G., Ramirez, O., Church, N., Boucher, R. C., Knowles, M. R., & King, M. (1993). Amiloride inhalation therapy in cystic fibrosis. Influence on ion content, hydration, and rheology of sputum. *The American Review of Respiratory Disease*, *148*(4 Pt 1), 1002–1007. https://doi.org/10.1164/ajrccm/148.4_Pt_1.1002

Torres, P., Ayala, J., Grande, C., Macías, M. J., & Grande, M. (1998). Furanoeremophilanes and a bakkenolide from Senecio auricula var. Major. *Phytochemistry*, *47*(1), 57–61. https://doi.org/10.1016/S0031-9422(97)00497-4

Toyang, N. J., Krause, M. A., Fairhurst, R. M., Tane, P., Bryant, J., & Verpoorte, R. (2013). Antiplasmodial activity of sesquiterpene lactones and a sucrose ester from Vernonia guineensis

Benth. (Asteraceae). *Journal of Ethnopharmacology*, *147*(3), 618–621. https://doi.org/10.1016/j.jep.2013.03.051

Trentin, A. P., Santos, A. R., Guedes, A., Pizzolatti, M. G., Yunes, R. A., & Calixto, J. B. (1999). Antinociception caused by the extract of Hedyosmum brasiliense and its active principle, the sesquiterpene lactone 13-hydroxy-8,9-dehydroshizukanolide. *Planta Medica*, *65*(6), 517–521. https://doi.org/10.1055/s-1999-14007

Tresnan, D. B., Levis, R., & Holmes, K. V. (1996). Feline aminopeptidase N serves as a receptor for feline, canine, porcine, and human coronaviruses in serogroup I. *Journal of Virology*, *70*(12), 8669–8674. https://doi.org/10.1128/JVI.70.12.8669-8674.1996

Truong, D.-H., Nguyen, D. H., Ta, N. T. A., Bui, A. V., Do, T. H., & Nguyen, H. C. (2019). Evaluation of the Use of Different Solvents for Phytochemical Constituents, Antioxidants, and In Vitro Anti-Inflammatory Activities of Severinia buxifolia. *Journal of Food Quality*, *2019*, 8178294. https://doi.org/10.1155/2019/8178294

Tundis, R., Loizzo, M. R., Statti, G. A., Houghton, P. J., Miljkovic-Brake, A., & Menichini, F. (2007). In vitro hypoglycemic and antimicrobial activities of Senecio leucanthemifolius Poiret. *Natural Product Research*, *21*(5), 396–400. https://doi.org/10.1080/14786410500520111

Tyrrell, D. A., & Bynoe, M. L. (1966). Cultivation of viruses from a high proportion of patients with colds. *Lancet (London, England)*, *1*(7428), 76–77. https://doi.org/10.1016/s0140-6736(66)92364-6

Uğur, A., Ertem, H., & Beyatlı, Y. (2006). Antibacterial Properties of Senecio sandrasicus. On Multidrug-Resistant Stenotrophomonas maltophilia. *Pharmaceutical Biology*, *44*(4), 253–257. https://doi.org/10.1080/13880200600713865

Ugur, A., Sarac, N., & Duru, M. E. (2009). Antimicrobial activity and chemical composition of Senecio sandrasicus on antibiotic resistant staphylococci. *Natural Product Communications*, *4*(4), 579–584.

Unal, M. A., Bitirim, C. V., Summak, G. Y., Bereketoglu, S., Cevher Zeytin, I., Besbinar, O., Gurcan, C., Aydos, D., Goksoy, E., Kocakaya, E., Eran, Z., Murat, M., Demir, N., Aksoy Ozer, Z. B., Somers, J., Demir, E., Nazir, H., Ozkan, S. A., Ozkul, A., … Akcali, K. C. (2021). Ribavirin shows antiviral activity against SARS-CoV-2 and downregulates the activity of TMPRSS2 and the expression of

ACE2 in vitro. *Canadian Journal of Physiology and Pharmacology*, *99*(5), 449–460. https://doi.org/10.1139/cjpp-2020-0734

Unasylva. (1993). *La foresterie urbaine et périurbaine—Table des matières*. https://www.fao.org/3/u9300F/u9300f00.htm

Upadhyay, N. K., Kumar, M. S. Y., & Gupta, A. (2010). Antioxidant, cytoprotective and antibacterial effects of Sea buckthorn (Hippophae rhamnoides L.) leaves. *Food and Chemical Toxicology: An International Journal Published for the British Industrial Biological Research Association*, *48*(12), 3443–3448. https://doi.org/10.1016/j.fct.2010.09.019

Upadhyay, N. K., Kumar, R., Siddiqui, M. S., & Gupta, A. (2011). Mechanism of Wound-Healing Activity of Hippophae rhamnoides L. Leaf Extract in Experimental Burns. *Evidence-Based Complementary and Alternative Medicine : eCAM*, *2011*, 659705. https://doi.org/10.1093/ecam/nep189

Valese, A. C., Daguer, H., Muller, C. M. O., Molognoni, L., da Luz, C. F. P., de Barcellos Falkenberg, D., Gonzaga, L. V., Brugnerotto, P., Gorniak, S. L., Barreto, F., Fett, R., & Costa, A. C. O. (2021). Quantification of pyrrolizidine alkaloids in Senecio brasiliensis, beehive pollen, and honey by LC-MS/MS. *Journal of Environmental Science and Health, Part B*, *56*(7), 685–694. https://doi.org/10.1080/03601234.2021.1943257

van Boheemen, S., de Graaf, M., Lauber, C., Bestebroer, T. M., Raj, V. S., Zaki, A. M., Osterhaus, A. D. M. E., Haagmans, B. L., Gorbalenya, A. E., Snijder, E. J., & Fouchier, R. A. M. (2012). Genomic characterization of a newly discovered coronavirus associated with acute respiratory distress syndrome in humans. *mBio*, *3*(6), e00473-12. https://doi.org/10.1128/mBio.00473-12

van der Hoek, L., Sure, K., Ihorst, G., Stang, A., Pyrc, K., Jebbink, M. F., Petersen, G., Forster, J., Berkhout, B., & Überla, K. (2005). Croup Is Associated with the Novel Coronavirus NL63. *PLoS Medicine*, *2*(8), e240. https://doi.org/10.1371/journal.pmed.0020240

Van Schalkwyk, F. J., Stander, M. A., Nsizwane, M., Mathee, A., & Van Wyk, B.-E. (2021). Fatal pyrrolizidine alkaloid poisoning of infants caused by adulterated Senecio coronatus. *Forensic Science International*, *320*, 110680. https://doi.org/10.1016/j.forsciint.2020.110680

Van Wyk, B.-E., Stander, M. A., & Long, H. S. (2017). Senecio angustifolius as the major source of pyrrolizidine alkaloid contamination of rooibos tea (Aspalathus linearis). *South African Journal of Botany*, *110*, 124–131. https://doi.org/10.1016/j.sajb.2017.01.013

Vanaparthy, R., Mohan, G., Vasireddy, D., & Atluri, P. (2021). Review of COVID-19 viral vector-based vaccines and COVID-19 variants. *Le Infezioni in Medicina*, *29*(3), 328–338. https://doi.org/10.53854/liim-2903-3

Vangeel, L., Chiu, W., De Jonghe, S., Maes, P., Slechten, B., Raymenants, J., André, E., Leyssen, P., Neyts, J., & Jochmans, D. (2022). Remdesivir, Molnupiravir and Nirmatrelvir remain active against SARS-CoV-2 Omicron and other variants of concern. *Antiviral Research*, *198*, 105252. https://doi.org/10.1016/j.antiviral.2022.105252

Velusamy, P., Kiruba, K., Su, C.-H., Arun, V., Anbu, P., Gopinath, S. C. B., & Vaseeharan, B. (2021). SARS-CoV-2 spike protein: Site-specific breakpoints for the development of COVID-19 vaccines. *Journal of King Saud University - Science*, *33*(8), 101648. https://doi.org/10.1016/j.jksus.2021.101648

Vercauteren, D., Vandenbroucke, R. E., Jones, A. T., Rejman, J., Demeester, J., De Smedt, S. C., Sanders, N. N., & Braeckmans, K. (2010). The use of inhibitors to study endocytic pathways of gene carriers: Optimization and pitfalls. *Molecular Therapy: The Journal of the American Society of Gene Therapy*, *18*(3), 561–569. https://doi.org/10.1038/mt.2009.281

Vijgen, L., Keyaerts, E., Lemey, P., Moës, E., Li, S., Vandamme, A.-M., & Van Ranst, M. (2005). Circulation of genetically distinct contemporary human coronavirus OC43 strains. *Virology*, *337*(1), 85–92. https://doi.org/10.1016/j.virol.2005.04.010

Vijgen, L., Keyaerts, E., Moës, E., Thoelen, I., Wollants, E., Lemey, P., Vandamme, A.-M., & Van Ranst, M. (2005). Complete genomic sequence of human coronavirus OC43: Molecular clock analysis suggests a relatively recent zoonotic coronavirus transmission event. *Journal of Virology*, *79*(3), 1595–1604. https://doi.org/10.1128/JVI.79.3.1595-1604.2005

V'kovski, P., Kratzel, A., Steiner, S., Stalder, H., & Thiel, V. (2021). Coronavirus biology and replication: Implications for SARS-CoV-2. *Nature Reviews Microbiology*, *19*(3), Article 3. https://doi.org/10.1038/s41579-020-00468-6

Vlasak, R., Luytjes, W., Spaan, W., & Palese, P. (1988). Human and bovine coronaviruses recognize sialic acid-containing receptors similar to those of influenza C viruses. *Proceedings of the National Academy of Sciences of the United States of America*, *85*(12), 4526–4529. https://doi.org/10.1073/pnas.85.12.4526

Walker, A. S., Vihta, K.-D., Gethings, O., Pritchard, E., Jones, J., House, T., Bell, I., Bell, J. I., Newton, J. N., Farrar, J., Diamond, I., Studley, R., Rourke, E., Hay, J., Hopkins, S., Crook, D., Peto, T., Matthews, P. C., Eyre, D. W., … Pouwels, K. B. (2021). Tracking the Emergence of SARS-CoV-2 Alpha Variant in the United Kingdom. *New England Journal of Medicine*, *385*(27), 2582–2585. https://doi.org/10.1056/NEJMc2103227

Walsh, E. E., Shin, J. H., & Falsey, A. R. (2013). Clinical Impact of Human Coronaviruses 229E and OC43 Infection in Diverse Adult Populations. *The Journal of Infectious Diseases*, *208*(10), 1634–1642. https://doi.org/10.1093/infdis/jit393

Wang, D., Hu, B., Hu, C., Zhu, F., Liu, X., Zhang, J., Wang, B., Xiang, H., Cheng, Z., Xiong, Y., Zhao, Y., Li, Y., Wang, X., & Peng, Z. (2020). Clinical Characteristics of 138 Hospitalized Patients With 2019 Novel Coronavirus-Infected Pneumonia in Wuhan, China. *JAMA*, *323*(11), 1061–1069. https://doi.org/10.1001/jama.2020.1585

Wang, M.-Y., Zhao, R., Gao, L.-J., Gao, X.-F., Wang, D.-P., & Cao, J.-M. (2020). SARS-CoV-2: Structure, Biology, and Structure-Based Therapeutics Development. *Frontiers in Cellular and Infection Microbiology*, *10*. https://www.frontiersin.org/articles/10.3389/fcimb.2020.587269

Wang, Q., Vlasova, A. N., Kenney, S. P., & Saif, L. J. (2019). Emerging and re-emerging coronaviruses in pigs. *Current Opinion in Virology*, *34*, 39–49. https://doi.org/10.1016/j.coviro.2018.12.001

Wd, I., J, L., Sd, J., Sr, K., & R, C. (1999). Antihyperglycemic sesquiterpenes from Psacalium decompositum. *Journal of Natural Products*, *62*(8). https://doi.org/10.1021/np990023v

Whitaker, H. J., Tsang, R. S. M., Byford, R., Andrews, N. J., Sherlock, J., Sebastian Pillai, P., Williams, J., Button, E., Campbell, H., Sinnathamby, M., Victor, W., Anand, S., Linley, E., Hewson, J., DArchangelo, S., Otter, A. D., Ellis, J., Hobbs, R. F. D., Howsam, G., … Lopez Bernal, J. (2022). Pfizer-BioNTech and Oxford AstraZeneca COVID-19 vaccine effectiveness and immune response amongst individuals in clinical risk groups. *The Journal of Infection*, *84*(5), 675–683. https://doi.org/10.1016/j.jinf.2021.12.044

Williams, G. M., Mori, H., Hirono, I., & Nagao, M. (1980). Genotoxicity of pyrrolizidine alkaloids in the hepatocyte primary culture/DNA-repair test. *Mutation Research*, *79*(1), 1–5. https://doi.org/10.1016/0165-1218(80)90141-x

Williams, R. K., Jiang, G. S., & Holmes, K. V. (1991). Receptor for mouse hepatitis virus is a member of the carcinoembryonic antigen family of glycoproteins. *Proceedings of the National Academy of Sciences of the United States of America*, *88*(13), 5533–5536.

Williamson, B. N., Feldmann, F., Schwarz, B., Meade-White, K., Porter, D. P., Schulz, J., van Doremalen, N., Leighton, I., Yinda, C. K., Pérez-Pérez, L., Okumura, A., Lovaglio, J., Hanley, P. W., Saturday, G., Bosio, C. M., Anzick, S., Barbian, K., Cihlar, T., Martens, C., … de Wit, E. (2020). Clinical benefit of remdesivir in rhesus macaques infected with SARS-CoV-2. *Nature*, *585*(7824), Article 7824. https://doi.org/10.1038/s41586-020-2423-5

Wong, H. R., & Menendez, I. Y. (1999). Sesquiterpene lactones inhibit inducible nitric oxide synthase gene expression in cultured rat aortic smooth muscle cells. *Biochemical and Biophysical Research Communications*, *262*(2), 375–380. https://doi.org/10.1006/bbrc.1999.1207

Wong, R. S. M., & Hui, D. S. (2004). Index Patient and SARS Outbreak in Hong Kong. *Emerging Infectious Diseases*, *10*(2), 339–341. https://doi.org/10.3201/eid1002.030645

Woo, P. C. Y., Huang, Y., Lau, S. K. P., & Yuen, K.-Y. (2010). Coronavirus Genomics and Bioinformatics Analysis. *Viruses*, *2*(8), 1804–1820. https://doi.org/10.3390/v2081803

Woo, P. C. Y., Lau, S. K. P., Chu, C., Chan, K., Tsoi, H., Huang, Y., Wong, B. H. L., Poon, R. W. S., Cai, J. J., Luk, W., Poon, L. L. M., Wong, S. S. Y., Guan, Y., Peiris, J. S. M., & Yuen, K. (2005). Characterization and complete genome sequence of a novel coronavirus, coronavirus HKU1, from patients with pneumonia. *Journal of Virology*, *79*(2), 884–895. https://doi.org/10.1128/JVI.79.2.884-895.2005

Woo, P. C. Y., Lau, S. K. P., Lam, C. S. F., Lau, C. C. Y., Tsang, A. K. L., Lau, J. H. N., Bai, R., Teng, J. L. L., Tsang, C. C. C., Wang, M., Zheng, B.-J., Chan, K.-H., & Yuen, K.-Y. (2012). Discovery of Seven Novel Mammalian and Avian Coronaviruses in the Genus Deltacoronavirus Supports Bat Coronaviruses as the Gene Source of Alphacoronavirus and Betacoronavirus and Avian Coronaviruses as the Gene Source of Gammacoronavirus and Deltacoronavirus. *Journal of Virology*, *86*(7), 3995–4008. https://doi.org/10.1128/JVI.06540-11

Wood, E. N., Pritchard, G. C., & Gibson, E. A. (1981). Transmissible gastroenteritis of pigs. *The Veterinary Record*, *108*(2), 41. https://doi.org/10.1136/vr.108.2.41

World Flora Online. (2023). *Hippophae L.* https://www.worldfloraonline.org/taxon/wfo-4000017969

World Health Organization. (2015, July 24). *Summary of probable SARS cases with onset of illness from 1 November 2002 to 31 July 2003*. https://www.who.int/publications/m/item/summary-of-probable-sars-cases-with-onset-of-illness-from-1-november-2002-to-31-july-2003

World Health Organization. (2020a). *"Solidarity" clinical trial for COVID-19 treatments*. https://www.who.int/emergencies/diseases/novel-coronavirus-2019/global-research-on-novel-coronavirus-2019-ncov/solidarity-clinical-trial-for-covid-19-treatments

World Health Organization. (2020b, January 30). *IHR Emergency Committee on Novel Coronavirus (2019-nCoV)*. https://www.who.int/director-general/speeches/detail/who-director-general-s-statement-on-ihr-emergency-committee-on-novel-coronavirus-(2019-ncov)

World Health Organization. (2020c, March 11). *WHO Director-General's opening remarks at the media briefing on COVID-19—11 March 2020*. https://www.who.int/director-general/speeches/detail/who-director-general-s-opening-remarks-at-the-media-briefing-on-covid-19---11-march-2020

World Health Organization. (2023a, January 30). *Integrating Traditional Medicine in Health Care*. https://www.who.int/southeastasia/news/feature-stories/detail/integrating-traditional-medicine

World Health Organization. (2023b, May). *MERS outbreaks*. World Health Organization - Regional Office for the Eastern Mediterranean. http://www.emro.who.int/health-topics/mers-cov/mers-outbreaks.html

World Health Organization. (2023c, November 16). *WHO Coronavirus (COVID-19) Dashboard*. https://covid19.who.int

Wu, B., Lin, W. H., Gao, H. Y., Zheng, L., Wu, L. J., & Kim, C. S. (2006). Four New Antibacterial Constituents from Senecio cannabifolius. *Pharmaceutical Biology*, *44*(6), 440–444. https://doi.org/10.1080/13880200600798502

Wu, C.-Y., Jan, J.-T., Ma, S.-H., Kuo, C.-J., Juan, H.-F., Cheng, Y.-S. E., Hsu, H.-H., Huang, H.-C., Wu, D., Brik, A., Liang, F.-S., Liu, R.-S., Fang, J.-M., Chen, S.-T., Liang, P.-H., & Wong, C.-H. (2004). Small molecules targeting severe acute respiratory syndrome human coronavirus. *Proceedings of the National Academy of Sciences*, *101*(27), 10012–10017. https://doi.org/10.1073/pnas.0403596101

Wu, K., Li, W., Peng, G., & Li, F. (2009). Crystal structure of NL63 respiratory coronavirus receptor-binding domain complexed with its human receptor. *Proceedings of the National Academy of Sciences*, *106*(47), 19970–19974. https://doi.org/10.1073/pnas.0908837106

Wu, W., Cheng, Y., Zhou, H., Sun, C., & Zhang, S. (2023). The SARS-CoV-2 nucleocapsid protein: Its role in the viral life cycle, structure and functions, and use as a potential target in the development of vaccines and diagnostics. *Virology Journal*, *20*(1), 6. https://doi.org/10.1186/s12985-023-01968-6

Xian, Y., Zhang, J., Bian, Z., Zhou, H., Zhang, Z., Lin, Z., & Xu, H. (2020). Bioactive natural compounds against human coronaviruses: A review and perspective. *Acta Pharmaceutica Sinica. B*, *10*(7), 1163–1174. https://doi.org/10.1016/j.apsb.2020.06.002

Xiong, Q., Cao, L., Ma, C., Tortorici, M. A., Liu, C., Si, J., Liu, P., Gu, M., Walls, A. C., Wang, C., Shi, L., Tong, F., Huang, M., Li, J., Zhao, C., Shen, C., Chen, Y., Zhao, H., Lan, K., … Yan, H. (2022). Close relatives of MERS-CoV in bats use ACE2 as their functional receptors. *Nature*, *612*(7941), 748. https://doi.org/10.1038/s41586-022-05513-3

Xu, C., Wang, A., Geng, K., Honnen, W., Wang, X., Bruiners, N., Singh, S., Ferrara, F., D'Angelo, S., Bradbury, A. R. M., Gennaro, M. L., Liu, D., Pinter, A., & Chang, T. L. (2021). Human Immunodeficiency Viruses Pseudotyped with SARS-CoV-2 Spike Proteins Infect a Broad Spectrum of Human Cell Lines through Multiple Entry Mechanisms. *Viruses*, *13*(6), 953. https://doi.org/10.3390/v13060953

Yadav, R., Chaudhary, J. K., Jain, N., Chaudhary, P. K., Khanra, S., Dhamija, P., Sharma, A., Kumar, A., & Handu, S. (2021). Role of Structural and Non-Structural Proteins and Therapeutic Targets of SARS-CoV-2 for COVID-19. *Cells*, *10*(4), 821. https://doi.org/10.3390/cells10040821

Yang, X., Yang, L., Xiong, A., Li, D., & Wang, Z. (2011). Authentication of Senecio scandens and S. vulgaris based on the comprehensive secondary metabolic patterns gained by UPLC-DAD/ESI-MS. *Journal of Pharmaceutical and Biomedical Analysis*, *56*(2), 165–172. https://doi.org/10.1016/j.jpba.2011.05.004

Yang, Z.-G., Li, H.-R., Wang, L.-Y., Li, Y.-H., Lu, S.-G., Wen, X.-F., Wang, J., Daikonya, A., & Kitanaka, S. (2007). Triterpenoids from *Hippophae rhamnoides* L. and Their Nitric Oxide Production-Inhibitory and DPPH Radical-Scavenging Activities. *Chemical and Pharmaceutical Bulletin*, *55*(1), 15–18. https://doi.org/10.1248/cpb.55.15

Yang, Z.-G., Wen, X.-F., Li, Y.-H., Matsuzaki, K., & Kitanaka, S. (2013). Inhibitory effects of the constituents of Hippophae rhamnoides on 3T3-L1 cell differentiation and nitric oxide production in RAW264.7 cells. *Chemical & Pharmaceutical Bulletin*, *61*(3), 279–285. https://doi.org/10.1248/cpb.c12-00835

Yongshan, L., Xuelin, C., Kun, S., & Ruijun, M. (2003). A New Subspecies of Hippophae (Elaeagnaceae) from China. *Novon*, *13*(2), 200–202. https://doi.org/10.2307/3393519

Yu, F., Wang, Q., Zhang, Z., Peng, Y., Qiu, Y., Shi, Y., Zheng, Y., Xiao, S., Wang, H., Huang, X., Zhu, L., Chen, K., Zhao, C., Zhang, C., Yu, M., Sun, D., Zhang, L., & Zhou, D. (2013). Development of Oleanane-Type Triterpenes as a New Class of HCV Entry Inhibitors. *Journal of Medicinal Chemistry*, *56*(11), 4300–4319. https://doi.org/10.1021/jm301910a

Yu, M., Si, L., Wang, Y., Wu, Y., Yu, F., Jiao, P., Shi, Y., Wang, H., Xiao, S., Fu, G., Tian, K., Wang, Y., Guo, Z., Ye, X., Zhang, L., & Zhou, D. (2014). Discovery of Pentacyclic Triterpenoids as Potential Entry Inhibitors of Influenza Viruses. *Journal of Medicinal Chemistry*, *57*(23), 10058–10071. https://doi.org/10.1021/jm5014067

Zaffagni, M., Harris, J. M., Patop, I. L., Pamudurti, N. R., Nguyen, S., & Kadener, S. (2022). SARS-CoV-2 Nsp14 mediates the effects of viral infection on the host cell transcriptome. *eLife*, *11*, e71945. https://doi.org/10.7554/eLife.71945

Zaki, A. M., van Boheemen, S., Bestebroer, T. M., Osterhaus, A. D. M. E., & Fouchier, R. A. M. (2012). Isolation of a novel coronavirus from a man with pneumonia in Saudi Arabia. *The New England Journal of Medicine*, *367*(19), 1814–1820. https://doi.org/10.1056/NEJMoa1211721

Zakynthinos, G., & Varzakas, T. (2015). Hippophae rhamnoides: Safety and nutrition. *Current Research in Nutrition and Food Science Journal*, *3*(2), 89–97.

Zandi, K., Musall, K., Oo, A., Cao, D., Liang, B., Hassandarvish, P., Lan, S., Slack, R. L., Kirby, K. A., Bassit, L., Amblard, F., Kim, B., AbuBakar, S., Sarafianos, S. G., & Schinazi, R. F. (2021). Baicalein and Baicalin Inhibit SARS-CoV-2 RNA-Dependent-RNA Polymerase. *Microorganisms*, *9*(5), 893. https://doi.org/10.3390/microorganisms9050893

Zannella, C., Giugliano, R., Chianese, A., Buonocore, C., Vitale, G. A., Sanna, G., Sarno, F., Manzin, A., Nebbioso, A., Termolino, P., Altucci, L., Galdiero, M., de Pascale, D., & Franci, G. (2021). Antiviral Activity of Vitis vinifera Leaf Extract against SARS-CoV-2 and HSV-1. *Viruses*, *13*(7), 1263. https://doi.org/10.3390/v13071263

Zeng, Q., Langereis, M. A., van Vliet, A. L. W., Huizinga, E. G., & de Groot, R. J. (2008). Structure of coronavirus hemagglutinin-esterase offers insight into corona and influenza virus evolution. *Proceedings of the National Academy of Sciences of the United States of America*, *105*(26), 9065–9069. https://doi.org/10.1073/pnas.0800502105

Zhan, Y., Ta, W., Tang, W., Hua, R., Wang, J., Wang, C., & Lu, W. (2021). Potential antiviral activity of isorhamnetin against SARS-CoV-2 spike pseudotyped virus in vitro. *Drug Development Research*, *82*(8), 1124–1130. https://doi.org/10.1002/ddr.21815

Zhang, S., Qiao, S., Yu, J., Zeng, J., Shan, S., Tian, L., Lan, J., Zhang, L., & Wang, X. (2021). Bat and pangolin coronavirus spike glycoprotein structures provide insights into SARS-CoV-2 evolution. *Nature Communications*, *12*, 1607. https://doi.org/10.1038/s41467-021-21767-3

Zhang, Y., Geng, X., Tan, Y., Li, Q., Xu, C., Xu, J., Hao, L., Zeng, Z., Luo, X., Liu, F., & Wang, H. (2020). New understanding of the damage of SARS-CoV-2 infection outside the respiratory system. *Biomedicine & Pharmacotherapy*, *127*, 110195. https://doi.org/10.1016/j.biopha.2020.110195

Zhang, Y., Li, J., Xiao, Y., Zhang, J., Wang, Y., Chen, L., Paranhos-Baccalà, G., Ren, L., & Wang, J. (2015). Genotype shift in human coronavirus OC43 and emergence of a novel genotype by natural recombination. *Journal of Infection*, *70*(6), 641–650. https://doi.org/10.1016/j.jinf.2014.12.005

Zhang, Z., Nomura, N., Muramoto, Y., Ekimoto, T., Uemura, T., Liu, K., Yui, M., Kono, N., Aoki, J., Ikeguchi, M., Noda, T., Iwata, S., Ohto, U., & Shimizu, T. (2022). Structure of SARS-CoV-2 membrane protein essential for virus assembly. *Nature Communications*, *13*(1), Article 1. https://doi.org/10.1038/s41467-022-32019-3

Zhao, G., Cao, Z., Zhang, W., & Zhao, H. (2015). The sesquiterpenoids and their chemotaxonomic implications in Senecio L. (Asteraceae). *Biochemical Systematics and Ecology*, *59*, 340–347. https://doi.org/10.1016/j.bse.2015.02.001

Zheng, J., Miao, J., Guo, R., Guo, J., Fan, Z., Kong, X., Gao, R., & Yang, L. (2022). Mechanism of COVID-19 Causing ARDS: Exploring the Possibility of Preventing and Treating SARS-CoV-2. *Frontiers in Cellular and Infection Microbiology*, *12*, 931061. https://doi.org/10.3389/fcimb.2022.931061

Zheng, R.-X., Xu, X.-D., Tian, Z., & Yang, J.-S. (2009). Chemical constituents from the fruits of Hippophae rhamnoides. *Natural Product Research*, *23*(15), 1451–1456. https://doi.org/10.1080/14786410903075457

Zhong, N., Zheng, B., Li, Y., Poon, L., Xie, Z., Chan, K., Li, P., Tan, S., Chang, Q., Xie, J., Liu, X., Xu, J., Li, D., Yuen, K., Peiris, J., & Guan, Y. (2003). Epidemiology and cause of severe acute respiratory syndrome (SARS) in Guangdong, People's Republic of China, in February, 2003. *The Lancet*, *362*(9393), 1353–1358. https://doi.org/10.1016/S0140-6736(03)14630-2

Zhou, L., Li, Q. N., Su, J. N., Chen, G. H., Wu, Z. X., Luo, Y., Wu, R. T., Sun, Y., Lan, T., & Ma, J. Y. (2019). The re-emerging of SADS-CoV infection in pig herds in Southern China. *Transboundary and Emerging Diseases*, *66*(5), 2180–2183. https://doi.org/10.1111/tbed.13270

Zhou, P., Fan, H., Lan, T., Yang, X.-L., Shi, W.-F., Zhang, W., Zhu, Y., Zhang, Y.-W., Xie, Q.-M., Mani, S., Zheng, X.-S., Li, B., Li, J.-M., Guo, H., Pei, G.-Q., An, X.-P., Chen, J.-W., Zhou, L., Mai, K.-J., … Ma, J.-Y. (2018). Fatal swine acute diarrhoea syndrome caused by an HKU2-related coronavirus of bat origin. *Nature*, *556*(7700), 255–258. https://doi.org/10.1038/s41586-018-0010-9

Zhu, W., Chen, C. Z., Gorshkov, K., Xu, M., Lo, D. C., & Zheng, W. (2020). RNA-Dependent RNA Polymerase as a Target for COVID-19 Drug Discovery. *Slas Discovery*, *25*(10), 1141–1151. https://doi.org/10.1177/2472555220942123

Zielińska, A., & Nowak, I. (2017). Abundance of active ingredients in sea-buckthorn oil. *Lipids in Health and Disease*, *16*(1), 95. https://doi.org/10.1186/s12944-017-0469-7

Żuchowski, J. (2023). Phytochemistry and pharmacology of sea buckthorn (Elaeagnus rhamnoides; syn. Hippophae rhamnoides): Progress from 2010 to 2021. *Phytochemistry Reviews*, *22*(1), 3–33. https://doi.org/10.1007/s11101-022-09832-1

VII.Annexes

Part I: Discovery of Anti-Coronavirus Cinnamoyl Triterpenoids Isolated from *Hippophae rhamnoides* during a Screening of Halophytes from the North Sea and Channel Coasts in Northern France

Figure S1. Purity of cinnamoyl triterpenoids isolated from HR DCM SE on the basis of PDA chromatograms.

(F2-1) 2-*O*-trans-*p*-coumaroylmaslinic acid

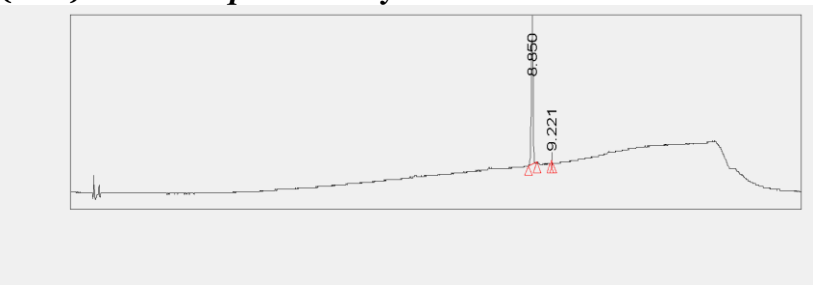

	Name	Retention Time	Area	% Area	Height
1		8.850	99425	**98.81**	43699
2		9.221	1199	1.19	788

(F2-2) 3β-hydroxy-2α-*trans*-*p*-coumaryloxy-urs-12-en-28-oic acid

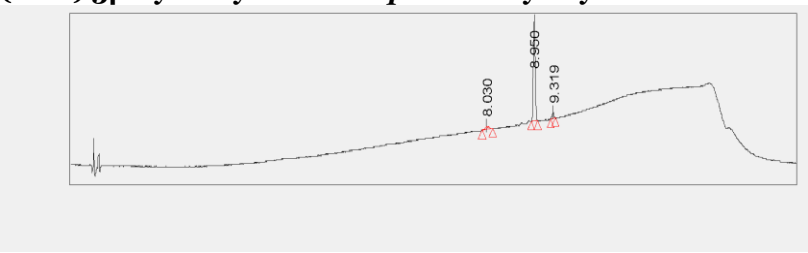

	Name	Retention Time	Area	% Area	Height
1		8.030	3263	5.69	739
2		8.950	50829	**88.63**	19645
3		9.319	3255	5.68	1318

(F2-3) 3β-hydroxy-2α-cis-*p*-coumaryloxy-urs-12-en-28-oic acid

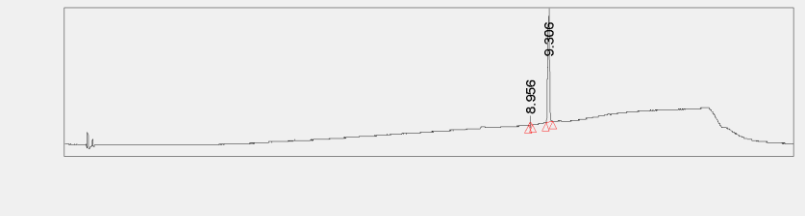

	Name	Retention Time	Area	% Area	Height
1		8.956	3109	2.86	1299
2		9.306	105645	**97.14**	47118

(F4-1) Mixture 3-*O-trans*-caffeoyl oleanolic acid / 3-*O-cis*-caffeoyl oleanolic acid (70/30)

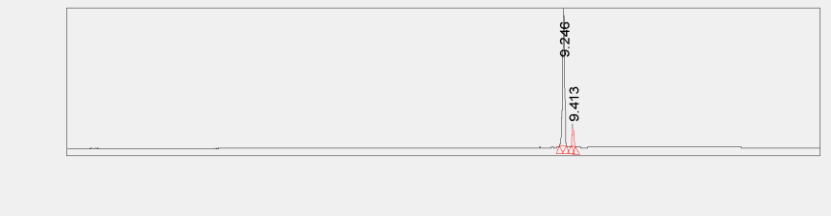

	Name	Retention Time	Area	% Area	Height
1		9.246	3197867	**90.71**	1228338
2		9.413	327318	9.29	159315

(F4-2) Oleanolic acid caffeate = 3-*O-trans*-caffeoyl oleanolic acid

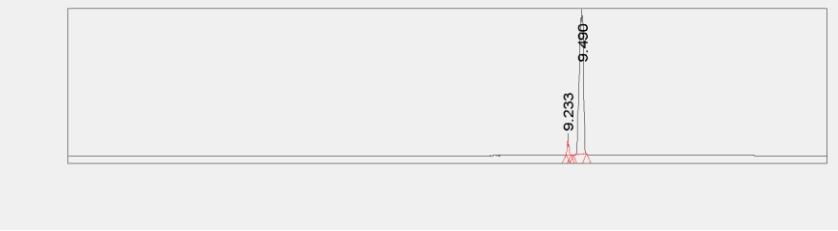

	Name	Retention Time	Area	% Area	Height
1		9.233	591875	3.64	284740
2		9.490	15686611	**96.36**	2716586

(F7-1) 3-O-*trans-p*-coumaroyl oleanolic acid

	Name	Retention Time	Area	% Area	Height
1		9.649	69990	7.26	34654
2		9.811	884184	**91.68**	353043
3		9.915	10293	1.07	7280

Figure S2. NMR data of cinnamoyl triterpenoids isolated from DCM sub-extract of *Hippophae rhamnoides*.

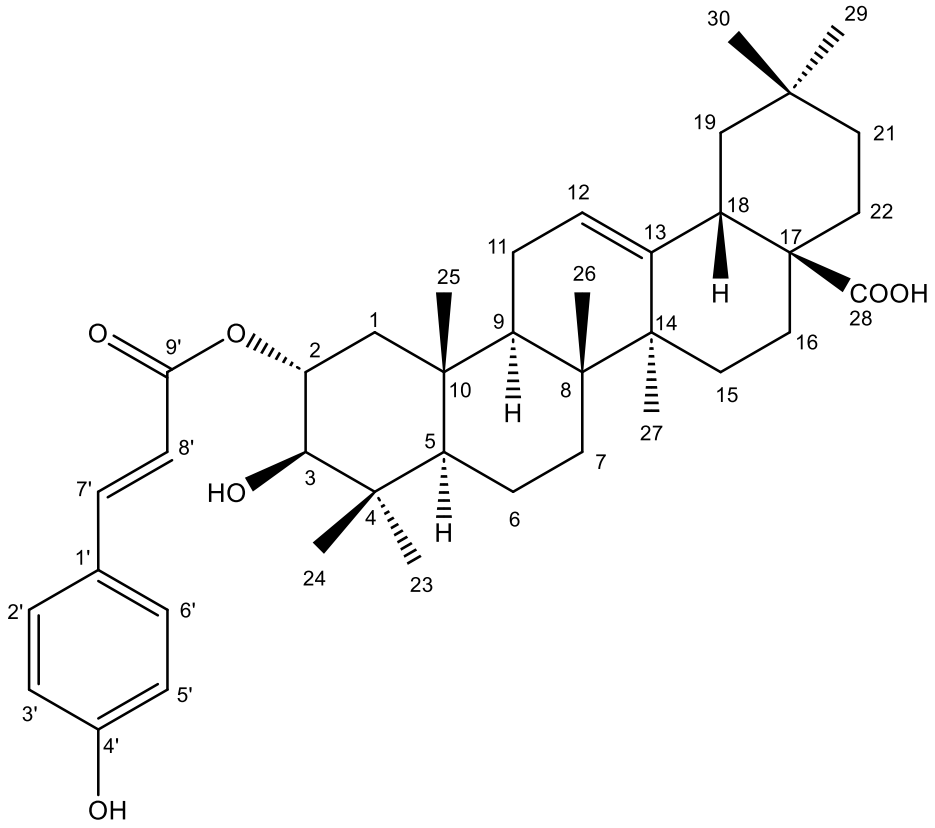

(F2-1) 2-*O*-trans-*p*-coumaroyl-maslinic acid ($C_{39}H_{54}O_6$, 618 g.mol^{-1})

White amorphous powder; ESI-MS (negative-ion mode) *m/z*: 617 [M-H]$^-$; HR-ESI-Orbitrap-MS (negative-ion mode) *m/z*: 617.3863 [M-H]$^-$; (calcd. 617.3837 for $C_{39}H_{53}O_6$ [M-H]$^-$); ^{1}H-NMR spectrum (MeOD ; 500 MHz): δ 7.65 (C**H**, *d*, *J* = 16 Hz, H-7′), 7.48 (C**H**, *d*, *J* = 8.2 Hz, H-2′), 7.48 (C**H**, *d*, *J* = 8.2 Hz, H-6′), 6.82 (C**H**, *d*, *J* = 8.2 Hz; H-3′), 6.82 (C**H**, *d*, *J* = 8.2 Hz; H-5′), 6.36 (C**H**, d, *J* = 16 Hz, H-8′), 5.26 (C**H**, *br.s*, H-12), 5.07 (C**H**, *ddd*, *J* = 11.8, 10.3, 4.6 Hz, H-2), 3.27 (C**H**, *d*, *J* = 10.3 Hz, H-3), 2.87 (C**H**, *dd*, *J* = 14.5, 4.9 Hz, H-18), 2.07 (C**H$_2$**, *m*, H-1β), 2.03 (C**H$_2$**, *m*, H-16β), 1.96 (C**H$_2$**, *m*, H-11β), 1.90 (C**H$_2$**, *m*, H-11α), 1.81 (C**H$_2$**, *m*, H-15β), 1.75 (C**H$_2$**, *m*, H-7β), 1.71 (C**H$_2$**, *m*, H-19β), 1.69 (C**H**, *m*, H-9), 1.63 (C**H$_2$**, *m*, H-6β), 1.63 (C**H$_2$**, *m*, H-16α), 1.55 (C**H$_2$**, *m*, H-22β), 1.55 (C**H$_2$**, *m*, H-7α), 1.50 (C**H$_2$**, *m*, H-6α), 1.41 (C**H$_2$**, *m*, H-21β), 1.37 (C**H$_2$**, m, H-22α), 1.23 (C**H$_2$**, *m*, H-21α), 1.19 (C**H$_3$**, *s*, H-27), 1.15 (C**H$_2$**, *m*, H-19α), 1.12 (C**H$_3$**, *s*, H-25), 1.12 (C**H$_2$**, *m*, H-15α), 1.09 (C**H$_3$**, *s*, H-23), 1.03 (C**H$_2$**, *m*, H-1α), 0.95 (C**H$_3$**, s, H-30), 0.95 (C**H**, *m*, H-5), 0.92 (C**H$_3$**, *s*, H-29), 0.90 (C**H$_3$**, *s*, H-24), 0.85 (C**H$_3$**, *s*, H-26), and ^{13}C-NMR spectrum (MeOD, 125 MHz): 182.16 (C-28), 169.29 (C-9′), 161.20 (C-4′), 146.23 (C-7′), 145.39 (C-13), 131.09 (C-6′), 131.09 (C-2′), 127.30 (C-1′), 123.31 (C-12), 116.81 (C-5′), 116.81 (C-3′), 115.87 (C-8′), 81.10 (C-3), 73.82 (C-2), 56.58 (C-5), 49.36 (C-9), 47.68 (C-17), 47.29 (C-19), 45.18 (C-1), 42.93 (C-8), 42.75 (C-18), 40.98 (C-4), 40.60 (C-14), 39.47 (C-10), 34.91 (C-21), 33.82 (C-7), 33.82 (C-22), 33.58 (C-29), 31.63 (C-20), 29.20 (C-23), 28.82 (C-15), 26.41 (C-27), 24.56 (C-11), 24.07 (C-16), 23.99 (C-30), 19.56 (C-6), 17.70 (C-26), 17.42 (C-24), 16.92 (C-25)

^{1}H spectrum

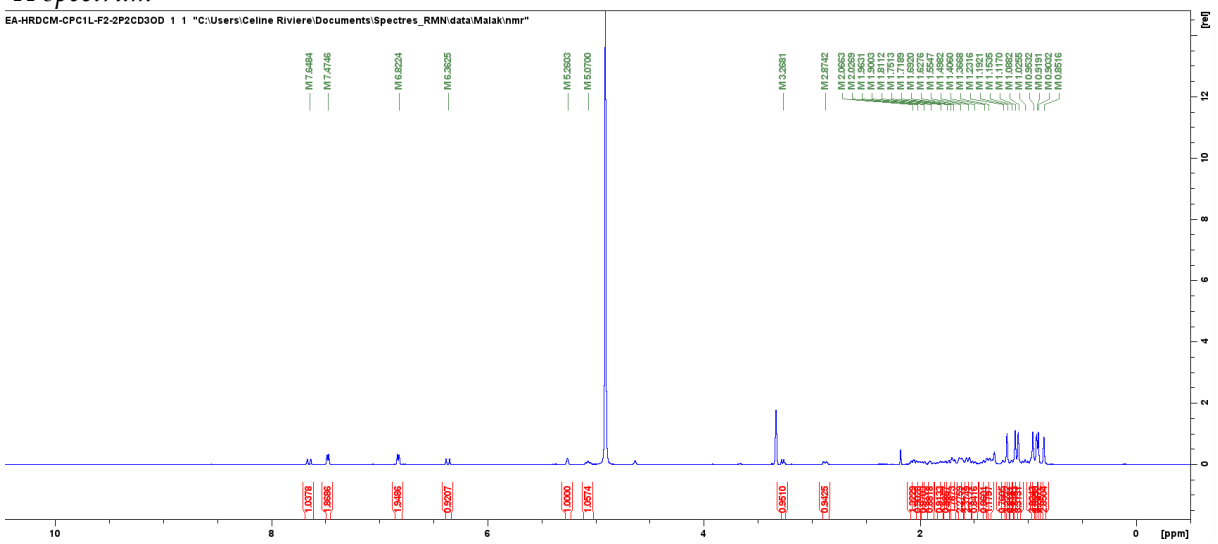

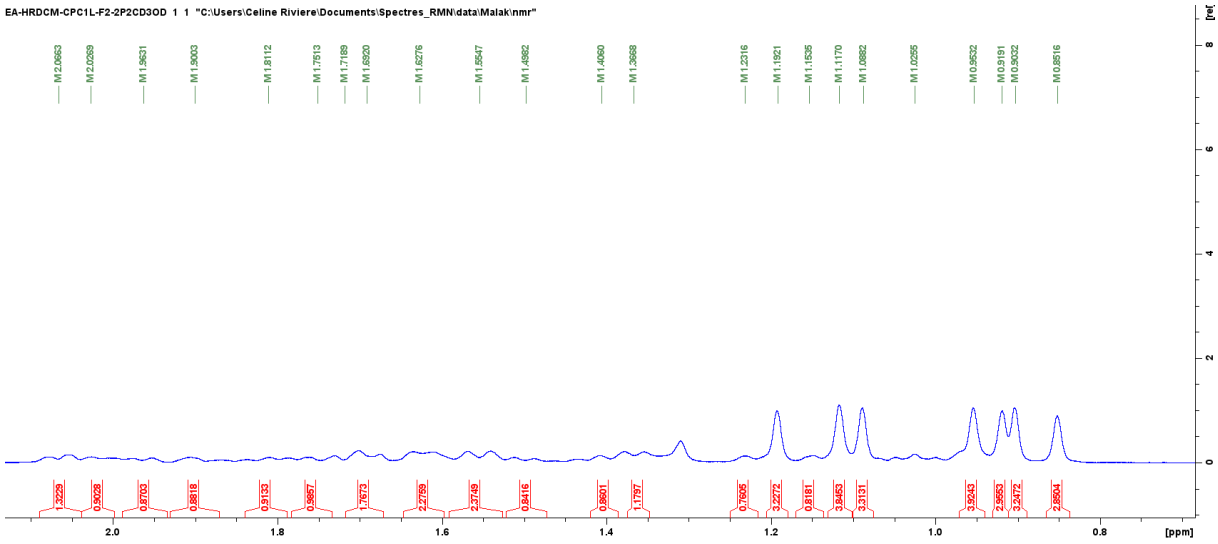

^{13}C spectrum

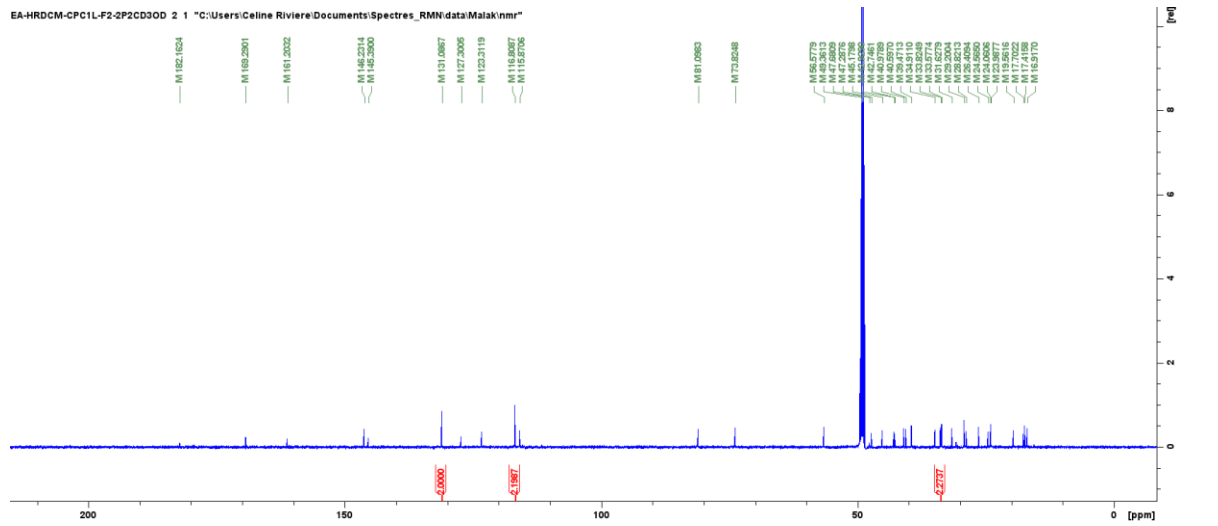

COSY spectrum

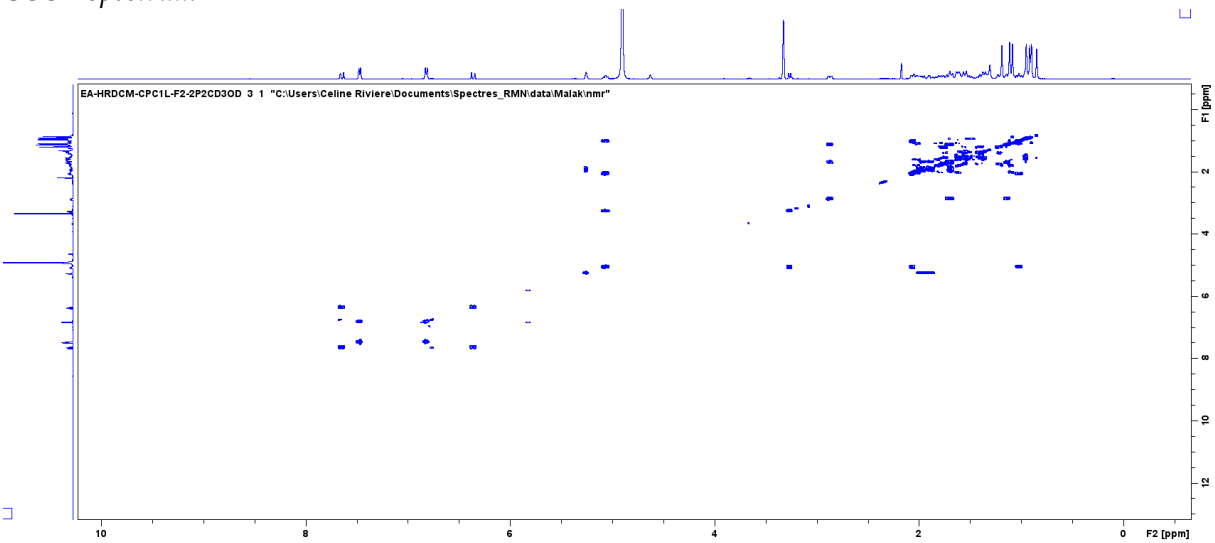

HSQC spectrum

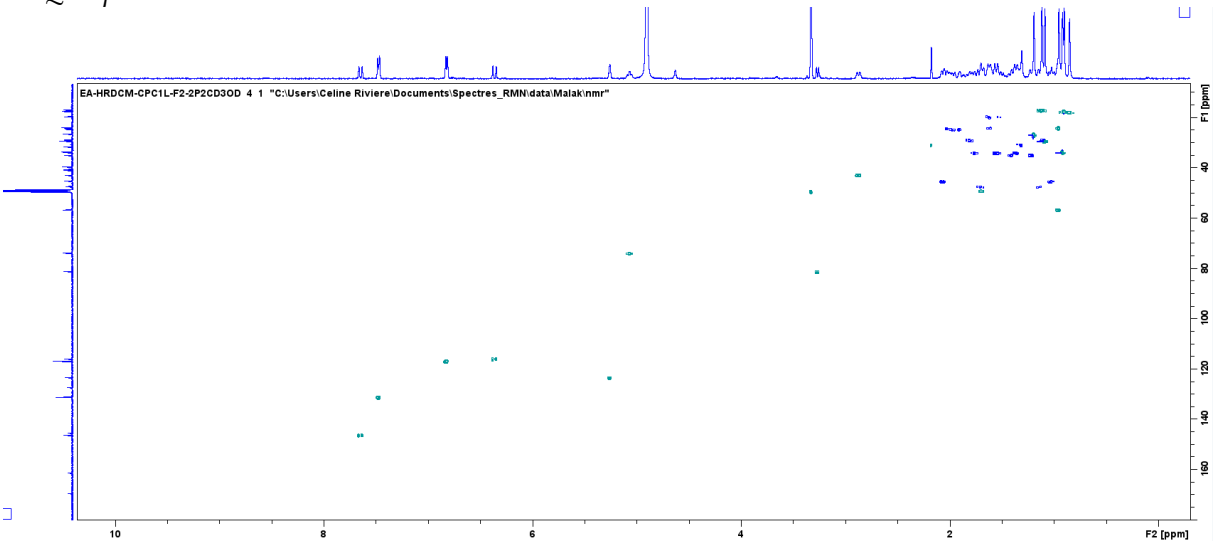

HMBC spectrum

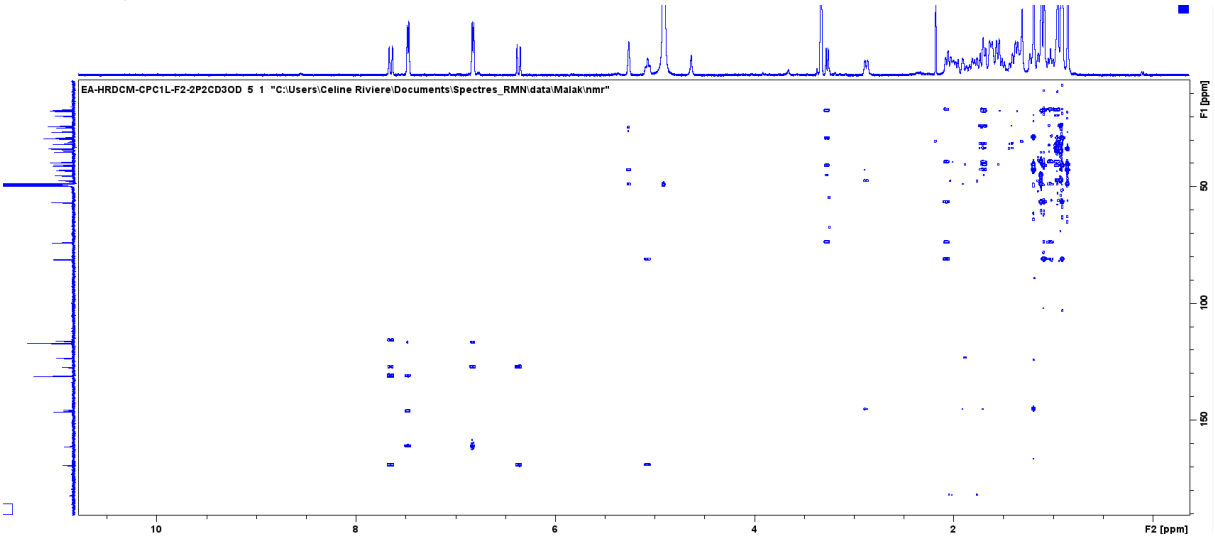

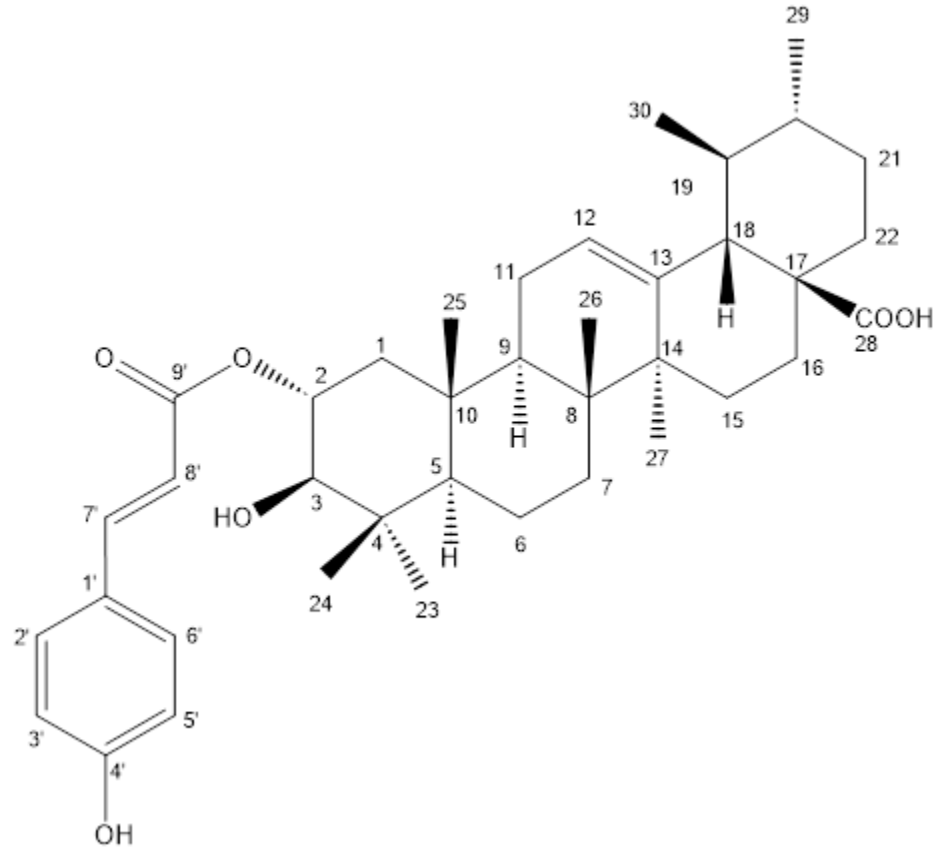

(F2-2) 3β-hydroxy-2*α*-*trans*-*p*-coumaryloxy-urs-12-en-28-oic acid ($C_{39}H_{54}O_6$, 618 g.mol^{-1})

White amorphous powder; ESI-MS (negative-ion mode) *m*/*z*: 617.63 [M-H]$^-$; HR-ESI-Orbitrap-MS (negative-ion mode) *m*/*z*: 617.3848 [M-H]$^-$; (calcd. 617.3837 for $C_{39}H_{53}O_6$ [M-H]$^-$) ; ^{1}H-NMR spectrum (MeOD ; 500 MHz): *δ* 7.65 (C**H**, *d*, *J* = 16 Hz, H-7′), 7.47 (C**H**, *d*, *J* = 8.2 Hz, H-2′), 7.47 (C**H**, d, *J* = 8.2 Hz, H-6′), 6.82 (C**H**, *d*, *J* = 8.2 Hz, H-3′), 6.82 (C**H**, *d*, *J* = 8.2 Hz, H-5′), 6.36 (C**H**, *d*, *J* = 16 Hz, H-8′), 5.24 (C**H**, *br. s*, H-12), 5.08 (C**H**, *ddd*, *J* = 11.56, 10.20, 4.45 Hz , H-2), 3.27 (C**H**, *d*, *J* = 10.20 Hz, H-3), 2.23 (C**H**, *d*, *J* = 11.04 Hz, H-18), 2.09 (C**H$_2$**, *m*, H-1β), 2.04 (C**H$_2$**, *m*, H-16β), 2.00 (C**H$_2$**, *m*, H-15β), 1.96 (C**H$_2$**, *m*, H-11), 1.72 (C**H$_2$**, *m*, H-22β), 1.66 (C**H$_2$**, *m*, H-16*α*), 1.66 (C**H$_2$**, *m*, H-22*α*), 1.64 (C**H**, *m*, H-9), 1.61 (C**H$_2$**, *m*, H-6β), 1.59 (C**H$_2$**, *m*, H-7β), 1.53 (C**H$_2$**, *m*, H-21β), 1.50 (C**H$_2$**, m, H-6*α*), 1.40 (C**H$_2$**, *m*, H-7*α*), 1.39 (C**H**, *m*, H-20), 1.36 (C**H$_2$**, *m*, H-21*α*), 1.15 (C**H$_3$**, *s*, H-27), 1.13 (C**H$_3$**, *s*, H-25), 1.12 (C**H$_2$**, *m*, H-15*α*), 1.09 (C**H$_3$**, *s*, H-23), 1.05 (C**H$_2$**, *m*, H-1*α*), 1.02 (C**H**, *m*, H-19), 0.98 (C**H$_3$**, *s*, H-29), 0.95 (C**H**, *m*, H-5), 0.90 (C**H$_3$**, *s*, H-24), 0.90 (C**H$_3$**, s, H-30), 0.88 (C**H$_3$**, *s*, H-26), and ^{13}C-NMR spectrum (MeOD, 125 MHz): 181.12 (C-28), 169.35 (C-9′), 161.22 (C-4′), 146.23 (C-7′), 139.86 (C-13), 131.10 (C-2′), 131.10 (C-6′), 127.31 (C-1′), 126.49 (C-12), 116.80 (C-3′), 116.80 (C-5′), 115.89 (C-8′), 81.11 (C-3), 73.81 (C-2), 56.57 (C-5), 54.38 (C-18), 49.36 (C-17), 49.21 (C-9), 45.35 (C-1), 43.30 (C-8), 40.98 (C-4), 40.83 (C-14), 40.47 (C-20), 40.42 (C-19), 39.41 (C-10), 38.15 (C-22), 34.15 (C-7), 31.81 (C-21), 29.24 (C-15), 29.21 (C-23), 25.34 (C-16), 24.42 (C-11), 24.11 (C-27), 21.60 (C-29), 19.54 (C-6), 17.80 (C-26), 17.70 (C-30), 17.48 (C-24), 17.06 (C-25)

[1]H spectrum

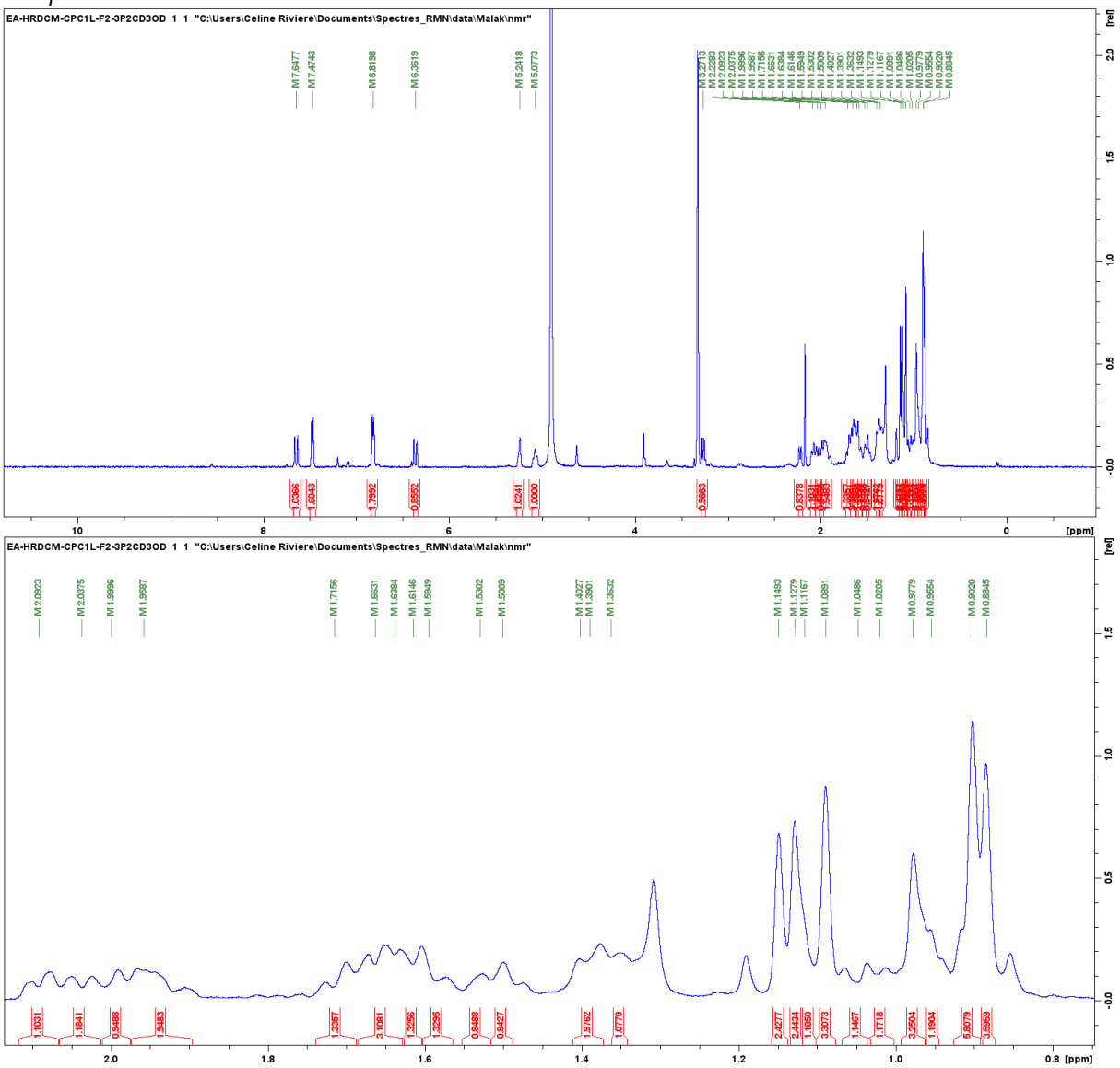

[13]C spectrum

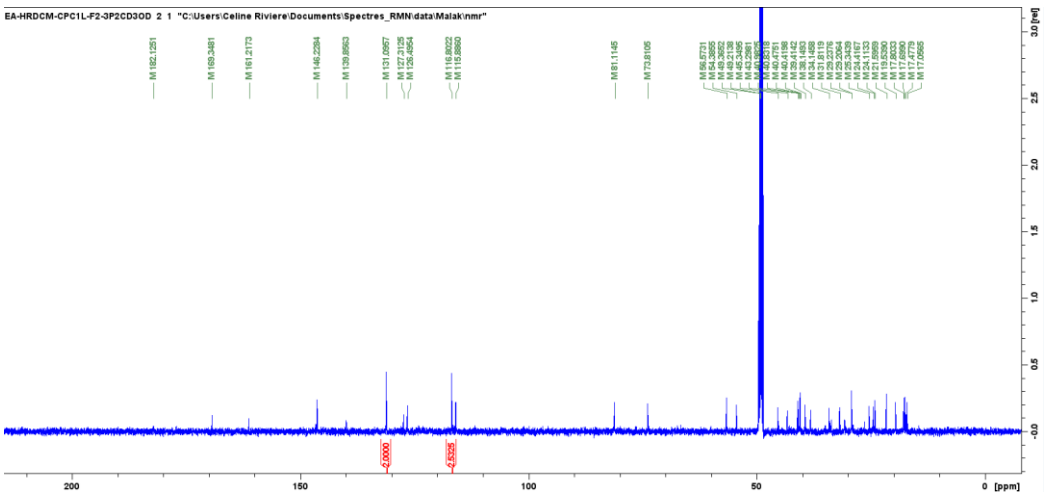

COSY spectrum

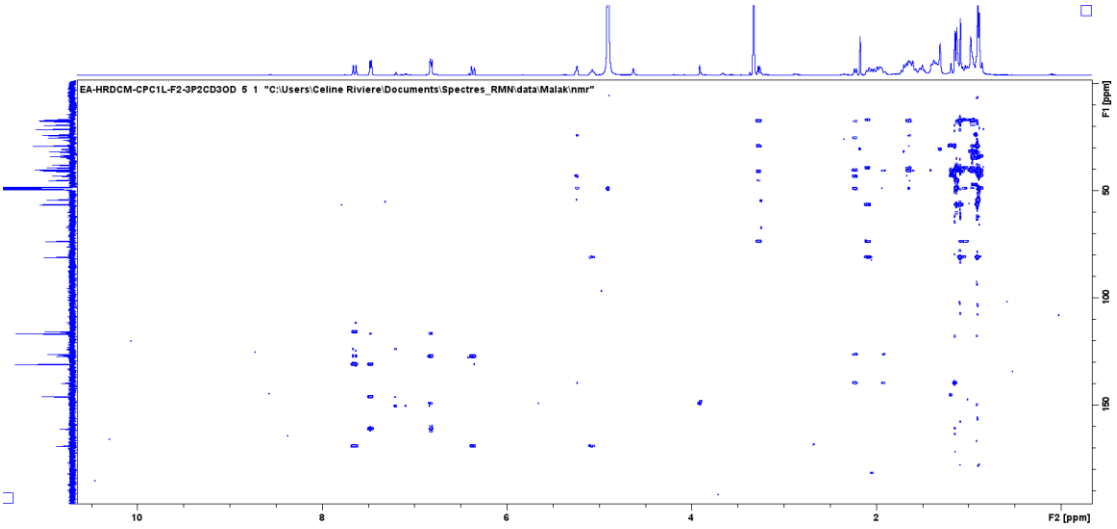

HSCQ spectrum

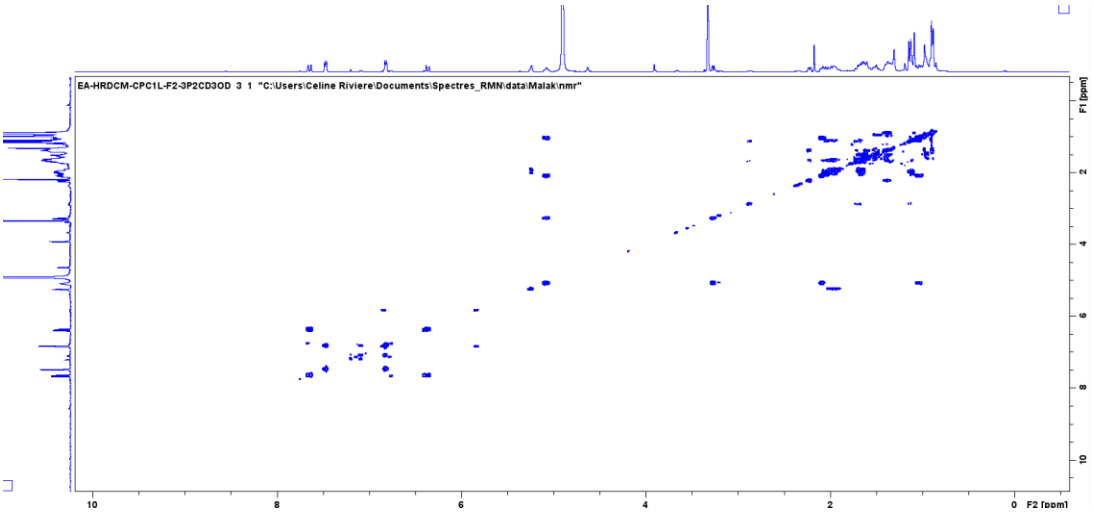

HMBC spectrum

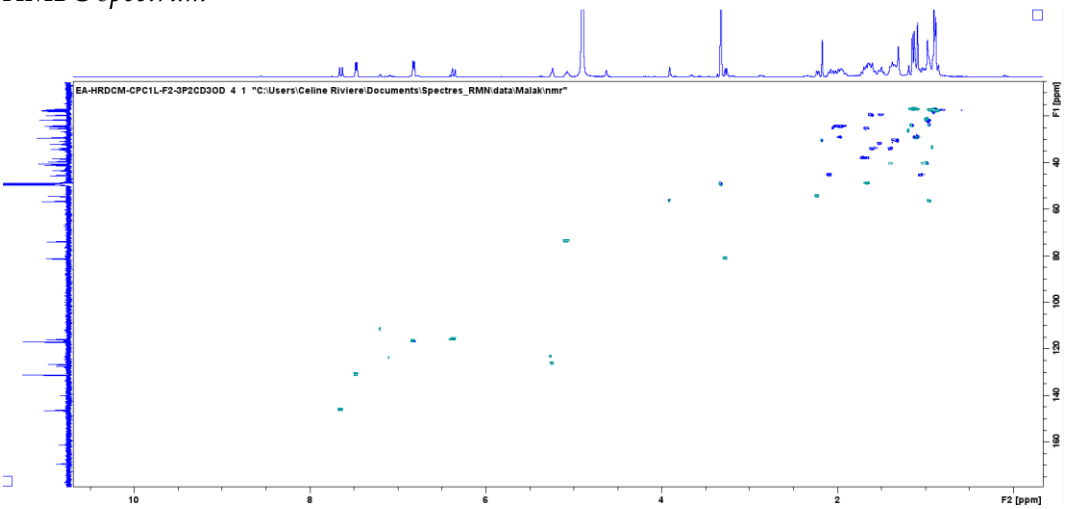

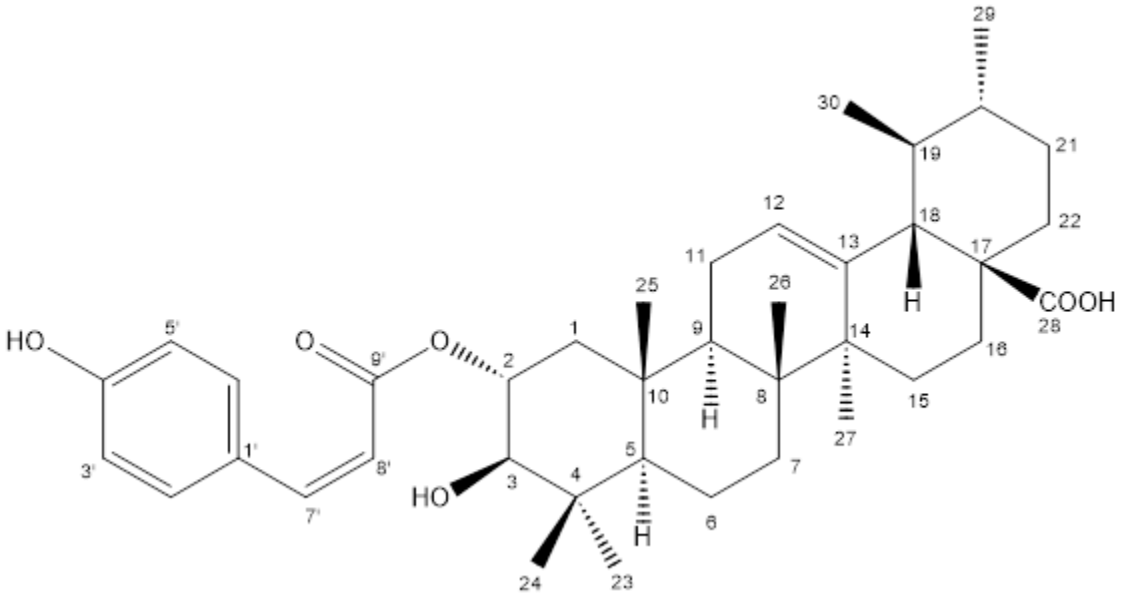

(F2-3) 3β-hydroxy-2*α*-cis-*p*-coumaryloxy-urs-12-en-28-oic acid ($C_{39}H_{54}O_6$, 618 g.mol^{-1})

White amorphous powder; ESI-MS (negative-ion mode) *m*/*z*: 617.63 [M-H]$^-$; HR-ESI-Orbitrap-MS (negative-ion mode) *m*/*z*: 617.3848 [M-H]$^-$; (calcd. 617.3837 for $C_{39}H_{53}O_6$ [M-H]$^-$); **^{1}H-NMR spectrum** (MeOD ; 500 MHz): *δ* 7.67 (C**H**, *d*, *J* = 8.45 Hz, H-2′), 7.67 (C**H**, *d*, *J* = 8.45 Hz, H-6′), 6.86 (C**H**, d, *J* = 12.90 Hz, H-7′), 6.77 (C**H**, *d*, *J* = 8.45 Hz, H-3′), 6.77 (C**H**, *d*, *J* = 8.45 Hz, H-5′), 5.83 (C**H**, d, *J* = 12.90 Hz, H-8′), 5.25 (C**H**, t, *J* = 3.66 Hz, H-12), 5.05 (C**H**, *ddd*, *J* = 11.56, 10.20, 4.45 Hz , H-2), 3.20 (C**H**, *d*, *J* = 10.20 Hz, H-3), 2.23 (C**H**, *d*, *J* = 11.04 Hz, H-18), 2.07 (C**H$_2$**, *m*, H-1β), 2.05 (C**H$_2$**, *m*, H-16β), 1.99 (C**H$_2$**, *m*, H-11), 1.96 (C**H$_2$**, *m*, H-15β), 1.72 (C**H$_2$**, *m*, H-22β), 1.67 (C**H$_2$**, *m*, H-16*α*), 1.67 (C**H$_2$**, *m*, H-22*α*), 1.64 (C**H**, *m*, H-9), 1.61 (C**H$_2$**, *m*, H-6β), 1.58 (C**H$_2$**, *m*, H-7β), 1.53 (C**H$_2$**, *m*, H-21), 1.48 (C**H$_2$**, m, H-6*α*), 1.40 (C**H**, m, H-20), 1.38 (C**H$_2$**, *m*, H-7*α*), 1.15 (C**H$_3$**, *s*, H-27), 1.12 (C**H$_3$**, *s*, H-25), 1.09 (C**H$_2$**, *m*, H-15*α*), 1.07 (C**H$_3$**, *s*, H-23), 1.01 (C**H**, *m*, H-19), 0.98 (C**H$_2$**, *m*, H-1*α*), 0.98 (C**H$_3$**, *s*, H-29), 0.93 (C**H**, *m*, H-5), 0.90 (C**H$_3$**, *s*, H-24), 0.90 (C**H$_3$**, *s*, H-30), 0.88 (C**H$_3$**, *s*, H-26), and **^{13}C-NMR spectrum** (MeOD, 125 MHz): 181.79 (C-28), 169.34 (C-9′), 159.99 (C-4′), 144.47 (C-7′), 139.75 (C-13), 133.65 (C-2′), 133.65 (C-6′), 127.73 (C-1′), 126.61 (C-12), 117.46 (C-8′), 115.79 (C-3′), 115.79 (C-5′), 81.05 (C-3), 73.48 (C-2), 56.50 (C-5), 54.33 (C-18), 48.63 (C-17), 49.18 (C-9), 45.26 (C-1), 43.27 (C-8), 40.98 (C-4), 40.82 (C-14), 40.43 (C-20), 40.42 (C-19), 39.39 (C-10), 38.12 (C-22), 34.11 (C-7), 31.77 (C-21), 29.20 (C-15), 29.18 (C-23), 25.31 (C-16), 24.41 (C-11), 24.10 (C-27), 21.57 (C-29), 19.53 (C-6), 17.76 (C-26), 17.69 (C-30), 17.48 (C-24), 17.06 (C-25)

^{1}H spectrum

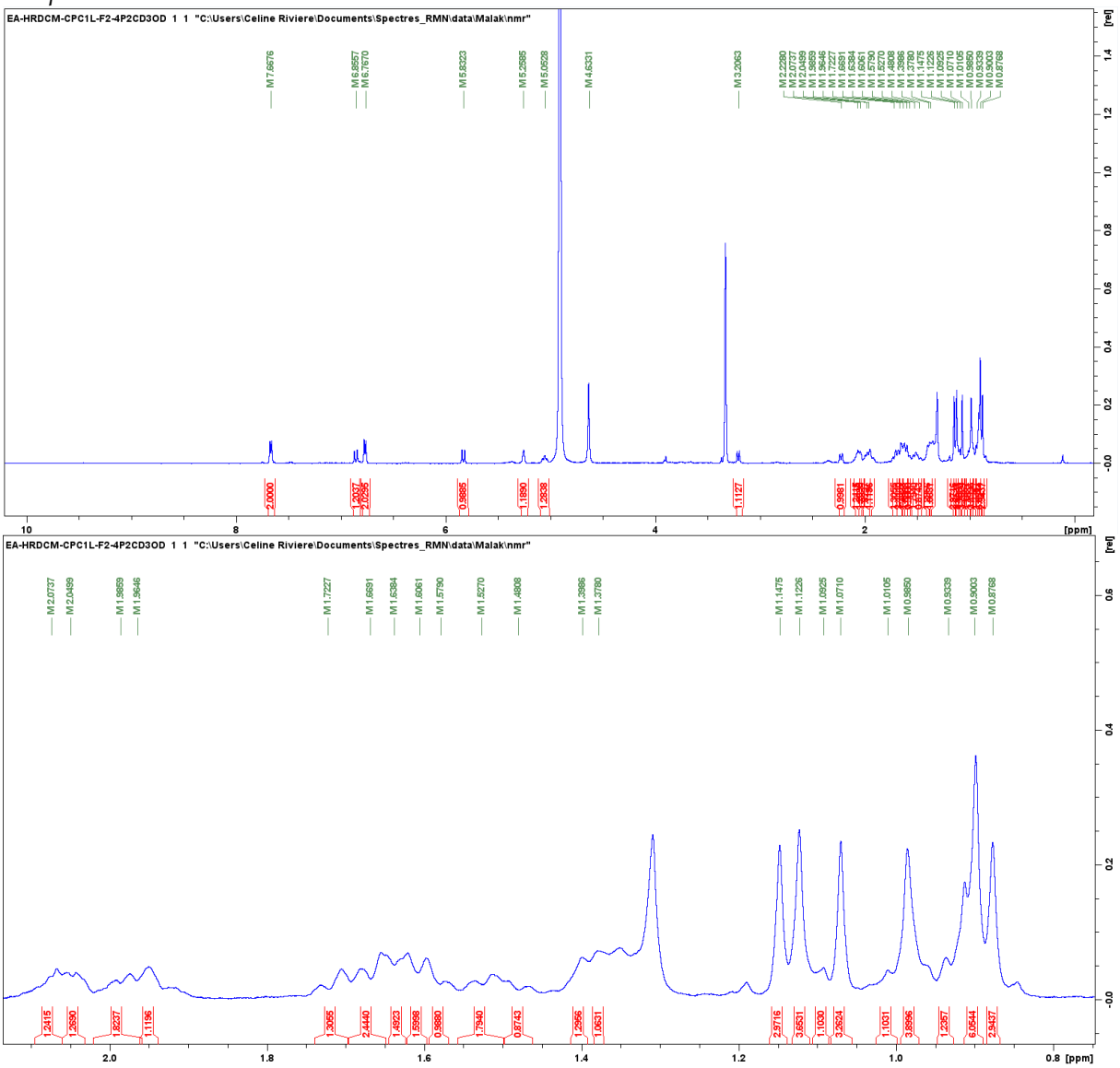

^{13}C spectrum

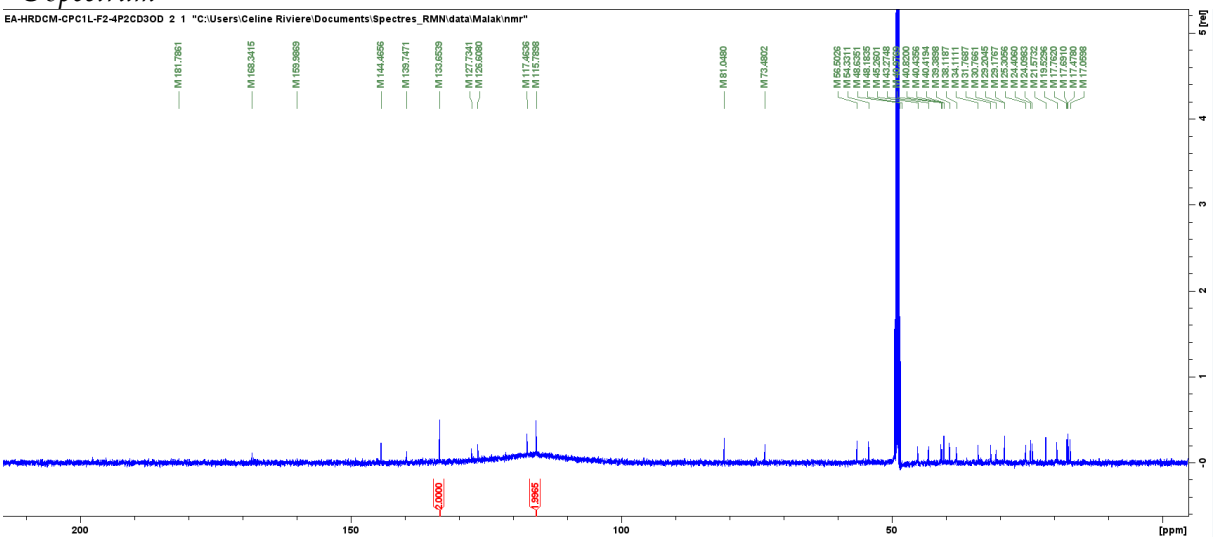

COSY spectrum

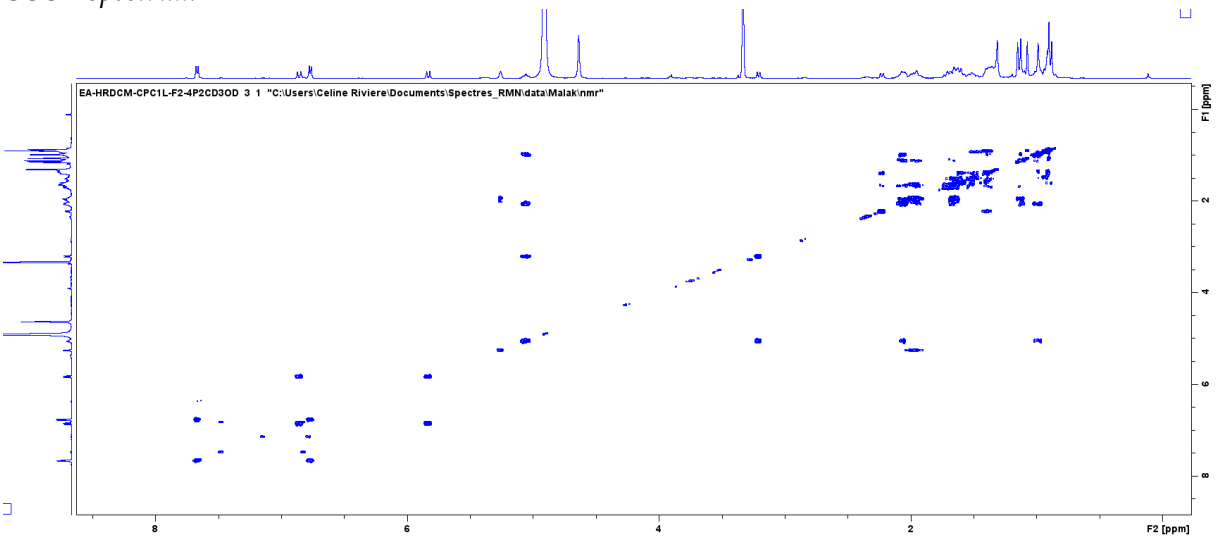

HSQC spectrum

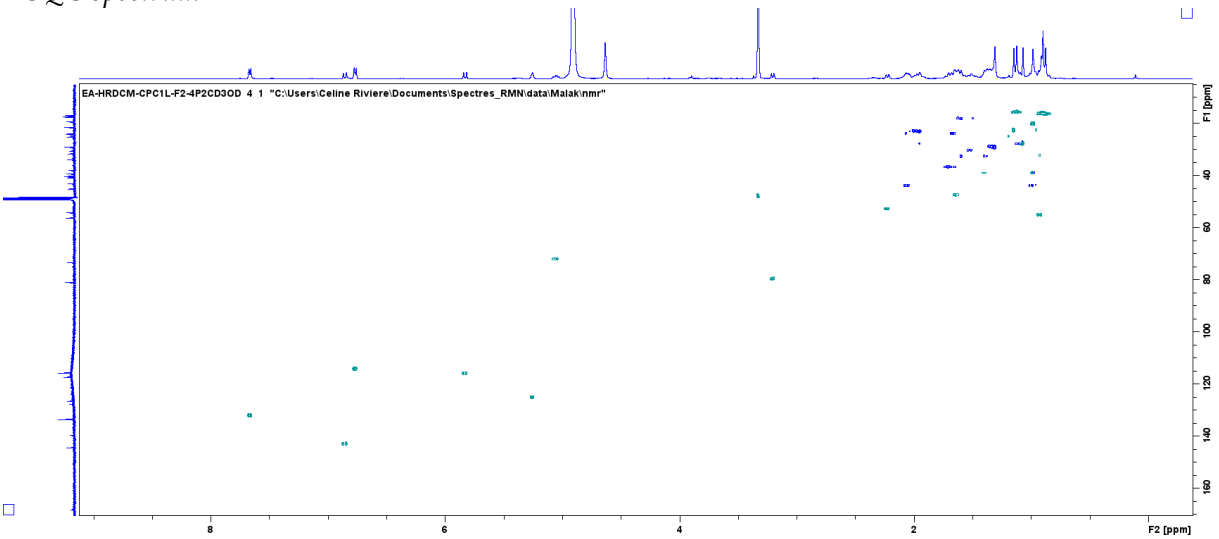

HMBC spectrum

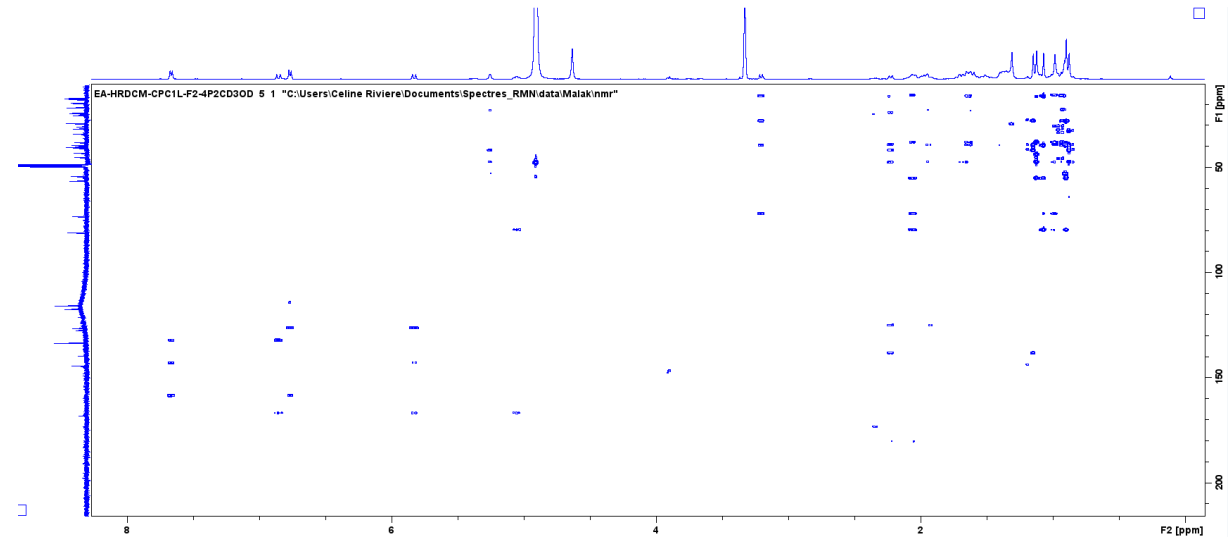

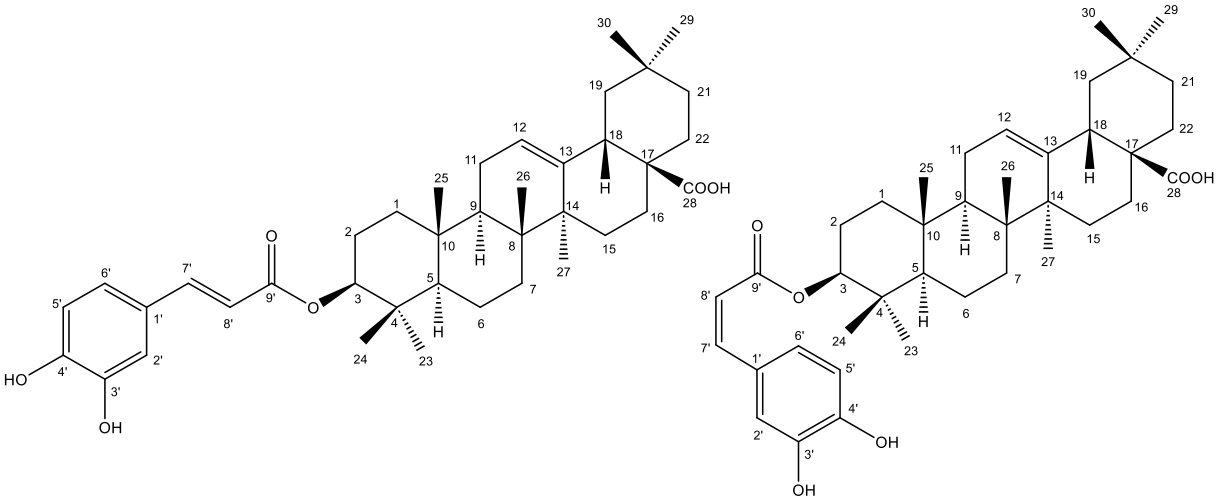

(F4-1) Mixture 3-*O-trans*-caffeoyl oleanolic acid / 3-*O-cis*-caffeoyl oleanolic acid (70/30) ($C_{39}H_{54}O_6$, 618 g.mol^{-1})

White amorphous powder; **ESI-MS** (negative-ion mode) *m*/z: 617 [M-H]$^-$; **HR-ESI-Orbitrap-MS** (negative-ion mode) *m*/z: 617.3841 [M-H]$^-$; (calcd. 617.3837 for $C_{39}H_{53}O_6$ [M-H]$^-$); **^{1}H-NMR spectrum of 3-*O-cis*-caffeoyl oleanolic acid** (MeOD ; 500 MHz): δ 7.32 (C**H**, *d*, *J* = 2.08 Hz, H-2′), 7.02 (C**H**, *dd*, *J* = 8.18, 2.08 Hz; H-6′), 6.82 (C**H**, d, *J* = 12.6 Hz, H-7′), 6.74 (C**H**, *d*, *J* = 8.18 Hz, H-5′), 5.76 (C**H**, d, *J* = 12.6 Hz, H-8′), 5.27 (C**H**, t, *J* = 3.66 Hz, H-12), 4.59 (C**H**, *dd*, *J* = 11.72, 4.76 Hz, H-3), 2.88 (C**H**, *dd*, *J* = 14.04, 4.59 Hz , H-18), 2.04 (C**H$_2$**, *m*, H-16β), 1.95 (C**H**, *m*, H-9), 1.94 (C**H$_2$**, *m*, H-11), 1.82 (C**H$_2$**, *m*, H-15β), 1.80 (C**H$_2$**, *m*, H-22β), 1.77 (C**H$_2$**, *m*, H-2β), 1.73 (C**H$_2$**, m, H-19β), 1.72 (C**H$_2$**, *m*, H-1β), 1.71 (C**H$_2$**, *m*, H-2α), 1.62 (C**H$_2$**, *m*, H-16α), 1.60 (C**H$_2$**, *m*, H-6β), 1.57 (C**H$_2$**, *m*, H-7β), 1.55 (C**H$_2$**, *m*, H-22α), 1.49 (C**H$_2$**, m, H-6α), 1.42 (C**H$_2$**, *m*, H-21β), 1.36 (C**H$_2$**, *m*, H-7α), 1.24 (C**H$_2$**, m, H-21α), 1.21 (C**H$_3$**, *s*, H-27), 1.16 (C**H$_2$**, *m*, H-19α), 1.12 (C**H$_2$**, *m*, H-1α), 1.09 (C**H$_2$**, *m*, H-15α), 1.03 (C**H$_3$**, *s*, H-25), 0.99 (C**H$_3$**, *s*, H-26), 0.97 (C**H$_3$**, *s*, H-30), 0.93 (C**H**, *m*, H-5), 0.93 (C**H$_3$**, *s*, H-23), 0.93 (C**H$_3$**, *s*, H-29), 0.86 (C**H$_3$**, *s*, H-24),

Comparison of ^{1}H spectrum of 3-O-trans-caffeoyl oleanolic acid (red spectrum) and mixture 3-O-trans-caffeoyl oleanolic acid / 3-O-cis-caffeoyl oleanolic acid (70/30) (blue spectrum)

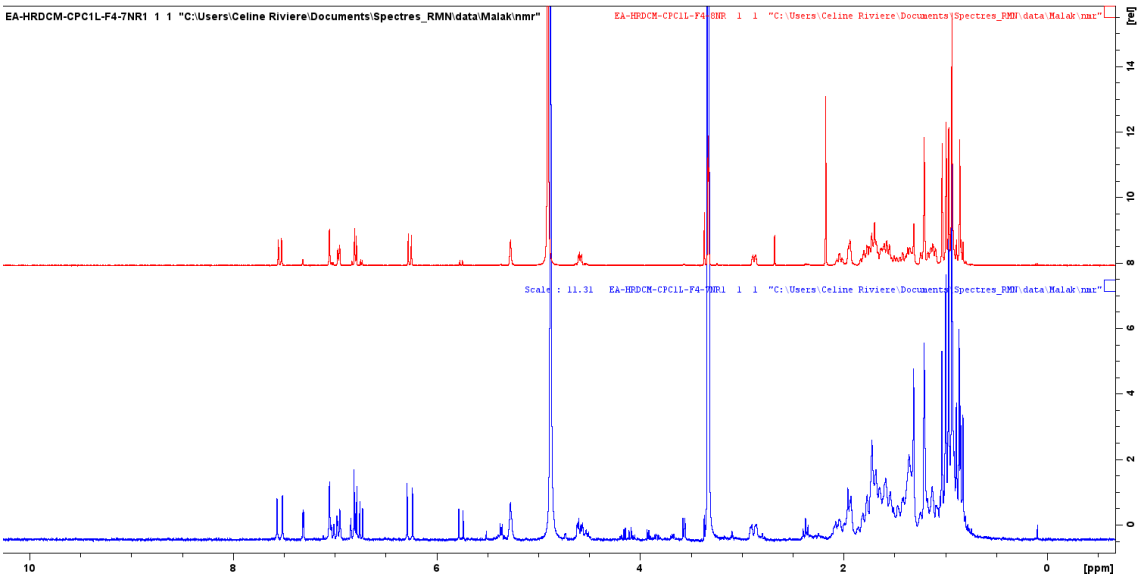

[1]H spectrum of mixture 3-*O*-*trans*-caffeoyl oleanolic acid / 3-*O*-*cis*-caffeoyl oleanolic acid (70/30) (peak picking of protons belonging to the cis-caffeoyl moiety and integration).

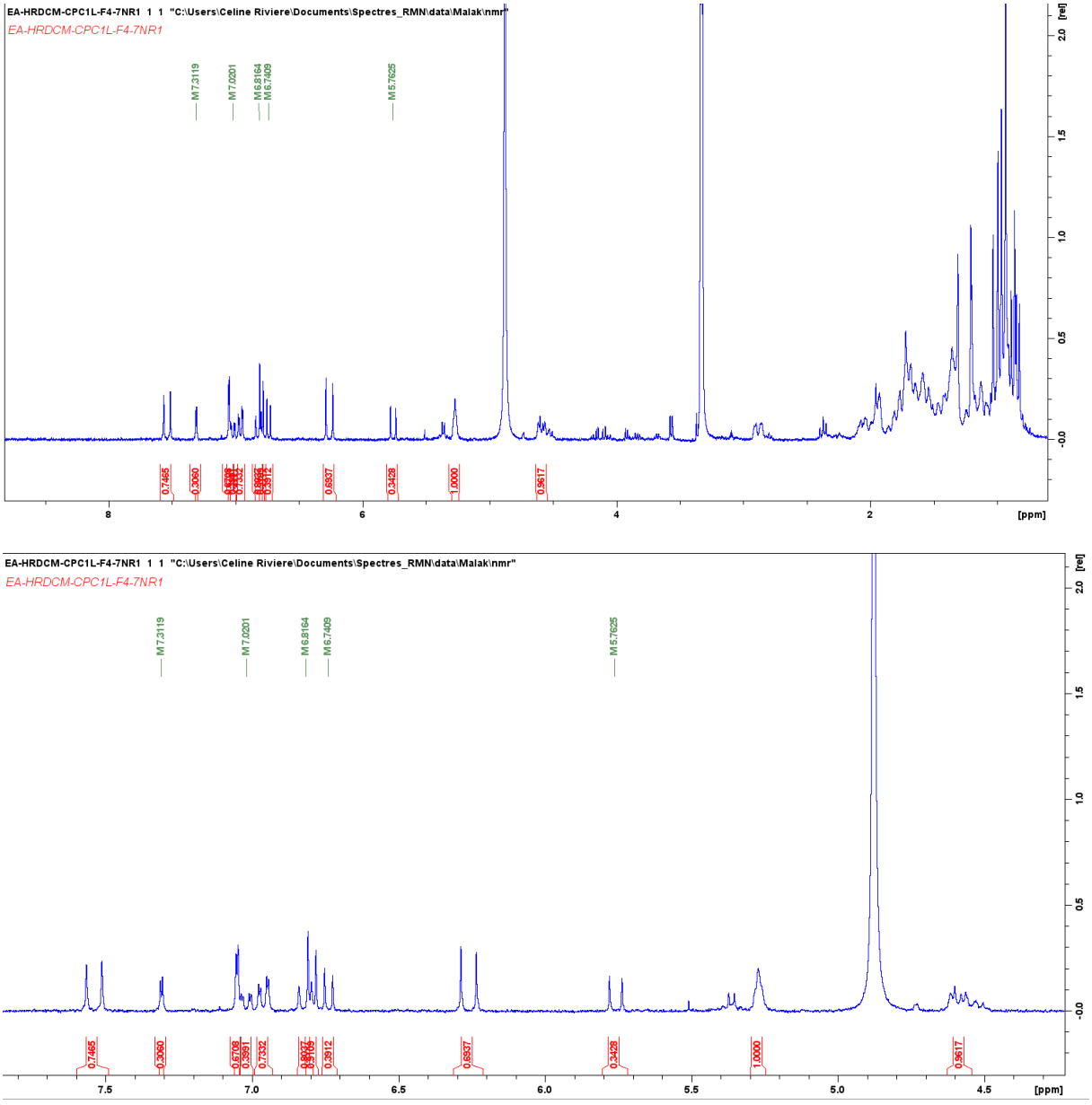

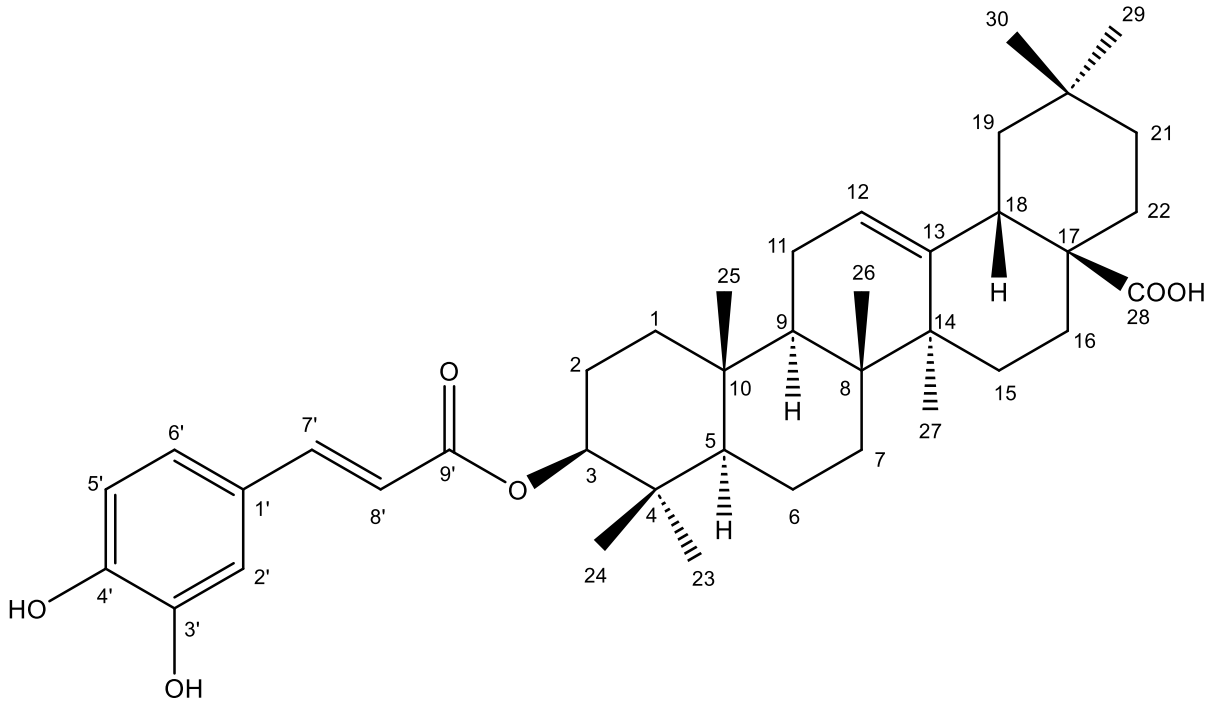

(F4-2) Oleanolic acid caffeate = 3-*O-trans*-caffeoyl oleanolic acid ($C_{39}H_{54}O_6$, 618 g.mol^{-1})
White amorphous powder; **ESI-MS** (negative-ion mode) *m*/*z*: 617 [M-H]$^-$; **HR-ESI-Orbitrap-MS** (negative-ion mode) *m*/*z*: 617.3841 [M-H]$^-$; (calcd. 617.3837 for $C_{39}H_{53}O_6$ [M-H]$^-$) ; **^{1}H-NMR spectrum** (MeOD ; 500 MHz): δ 7.54 (C**H**, d, *J* = 15.9 Hz, H-7′), 7.05 (C**H**, *d*, *J* = 2.08 Hz, H-2′), 6.96 (C**H**, *dd*, *J* = 8.18, 2.08 Hz; H-6′), 6.80 (C**H**, *d*, *J* = 8.18 Hz, H-5′), 6.26 (C**H**, d, *J* = 15.9 Hz, H-8′), 5.27 (C**H**, t, *J* = 3.66 Hz, H-12), 4.59 (C**H**, *dd*, *J* = 11.72, 4.76 Hz, H-3), 2.88 (C**H**, *dd*, *J* = 14.04, 4.59 Hz , H-18), 2.04 (C**H$_2$**, *m*, H-16β), 1.95 (C**H**, *m*, H-9), 1.94 (C**H$_2$**, *m*, H-11), 1.82 (C**H$_2$**, *m*, H-15β), 1.80 (C**H$_2$**, *m*, H-22β), 1.77 (C**H$_2$**, *m*, H-2β), 1.73 (C**H$_2$**, m, H-19β), 1.72 (C**H$_2$**, *m*, H-1β), 1.71 (C**H$_2$**, *m*, H-2α), 1.62 (C**H$_2$**, *m*, H-16α), 1.60 (C**H$_2$**, *m*, H-6β), 1.57 (C**H$_2$**, *m*, H-7β), 1.55 (C**H$_2$**, *m*, H-22α), 1.49 (C**H$_2$**, m, H-6α), 1.42 (C**H$_2$**, *m*, H-21β), 1.36 (C**H$_2$**, *m*, H-7α), 1.24 (C**H$_2$**, m, H-21α), 1.21 (C**H$_3$**, *s*, H-27), 1.16 (C**H$_2$**, *m*, H-19α), 1.12 (C**H$_2$**, *m*, H-1α), 1.09 (C**H$_2$**, *m*, H-15α), 1.03 (C**H$_3$**, *s*, H-25), 0.99 (C**H$_3$**, *s*, H-26), 0.97 (C**H$_3$**, *s*, H-30), 0.93 (C**H**, *m*, H-5), 0.93 (C**H$_3$**, *s*, H-23), 0.93 (C**H$_3$**, *s*, H-29), 0.86 (C**H$_3$**, *s*, H-24), and **^{13}C-NMR spectrum** (MeOD, 125 MHz): 182.04 (C-28), 169.20 (C-9′), 149.57 (C-4′), 146.84 (C-3′), 146.69 (C-7′), 145.28 (C-13), 127.74 (C-1′), 123.53 (C-12), 122.95 (C-6′), 116.50 (C-5′), 115.57 (C-8′), 115.07 (C-2′), 82.28 (C-3), 56.82 (C-5), 49.19 (C-9), 47.66 (C-17), 47.26 (C-19), 42.92 (C-14), 42.74 (C-18), 40.58 (C-8), 39.35 (C-1), 38.99 (C-4), 38.16 (C-10), 34.91 (C-21), 33.91 (C-7), 33.84 (C-22), 33.58 (C-29), 31.63 (C-20), 28.85 (C-15), 28.67 (C-23), 26.41 (C-27), 24.70 (C-2), 24.53 (C-11), 24.07 (C-30), 23.99 (C-16), 19.37 (C-6), 17.73 (C-26), 17.36 (C-24), 15.94 (C-25)

^{1}H spectrum

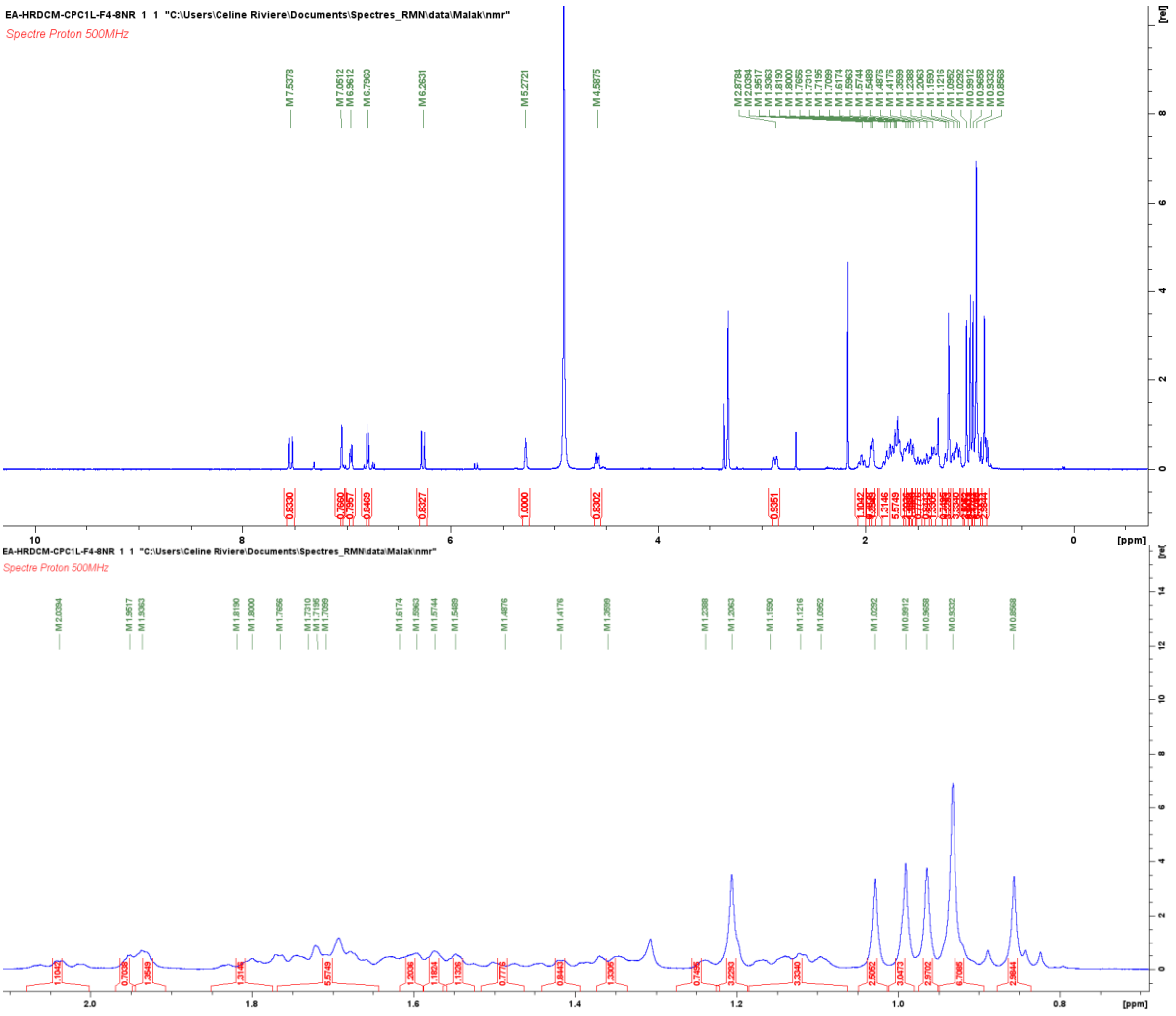

^{13}C spectrum

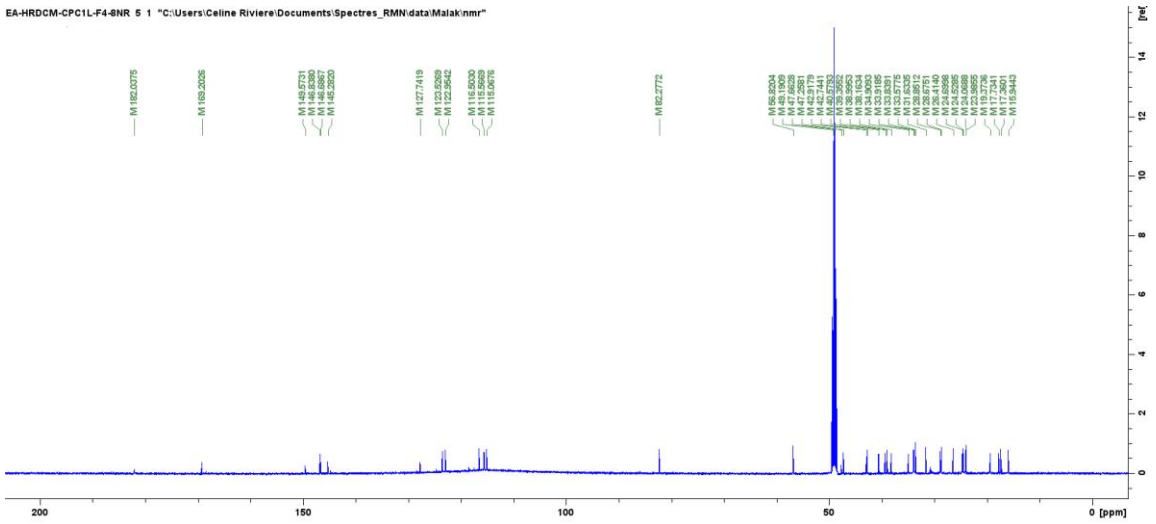

COSY spectrum

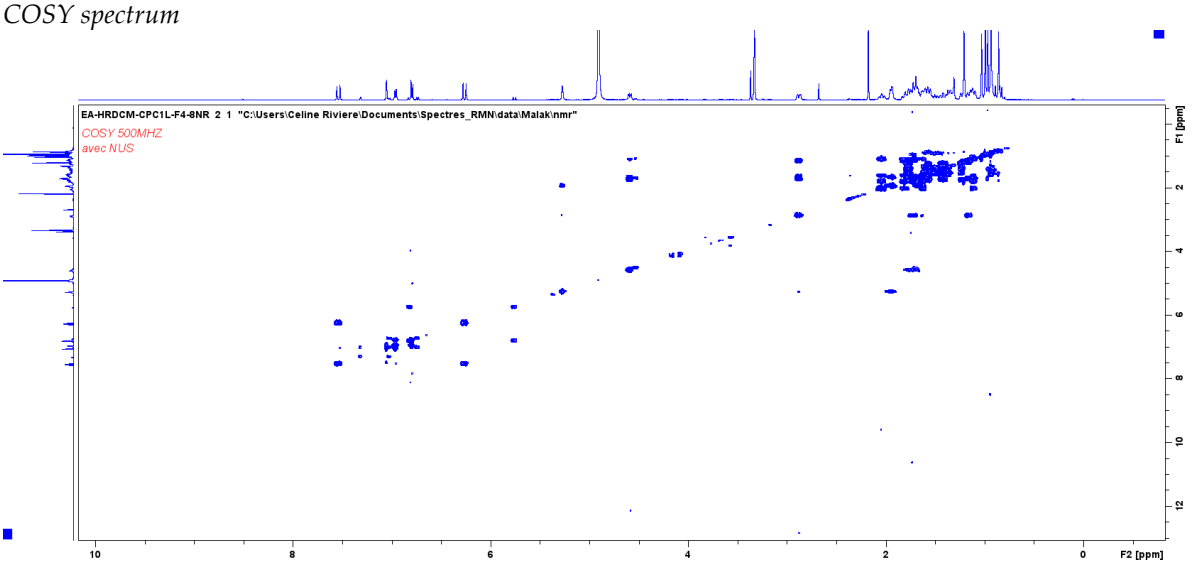

HSQC spectrum

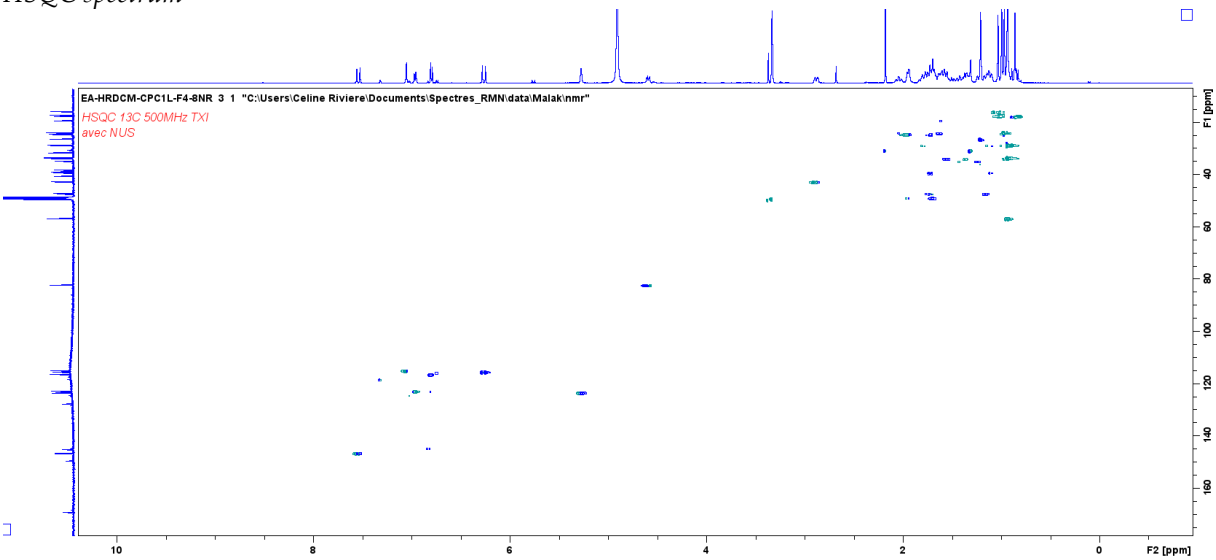

HMBC spectrum

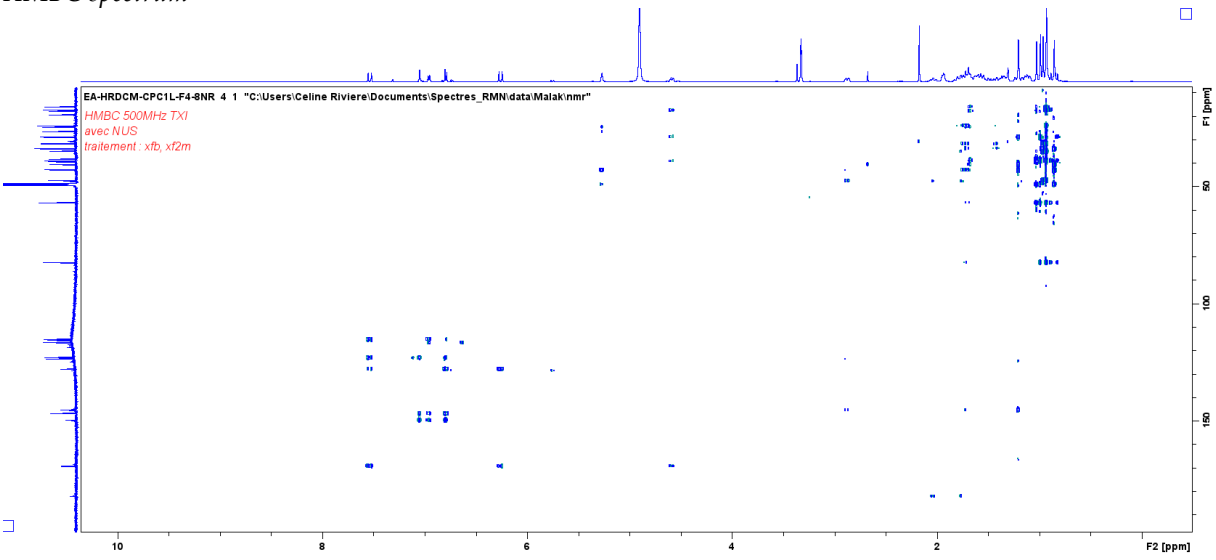

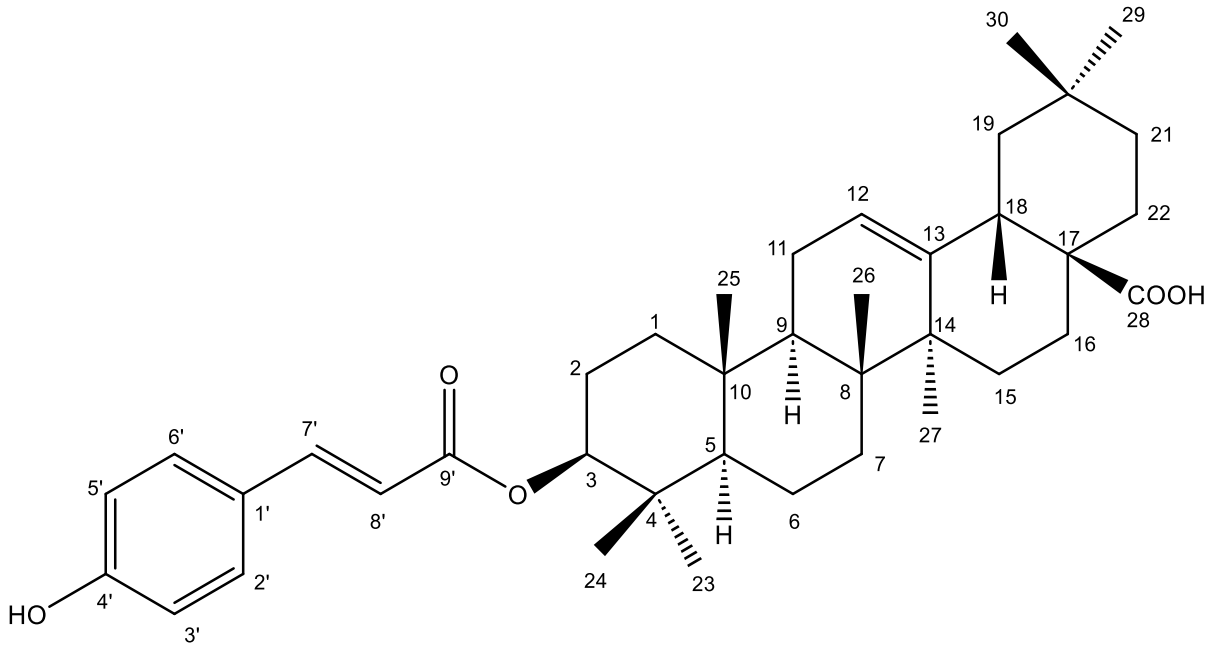

(F7-1) 3-O-*trans-p*-coumaroyl oleanolic acid ($C_{39}H_{54}O_5$, 602 g.mol^{-1})

White amorphous powder; ESI-MS (negative-ion mode) *m*/z: 601.72 [M-H]$^-$; HR-ESI-Orbitrap-MS (negative-ion mode) *m*/z: 601.3899 [M-H]$^-$; (calcd. 601.3888 for $C_{39}H_{53}O_5$ [M-H]$^-$); **^{1}H-NMR spectrum** (MeOD ; 500 MHz): δ 7.61 (C**H**, d, *J* = 15.91 Hz, H-7′), 7.48 (C**H**, *d*, *J* = 8.68 Hz, H-2′), 7.48 (C**H**, *d*, *J* = 8.68 Hz, H-6′), 6.83 (C**H**, *d*, *J* = 8.68 Hz, H-3′), 6.83 (C**H**, *d*, *J* = 8.68 Hz, H-5′), 6.33 (C**H**, d, *J* = 15.91 Hz, H-8′), 5.27 (C**H**, t, *J* = 3.59 Hz, H-12), 4.59 (C**H**, *dd*, *J* = 11.72, 4.67 Hz, H-3), 2.88 (C**H**, *dd*, *J* = 14.10, 4.59 Hz, H-18), 2.02 (C**H$_2$**, *m*, H-16β), 1.94 (C**H**, *m*, H-9), 1.93 (C**H$_2$**, *m*, H-11β), 1.80 (C**H$_2$**, *m*, H-15β), 1.77 (C**H$_2$**, *m*, H-22β), 1.75 (C**H$_3$**, *m*, H-2β), 1.72 (C**H$_2$**, m, H-19β), 1.70 (C**H$_2$**, *m*, H-1β), 1.70 (C**H$_3$**, *m*, H-2α), 1.68 (C**H$_2$**, *m*, H-11α), 1.63 (C**H$_2$**, *m*, H-16α), 1.60 (C**H$_2$**, *m*, H-6β), 1.58 (C**H$_2$**, *m*, H-7β), 1.55 (C**H$_2$**, *m*, H-22α), 1.49 (C**H$_2$**, m, H-6α), 1.42 (C**H$_2$**, *m*, H-21β), 1.35 (C**H$_2$**, *m*, H-7α), 1.24 (C**H$_2$**, m, H-21α), 1.21 (C**H$_3$**, *s*, H-27), 1.14 (C**H$_2$**, m, H-19α), 1.12 (C**H$_2$**, *m*, H-1α), 1.09 (C**H$_2$**, *m*, H-15α), 1.04 (C**H$_3$**, *s*, H-25), 0.99 (C**H$_3$**, *s*, H-24), 0.97 (C**H$_3$**, *s*, H-30), 0.93 (C**H$_3$**, *s*, H-23), 0.93 (C**H$_3$**, *s*, H-29), 0.89 (C**H**, *m*, H-5), 0.86 (C**H$_3$**, *s*, H-26) and **^{13}C-NMR spectrum** (MeOD, 125 MHz): 180.75 (C-28), 167.79 (C-9′), 159.87 (C-4′), 144.90 (C-13), 143.95 (C-7'), 129.75 (C-2′), 129.75 (C-6′), 125.77 (C-1′), 122.06 (C-12), 115.43 (C-3′), 115.43 (C-5′), 114.25 (C-8′), 80.90 (C-3), 55.41 (C-5), 48.45 (C-9), 46.32 (C-17), 45.90 (C-19), 41.51 (C-14), 41.38 (C-18), 39.16 (C-8), 37.95 (C-10), 37.58 (C-4), 37.40 (C-1), 33.53 (C-21), 32.51 (C-22), 32.45 (C-7), 32.18 (C-29), 30.23 (C-20), 27.46 (C-15), 27.26 (C-23), 25.00 (C-27), 23.29 (C-11), 23.12 (C-2), 22.68 (C-30), 22.59 (C-16), 17.97 (C-6), 16.34 (C-26), 15.94 (C-25), 14.53 (C-24)

^{1}H spectrum

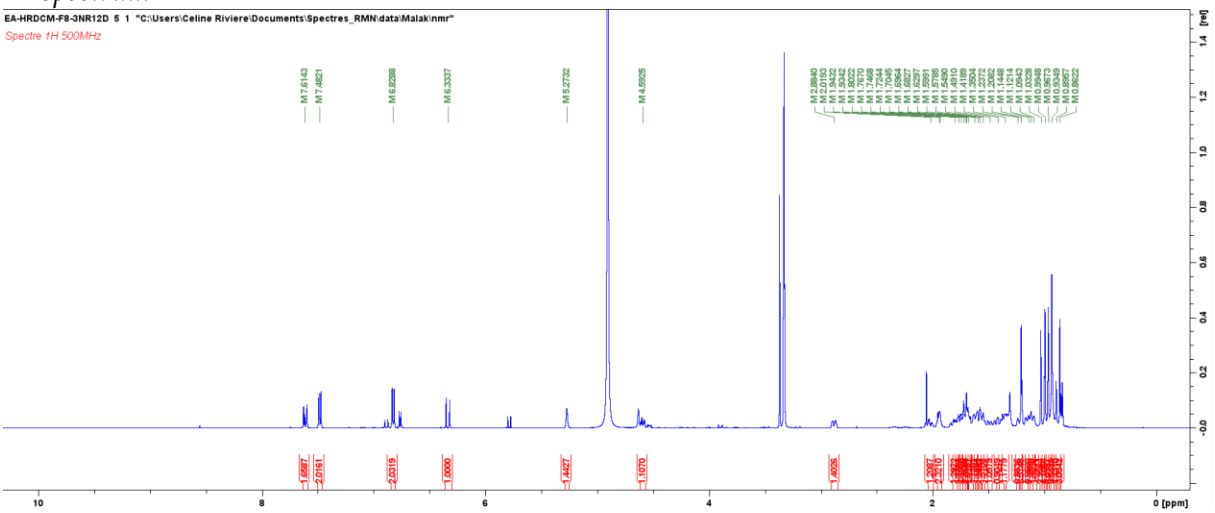

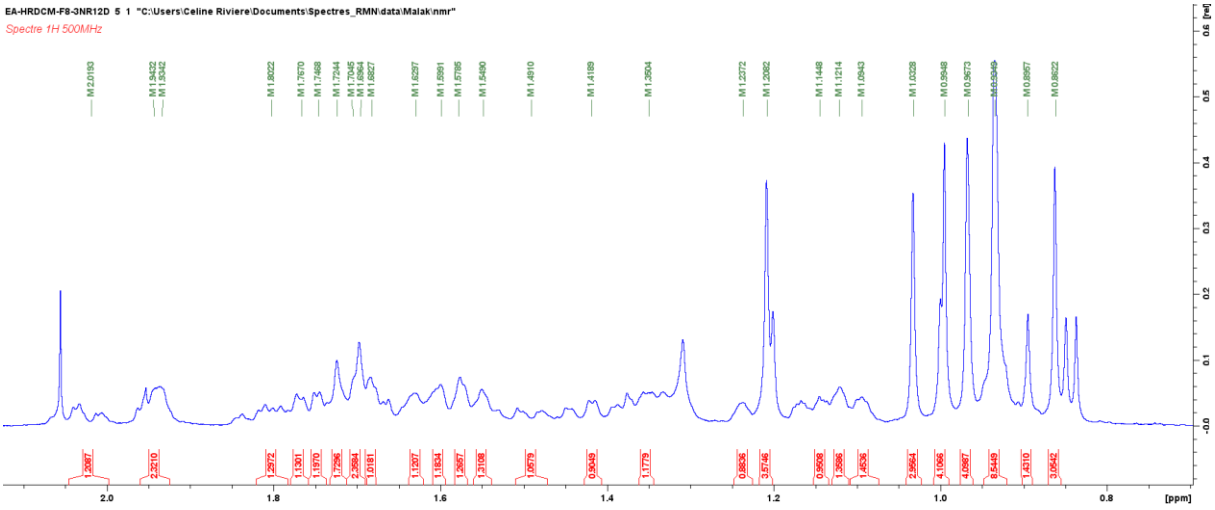

^{13}C spectrum

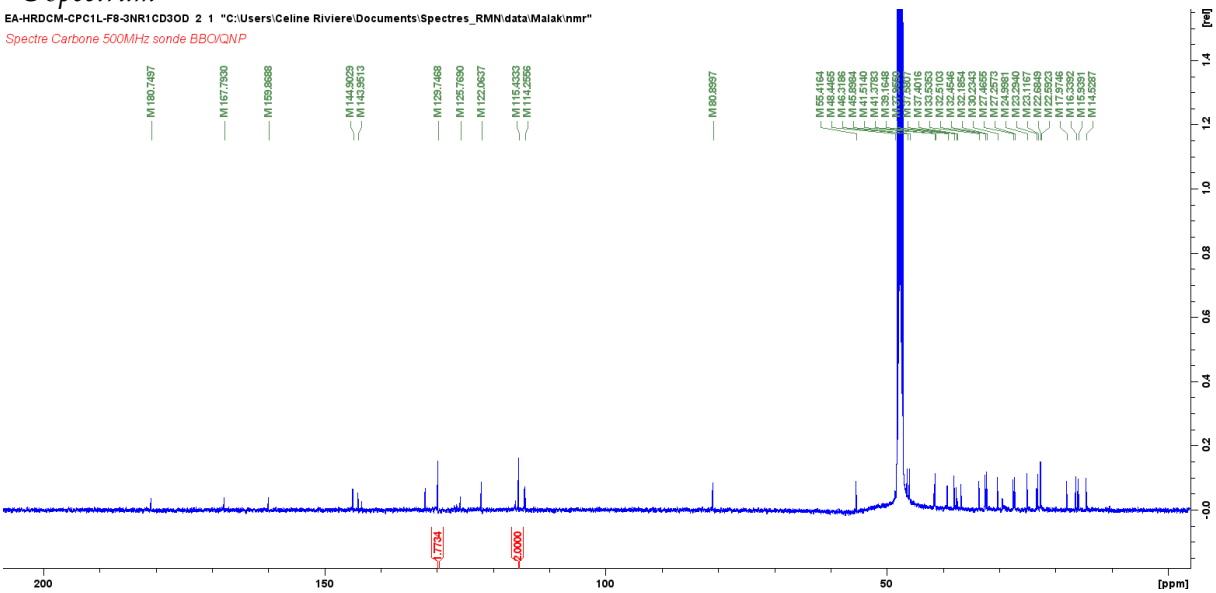

COSY spectrum

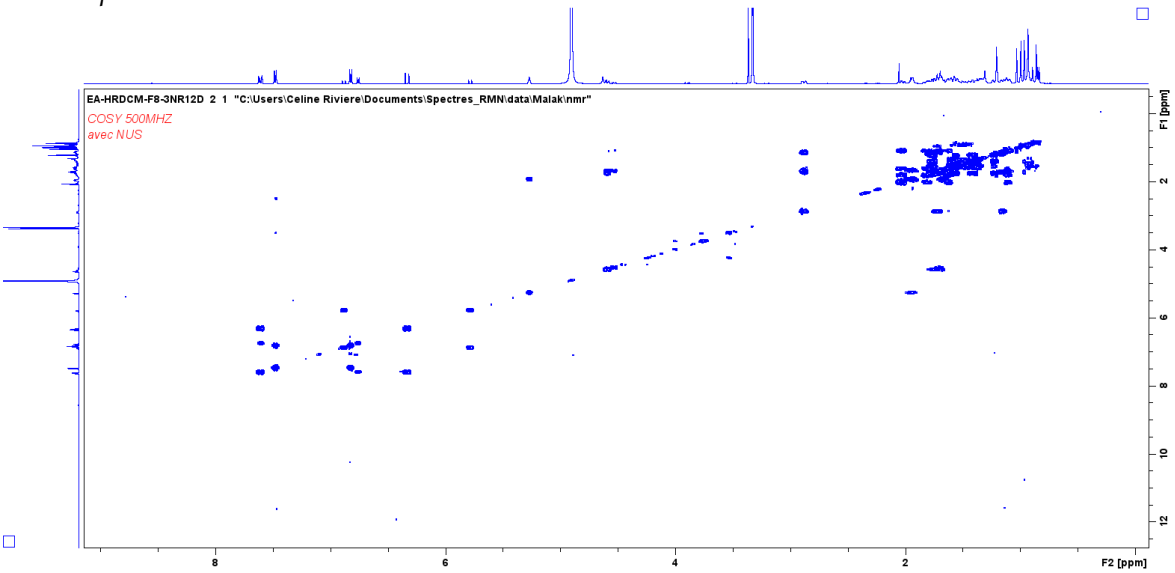

HSQC spectrum

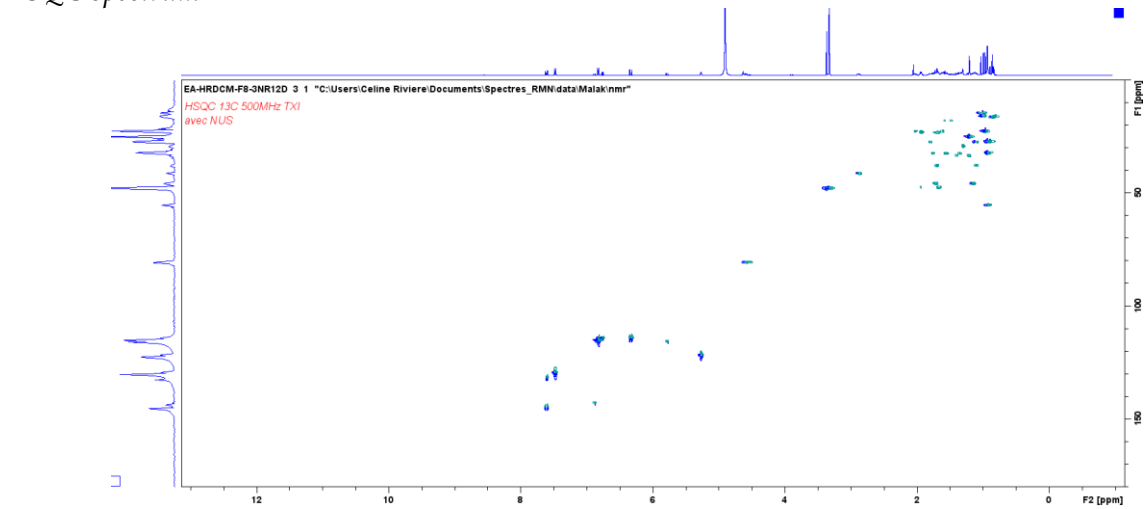

HMBC spectrum

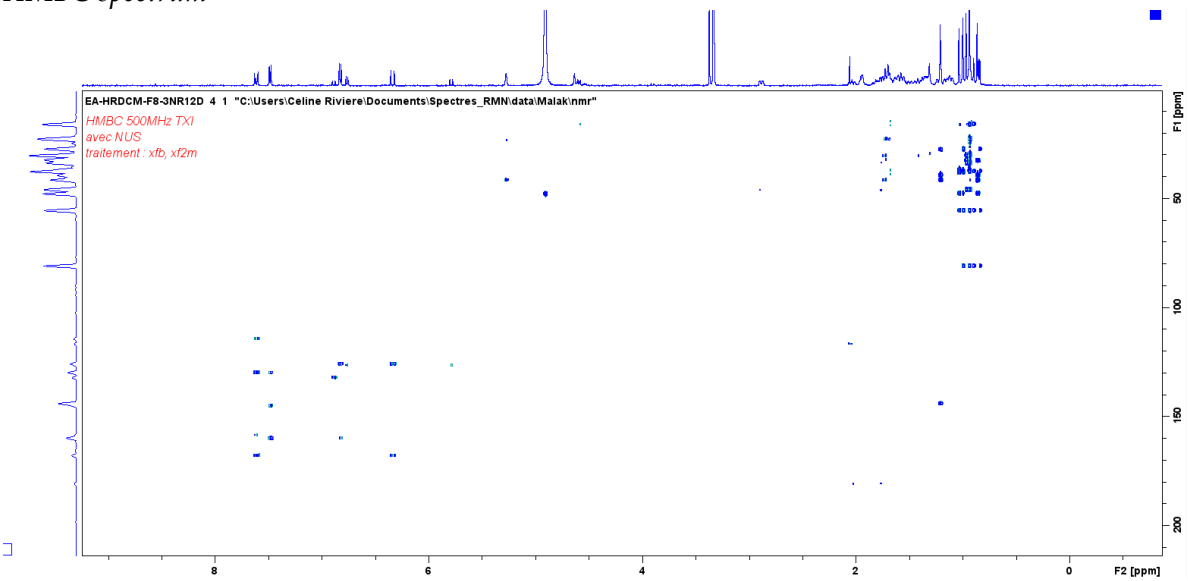

Part II: Exploring the Antiviral Potential of the Invasive Plant *Senecio inaequidens* Against Coronaviruses

Figure S3. Purity of sesquiterpenoids isolated from SI DCM on the basis of PDA chromatograms.

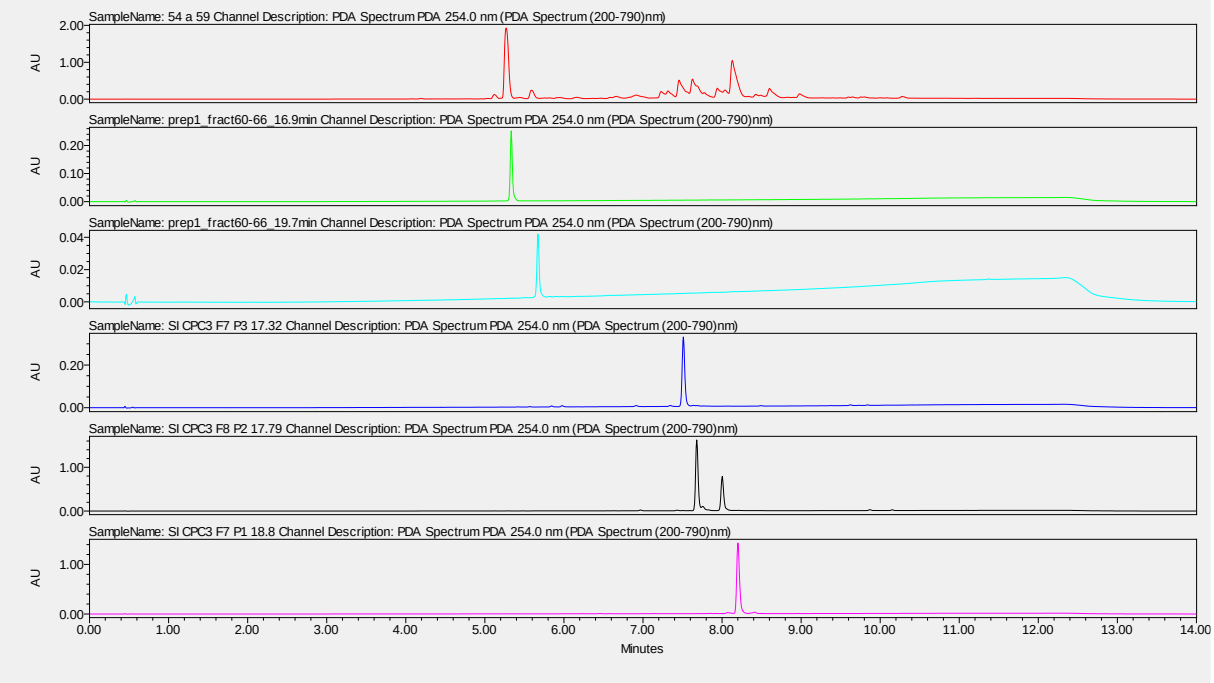

(**F4-1**) 2-methoxy-*O*-methyl-1-oxo-2,3-dehydrocacalol

	Name	Retention Time	Area	% Area	Height
1		5.176	1050	0.22	505
2		5.334	485176	**99.71**	249629
3		5.530	343	0.07	247

(**F4-2 = F11-2**) (6*R*) 1-hydroxy-2-methoxy-1,2,3,4-dehydrocacalone

	Name	Retention Time	Area	% Area	Height
1		5.489	180	0.22	156
2		5.672	80994	**99.17**	39335
3		5.816	494	0.61	271

(**F4-3**) Cacalol

	Name	Retention Time	Area	% Area	Height
1		5.418	2133	0.25	1015
2		5.507	123	0.01	161
3		5.567	3760	0.44	1790
4		5.844	10318	1.21	4611
5		5.977	12464	1.46	5628
6		6.913	11614	1.36	4591
7		7.222	961	0.11	475
8		7.345	10214	1.20	4472
9		7.511	771024	**90.56**	326291
10		7.641	11724	1.38	4275
11		7.684	8949	1.05	3230

12		7.765	3130	0.37	1034
13		8.490	4987	0.59	1947

(F4-4) Not determined

	Name	Retention Time	Area	% Area	Height
1		7.281	1512	0.03	685
2		7.433	31460	0.53	13209
3		7.507	13092	0.22	4629
4		7.593	5571	0.09	2422
5		7.680	3610394	**60.48**	1618985
6		7.756	341845	5.73	98005
7		8.002	1920971	**32.18**	781829
8		8.153	13938	0.23	4980
9		8.211	21646	0.36	6780
10		8.334	2446	0.04	918
11		8.361	1484	0.02	910
12		8.491	4911	0.08	1901

(**F4-5)** Butanoic acid, 3-methyl-, 4,4a,5,6,7,9-hexahydro-3,4a,5-trimethyl-9-oxonaphtho[2,3-*b*]furan-4-yl ester, [4*S*-(4α,4aα,5α)]- (9CI)

	Name	Retention Time	Area	% Area	Height
1		7.033	1511	0.04	865
2		7.142	8488	0.22	2504
3		7.372	1536	0.04	688
4		7.506	760	0.02	364
5		7.587	1151	0.03	565
6		7.696	2494	0.07	1072
7		7.842	9106	0.24	3972
8		7.918	1882	0.05	1421
9		7.939	3553	0.09	1586
10		8.010	918	0.02	628
11		8.073	75984	1.99	20681
12		8.201	3608887	**94.31**	1425469
13		8.413	107429	2.81	28142
14		8.491	1618	0.04	992
15		8.982	1106	0.03	400

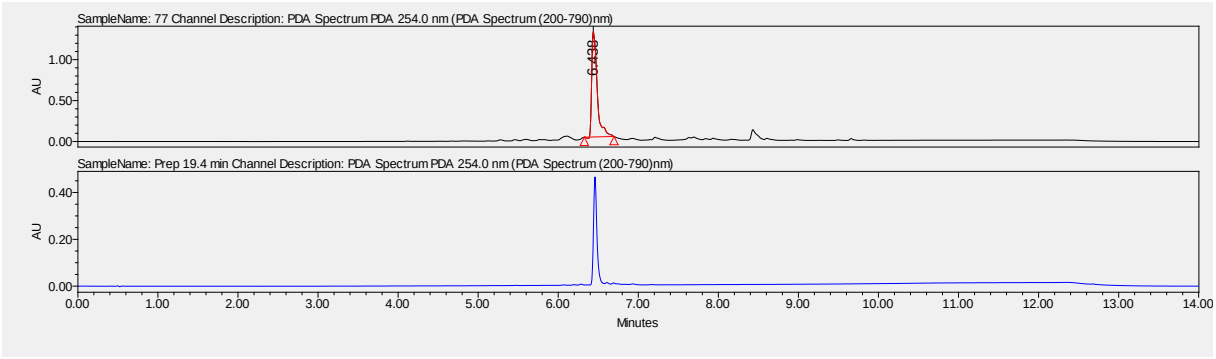

(**F7-1**) 1-hydroxy-2-methoxy-1,2,3,4-dehydro-6-dehydroxycacalone

	Name	Retention Time	Area	% Area	Height
1		6.070	4019	0.27	1471
2		6.199	6284	0.42	2307
3		6.285	12763	0.84	4230
4		6.373	3094	0.20	1209
5		6.459	1373170	**90.87**	462453
6		6.608	35669	2.36	10515
7		6.693	27689	1.83	8753
8		6.743	15383	1.02	5166
9		6.811	14038	0.93	2915
10		6.932	19046	1.26	4579

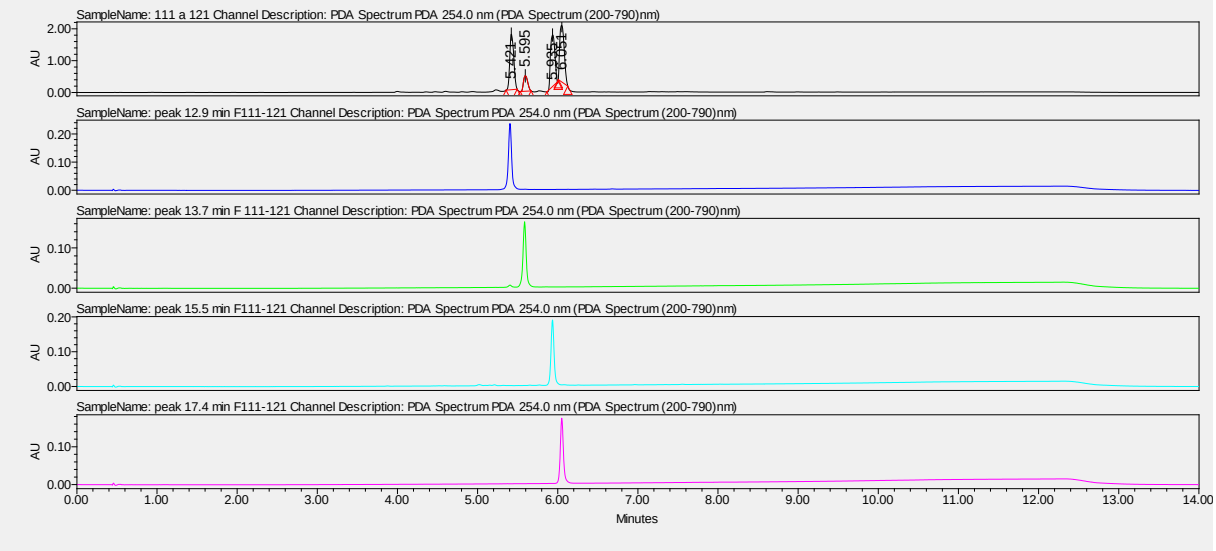

(**F11-1**) (6*S*) 1-hydroxy-2-methoxy-1,2,3,4-dehydrocacalone

	Name	Retention Time	Area	% Area	Height
1		5.405	683106	**98.89**	234904
2		5.587	3389	0.49	882
3		6.056	316	0.05	158
4		6.457	1348	0.20	320
5		6.682	2612	0.38	904

(**F11-2 = F4-2)** (6*R*) 1-hydroxy-2-methoxy-1,2,3,4-dehydrocacalone

	Name	Retention Time	Area	% Area	Height
1		5.405	15502	3.22	5386
2		5.587	465591	**96.74**	162338
3		6.415	45	0.01	57
4		6.576	143	0.03	85

(**F11-3)** 1,2-dimethoxy-1,2,3,4-dehydro-6-dehydroxycacalone

	Name	Retention Time	Area	% Area	Height
1		5.019	11553	2.05	3352
2		5.098	2647	0.47	1192
3		5.150	4679	0.83	1663
4		5.211	6733	1.19	2626
5		5.323	2807	0.50	938
6		5.378	1251	0.22	394
7		5.508	539	0.10	232
8		5.581	339	0.06	178
9		5.650	2812	0.50	960
10		5.769	3933	0.70	1360
11		5.935	515991	**91.40**	188113
12		6.081	7354	1.30	1760
13		6.259	1983	0.35	686
14		6.961	1940	0.34	711

(**F11-4)** 2,3-dehydro-2-methoxy-1-oxocacalol methyl ether

	Name	Retention Time	Area	% Area	Height
1		5.898	230	0.05	129
2		6.051	472354	**99.95**	172396

Figure S4. NMR data of cacalolides isolated from DCM sub-extract of *Senecio inaequidens*.

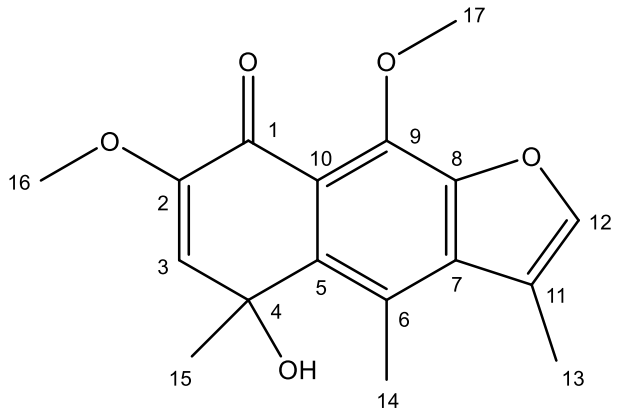

(F4-1) 2-methoxy-*O*-methyl-1-oxo-2,3-dehydrocacalol (= 5-hydroxy-7,9-dimethoxy-3,4,5-trimethylnaphtho[2,3-b]furan-8(5H)-one, CAS number 908102-41-0) ($C_{17}H_{18}O_5$, 302 g.mol^{-1})

White amorphous powder; **ESI-MS** (positive-ion mode) *m/z* 303 $[M+H]^+$; **HR-ESI-Orbitrap-MS** (positive-ion mode) *m/z*: 308.1012 $[M+Na]^+$; (calcd. 308.1019 for $C_{17}H_{17}O_4Na$ $[M+Na]^+$), **^{1}H-NMR spectrum** (500 MHz, $CDCl_3$): 7.71 (C**H**, *q*, *J* = 1.25 Hz, H-**12**), 6.03 (C**H**, d, *J* = 5.45 Hz, H-**3**), 4.05 (C**H$_3$**, s, H-**17**), 3.78 (C**H$_3$**, *s*, H-**16**), 2.98 (C**H$_3$**, *s*, H-**14**), 2.49 (C**H$_3$**, *d*, *J* = 1.25 Hz, H-**13**), 1.72 (C**H$_3$**, *s*, H-**15**), and **^{13}C-NMR spectrum** (500 MHz, $CDCl_3$): 181.19 (C-**1**), 149.77 (C-**2**), 147.05 (C-**8**), 145.57 (C-**12**), 144.77 (C-**9**), 136.03 (C-**5**), 134.56 (C-**7**), 126.84 (C-**6**), 120.05 (C-**10**), 119.57 (C-**3**), 117.70 (C-**11**), 81.97 (C-**4**), 60.54 (C-**17**), 54.19 (C-**16**), 25.60 (C-**15**), 15.67 (C-**14**), 10.23 (C-**13**)

^{1}H-NMR spectrum of 2-methoxy-O-methyl-1-oxo-2,3-dehydrocacalol in MeOD (sonde TXI)

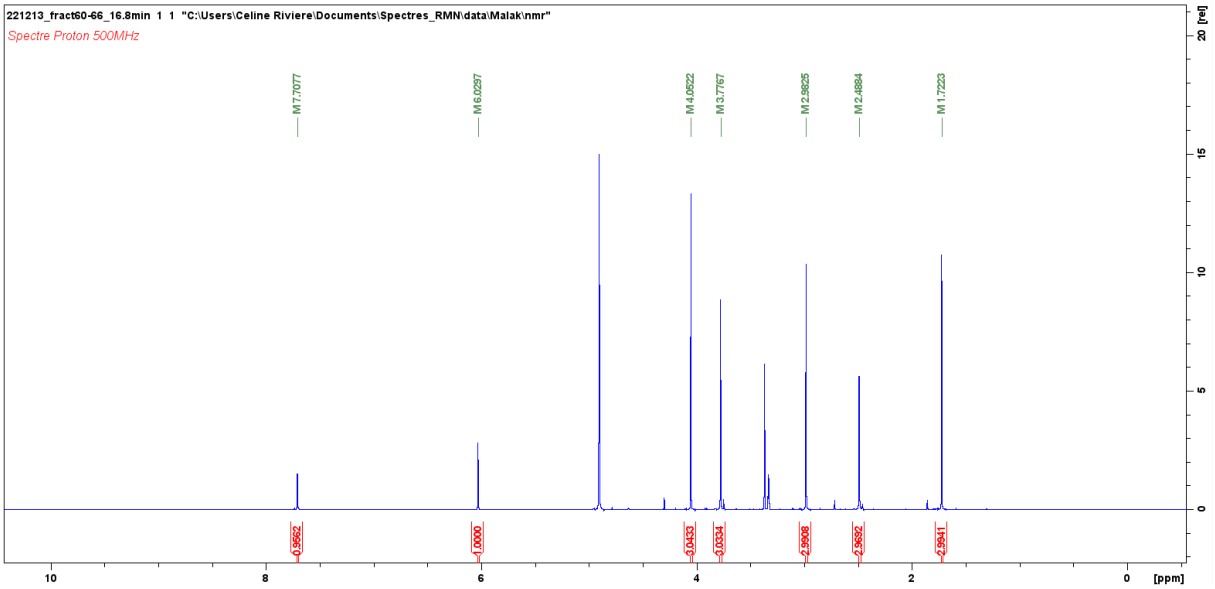

^{13}C-NMR spectrum of 2-methoxy-O-methyl-1-oxo-2,3-dehydrocacalol in MeOD (sonde TXI)

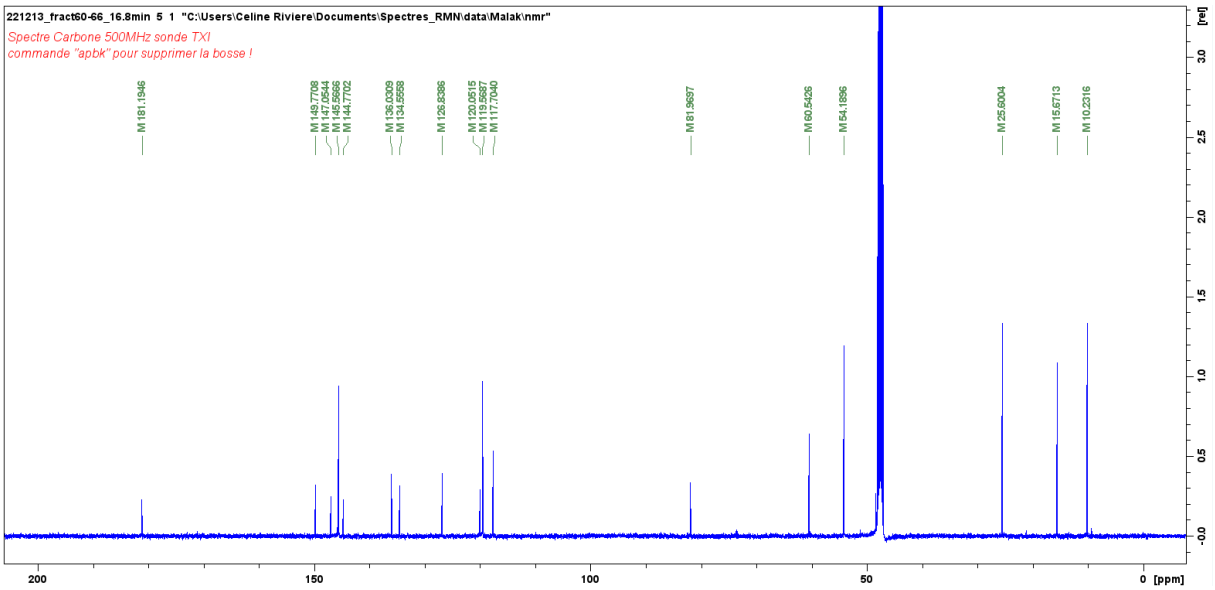

COSY spectrum of 2-methoxy-O-methyl-1-oxo-2,3-dehydrocacalol in MeOD (sonde TXI)

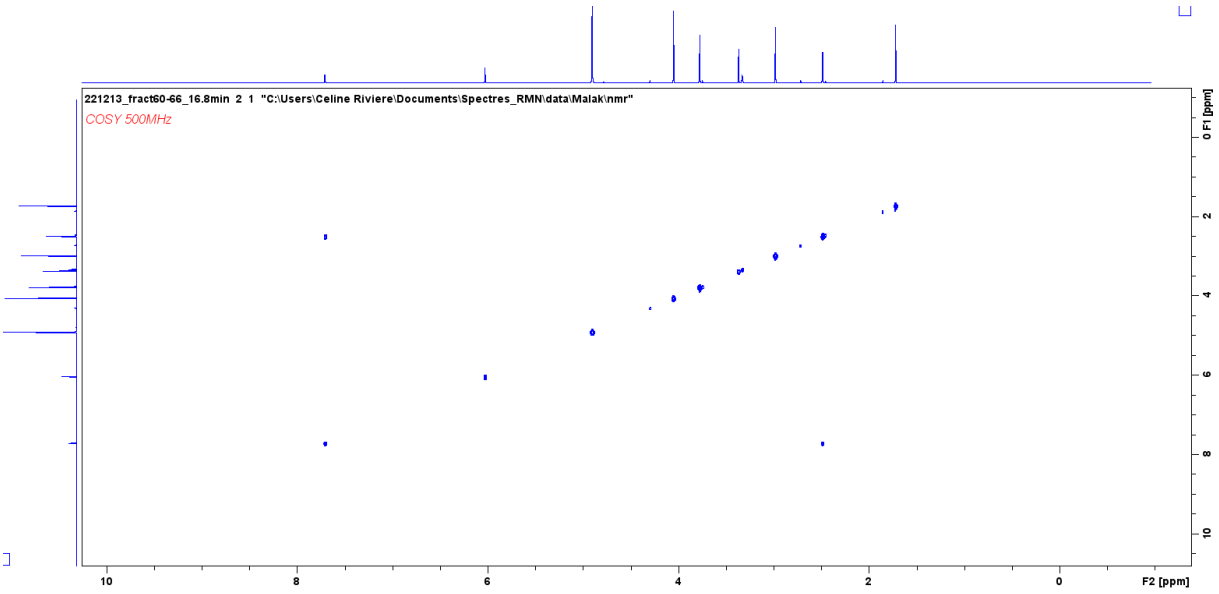

HSQC-DEPT spectrum of 2-methoxy-O-methyl-1-oxo-2,3-dehydrocacalol in MeOD (sonde TXI)

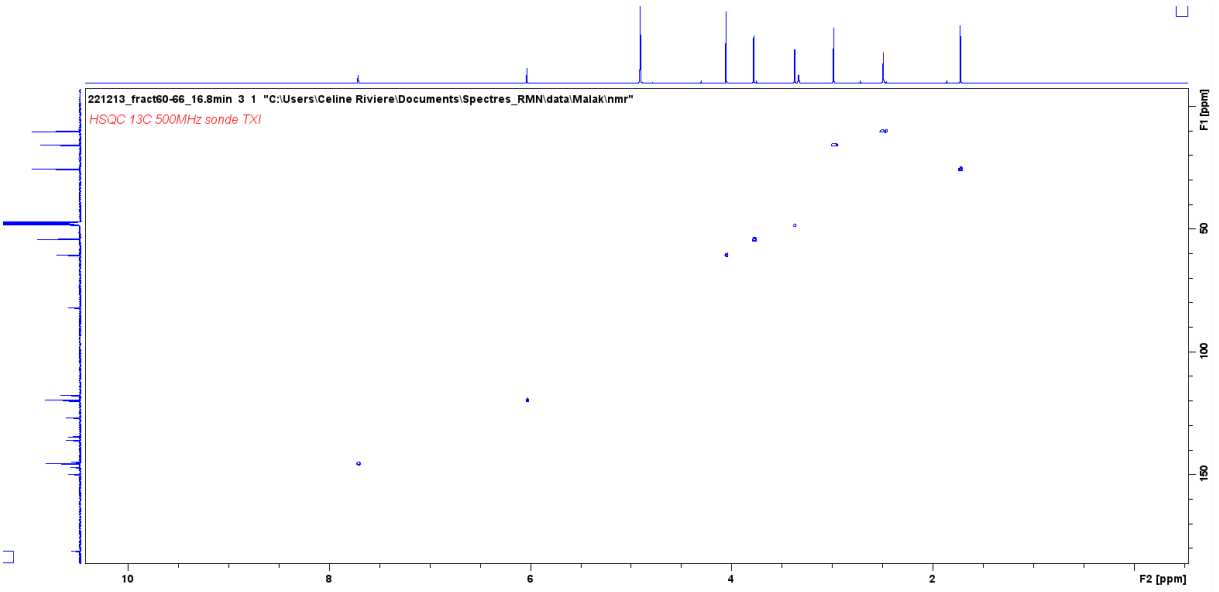

HMBC spectrum of 2-methoxy-O-methyl-1-oxo-2,3-dehydrocacalol in MeOD (sonde TXI)

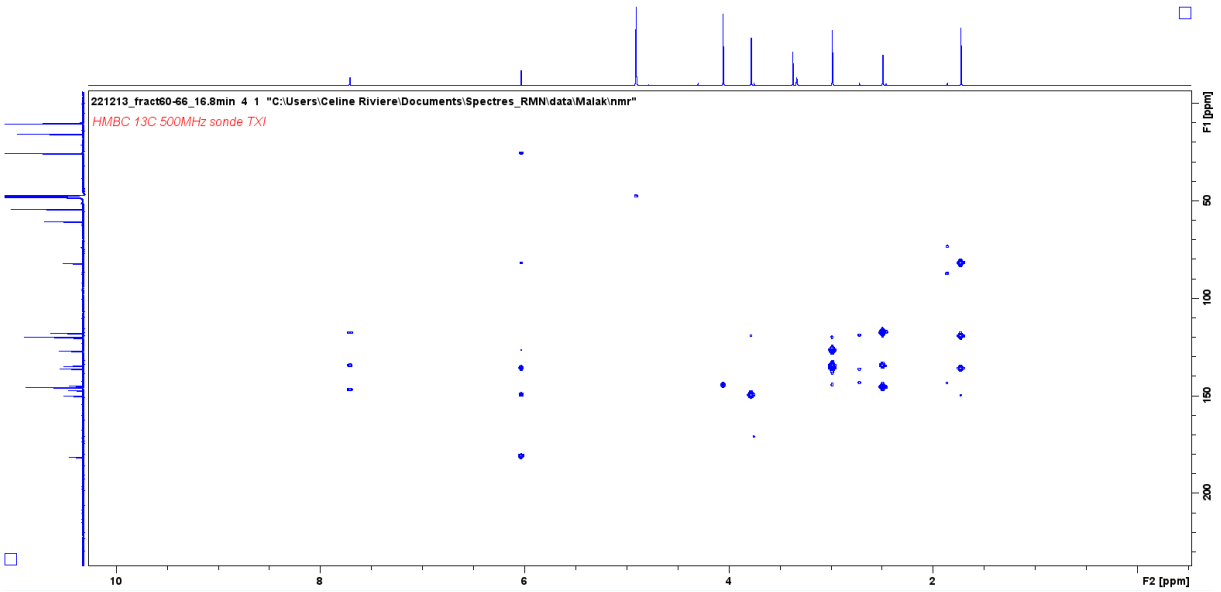

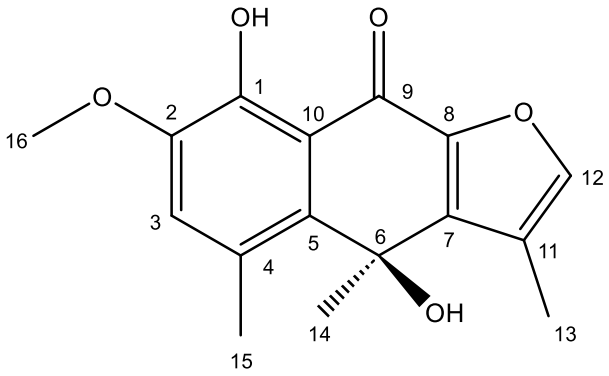

F4-2 (= F11-2) **(6*R*) 1-hydroxy-2-methoxy-1,2,3,4-dehydrocacalone** (= naphtho[2,3-b]furan-9(4H)-one,4,8-dihydroxy-7-methoxy-3,4,5-trimethyl-,(4R)-(9CI, ACI), CAS number 337513-79-8)($C_{16}H_{16}O_5$, 288 g.mol^{-1})

White amorphous powder; **ESI-MS** (positive-ion mode) *m/z* 305 $[M+H]^+$; **HR-ESI-Orbitrap-MS** (positive-ion mode) *m/z* 327.08389 $[M+Na]^+$; (calcd 327.08391 for $C_{16}H_{16}O_6Na$ $[M+Na]^+$), **^{1}H-NMR spectrum** (500 MHz, MeOD): 7.74 (C**H**, *q*, *J* = 1.15 Hz, H-**12**), 7.06 (C**H**, *s*, H-**3**), 3.91 (C**H$_3$**, *s*, H-**16**), 2.69 (C**H$_3$**, *s*, H-**15**), 2.32 (C**H$_3$**, *d*, *J* = 1.15 Hz, H-**13**), 1.79 (C**H$_3$**, *s*, H-**14**), and **^{13}C-NMR spectrum** (500 MHz, MeOD): 178.78 (C-**9**), 151.72 (C-**1**), 147.28 (C-**12**), 147.27 (C-**2**), 145.02 (C-**8**), 142.99 (C-**7**), 134.17 (C-**5**), 127.88 (C-**4**), 121.39 (C-**11**), 121.03 (C-**3**), 115.70 (C-**10**), 82.07 (C-**6**), 55.21 (C-**16**), 23.70 (C-**14**), 19.65 (C-**15**), 7.35 (C-**13**)

^{1}H-NMR spectrum of (6R) 1-hydroxy-2-methoxy-1,2,3,4-dehydrocacalone in MeOD (sonde TXI)

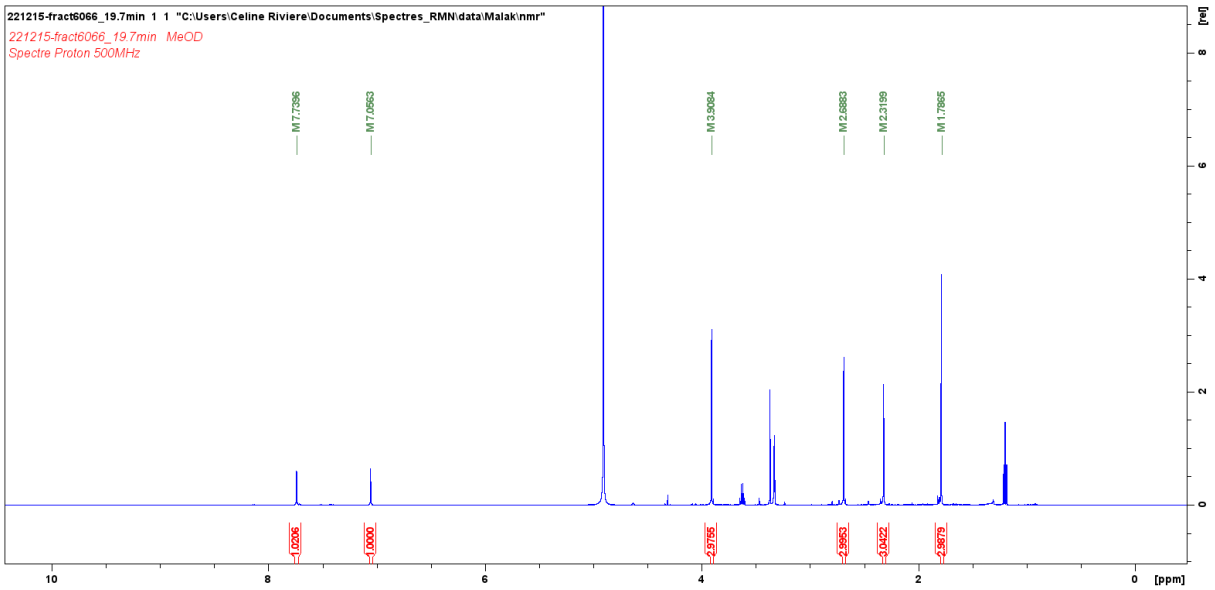

^{13}C-NMR spectrum of (6R) 1-hydroxy-2-methoxy-1,2,3,4-dehydrocacalone in MeOD (sonde TXI)

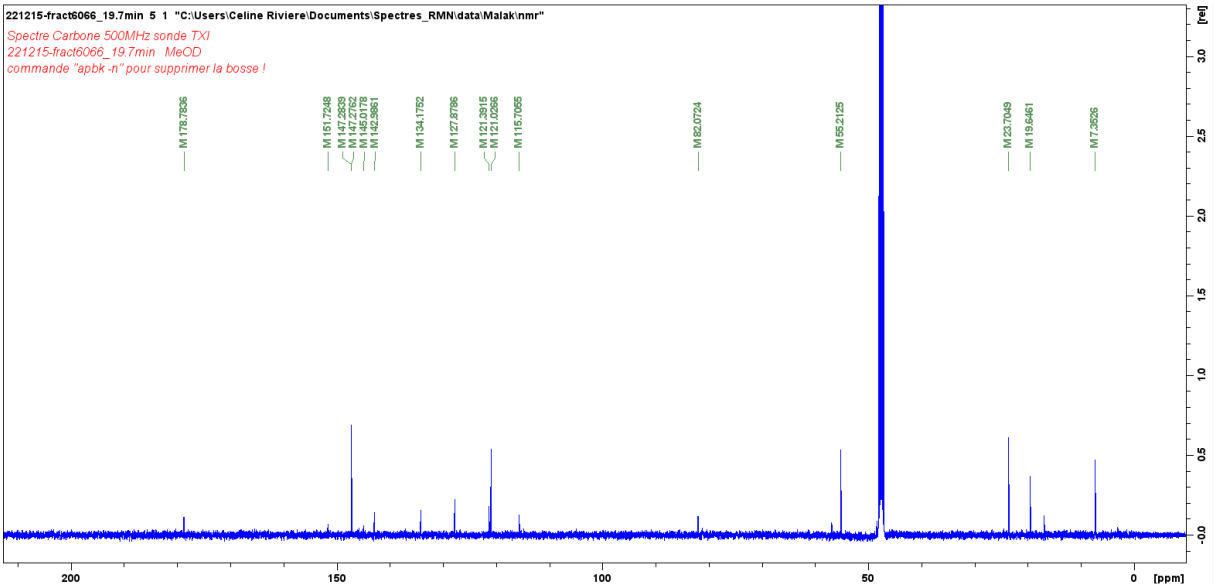

COSY spectrum of (6R) 1-hydroxy-2-methoxy-1,2,3,4-dehydrocacalone in MeOD (sonde TXI)

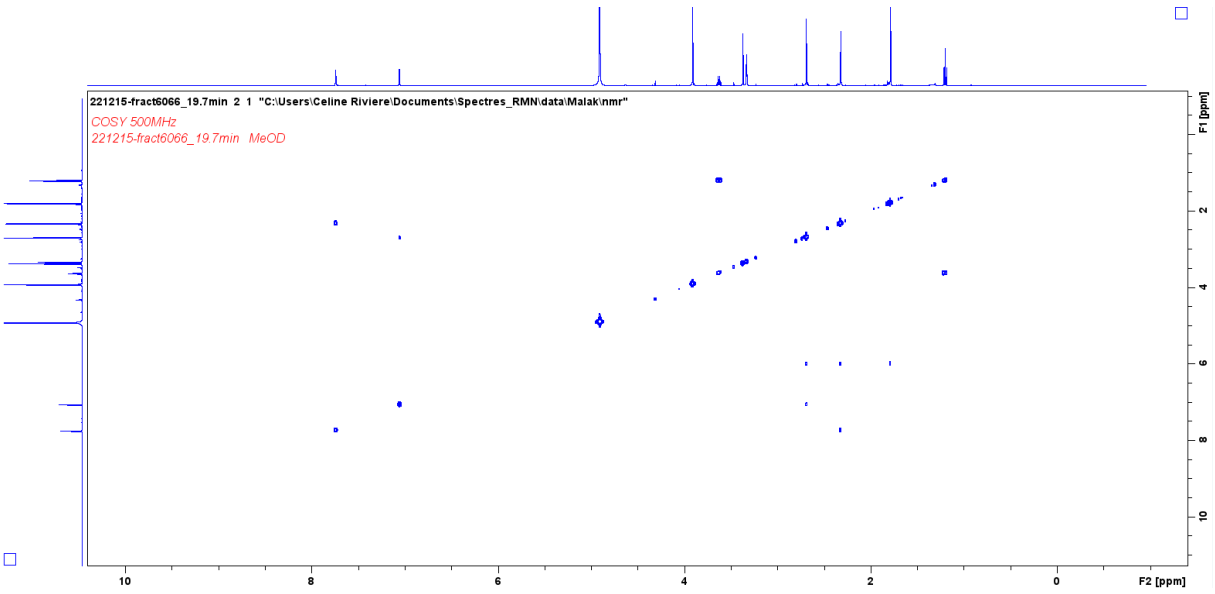

HSQC spectrum of (6R) 1-hydroxy-2-methoxy-1,2,3,4-dehydrocacalone in MeOD (sonde TXI)

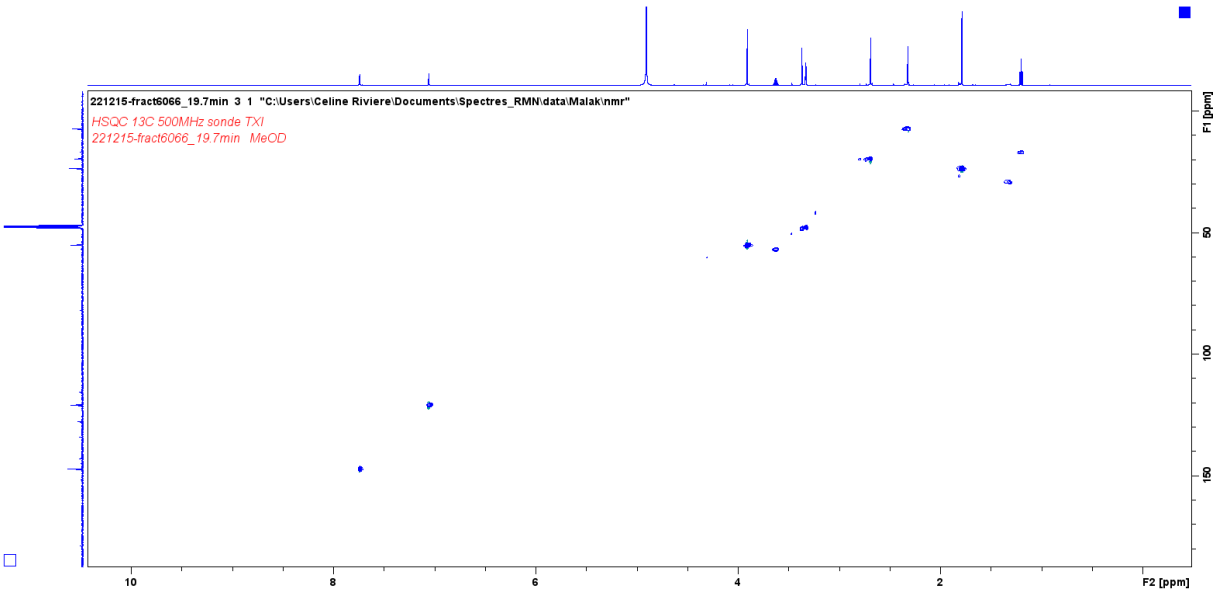

HMBC spectrum of (6R) 1-hydroxy-2-methoxy-1,2,3,4-dehydrocacalone in MeOD (sonde TXI)

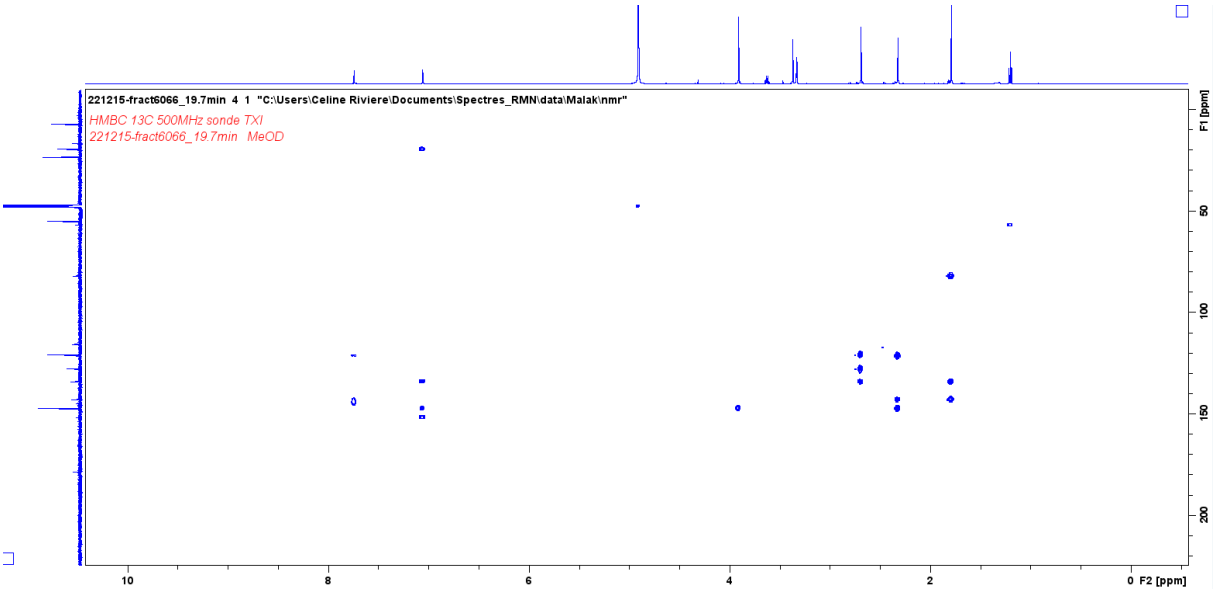

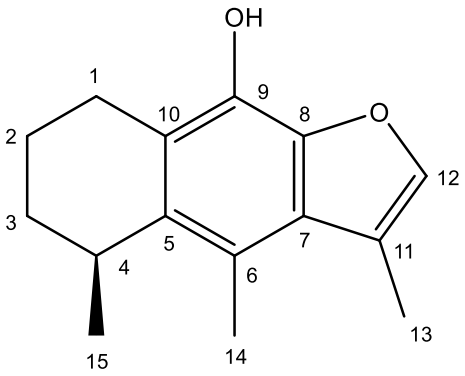

(F4-3) cacalol (= naphtho[2,3-b]furan-9-ol, 5,6,7,8-tetrahydro-3,4,5-trimethyl-, (5S)- (9CI, ACI), CAS number 24393-79-1) ($C_{15}H_{18}O_2$, 230 g.mol^{-1})

White amorphous powder; **ESI-MS** (positive-ion mode) *m/z* 231 $[M+H]^+$; **HR-ESI-Orbitrap-MS** (negative-ion mode) *m/z*: 229,12311 $[M-H]^-$; (calcd. 229.12231 for $C_{15}H_{17}O_2$ $[M-H]^-$), **^{1}H-NMR spectrum** (500 MHz, MeOD): 7.33 (C**H**, *q*, *J* = 1.15 Hz, H-**12**), 3.23 (C**H**, *m*, H-**4**), 2.97 (C**H$_2$**, *dd*, *J* = 17.35, 5.75 Hz H-**1a**), 2.58 (C**H$_2$**, *m*, H-**1b**), 2.52 (C**H$_3$**, *s*, H-**14**), 2.39 (C**H$_3$**, *d*, *J* = 1.15 Hz, H-**13**), 1.90 (C**H$_2$**, *m*, H-**2a**), 1.81 (C**H$_2$**, *m*, H-**2b**), 1.81 (C**H$_2$**, *m*, H-**3**), 1.19 (C**H$_3$**, *d*, *J* = 6.95 Hz, H-**15**), and **^{13}C-NMR spectrum** (500 MHz, $CDCl_3$): 144.39 (C-**8**), 141.97 (C-**12**), 138.25 (C-**9**), 136.25 (C-**5**), 127.42 (C-**7**), 120.42 (C-**10**), 120.20 (C-**6**), 117.95 (C-**11**), 31.41 (C-**3**), 30.21 (C-**4**), 24.37 (C-**1**), 21.93 (C-**15**), 18.02 (C-**2**), 14.09 (C-**14**), 11.49 (C-**13**)

^{1}H-NMR spectrum of cacalol in MeOD (sonde TXI)

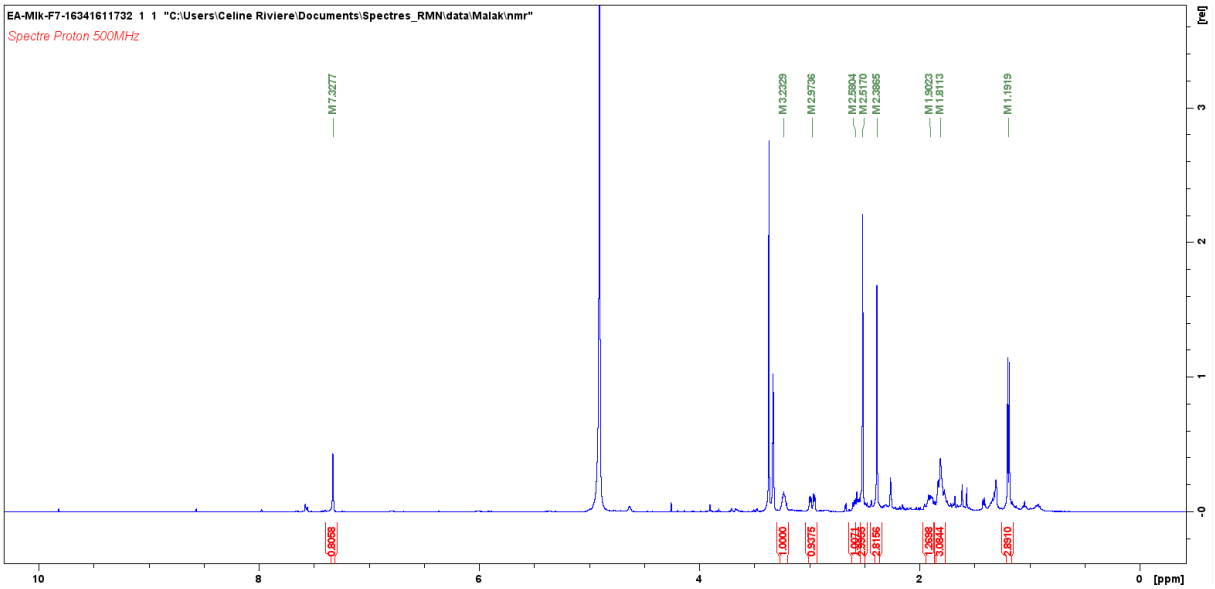

^{13}C-NMR spectrum of cacalol in MeOD (sonde TXI)

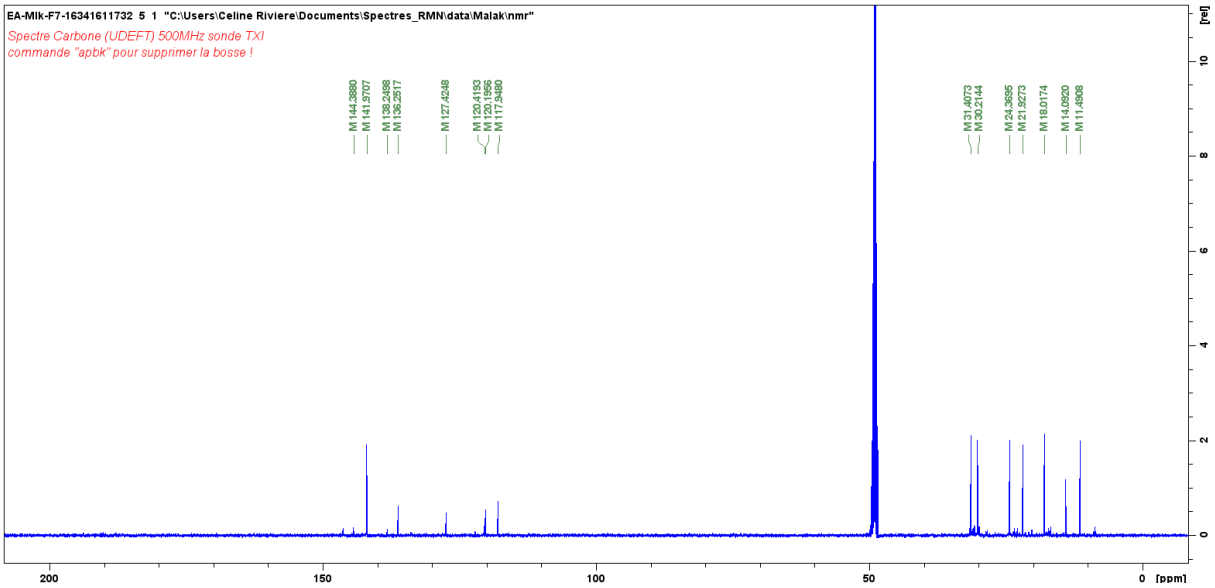

COSY spectrum of cacalol in MeOD (sonde TXI)

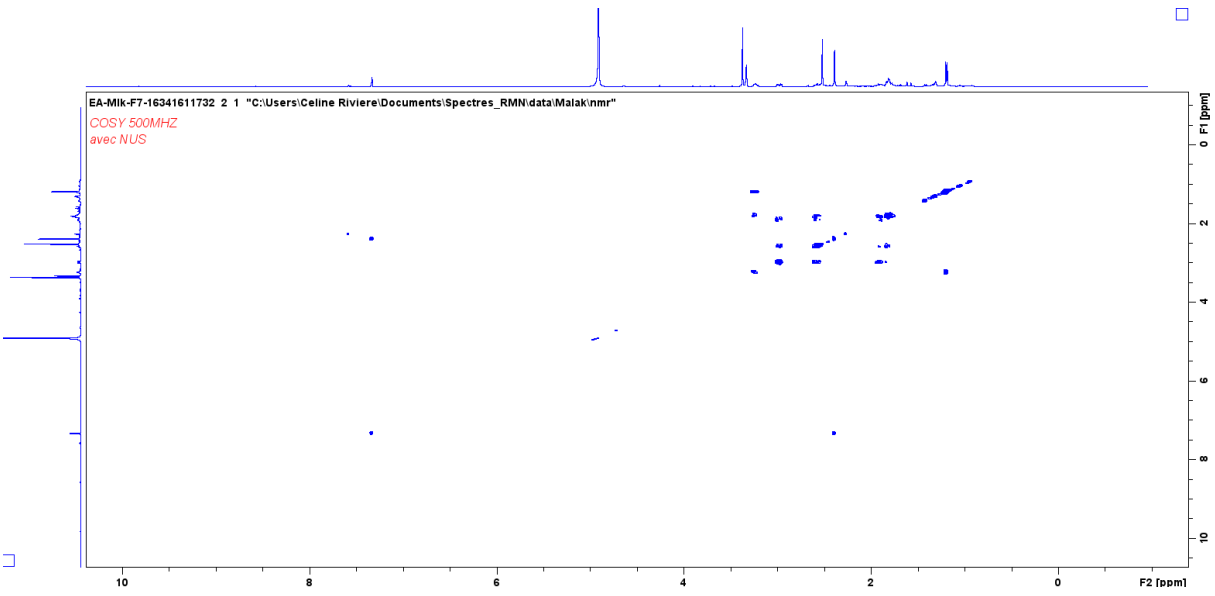

HSQC spectrum of cacalol in MeOD (sonde TXI)

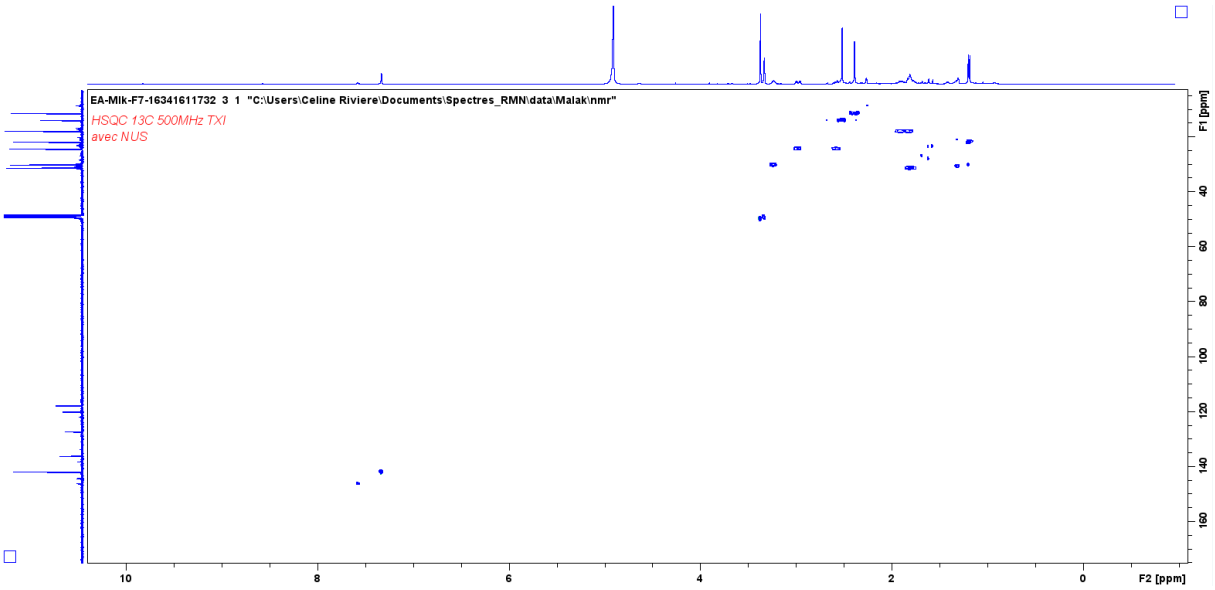

HMBC spectrum of cacalol in MeOD (sonde TXI)

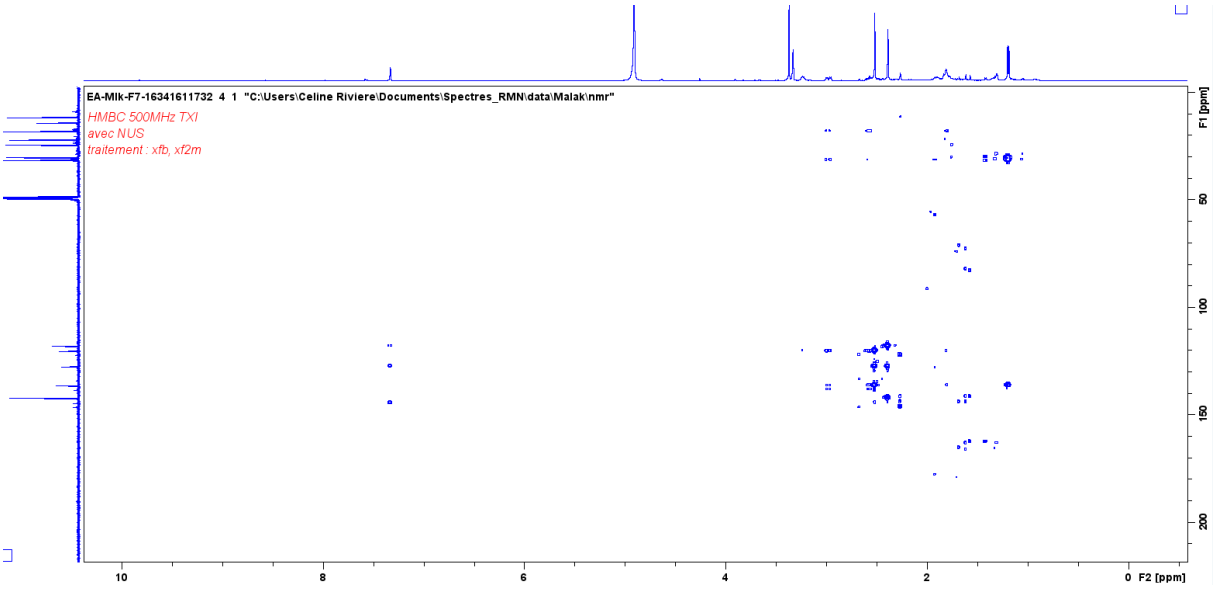

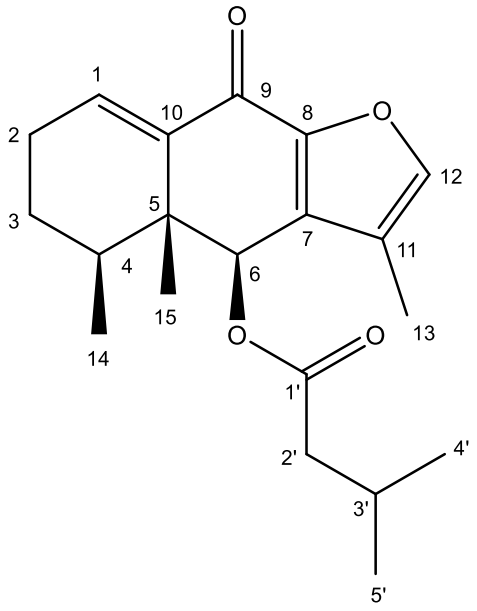

(F4-5) Butanoic acid, 3-methyl-,4,4a,5,6,7,9-hexahydro-3,4a,5-trimethyl-9-oxonaphtho[2,3-*b*]furan-4-yl ester, [4*S*-(4α,4aα,5α)]-(9CI), CAS number 59742-02-8 ($C_{20}H_{26}O_4$, 330 g.mol^{-1})

White amorphous powder; **ESI-MS** (positive-ion mode) *m/z* 331 $[M+H]^+$; **HR-ESI-Orbitrap-MS** (positive-ion mode) *m/z*: 353,17175 $[M+Na]^+$; (calcd. 353.17233 for $C_{20}H_{26}O_4$ Na $[M+H]^+$), **^{1}H-NMR spectrum** (500 MHz, MeOD): 7.69 (C**H**, q, *J* = 0.95 Hz, H-**12**), 6.99 (C**H**, t, *J* = 4.05, 4.30 Hz, H-**1**), 6.38 (C**H**, *s*, H-**6**), 2.44 (C**H$_2$**, *dd*, *J* = 7.20, 2.75, 2.25 Hz, H-**3**), 2.30 (C**H$_2$**, *m*, H-**2**), 2.21 (C**H**, m, H-3'), 2.01 (C**H**, m, H-5), 1.97 (C**H$_3$**, d, *J* = 1.12 Hz, H-10), 1.61 (C**H$_{6a}$**, m, H-6a), 1.51 (C**H$_{6b}$**, d, H-6b), 1.12 (C**H$_3$**, s, H-11), 1.07 (C**H$_3$**, d, *J* = 1.31 Hz H-5'), 1.05 (C**H$_3$**, d, *J* = 1.31 Hz H-4'), 1.06/1.04 (C**H$_3$**, d, *J* = 6.84 Hz, H-12) and **^{13}C-NMR spectrum** (500 MHz, MeOD): 176.9 (C-9), 172.7 (C-1'), 147.0 (C-2), 146.5 (C-1), 141.2 (C-8a), 138.3 (C-8), 136.8 (C-3a), 121.3 (C-3), 73.9 (C-4), 46.4 (C-4a), 42.7 (C-2'), 37.2 (C-5), 27.4 (C-6), 24.6 (C-3'), 24.4 (C-7), 21.5 (C-5'), 21.4 (C-4'), 16.5 (C-12), 14.5 (C-11), 7.4 (C-10)

[1]H-NMR spectrum of Butanoic acid, 3-methyl-,4,4a,5,6,7,9-hexahydro-3,4a,5-trimethyl-9-oxonaphtho[2,3-b]furan-4-yl ester, [4S-(4a,4aa,5a)]-(9CI) in MeOD (sonde TXI)

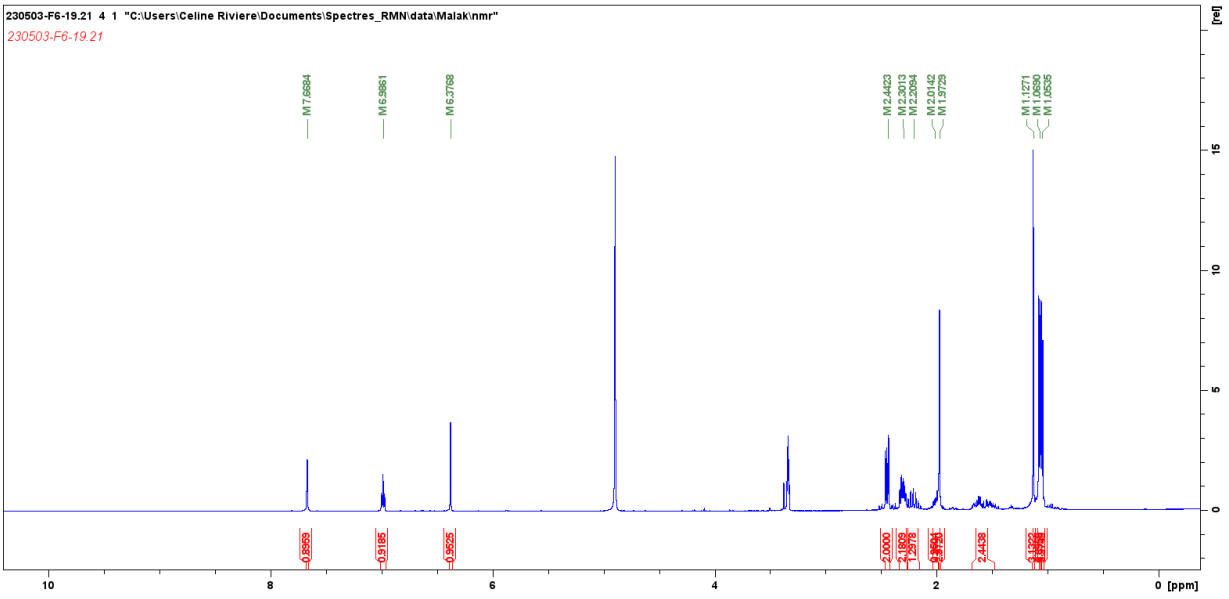

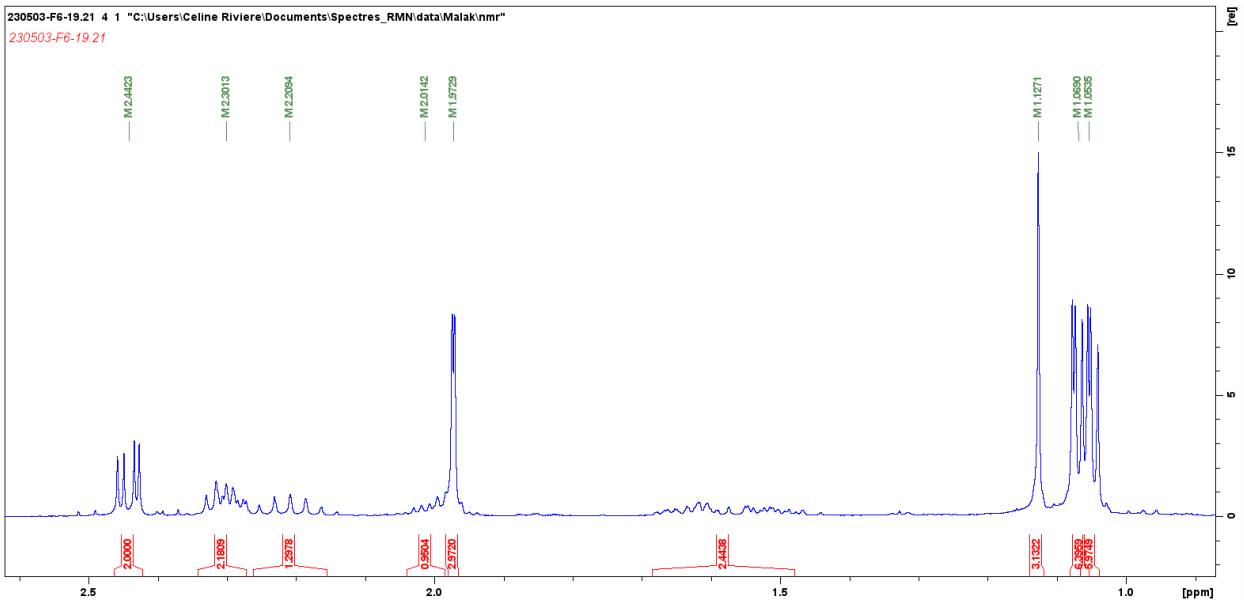

^{13}C-NMR spectrum of Butanoic acid, 3-methyl-,4,4a,5,6,7,9-hexahydro-3,4a,5-trimethyl-9-oxonaphtho[2,3-b]furan-4-yl ester, [4S-(4a,4aa,5a)]-(9CI) in MeOD (sonde TXI)

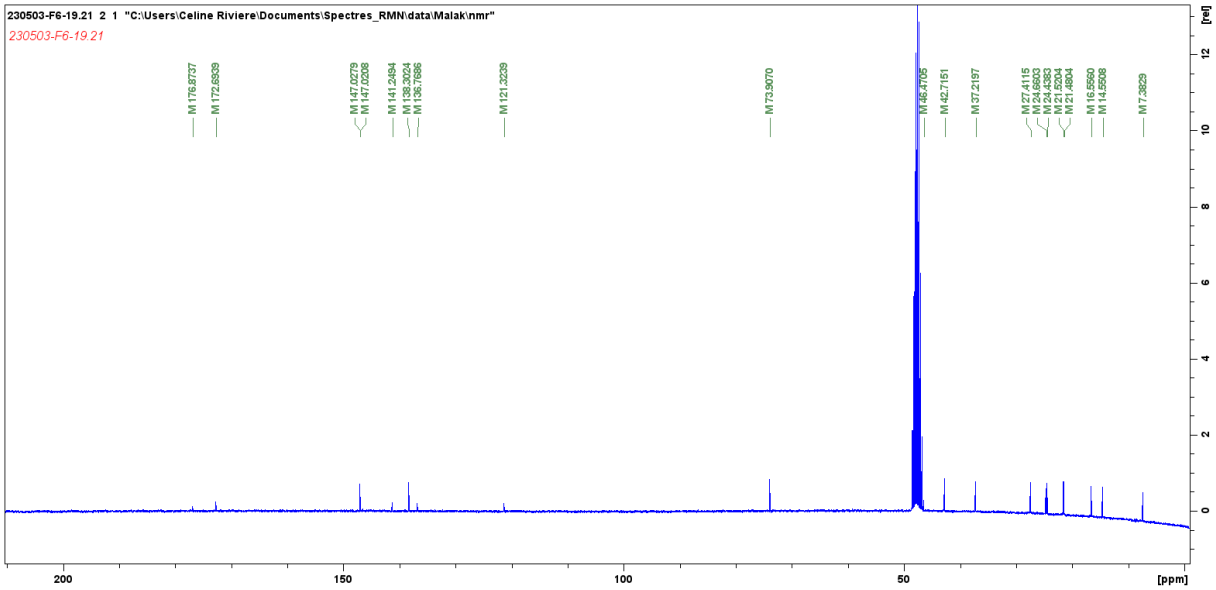

COSY spectrum of Butanoic acid, 3-methyl-,4,4a,5,6,7,9-hexahydro-3,4a,5-trimethyl-9-oxonaphtho[2,3-b]furan-4-yl ester, [4S-(4a,4aa,5a)]-(9CI) in MeOD

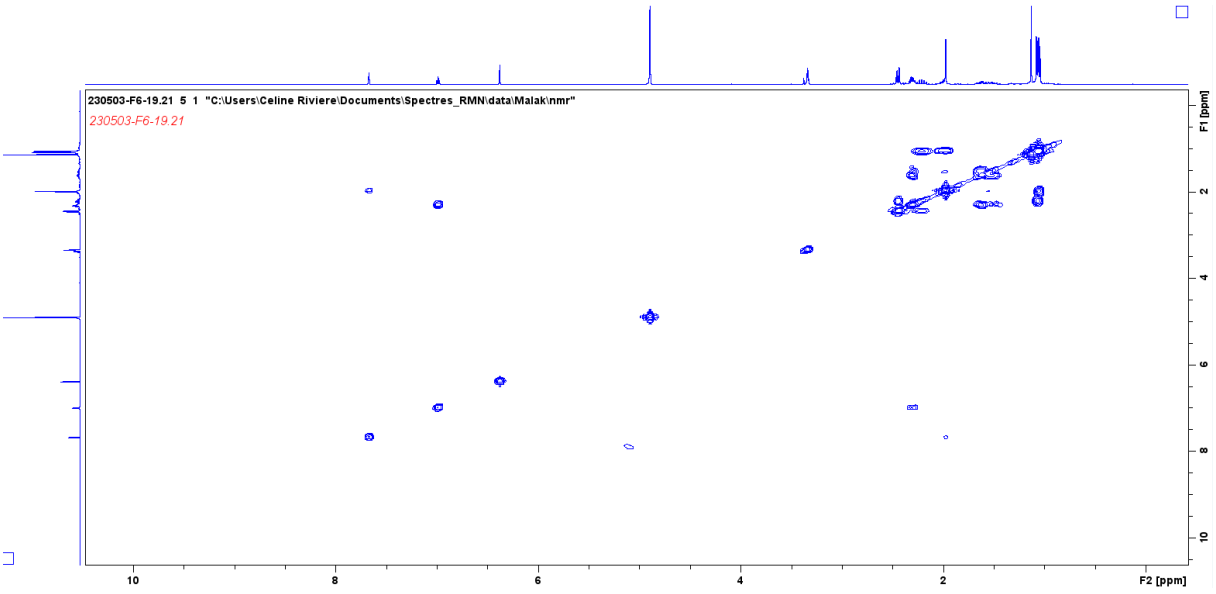

HSQC spectrum of Butanoic acid, 3-methyl-,4,4a,5,6,7,9-hexahydro-3,4a,5-trimethyl-9-oxonaphtho[2,3-b]furan-4-yl ester, [4S-(4a,4aa,5a)]-(9CI) in MeOD

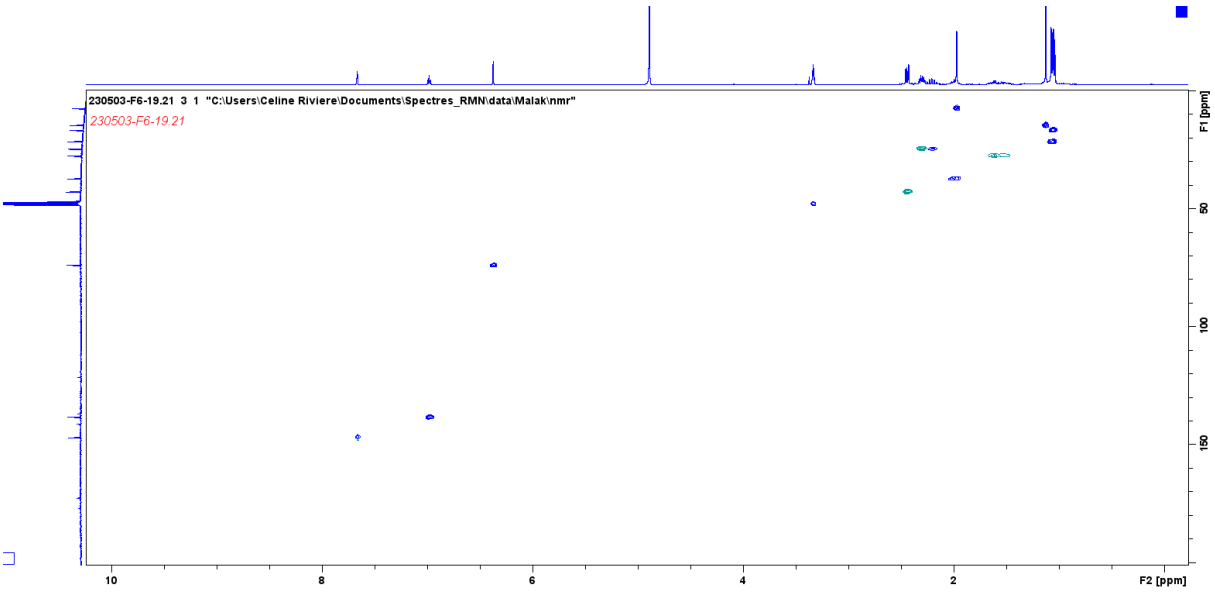

HMBC spectrum of Butanoic acid, 3-methyl-,4,4a,5,6,7,9-hexahydro-3,4a,5-trimethyl-9-oxonaphtho[2,3-b]furan-4-yl ester, [4S-(4a,4aa,5a)]-(9CI) in MeOD

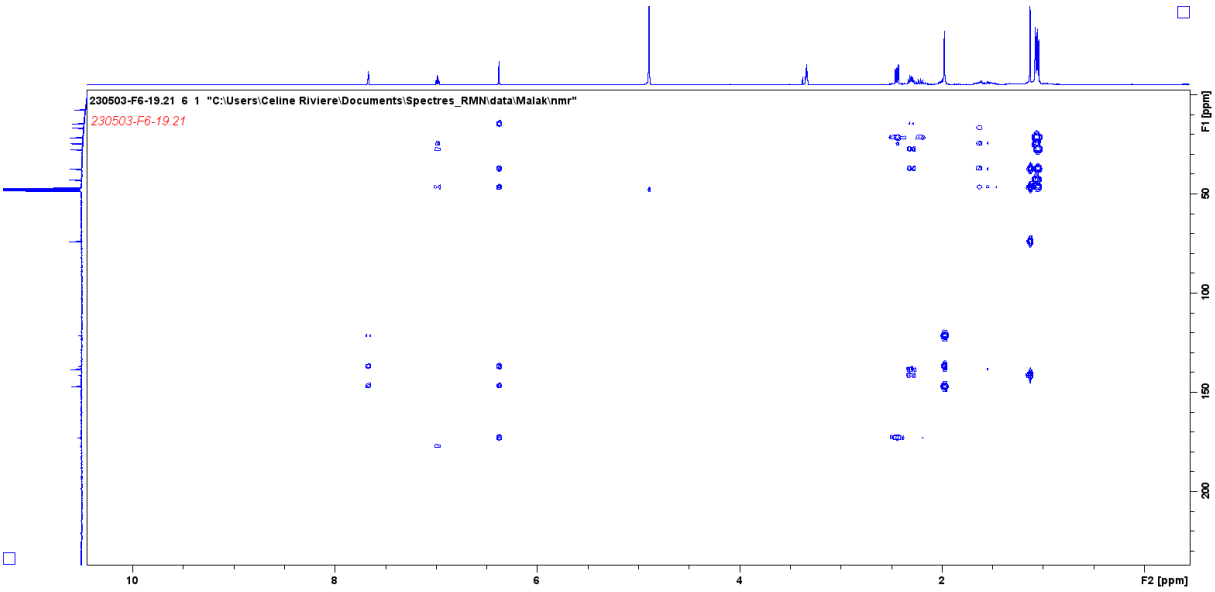

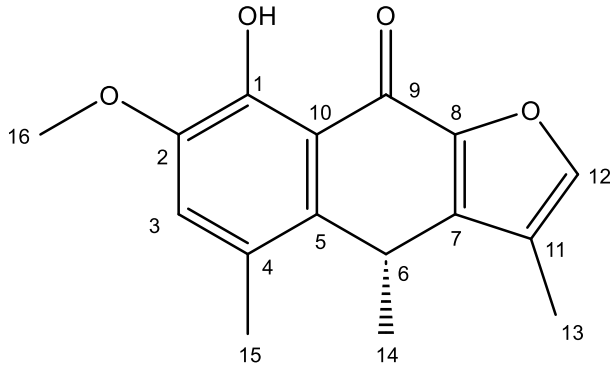

(F7-1) 1-hydroxy-2-methoxy-1,2,3,4-dehydro-6-dehydroxycacalone (= (4S)-8-Hydroxy-7-methoxy-3,4,5-trimethylnaphtho[2,3-b]furan-9(4H)-one (ACI),CAS number 337513-78-7) ($C_{16}H_{16}O_4$, 272 g.mol^{-1})

White amorphous powder; **ESI-MS** (positive-ion mode) *m/z* 273 $[M+H]^+$; **HR-ESI-Orbitrap-MS** (positive-ion mode) *m/z* 295.0937 $[M+Na]^+$; (calcd. 295.0941for $C_{16}H_{16}O_4Na$ $[M+Na]^+$), **^{1}H-NMR spectrum** (500 MHz, MeOD): 7.72 (C**H**, *q*, *J* = 1.15 Hz, H-**12**), 7.04 (C**H**, *s*, H-**3**), 4.24 (C**H**, *q*, *J* = 7.15 Hz, H-**6**), 3.88 (C**H$_3$**, *s*, H-**16**), 2.42 (C**H$_3$**, *s*, H-**15**), 2.20 (C**H$_3$**, *d*, *J* = 1.15 Hz, H-**13**), 1.35 (C**H$_3$**, *d*, *J* = 7.15 Hz, H-**14**), and **^{13}C-NMR spectrum** (500 MHz, MeOD): 178.56 (C-**9**), 151.15 (C-**1**), 146.98 (C-**12**), 146.19 (C-**2**), 144.72 (C-**8**), 144.53 (C-**7**), 136.12 (C-**5**), 125.90 (C-**4**), 121.02 (C-**11**), 119.41 (C-**3**), 115.57 (C-**10**), 55.31 (C-**16**), 30.64 (C-**6**), 20.95 (C-**14**), 17.59 (C-**15**), 6.46 (C-**13**)

^{1}H-NMR spectrum of 1-hydroxy-2-methoxy-1,2,3,4-dehydro-6-dehydroxycacalone in MeOD (sonde TXI)

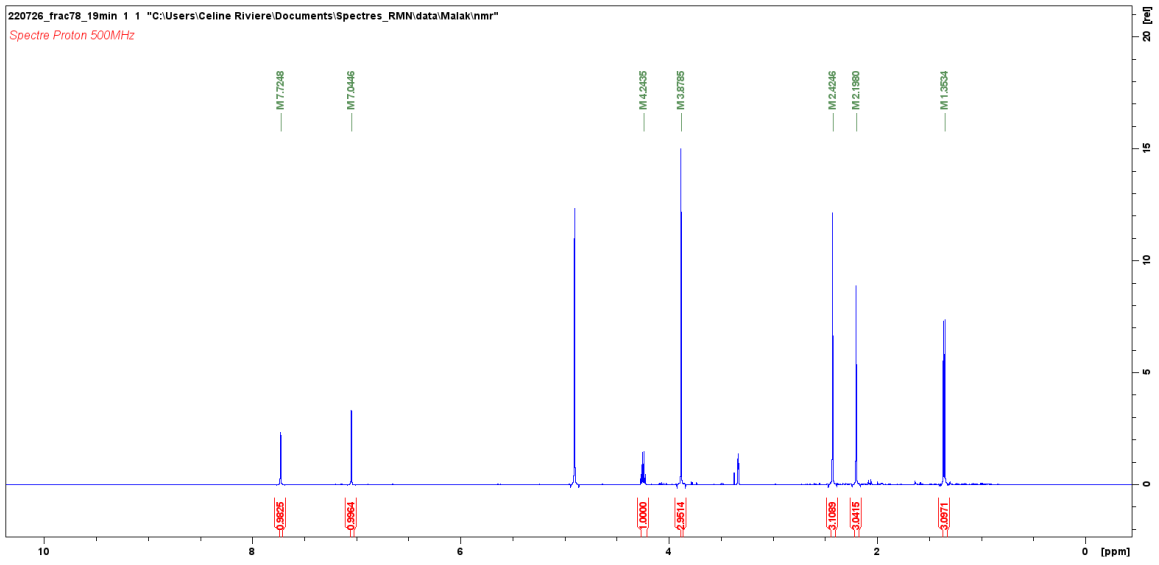

^{13}C-NMR spectrum of 1-hydroxy-2-methoxy-1,2,3,4-dehydro-6-dehydroxycacalone in MeOD (sonde TXI)

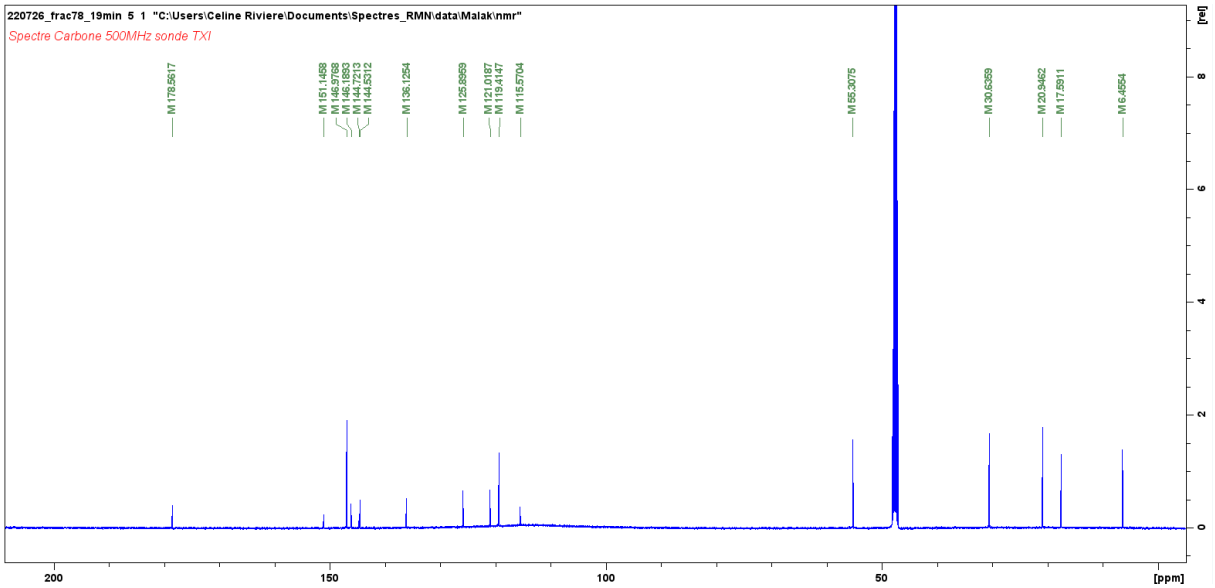

COSY spectrum of 1-hydroxy-2-methoxy-1,2,3,4-dehydro-6-dehydroxycacalone in MeOD (sonde TXI)

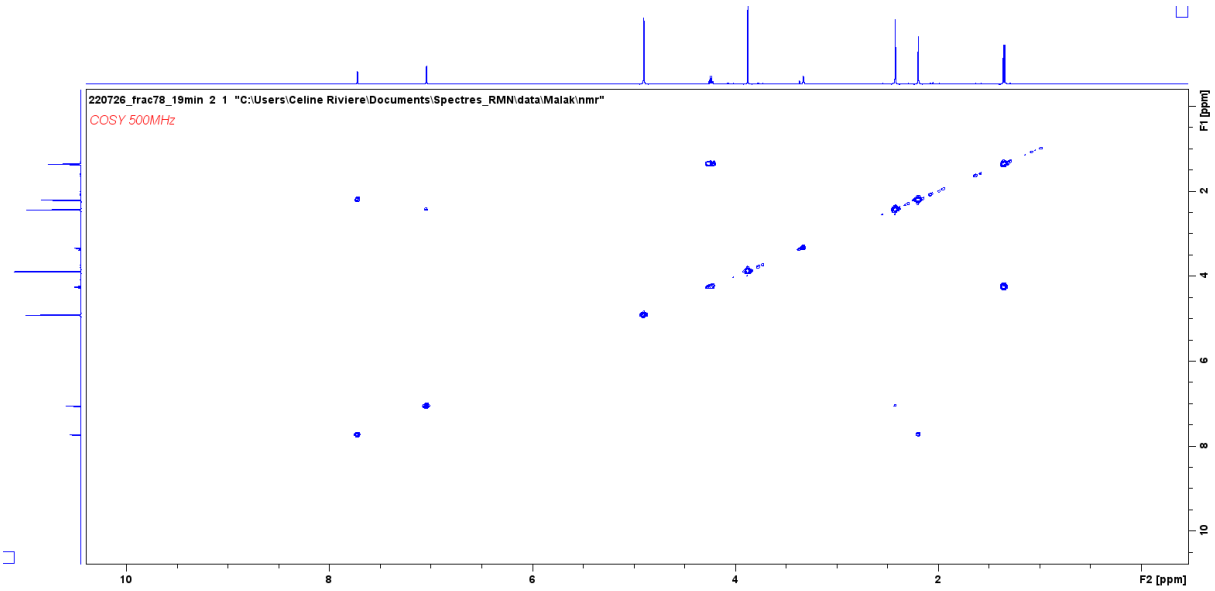

HSQC-DEPT spectrum of 1-hydroxy-2-methoxy-1,2,3,4-dehydro-6-dehydroxycacalone in MeOD (sonde TXI)

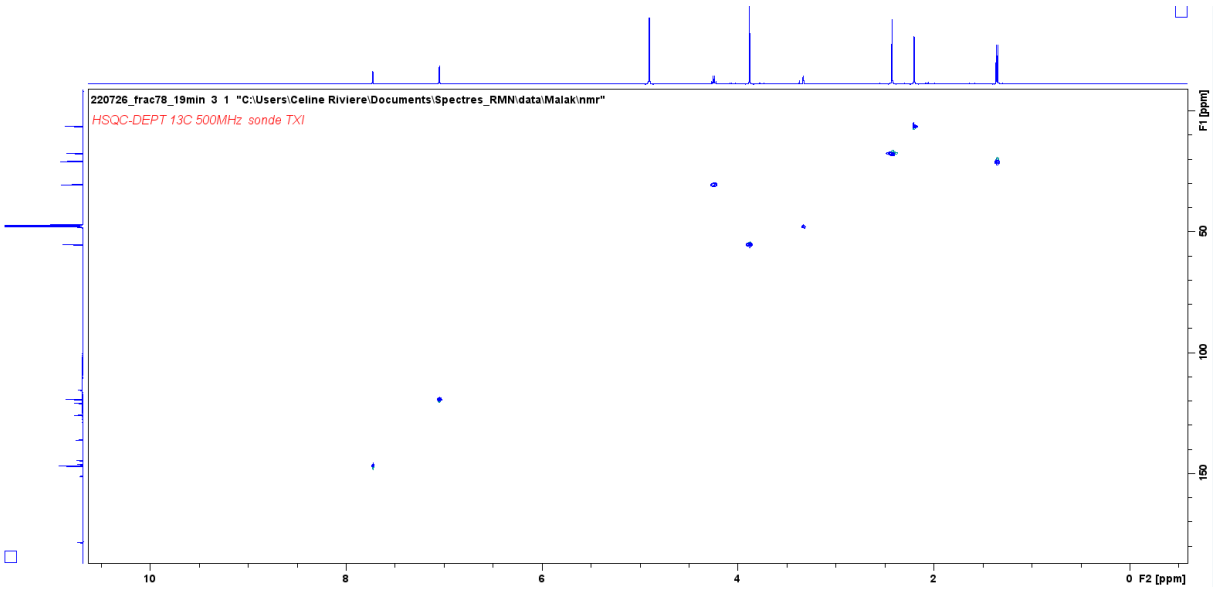

HMBC spectrum of 1-hydroxy-2-methoxy-1,2,3,4-dehydro-6-dehydroxycacalone in MeOD (sonde TXI)

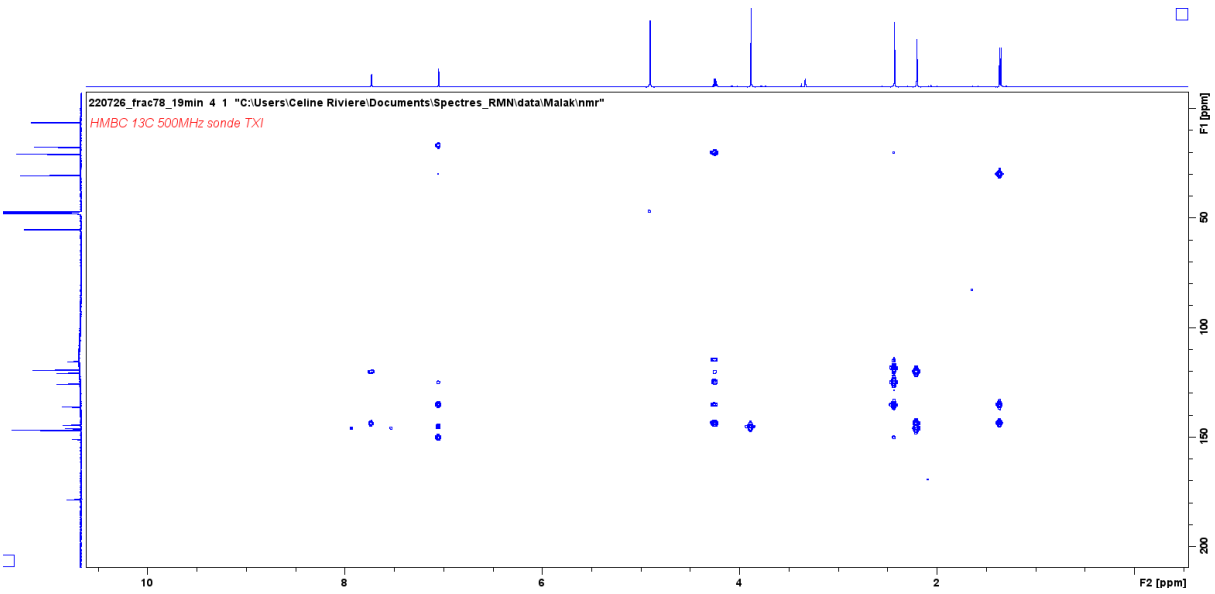

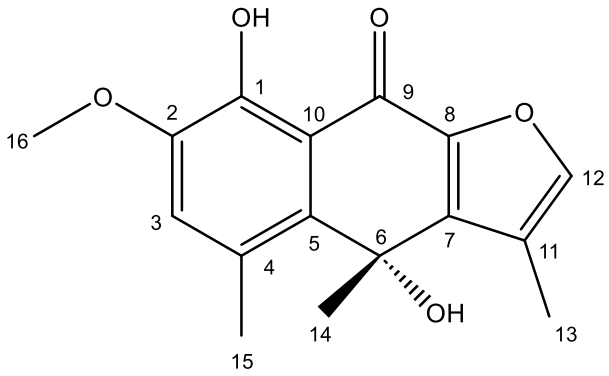

(F11-1) (6S) 1-hydroxy-2-methoxy-1,2,3,4-dehydrocacalone (= naphtho[2,3-b]furan-9(4H)-one,4,8-dihydroxy-7-methoxy-3,4,5-trimethyl-,(4S)-(9CI, ACI) ($C_{16}H_{16}O_5$, 288 g.mol^{-1})

White amorphous powder; **ESI-MS** (positive-ion mode) *m/z* 289 $[M+H]^-$; **^{1}H-NMR spectrum** (500 MHz, $CDCl_3$): 13.19 (1-O**H**) 7.47 (C**H**, *brs*, H-**12**), 6.71 (C**H**, *brs,* H-**3**), 3.74 (C**H$_3$**, *s*, H-**16**), 2.71 (C**H$_3$**, *s*, H-**15**), 2.33 (C**H$_3$**, *d*, *J* = 0.95 Hz, H-**13**), 1.79 (C**H$_3$**, *s*, H-**14**), and **^{13}C-NMR spectrum** (500 MHz, $CDCl_3$): 178.45 (C-**9**), 151.48 (C-**1**), 146.91 (C-**2**), 146.82 (C-**12**), 144.28 (C-**8**), 143.08 (C-**7**), 136.24 (C-**5**), 128.10 (C-**4**), 121.59 (C-**11**), 120.60 (C-**3**), 114.42 (C-**10**), 71.21 (C-**6**), 55.69 (C-**16**), 27.25 (C-**14**), 21.33 (C-**15**), 8.90 (C-**13**)

^{1}H-NMR spectrum of (6S) 1-hydroxy-2-methoxy-1,2,3,4-dehydrocacalone in $CDCl_3$ (sonde TXI)

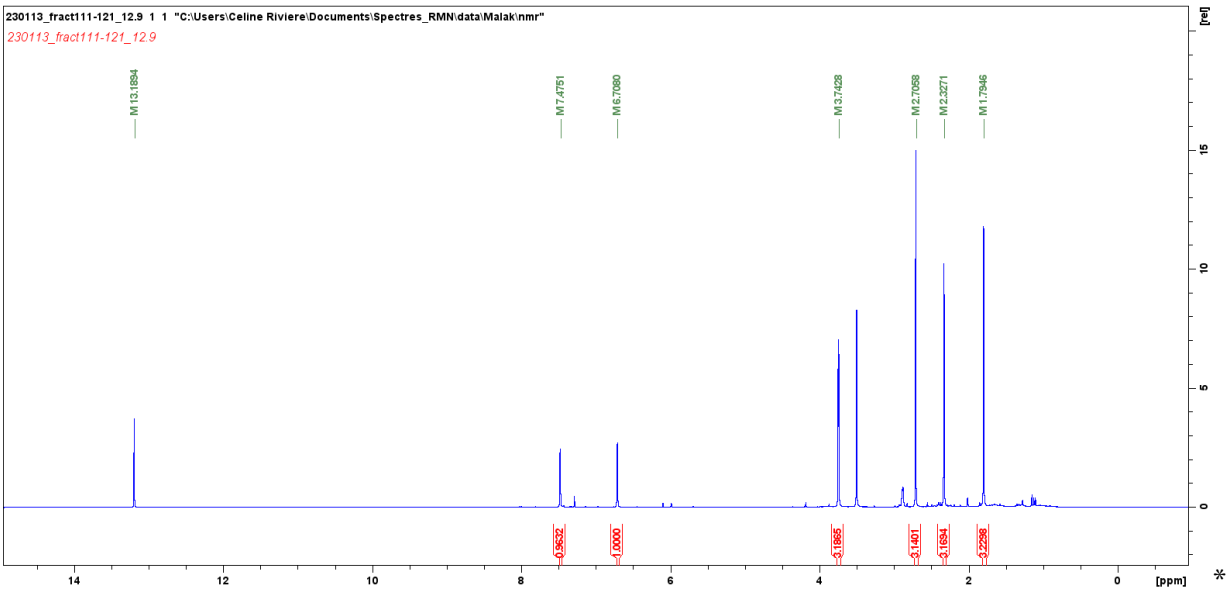

^{13}C-NMR spectrum of (6S) 1-hydroxy-2-methoxy-1,2,3,4-dehydrocacalone in $CDCl_3$ (sonde TXI)

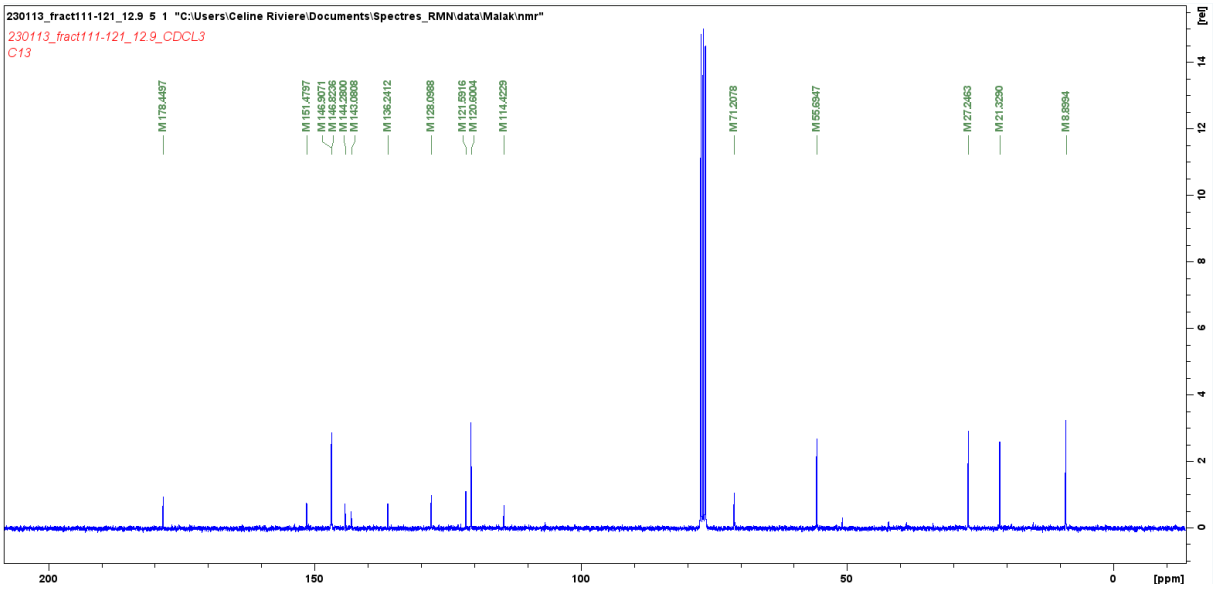

COSY spectrum of (6S) 1-hydroxy-2-methoxy-1,2,3,4-dehydrocacalone in $CDCl_3$ (sonde TXI)

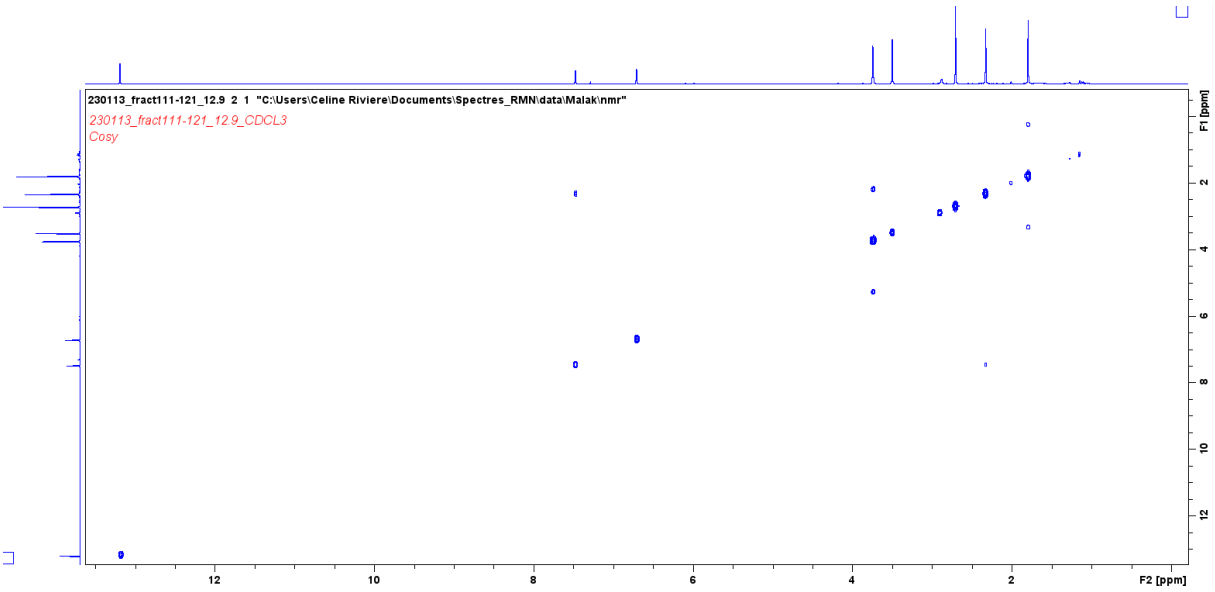

HSQC spectrum of (6S) 1-hydroxy-2-methoxy-1,2,3,4-dehydrocacalone in $CDCl_3$ (sonde TXI)

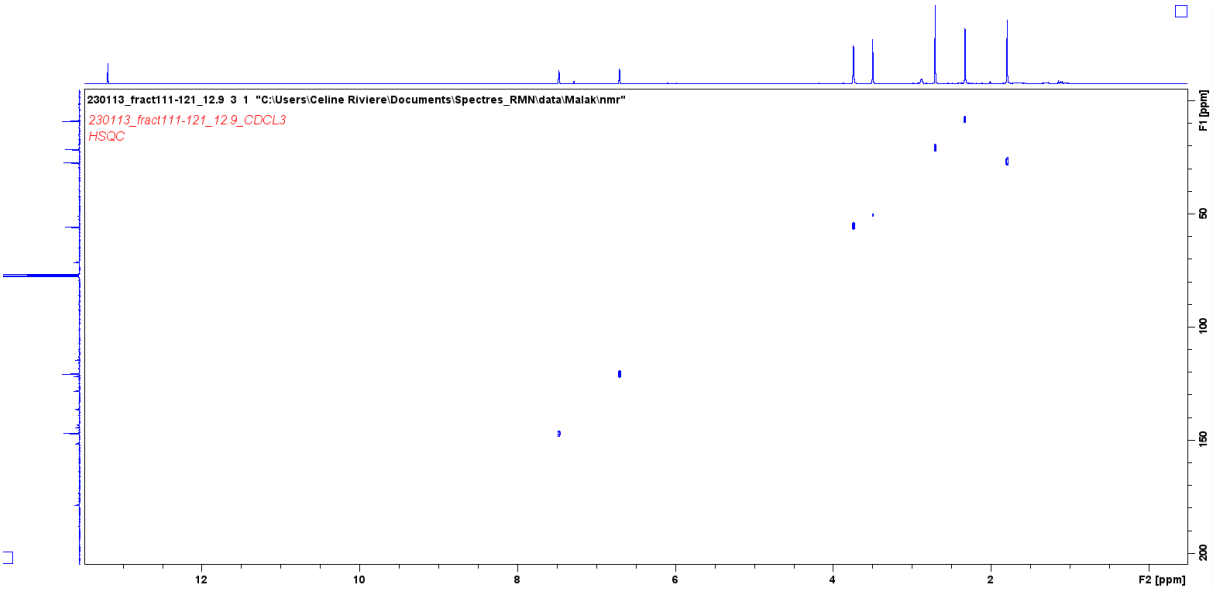

HMBC spectrum of (6S) 1-hydroxy-2-methoxy-1,2,3,4-dehydrocacalone in $CDCl_3$ (sonde TXI)

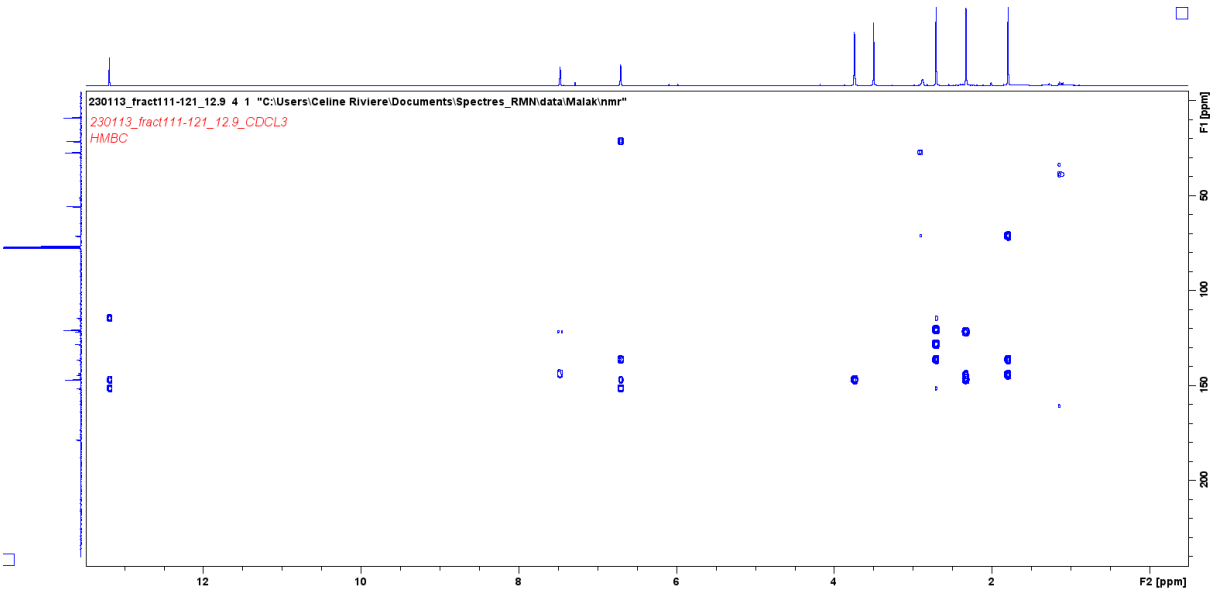

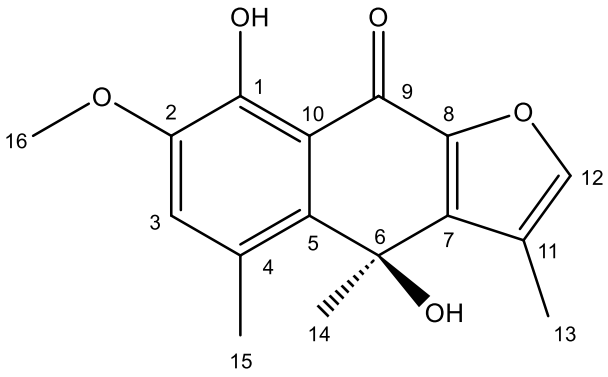

(F11-2) (= F4-2) **(6*R*) 1-hydroxy-2-methoxy-1,2,3,4-dehydrocacalone** (= naphtho[2,3-b]furan-9(4H)-one,4,8-dihydroxy-7-methoxy-3,4,5-trimethyl-,(4R)-(9CI, ACI), CAS number 337513-79-8) ($C_{16}H_{16}O_5$, 288 g.mol^{-1})

White amorphous powder; **ESI-MS** (positive-ion mode) *m/z* 289 $[M+H]^+$; **^{1}H-NMR spectrum** (500 MHz, $CDCl_3$): 13.32 (1-O**H**) 7.55 (C**H**, *q*, *J* = 1.15 Hz H-**12**), 6.87 (C**H**, *s,* H-**3**), 3.92 (C**H$_3$**, *s*, H-**16**), 2.68 (C**H$_3$**, *s*, H-**15**), 2.32 (C**H$_3$**, *d*, *J* = 1.15 Hz, H-**13**), 1.83 (C**H$_3$**, *s*, H-**14**), and **^{13}C-NMR spectrum** (500 MHz, $CDCl_3$): 178.53 (C-**9**), 152.83 (C-**1**), 146.90 (C-**2**), 146.88 (C-**12**), 145.36 (C-**8**), 141.20 (C-**7**), 132.21 (C-**5**), 126.82 (C-**4**), 120.79 (C-**11**), 120.51 (C-**3**), 116.08 (C-**10**), 83.40 (C-**6**), 56.07 (C-**16**), 24.73 (C-**14**), 20.72 (C-**15**), 8.70 (C-**13**)

^{1}H-NMR spectrum of (6R) 1-hydroxy-2-methoxy-1,2,3,4-dehydrocacalone in $CDCl_3$ (sonde TXI)

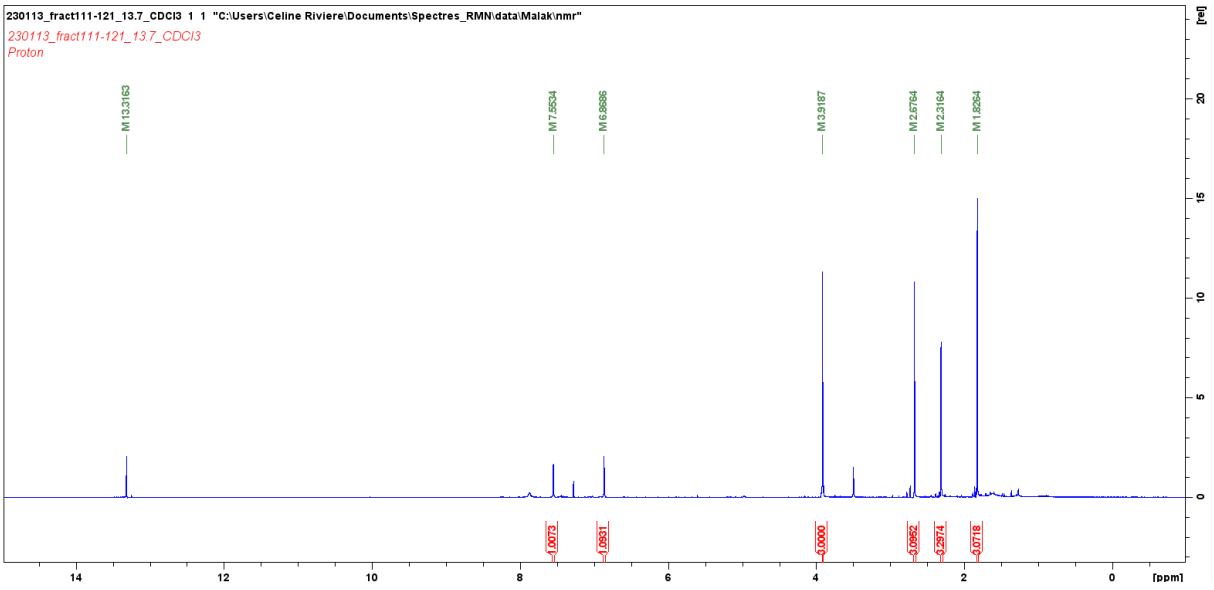

^{13}C-NMR spectrum of (6R) 1-hydroxy-2-methoxy-1,2,3,4-dehydrocacalone in $CDCl_3$ (sonde TXI)

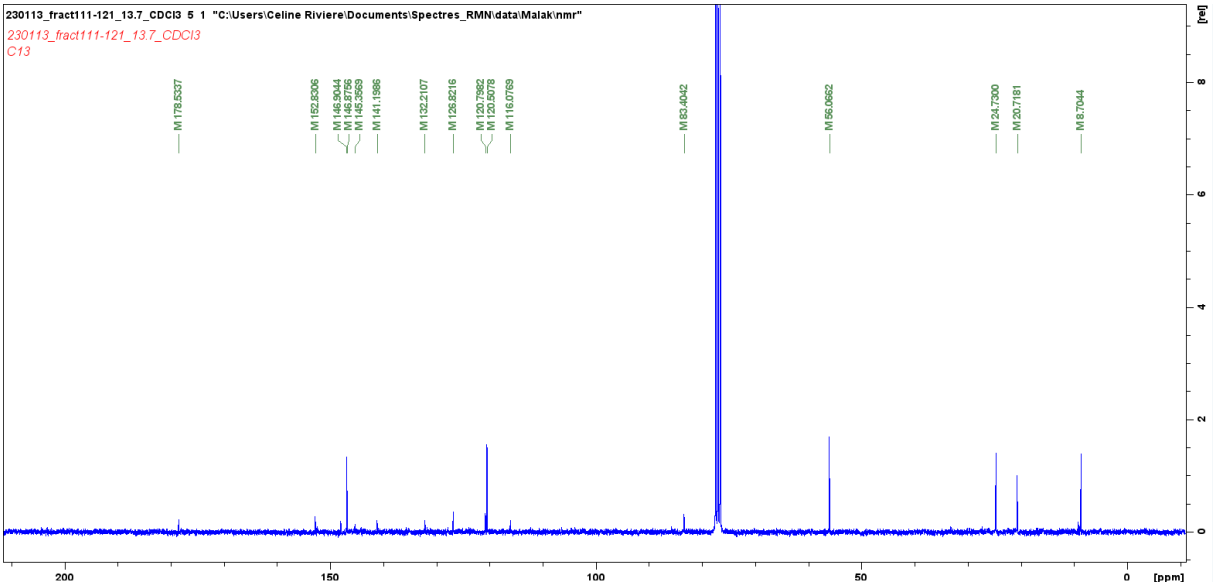

COSY spectrum of (6R) 1-hydroxy-2-methoxy-1,2,3,4-dehydrocacalone in $CDCl_3$ (sonde TXI)

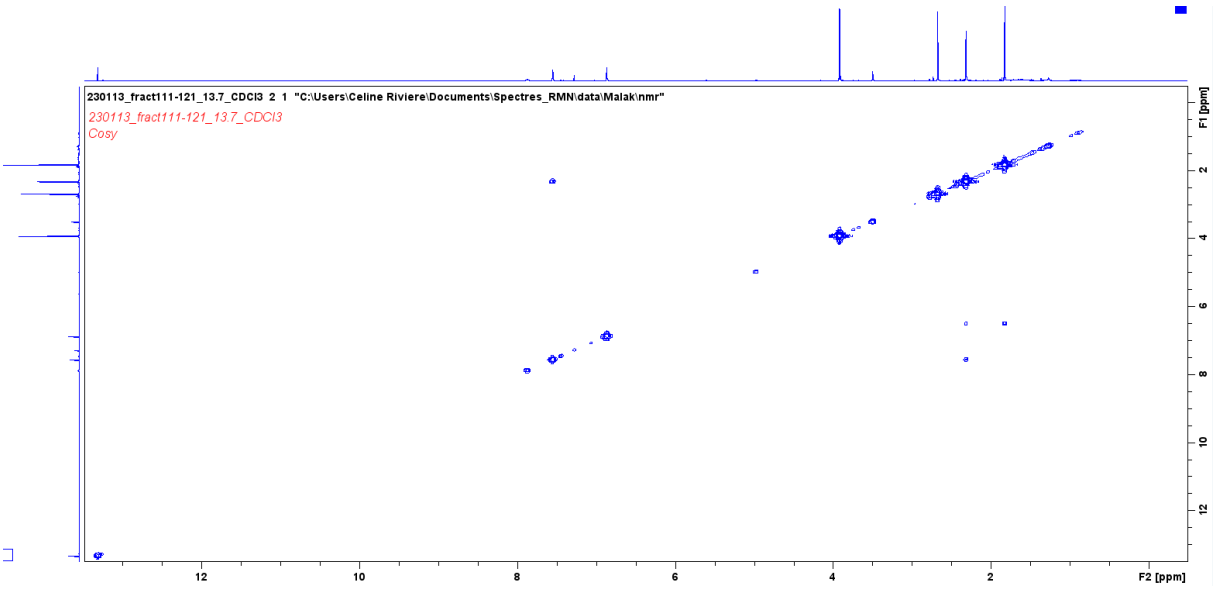

HSQC spectrum of (6R) 1-hydroxy-2-methoxy-1,2,3,4-dehydrocacalone in $CDCl_3$ (sonde TXI)

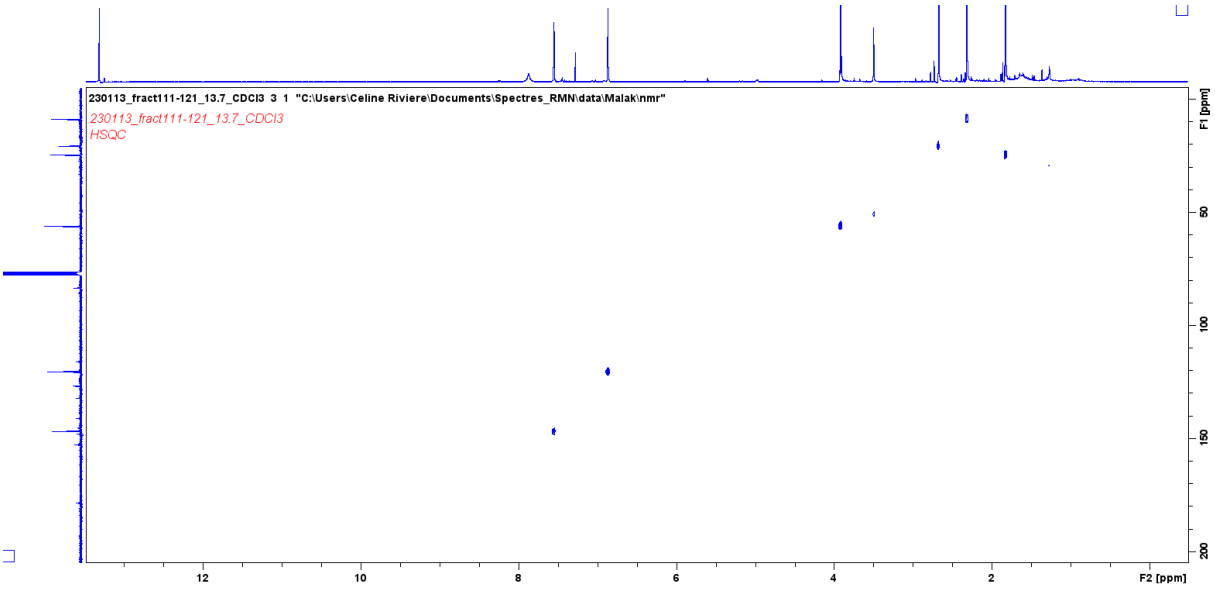

HMBC spectrum of (6R) 1-hydroxy-2-methoxy-1,2,3,4-dehydrocacalone in $CDCl_3$ (sonde TXI)

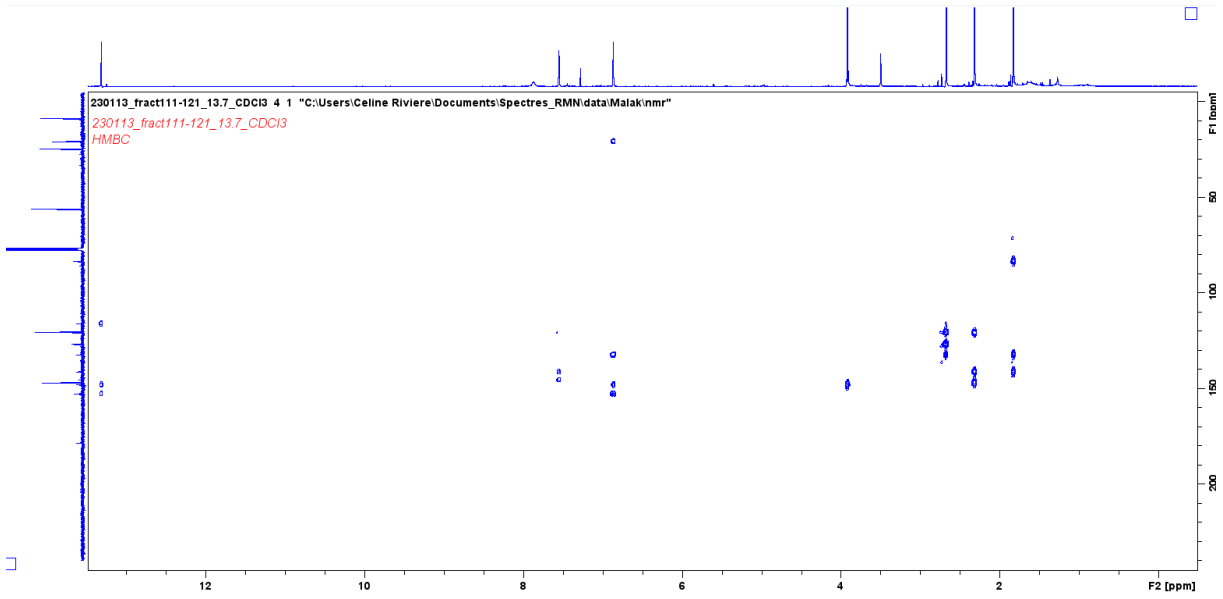

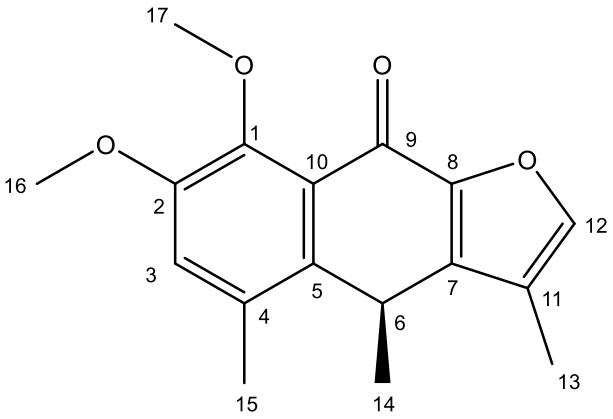

(F11-3) 1,2-dimethoxy-1,2,3,4-dehydro-6-dehydroxycacalone (= naphtho[2,3-b]furan-9(4H)-one, 7,8-dimethoxy-3,4,5-trimethyl-, (4S)- (9CI, ACI), CAS Number 337513-80-1) ($C_{17}H_{18}O_4$, 286 g.mol^{-1})

White amorphous powder; **ESI-MS** (positive-ion mode) *m/z* 287 $[M+H]^+$; **HR-ESI-Orbitrap-MS** (positive-ion mode) *m/z* 309.1089 $[M+Na]^+$; (calcd. 309.1097 for $C_{17}H_{18}O_4Na$ $[M+Na]^+$), **^{1}H-NMR spectrum** (500 MHz, MeOD): 7.65 (C**H**, *q*, *J* = 0.95 Hz, H-**12**), 7.19 (C**H**, *s*, H-**3**), 4.29 (C**H**, *q*, *J* = 6.95 Hz, H-**6**), 3.90 (C**H$_3$**, *s*, H-**16**), 3.84 (C**H$_3$**, *s*, H-**17**), 2.53 (C**H$_3$**, *s*, H-**15**), 2.20 (C**H$_3$**, *s*, *d*, *J* = 0.95 Hz H-**13**), 1.38 (C**H$_3$**, *d*, *J* = 6.95 Hz, H-**14**), and **^{13}C-NMR spectrum** (500 MHz, MeOD): 172.34 (C-**9**), 150.36 (C-**2**), 147.08 (C-**1**), 145.27 (C-**8**), 144.12 (C-**12**), 139.79 (C-**7**), 136.52 (C-**5**), 130.67 (C-**4**), 124.07 (C-**10**), 118.75 (C-**11**), 117.52 (C-**3**), 58.66 (C-**17**), 53.67 (C-**16**), 28.91 (C-**6**), 20.11 (C-**14**), 16.79 (C-**15**), 4.90 (C-**13**)

^{1}H-NMR spectrum of 1,2-dimethoxy-1,2,3,4-dehydro-6-dehydroxycacalone in MeOD (sonde TXI)

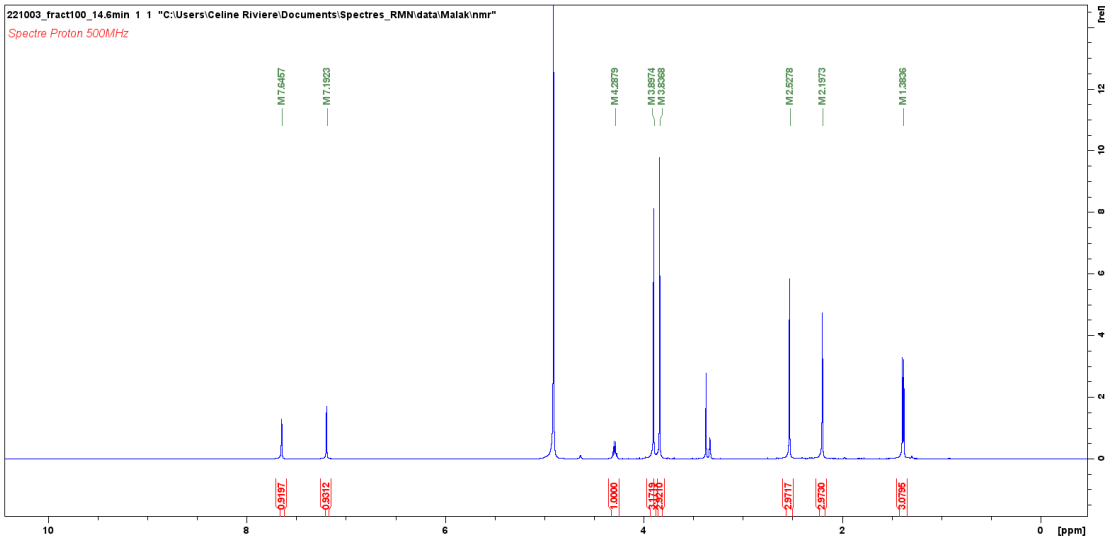

^{13}C-NMR spectrum of 1,2-dimethoxy-1,2,3,4-dehydro-6-dehydroxycacalone in MeOD (sonde TXI)

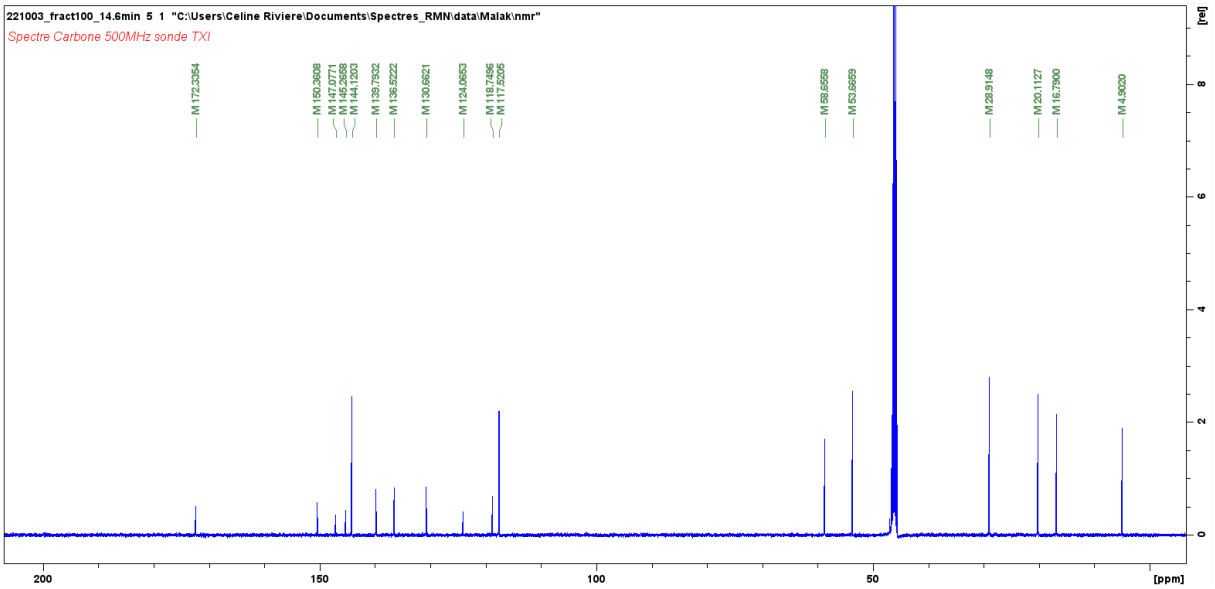

COSY spectrum of 1,2-dimethoxy-1,2,3,4-dehydro-6-dehydroxycacalone in MeOD (sonde TXI)

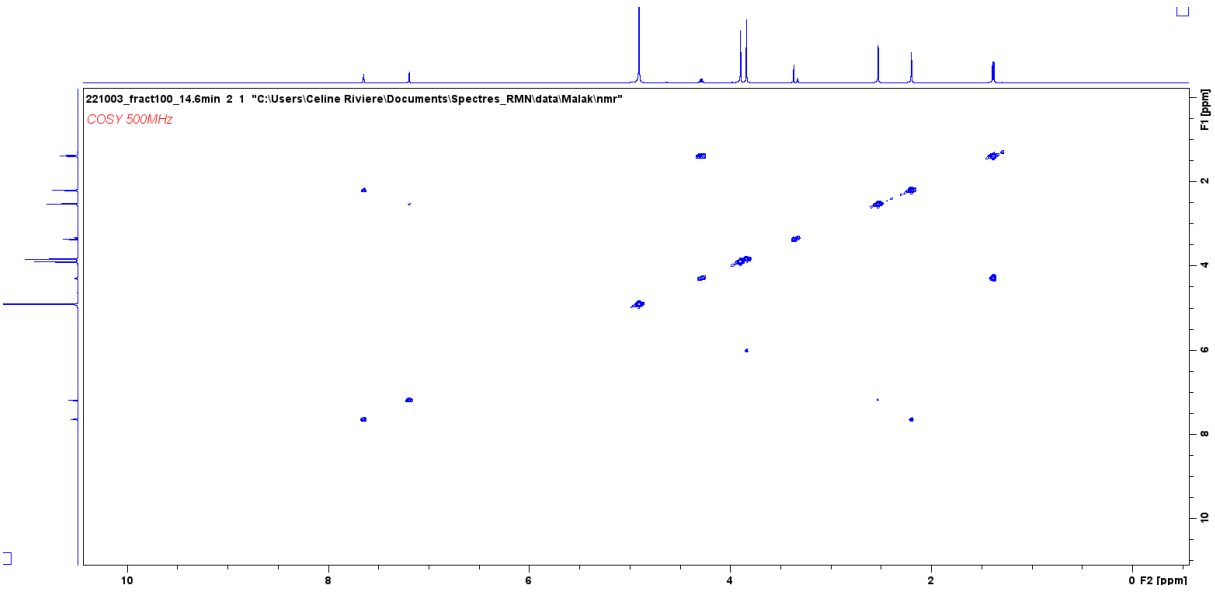

HSQC-DEPT spectrum of 1,2-dimethoxy-1,2,3,4-dehydro-6-dehydroxycacalone in MeOD (sonde TXI)

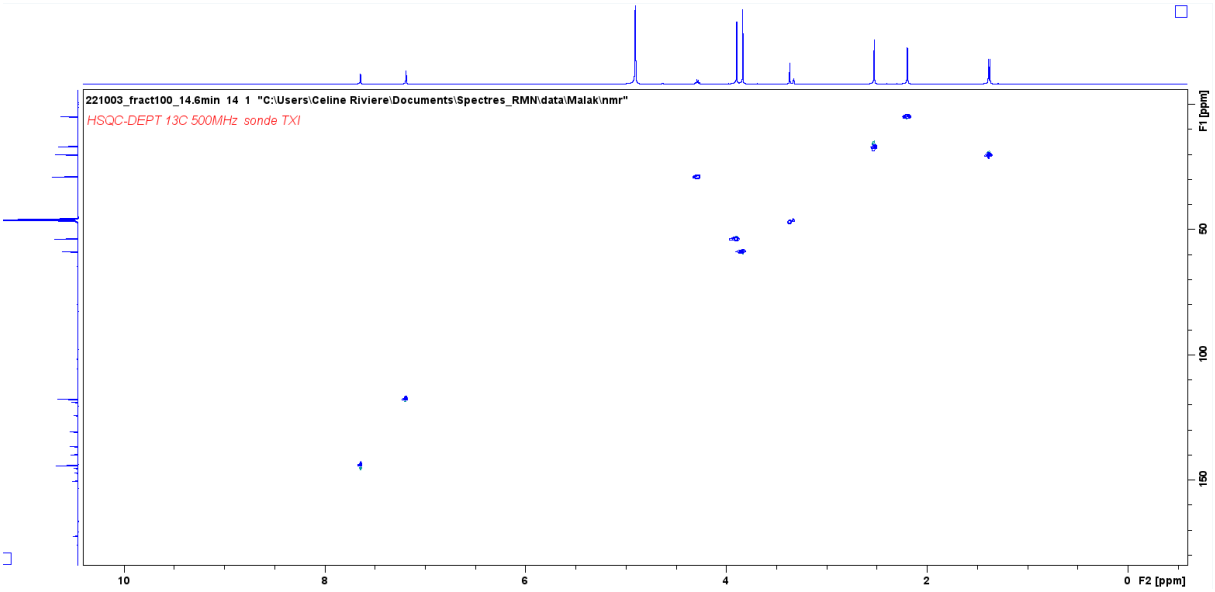

HMBC spectrum of 1,2-dimethoxy-1,2,3,4-dehydro-6-dehydroxycacalone in MeOD (sonde TXI)

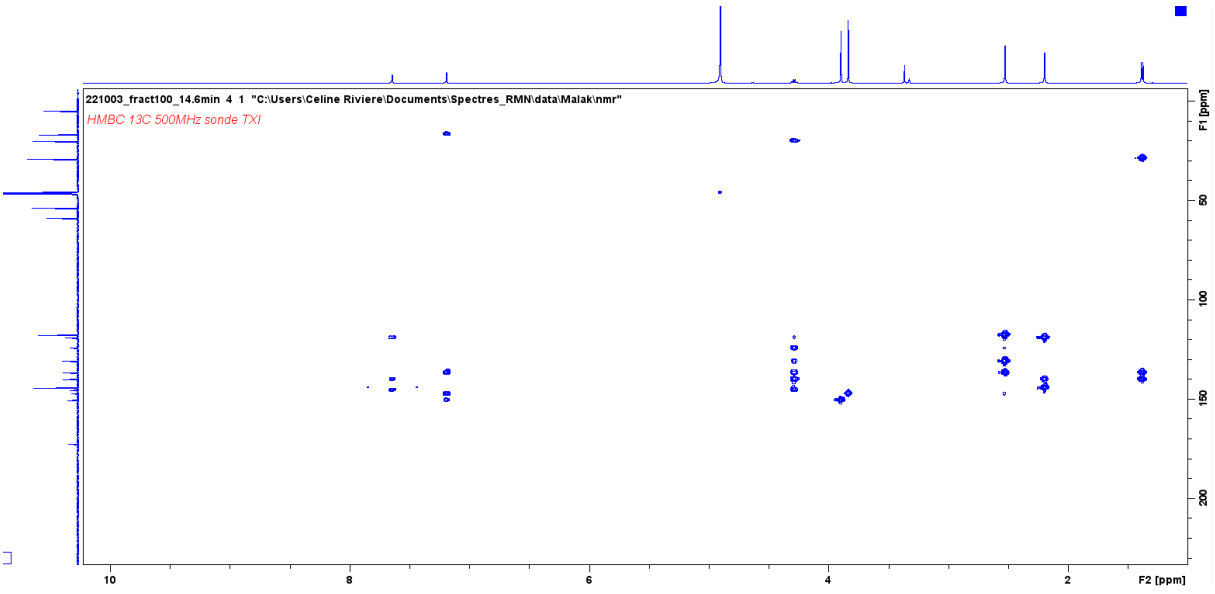

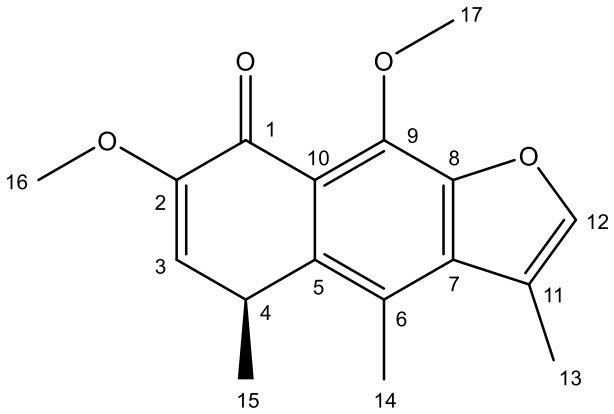

(F11-4) 2,3-dehydro-2-methoxy-1-oxocacalol methyl ether (= naphtho[2,3-b]furan-8(5H)-one, 7,9-dimethoxy-3,4,5-trimethyl-, (S)- (9CI), CAS number 64209-74-1) ($C_{17}H_{18}O_4$, 286 g.mol^{-1})

White amorphous powder; **ESI-MS** (positive-ion mode) *m/z* 287 $[M+H]^-$; **HR-ESI-Orbitrap-MS** (positive-ion mode) *m/z* 309,1087 $[M+Na]^+$; (calcd. 309,1097 for $C_{17}H_{18}O_4Na$ $[M+Na]^+$), **^{1}H-NMR spectrum** (500 MHz, $CDCl_3$): 7.50 (C**H**, *q*, *J* = 1.25 Hz, H-**12**), 6.00 (C**H**, d, *J* = 5.45 Hz, H-**3**), 4.13 (C**H$_3$**, s, H-**17**), 3.99 (C**H**, *m*, *J* = 5.45, 6.95 Hz, H-**4**), 3.75 (C**H$_3$**, *s*, H-**16**), 2.66 (C**H$_3$**, *s*, H-**14**), 2.45 (C**H$_3$**, *d*, *J* = 1.25 Hz, H-**13**), 1.35 (C**H$_3$**, *d*, *J* = 6.95 Hz, H-**15**), and **^{13}C-NMR spectrum** (500 MHz, $CDCl_3$): 180.62 (C-**1**), 151.33 (C-**2**), 146.75 (C-**8**), 144.87 (C-**12**), 144.83 (C-**9**), 139.27 (C-**5**), 133.16 (C-**7**), 122.91 (C-**6**), 120.93 (C-**10**), 116.82 (C-**11**), 116.09 (C-**3**), 61.92 (C-**17**), 55.14 (C-**16**), 32.18 (C-**4**), 24.45 (C-**15**), 14.69 (C-**14**), 11.23 (C-**13**)

^{1}H-NMR spectrum of 2,3-dehydro-2-methoxy-1-oxocacalol methyl ether in CDCl3 (sonde TXI)

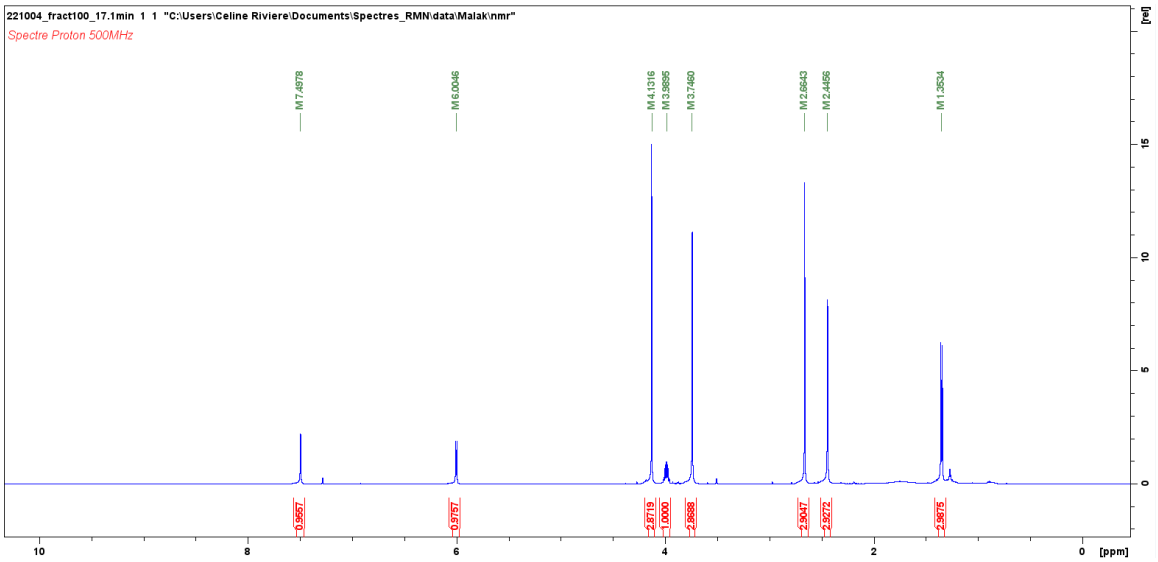

^{13}C-NMR spectrum of 2,3-dehydro-2-methoxy-1-oxocacalol methyl ether in CDCl3 (sonde TXI)

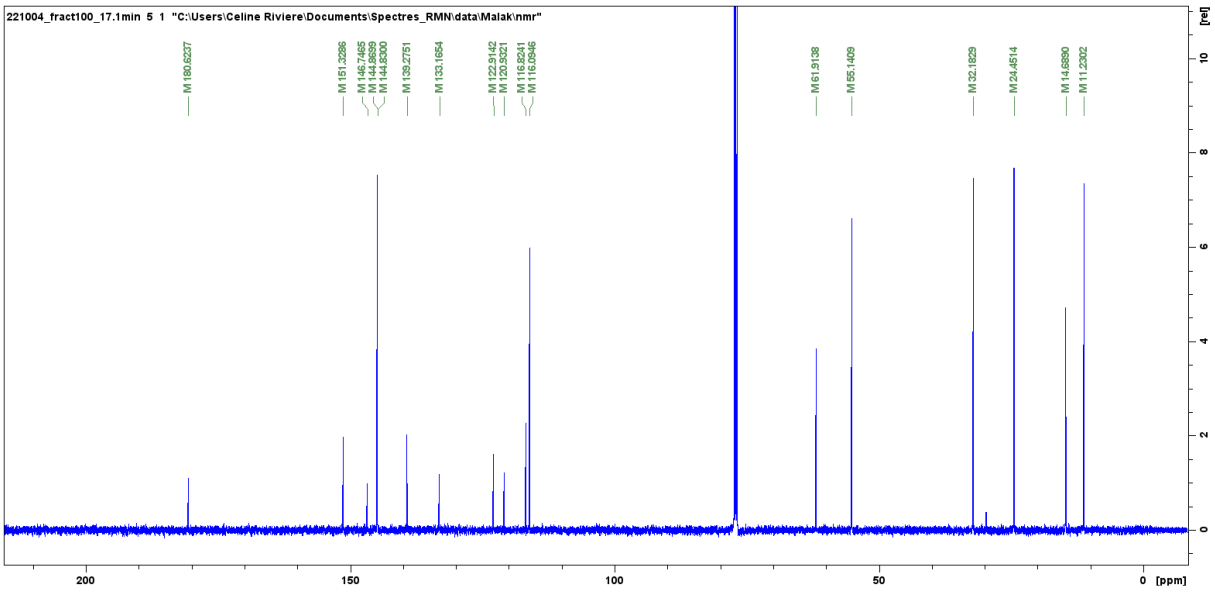

COSY spectrum of 2,3-dehydro-2-methoxy-1-oxocacalol methyl ether in CDCl3 (sonde TXI)

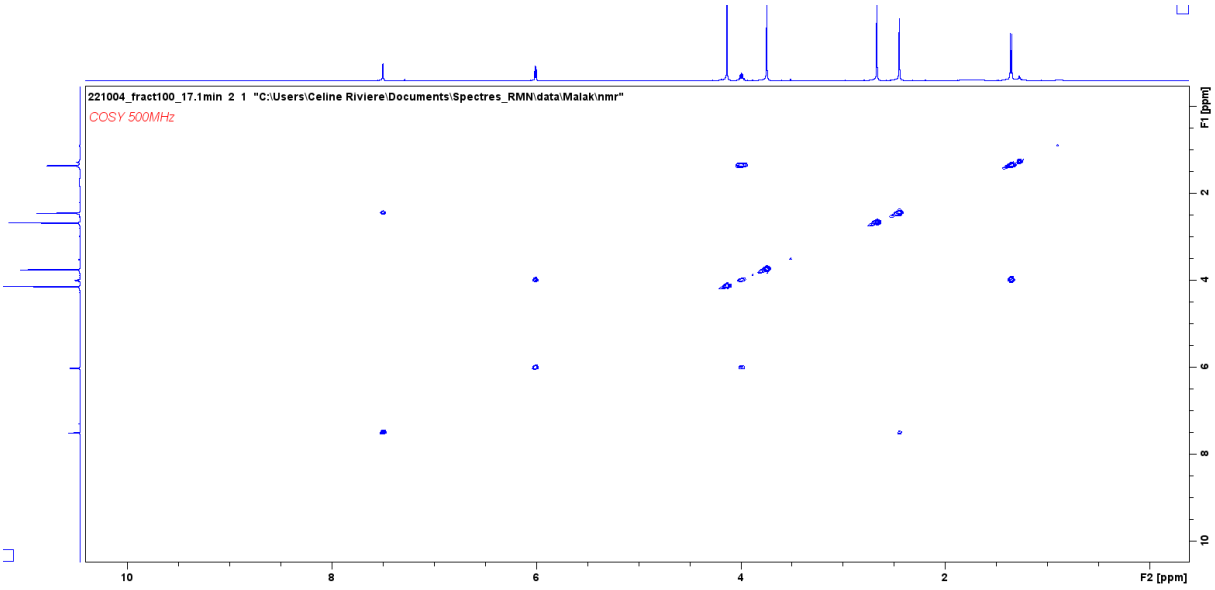

HSQC-DEPT spectrum of 2,3-dehydro-2-methoxy-1-oxocacalol methyl ether in CDCl3 (sonde TXI)

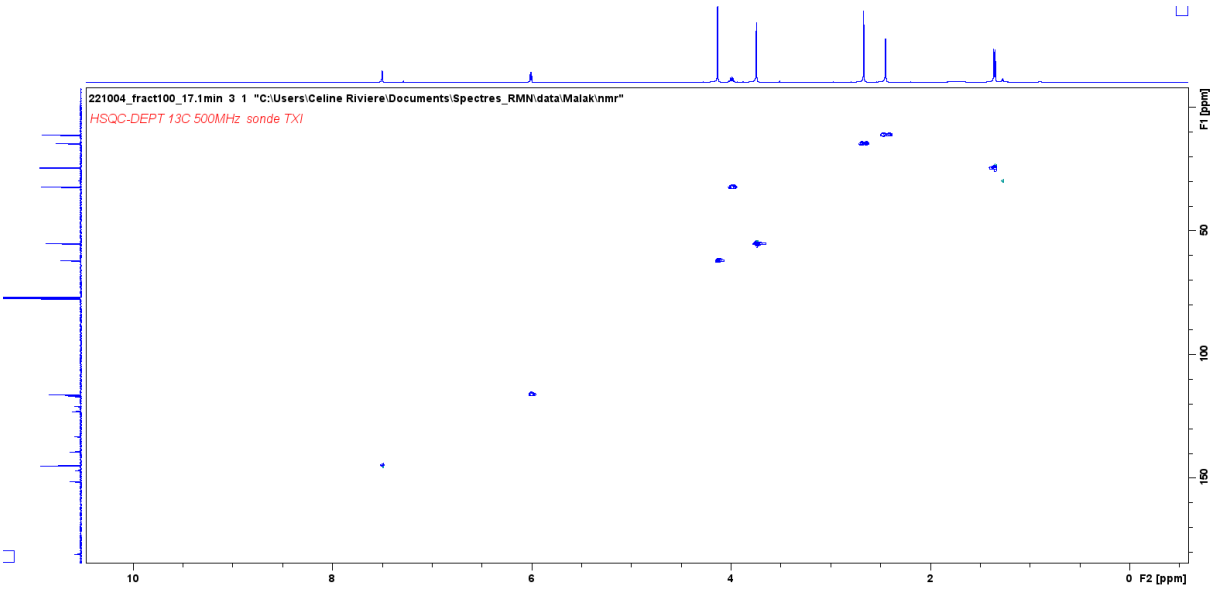

HMBC spectrum of 2,3-dehydro-2-methoxy-1-oxocacalol methyl ether in CDCl3 (sonde TXI)

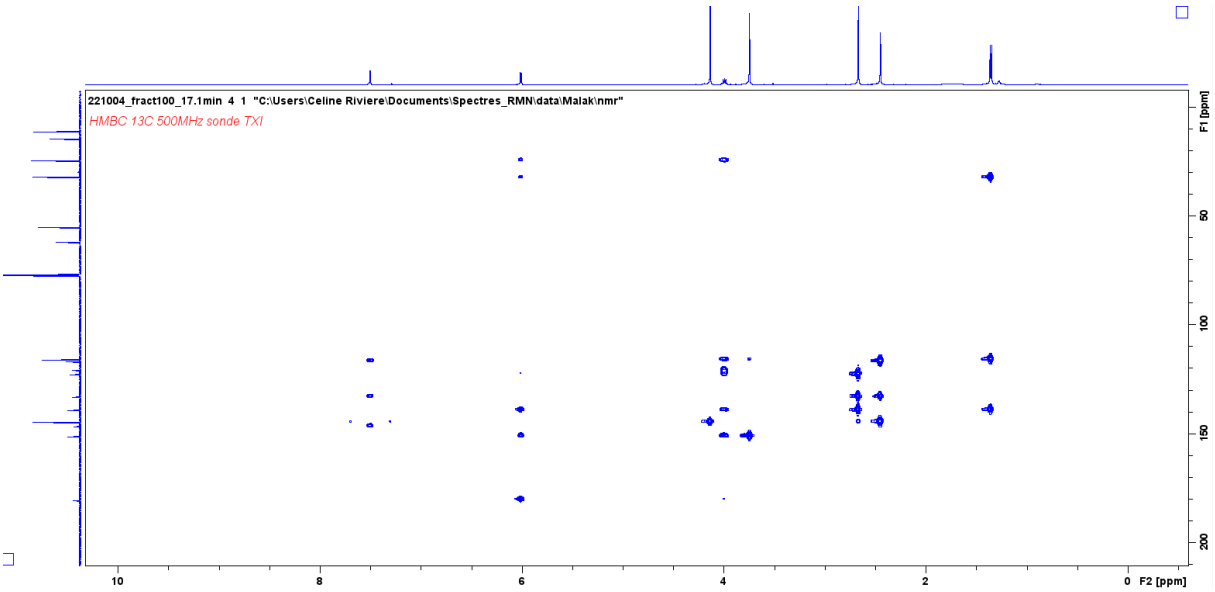

International Journal of
Molecular Sciences

MDPI

Article

Discovery of Anti-Coronavirus Cinnamoyl Triterpenoids Isolated from *Hippophae rhamnoides* during a Screening of Halophytes from the North Sea and Channel Coasts in Northern France

Malak Al Ibrahim [1,2], Zachee Louis Evariste Akissi [2,†], Lowiese Desmarets [1,†], Gabriel Lefèvre [2], Jennifer Samaillie [2], Imelda Raczkiewicz [1], Sevser Sahpaz [2], Jean Dubuisson [1], Sandrine Belouzard [1], Céline Rivière [2,*,‡] and Karin Séron [1,*,‡]

[1] University of Lille, CNRS, Inserm, CHU Lille, Institut Pasteur de Lille, U1019—UMR9017—Center for Infection and Immunity of Lille (CIIL), F-59000 Lille, France; malak.alibrahim.etu@univ-lille.fr (M.A.I.); lowiese.desmarets@ibl.cnrs.fr (L.D.); imelda.raczkiewicz.etu@univ-lille.fr (I.R.); jean.dubuisson@ibl.cnrs.fr (J.D.); sandrine.belouzard@ibl.cnrs.fr (S.B.)

[2] BioEcoAgro, Joint Research Unit 1158, University of Lille, INRAE, University of. Liège, UPJV, YNCREA, University of Artois, University Littoral Côte d'Opale, ICV—Institut Charles Viollette, F-59650 Villeneuve d'Ascq, France; zachee.akissi@univ-lille.fr (Z.L.E.A.); gabriel.lefevre@univ-lille.fr (G.L.); jennifer.samaillie@univ-lille.fr (J.S.); sevser.sahpaz@univ-lille.fr (S.S.)

* Correspondence: celine.riviere@univ-lille.fr (C.R.); karin.seron@ibl.cnrs.fr (K.S.)

† These authors contributed equally to this work.

‡ These authors contributed equally to this work.

check for updates

Citation: Al Ibrahim, M.; Akissi, Z.L.E.; Desmarets, L.; Lefèvre, G.; Samaillie, J.; Raczkiewicz, I.; Sahpaz, S.; Dubuisson, J.; Belouzard, S.; Rivière, C.; et al. Discovery of Anti-Coronavirus Cinnamoyl Triterpenoids Isolated from *Hippophae rhamnoides* during a Screening of Halophytes from the North Sea and Channel Coasts in Northern France. *Int. J. Mol. Sci.* **2023**, *24*, 16617. https://doi.org/10.3390/ijms242316617

Academic Editor: David Arráez-Román

Received: 31 October 2023
Revised: 9 November 2023
Accepted: 16 November 2023
Published: 22 November 2023

Abstract: The limited availability of antiviral therapy for severe acute respiratory syndrome coronavirus 2 (SARS-CoV-2) has spurred the search for novel antiviral drugs. Here, we investigated the potential antiviral properties of plants adapted to high-salt environments collected in the north of France. Twenty-five crude methanolic extracts obtained from twenty-two plant species were evaluated for their cytotoxicity and antiviral effectiveness against coronaviruses HCoV-229E and SARS-CoV-2. Then, a bioguided fractionation approach was employed. The most active crude methanolic extracts were partitioned into three different sub-extracts. Notably, the dichloromethane sub-extract of the whole plant *Hippophae rhamnoides* L. demonstrated the highest antiviral activity against both viruses. Its chemical composition was evaluated by ultra-high performance liquid chromatography (UHPLC) coupled with mass spectrometry (MS) and then it was fractionated by centrifugal partition chromatography (CPC). Six cinnamoyl triterpenoid compounds were isolated from the three most active fractions by preparative high-performance liquid chromatography (HPLC) and identified by high resolution MS (HR-MS) and mono- and bi-dimensional nuclear magnetic resonance (NMR). Specifically, these compounds were identified as 2-*O*-*trans*-*p*-coumaroyl-maslinic acid, 3β-hydroxy-2α-*trans*-*p*-coumaryloxy-urs-12-en-28-oic acid, 3β-hydroxy-2α-*cis*-*p*-coumaryloxy-urs-12-en-28-oic acid, 3-*O*-*trans*-caffeoyl oleanolic acid, a mixture of 3-*O*-*trans*-caffeoyl oleanolic acid/3-*O*-*cis*-caffeoyl oleanolic acid (70/30), and 3-*O*-*trans*-*p*-coumaroyl oleanolic acid. Infection tests demonstrated a dose-dependent inhibition of these triterpenes against HCoV-229E and SARS-CoV-2. Notably, cinnamoyl oleanolic acids displayed activity against both SARS-CoV-2 and HCoV-229E. Our findings suggest that *Hippophae rhamnoides* could represent a source of potential antiviral agents against coronaviruses.

Keywords: SARS-CoV-2; HCoV-229E; antiviral agents; halophytes; *Hippophae rhamnoides*; triterpenoids

1. Introduction

Coronaviruses belonging to the sub-family *Orthocoronavirinae* of the *Coronaviridae* family are enveloped viruses with a positive-strand RNA genome. To date, seven human coronaviruses (HCoVs) have been identified, including HCoV-NL63, HCoV-229E,

HCoV-HKU1, HCoV-OC43, SARS-CoV, Middle East respiratory syndrome coronavirus (MERS-CoV), and SARS-CoV-2 [1]. Coronaviruses have shown high transmissibility potential with varying mortality rates. Four viruses, HCoV-NL63, -229E, -HKU1, and -OC43, are known to cause mild to moderate respiratory diseases in immunocompetent individuals [2]. The remaining three, SARS-CoV, MERS-CoV, and SARS-CoV-2, are highly pathogenic, with significantly higher mortality rates. To date, three coronavirus outbreaks have occurred, including the 2002–2003 SARS epidemic caused by SARS-CoV, the 2012 MERS epidemic caused by MERS-CoV, and the 2019-current SARS-CoV-2 pandemic (COVID-19) [3]. This pandemic has posed profound unprecedented challenges on the global economy and healthcare sectors. While several vaccines have been manufactured and licensed, nearly 4 years into the pandemic, only three drugs, paxlovid (nirmatrelvir and ritonavir), remdesivir, and molnupiravir, have been granted authorization by the Food and Drug Administration (FDA) [4]. However, the European Medicines Agency considered that the benefit/risk balance of molnupiravir in the treatment of COVID-19 had not been established and refused its marketing authorization [5]. Moreover, inequitable access to COVID-19 therapies and vaccines, particularly in lower-income countries, persists [6]. Thus, the need to search for new low-cost and effective antivirals against COVID-19 is crucial.

Some of the current studies on drug therapies against COVID-19 are investigating plant secondary metabolites for their potential antiviral capacity against SARS-CoV-2. According to the WHO, around 80% of the world's population relies on traditional plants or herbs to fulfill their basic health needs. Several countries worldwide have started to study the antiviral role of their traditional medicinal plants in combating COVID-19 [6–9]. Secondary metabolites found in plants play a significant biological and ecological function, particularly in chemical defense because of their anti-oxidative and antimicrobial activities. Plants subjected to abiotic stresses such as soil drought and salinity are considered rich sources of bioactive molecules due to their anti-oxidative systems and biochemical and molecular mechanisms that can survive in abiotic environments. The separation of halophytes from more sensitive plants, called glycophytes, is most often based on the salt (NaCl) concentration, which was typically set at 86 mM (0.5% NaCl). However, more recent studies have suggested a limit of 200 mM NaCl in order to separate true halophytes (euhalophytes) from relatively tolerant species. Some species, such as *Tecticornia* spp., are capable of withstanding NaCl concentrations of 10 mM to 2 M [10–12]. A plethora of definitions have been attributed to halophytes due to their taxonomical and ecological complexity, and the definition remains debated. Succulence, a common feature in halophytes, is associated with the existence of salt secretory glands, which are modified trichomes that were originally epidermal cells. The coastline of northern France (Hauts-de-France region) harbors some halophilic vegetations that belong to different botanical families, including Amaranthaceae, Apiaceae, Asteraceae, Brassicaceae, Caryophyllaceae, Convolvulaceae, Cyperaceae, Euphorbiaceae, Gentianaceae, Juncaceae, Juncaginaceae, Papaveraceae, Plantaginaceae, Plumbaginaceae, Poaceae, Polygonaceae, Primulaceae, and Ruppiaceae [13]. Studies have shown that halophilic plants possess a broad spectrum of antiviral activity against different viruses, including herpes simplex virus-2, influenza virus, and adenoviruses, due to their specialized metabolites such as saponins, alkaloids, tannins, and flavonoids [13–16]. Moreover, we previously published that a phenanthrene derivative, dehydrojuncusol, isolated from a halophyte, *Juncus maritimus* L. (Juncaceae), has been shown to be an inhibitor of hepatitis C virus replication [17]. Hence, in our work, different halophytes and less salt-tolerant plants collected from northern France were first screened for their antiviral activity against human coronavirus HCoV-229E in vitro. The most active extracts and fractions were then tested against SARS-CoV-2 in order to identify potential pan-coronavirus antiviral agents. Bioguided fractionation was performed on the most active plant species, *Hippophae rhamnoides* L. (Eleagnaceae), in order to identify natural bioactive compounds.

2. Results

2.1. Sampling and Classification of the Collected Plant Species

Twenty-two plant species, including strictly halophytes and relatively salt-tolerant species, were selected and collected from five different locations (Étaples, Dannes, Le Portel, Gravelines, Zuydcoote) distributed across the coastline of the North Sea and the English Channel in northern France (Hauts-de-France region). The whole plant or, in some cases, different parts of the plants (leaves (L), stems (S), roots (R)) were powdered to produce twenty-five crude methanolic extracts. The majority of these plants are representative of the botanical families of salt-tolerant plants distributed on the coasts of the North Sea and the English Channel. Some of them are considered strictly halophytes and were found in a schorre or at the base of an incipient dune, such as the Amaranthaceae species, *Cakile maritima* Scop. subsp. *integrifolia* (Brassicaceae), and *Lysimachia maritima* (Primulaceae). The majority of the collected plants belong to the families of Asteraceae and Amaranthaceae, each representing 18% (n = 4) of all the plants collected. This repartition is logical with regard to Amaranthaceae since they are the most representative family of halophytes from the coast in the region [13]. Cyperaceae and Poaceae each represent 9% (n = 2). The remaining families (Apiaceae, Berberidaceae, Convolvulaceae, Brassicaceae, Elaeagnaceae, Euphorbiaceae, Onagraceae, Primulaceae, Rosaceae, and Salicaceae) each represent 4.5% (n = 1) of the collected plants (Figures 1 and S1 and Table 1).

Figure 1. Pictures of some collected plant species (Lefèvre G. and Rivière C., 2020): (**A**) *Salicornia procumbens* Sm. and *Suaeda maritima* (L.) Dumort. (Etaples), (**B**) *Salsola kali* L. (Dannes), (**C**) *Tripleurospermum maritimum* (L.) W. D. J. Koch (Le Portel), (**D**) *Crithmum maritimum* L. (Le Portel), (**E**) *Cakile maritima* Scop. subsp. *integrifolia* (Hornem.) Greuter and Burdet (Dannes), (**F**) *Ammophila arenaria* subsp. *arenaria* (L.) Link (Dannes), (**G**) *Convolvulus soldanella* L. (Dannes), and (**H**) *Hippophae rhamnoides* L. (Dannes).

2.2. Cytotoxicity and Antiviral Activity of Plant Crude Methanolic Extracts

2.2.1. Effect of Crude Methanolic Extracts on Cell Viability

The cytotoxicity of 25 crude methanolic extracts was tested on Huh-7 cells using an [3-(4,5-dimethylthiazol-2-yl)-5-(3-carboxymethoxyphenyl)-2-(4-sulfophenyl)-2H-tetrazolium]- based (MTS) viability assay. Huh-7 cells were treated with two different concentrations of the crude methanolic extracts (25 and 100 µg/mL) for 24 h. Non-treated control cells were incubated with

0.1% dimethyl sulfoxide (DMSO) in the media. The concentration of 25 µg/mL of all crude methanolic extracts was tolerated by Huh-7 cells after 24 h treatment. Similarly, no cellular cytotoxicity was observed using a concentration of 100 µg/mL of the crude methanolic extracts on Huh-7 cells, except for *Convolvulus soldanella*, *Berberis aquifolium* (R), and *Lysimachia maritima*, causing a decrease in cell viability by 53%, 60%, and 72.6%, respectively (Figure 2).

Table 1. List of plant species used in this study.

Botanical Family	Plant Species	Parts	Place of Collection	Voucher Code
Amaranthaceae	*Atriplex prostrata* Boucher ex DC.	Whole plant	Dannes (at the base of an incipient dune)	LIP007584
	Salicornia procumbens Sm.	Whole plant	Etaples (in the schorre)	LIP007585
	Salsola kali L.	Whole plant	Dannes (at the base of an incipient dune)	LIP007586
	Suaeda maritima (L.) Dumort.	Whole plant	Etaples (in the schorre)	LIP007587
Apiaceae	*Crithmum maritimum* L.	Aerial parts	Le Portel (on a coastal cliff)	LIP007588
	Baccharis halimifolia L.	Leaves (L), stems (S)	Gravelines (planted in a roadside hedge)	LIP007589
Asteraceae	*Centaurea aspera* L.	Whole plant	Zuydcoote (on a relict foredune)	LIP007590
	Tripleurospermum maritimum (L.) W. D. J. Koch	Whole plant	Le Portel (on a coastal cliff)	LIP007591
	Tripolium pannonicum (Jacq.) Dobroc.	Whole plant	Dannes (in the schorre)	LIP007592
Berberidaceae	*Berberis aquifolium* Pursh	Leaves (L), roots (R)	Zuydcoote (on a relict foredune)	LIP007593
Brassicaceae	*Cakile maritima* Scop. subsp. *integrifolia* (Hornem.) Greuter and Burdet	Whole plant	Dannes (at the base of an incipient dune)	LIP007594
Convolvulaceae	*Convolvulus soldanella* L.	Whole plant	Dannes (on an incipient dune)	LIP007595
Cyperaceae	*Bolboschoenus maritimus* (L.) Palla	Whole plant	Dannes (in the schorre)	LIP007596
	Carex arenaria L.	Whole plant	Dannes (in the schorre)	LIP007597
Elaeagnaceae	*Hippophae rhamnoides* L.	Whole plant	Dannes (on an established foredune)	LIP007598
Euphorbiaceae	*Euphorbia paralias* L.	Whole plant	Dannes (on an incipient foredune)	LIP007599
Onagraceae	*Oenothera biennis* L.	Whole plant	Zuydcoote (on a relict foredune)	LIP007600
Poaceae	*Ammophila arenaria* subsp. *arenaria* (L.) Link	Whole plant	Dannes (on an established foredune)	LIP007601
	Elytrigia acuta (DC.) Tzvelev	Whole plant	Zuydcoote (on an incipient foredune)	LIP007602
Primulaceae	*Lysimachia maritima* (L.) Galasso, Banfi, and Soldano	Whole plant	Dannes (in the schorre)	LIP007603
Rosaceae	*Rosa rugosa* Thumb.	Aerial parts	Dannes (on an established foredune)	LIP007604
Salicaceae	*Salix repens* subsp. *dunensis* Rouy	Stems (S), roots (R)	Zuydcoote (on a relict foredune)	LIP007605

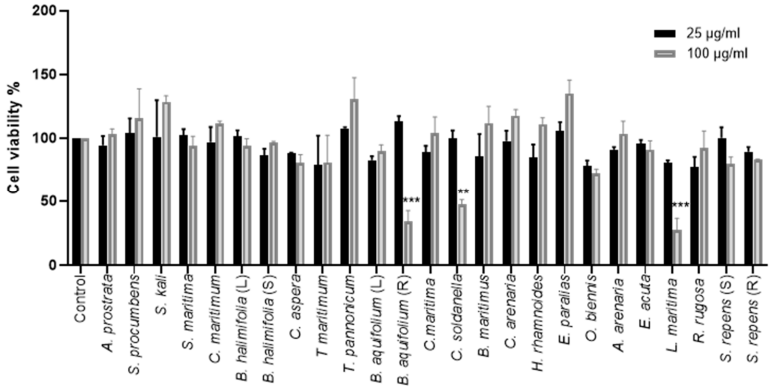

Figure 2. Cytotoxicity of the methanolic crude extracts on Huh-7 cells. Huh-7 cells were treated with two concentrations, 25 and 100 µg/mL, of crude extracts. Control cells were treated with 0.1% DMSO only. The cells were incubated for 24 h, and an MTS assay was then performed to determine the cell viability. The data bars represent the mean ± standard error of the mean (SEM) of three experiments performed in triplicate. The asterisk indicates a statistical difference compared to the control. (**, $p < 0.01$; ***, $p < 0.001$). (L) = Leaves, (S) = Stem, (R) = Roots.

2.2.2. Antiviral Screening of the Plant Crude Methanolic Extracts on HCoV-229E

Following the identification of the toxicity, we studied the antiviral activity of the extract on HCoV-229E infection. A coronavirus enters the cells through one of two pathways: by endocytosis or by direct fusion with the plasma membrane. The host-cell protease transmembrane serine protease 2 (TMPRSS2) is necessary for the plasma membrane fusion of many coronaviruses, including HCoV-229E, whereas cathepsins are often involved in fusion processes at endosomal membranes [18]. We screened the antiviral activity of the crude methanolic extracts at a concentration of 25 µg/mL by quantifying the infection of HCoV-229E-Luc in Huh-7 cells, whether they expressed the TMPRSS2 protease or not. A significant decrease in the luciferase activity representing an antiviral effect was observed using *Hippophae rhamnoides*, *Salix repens* (R), *Salix repens* (S), *Berberis aquifolium* (R), and *Baccharis halimifolia* (L) in Huh-7/TMPRSS2 cells. Similarly, an antiviral effect was observed with *Hippophae rhamnoides*, *Salix repens* (R), *Salix repens* (S), *Berberis aquifolium* (R), and *Baccharis halimifolia* (L) in Huh-7 cells (Figure 3). Since *Berberis aquifolium* (R) crude methanolic extracts showed cytotoxicity at 100 µg/mL, we decided not to study it further.

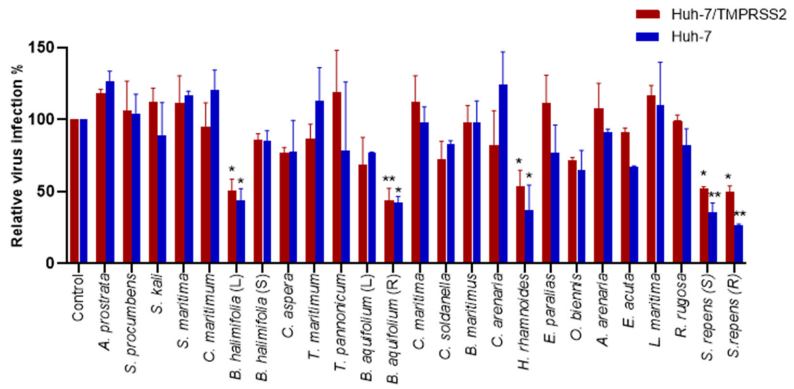

Figure 3. Screening of the antiviral activity of crude methanolic extracts on HCoV-229E-Luc. Huh-7 or Huh-7/TMPRSS2 cells were inoculated with HCoV-229E-Luc in the presence of various plant extracts at 25 µg/mL. Cells were lysed 7 h post-inoculation, and luciferase activity was quantified. Experiments were performed in triplicate, with each experiment being repeated thrice. The data bars represent the mean ± SEM. The asterisk indicates a statistical difference compared to the control (*, $p < 0.05$; **, $p < 0.01$).

2.3. Dose-Response Antiviral Activity of Plant Extracts

In order to confirm the antiviral activity of *Hippophae rhamnoides*, *Salix repens* (R), *Salix repens* (S), and *Baccharis halimifolia* (L) extracts on HCoV-229E, dose-response experiments were conducted. Antiviral assays were conducted in Huh-7 and Huh-7/TMPRSS2 cells to cover the two entry pathways. Cytotoxicity was also evaluated in parallel. The results presented in (Figure S2) show that the four selected extracts were able to decrease HCoV-229E infection in a dose-dependent manner, confirming their antiviral capacity. These results allowed us to determine the 50% cytotoxic concentration (CC_{50}) and the 50% inhibitory concentration (IC_{50}) of each extract and calculate their selectivity index (SI), which is the ratio between CC_{50} and IC_{50} (Table 2).

Table 2. Cytotoxicity, antiviral activity, and SI of each of the crude methanolic extracts against HCoV-229E.

Crude Extract	CC_{50} (µg/mL) Vero-81	CC_{50} (µg/mL) Huh-7	Huh-7		Huh-7/TMPRSS2	
			IC_{50} (µg/mL)	SI	IC_{50} (µg/mL)	SI
H. rhamnoides	499	621	19.7	31.5	27.2	22
S. repens (R)	441	149	29.1	5.1	15.5	9
S. repens (S)	438	285	15.1	28.9	14.7	19
B halimifolia (L)	820	>1000	65.3	>15	11.2	>89

Hippophae rhamnoides showed the highest CC_{50} in Huh-7 cells (621 µg/mL), whereas *Salix repens* (R) showed the lowest CC_{50} of 149 µg/mL. For antiviral activity, *Salix repens* (S) demonstrated the lowest IC_{50} in both Huh-7 and Huh-7/TMPRSS2 cells (15.1 and 14.7 µg/mL, respectively). However, *Baccharis halimifolia* (L) extract was the most active among the extracts but only in Huh-7/TMPRSS2 cells, with an IC_{50} of 11.2 µg/mL, showing that it might inhibit the TMPRSS2 entry pathway. Finally, for the four extracts, antiviral activity was not due to cytotoxicity, with the calculated SIs ranging from 5 to 35.

As a next step, we wondered if the extracts could have antiviral activity against other HCoVs and examined their antiviral capacity against SARS-CoV-2 in Vero-81 cells. Cytotoxicity was first evaluated (Table 2, Figure S3). Vero-81 cells showed higher tolerance to the crude methanolic extracts compared to Huh-7 cells due to the presence of a P-glycoprotein efflux pump [19]. Vero-81 cells infected with the SARS-CoV-2 were treated with two concentrations, 25 and 50 µg/mL, of the crude methanolic extracts, and chloroquine, an inhibitor of the endocytic entry pathway, was added as control. Western blot analyses showed a dose-dependent decrease in the SARS-CoV-2 N protein expression levels for the four extracts, indicating an antiviral effect (Figure 4). Three crude methanolic extracts, *Hippophae rhamnoides*, *Salix repens* (R), and *Baccharis halimifolia* (L), showed a high antiviral effect at both concentrations. Even though *Salix repens* (S) showed an antiviral effect at 50 µg/mL, the antiviral activity at 25 µg/mL was weaker (Figure 4).

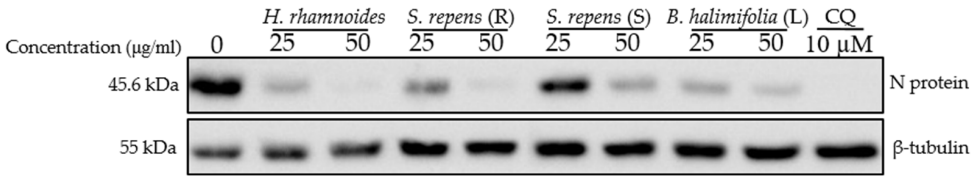

Figure 4. Antiviral activity on SARS-CoV-2 of crude methanolic extract of *Hippophae rhamnoides*, *Salix repens* (R), *Salix repens* (S), and *Baccharis halimifolia* (L). Vero-81 cells were infected with SARS-CoV-2 in the presence of different plant extracts at 25 and 50 µg/mL, or 10 µM chloroquine (CQ). Cell lysates were collected after 16 h and subjected to immunoblotting analysis using an anti-SARS-CoV-2 N antibody and an anti-ß-tubulin antibody to show an equal amount of cellular protein in each lane. This immunoblot is representative of two independent experiments.

Taken together, these results show that the four crude methanolic extracts of salt-tolerant species might be a source of antiviral compounds against human coronaviruses HCoV-229E and SARS-CoV-2.

2.4. Bioguided Fractionation Assay to Determine the Active Sub-Extracts

A bioguided fractionation assay was conducted in order to isolate the active compounds present in the active crude methanolic extracts. The four extracts were partitioned using three solvents of different polarities, yielding dichloromethane (DCM), ethyl acetate (EtOAc), and aqueous (Aq) sub-extracts. The different partitions obtained were tested for cytotoxicity at 25 and 100 µg/mL through the MTS assay. None of the tested sub-extracts appeared to be cytotoxic at 25 µg/mL (Figure S4).

Then, the antiviral activity of each sub-extract at 25 µg/mL was tested against HCoV-229E (Figure 5). The DCM sub-extract was the most active for *Hippophae rhamnoides* in both Huh-7 and Huh-7/TMPRSS2 cells. The Aq sub-extract was the most active in *Salix repens* (S) in both Huh-7 and Huh-7/TMPRSS2 cells. All sub-extracts of *Salix repens* (R) showed an antiviral effect against HCoV-229E. Surprisingly, for *Baccharis halimifolia* (L), fractionation did not permit the identification of a very active sub-extract. We selected *H. rhamnoides* DCM, *S. repens* (R) EtOAc, *S. repens* (S) Aq, and *B. halimifolia* DCM for further investigations.

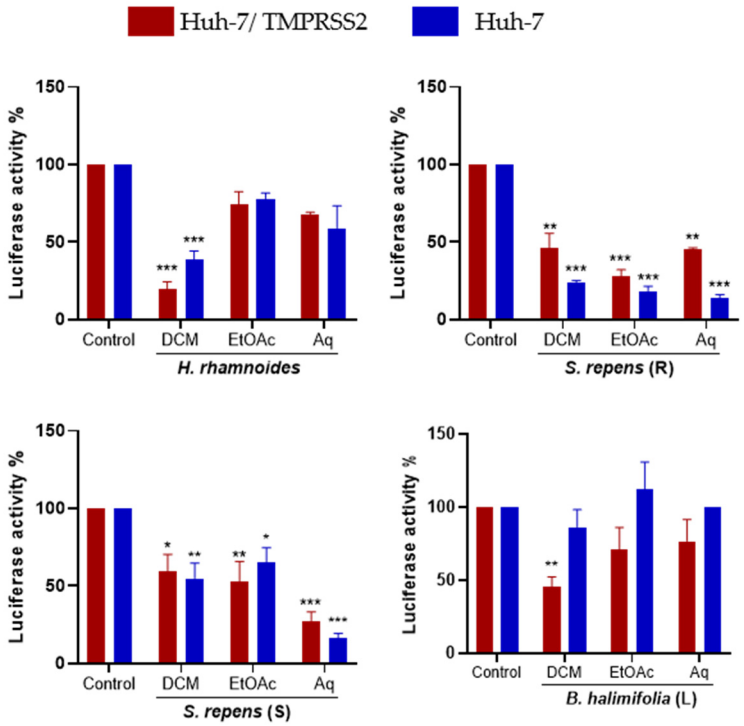

Figure 5. Inhibitory activity of the three partitions obtained from each plant's crude methanolic extract on HCoV-229E-Luc infection. Experiments were conducted as described earlier. Data are represented as the mean ± SEM of three independent experiments. (*, $p < 0.05$; **, $p < 0.01$; ***, $p < 0.001$).

In order to confirm the antiviral activity of the selected sub-extracts and determine their cytotoxicity, dose-response experiments were performed as described. This allowed us to calculate the CC_{50}, IC_{50}, and SI values (Table 3, Figure S5). All the tested sub-extracts showed a dose-dependent reduction in infection with a high SI (SI > 10). The EtOAc sub-extract of *Salix repens* (R) displayed the lowest IC_{50} in Huh-7/TMPRSS2 cells (IC_{50} = 28.8 µg/mL), whereas the Aq sub-extract of *Salix repens* (S) showed the lowest IC_{50} value in Huh-7 cells (IC_{50} = 7.6 µg/mL). On the other hand, the DCM sub-extract

of *Baccharis halimifolia* showed the highest IC_{50} values of 38.3 µg/mL and 31.1 µg/mL in Huh-7/TMPRSS2 and Huh-7 cells, respectively.

Table 3. Cytotoxicity, activity, and SI of each of the sub-extracts against HCoV-229E.

Sub-Extract	Vero-81 CC_{50} (µg/mL)	Huh-7 CC_{50} (µg/mL)	Huh-7		Huh-7/TMPRSS2	
			IC_{50} (µg/mL)	SI	IC_{50} (µg/mL)	SI
H. rhamnoides DCM	264	410	18.7	21	36.	11
S. repens (R) EtOAc	344	500	15.8	31	28.87	17
S. repens (S) Aq	262	550	7.6	71	30.5	18
B. halimifolia (L) DCM	347	368	31.1	11	38.3	9

We then tested the antiviral activity of the sub-extracts on SARS-CoV-2. A dose-dependent inhibitory effect was observed for all extracts (Figure 6). Treatment with the DCM sub-extract of *Hippophae rhamnoides* (HR DCM SE) at a concentration of 50 µg/mL led to a strong reduction in SARS-CoV-2 infection by showing a complete decrease in N protein expression levels in the cell lysate. The DCM sub-extract of *Baccharis halimifolia* showed the lowest inhibitory activity against SARS-CoV-2 at both concentrations. Both the EtOAc sub-extract of *Salix repens* (R) and the Aq sub-extract of *Salix repens* (S) showed similar inhibitory effects against SARS-CoV-2; however, it was lower than that of HR DCM SE.

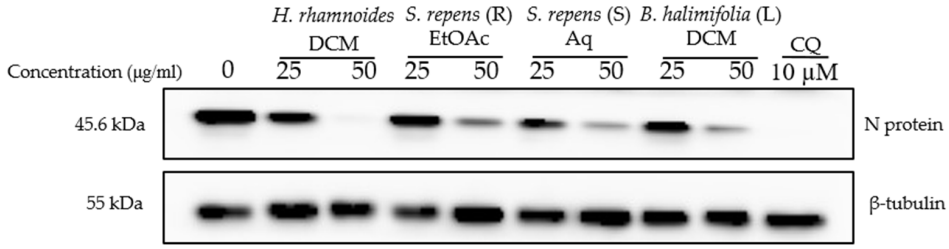

Figure 6. Antiviral activity on SARS-CoV-2 of sub-extracts. Vero-81 cells were infected with SARS-CoV-2 in the presence and absence of different plant sub-extracts at 25 and 50 µg/mL, or 10 µM chloroquine. Cell lysates were collected after 16 h and subjected to immunoblotting as described. This blot is representative of two independent experiments.

Since the HR DCM SE showed a strong antiviral effect against both HCoV-229E and SARS-CoV-2, we decided to study this plant in depth to determine the major bioactive compounds responsible for the anti-coronavirus effect.

2.5. Characterization of HR DCM SE by UHPLC UV-MS

The analysis of HR DCM SE by UHPLC-UV-MS showed different compounds with different levels and polarities. HR DCM SE was fractionated by CPC with the Arizona R system in descending mode. The collected fractions were dried and analyzed by UHPLC-UV-MS. The fractions that showed the same chromatographic profile were pooled together. Thus, we ended up with 10 fractions (Figure S6).

2.6. Cytotoxicity of Ten Fractions Prepared from HR DCM SE

The cytotoxicity of the ten fractions of HR DCM SE obtained through CPC was assessed in Huh-7 cells and Vero-81 cells at 25 and 100 µg/mL. Generally, a dose-dependent decrease in cell viability was observed upon testing the fractions at increasing concentrations. However, at 25 µg/mL, all fractions showed no cytotoxicity on Huh-7 cells. At 100 µg/mL, fractions F2, F3, F4, F6, and F7 were considered cytotoxic upon treating the cells, causing a decrease in cell viability by 41.7%, 44.2%, 61.4%, 30.9%, and 70.4%, respectively. However, fractions F1, F2, F9, and F10, did not show cellular toxicity. Similar to Huh-7, these fractions were not cytotoxic on Vero-81 cells when tested at 25 µg/mL. Fractions F2, F4, F6, and F7, which showed cytotoxicity

on Huh-7 cells, were also toxic on Vero-81 cells at 100 µg/mL, decreasing the viability by 55.7%, 75.7%, 81.7%, and 66.4%, respectively (Figure S7).

2.7. Antiviral Screening of Ten Fractions Obtained from HR DCM SE against HCoV-229E and SARS-CoV-2

After identifying a concentration that could be tolerated by Huh-7 cells, the antiviral activity on HCoV-229E-Luc in Huh-7 and Huh-7/TMPRSS2 cells was monitored. Huh-7 cells were infected with the virus and treated simultaneously with the different fractions at 10 and 25 µg/mL. Three fractions (F3, F4, and F7) showed a 10-fold decrease in virus infection levels compared to the control, indicating an antiviral effect against HCoV-229E (Figure 7A).

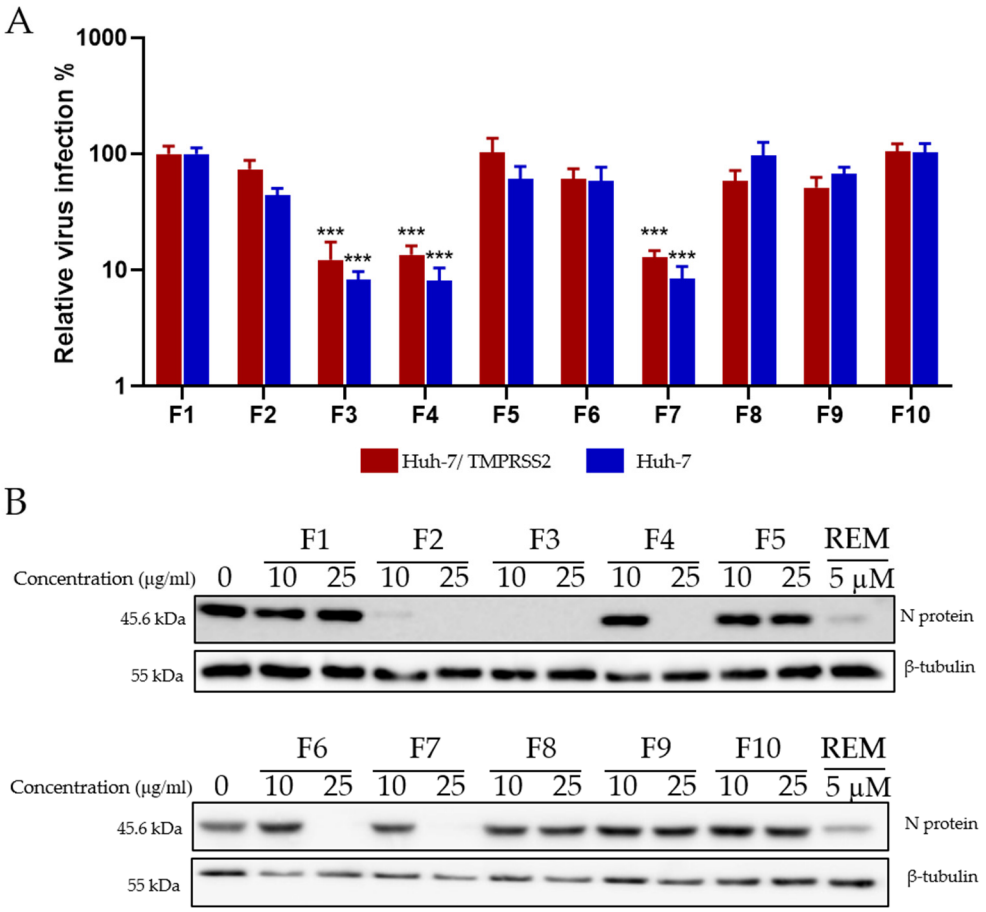

Figure 7. Antiviral activity of *Hippophae rhamnoides* fractions. (**A**) Screening of the antiviral activity of the fractions of *Hippophae rhamnoides* with HCoV-229E-Luc. The different fractions were tested at 25 µg/mL. (**B**) Western blotting analysis showing the effects of the different fractions of *Hippophae rhamnoides* on N protein expression in Vero-81 cells. Vero-81 cells were infected with SARS-CoV-2 in the presence of the different fractions at 10 and 25 µg/mL. Cell lysates were collected after 16 h and subjected to Western blotting. (***, $p < 0.001$).

Similarly, the ten fractions were tested for antiviral activity against SARS-CoV-2. The results presented in (Figure 7B) show that, interestingly, fractions F2 and F6, which were not active on HCoV-229E, were able to inhibit the expression of the SARS-CoV-2 N protein. Similar to HCoV-229E, fractions F3, F4, and F7 were able to inhibit SARS-CoV-2 replication, showing a dose-dependent decrease in antiviral activity (Figure 7B).

2.8. Isolation of Compounds by Preparative HPLC and Identification by HRMS and NMR

To isolate the active compounds responsible for an antiviral effect against both viruses, a preparative HPLC was performed. Fractions F2, F4, and F7 were first analyzed by analytical

HPLC to find the best purification method. We chose not to purify compounds from F3 due to their high complexity and because the compounds of interest were also found in the less complex fractions, F2 and F4 (Figure S6). Then, the major compounds were purified by preparative HPLC using the same stationary phase. Fraction 2 was purified with a gradient system (60–100% CH_3CN, 30 min), providing compounds F2-1 (tr = 23.00 min, 2.41 mg), F2-2 (tr = 23.55 min, 2 mg), F2-3 (tr = 26.00 min, 2 mg), and F2-4 (tr = 9.830 min, 3 mg) (Figure 8). F2-1, F2-2, and F2-3 have a molecular mass of 618 $g.mol^{-1}$. Two compounds, F4-1 (tr = 16.507 min, 3 mg) and F4-2 (tr = 18.946 min, 8 mg), with a molecular mass of 618 $g.mol^{-1}$, were purified from F4 with a gradient system (80–100% CH_3CN, 30 min) (Figure 8). Compound F4-1 was isolated as a mixture (30:70) with compound F4-2. F7 was fractionated with a gradient system (80–100% CH_3CN, 30 min) to give compound F7-1 (tr = 19.030 min, 3.4 mg) with a molecular mass of 602 $g.mol^{-1}$ (Figure 8).

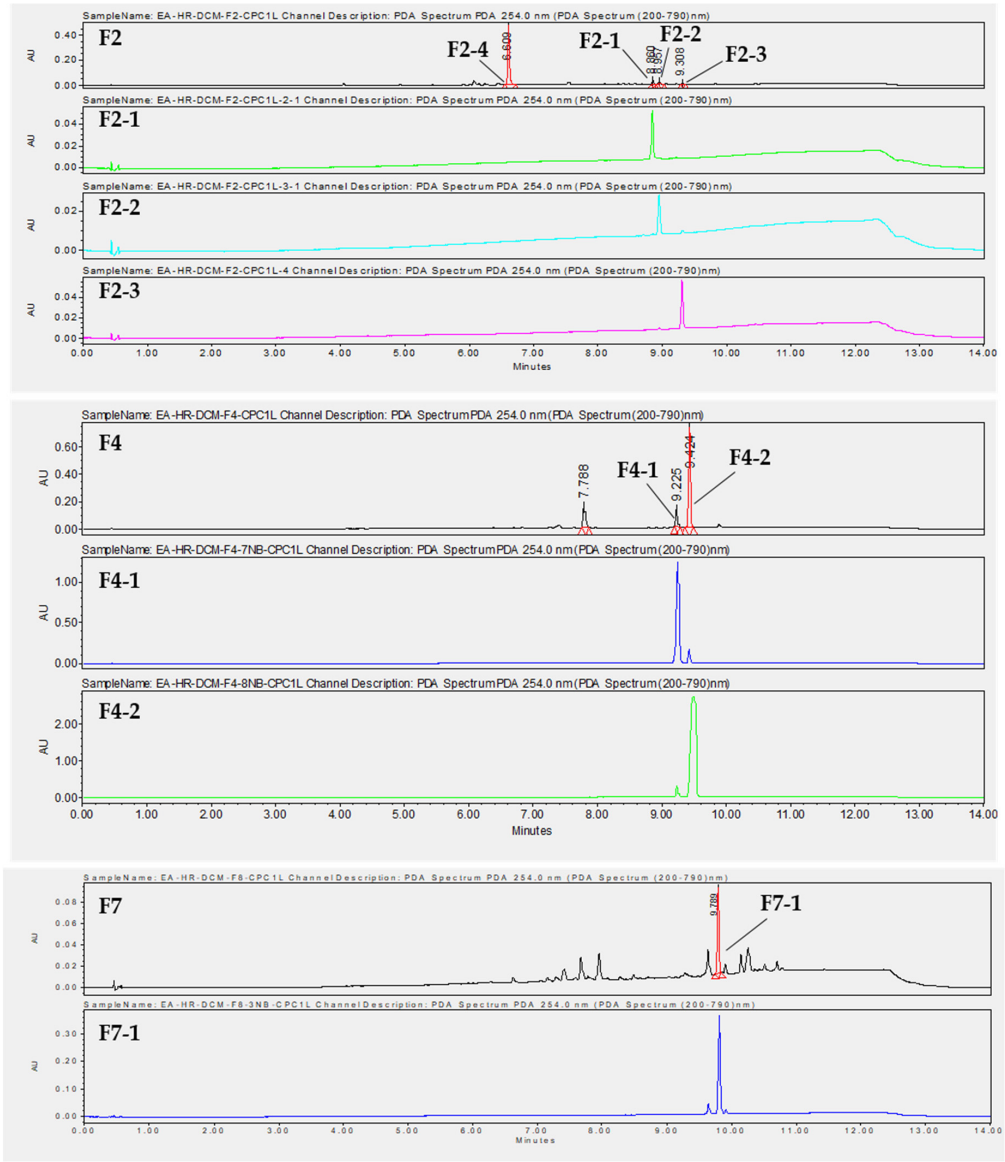

Figure 8. Chromatograms at λ = 254 nm obtained by UHPLC-UV-MS of F2, F4, and F7, as well as purified compounds obtained by preparative HPLC.

Taken together, F2-1, F2-2, F3-2, F4-1, F4-2, and F7-1 were identified as six cinnamoyl triterpenoids. Their purities were, respectively, estimated at 98.8, 88.6, 97.1, 90.7, 96.4, and 91.7% on the basis of PDA chromatograms (Figure S10). Their structures were established through a com-

parison of their physical and spectral data, including HRMS and extensive 1D- and 2D-NMR data, with reported values of 2-*O*-*trans*-*p*-coumaroyl-maslinic acid (F2-1) [20], 3β-hydroxy-2α-*trans*-*p*-coumaryloxy-urs-12-en-28-oic acid (F2-2) [21], 3β-hydroxy-2α-*cis*-*p*-coumaryloxy-urs-12-en-28-oic acid (F2-3) [21], 3-*O*-*cis*-caffeoyl-oleanolic acid (F4-1), 3-*O*-*trans*-caffeoyl-oleanolic acid (F4-2) [22], and 3-*O*-*trans*-*p*-coumaroyl-oleanolic acid (F7-1) [23] (Figures 9 and S11). Unfortunately, F2-4 could not be precisely identified due to the lack of a mass response and poor NMR resolution. It was not a triterpenoid and seemed to be a flavonoid due to a positive response to Neu's reagent.

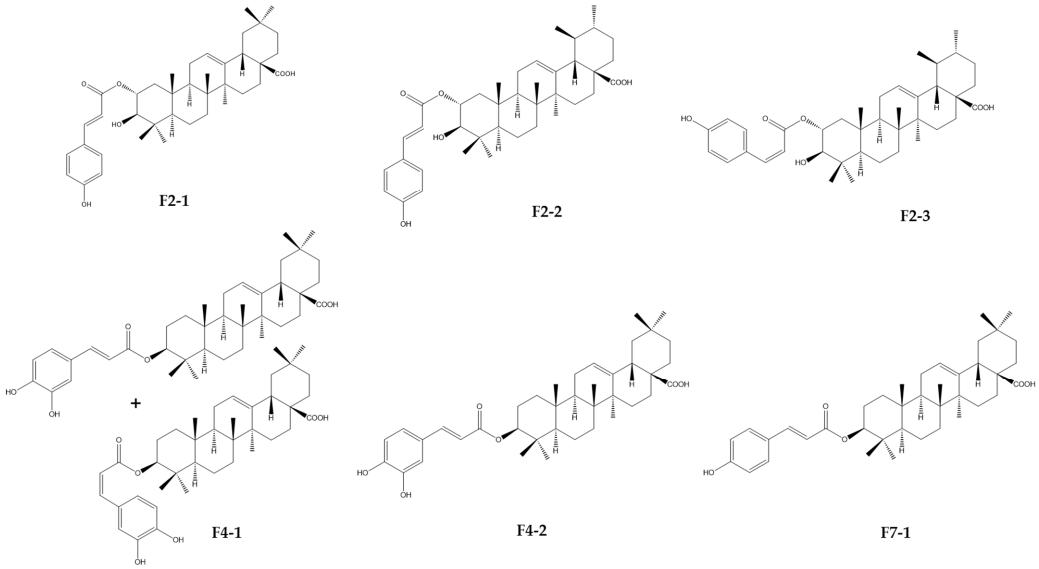

Figure 9. Chemical structures of cinnamoyl triterpenoids purified from fractions F2, F4, and F7 resulting from CPC fractionation of the DCM sub-extract of *Hippophae rhamnoides*.

2.9. Cytotoxicity and Antiviral Activity of the Purified Compounds on HCoV-229E and SARS-CoV-2

To determine whether the purified compounds were responsible for the antiviral effects on both coronaviruses, we conducted cytotoxicity and antiviral dose-response experiments. Huh-7 cells were treated with the various compounds at different concentrations of up to 100 µM for 24 h, and the cytotoxicity was quantified using an MTS assay. Among the compounds, F4-2 displayed the highest CC_{50} value of 81.4 µM. Conversely, the mixture F4-1 exhibited the lowest CC_{50} value of 21 µM. The CC_{50} values for F2-2 and F2-3 were found to be 44.4 and 52.1 µM, respectively. Both F2-1 and F7-1 demonstrated similar CC_{50} values of 39.9 µM and 39.3 µM, respectively (Table 4, Figure S8).

Antiviral testing against HCoV-229E showed that the six compounds isolated from the three fractions (F2, F4, and F7) demonstrated a dose-dependent antiviral activity in both Huh-7 and Huh-7/TMPRSS2 cells (Table 4, Figure S8). F2-1 displayed the most promising performance, showing IC_{50} values of 8.6 and 9.1 µM in Huh-7 and Huh-7/TMPRSS2 cells, respectively, with an SI of approximately 4. It is noteworthy that the major compound F2-4 of fraction 2, which was not chemically characterized, did not exhibit either cytotoxicity or antiviral effects on HCoV-229E (Figure S9). F4-2 also displayed interesting antiviral activities and the highest SI of 7. F4-1 was the most active but only in Huh-7 cells with an IC_{50} value of 7.6 µM.

Finally, we explored the antiviral impact of the three cinnamoyl oleanolic acids, F4-1, F4-2, and F7-1, on SARS-CoV-2 at various concentrations. The inhibitory activity was assessed by quantifying the levels of N protein expression (Figure 10). A noticeable, dose-dependent reduction in N protein levels, indicative of an antiviral effect, was observed for all three compounds. Specifically, F4-1 exhibited the highest antiviral activity, significantly inhibiting SARS-CoV-2 by 54% at 12.5 µM, 68% at 25 µM, and 93.3% at 50 µM. In

contrast, both F4-2 and F7-1 demonstrated significant inhibitory effects, reaching 54% and 55.5%, respectively, but only at the concentration of 50 µM (Figure 10). The difference in activity observed between F4-1 and F4-2 could suggest better activity for 3-*O*-*cis*-caffeoyl oleanolic acid. Unfortunately, this compound could not be obtained in pure form due to a spontaneous conversion to the *trans* isomer during the purification process.

Table 4. Cytotoxicity, antiviral activity, and SI of each purified compound against HCoV-229E.

Sub-Extract	Huh-7 CC_{50} (µM)	Huh-7		Huh-7/TMPRSS2	
		IC_{50} (µM)	SI	IC_{50} (µM)	SI
F2-1 (2-*O*-*trans*-*p*-coumaroyl-maslinic acid)	39.9	8.6	4	9.1	4
F2-2 (3β-hydroxy-2α-*trans*-*p*-coumaryloxy-urs-12-en-28-oic acid)	44.4	12.0	3	11.4	3
F2-3 (3β-hydroxy-2α-*cis*-*p*-coumaryloxy-urs-12-en-28-oic acid)	52.1	14.5	3	14.1	3
F4-1 Mixture 3-*O*-*trans*-caffeoyl oleanolic acid / 3-*O*-*cis*-caffeoyl oleanolic acid (70/30)	21.0	7.6	2	12.0	1
F4-2 (3-*O*-*trans*-caffeoyl-oleanolic acid)	81.4	11.6	6	11.5	7
F7-1 (3-*O*-*trans*-*p*-coumaroyl-oleanolic acid)	39.3	11.4	3	10.7	3

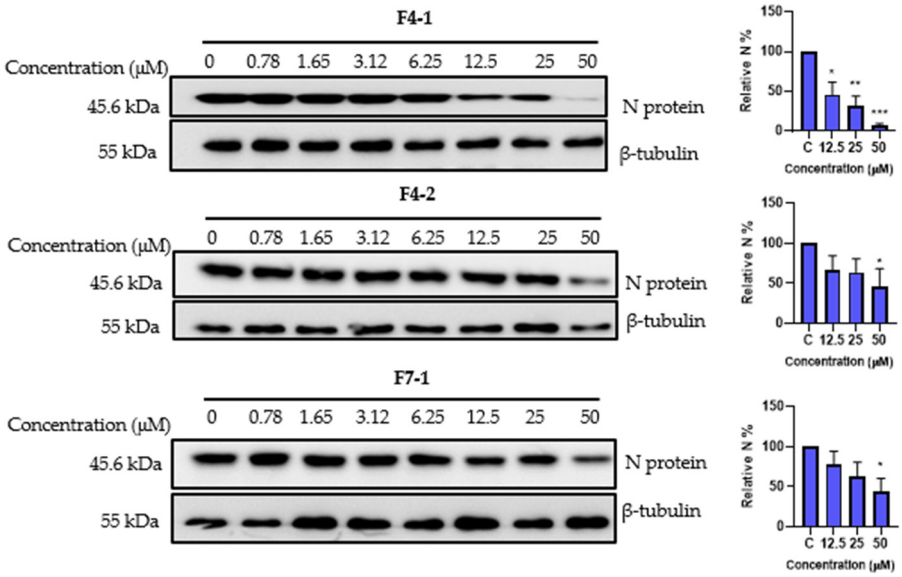

Figure 10. Antiviral activity of cinnamoyl oleanolic acids against SARS-CoV-2. The antiviral effect of F4-1 (3-O-cis-caffeoyl-oleanolic acid), F4-2 (3-O-trans-caffeoyl-oleanolic), and F7-1 (3-O-trans-p-coumaroyl-oleanolic acid) against SARS-CoV-2 was determined by Western blot. Vero-81 cells were treated with the different compounds at different concentrations for 16 h. Cell lysates were collected after 16 h and subjected to Western blotting. Data values represent the mean ± standard deviation from 3 independent experiments, (*, $p < 0.05$; **, $p < 0.01$; ***, $p < 0.001$).

Taken together, the results show that several cinnamoyl triterpenoids, isolated from three different fractions of HR DCM SE, have antiviral activities against both HCoV-229E and SARS-CoV-2.

3. Discussion

In light of the emergence of coronavirus outbreaks and the predictability of future epidemics and pandemics, it has become imperative to discover effective antiviral solutions. Despite the development of vaccines and antiviral drugs, several significant challenges hinder progress, such as unequal access to treatments and vaccines, the emergence of variant strains, and more. Therefore, there is a critical need for effective, accessible, and cost-effective antiviral treatments targeting SARS-CoV-2, especially in low-income countries.

Natural products have played a crucial role in the field of drug discovery, particularly in the discovery of antibacterial and antitumoral agents. Halophytes and salt-tolerant plants

are recognized as abundant sources of specialized metabolites that exhibit a wide range of biological functions, including survival under challenging environmental conditions and defense mechanisms against microorganisms. In our study, we explored the antiviral potential of halophytes and salt-tolerant plants collected from the North Sea and English Channel coasts in northern France against various coronaviruses.

The crude methanolic extracts of *Hippophae rhamnoides*, *Salix repens* (S and R), and *Baccharis halimifolia* exhibited significant antiviral effects against HCoV-229E and SARS-CoV-2. A recent paper demonstrated the antiviral activity of *Salix* spp against both seasonal and pandemic coronaviruses; however [24]. Furthermore, a flavonoid compound, isorhamnetin, isolated from *Hippophae rhamnoides* fruits, displayed antiviral activity against the SARS-CoV-2 spike pseudotyped virus in vitro [25]. However, no prior research has investigated the antiviral activity of these plants against HCoV-229E.

Hippophae rhamnoides belongs to the Elaeagnaceae family and is native to the cold-temperate regions of Europe and Asia [26]. Sea buckthorn berries are known for their rich nutritional content, including vitamins and specialized metabolites like tocopherols, phenolic acids, carotenoids, flavonoids, tocopherols, and phytosterols [27,28]. Traditional medicine in China and Russia has previously employed this plant to treat dermatological diseases. Additionally, numerous studies have highlighted the pharmacological effects of *Hippophae rhamnoides*, including its antioxidant [29], antimicrobial [30], anti-atherogenic [31], cardioprotective [31], hepatoprotective [32], radioprotective [33], and tissue regeneration properties [34]. Nonetheless, research on the antiviral activity of *Hippophae rhamnoides* remains limited.

Liquid–liquid partitioning, combined with simultaneous biological testing, revealed that the HR DCM SE exhibited the most substantial antiviral effect against coronaviruses. Consequently, we decided to narrow our investigation to this specific sub-extract to pinpoint the active fraction and subsequently isolate the bioactive compounds responsible for the antiviral effect against coronaviruses. The nonpolar nature of this sub-extract suggests that the active compounds are rather lipophilic.

Using a bioguided fractionation approach combining fractionation by CPC and antiviral testing, we identified F3, F4, and F7 as the most potent fractions against HCoV-229E, whereas F2, F3, F4, and F7 were the most effective against SARS-CoV-2. UHPLC-UV-MS analysis revealed the presence of compounds, with a similar absorbance and molecular mass of around 600 g.mol^{-1} found in several fractions, suggesting that analogs contribute to the antiviral activity in different fractions.

Six compounds were isolated from HR DCM SE and identified through NMR and HR-MS analysis as cinnamoyl triterpenoids. Among these, three compounds—2-*O*-*trans*-*p*-coumaroyl-maslinic acid, 3β-hydroxy-2α-*trans*-*p*-coumaryloxy-urs-12-en-28-oic acid, and 3β-hydroxy-2α-*cis*-*p*-coumaryloxy-urs-12-en-28-oic acid—were isolated from F2 and are derivatives of maslinic acid (MA) and ursolic acid (UA), respectively. The remaining compounds were cinnamoyl derivatives of oleanolic acid (OA), obtained from F4 (mixture of 3-*O*-*trans*-caffeoyl oleanolic acid/3-*O*-*cis*-caffeoyl oleanolic acid (70/30) and 3-*O*-*trans*-caffeoyl oleanolic acid) and F7 (3-*O*-*trans*-*p*-coumaroyl oleanolic acid). MA, UA, and OA are common triterpenoids and are known to be abundant in *Hippophae rhamnoides* [28].

Despite F2 not demonstrating an antiviral effect against HCoV-229E, the UHPLC-UV-MS analysis indicated the presence of a major compound, seemingly a flavonoid, which also proved to be inactive when tested at different doses. However, the antiviral impact of F2 on SARS-CoV-2 prompted us to isolate three other compounds, which are cinnamoyl derivatives of MA and UA. Unexpectedly, these compounds exhibited inhibitory activity against HCoV-229E following separation and isolation, whereas F2 was inactive. This might be due to the fact that these three compounds were present at low levels in F2.

Triterpenoids represent the most widely distributed category of natural compounds, typically originating from the C30 molecular structure, which is synthesized by rearranging six isoprene units following the isoprene rule. They are found in plants either in their free form or as glycosides (saponins). Some of these triterpenoids can, in some cases, be

acylated. Among triterpenoids, the tricyclic and pentacyclic varieties are the most abundant [32,33]. Previous phytochemical studies conducted on different parts of *Hippophae rhamnoides* highlighted the presence of pentacyclic triterpenoids, mostly the oleanane and ursane types, with different biological activities [28]. Some cinnamoyl triterpenoids, including 2-*O*-*trans*-p-coumaroyl maslinic acid, 2-*O*-*trans*caffeoyl maslinic acid, 3-*O*-*trans*-*p*-coumaroyl oleanolic acid, and 3-*O*-*trans*-caffeoyl oleanolic acid have already been isolated from the branch bark of this plant [20]. Some other derivatives have been tentatively identified in different parts of *Hippophae rhamnoides* by LC-HRMS [35].

Pentacyclic triterpenes, such as analogs or derivatives of OA, have demonstrated various inhibitory activities against viruses, primarily linked to their structures. They have been found to be effective against the influenza virus and hepatitis C virus (HCV) infections. These triterpenes work by binding to viral fusion proteins like hemagglutinin (HA2) of influenza [36], E2 of HCV [37], and GP41 of human immunodeficiency virus-1, thus disrupting the entry of the virus into host cells. Further exploration of OA revealed that it can interact with heptad repeat-2 and hinder Ebola virus–cell fusion [38], shedding light on its mechanism of action against SARS-CoV-2. Additionally, research suggests that OA may act as an inhibitor of viral replication by blocking the activity of SARS-CoV 3CLpro [39]. Moreover, friedlane-type triterpenoids isolated from *Euphorbia neriifolia* L. leaves, a drought-tolerant plant, exhibited potent antiviral activity against HCoV-229E cultured in MRC-5 cells [40]. The friedelane skeleton could act on multiple targets simultaneously, making it a potential candidate for exerting an antiviral effect against various human coronaviruses.

MA is a commonly occurring triterpenoid abundant in the fruits of *Hippophae rhamnoides* [41]. MA has demonstrated a wide spectrum of biological activities, including antibacterial, anti-inflammatory, and antitumor properties. Moreover, in another study, a cinnamoyl maslinic acid named 3-β -O-(*trans*-*p*-coumaroyl)maslinic acid, demonstrated broad antimicrobial activity against Gram-positive bacteria and yeasts, with a minimum inhibitory concentration of 12.5 µg/mL against *Staphylococcus capitis* and *Candida albicans* [42].

UA and OA share similar chemical structures but differ in the position of one methyl group on ring E. UA has been recognized for its anti-inflammatory, antibacterial, antioxidant, anti-diabetic, and anticancer properties. While there are limited data regarding the antiviral activity of UA against HCoV-229E, there are several reports related to its potential against SARS-CoV-2, given their similar morphologies, replication cycles, and symptoms. It has been tested against the SARS-CoV-2 Mpro enzyme and successfully inhibited its activity [43]. Additionally, molecular docking (MD) and molecular dynamic simulation studies have confirmed the ability of UA and its derivatives to interact with SARS-CoV-2 protease during 50 nanoseconds of MD simulation [44]. UA exhibits high binding affinity, forming a hydrogen bond with the amino group of Asp 108 in the PLpro protease enzyme and engaging in hydrophobic interactions with Ala 107, Pro 248, and Tyr 264 of the same enzyme [45]. In silico studies suggest that UA could inhibit the interaction between SARS-CoV-2 spike proteins and the receptor, angiotensin-converting enzyme 2 (ACE-2) [46]. However, further confirmation is needed through in vitro or in vivo studies.

In this study, we showed that the antiviral activity of cinnamoyl terpenoids on human coronaviruses is promising. However, they display relatively low SIs (between 1 and 7) due to their cytotoxicity. The toxicity and antiviral assays were performed in Huh-7 cells, which is a hepatoma cell line. It would be interesting to evaluate the cytotoxicity of the compounds in respiratory cell lines or in animal models (in vivo). Few studies exist on this type of compound. Furthermore, if the cytotoxicity is high in other cell lines, one could envisage administrating the compound via aerosols (orally or nasally), limiting any toxic side effects. This mode of administration would reach the nasal or bronchial epithelial cells, the sites of viral replication.

Additional work is necessary to determine the mechanism of action of the active isolated compounds against SARS-CoV-2 and HCoV-229E. It would be necessary to determine if they act in the entry or replication step. It is unlikely that one compound could act in both steps; however, it would be very interesting to show that *Hippophae rhamnoides* extract

contains a mixture of compounds, with some active on entry and others on replication. It would also be interesting to perform combination assays with the different compounds to determine if the mixture of all these compounds is more active than each isolated molecule.

Considering all the aforementioned information, it is evident that pentacyclic triterpenoids exhibit anti-coronavirus activity, perhaps due to their structural properties. The presence of cinnamoyl triterpenoid derivatives like MA, UA, and OA, which share structural similarities, in plants like *Hippophae rhamnoides* points to potential antiviral activity, particularly against SARS-CoV-2. Further in-depth investigations are necessary to gain a deeper understanding of their specific targets and mechanisms of action, facilitating their development and ensuring safety, and fully exploring their therapeutic efficacy.

4. Materials and Methods

4.1. Plant Material

Plant species, mainly halophytes, were selected and collected between July 2020 and November 2020 from five different locations (Étaples, Dannes, Le Portel, Gravelines, Zuydcoote) distributed across the coastline region of northern France (Hauts-de-France region) in conjunction with the managers of the natural sites (Figure 11). Plants were mainly collected from schorres; coastal cliffs; and incipient, established, and relict dunes [46–48]. All these operations, followed by the identification of plant materials, were conducted by Prof. Céline Rivière and Dr. Gabriel Lefèvre from the Faculty of Pharmacy in Lille (UMRt BioEcoAgro). These samples were collected in accordance with the rules of the Nagoya Protocol and the French biodiversity law of 2017 (decision of 23 September 2020 issued by the Ministry of Ecological and Inclusive Transition; NOR: TREL2002508 S/342 and ABSCH-IRCC-FR-252501-1). Specific authorizations were also granted by the "Direction Interrégionale de la Mer Manche Est- Mer du Nord" (Decision n°778/2020) and by the prefect of the region of Normandy (regulation service for maritime activities). Harvested plant species were dried at 30 °C in an oven for a maximum of one week and protected from light. Different parts of these plants (leaves, stems, roots) were pulverized separately using a crushed Retsh Cutting Mill SM200.

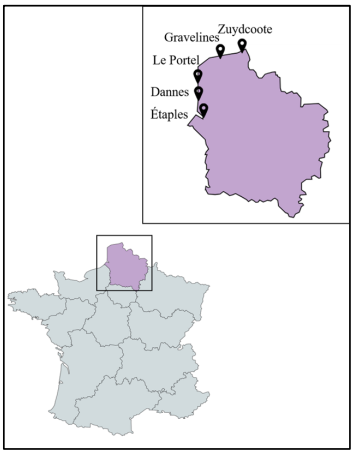

Figure 11. Map showing the sites of collection of the studied plant species.

4.2. Solid/Liquid Extraction

Crude methanolic extracts were prepared by maceration by soaking the powder in 10 mL/g of methanol for 24 h, and the mixtures were then filtered through Whatman filter paper (11 µm pore size). The process was repeated three times. The resulting extracts were then dried in vacuum at 35 °C using a rotary evaporator and stored at −20 °C until tested. For cytotoxicity and antiviral assays, extracts were re-suspended in DMSO at 25 mg/mL, aliquoted, and stored at −20 °C.

4.3. Liquid/Liquid Extraction

The active crude methanolic extracts were subjected to bioguided fractionation using liquid–liquid partitioning. An amount of 3 g of crude methanolic extract was dissolved in water and then partitioned with DCM and EtOAc (3 × 300 mL) to obtain three solvent partitions. The partitions were evaporated using a rotary evaporator and transferred to vials for storage. The apolar partitions (DCM and EtOAc) were evaporated at an ambient temperature and then desiccated under vacuum (desiccator); the polar (Aq) partitions were dried by lyophilization (freeze-drying).

4.4. Fractionation of the DCM Sub-Extract of Hippophae Rhamnoides

The DCM extract of *Hippophae rhamnoides* (HR DMC SE) was fractionated by centrifugal partition chromatography (Armen instruments®, Saint-Avé, France) with a capacity of 1 L. The liquid phases were pumped with a Shimazu® pump (LC-20AP, Kyoto, Japan). The column was coupled online with a DAD detector (SPD-M20A). Fractions were collected with an automated fraction collector (Gilson® FC 204, Villiers-le-Bel, France). The elution profile was recorded using LabSolutions™ software version 1.25. The solvent system was composed of heptane, EtOAc, methanol, and water (2:1:2:1) (Arizona R system). The CPC rotor was first filled with the stationary phase (upper phase) at a flow rate of 50 mL.min^{-1} (500 rpm) in descending mode. Equilibrium was reached by introducing the mobile phase (lower phase) at 1200 rpm and a flow rate of 30 mL.min^{-1}. An amount of 5.9 g of the HR DCM SE (obtained from the whole plant) was dissolved in 46 mL of the organic/aqueous phase mixture (1:1, v/v) and filtered through a Millipore syringe filter (0.45 µm). The filtered solution was injected immediately after displacement of the stationary phase (170 mL). The elution was carried out at 30 mL.min^{-1} for 60 min and monitored at λ = 254 nm. After that, extrusion mode was performed to allow for the recovery of highly retained molecules in the stationary phase. At the end of the CPC cycle, the 193 tubes obtained were characterized by UHPLC-UV-MS and then grouped into 10 fractions according to their phytochemical profiles. The 10 fractions were then concentrated by a centrifugal concentrator (Genevac™, Fisher Scientific, Illkirch, France).

4.5. UHPLC-UV-MS Analysis

The Acquity UPLC H-Class Waters® System (Guyancourt, France) apparatus was equipped with two independent pumps, a controller, a diode array detector (DAD), and a QDa electrospray quadrupole mass spectrometer. The stationary phase was a C18 BEH (2.1 × 50 mm, 1.7 µm) reverse column. The mobile phase was composed of two solvents: (A) ultrapure water + 0.1% formic acid (Carlo Erba Reagents®, Val de Reuil, France) and (B) Acetonitrile (Carlo Erba Reagents®, Val de Reuil, France) + 0.1% formic acid. The flow rate and column temperature were set at 0.3 mL.min^{-1} and 30 °C, respectively. The wavelength range was fixed at 200–790 nm with a resolution of 1.2 nm. Ionization was carried out in both negative and positive modes, with the mass ranging from 50 to 1250 Da. The cone voltage and capillary voltage values were 15 V and 0.8 kV, respectively. The injection volume was set at 2 µL. UHPLC-UV-MS analysis was executed following the elution program: 10%→100% (B) (0–9 min), 100% (B) (9–11.5 min), and 10% (B) (11.5–14 min). All samples were prepared at 1 mg·mL^{-1} in analytical grade MeOH and filtered through a PTFE 0.4 µm membrane before injection.

4.6. Preparative HPLC

The equipment consisted of Shimadzu® LC-20AP binary high-pressure pumps, an SPD-M20A photodiode array detector, and a CBM-20A controller. A column Interchim US5C18HQ-250/212 Uptisphere Strategy C18-HQ 5 µm (250 × 21.2 mm) prep-LC was used in this experiment as the stationary phase. The mobile phase was composed of ultra-pure water (Millipore Integral 5 Milli-Q, Merck™, Trosly-Breuil, France) + 0.1% formic acid (Merck™, Darmstadt, Germany) (solvent A) and acetonitrile (Carlo Erba Reagents®, Val de Reuil, France) (solvent B). The flow rate was set at 15 mL·min^{-1}. The purification monitoring was carried out at two main

wavelengths: 247 nm and 254 nm. Preparative HPLC was performed on fractions F2, F4, and F7 obtained from HR DCM SE after CPC. The gradients used were 60% B (0.01 min), 60% to 100% B (0.01–25 min), 100% B (25.01–28.99 min), and 60% B (29–30 min) for fraction 2, and 80% B (0.01 min), 80% to 100% B (0.01–25 min), 100% B (25.01–28.99 min), and 80% B (29–30 min) for fractions 4 and 7.

4.7. NMR and HRMS

The structures of the purified compounds were determined using NMR and HR-MS. NMR spectra (mono- and bi-dimensional) were recorded on a Bruker ® DPX-500 spectrometer (^{1}H- and ^{13}C-NMR at 500 and 125 MHz) (Bruker, Bremen, Germany). High-Resolution Mass Spectrometry (HR-MS) analyses were carried out using a Thermo Fisher Scientific® Exactive Orbitrap Mass Spectrometer (Thermo Fisher Scientific, Waltham, MA, USA) equipped with an electrospray ion source. The pure compounds were analyzed in deuterated methanol, MeOD (Euriso-Top®, Gif-sur-Yvette, France). HR-MS analyses were carried out in negative mode with a range of m/z 100–1000 amu. Products were solubilized in methanol.

4.8. Virus and Cell Lines

The human hepatoma cell line (Huh-7), whether expressing the TMPRSS2 protease or not [18], and the African green monkey kidney Vero-81 cells were grown in DMEM supplemented with GlutaMax-I and 10% fetal bovine serum and cultured at 37 °C in 5% CO_2 in a humidified incubator. All cell lines used in this study were regularly screened for mycoplasma contamination using the MycoAlert™ Mycoplasma Detection Kit (Lonza Bioscience, Basel, Switzerland).

The viruses used were HCoV-229E strain VR-740 (ATCC), a recombinant HCoV-229E-Luc (kind gift of Volker Thiel), and SARS-CoV-2 (isolate SARS-CoV- 536 2/human/FRA/Lille_Vero-81-TMPRSS2/2020, NCBI MW575140).

4.9. Cell Viability Assay

Huh-7 cells and Vero-81 cells were seeded in 96-well plates and incubated with 100 µL of culture medium containing increasing concentrations of our compounds for 24 h. An MTS based viability assay (CellTiter 96 aqueous nonradioactive cell proliferation assay, Promega, Madison WI, USA) was performed, as recommended by the manufacturer. The absorbance of formazan at 490 nm was detected using ELx808 plate reader (BioTek Instruments Inc., Winooski, VT, USA). Each measurement was performed in triplicate.

4.10. Virus Infection Assay

4.10.1. HCoV-229E

Huh-7 and Huh-7/TMPRSS2 cells, were seeded in 96-well plates and inoculated with HCoV-229E-Luc at an MOI of 0.3 simultaneously with the compounds for 7 h and then lysed in 20 µL of 1× luciferase lysis buffer (Promega) as described [49]. The luciferase activity was quantified in a TriStar LB 941 luminometer (Berthold Technologies, Bad Wildbad, Germany) using the Renilla luciferase assay system (Promega), as recommended by the manufacturer.

4.10.2. SARS-CoV-2

Vero-81 cells were seeded in 24-well plates, inoculated with SARS-CoV-2, and incubated simultaneously with the different compounds for 16 h [50]. Cells were lysed in ice-cold lysis buffer (Tris HCl, 50 mM; NaCl, 100 mM; EDTA, 2 mM; Triton X-100, 1%; SDS, 0.1%) on ice for 20 min. Lysates were collected and analyzed by Western blotting using rabbit polyclonal anti-SARS-CoV-2 nucleocapsid antibodies (Novus Biologicals, Littleton, CO, USA) and mouse anti-β-tubulin monoclonal antibody (TUB 2.1) from Sigma. Horse-radish peroxidase-conjugated goat anti-rabbit and anti-mouse secondary antibodies (Jackson ImmunoResearch, West Grove, PA, USA) were used for the revelation using an

enhanced chemiluminescence (ECL) Western blotting substrate (Thermo Fisher Scientific). The intensity of the bands was quantified using ImageJ software version 1.53i.

4.10.3. Statistical Analysis

The results were presented as the means ± SEM of three independent experiments performed in triplicate. The data were analyzed using GraphPad Prism software version 10.0.3 (Boston, MA, USA) by comparing each treated group and untreated group (DMSO control).

Supplementary Materials: The following supporting information can be downloaded at https://www.mdpi.com/article/10.3390/ijms242316617/s1.

Author Contributions: Conceptualization, K.S. and C.R., M.A.I. and G.L.; methodology, M.A.I., Z.L.E.A., L.D., G.L., J.S., I.R., S.B., K.S. and C.R.; validation, K.S. and C.R.; formal analysis, M.A.I., K.S., Z.L.E.A. and C.R.; investigation, M.A.I., G.L., Z.L.E.A., L.D., J.S., I.R. and C.R.; resources, G.L., C.R. and K.S.; writing—original draft preparation, M.A.I.; writing—review and editing, Z.L.E.A., G.L., L.D., J.S., I.R., S.S., J.D., S.B., K.S. and C.R.; supervision, K.S. and C.R.; project administration, K.S. and C.R.; funding acquisition, K.S. and C.R. All authors have read and agreed to the published version of the manuscript.

Funding: The authors gratefully thank the European Union's Horizon 2020 Research and Innovation program and I-Site ULNE under the Marie Sklodowska-Curie grant agreement (PEARL program No. 847568) for the funding of the Ph.D. fellowship of Malak Al Ibrahim. This work was also supported by the Centre National de la Recherche Scientifique (CNRS: COVID and ViroCrib programs), FEDER-FSE Hauts-de-France region (AP09 REACT-EU 22003058), and CPER BiHauts Eco de France funded by both the French State and the Hauts-de-France region.

Institutional Review Board Statement: Not applicable.

Informed Consent Statement: Not applicable.

Data Availability Statement: Data are contained within the article and Supplementary Materials. Raw data are available on request from the corresponding author.

Acknowledgments: We thank Charline Camuzet and Nathan François for their technical assistance. We also warmly thank the natural park managers for their help in identifying the collection sites of salt-tolerant and invasive species, in particular Hubert Brabant and Dominique Derout (Eden 62), Aline Bue, Lucien Lefebvre, and Virginie Helin (département du Nord), Christophe Blondel (CBNBL), as well as Frédérique Fauré and Henri D'Hour. We are also grateful to the LARMN (Nathalie Azaroual and Vincent Ultré) and GRITA platforms (Jean-François Goossens and Mostafa Kouach) for the access to equipment (UFR3S Faculty of Pharmacy). We also thank the Laboratory of Botany and Mycology (UFR3S Faculty of Pharmacy) for access to their herbarium to deposit our samples (LIP), in particular Alexandre Fruleux and Pierre-Arthur Moreau, as well as Damien Cuny.

Conflicts of Interest: The authors declare no conflict of interest.

References

1. Kesheh, M.M.; Hosseini, P.; Soltani, S.; Zandi, M. An overview on the seven pathogenic human coronaviruses. *Rev. Med. Virol.* **2022**, *32*, e2282. [CrossRef] [PubMed]
2. Liu, D.X.; Liang, J.Q.; Fung, T.S. Human Coronavirus-229E, -OC43, -NL63, and -HKU1 (*Coronaviridae*). *Encycl. Virol.* **2021**, *2*, 428–440. [CrossRef]
3. Zhu, Z.; Lian, X.; Su, X.; Wu, W.; Marraro, G.A.; Zeng, Y. From SARS and MERS to COVID-19: A brief summary and comparison of severe acute respiratory infections caused by three highly pathogenic human coronaviruses. *Respir. Res.* **2020**, *21*, 224. [CrossRef] [PubMed]
4. Agarwal, A.; Hunt, B.J.; Stegermann, M.; Rochwerg, B.; Lamontagne, F.; Siemieniuk, R.A.; Agoritsas, T.; Askie, L.; Lytvyn, L.; Leo, Y.-S.; et al. A living WHO guideline on drugs for COVID-19. *BMJ* **2020**, *370*, m3379. [CrossRef] [PubMed]
5. EMA (European Medicines Agency). Lagevrio: Withdrawn Application. Available online: https://www.ema.europa.eu/en/medicines/human/withdrawn-applications/lagevrio (accessed on 15 October 2023).
6. Duroseau, B.; Kipshidze, N.; Limaye, R.J. The impact of delayed access to COVID-19 vaccines in low- and lower-middle-income countries. *Front. Public Health* **2023**, *10*, 1087138. [CrossRef] [PubMed]
7. Lee, D.Y.; Li, Q.Y.; Liu, J.; Efferth, T. Traditional Chinese herbal medicine at the forefront battle against COVID-19: Clinical experience and scientific basis. *Phytomedicine* **2021**, *80*, 153337. [CrossRef] [PubMed]

8. Villena-Tejada, M.; Vera-Ferchau, I.; Cardona-Rivero, A.; Zamalloa-Cornejo, R.; Quispe-Florez, M.; Frisancho-Triveño, Z.; Abarca-Meléndez, R.C.; Alvarez-Sucari, S.G.; Mejia, C.R.; Yañez, J.A. Use of medicinal plants for COVID-19 prevention and respiratory symptom treatment during the pandemic in Cusco, Peru: A cross-sectional survey. *PLoS ONE* **2021**, *16*, e0257165. [CrossRef]
9. Khadka, D.; Dhamala, M.K.; Li, F.; Aryal, P.C.; Magar, P.R.; Bhatta, S.; Thakur, M.S.; Basnet, A.; Cui, D.; Shi, S. The use of medicinal plants to prevent COVID-19 in Nepal. *J. Ethnobiol. Ethnomed.* **2021**, *17*, 26. [CrossRef]
10. Duan, Q.; Zhu, Z.; Wang, B.; Chen, M. Recent Progress on the Salt Tolerance Mechanisms and Application of Tamarisk. *Int. J. Mol. Sci.* **2022**, *23*, 3325. [CrossRef]
11. Santos, J.; Al-Azzawi, M.; Aronson, J.; Flowers, T.J. eHALOPH a Database of Salt-Tolerant Plants: Helping put Halophytes to Work. *Plant Cell Physiol.* **2016**, *57*, e10. [CrossRef]
12. Cheeseman, J.M. The evolution of halophytes, glycophytes and crops, and its implications for food security under saline conditions. *New Phytol.* **2015**, *206*, 557–570. [CrossRef] [PubMed]
13. Lefèvre, G.; Rivière, C. Amaranthaceae halophytes from the French Flanders coast of the North Sea: A review of their phytochemistry and biological activities. *Phytochem. Rev.* **2020**, *19*, 1263–1302. [CrossRef]
14. Kuo, Y.-C.; Lin, L.-C.; Tsai, W.-J.; Chou, C.-J.; Kung, S.-H.; Ho, Y.-H. Samarangenin B from *Limonium sinense* Suppresses Herpes Simplex Virus Type 1 Replication in Vero Cells by Regulation of Viral Macromolecular Synthesis. *Antimicrob. Agents Chemother.* **2002**, *46*, 2854–2864. [CrossRef] [PubMed]
15. Medini, F.; Legault, J.; Pichette, A.; Abdelly, C.; Ksouri, R. Antiviral efficacy of Limonium densiflorum against HSV-1 and influenza viruses. *S. Afr. J. Bot.* **2014**, *92*, 65–72. Available online: https://cyberleninka.org/article/n/390317 (accessed on 7 September 2021). [CrossRef]
16. Chiang, L.; Chiang, W.; Chang, M.; Ng, L.; Lin, C. Antiviral activity of Plantago major extracts and related compounds in vitro. *Antivir. Res.* **2002**, *55*, 53–62. [CrossRef]
17. Sahuc, M.-E.; Sahli, R.; Rivière, C.; Pène, V.; Lavie, M.; Vandeputte, A.; Brodin, P.; Rosenberg, A.R.; Dubuisson, J.; Ksouri, R.; et al. Dehydrojuncusol, a Natural Phenanthrene Compound Extracted from *Juncus maritimus*, Is a New Inhibitor of Hepatitis C Virus RNA Replication. *J. Virol.* **2019**, *93*, e02009-18. [CrossRef] [PubMed]
18. Belouzard, S.; Millet, J.K.; Licitra, B.N.; Whittaker, G.R. Mechanisms of Coronavirus Cell Entry Mediated by the Viral Spike Protein. *Viruses* **2012**, *4*, 1011–1033. [CrossRef] [PubMed]
19. Zhu, Y.; Binder, J.; Yurgelonis, I.; Rai, D.K.; Lazarro, S.; Costales, C.; Kobylarz, K.; McMonagle, P.; Steppan, C.M.; Aschenbrenner, L.; et al. Generation of a VeroE6 Pgp gene knock out cell line and its use in SARS-CoV-2 antiviral study. *Antivir. Res.* **2022**, *208*, 105429. [CrossRef]
20. Yang, Z.-G.; Li, H.-R.; Wang, L.-Y.; Li, Y.-H.; Lu, S.-G.; Wen, X.-F.; Wang, J.; Daikonya, A.; Kitanaka, S. Triterpenoids from *Hippophae rhamnoides* L. and Their Nitric Oxide Production-Inhibitory and DPPH Radical-Scavenging Activities. *Chem. Pharm. Bull.* **2007**, *55*, 15–18. [CrossRef]
21. Siddiqui, S.; Siddiqui, B.S.; Hafeez, F.; Begum, S. Isolation and Structure of Neriucoumaric and Isoneriucoumaric Acids from the Leaves of *Nerium oleander*. *Planta Medica* **1987**, *53*, 424–427. [CrossRef]
22. Fuchino, H.; Satoh, T.; Tanaka, N. Chemical Evaluation of Betula Species in Japan. I.Constituents of *Betula ermanii*. *Chem. Pharm. Bull.* **1995**, *43*, 1937–1942. [CrossRef]
23. Takahashi, H.; Iuchi, M.; Fujita, Y.; Minami, H.; Fukuyama, Y. Coumaroyl triterpenes from *Casuarina equisetifolia*. *Phytochemistry* **1999**, *51*, 543–550. [CrossRef]
24. Reshamwala, D.; Shroff, S.; Liimatainen, J.; Tienaho, J.; Laajala, M.; Kilpeläinen, P.; Viherä-Aarnio, A.; Karonen, M.; Jyske, T.; Marjomäki, V. Willow (*Salix* spp.) bark hot extracts inhibit both enveloped and nonenveloped viruses: Study on its anti-coronavirus and anti-enterovirus activities. *Front. Microbiol.* **2023**, *14*, 1249794. [CrossRef]
25. Zhan, Y.; Ta, W.; Tang, W.; Hua, R.; Wang, J.; Wang, C.; Lu, W. Potential antiviral activity of isorhamnetin against SARS-CoV-2 spike pseudotyped virus in vitro. *Drug Dev. Res.* **2021**, *82*, 1124–1130. [CrossRef] [PubMed]
26. Rousi, A. The genus Hippophaë L. A taxonomic study. *Ann. Bot. Fenn.* **1971**, *8*, 177–227.
27. Zakynthinos, G.; Varzakas, T. *Hippophae rhamnoides*: Safety and nutrition. *Curr. Res. Nutr. Food Sci. J.* **2015**, *3*, 89–97. [CrossRef]
28. Żuchowski, J. Phytochemistry and pharmacology of sea buckthorn (*Elaeagnus rhamnoides*; syn. *Hippophae rhamnoides*): Progress from 2010 to 2021. *Phytochem. Rev.* **2023**, *22*, 3–33. [CrossRef]
29. Kim, S.-J.; Hwang, E.; Yi, S.S.; Song, K.D.; Lee, H.-K.; Heo, T.-H.; Park, S.-K.; Jung, Y.J.; Jun, H.S. Sea Buckthorn Leaf Extract Inhibits Glioma Cell Growth by Reducing Reactive Oxygen Species and Promoting Apoptosis. *Appl. Biochem. Biotechnol.* **2017**, *182*, 1663–1674. [CrossRef]
30. Upadhyay, N.K.; Kumar, M.Y.; Gupta, A. Antioxidant, cytoprotective and antibacterial effects of Sea buckthorn (*Hippophae rhamnoides* L.) leaves. *Food Chem. Toxicol.* **2010**, *48*, 3443–3448. [CrossRef]
31. Basu, M.; Prasad, R.; Jayamurthy, P.; Pal, K.; Arumughan, C.; Sawhney, R. Anti-atherogenic effects of seabuckthorn (*Hippophaea rhamnoides*) seed oil. *Phytomed. Int. J. Phytother. Phytopharm.* **2007**, *14*, 770–777. [CrossRef]
32. Solcan, C.; Gogu, M.; Floristean, V.; Oprisan, B.; Solcan, G. The hepatoprotective effect of sea buckthorn (*Hippophae rhamnoides*) berries on induced aflatoxin B1 poisoning in chickens. *Poult. Sci.* **2013**, *92*, 966–974. [CrossRef] [PubMed]
33. Goel, H.; Kumar, I.P.; Samanta, N.; Rana, S. Induction of DNA-protein cross-links by *Hippophae rhamnoides*: Implications in radioprotection and cytotoxicity. *Mol. Cell. Biochem.* **2003**, *245*, 57–67. [CrossRef] [PubMed]

34. Upadhyay, N.K.; Kumar, R.; Siddiqui, M.S.; Gupta, A. Mechanism of Wound-Healing Activity of *Hippophae rhamnoides* L. Leaf Extract in Experimental Burns. *Evid.-Based Complement. Altern. Med.* **2011**, *2011*, 659705. [CrossRef] [PubMed]
35. Marciniak, B.; Kontek, R.; Żuchowski, J.; Stochmal, A. Novel bioactive properties of low-polarity fractions from sea-buckthorn extracts (*Elaeagnus rhamnoides* (L.) A. Nelson)—(in vitro). *Biomed. Pharmacother.* **2021**, *135*, 111141. [CrossRef] [PubMed]
36. Yu, M.; Si, L.; Wang, Y.; Wu, Y.; Yu, F.; Jiao, P.; Shi, Y.; Wang, H.; Xiao, S.; Fu, G.; et al. Discovery of Pentacyclic Triterpenoids as Potential Entry Inhibitors of Influenza Viruses. *J. Med. Chem.* **2014**, *57*, 10058–10071. [CrossRef] [PubMed]
37. Yu, F.; Wang, Q.; Zhang, Z.; Peng, Y.; Qiu, Y.; Shi, Y.; Zheng, Y.; Xiao, S.; Wang, H.; Huang, X.; et al. Development of Oleanane-Type Triterpenes as a New Class of HCV Entry Inhibitors. *J. Med. Chem.* **2013**, *56*, 4300–4319. [CrossRef] [PubMed]
38. Si, L.; Meng, K.; Tian, Z.; Sun, J.; Li, H.; Zhang, Z.; Soloveva, V.; Li, H.; Fu, G.; Xia, Q.; et al. Triterpenoids manipulate a broad range of virus-host fusion via wrapping the HR2 domain prevalent in viral envelopes. *Sci. Adv.* **2018**, *4*, eaau8408. [CrossRef] [PubMed]
39. Ryu, Y.B.; Park, S.-J.; Kim, Y.M.; Lee, J.-Y.; Seo, W.D.; Chang, J.S.; Park, K.H.; Rho, M.-C.; Lee, W.S. SARS-CoV 3CLpro inhibitory effects of quinone-methide triterpenes from *Tripterygium regelii*. *Bioorganic Med. Chem. Lett.* **2010**, *20*, 1873–1876. [CrossRef]
40. Darshani, P.; Sarma, S.S.; Srivastava, A.K.; Baishya, R.; Kumar, D. Anti-viral triterpenes: A review. *Phytochem. Rev.* **2022**, *21*, 1761–1842. [CrossRef]
41. Tkacz, K.; Wojdyło, A.; Turkiewicz, I.P.; Nowicka, P. Triterpenoids, phenolic compounds, macro- and microelements in anatomical parts of sea buckthorn (*Hippophaë rhamnoides* L.) berries, branches and leaves. *J. Food Compos. Anal.* **2021**, *103*, 104107. [CrossRef]
42. Braca, A.; Morelli, I.; Mendez, J.; Battinelli, L.; Braghiroli, L.; Mazzanti, G. Antimicrobial Triterpenoids from *Licania heteromorpha*. *Planta Medica* **2000**, *66*, 768–769. [CrossRef] [PubMed]
43. Ali, S.; Alam, M.; Khatoon, F.; Fatima, U.; Elasbali, A.M.; Adnan, M.; Islam, A.; Hassan, I.; Snoussi, M.; De Feo, V. Natural products can be used in therapeutic management of COVID-19: Probable mechanistic insights. *Biomed. Pharmacother.* **2022**, *147*, 112658. [CrossRef] [PubMed]
44. Kumar, A.; Choudhir, G.; Shukla, S.K.; Sharma, M.; Tyagi, P.; Bhushan, A.; Rathore, M. Identification of phytochemical inhibitors against main protease of COVID-19 using molecular modeling approaches. *J. Biomol. Struct. Dyn.* **2021**, *39*, 3760–3770. [CrossRef]
45. Mitra, D.; Verma, D.; Mahakur, B.; Kamboj, A.; Srivastava, R.; Gupta, S.; Pandey, A.; Arora, B.; Pant, K.; Panneerselvam, P.; et al. Molecular docking and simulation studies of natural compounds of *Vitex negundo* L. against papain-like protease (PL^{pro}) of SARS-CoV-2 (coronavirus) to conquer the pandemic situation in the world. *J. Biomol. Struct. Dyn.* **2022**, *40*, 5665–5686. [CrossRef] [PubMed]
46. Anbazhagan, S.; Muthu, S.; Singh, R.K.; Pallab, C. In silico molecular docking analysis targeting SARS-CoV-2 spike protein and selected herbal constituents. *J. Pure Appl. Microbiol.* **2020**, *14*, 989–998.
47. Duhamel, F.; Farvacques, C.; Blondel, C.; Delplanque, S.; Catteau, E.; Gelez, W.; Francois, R.; Prey, T.; Cholet, J.; Buchet, J.; et al. Guide des Végétations Littorales du Nord-Ouest de la France. CBN de Bailleul. Available online: https://www.cbnbl.org/guide-vegetations-littorales-du-nord-ouest-france (accessed on 15 October 2023).
48. Hesp, P. Foredunes and blowouts: Initiation, geomorphology and dynamics. *Geomorphology* **2002**, *48*, 245–268. [CrossRef]
49. Belouzard, S.; Machelart, A.; Sencio, V.; Vausselin, T.; Hoffmann, E.; Deboosere, N.; Rouillé, Y.; Desmarets, L.; Séron, K.; Danneels, A.; et al. Clofoctol inhibits SARS-CoV-2 replication and reduces lung pathology in mice. *PLoS Pathog.* **2022**, *18*, e1010498. [CrossRef]
50. Meunier, T.; Desmarets, L.; Bordage, S.; Bamba, M.; Hervouet, K.; Rouillé, Y.; François, N.; Decossas, M.; Sencio, V.; Trottein, F.; et al. A Photoactivable Natural Product with Broad Antiviral Activity against Enveloped Viruses, Including Highly Pathogenic Coronaviruses. *Antimicrob. Agents Chemother.* **2022**, *66*, e0158121. [CrossRef]